Gas Phase Chemical Physics Program

DOE Principal Investigators'
Abstracts

October 24 – October 25, 2024

Chemical Sciences, Geosciences, and Biosciences Division
Office of Basic Energy Sciences
Office of Science
U.S. Department of Energy

The research grants and contracts described in this document are supported by the U.S. DOE Office of Science, Office of Basic Energy Sciences, Chemical Sciences, Geosciences and Biosciences Division.

Foreword

The 43rd Annual Gas Phase Chemical Physics (GPCP) Principal Investigators' Meeting sponsored by the U. S. Department of Energy (DOE), Office of Basic Energy Sciences (BES) provides a forum for DOE laboratory and university principal investigators (PIs) within the BES GPCP Program to share recent research findings supported by the program. This meeting will facilitate scientific interchange among PIs and afford opportunities for research collaboration.

The GPCP program explores chemical reactivity, kinetics, and dynamics at the level of electrons, atoms, molecules, and nanoparticles in support of the BES mission to understand, predict, and ultimately control matter and energy. The program continues to evolve by identifying new growth areas, including plasma chemistry, chemistry for high value products, and emergent molecular complexity. This is driven by the need to address compelling knowledge gaps in GPCP and accomplished via the development of novel modeling, experimental, and theoretical approaches.

This collection of abstracts presents innovative state-of-the-art research aligned with several themes: chemical dynamics and reaction kinetics, spectroscopy and molecular characterization, gas-surface reactions and heterogeneous catalysis, combustion chemistry, atmospheric chemistry, and computational chemistry and modeling. These investigations advance gas phase chemical physics and align with the research objectives of the Department of Energy's Office of Basic Energy Sciences (BES). We thank all the researchers whose dedication and innovation have advanced DOE BES research. We look forward to our assembly in 2025 for our 44th annual meeting.

Wade Sisk
Tom Settersten

Table of Contents

Nanoparticle Surface Kinetics and Dynamics by Single Nanoparticle Mass Spectrometry

Scott L. Anderson, Chemistry Department, University of Utah
315 S. 1400 E. Salt Lake City, UT 84112 anderson@chem.utah.edu

Program Scope

This project is focused on reaction kinetics and emission spectroscopy for individual nanoparticles (NPs) at high temperatures (T_{NP}), using a single NP mass spectrometry (NPMS) technique. The method allows measurement of absolute kinetics for reactions that change the NP mass, and observation of how kinetics vary from NP-to-NP, or over time as an NP is transformed by reaction, with resolution corresponding to a few percent of a monolayer's work of change. However, NPMS does not directly reveal what reactions are occurring. Past experiments have examined carbon and silicon chemistry, where it was clear from surface science results at lower temperatures, what kinds of elementary reactions occur, and what might remain on the surface under different conditions.

During the current grant period, work has focused on the high T_{NP} sublimation and oxidation chemistry of hafnium-based high temperature materials, including HfC (mp = 4170 K) HfO_2 (mp = 3030 K) and Hf (mp = 2506 K). These systems were chosen to test how well the NPMS method is able to work out what chemistry is occurring, for materials where the literature has little information about the elementary chemistry.

Methodology

Details of the methodology for measuring kinetics are in papers 3, 5, and 6, below, and the approach to measuring NP temperature (T_{NP}) has been discussed previously.[1, 2] Briefly, a single NP of the material of interest is injected into an electrodynamic trap and held at reduced pressure (to slow reaction kinetics). The NP is laser heated with T_{NP} determined by fitting its blackbody-like emission spectrum, and the NP mass is determined with 0.1% precision from the frequency of NP motion in the trap. By monitoring the NP mass vs. time when the NP is held at elevated T_{NP} in either inert or reactive atmosphere, the kinetics for mass-changing processes, such as sublimation, pyrolysis, oxidation, or growth, can be determined with high sensitivity. In addition to being used to determine T_{NP}, the emission spectra and laser heating power provide information about changes in the emissivity and absorptivity of the NP caused by the chemical process being studied.

The single NP approach avoids ensemble averaging, thus providing unique insights into heterogeneity and structure-reactivity relationships, but it is a slow method. Therefore, the experiments are highly automated, allowing operation with just occasional operator input, which can be done remotely. Current improvements in methodology are aimed at reaching higher temperatures to allow studies of refractory NPs of interest for high temperature materials applications.

Recent Progress

Highlights of this research include:

- Measurement of the effects of NP-to-NP variations on reactivity, and on the evolution of reactivity under reaction conditions, for many different NP types and several reactions, including sublimation, oxidation by O_2 and N_2O, and growth by C_2H_2 addition.
- Use of O_2 etching kinetics to monitor changes in the numbers of reactive surface sites for NPs under active etching, allowing correlations with other chemistry, e.g. formation of passivation layers, annealing to low-defect surface structures, etc.
- Characterization of the effects of NP feedstock structure on initial reactivity toward growth, etching, and sublimation reactions.
- Measurement of the kinetics for transformation to a partially passivated state under different temperature/pressure conditions for HfC, HfO_2, and Hf NPs, building on previous studies of structural effect on reactivity for carbon and silicon-based NPs
- Measurements of absolute etching and sublimation kinetics for HfC, HfO_2, and Hf NPs for T_{NP} ranging from 1200 to 2500 K.

- Observation that Hf-based NPs passivate under low O_2 pressure/high temperature conditions but that both initial reaction rates and passivation time scale and completeness depend strongly the NP composition and pre-treatment.
- Comparison of etching and passivation kinetics for Hf NPs with and without melting, with the analogous kinetics for surface-reduced HfO_2 NPs (Hf-rich surface/HfO_2 core), confirming the importance of core oxygen in passivation.
- Development of T-pulse methods to study chemistry at ultra-high T_{NP}, above the range where steady state kinetics measurement methods can be used, due to fast NP sublimation/decomposition.
- Observation of correlations between evolution of sublimation or etching rates and thermal emission spectral properties for Hf-based NPs.

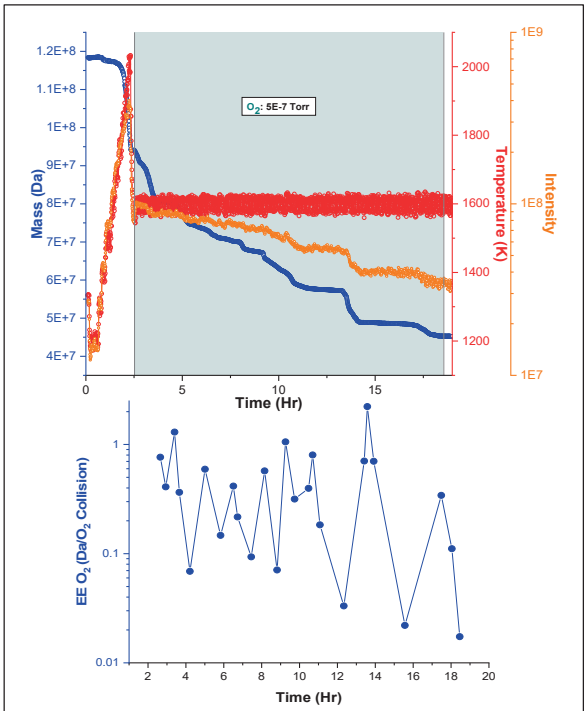

Fig. 1.Etching of an Hf NP at 1600 K.

Recent (not yet published) examples:
Etching and sublimation of Hf NPs.

A typical experiment measuring 1600 K O_2 etching of an Hf NP is shown the figure. The NP was trapped, then first heated to 2000 K in argon atmosphere (white background) to remove surface oxides and other contaminants, resulting in loss of ~20 MDa of mass, then T_{NP} was set to 1600K resulting in stable NP mass in a ~15 minute measuring period. Then, 5 x 10^{-7} Torr of O_2 was added to the atmosphere (cyan background) resulting in substantial additional mass loss due to etching. It is known that HfO_2 essentially non-volatile in this temperature range, but HfO_2 can decompose at high T to liberate $HfO_{(g)}$ and excess oxygen (O/O_2).[3] Therefore, the net etching reaction for Hf corresponds to $2Hf + O_2 \rightarrow 2\ HfO_{(g)}$. The interesting aspect of the etching is that it is unsteady, gradually slowing by roughly an order of magnitude, but with substantial fluctuations in the etching kinetics, as shown in the lower frame of the figure which plots the etching efficiency (EE_{O2} = Da of mass loss/O_2 collision). Over the etching period, this NP lost ~half its mass, corresponding to a decrease from ~28 nm to ~22 nm diameter if the NP were spherical, i.e., the interesting kinetics occurred as the NP lost ~3 nm from its surface. The gradual slowing is attributed to increasing coverage by HfO_2 (more thermally stable than HfO), and the fluctuations indicate that formation of this passivating layer is unsteady, with passivated areas growing and shrinking due to competition between HfO desorption and nucleation and growth of HfO_2 islands.

Etching and sublimation of surface-reduced HfO_2.

Hf NPs eventually passivate at low etching temperatures due to formation of a stable HfO_2 surface layer capping the Hf-rich core. Another starting point to probe the etching and passivation kinetics is NPs with an HfO_2 core capped by an Hf-rich surface layer. Such surface-reduced HfO_2 NPs can be prepared simply by briefly heating HfO_2 NPs in vacuum, taking advantage of the fact that HfO_2 decomposes at high T to liberate excess oxygen, in addition to HfO.[3] The figure shows an example experiment in which a ~23nm dia. HfO_2 NP was trapped, briefly heated by a CO_2 laser, then subjected to sequential T_{NP} ramps to study the sublimation kinetics (top frame), and finally studied by constant temperature (1500K) O_2 etching at P_{O2} = 4 x 10^{-5} Torr (~two orders of magnitude higher than in fig. 1).

Roughly 5.7 MDa of mass was lost to sublimation during that phase of the experiment, corresponding to only ~0.65 nm from the NP surface. Then, during the etching phase the NP lost ~40% of the mass at the start of the etching phase, but then abruptly passivated, having lost roughly ~1.9 nm worth of material from its surface. Passivation of surface-reduced HfO_2 is more rapid than that for Hf and HfC NPs, and similar behavior was observed surface-resulted SiO_2 and Si NPs (publications 3 and 5). The rapid passivation is attributed to the presence of oxygen in the core of the surface-reduced oxide NPs, which inhibits O diffusion from the surface to the core, blocking a minor-but-important mechanism for O loss from the surface layer that slows the formation of surface SiO_2 or HfO_2.

Etching and sublimation of HfC

The material of greatest interest for high temperature applications is HfC, which has the second highest known melting point. Fig. 3 shows an example experiment, looking at O_2 etching and passivation of a ~37 nm HfC NP. The NP was first heated to 2000 K to desorb oxides or other contaminants, and then exposed to O_2 at 1500 K for ~20 hours. The initial etching rate was fast, reflecting the net reaction: $HfC + O_2 \rightarrow HfO_{(g)} + CO_{(g)}$, but after losing ~5nm from the NP surface, the etching rate slowed abruptly, signaling formation of a passivating HfO_2 layer. Closer examination of the mass vs. time for the "passivated" particle (upper right plot) shows that in fact, the NP continued to react, albeit slowly and in an unsteady fashion. The EE_{O2} plot at the lower right shows that the etching kinetics slowed by three orders of magnitude, but there continued to be periodic waves of additional etching. In etching of bulk HfC at high temperatures, the oxide layer that forms is quite porous, allowing formation of oxidized layers hundreds of microns thick, and the

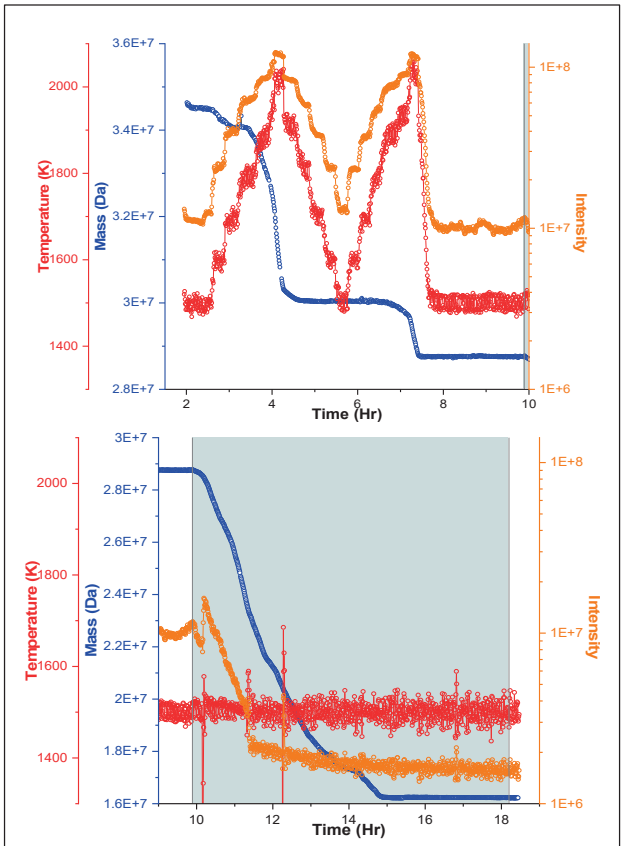

Fig. 2. Sublimation (top) and etching (bottom) of a partially reduced HfO_2 NP.

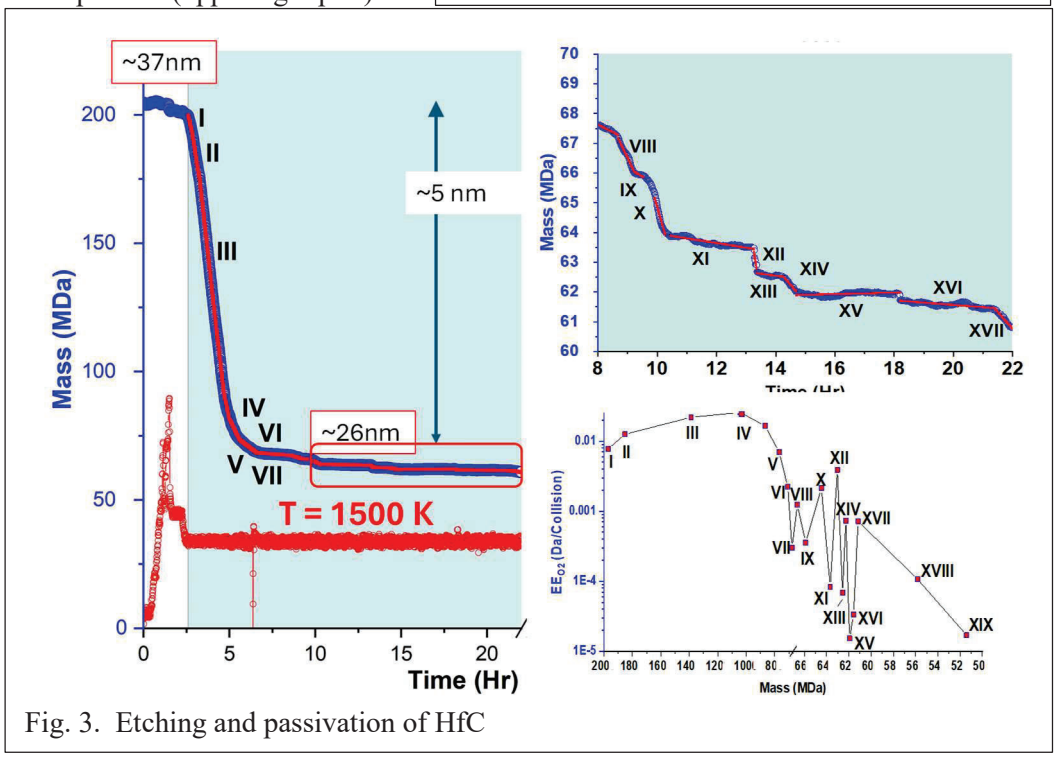

Fig. 3. Etching and passivation of HfC

unsteady etching observed here is attributed to a nano-scale version of porosity, i.e., to cracks opening in the growing HfO_2 layer, allowing additional etching and thickening the oxide layer.

Plans for the coming year:

The grant period expires at the end of February, and during the remaining time, I anticipate finishing the study of HfC, HfO_2, and Hf NPs. In addition to more NP experiments, we have grown some HfC and HfO_2 thick film samples and plan to carry out surface science studies that will show the surface composition and the identity of molecules desorbing from the surface under etching conditions. This should allow us to put together a mechanism and to extract absolute rates for the elementary processes responsible for the initial stages of HfC etching and passivation.

Publications 2022-2024 acknowledging support from the DOE GPCP program

Published or in press:

1. "High Temperature Reaction of Individual Graphite Nanoparticles with N_2O: Etching, Passivation, Sublimation, and Comparison to O_2", Chris Y. Lau, Abigail M. Friese, and Scott L. Anderson, J. Phys. Chem. C 127, 15157-15168 (2023). https://doi.org/10.1021/acs.jpcc.3c02806, and Chemrxiv 10.26434/chemrxiv-2023-6894f)
2. "Growth and Passivation of Individual Carbon Nanoparticles by C_2H_2 addition at High Temperatures: Dependence of Growth Rate and Evolution on Material and Size", Chris Y. Lau, Daniel J. Rodriguez, Abigail M. Friese, and Scott L. Anderson, J. Chem. Phys. 158, 194706 (2023) https://doi.org/10.1063/5.0143948, and ChemRxiv DOI:10.26434/chemrxiv-2023-g9sm2
3. "High Temperature Transformation, O_2 Etching, and Passivation of Single SiO_x Nanoparticles: Kinetics and Optical Properties as Structure Probes", Daniel J. Rodriguez, Chris Y. Lau, Abigail M. Friese, and Scott L. Anderson, Mol. Phys. (2023) p. e2184652 DOI: 10.1080/00268976.2023.2184652, and ChemRxiv DOI: 10.26434/chemrxiv-2023-cs6vh.
4. "Methods for Non-Destructive, High Precision Mass/Charge Determination for Single, Trapped, GigaDalton Nanoparticles", David M. Bell, Collin R. Howder, Bryan A, Long, Scott L. Anderson, ChemRxiv (December 2022) DOI: 10.26434/chemrxiv-2022-1n56p Note: this is a "how-to" article which we decided to make available online to help others get started with NP mass measurements.
5. "O_2 Oxidation and Sublimation Kinetics of Single Silicon Nanoparticles at 1200 to 2050 K: Variation of Reaction Rates, Evolution of Structural and Optical Properties, and the Active-to-Passive Transition", Daniel J. Rodriguez, Chris Y. Lau, Abigail M. Friese, Bryan A. Long, and Scott L. Anderson, J. Phys. Chem. C (2023)126, 18716–18733, DOI: 10.1021/acs.jpcc.2c05985. Also ChemRxiv DOI: 10.26434/chemrxiv-2022-2ll5c
6. "High Temperature Oxidation of Single Carbon Nanoparticles: Dependence on Surface Structure, and Probing Real-Time Structural Evolution via Kinetics", Daniel J. Rodriguez, Chris Y. Lau, Abigail M. Friese, Alexandre Magasinski, Gleb Yushin, and Scott L. Anderson*, J. Am. Chem. Soc. (2022), 144, 4897–4912, DOI: 10.1021/jacs.1c12698. Also ChemRxiv: 10.26434/chemrxiv-2022-3b3h8

References

(1) Long, B. A.; Rodriguez, D. J.; Lau, C. Y.; Anderson, S. L. Thermal emission spectroscopy for single nanoparticle temperature measurement: optical system design and calibration. *Appl. Opt.* **2019**, *58* (3), 642-649. DOI: 10.1364/AO.58.000642.

(2) Long, B. A.; Rodriguez, D. J.; Lau, C. Y.; Schultz, M.; Anderson, S. L. Thermal Emission Spectroscopy of Single, Isolated Carbon Nanoparticles: Effects of Particle Size, Material, Charge, Excitation Wavelength, and Thermal History. *J. Phys. Chem. C* **2020**, *124*, 1704-1716. DOI: 10.1021/acs.jpcc.9b10509.

(3) Panish, M. B.; Reif, L. Thermodynamics of the Vaporization of Hf and HfO2: Dissociation Energy of HfO. *The Journal of Chemical Physics* **1963**, *38* (1), 253-256. DOI: 10.1063/1.1733473 (acccessed 9/18/2024).

Chemical Dynamics in the Gas Phase at Argonne: Chemical Dynamics Subtask

Ahren W. Jasper (ajasper@anl.gov), Stephen T. Pratt (stpratt@anl.gov),
and Kirill Prozument (prozument@anl.gov)
Chemical Sciences and Engineering Division, Argonne National Laboratory

Program Scope

Complementary experimental and theoretical studies of gas phase dynamics are performed to explore unimolecular and bimolecular reactivity, energy flow within molecules and between collision partners, and the detailed mechanisms through which chemistry takes place. The studies produce improved theoretical methods and new fundamental descriptions of chemical dynamics at the molecular scale and are carried out in close coordination with work in the Thermochemistry, Kinetics, and Methods and Modeling Subtasks of the Chemical Dynamics in the Gas Phase Group at Argonne. The theoretical component is supplied by Jasper who emphasizes methods development and applications for predicting pressure-dependent, nonthermal, and electronically nonadiabatic chemistry, with recent studies taking advantage of high-performance computing. The experimental component is supplied by Pratt and Prozument. Pratt uses photoionization and photodissociation experiments to elucidate the spectroscopy and dynamics of highly excited molecules and radicals, with recent work focusing on resonant processes in core-excited molecules and new experiments using ultrafast free-electron laser sources. Prozument develops and applies chirped-pulse millimeter-wave spectroscopy to probe chemical dynamics and kinetics as well as artificial intelligence methods to assign rotational spectra. His future work involves a multi-experiment approach to understanding dynamical phenomena at different energy scales and in varied environments through the quantification of time- and vibrational-state-dependent branching ratios.

Recent Progress

Theory. Trajectory studies benefit from robust and convenient strategies for parametrizing global potential energy surfaces (PESs). We continued automating and validating methods for constructing permutationally invariant polynomial (PIP) expansions of PESs for reactive molecular systems. In earlier work with Davis, we used greedy subset selection to significantly (>10x) reduce PIP expansions, recovering nearly linear scaling with respect to dimensionality. In recent work, we demonstrated >100x speedups in PIP evaluations using GPUs, and similar speedups are being pursued for our greedy subset selection algorithm. As an example of a recent application, we fit a global PES for $CH_3 + CH_2 = C_2H_5 = C_2H_4 + H$. The 6th order PIP expansion for this system has nearly 250k terms, 2177 free parameters using full permutational symmetry, and a weighted fitting error of ~3 kcal/mol for training data spanning 300 kcal/mol. Greedy subset selection using a PIP7 dictionary resulted in a PIP expansion with a similar error and just 35k terms.

Sometimes it is more convenient to skip PES fitting and instead evaluate forces via direct calls to electronic structure codes. In support of experimental work from Prozument, we ran direct trajectories for a key step in the photodissociation of formamide, NH_2CHO.[10] Trajectories were initiated in the NHCHOH well with a total energy of 148 kcal/mol, far in excess of the thresholds for the direct products (44, 74, and 83 kcal/mol for the NH_2CHO, H_2O + HCN, and H_2O + HNC channels, respectively). The goal was to compute the HNC/HCN branching ratio, and these products were formed after only a few ps. The PBE0/aug-cc-pVTZ level of theory was identified as a good compromise of efficiency and accuracy, and, despite the short simulation times, each of the 500 trajectories took ~20 hours, on

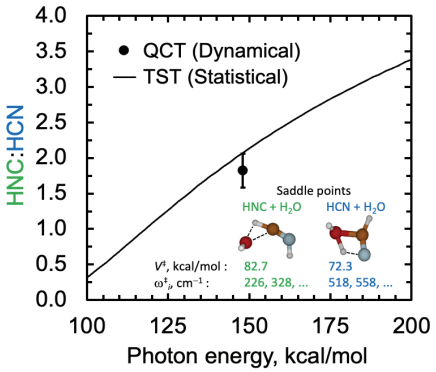

Fig. 1. HNC to HCN branching ratio predicted using QCT and TST. The key saddle points for these processes are shown along with their energies and lowest frequencies. The HNC saddle point is higher-energy but less rigid.

average. In subsequent work, we developed a PIP6 expansion for this system with 50k terms, a fitting error of 1.5 kcal/mol, and trajectories that each took only a few seconds. Notably, the direct dynamics study required almost no human effort to set up, whereas PIP development required significant human intervention such that both strategies took about the same number of overall calendar days.

A major goal of this work is to develop, apply, and demonstrate the accuracy of dynamics for studying collisional energy transfer (CET) and intramolecular vibrational energy redistribution (IVR) and for predicting pressure dependent and nonthermal kinetics. Numerous applications were carried out to test our approaches and to support experimentalists and modelers, including: ionization energy studies for Criegee chemistry with Popolan-Vaida, carbene chemistry kinetics with Sivaramakrishnan and Tranter, QOOH(+M) kinetics with Lester and co-workers, PAH chemistry with Frenklach and Mebel, energy transfer in vdW dimers with Caravan, O_3(+M) kinetics with Glarborg, astrochemistry with Galvão and Kaiser, and a dynamics study of CO_2 superrotors with Kliewer.

Experimental Photoionization and Photodissociation. Over the past year, Pratt has focused on electronic autoionization and resonant Auger decay in small molecules. Two papers were published on resonant Auger decay near the I $4d^{-1}$ edge of CH_3I and C_6H_5I. Participator decay, which involves the excited electron, accesses the regular valence states of the molecular cation, while spectator decay accesses the two-hole one-particle (2h-1p) states that tend to be highly correlated and difficult to calculate. Pratt has worked to develop complementary approaches to access such states and improve the ability to characterize them.

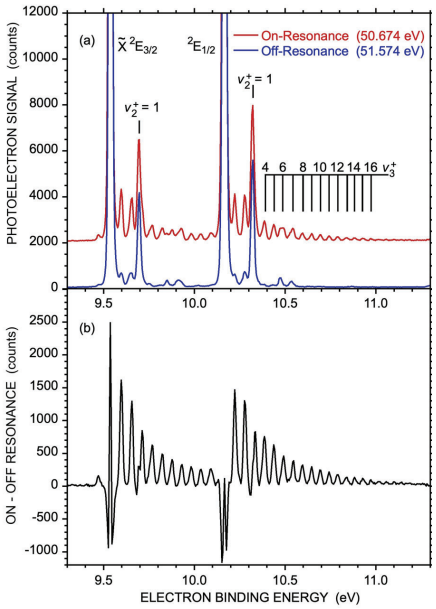

Fig. 2. Resonant Auger spectra of CH_3I with participator decay populating a long progression in the C-I stretch of the CH_3I^+ ground state.

Over the past year, a considerable effort has been spent analyzing time-resolved photoelectron spectra of the A ^1A_u state of acetylene recorded at the FERMI free electron laser (FEL) facility. This work was performed by a large international collaboration of experimentalists and theoreticians led by Pratt. By pumping the A ^1A_u state with 6.2 eV photons and ionizing it with 20.8 eV photons from the FEL, the excitation process accessed not only the X $^2\Pi_u$ and A $^2\Sigma_g^+$ valence states of the cation, but also the previously predicted, but unobserved, 2h-1p 1 $^2\Pi_g$ state of the cation. In agreement with theoretical predictions, the latter state is the most intense in the two-photon spectrum, even though it is nominally forbidden in the single-photon ionization spectrum. As discussed above, such 2h-1p states are often observed in resonant Auger spectra, but the ability to access them directly in two-photon excitation will ultimately provide a powerful tool for their characterization. A paper will be submitted in the near future.

In the past year, Pratt also coauthored two papers involving an earlier collaboration at the FERMI FEL to study the photoionization of atomic He and N_2 using phase-control methods. The work on N_2 has been published and the work on He is currently under review at the journal.

Pratt has had two new beamtimes at the FERMI FEL since the last annual report. In the first, he led a team studying the two-photon ionization of Xe and XeF_2 near the Xe $4p^{-1}$ edge at ~148 eV. This region is interesting because the $4p^{-1}$ edge is at almost exactly the same energy as the $4d^{-2}$ edge, so that there is a high density of Xe^+ $4d^{-2}$nl 2h-1p states near the Xe^+ $4p^{-1}$ single hole state. The configuration mixing amongst these states is extremely strong, and results in unexpectedly complex structure in single-photon studies near the $4p^{-1}$ edge. By exciting into this region with two 74 eV photons, the goal was to enhance the excitation of the Xe $4d^{-2}$ component of these states, and to allow a more complete characterization of the configuration mixing. The molecular character of the XeF_2 adds to the expected complexity but should provide insight into how the molecular character affects the configuration mixing. The extraction of the desired signal in FEL experiments is typically quite involved, and the analysis of the data is still ongoing, Nevertheless, we

do appear to see clear evidence for the two-photon process in Xe, and we are making progress on a more comprehensive analysis of the data.

In the second set of experiments, Pratt collaborated on time-resolved ultrafast experiments led by Russell Minns (University of Southampton, UK) to study the near ultraviolet (267 nm) photodissociation of 2-iodothiophene. In these experiments, photoelectron spectroscopy following ionization from either the S 2p or I 4d shells provided a probe of the local environment around these two atoms as a function of time-delay following the ultraviolet excitation of the molecule. In particular, changes in the I 4d photoelectron spectrum shows the effects of breaking the C-I bond, while changes in the S 2p photoelectron spectrum reflect torsional motion and opening of the five-member thiophene ring. In these experiments, it appears the decay processes were dominated by C-I bond fission, but the full analysis of the data is still underway. We have proposed new experiments on 2-bromothiophene at shorter wavelengths that should provide better access to the ring opening dynamics.

Finally, Pratt and collaborators from Daresbury Laboratory and Universite Paris-Saclay published a comprehensive vacuum ultraviolet absorption spectrum of ammonia recorded at the Fourier Transform Spectrometer (FTS) at SOLEIL. The data included absolute absorption cross sections recorded with a resolution of ~0.23 cm^{-1} at both room temperature and ~70K, and are of significantly higher quality than the previously existing data. In the past year, the team had beamtime to record the analogous spectra of ND_3, NH_2D, and NHD_2. The analysis of these data will be pursued in the coming year.

Chirped-pulse millimeter-wave spectroscopy: Thermal reactions. Thermally induced oxidation reactions continue to be studied with a recently developed SiO_2/SiC microreactor.[11] The reactor is coupled to a CP-FTmmW spectrometer with fast digitizer that can average up to 1 billion free induction decay traces in 2 hours and achieves superior sensitivity. We are observing the CH_2OO Criegee intermediate (CI) emerging from a heated reactor. Observation of the CI in an environment that is relevant to low-temperature combustion and flames is surprising, but unambiguous. We think that CH_2OO is formed in a cooler region near the exit of the reactor, with the temperature of 650 K or lower, where the predicted lifetime of this species is > 1 μs. It is plausible that the reaction mechanism proposed for a discharge environment [T. L. Nguyen, M. C. McCarthy, and J. F. Stanton, J. Phys. Chem. A **119**, 7197 (2015)] is applicable to this work. It involves recombination of methyl radicals and molecular oxygen to form energized CH_3OO radical, which then forms a complex with O_2 and dissociates to CH_2OO and HO_2, possibly via tunneling under a 9.7 kcal/mol barrier. The pathway results in a CH_2OO that does not have sufficient energy to further isomerize do dioxirane and formic acid.

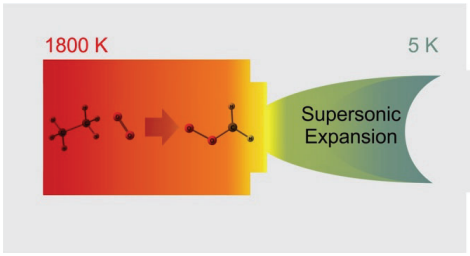

Chirped-pulse millimeter-wave spectroscopy: Photodissociation dynamics. The photodissociation dynamics of formamide, NH_2CHO, following absorption of a 193 nm photon has been analyzed.[10] As discussed above, theoretical branching ratios of the HCN and HNC photoproducts provided by Jasper agree with the experiment. Underestimation by theory of the HNCO yield led to an understanding that formation of most of HNCO in this 193 nm photodissociation is initiated on the S_1 electronic surface. As described in the literature [I. Antol, M. Eckert-Maksic, M. Barbatti, and H. Lischka, J. Chem. Phys. **127**, 234303 (2007)], dissociation to NH_2CO + H along the (S_1/S_0) conical intersection with subsequent dissociation to HNCO + H on S_0 is quantitatively consistent with our experimental branching to HNCO.

Chirped-pulse millimeter-wave spectroscopy: AI for spectroscopy. This branch of our Program resulted in a curious work where we posed a question of whether a rotational spectrum uniquely identifies a molecular structure. For decades it has been assumed that this inverse problem is well-posed. With the new opportunities offered by the vast datasets of chemical species with calculated properties, in collaboration with Davis, Schwarting, Seifert, Blaiszik and Foster, we demonstrate that there are multiple

Category	Molecule 1	Molecule 2
Lewis Structure	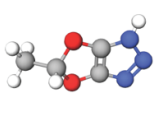	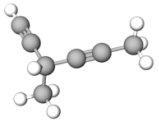
R, MHz	4948.75	4970.63
A, MHz	4611.44	4631.89
B, MHz	1393.04	1403.50
C, MHz	1133.22	1132.71

instances where two structurally distinct species have almost identical rotational constants and spectra.[6] An example of such *twins* is shown in the Figure. Although their spectra would probably be experimentally resolved, the chemical identity of the species could not be distinguished using standard theoretical methods for structure calculation. This work has consequences for the efforts of many research groups, including ours, to automatically assign rotational spectra *and* perceive the molecular identity of the carrier. There will be instances where such an inverse problem is ill-posed and additional measurements may need to be performed to solve it.

Future Work

Theory. We will continue to generalize, improve, and test our dynamics and transition state theory (TST) methods. With Skodje, we are developing TST methods for predicting nonthermal and nonequilibrium kinetics involving generalized transition states with energy- (or momentum-) dependent dividing surfaces. QCTs are being run on a variety of systems to test assumptions inherent in TST, including statistical assumptions about IVR, dynamical recrossing, and incomplete equilibration at the transition state. In an ongoing study, we identified a dynamical correction to TST using QCTs that quantifies incomplete IVR in the H + HO_2 reaction. The magnitude of this correction was shown to increase with the internal energy of HO_2, leading to an overall negative energy dependence in the rate constant. While inefficient IVR is often invoked, it does not often have such a big impact on the overall kinetics. Its importance here is likely due to the presence of a deep intermediate well (H_2O_2) and barrierless bimolecular channels. To further explore this physics, we prepared two artificial sets of PESs for this reaction. In one set, we modified the location and depth of the intermediate well without significantly altering the repulsive wall relevant to the initial H + HO_2 collision. The amount of inefficient IVR observed for this set of artificial PESs was very similar to the unmodified PES. In a second set of artificial PESs, we altered the shape of the repulsive wall around without significantly affecting the intermediate well. By "rounding out" the repulsive wall, we found we could promote energy sharing and largely turn off inefficient IVR.

Experimental Photoionization and Photodissociation. In the coming year, Pratt will work on the analysis of two-photon photoelectron spectra of Xe and XeF_2 near the 4p edge that were recorded at the FERMI FEL. This work has been discussed with two theoretical chemists, Lan Cheng (Johns Hopkins) and Phay Ho (Argonne), who are interested in modeling the spectra if definitive results can be extracted from the data. Pratt will also be involved in the analysis of the FEL experiments on 2-iodothiophene. As mentioned above, a beamtime proposal for new work on 2-bromothiophene has been submitted, and the outcome will be known in the coming months. Several new collaborative beamtime proposals have also been submitted to record high-resolution resonant Auger electron spectra at the SOLEIL Synchrotron. The first of these is focused on resonant Auger decay near the C 1s edge of acetylene, with the goal of observing spectator decay to the 2h-1p 1 $^2\Pi_g$ state that was first observed in our experiments at FERMI. These experiments would close the cycle for the 1 $^2\Pi_g$ state by demonstrating it can be accessed from below or above. Two additional proposals are two study resonant Auger processes in small heteronuclear ring compounds (pyrrole, furan, and thiophene) and Cr-carbonyl compounds. In each case, the resonant processes will be studies at energetically accessible edges for two or three elements, and which should provide a more detailed understanding of the bonding and electronic structure of these molecules.

This past year, Ch. Jungen (Universite Paris-Saclay, France) and Pratt published a new approach to assign molecular Rydberg spectra using theoretical photoionization phase shifts and transition moments, with an application to the 2-butyne spectrum. By working from the continuum back into the discrete spectrum, this approach avoids some of the difficulties of traditional bottom up approaches. In the future, we hope to apply this approach to the analysis of a number of absorption spectra recorded previously at SOLEIL on molecules including ammonia isotopomers, and pentynes and hexynes.

Chirped-pulse millimeter-wave spectroscopy: We plan to explore whether oxidation of other fuels would show presence of the CH_2OO CI. For example, the C–O bond energy in dimethyl ether is slightly lower than the C–C bond energy in ethane. Hence, it would produce more CH_3 radicals and CH_2OO if our understanding of the mechanism is correct. Experiments with deuterated precursors will help to confirm the proposed pathway for CI formation as it involves reaction through tunneling. We also plan to conduct

a nutation experiment to determine the *a*-axis projection of the dipole moment of CH_2OO, which is now known solely from theory. Analysis of the novel photodissociation data where HCCCN products of the 193 nm photolysis of CH_2CHCN show vibrational state-dependent rates of formation will continue.

Publications supported by this project since 2022.

1. R. A. Shaik, A. W. Jasper, P. T. Lynch, R. Sivaramakrishnan, and R. S. Tranter, Initiation and carbene induced radical chain reactions in CH_2F_2 pyrolysis. *ChemPhysChem*, online (2024). DOI:10.1002/cphc.202400362
2. H. Zhao, C. Yan, G. Song, Z. Wang, A. W. Jasper, S. J. Klippenstein, Y. Ju, High-pressure oxidation of hydrogen diluted in N_2 with added H_2O or CO_2 at 100 atm in a supercritical-pressure jet-stirred reactor. *Combust. Flame* **226**, 113543 (2024).
3. Y. Qian, T. K. Roy, A. W. Jasper, C. A. Sodjak, M. C. Kozlowski, S. J. Klippenstein, and M. I. Lester, Isomer-resolved unimolecular dynamics of the hydroperoxyalkyl intermediate (•QOOH) in cyclohexane oxidation*. Proc. Natl. Acad. Sci.* **121**, e2401148121 (2024). DOI:10.1073/pnas.2401148121
4. Z. Shi, A. D. Lele, A. W. Jasper, S. J. Klippenstein, and Y. Ju, Quasiclassical trajectory calculation of rate constants using an ab initio trained machine learning model (aML-MD) with multifidelity data. *J. Phys. Chem. A* **128***,* 3449–3457 (2024). DOI:10.1021/acs.jpca.4c00750
5. M. Frenklach, A. W. Jasper, and A. M. Mebel, Phenalenyl growth reactions and implications to prenucleation chemistry of aromatics in flames*. Phys. Chem. Chem. Phys.* **26***,* 13034-13048 (2024). DOI:10.1039/D4CP00096J
6. M. Schwarting, N. A. Seifert, M. J. Davis, B. Blaiszik, I. Foster, K. Prozument, Twins in rotational spectroscopy: Does a rotational spectrum uniquely identify a molecule? J. Chem. Phys. **161**, 044309 (2024). https://doi.org/10.1063/5.0212632
7. R. L. Caravan, T. J. Bannan, F. A. F. Winiberg, M. A. H. Khan, A. C. Rousso, A. W. Jasper, S. D. Worrall, A. Bacak, P. Artaxo, J. Brito, M. Priestley, J. D. Allan, H. Coe, Y. Ju, D. L. Osborn, N. Hansen, S. J. Klippenstein, D. E. Shallcross, C. A. Taatjes & C. J. Percival, Observational evidence for Criegee intermediate oligomerization reactions relevant to aerosol formation in the troposphere*. Nat. Geosci.* **17**, 219–226 (2024). DOI:10.1038/s41561-023-01361-6
8. J. Jian, H. Hashemi, H. Wu, P. Glarborg, A. W. Jasper, and S. J. Klippenstein, An experimental, theoretical, and kinetic modeling study of post-flame oxidation of ammonia*. Combust. Flame* **261**, 113325 (2024). DOI:10.1016/j.combustflame.2024.113325
9. Y. Shu, Z. Varga, A. W. Jasper, J. Espinosa-Garcia, J. C. Corchado, and D. G. Truhlar, PotLib 2023: New version of a potential energy surface library for chemical systems. *Comput. Phys. Comm.* **294**, 108937 (2024). DOI:10.1016/j.cpc.2023.108937
10. K. L. Caster, N. A. Seifert, B. Ruscic, A. W. Jasper, and K. Prozument, Dynamics of HCN, HNC, and HNCO formation in the 193 nm photodissociation of formamide. *J. Phys. Chem. A*, online (2024). DOI:10.1021/acs.jpca.4c02232
11. N. A Seifert, B. Ruscic, R. Sivaramakrishnan, and K. Prozument, The C_2H_4O isomers in the oxidation of ethylene. J. Mol. Spectrosc. **398**, 111847/1-8 (2023); https://doi.org/10.1016/j.jms.2023.111847
12. N. A. Seifert, K. Prozument, and M. J. Davis, Computational optimal transport for molecular spectra: The fully continuous case, J. Chem. Phys. **159**, 164110 (2023). doi: 10.1063/5.0166469
13. S. T. Pratt, U. Jacovella, S. Boyé-Péronne, M. N. R. Ashfold, D. Joyeux, N. De Oliveira, and D. M. P. Holland, High-resolution absorption spectroscopy of reoom-temperature and jet-cooled ammonia between 59,000 and 93,000 cm^{-1}, J. Mol. Spectrosc. 396, 111810 (2023). https://doi.org/10.1016/j.jms.2023.111810
14. Ch. Jungen and S. T. Pratt, An energy-modfied quantum defect method for the analysis of Rydberg spectra: application to 2-butyne, J. Chem. Phys. in press (2024). DOI: 10.1063/5.0224294
15. S. T. Pratt, U. Jacovella, B. Gans, J. D. Bozek, and D. M. P. Holland, Resonant Auger decay of dissociating CH_3I near the I 4d threshold, J. Chem. Phys.**160**, 074304 (2024) https://doi.org/10.1063/5.0190794
16. S. T. Pratt, U. Jacovella, B. Gans, J. D. Bozek, and D. M. P. Holland, Resonant Auger decay of iodobenzene below the I 4d edge, J. Chem. Phys. **160**, 174309 (2024). https://doi.org/10.1063/5.0203661
17. M. Fushitani, H. Fujise, A. Hishikawa, D. You, S. Saito, Y. Luo, K. Ueda, H. Ibrahim, F. Légaré, S. T. Pratt, P. Eng-Johnsson, J. Mauritsson, A. Olofsson, J. Peschel, E. R. Simpson, P. A. Carpeggiani, D. Ertel, P. K. Marojou, M. Moioli, G. Sansone, R. Shah, T. Csizmadia, M. Dumergue, N. G. Harshitha, S. Kühn, C. Callegari, M. Danailov, A.Demidovich, L. Raimondi, M. Zangrando, G. De Ninno, M. Di Fraia, L. Giannessi, O. Plekan, P.

Rebernik Ribic, and K.C. Prince, Wave packet dynamics and control in excited states of molecular nitrogen, J. Chem. Phys. **160**, 104203 (2024). https://doi.org/10.1063/5.0188182

18. A. C. DeCecco, A. R. Conrad, A. M. Floyd, A. W. Jasper, N. Hansen, P. Dagaut, N.-E. Moody, and D. M. Popolan-Vaida, Tracking the reaction networks of acetaldehyde oxide and glyoxal oxide Criegee intermediates in the ozone-assisted oxidation reaction of crotonaldehyde**.** *Phys. Chem. Chem. Phys.*, online (2024). DOI: 10.1039/D4CP01942C\
19. T. Y. Chen, S. A. Steinmetz, B. D. Patterson, A. W. Jasper, and C. J. Kliewer. Direct observation of coherence transfer and rotational-to-vibrational energy exchange in optically centrifuged CO_2 super-rotors. *Nature Comm.*, accepted (2023).
20. T. M. Selby, F. Goulay, S. Soorkia, A. Ray, A. W. Jasper, S. J. Klippenstein, A. N. Morozov, A. M. Mebel,
21. J. D. Savee, C. A. Taatjes, and D. L. Osborn, Radical-radical reactions in molecular weight growth: The phenyl + propargyl reaction. *J. Phys. Chem. A* 127, 2577–2590 (2023).
22. A. C. R. Gomes, A. C. Souza, A. W. Jasper, and B. R. L. Galvão, The P(^{4}S) + NH($^3\mathbf{\Sigma}^-$) and N(^{4}S) + PH($^3\mathbf{\Sigma}^-$) reactions as sources of interstellar phosphorus nitride. *Pub. Astron. Soc. Aus.* 40, e011 (2023).
23. D. E. Couch, A. W. Jasper, G. Kukkadapu, M. M. San Marchi, A. J. Zhang, C. A. Taatjes, and Nils Hansen, Molecular weight growth by the phenyl + cyclopentadienyl reaction: Well-skipping, ring-opening, and dissociation. *Combust. Flame*, 112502 (2022).
24. J. Cho, A. W. Jasper, Y. Georgievskii, S. J. Klippenstein, and R. Sivaramakrishnan, The role of energy transfer and competing bimolecular reactions in characterizing the unimolecular dissociations of allylic radicals. *Combust. Flame*, online (2022).
25. D. E. Couch, G. Kukkadapu, A. J. Zhang, A. W. Jasper, C. A. Taatjes, and Nils Hansen, The role of radical-radical chain propagating pathways in the phenyl + propargyl reaction. *Proc. Combust. Inst.*, online (2022).
26. J. Cho, Y. Tao, Y. Georgievskii, S. J. Klippenstein, A. W. Jasper, and R. Sivaramakrishnan, The role of collisional energy transfer on the thermal and prompt dissociation of 1-methyl allyl. *Proc. Combust. Inst.*, online (2022).
27. Z. Wang, H. Zhao, C. Yan, Y. Lin, A. D. Lele, W. Xu, B. Rotavera, A. W. Jasper, S. J. Klippenstein, and Yiguang Ju, Methanol oxidation up to 100 atm in a supercritical pressure jet-stirred reactor. *Proc. Combust. Inst.*, online (2022).
28. A. W. Jasper, D. R. Moberg, Y. Tao, S. J. Klippenstein, and R. Sivaramakrishnan, Inefficient intramolecular vibrational energy redistribution for the H + HO_2 reaction and negative internal energy dependence for its rate constant. *Frontiers Phys.* **10**, 1003010 (2022).
29. Z. Yang, S. Doddipatla, C. He, S. J. Goettl, R. I. Kaiser, A. W. Jasper, A. C. R. Gomes, and B. R. L. Galvão, Can third-body stabilization of bimolecular collision complexes in cold molecular clouds happen? *Mol. Phys.* **120**, e2134832 (2022).
30. A. C. R. Gomes, C. M. R. Rocha, A. W. Jasper, and B. R. L. Galvão, Formation of phosphorus monoxide through the P(^{4}S) + O_2($^3\Sigma^-$) → O(^{3}P) + PO($^2\Pi$) reaction. *J. Molec. Model.* **28**, 259 (2022).
31. J. Jian, H. Hashemi, H. Wu, A. W. Jasper, and P. Glarborg, A reaction mechanism for ozone dissociation and reaction with hydrogen at elevated temperature. *Fuel* 322, 124138 (2022).
32. A. W. Jasper, Predicting third-body collision efficiencies for water and other polyatomic baths. *Faraday Discuss.* **238**, 68–86 (2022).
33. C. Yan, H. Zhao, Z. Wang, G. Song, Y. Lin, C. R. Mulvihill, A. W. Jasper, S. J. Klippenstein, and Y. Ju, Low- and intermediate-temperature oxidation of dimethyl ether up to 100 atm in a supercritical pressure jet-stirred reactor. *Combust. Flame* **243**, 112059 (2022).\
34. A. Al-Haddad, S. Oberli, J. González-Vázquez, M. Bucher, G. Doumy, P. Ho, J. Krzywinski, T. J. Lane, A. Lutman, A. Marinelli, T. J. Maxwell, S. Moeller, S. T. Pratt, D. Ray, R. Shepard, S. H. Southworth, A. Vazquez-Mayagoitia, P. Walter, L. Young, A. Picón, and C. Bostedt, Observation of site-selective chemical bond changes via ultrafast chemical shifts, *Nature Comm.* **13**, 7170 (2022).
35. R. Forbes, P. Hockett, I. Powis, J. D. Bozek, S. T. Pratt, and D. M. P. Holland, Auger electron angular distributions following excitation or ionization from the Xe 3d and F 1s levels in xenon difluoride, *Phys. Chem. Chem. Phys.* **24**, 1367-1379 (2022).
36. I. Fischer and S. T. Pratt, Photoelectron spectroscopy in molecular physical chemistry, *Phys. Chem. Chem. Phys.* **24**, 1944-1959 (2022).
37. N. A. Seifert, K. Prozument, and M. J. Davis, Computational optimal transport for molecular spectra: The semi-discrete case, J. Chem. Phys. 156, 134117, 16 pages. (2022) https://doi.org/10.1063/5.0087385

Chemical Dynamics in the Gas Phase – Chemical Kinetics Subtask

Rebecca L. Caravan, Stephen J. Klippenstein, Robert S. Tranter
**Chemical Sciences and Engineering Division, Argonne National Laboratory, Lemont, IL, 60439*

caravarl@anl.gov; sjk@anl.gov; tranter@anl.gov

Program Scope

The goal of this program is to explore foundational problems in gas phase chemical kinetics through a combination of experimental studies and *ab initio* chemical kinetics calculations. We use these methods to explore reactions on complex potential energy surfaces (PESs), which includes assessments of the reaction rates, the role of incomplete thermalization in kinetics, the potential importance of novel classes of reactions, and the role of all aspects of the global PES. The close linkage of experimental and theoretical studies of prototypical reactions allows us to deeply explore key kinetic questions, while generating kinetic data of relevance to a variety of complex, chemically reactive, non-equilibrium systems such as combustion, atmospheric chemistry, and atomic layer deposition. Our efforts to address these key science questions benefit from continued development of unique experimental and theoretical methods. The experimental approach spans a wide range of reaction conditions using a combination of shock tube and flow reactor methods. A suite of optical and mass spectrometric diagnostics allow in-depth interrogation of reactions. Extensive use of synchrotron (VUV and x-ray) techniques enhances the laboratory capabilities.

Recent Progress

Ammonia Oxidation Chemistry: Ammonia continues to be of considerable interest as a prospective zero-carbon fuel. To that end, we collaborated with Glarborg (DTU), with Ju (Princeton), and with Curran (Galway) in the development of high-quality mechanisms for its oxidation both in isolation and as a co-fuel. We published ab initio (TST) state theory based rate predictions for the reaction of NH_2 with NO_2 (as part of an analysis of post flame oxidation of NH_3), for the reaction of HNNO + H (as part of a study on the NOx behavior in H_2/NNO mixtures, which is important due to the extraordinarily large global warming potential of NNO) for the reactions of NH_2 with CH_3OH and CH_2O (as part of a study on the oxidation of ammonia/methanol cofuel at pressures up to 100 atm), and for the reaction of NH_2 with CH_3 (as part of a study on oxidation of CH_4/NH_3 mixtures). Each of these studies employed high level (ANL style) potential energy surfaces and direct CASPT2 variable reaction coordinate (VRC)-TST (as appropriate) within ab initio TST based master equation treatments. For the H_2/NNO system the inclusion of the HNNO chemistry, as first expounded on by Burke (Columbia), yields a marked improvement in the quality of the modeling predictions. Resonant stabilization yields a remarkable set of barrierless channels for the H + HNNO reaction, all of which were treated with VRC-TST.

Criegee Intermediate Reactivity*:* We have continued our studies of stabilized Criegee intermediates (sCIs) with our collaborators including Taatjes, Osborn, Hansen, and Sheps (Sandia), Jasper, Lester (Penn), Percival and Winiberg (JPL), Vansco (Coastal Carolina University, CCU), Bannan (Manchester) and Shallcross (Bristol). Details of several projects are given below.

Reactivity with SO_2: We led a combined experimental and theoretical study to investigate the influence of size, structure, and resonance stabilization on the reactivity of more highly functionalized sCIs. We performed experiments on the bimolecular reaction of SO_2 with methyl ethyl substituted Criegee intermediate (MECI). MECI –is structurally similar to the isoprene-derived sCI methyl vinyl ketone oxide (MVK-oxide, previously studied by our team), but lacks resonance stabilization. We find that MECI reacts about a factor of 3 faster with SO_2 than MVK-oxide does, indicating the strong influence of resonance stabilization on sCI reactivity. We have calculated and compared the minimum energy pathways for select sCI + SO_2 reactions. Our findings emphasize the sensitivity of the reaction energetics to a combination of the overall sCI size, resonance stabilization, and conformational form. These combined influences are reflected in the prior experimental determinations of various sCI + SO_2 bimolecular rate coefficients. As such, these parameters should be considered in the development of structure−activity relationship parameters for the reactions of SO_2 with more complex, functionalized sCIs which are not directly accessible experimentally at present.

Oligomerization: With Percival, we led an expansive study to investigate the kinetics and mechanisms of an oligomerization sequence of the CH_2OO sCI, and its persistence in chemically complex environments. Mass spectrometric measurements in the ambient Amazonian troposphere by our collaborators at Manchester revealed signatures of species consistent with sequential insertion of CH_2OO into formic acid. sCI oligomerization sequences have been implicated in gas-particle interconversion in prior laboratory-based chamber experiments, but deducing the viability of these sequences in more chemically complex environments requires understanding the kinetics and mechanisms of key reaction steps. Our theoretical kinetics investigations reveal that the sequence, initiated by 1,4-insertion of CH_2OO into formic acid, is energetically downhill and involves a cycloaddition step followed by sequential 1,2-insertion reactions into functionalized organic hydroperoxide (ROOH) reaction products. Some of these insertion steps have multiple possible product channels, and the predicted yields are sensitive to energy transfer parameters (determined by Jasper). Our theoretical predictions are in accord with our direct kinetic studies of CH_2OO reactions with experimentally accessible analogues of ROOH. Comparison of spectroscopic signatures of the products from these direct studies with those from ozonolysis experiments (Hansen) indicates that sCI reactions are indeed persistent and driving molecular weight growth in these more chemically complex systems. The present and prior ozonolysis experiments by Hansen have revealed the operation of multiple concurrent sCI insertion sequences, including that derived from formic acid. Global chemical modelling that incorporates the newly characterized oligomerization sequence beginning from formic acid captures only a relatively small fraction of the amplitude of the field measurements. Our future work will investigate the chemical kinetics and mechanisms underlying one potential contribution to this discrepancy.

Roaming in the Multistep Decomposition of CIs: Previously we studied OH roaming in the multistep decomposition of smaller Criegee intermediates. We extended the theoretical component of the work to a treatment of the OH roaming induced pathways in the ozonolysis of α-pinene (the dominant monoterpene, which are a major component of biogenic volatile organic compounds). The relatively large size of α-pinene made the use of multireference methods somewhat challenging, but the replacement of two spectator methyl groups with H atoms made them just feasible. These multireference ab initio transition state theory calculations indicate that the OH roaming pathways from the relevant vinylhydroperoxides are kinetically significant with a branching that generally increases from ~20% at room temperature up to a remarkably large ~70% at the lower temperatures representative of the troposphere. An interesting fundamental question for this system relates to how and when the butane ring gets broken, which is required to proceed on to further oxidation and lower volatility products. The calculations provided novel speculation for how this might occur following roaming.

Hydroxy-functionalized Peroxy Radical Reactions: We have continued to lead studies on the reactions of β-hydroxy functionalized peroxy radicals ($HO\text{-}RO_2$). With Winiberg, Percival, Vansco, Taatjes, and Osborn, we have performed studies on the self-reactions of targeted functionalized $HO\text{-}RO_2$, with a focus on possible evidence for the dialkyl hydroperoxide ($HO\text{-}RO_2R\text{-}OH$) reaction product in our experimental data, and the influence of $HO\text{-}RO_2$ structure on the yield of this reaction product. Inspired by the heterogenous work of Wilson (LBNL), in which his group found compelling evidence of conversion of $HO\text{-}RO_2$ to CI, we have continued our analysis of our experimental data to examine whether this mechanism is also operative in the gas phase. In our experiments, we probed: possible $HO\text{-}RO_2$ self-reaction vs. unimolecular mechanisms, the effect of $HO\text{-}RO_2$ structure, and the possibility of facilitating sCI formation by complexation of $HO\text{-}RO_2$ with water. sCI scavenging was attempted using SO_2 or formic acid. Examination of our experimental data indicates that the $HO\text{-}RO_2$ to sCI interconversion pathway identified in the heterogenous work of Wilson is minor in the gas phase, emphasizing the interesting differences in reactivity of intermediates in different environments.

Isopropanol Dissociation: We have continued our collaboration with Wooldridge on the dissociation of iso-propanol (IPA). We previously reported on laser schlieren and modeling studies to investigate the multi-channel dissociations of IPA. Several inadequacies in chemical mechanisms were identified. We have subsequently performed shock tube/TOF-MS studies to determine the reaction intermediates and inform development of the mechanism. The experiments were performed at low pressures (200-300 Torr) using electron impact ionization (EI) in the lab and at high pressures (~5 atm) with VUV-photoionization (PI) at

the Advanced Light Source. The results indicate that the dehydrogenation channel is the dominant dissociation path for IPA but that the minor channel, elimination of a CH_3 group, is not negligible as the co-product, CH_3CHOH, rapidly eliminates H-atoms that readily attack IPA initiating a new reaction branch. The mass spectra yielded relative concentrations of species and their time dependencies, which were key to elucidating the mechanistic steps. It is notable that there are several significant differences in the concentrations of secondary species observed in the EI and PI datasets, particularly for allene, propyne, and propene. While this might be partially attributable to enhanced fragmentation of species in the EI work compared to the PI studies this cannot be the sole explanation. The major source could be reduced bimolecular reaction rates at low pressures, although this is an area of ongoing study.

Microcanonical Rate Measurements and RRKM Theory: Recent groundbreaking experimental efforts in the Lester lab (Penn) and separately in the Davis lab (Cornell) have provided microcanonical dissociation rate constants across a range of energy for some interesting new chemical systems. We have collaborated with these experimental efforts in making state-of-the-art ab initio RRKM predictions for comparison with their observations.

QOOH Decomposition: As described in her abstract, Lester extended her observations of hydroperoxyalkyl radical (QOOH) dissociation dynamics to the cyclohexyl and cyclopentyl oxidation systems, thereby examining the effect of rings on the OO fission process. The larger molecular size of these systems presented some challenges to obtaining high accuracy a priori barrier and rate estimates. We employed a bootstrapping method to extrapolate benchmark calculations for the smaller C_2H_4OOH system to the $C_6H_{10}OOH$ and C_5H_8OOH dissociations. For both systems, detailed comparisons between theory and experiment demonstrated that the observed dissociation process initiates from the β-QOOH form, where the radical is on the carbon next to the OOH group. For the C_5H_8OOH system, the full set of ring-puckered and torsional states were explicitly considered, while axial and equatorial geometries were considered for $C_6H_{10}OOH$. In both cases, the ab initio RRKM theory predicted dissociation rate constants agreed with the experimental measurements to within the expected accuracy of the calculations. With this confirmation of the accuracy of the theoretical methodology, the microcanonical rate predictions were then extended to thermal (T and P dependent) rate predictions via master equation modeling for a range of related chemical processes on the $C_6H_{11}O_2$ and $C_5H_9O_2$ potential energy surfaces.

Acrolein/Methylketene Dissociation: As described in his abstract, Davis's experiments focus on the photodissociation of acrolein and methylketene at energies near the dissociation threshold (within about 10 kcal/mol). Their observations provide measures of the microcanonical rates for isomerization from acrolein to methylketene and for dissociation of methylketene. Notably, the isomerization appears to involve contributions from two distinct pathways (either via a direct H-transfer or via H-transfers to and from an intermediary CH_3CCHO carbene), while the dissociation appears to produce a mixture of $^1CH_3CH + CO$, $^3CH_3CH + CO$, and $C_2H_4 + CO$. We are currently in the process of making detailed comparisons between ab initio RRKM predictions and the experimentally observed rise and fall times for the methylketene photoionization signal. Preliminary results indicate good agreement. The ab initio RRKM calculations employed ANL0 quality barrier estimates (i.e., a high-level composite method with uncertainties of ~ 0.2 kcal/mol) in combination with variational RRKM theory. For the $^1CH_3CH + CO$ channel we include a direct CCSD(T)/cc-pVTZ based variable reaction coordinate (VRC)-RRKM analysis.

***Pyrolysis of Fluorinated Alkanes*:** We have previously reported initial results from an experiment, theory, and modeling investigation with Sivaramakrishnan and Jasper on the dissociation of difluoromethane (DFM) which are now published. A key feature was accurately characterizing the reactions of CHF as well as the secondary reactions they initiate. The work also provides a foundation for understanding the production of CF_2, which has previously been observed from DFM. In collaboration with Goldsmith (Brown) we have broadened our studies of fluorinated alkanes to include the canonical series of perfluorinated alkanes (PFA) C_2F_6, C_3F_8, and C_4F_{10}. Shock tube laser schlieren densitometry experiments cannot be simulated with existing PFA models. Consequently, Goldsmith's group are using theoretical methods to develop pressure dependent chemical kinetic models, see Goldsmith's abstract. So far satisfactory results have been achieved for C_2F_6 and indicate the initial step is scission of the C-C bond yielding CF_3 radicals which rapidly dissociate to CF_2. Thus, similar to DFM, it is likely that the chemistry

of CF_2 radicals will be critical to the gas phase chemistry of fluorinated alkanes and is an ongoing target for theoretical work.

X-ray Fluorescence (XRF): We have continued to use the krypton XRF method to obtain highly spatially resolved measurements of gas temperatures in a variety of flames. With Wooldridge (U. Michigan) we have studied the initiation steps of Si-nanoparticle production when particle precursors (hexamethyldisiloxane and trimethylsilanol) entrained in an inert gas jet are introduced into a flame, see also Wooldridge's abstract. The XRF method provided temperature maps of the complete flame and jet and revealed that, in the absence of precursors, mixing between the jet and flame gases was minimal and the jet temperature remained low (height above burner, HAB, < 15 mm, T < 1000 K) despite the surrounding flame being at ~1700 K. When precursors were added to the inert jet, a rapid increase in the jet temperature was observed within 1-2 mm HAB reaching the primary flame temperature at ~ 5 mm HAB. Thus, rapid reaction is occurring in an apparently inert jet at temperatures too low for pyrolysis of the precursors. We performed femtosecond two photon H-atom laser induced fluorescence studies of the flames in collaboration with Kulatilaka (Texas A&M), which validated our hypothesis that H-atoms diffuse from the primary flame into the jet close to the burner surface and are likely the main initiator of precursor decomposition.

Future Work

Criegee Intermediate Reactivity and Oligomerization*:* We will continue our explorations of sCI reactivity and their molecular weight growth reactions with our collaborators. Building on our work on CH_2OO oligomerization, we are examining the impact of water complexation on sCI reactions with organic hydroperoxides. The oligomerization sequence we previously characterized in the absence of water involves 1,2-insertion reactions: a class of reactions which have been shown to be enhanced by water complexation. We are using experiment and theory to understand the effects of water complexation on the reactivity of sCIs, with a focus on how this complexation influences the kinetics and product branching of such molecular weight growth sequences. We will work with our modelling collaborators to assess the propensity for these complexes to impact our understanding of molecular weight growth sequences in chemically complex regions of Earth's troposphere. We are also exploring the impact of sCI structure, size, conformer, and resonance stabilization on these molecular weight growth sequences. For example, we are examining the reactions of organic hydroperoxides with CH_3CHOO, MVK-oxide, and MACR-oxide through direct experiment and theoretical kinetics. In the case of the four-carbon, resonance stabilized sCIs, we are connecting to ozonolysis studies (Hansen) and measurements in Earth's lower atmosphere (Bannan) to interrogate the persistence of these mechanisms in highly chemically complex environments that involve large reaction networks.

Fluorinated Alkanes: We will extend our studies of PFA to obtain EI and PI TOF-MS data over a broad pressure range to further constrain the chemical kinetic models being developed by Goldsmith. These data will also probe the secondary chemistry more than the existing laser schlieren experiments that focus on the initial decomposition processes. In practical systems, PFA react in complex mixtures of radical and stable species. A key reaction that is poorly characterized is H + PFA$\rightarrow$ products. We intend to study this reaction over a broad range of pressures and temperatures experimentally and theoretically in collaboration with Goldsmith. We are also examining with VRC-TST the kinetics of barrierless reactions of relevance to the decomposition of PFAs.

Hydroxy-functionalized Peroxy Radical Reactions*:* With our collaborators, we will continue our investigations of HO-RO_2 self-reactions. With Sheps (Sandia) we will perform higher pressure experiments to examine the pressure dependence of the product channels, with a focus on HO-RO_2R-OH.

Theoretical Studies**:** In collaboration with Bourgalais and Battin-Leclerc (Nancy) we plan to examine the formation of ketohydroperoxides (KHPs) in alkene ozonolysis through diradical channels, with a particular focus on the branching between CI formation and KHP formation, and on the dissociation of the KHPs. Water complexation can have various roles in atmospheric kinetics including (i) acting as a spectator in modulating barrier properties, (ii) directly catalyzing chemical conversions through H shuttling, and/or (iii) facilitating a swapping amongst various dimer complexes. We are exploring these various roles with illustrative calculations. We also plan to explore RO_2 recombination kinetics for some simple dimers

including for the HO-RO_2 being studied experimentally. We intend to continue collaborating with Lester and Davis in providing high quality ab initio RRKM predictions for the systems that they probe experimentally. Each of these studies are motivated by the desire to better understand unique fundamental aspects of the kinetics.

Water Enhancement of Alkoxy Radical Chemistry*:* With Winiberg, Sander, and Percival (JPL), Vereecken (Jülich), Okumura (Caltech), Taatjes and Osborn (Sandia), and Jasper, we are investigating the impact of water vapor on the unimolecular decay of hydroxy-functionalized alkoxy radicals (HO-RO). Preliminary analysis of our experimental measurements indicates a substantial water-mediated enhancement in the unimolecular decay rate of hydroxyethyl peroxy, which early theoretical investigations support. Further experimental analysis and master equation calculations with rigorous treatment of energy transfer parameters will be performed to elucidate the mechanism responsible for our observations. Future investigations on the influence of HO-RO structure will also be undertaken.

DOE Supported Publications 2022 - present

1. **Theoretical Kinetics Predictions for NH_2 + HO_2**, S. J. Klippenstein, P. Glarborg, *Combust. Flame*, **236**, 111787 (2022).
2. **Dramatic Conformer-Dependent Reactivity of Acetaldehyde Oxide Criegee Intermediate with Dimethylamine via a 1,2-Insertion Mechanism,** M. F. Vansco, M. Zou, I. O. Antonov, K. Ramasesha, B. Rotavera, D. L. Osborn, Y. Georgievskii, C. J. Percival, S. J. Klippenstein, C. A. Taatjes, M. I. Lester, R. L. Caravan, *J. Phys. Chem. A*, **126**, 710-719 (2022).
3. **Infrared Spectroscopic Signature of a Hydroperoxyalkyl Radical (•QOOH),** A. S. Hansen, T. Bhagde, Y. Qian, A. Cavazos, R. M. Huchmala, M. A. Boyer, C. F. Gavin-Hanner, S. J. Klippenstein, A. B. McCoy, M. I. Lester**,** *J. Chem. Phys*., **156**, 014301 (2022).
4. **Rapid Allylic 1,6 H-Atom Transfer in an Unsaturated Criegee Intermediate,** A. S. Hansen, Y. Qian, C. A. Sojdak, M. Kozlowski, V. J. Esposito, J. S. Francisco, S. J. Klippenstein, M. I. Lester**,** *J. Am. Chem. Soc*., **144**, 5945-5955 (2022).
5. **Spiers Memorial Lecture: Theory of Unimolecular Reactions,** S. J. Klippenstein**,** *Faraday Disc.*, **238**, 11-67 (2022).
6. **Energy-Resolved and Time-Dependent Unimolecular Dissociation of Hydroperoxyalkyl Radicals (•QOOH),** T. Bhagde, A. S. Hansen, S. Chen, P. J. Walsh, S. J. Klippenstein, M. I. Lester**,** *Faraday Disc.*, **238**, 575-588 (2022).
7. **In Situ Temperature Measurements in Sooting Methane/Air Flames Using Synchrotron X-Ray Fluorescence of Seeded Krypton Atoms,** M. J. Montgomery, H. Kwon, A. L. Kastengren, L. D. Pfefferle, T. Sikes, R. S. Tranter, Y. Xuan, C. S. McEnally, *Sci. Adv.,* **8**, eabm7947 (2022).
8. **Formation of Organic Acids and Carbonyl Compounds in n-Butane Oxidation via ɣ-Ketohydroperoxide Decomposition**, D. M. Popolan-Vaida, A. J. Eskola, B. Rotavera, J. F. Lockyear, Z. Wang, S. M. Sarathy, R. L. Caravan, J. Zádor, L. Sheps, A. Lucassen, K. Moshammer, P. Dagaut, D. L. Osborn, N. Hansen, S. R. Leone, C. A. Taatjes, *Angew. Chem. Int. Ed.* **61**, e202209168 (2022).
9. **Temperature Measurements in Heavily Sooting Ethylene/Air Flames Using Synchrotron X-Ray Fluorescence of Krypton,** C. Banyon, M. J. Montgomery, H. Kwon, A. L. Kastengren, L. D. Pfefferle, T. Sikes, Y. Xuan. C. S. McEnally, R. S. Tranter, *Combust. Flame*. **257,** 112494 (2023).
10. **A Wide Range Experimental Study and Further Development of a Kinetic Model Describing Propane Oxidation,** L. Zhu, S. Panigraphy, S. N. Elliott, S. J. Klippenstein, M. Baigmohammadi, A. A. El-Sabor Mohamed, J. W. Hargis, S. Alturaifi, O. Mathieu, E. L. Petersen, K. A. Heufer, A. Ramalingam, Z. Wang, H. J. Curran**,** *Combust. Flame.*, **248**, 112562 (2023).
11. **Automated Identification and Calculation of Prompt Effects in Kinetic Mechanisms using Statistical Models,** L. Pratali Maffei, K. B. Moore III, Y. Georgievskii, C. R. Mulvihill, S. N. Elliott, J. Cho, Raghu Sivaramakrishnan, T. Faravelli, S. J. Klippenstein**,** *Combust. Flame*, **257**, 112422 (2023).
12. **Dedication to James A. Miller,** S. J. Klippenstein, J. Zador, *Combust. Flame*, **257**, 113013 (2023)**.**
13. **Radical-Radical Reactions in Molecular Weight Growth: The Phenyl + Propargyl Reaction,** T. M. Selby, F. Goulay, S. Soorkia, A. Ray, A. W. Jasper, S. J. Klippenstein, A. N. Morozov, A. M. Mebel, J. D. Savee, C. A. Taatjes, D. L. Osborn**,** *J. Phys. Chem.* A, **127**, 2577-2590 (2023).
14. **Combustion in a Sustainable World: From Molecules to Processes,** S. J. Klippenstein, K. Kohse-Hoinghaus, *J. Phys. Chem. A*, **127**, 3737-3742 (2023).

15. **OH Roaming and Beyond in the Unimolecular Decay of the Methyl-Ethyl Substituted Criegee Intermediate: Observations and Predictions,** T. Liu, S. N. Elliott, M. Zou, M. F. Vansco, C. A. Sojdak, C. R. Markus, R. Almeida, K. Au, L. Sheps, D. L. Osborn, F. A. F. Winiberg, C. J. Percival, C. A. Taatjes, R. L. Caravan, S. J. Klippenstein, M. I. Lester, *J. Am. Chem. Soc.*, **145**, 19405-19420 (2023). Correction; *J. Am. Chem. Soc.* **146**, 18184-18185 (2024).
16. **Uncovering Novel Liquid Organic Hydrogen Carriers: A Systematic Exploration of Chemical Compound Space Using Cheminformatics and Quantum Chemical Methods,** H. Harb, S. N. Elliott, L. Ward, I. T. Foster, S. J. Klippenstein, L. A. Curtiss, R. S. Assary, *Dig. Disc*., **2**, 1813-1830 (2023).
17. **Bimolecular Reactions of Methyl-Ethyl-Substituted Criegee Intermediate with SO_2,** M. Zou, T. Liu, M. F. Vansco, C. A. Sojdak, C. R. Markus, R. Almeida, K. Au, L. Sheps, D. L. Osborn, F. A. F. Winiberg, C. J. Percival, C. A. Taatjes, S. J. Klippenstein, M. I. Lester, R. L. Caravan, *J. Phys. Chem. A*, **127**, 8994-9002 (2023).
18. **OH Roaming During the Ozonolysis of a-Pinene: A New Route to Highly Oxygenated Molecules?** S. J. Klippenstein, S. N. Elliott, *J. Phys. Chem. A*, **127**, 10647-10662 (2023).
19. **Experimental Measurement of the Rapid Mixing of Fuel and Air in a Multi-Element Diffusion (Hencken) Burner,** Q. Meng, C. Banyon, A. L. Kastengren, M. S. Wooldridge, R. S. Tranter, *Combust. Flame,* **251**, 112686 (2023).
20. **Conformer-Dependent Chemistry: Experimental Product Branching of the Vinyl Alcohol + OH + O_2 Reaction,** D. Rösch, G. H. Jones, R. Almeida, R. L. Caravan, A. Hui, A. W. Ray, C. J. Percival, S. P. Sander, M. D. Smarte, F. A. F. Winiberg, M. Okumura, D. L. Osborn, *J. Phys. Chem. A*, **127**, 3221-3230 (2023).
21. **Tribute to Marsha I. Lester,** N. M. Kidwell, S. J. Klippenstein, J. H. Lehman, A. B. McCoy**,** *J. Phys. Chem. A*, **128**, 501-502 (2024).
22. **An Experimental, Theoretical, and Kinetic Modeling Study of Post-Flame Oxidation of Ammonia,** J. Jian, H. Hashemi, H. Wu, P. Glarborg, A. W. Jasper, S. J. Klippenstein**,** *Combust. Flame*, **261**, 113325 (2024).
23. **Observational Evidence for Criegee Intermediate Oligomerization Reactions Relevant to Aerosol Formation in the Troposphere,** R. L. Caravan, T.J. Bannan, F. A. F. Winiberg, M. A. H. Khan, A. C. Rousso, A. W. Jasper, S. D. Worrall, A. Bacak. P. Artaxo, J. Brito, M. Priestley, J. D. Allan, H. Coe, Y. Ju, D. L. Osborn, N. Hansen, S. J. Klippenstein, D. E. Shallcross, C. A. Taatjes, C. J. Percival**,** *Nature Geo.*, **17**, 219-226 (2024).
24. **The Role of Stereochemistry in Combustion Processes,** S. N. Elliott, K. B. Moore III, C. R. Mulvihill, A. V. Copan, L. Pratali Maffei, S. J. Klippenstein**,** *WIREs, Comput. Mol. Sci.* **14**, e1710 (2024).
25. **Isomer-Resolved Unimolecular Dynamics of the Hydroperoxyalkyl Intermediate (•QOOH) in Cyclohexane Oxidation,** Y. Qian, T. K. Roy, A. W. Jasper, C. A. Sodjak, M. C. Kozlowski, S. J. Klippenstein, M. I. Lester**,** *Proc. Nat. Acad. Sci.* **121**, e2401148121 (2024).
26. **Radical Stereochemistry: Accounting for Diastereomers in Kinetic Mechanism Development,** A. V. Copan, K. B. Moore III, S. N. Elliott, C. R. Mulvihill, L. Pratali Maffei, S. J. Klippenstein**,** *J. Phys. Chem. A*, **128**, 3711-3725 (2024).
27. **Infrared Signature of the Hydroperoxyalkyl Intermediate (•QOOH) in Cyclohexane Oxidation: An Isomer-Resolved Spectroscopic Study,** T. K. Roy, Y. Qian, C. A. Sodjak, M. C. Kozlowski, S. J. Klippenstein, M. I. Lester**,** *J. Chem. Phys.* **161**, 034302 (2024).
28. **On the Prediction of Pressure Effects for the Combination Kinetics of Two Alkyl Radicals with the Geometric Mean Rule,** F. Citrangolo Destro, R. Fournet, B. Sirjean, S. J. Klippenstein, *Proc. Combust. Inst.* **40**, 105380 (2024).
29. **Resolving Theory and Experiment for the H + NCN Reaction,** R. Sivaramakrishnan, S. J. Klippenstein**,** *Proc. Combust. Inst.* **40**, 105403 (2024).
30. **Styrene Thermal Decomposition and its Reaction with Acetylene Under Shock Tube Pyrolysis Conditions: An Experimental and Kinetic Modeling Study,** A. Hamadi, R. Sivaramakrishnan, F. E. Cano Ardila, R. S. Tranter, S. Abid, N. Chaumeix, A. Comandini, *Proc. Combust. Inst.* **40**, 105481 (2024).
31. **Initiation and Carbene Induced Radical Chain Reactions in CH_2F_2 Pyrolysis,** R. A Shaik, A. W Jasper, P. T Lynch, R. Sivaramakrishnan, R. S Tranter, *Chem. Phys, Chem.*, **25**, e202400362 (2024).
32. **Hexamethyldisiloxane Pyrolysis: Probing H-Atom Initiation by Femtosecond Two-Photon LIF,** K. Kim, M. Hay, Q. Meng, M. S. Wooldridge, W. D., Kulatilaka, R. S. Tranter, *Proc. Combust. Inst*. **40**, 105640 (2024).
33. **In-Situ Two-Dimensional Temperature Measurements Using X-Ray Fluorescence Spectroscopy in Laminar Flames with High Silica Particle Concentrations,** Q. Meng, C. Banyon, K. Kim, J. H. Kim, M. S. Wooldridge, A. L. Kastengren, R. S Tranter, *Combust. Flame* **266**, 113564, (2024).
34. **Competing Radical and Molecular Channels in the Unimolecular Dissociation of Methylformate,** J. Cho, N. J. Labbe, L. B. Harding, S. J. Klippenstein, R. Sivaramakrishnan, *Proc. Combust. Inst.,* **40**, 105684 (2024).

Chemical Dynamics in the Gas Phase: Theory, Modeling, and Methods Subtask

Ron L. Shepard[1], Raghu Sivaramakrishnan[2], and Michael J. Davis[3]
Chemical Sciences and Engineering Division
Argonne National Laboratory
Lemont, IL 60439
Email:[1]shepard@tcg.anl.gov, [2]raghu@anl.gov,[3]davis@tcg.anl.gov

The Theory, Modeling, and Methods Subtask focuses on the development of three research areas corresponding to: electronic structure methods; the generation and analysis of chemical kinetic mechanisms for simulating complex systems; and the exploration of chemically reactive systems, including isolated chemical reactions, complex chemical kinetic mechanisms, and spectroscopy, through the methods of novel numerical analysis. These efforts are closely connected to the goals of the other three subtasks and result in substantial cross-fertilization.

Theoretical Studies of Potential Energy Surfaces and Computational Methods: Ron Shepard

Program Scope: This project involves the development, implementation, and application of theoretical methods for the calculation and characterization of potential energy surfaces (PES) and other molecular properties involving molecular species that occur in combustion, atmospheric, and general gas-phase chemistry. An accurate and balanced treatment of reactants, intermediates, and products for both ground and excited electronic states is required. This difficult challenge is met with general multiconfiguration self-consistent field (MCSCF) and multireference configuration interaction (MRCI) methods [see *Chem. Rev.* **112**, 108 (2012) and *J. Chem. Phys.* **152**, 134110 (2020)]. More recently, the *graphically contracted function* (GCF) method has been developed to address some of the practical limitations of the traditional MCSCF and MRCI approaches, including the number of active electrons that may be accommodated and the overall expense associated with the study of larger molecular systems [see *J. Chem. Phys.* **141**, 064105 (2014) and references therein]. These methods are developed and maintained within the COLUMBUS Program System.

Recent Progress:

In COLUMBUS, an electronic structure wave function may be represented as a linear expansion in configuration state functions (CSF), $|\psi\rangle = \sum_{m=1}^{N_{\mathrm{CSF}}} x_m |\widetilde{m}\rangle$, or as a linear expansion in graphically contracted functions (GCF), $|\psi\rangle = \sum_{P=1}^{N_{\mathrm{GCF}}} c_P |P\rangle$. Both representations are based on the Graphical Unitary Group Approach (GUGA). Each GCF is itself equivalent to a linear CSF expansion in which the CSF coefficients are computed as a product of matrices,

$$x_m^P = \langle \widetilde{m}|P\rangle = \boldsymbol{\alpha}^P_{k_0^m,k_1^m}\boldsymbol{\alpha}^P_{k_1^m,k_2^m}\ldots\boldsymbol{\alpha}^P_{k_{n-2}^m,k_{n-1}^m}\boldsymbol{\alpha}^P_{k_{n-1}^m,k_n^m}.$$

In this expression, $\boldsymbol{\alpha}^P_{k_{q-1}^m k_q^m}$ is the matrix of arc factors associated with the arc $\left(k_{q-1}^m, k_q^m\right)$ between node k_{q-1}^m at level (q–1) and node k_q^m at level q within the CSF m. In the GCF method, the computations are organized around this matrix product state (MPS) structure, so the underlying CSFs are never referenced directly. In contrast, in the MCSCF and MRCI codes within COLUMBUS, the CSF expansion coefficients are the central quantities of interest. It is therefore useful to convert a given wave function in one representation to the other, and particularly for large wave function expansions, this transformation should be as computationally efficient as possible.

Last year we developed algorithms and initial computer codes to perform these transformations. The GCF to CSF transformation proceeds by computing the x_m^P using the above matrix-product expression, and then combining these contributions for the CSF expansion coefficient $x_m = \langle \widetilde{m}|\psi\rangle = \sum_{P=1}^{N_{\mathrm{GCF}}} c_P x_m^P$. We use an efficient Depth-First Search (DFS) of the walks to compute these x_m coefficients. When computed in this way, the above matrix-product expression reduces to a sequence of matrix-vector products. The DFS procedure saves each matrix-vector product and reuses it to compute the x_m for all CSFs that share the same subsequence of

nodes and arcs. If $\bar{f}$ is taken as an average facet count within the GCF wave function, then the DFS reduces the total computational effort to compute the full CSF expansion vector **x** from $\sim 2n\bar{f}^2 N_{\mathrm{CSF}} N_{\mathrm{GCF}}$ to only $O\left(\bar{f}^2 N_{\mathrm{CSF}} N_{\mathrm{GCF}}\right)$; that is, it eliminates the $O(n^1)$ prefactor and replaces it with an $O(n^0)$ prefactor, the exact value of which depends on the complexity of the wave function expansion (e.g. PPMC, GVB-RCI, CAS, MRCI-SD, etc.).

For the CSF to GCF transformation, we developed two separate algorithms. The first is based on the fact that two GCFs may be merged together into a single GCF. This merge is denoted $|M\rangle \leftarrow c_P|P\rangle + c_Q|Q\rangle$. To effect the full transformation, this merge operation is invoked recursively. Each CSF is first converted into a GCF; this is a trivial operation since the only nonzero arc factors are the $\mathbb{R}^{1\times 1}$ matrices $\boldsymbol{\alpha}^P_{k^m_{q-1}k^m_q} = (1)$ for just the *n* nodes within CSF *m*. These GCFs are then merged pairwise as $|M\rangle \leftarrow x_m|m\rangle + x_{m+1}|m+1\rangle$ for odd *m*. Thus the initial N_{CSF} terms are merged to form $N_{\mathrm{CSF}}/2$ terms. These $N_{\mathrm{CSF}}/2$ terms are then merged pairwise into $N_{\mathrm{CSF}}/4$ terms, and so on, until the final step when they are merged into the final GCF representation of the original wave function. There are a total of $N_{\mathrm{CSF}} - 1$ merge operations performed, and the effort for each scales as $O\left(n\bar{f}^3\right)$ where $\bar{f}$ is the average facet count for the intermediate merged GCF, resulting in $O\left(n\bar{f}^3 N_{\mathrm{CSF}}\right)$ total effort. The facet counts are limited during each merge step according to numerical singular value tolerances and also subject to any imposed maximum facet count limits. Thus, this merge procedure can, in principle, reproduce the initial wave function exactly, or, with reduced computational effort and storage requirements, to within some specified tolerance. Our main improvement to this recursive merge operation is to perform the higher-level merge operations as soon as possible. This does not reduce the overall computational effort, but it reduces the intermediate GCF storage requirements from N_{CSF} to only $\mathrm{floor}\left((\log_2(N_{\mathrm{CSF}}) + 1)\right)$. We have subsequently improved this recursive pairwise merge algorithm to reduce the effort associated with the low-level memory allocation steps within each merge operation. This results in roughly an order of magnitude improvement in overall efficiency, and it also approximately eliminates a factor of *n*, the molecular orbital dimension, from the original implementation. Initial application of this merge procedure to a series of H_m molecules shows that the GCF wave functions can be represented well both with delocalized canonical Hartree-Fock orbitals and with localized molecular orbitals. For a given wave function complexity, as measured by the average facet count $\overline{f}$, the delocalized Hartree-Fock orbitals show smaller errors for small $\overline{f}$ values, while the localized orbitals show smaller errors for larger $\overline{f}$ values. Furthermore, we find with localized orbitals that the wave function errors are approximately independent of the molecule size; this suggests that larger-molecule wave functions can be constructed from smaller-molecule fragments for this kind of orbital basis, and this possibility will be explored in the future.

The second CSF to GCF transformation algorithm is based on least-squares fitting. We define the least squares error as $\mathcal{E} = \sum_{m=1}^{N_{\mathrm{CSF}}}(x_m - y_m)^2$ for the input expansion coefficients y_m and for $x_m \equiv x_m(\boldsymbol{\alpha})$ determined from the MPS expansion above. A nonlinear least-squares optimization of $\boldsymbol{\alpha}$ is then performed for the fixed-facet structure to minimize this error. This error is zero if and only if the two wave functions are identical, including overall normalizations and signs, and the facet count structure is then modified in order to reduce the error to below a specified tolerance. The x_m and $g_{j\mu,k\nu} \equiv \partial\mathcal{E}/\partial\alpha_{j\mu,k\nu}$ gradient computations are performed with a DFS procedure. The end result is that each combined $\mathcal{E}$ and **g** computation scales only as $O\left(\bar{f}^2 N_{\mathrm{CSF}}\right)$. Thus, the optimal choice between the merge algorithm and the iterative fitting algorithm depends on details such as the convergence tolerances and iterative convergence rates. For the initial implementation, the iterative process is slowly convergent, and the improved merge algorithm described above is usually the best choice. We are examining alternative iterative algorithms for this least-squares optimization in order to exploit the low-order scaling of the $\mathcal{E}$ and **g** computation steps.

Mechanisms and Models for Simulating Gas Phase Chemical Reactivity: Raghu Sivaramakrishnan

The scope of this program involves the development and analysis of detailed chemical kinetics mechanisms and models used for predictive simulations of gas phase reactivity in complex systems. Kinetics modeling has been used predominantly as an engineering tool for making predictions for practical applications in combustion and chemical conversions. However, within the context of the chemical physics BES program we have utilized a concerted Modeling-Experiment-Theory (MET) approach to further our understanding of the chemical kinetics of gas phase reactions.

Recent Progress

Resolving Discrepancies between Theory and Experiments for the NCN + H Reaction

Flame modeling studies have highlighted the role of branching in the kinetics for the prompt NO switch reaction, NCN + H. In this reaction, there is strong competition between the CH + N_2 (R1) and HCN + N (R2) product channels. Increased branching towards reaction R_2 promotes the subsequent formation of Fenimore or Prompt NO. Recent direct shock tube studies on this complex reaction conclude that branching to reaction R2 is much more favorable than the predicted branching from theoretical studies. The experimentally predicted prompt NO switch temperature (TS), i.e., the temperature at which $k_2/(k_1+k_2) = 0.5$, is at 1670 K, in contrast to theory that predicts Ts > 3200 K. The present theory/modeling work was initiated in collaboration with Klippenstein to highlight potential causes for this significant discrepancy between experiment and theory. Our analysis of the simulations reported in the experimental studies indicate that including a fall-off representation for C_2H_5 radical dissociation (with C_2H_5 produced from C_2H_5I dissociation and acting as an H-atom source) has a noticeable influence on the simulations for NCN decay and HCN formation in the shock tube studies. With the inclusion of a theory-based pressure fall-off representation for C_2H_5 dissociation, we show that this radical persists for much longer timescales even at the high-temperatures in the shock tube studies. This persistence then facilitates the rapid conversion of reactive H-atoms to CH_3 radicals at the shock tube conditions via the $H + C_2H_5 \rightarrow CH_3 + CH_3$ reaction. An updated theoretical analysis for this classic addition-elimination reaction is also provided in this work. The rapid formation of CH_3 radicals necessitates the inclusion of additional reactions to adequately simulate the NCN and HCN data. Our simulations conclude that, with the inclusion of these additional reactions, the NCN and HCN profiles can be reasonably well simulated by the most recent theoretical predictions.

Initiation and Carbene Induced Radical Chain Reactions in CH_2F_2 Pyrolysis

High temperature dissociations of organic molecules typically involve a competition between radical and molecular processes. In collaboration with Tranter, Jasper, and Lynch (University of Illinois-Chicago), we use a modeling, experiment, theory (MET) framework to characterize the high temperature thermal dissociation of CH_2F_2, a flammable hydrofluorocarbon (HFC) that finds widespread use as a refrigerant. Initiation in CH_2F_2 proceeds via a molecular elimination channel; $CH_2F_2 \rightarrow CHF+HF$. Here we show that the subsequent self-reactions of the singlet carbene, CHF, are fast multichannel processes and a facile source of radicals that initiate rapid chain propagation reactions. These have a marked influence on the decomposition kinetics of CH_2F_2. The inclusion of these reactions brings the simulations into better agreement with the present and literature experiments. Additionally, flame simulations indicate that inclusion of the CHF + CHF multichannel reaction leads to a noticeable enhancement in predictions of laminar flame speeds, a key parameter that is used to determine the flammability of a refrigerant.

The High Temperature Thermal Decomposition of Tetramethylsilane

Tetramethylsilane (TMS) is not only the simplest tetraalkylsilane but also the simplest of the organometallic analogs of neopentane among the group IVA metals. It finds widespread use as an ideal solvent for organic solution NMR. Additionally, it is also a well-known precursor for the formation of SiC (via pyrolysis and Chemical Vapor Deposition (CVD)) which is used as a ceramic and in the semiconductor industry. Recent studies indicate that kinetics and branching in this

thermal decomposition is poorly characterized. In collaboration with Tranter and Jasper, we have initiated theoretical studies to calculate the kinetics for bond fission and molecular channels in $(CH_3)_4Si$ dissociation. The PES for this dissociation indicated that molecular elimination to CH_4 was the lowest energy process followed by Si-C bond fission. The present VRC-TST based master equation analysis result in entropic considerations largely favoring initiation exclusively via Si-C bond fission. Ongoing work is in progress to address the kinetics for the subsequent dissociation of Si-radicals and interpret ongoing experimental studies by Tranter on the pyrolysis of this and other larger silicon containing molecules.

Exploration of Chemical Reactivity and Spectroscopy using Novel Numerical Analysis:
Michael J. Davis

This work involves the exploration of chemically reactive systems, including isolated chemical reactions and complex chemical-kinetics mechanisms, as well as molecular spectroscopy. The work relies on modern-day numerical analysis. The analysis is generally applicable, and we have been able to use it in work with other subtasks, as well as for projects outside our group.

Recent Progress

The work on computational optimal transport has been the focus of progress in the last period. This has included the completion of the project on continuous molecular spectra [16], the continued development and use of geodesics to define interesting probability density functions, and the extension of the previous discrete applications to multidimensional spectra. Particular attention has been made to the transport map as versions of it have been applied to many areas of science, most notably climate modeling where it is often used to correct the bias of simulations.

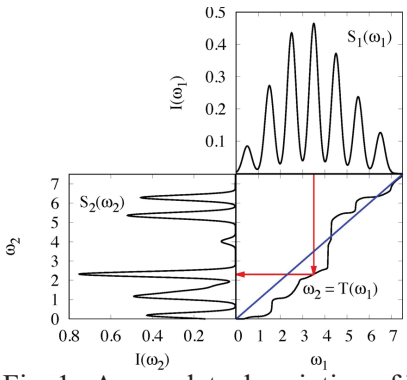

Fig. 1. A complete description of how the transport map on the bottom right transports density from one spectrum (top right) to another (bottom left).

The transport map which describes the transformation of one spectrum into another is:

$$\omega_2 = F_2^{-1}F_1(\omega_1),\ \omega_1 = F^{-1}F(\omega_1), \quad (1)$$

The second term in Eq. (1) shows that F^{-1} is an inverse transformation and not 1/F. F is defined:

$$F(\omega) = \int_{-\infty}^{\omega} S(\Omega)d\Omega\,, \quad (2)$$

and is the cumulative distribution. Equation (2) demonstrates how it is generated from the spectrum S. Figure 1 demonstrates how the map is used.

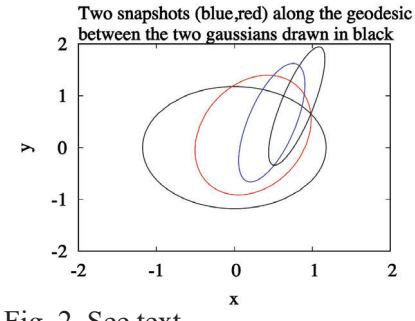

Fig. 2. See text.

Geodesics in the optimal-transport geometry can be utilized to design novel probability densities (e.g., Dalery *et al*, arXiv:2307.15423), for example, to be used in electronic structure calculations. Figure 2 shows blue and red Gaussians which lie along a geodesic between the black Gaussians.

As noted, computational optimal transport of molecular spectra is being extended to multidimensional spectra. This is first be carried out for discrete spectra and discretized versions of continuous spectra and requires a considerable change in the algorithm we have previously used.

We are using primal-dual first order methods to solve the optimal transport problem. Primal-dual methods for optimal transport solve the saddlepoint problem:

$$\min_{X \in R_+^{mxn}} \max_{u \in R^m, v \in R^n} L(x,y) := < C, X > - y^T A x + S_1^T u + S_2^T v. \quad (3a)$$

S_1 and S_2 are the intensities of the two spectra, which are vectorized versions of the two-dimensional intensities. The line positions are embedded in the cost matrix C. The transport plan is in the matrix X. The vectors u and v are dual vectors. The first term on the right-hand side is the matrix dot product between the cost and transport matrices. The middle term on the right hand of Eq. (3a) includes these two terms:

$$y = \begin{pmatrix} u \\ v \end{pmatrix}, Ax = \begin{pmatrix} X\mathbf{1}^n \\ X^T\mathbf{1}^m \end{pmatrix} \quad (3b)$$

Future Plans

Application to multidimensional spectra will be continued. Other applications of optimal transport geometry will be pursued which rely on the way the optimal transport map can be used to correct the difference between simulations and experiments or observations, as is done in climate modeling, where it is referred to as a "quantile map". One area where transport geometry may be useful is in molecular line shapes, where the geodesic between two different line shapes, can lead to a set of different line shapes, as shown in Fig. 3 for a geodesic between a Gaussian and Lorentzian line shape.

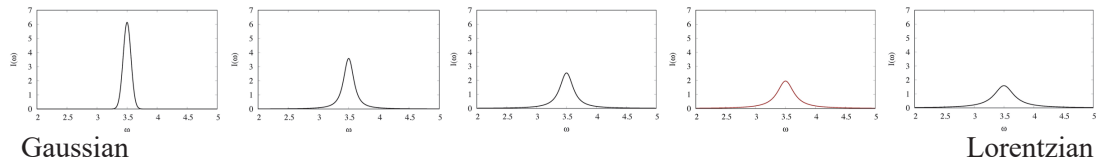

Fig. 3. Geodesic between Gaussian and Lorentzian line shapes.

Comparisons with other forms of line shapes such as the Voigt line shape, which is a convolution of a Gaussian and Lorentzian, will be made.

Publications (2022-2024)

1. R. Shepard, "Some Comments on Different-Orbitals-for-Different-Spins Determinants," The 10th OpenMolcas Developers' Workshop Abstracts (2022).
https://enccs.github.io/openmolcas-2022/posters/
2. A. Al-Haddad, S, Oberli, J, González-Vázquez, M. Bucher, G. Doumy, P. Ho, J. Krzywinski, T. J. Lane, A. Lutman, A. Marinelli, T. J. Maxwell, S. Moeller, S. T. Pratt, D. Ray, R. Shepard, S. H. Southworth, Á. Vázquez-Mayagoitia, P. Walter, L. Young, A. Picón, and C. Bostedt, "Observation of Site-Selective Chemical Bond Changes via Ultrafast Chemical Shifts," *Nature Communications* **13** (2022) 7170, 7 pages.
3. C. L. Cortes, P. Lefebvre, N. Lauk, M. J. Davis, S. K. Gray, N. Sinclair and D. Oblak,"Adaptive Calibration of Photon Indistinguishability in Quantum Networks Using Bayesian Optimization", Phys, Rev. Appl. **17** (2022) 034067, 17 pages.
4. N. A. Seifert, K. Prozument, and M. J. Davis, "Computational Optimal Transport for Molecular Spectra: The Semi-Discrete Case", J. Chem. Phys. **156** (2022) 134117, 16 pages.
5. R. Shepard, "The Cosine-Sine Decomposition with Different-Orbitals-for-Different-Spins Determinants", Mol. Phys. **121** (2023) e2077853, 9 pages.
6. R. F. K. Spada, M. P. Franco, R. Nieman, A. J. A. Aquino, R. Shepard, F. Plasser, and H. Lischka, "Spin-Density Calculation via the Graphical Unitary Group Approach", Mol. Phys. **121** (2023) e2091049, 17 pages .
7. The OpenMolcas Web: A Community-Driven Approach to Advancing Computational Chemistry," G. L. Manni, I. F. Galván, A. Alavi, F. Aleotti, F. Aquilante, J. Autschbach, D. Avagliano, A. Baiardi, J. J. Bao, S. Battaglia, L. Birnoschi, A. Blanco-González, S. I. Bokarev, R. Broer, R. Cacciari, P. B. Calio, R. K. Carlson, R. C. Couto, L. Cerdán, L. F. Chibotaru, N. F. Chilton, J. R. Church, I. Conti, S. Coriani, J. Cuéllar-Zuquin, R. E. Daoud, N. Dattani, P. Decleva, C. de Graaf, M. G. Delcey, L. De Vico, W. Dobrautz, S. S. Dong, R.

Feng, N. Ferré, M. Filatov(Gulak), L. Gagliardi, M. Garavelli, L. González, Y. Guan, M. Guo, M. R. Hennefarth, M. R. Hermes, C. E. Hoyer, M. Huix-Rotllant, V. K. Jaiswal, A. Kaiser, D. S. Kaliakin, M. Khamesian, D. S. King, V. Kochetov, M. Krośnicki, A. A. Kumaar, E. D. Larsson, S. Lehtola, M.-B. Lepetit, H. Lischka, P. L. Ríos, M. Lundberg, D. Ma, S. Mai, P. Marquetand, I. C. D. Merritt, F. Montorsi, M. Mörchen, A. Nenov, V. H. A. Nguyen, Y. Nishimoto, M. S. Oakley, M. Olivucci, M. Oppel, D. Padula, R. Pandharkar, Q. M. Phung, F. Plasser, G. Raggi, E. Rebolini, M. Reiher, I. Rivalta, D. Roca-Sanjuán, T. Romig, A. A. Safari, A. Sánchez-Mansilla, A. M. Sand, I. Schapiro, T. R. Scott, J. Segarra-Martí, F. Segatta, D.-C. Sergentu, P. Sharma, R. Shepard, Y. Shu, J. K. Staab, T. P. Straatsma, L. K. Sørensen, B. N. C. Tenorio, D. G. Truhlar, L. Ungur, M. Vacher, V. Veryazov, T. A. Voß, O. Weser, D. Wu, X. Yang, D. Yarkony, C. Zhou, J. P. Zobel, and R. Lindh, *J. Chem. Theory Comput.*, **19**, 6933-6991 (2023).

8. The Efficient Conversion Between Linear Wave Function Expansions and Nonlinear Graphically Contracted Function Expansions," 62nd Sanibel Symposium Proceedings (2023). http://qtp.ufl.edu/sanibel/abstracts.html.

9. A Perspective on Sustainable Computational Chemistry Software Development and Integration," R. Di Felice, M. L. Mayes, R. M. Richard, D. B. Williams-Young, G. K.-L. Chan, W. A. de Jong, N. Govind, M. Head-Gordon, M. R. Hermes, K. Kowalski, X. Li, H. Lischka, K. T. Mueller, E. Mutlu, A. M. N. Niklasson, M. R. Pederson, B. Peng, R. Shepard, E. F. Valeev, M. van Schilfgaarde, B. Vlaisavljevich, T. L. Windus, S. S. Xantheas, X. Zhang, and P. M. Zimmerman, *J. Chem. Theory Comput.*, **19** (2023) 7056-7076.

10. The Efficient Conversion Between Linear Wave Function Expansions and Nonlinear Graphically Contracted Function Expansions," R. Shepard, *Mol. Phys.*, (2023) e2231564 12 pages.

11. Quantification of the Ionic Character of Multiconfigurational Wave Functions: The Q_a^t Diagnostic, S. A. do Monte, R. F. K. Spada, R. L. R. Alves, L. Belcher, R. Shepard, H. Lischka, and F. Plasser, *J. Phys. Chem. A*, **127** (2023) 9842-9852.

12. The Efficient Conversion Between Linear Wave Function Expansions and Nonlinear Graphically Contracted Function Expansions, R. Shepard, *The 11th OpenMolcas Developers' Workshop Book of Abstracts*, (2023). https://eventi.unibo.it/openmolcas-workshop-2023/program

13. Graphically Contracted Function Construction with the Recursive Pairwise Merge Algorithm," R. Shepard, *J. Phys. Chem. A*, **127** (2023) 10334-10338.

14. J. Cho, C. R. Mulvihill, S. J. Klippenstein, R. Sivaramakrishnan, "Bimolecular Peroxy Radical (RO_2) Reactions and Their Relevance in Radical Initiated Oxidation of Hydrocarbons," J. Phys. Chem. A **127** (2023) 300-315.

15. N. A Seifert, B. Ruscic, R. Sivaramakrishnan, and K. Prozument, The C_2H_4O isomers in the oxidation of ethylene. J. Mol. Spectrosc. **398** (2023) 111847/1-8.

16. N. A. Seifert, K. Prozument, and M. J. Davis, "Computational Optimal Transport for Molecular Spectra: The Fully Continuous Case", J. Chem. Phys. **159** (2023) 164110, 19 pages.

17. Recent Progress with the Graphically Contracted Function Method, R. Shepard, *The Path of Quantum Chemistry in the 21st Century Abstracts for Invited Talks*, 23 (2024).

18. The Graphical Unitary Group Approach in COLUMBUS," 63rd Sanibel Symposium Proceedings (2024). https://sanibelsymposium.qtp.ufl.edu/resources/abstracts

19. A. Hamadi, R. Sivaramakrishnan, F. E. Cano Ardila, R. S. Tranter, S. Abid, N. Chaumeix, and A. Comandini, Styrene thermal decomposition and its reaction with acetylene under shock tube pyrolysis conditions: An experimental and kinetic modeling study. *Proc. Combust. Inst.* **40** (2024) 105481, 7 pages.

20. J. Cho, N. J. Labbe, L. B. Harding, S. J. Klippenstein, and R. Sivaramakrishnan, Competing radical and molecular channels in the unimolecular dissociation of methylformate. *Proc. Combust. Inst.* **40** (2024) 105684, 7 pages.

21. R. Sivaramakrishnan, and S. J. Klippenstein, Resolving discrepancies between theory and experiment for the NCN + H reaction. *Proc. Combust. Inst.* **40** (2024) 105403, 6 pages.

22. R. A. Shaik, A. W. Jasper, P. T. Lynch, R. Sivaramakrishnan, and R. S. Tranter, Initiation and carbene induced radical chain reactions in CH_2F_2 pyrolysis. *ChemPhysChem*, **25**, e202400362 (2024) 10 pages.

23. Y. Chen, C. Chen, I. Hwang, M. J. Davis, W. Yang, C. Sun, G.-H. Lee, D. McReynolds, D. Allan, J. M. Arias, S. P. Ong, and M. K. Y. Chan, "Robust Machine Learning Inference for X-Ray Absorption Near Edge Spectra Through Featurization", Chem. Mater. 36, (2024), 2304-2312.

24. M. Schwarting, N. A. Seifert, M. J. Davis, B. Blaiszik, I. Foster, and K. Prozument, "Twins in rotational spectroscopy: Does a rotational spectrum uniquely identify a molecule? ", J. Chem. Phys. 161, (2024) 044309, 15 pages.

Chemical Dynamics in the Gas Phase

Thermochemistry Subtask

Branko Ruscic, David H. Bross, and Stephen J. Klippenstein
Chemical Sciences and Engineering Division, Argonne National Laboratory,
9700 South Cass Avenue, Lemont, IL 60439
ruscic@anl.gov, dbross@anl.gov, sjk@anl.gov

Program Scope

The *spiritus movens* of the Thermochemistry Subtask of the Chemical Dynamics in the Gas Phase Program at Argonne is the need to provide the scientific community with accurate and reliable thermochemical information on chemical species that are relevant in energy-generating chemical processes or play prominent roles in subsequent environmental chemistry. Detailed knowledge of thermodynamic parameters for a broad array of stable and ephemeral chemical species is central to chemistry and essential in many industries. In particular, the availability of accurate, reliable, and internally consistent thermochemical values is a *conditio sine qua non* in quantitative areas of physical chemistry, such as kinetics, reaction dynamics, formulation of plausible reaction mechanisms, and construction of predictive models of complex chemical environments. Furthermore, the availability of accurate thermochemical values has historically been the prime driver for steady improvements in fidelity of increasingly sophisticated electronic structure theories.

The focus of the Thermochemistry Subtask is on bringing substantial innovations to the thermochemical field through development of novel methodologies and approaches, and utilizing them to the fullest in order to systematically improve both the quality and quantity of available thermochemical data relevant to the DOE mission. In order to achieve this, this program has developed, *inter alia*, a novel approach that is centered on analyzing and optimally utilizing the information content of *all available* thermochemically relevant determinations, both from theory and experiments. The aim is not only to dynamically produce the best currently possible thermochemical parameters for the targeted chemical species, but also to allow efficient updates as new knowledge becomes available, properly propagating its consequences through all affected chemical species, as well as providing critical tests of new experimental or theoretical data and, when possible, generating pointers to new determinations that are most likely to efficiently improve the overall thermochemical knowledge base. In order to provide a broad perspective of this area of science, the effort of the Thermochemistry Subtask is synergistically coordinated with related experimental and theoretical efforts within other Subtasks of the Chemical Dynamics in the Gas Phase Group at Argonne.

Recent Progress

Over the past year we have continued the development of various aspects of Active Thermochemical Tables (ATcT). The ATcT approach is the long-term centerpiece development of the Thermochemistry Subtask. ATcT has recently gained both additional nationwide and international prominence, as well as new responsibilities, thanks to a successful completion of a detailed scrutiny examining whether it fully satisfies a set of stringent requirements,[1] and its subsequent promotion (in 2023) to the status of a DOE Office of Science Public Reusable Research (DOE SC PuRe) Data Resource.[2-4] In order to ascend to this category, the candidate resource has to satisfy a number of criteria, such as being generally recognized by the scientific community as an authoritative provider of data, being publicly available and easily discoverable, maintaining detailed documentation on the provenance of data and providing adequate metadata, preserving strict versioning that maintains journal-like archival quality of published data, observing high standards for data management, curation, long-term preservation, etc. Pleasingly, the vast majority of these requirements were automatically satisfied by virtue of the original conceptual design of ATcT, allowing its ascension to SC PuRe status.

ATcT is currently capable of producing accurate, reliable, and internally consistent thermochemistry for both stable and ephemeral chemical species in a variety of aggregate states, including gas phase, condensed phases (both solids and liquids), aqueous solutions, and - as of recently - also species that are

adsorbed on various substrates, such as catalysts. In general, thermochemically-relevant determinations (such as reaction enthalpies, equilibrium constants, bond dissociation energies, etc.) by definition involve several chemical species, and thus help define (within the limitations of the associated error bars) the enthalpy of formation of the target chemical species only *relative* to other reactants and products in the underlying chemical reaction. Consequently, enthalpies of formation generally do not correspond, as such, to directly measured quantities; rather, they are indirectly defined via complex manifolds of thermochemical dependencies. The extraction of enthalpies of formation from intertwined (and frequently mutually inconsistent) dependencies among multiple species was historically an intractable proposition, resulting in a simplified *sequential* approach of inferring the relevant quantities one at a time (A begets B, B begets C, etc.), producing static sets of values that contain hidden progenitor-progeny relationships and cannot be updated with new knowledge without introducing new inconsistencies. In contrast, the ATcT approach relies on a unique paradigm that is rooted in assembling all relevant thermochemical determinations into complex Thermochemical Networks (TN). The TN effectively represent a set of qualified constraints that must be simultaneously satisfied to the maximum degree possible by the resulting thermochemistry. Categorizing the TN as a set of conditional constraints allows its detailed analysis using mathematical and statistical manipulations (enabling, for example, the isolation and remediation of internal inconsistencies). Once self-consistency is achieved across the TN, ATcT solves it simultaneously for the optimal enthalpies of formation of all included chemical species.

The most significant vehicle for disseminating the ATcT results is the ATcT website, ATcT.anl.gov, particularly after its ascension to the DOE SC PuRe status. The website continues to enjoy high popularity in the chemical community (netting a million pageviews each month) and continues to be hyped in peer-reviewed scientific literature as the most reliable source of accurate enthalpies of formation for species relevant in combustion, atmospheric chemistry, astrochemistry, as well as other areas.

In the past, the publicly released versions of ATcT results tended to suffer from a significant time-lag of a year or even more compared to the publication of scientific papers that were citing the results of a particular version. In order to correct that, we have made a concerted effort to catch up. Thus, in September 2023, we have published, as usual, two versions, 1.128 and 1.130. The last previous version (1.124) contained 2791 species, while ver. 1.130 describes 3003 chemical species, for a growth of more than 200 new species. However, in order to catch-up, we have very recently published six additional new versions (1.140, 1.148, 1.156, 1.172, 1.176, and 1.202). Compared to ver. 1.130, the latest published version as of September 2024, ver. 1.202, exhibits an additional growth of about 380 species and contains a total of 3384 chemical species, interconnected in the TN by >35,000 determinations.

Each of the above public versions is related to one or more peer reviewed papers that were intimately involved in driving the expansion for at least a portion of the new ATcT species. Thus, for example, vers. 1.128 and 1.130 were involved in producing the thermochemistry related to the ring opening mechanism of cyclopropyl radical and cation.[5] Of the most recent set of published versions of ATcT results, ver. 1.140 includes the most accurate (to within ± 10-15 cm^{-1}) state-of-the-art theoretical treatments in existence for several small molecules,[6] ver. 1.148 includes species relevant to the examination of the role of methanediol as a source of atmospheric formic acid,[7] ver. 1.156 is related both to a recent study of the oxidation of ethylene,[8] and to a new synchrotron-based experimental photoionization mass spectrometric measurements that led to refining the thermochemistry of both CF and SiF and their cations,[9] ver. 1.172 was generated to include species relevant to a study of photodissociation of formamide,[10] ver. 1.176 was expanded to include several species related to Criegee intermediates that are involved in an ongoing study conducted collaboratively within the ATcT Task Force One, and the most recent ver. 1.202 was instrumental in determining the correct thermochemistry of glycine.[11]

The latter is our most recent published study, the aim of which was to demonstrate the ATcT capabilities of efficiently arbitrating between significantly inconsistent (experimental) determinations of the enthalpy of formation of crystal α-glycine. The inconsistencies in the solid thermochemistry propagate to the thermochemistry for gas-phase glycine and are further amplified by inconsistencies in the available determinations of the sublimation enthalpy. Solid-phase and aqueous thermochemistry of glycine is

highly relevant in biochemistry, while gas-phase glycine is not only a suspected prebiotic molecule potentially formed in interstellar space, but is also a key thermochemical value for the determination of the thermochemistry of the remaining proteinogenic α-amino acids. Because of its three hindered rotors, gas-phase glycine has a rather complex potential energy surface with 8 different rotamers and 12 minima, (since 4 rotamers are enantiomeric). The ATcT analysis produces the best available enthalpies of formation: $\Delta_fH°_{298}$(glycine (g)) = -394.70 ± 0.55 kJ mol^{-1}, $\Delta_fH°_{298}$(α-glycine (cr)) = -528.37 ± 0.20 kJ mol^{-1}, $\Delta_fH°_{298}$(β-glycine (cr)) = -528.05 ± 0.22 kJ mol^{-1}, $\Delta_fH°_{298}$(γ-glycine (cr)) = -528.05 ± 0.22 kJ mol^{-1}, $\Delta_fH°_{298}$(glycine (aq, undissoc)) = -514.22 ± 0.20 kJ mol^{-1}, and $\Delta_fH°_{298}$(glycine (aq)) = -470.09 ± 0.20 kJ mol^{-1}. This work was presented to the ML community at the Faraday Discussion on Data-Driven Discovery in the Chemical Sciences; most of the participants were not previously aware of ATcT nor of its capabilities.

One of the studies mentioned above involves the experimental determination of the adiabatic ionization energies of CF and SiF, where the extraction of the experimental onset is rendered somewhat complex by spin-orbit effects, but the new value obtained for SiF improves the resulting ATcT SiF thermochemistry.

Another study mentioned above involves a broad multi-institutional collaboration (led by T. L. Nguyen and J. Stanton, U. Florida, and involving A. Perera from the same institution, J. Peters from U. Leuven, J.-F. Müller from Royal Belgian Institute for Space Aeronomy, and D. H. Bross and B. Ruscic, ANL), that carefully examined existing claims that the conversion of formaldehyde into methanediol within clouds could be a significant source of atmospheric formic acid. Based on accurate theoretical estimates of the related kinetic rate constants and aided by ATcT thermochemistry, we have conclusively shown that this mechanism contributes at most a rather small amount to the overall atmospheric formic acid.

In order to enhance the discoverability of ATcT results, we have recently expanded the description of each species by adding relevant metadata, such as synonymous names, InChI, InChIKey, etc.

Besides publishing updated versions of results on the ATcT website and steadfastly expanding the developmental ATcT TN, we have also continued a broad range of collaborations that involves researchers formally organized as the ATcT Task Force One (J. Stanton and T. L. Nguyen and their groups at UF, B. Ellison, UColorado, B. Changala, Harvard-Smithsonian, J. Baraban and his group at Ben-Gurion, M. J. L. Martin at Weizmann, and D. H. Bross, ANL). This Task Force continues to be very active, maintaining weekly teleconference meetings, and has a number of currently ongoing projects.

In collaboration with the ECC project (led by J. Zador, Sandia CRF), we have continued exploring and further developing various approaches that would allow a sensible and accurate description of partition function-based thermophysical properties of adsorbates, extending the studies to a polyatomic adsorbate, CH_3/Ni(111), and focusing in particular on the modes responsible for diffusion on the surface and libration of the adsorbate, resulting in a recent paper in *Phys. Chem. Chem. Phys*.

With respect to other activities within the Thermochemistry Subtask, our collaborative work with Curran was expanded to include thermochemical predictions for a large set of peroxy hydroperoxy-alkyl (OOQOOH) radicals. The set of molecules is comprised of 149 C_2–C_8 OOQOOH radicals, selected to encompass a wide variety of branching and substitution patterns, with the goal of exploring a wide range of interactions for use in group theory and/or machine learning based models. The thermochemistry for these radicals has a significant influence on the reactivity of fuels and on the formation of highly oxygenated molecules (HOMs) in the atmosphere. Theoretical characterization of these radicals is arduous due to their molecular size and complex fundamental interactions, such as hydrogen-bonding and torsional anharmonicity, and is difficult to validate in the absence of any direct experimental thermochemical data for such highly transient species.

The challenge of obtaining high accuracy predictions for the 0 K heat of formation for such large species was again met by coupling the connectivity based hierarchical (CBH) scheme of Raghavachari with the ANL scheme for calculating energies of a core set of reference species. Meanwhile, we systematically explored the thermodynamic properties for this set of radicals with five increasingly affordable approaches. In doing so, we presented a novel conformer selection approach suited to predict properties at

combustion temperatures. We also highlighted the shortcomings in the standard choice of the ground conformer as the reference. Comparisons amongst the approaches helped quantify the errors arising from various simplifying assumptions. For the largest of these radicals, and with the most affordable approach, final predictions of Gibbs energies were assigned a 2σ uncertainty of 4 kcal mol^{-1} in the negative temperature coefficient region.

Future Plans

Future plans of this program pivot around further development and expansion of the Active Thermochemical Tables approach, continuing to provide accurate thermochemistry to the scientific community and driving targeted thermochemically-relevant theoretical and experimental investigations of radicals and transient species that are intimately related to chemical processes of relevance to the DOE mission. A significant part of the effort will be focused on continued 'finalization' and dissemination of the resulting ATcT thermochemistry, typically involving groups of related chemical species. One important component of this process, focused on their enthalpies of formation, consists of testing and analyzing the TN dependencies, using tools such as the variance/covariance decomposition approach and analyses of the influence of relevant determinations via the hat-matrix, followed by improving the connectivity within the TN and adding new high-quality results (either virtual, i.e., computational, or actual, i.e., experimental) to coerce the resulting thermochemistry toward stable, 'release quality' values. This iterative process unavoidably results in additional expansion of the TN with new related chemical species, which is an added benefit. Another equally important component focuses on enhancing the accuracy of the thermophysical properties derived from the partition functions, typically by upgrading RRHO partition functions to NRRAO partition functions, which is also a currently ongoing effort.

The ascension of ATcT to the DOE SC PuRe Resource status provides a strong additional impetus for steadfast curation, aggressive expansion, and unfaltering long-term stewardship and maintenance. It also entails a careful evaluation of various suggestions proposed by users at large, as well as serious consideration of any and all requests for inclusion of particular additional species in ATcT. Thus, for example, we plan to gradually expand ATcT coverage to other relevant areas of chemistry (catalysis, energy storage, etc.), which, *inter alia*, involves the introduction of additional chemical elements to ATcT.

We are also in the process of developing additional CBH-ANL based theoretical thermochemistry databases (with systematic explorations of the thermodynamics) for a set of N_xH_y species (of relevance to ammonia synthesis), for a set of C_xF_y species (or relevance to PFAS kinetics), and for a set of alcohols and their related radical oxidation species. This theoretical thermochemistry work continues to make heavy use of the AutoMech software package. Appropriate extensions to AutoMech will be made for these and other new reaction classes as appropriate, including further developments of our treatments of low frequency modes such as torsions, ring puckering, and umbrella modes.

This work is supported by the U.S. Department of Energy, Office of Basic Energy Sciences, Division of Chemical Sciences, Geosciences, and Biosciences, under Contract No. DE–AC02–06CH11357.

References

[1] For DOE SC PuRe Resource requirements, see: https://science.osti.gov/Initiatives/PuRe-Data

[2] See: https://www.energy.gov/science/articles/active-thermochemical-tables-atct-advance-chemistry-pure-data-resource

[3] See: https://www.anl.gov/article/department-of-energy-recognizes-two-decades-worth-of-argonnes-highquality-thermochemical-data

[4] For a list of current PuRe Resources, see: https://science.osti.gov/Initiatives/PuRe-Data/Resources-at-a-Glance

[5] *Ring-Opening Dynamics of the Cyclopropyl Radical and Cation: The Transition State Nature of the Cyclopropyl Cation*, N. Genossar, P. B. Changala, B. Gans, J.-C. Loison, S. Hartweg, M.-A. Martin-Drumel, G. A. Garcia, J. F. Stanton, B. Ruscic, and J. H. Baraban, *J. Am. Chem. Soc.* 144, 18518-18525 (2022); DOI: 10.1021/jacs.2c07740

[6] *Elaborated Thermochemical Treatment of HF, CO, N2, and H2O: Insight into HEAT and Its Extensions,* J. H. Thorpe, J. L. Kilburn, D. Feller, P. B. Changala, D. H. Bross, B. Ruscic, and J. F. Stanton, *J. Chem. Phys.* **155**, 184109 (2021); DOI: 10.1063/5.0069322

[7] *Methanediol from Cloud-Processed Formaldehyde is Only a Minor Source of Atmospheric Formic Acid,* T. L. Nguyen, J. Peeters, J.-F. Müller, A. Perera, D. H. Bross, B. Ruscic, and J. F. Stanton, *Proc. Natl. Acad. Sci.* **120**, e2304650120/1-8 (2023); DOI: 10.1073/pnas.2304650120

[8] *The C2H4O Isomers in the Oxidation of Ethylene*, N. A. Seifert, B. Ruscic, R. Sivaramakrishnan, and K. Prozument, *J. Mol. Spectrosc.* **398**, 111847/1-8 (2023); DOI: 10.1016/j.jms.2023.111847

[9] *Refining Thermochemical Properties of CF, SiF, and Their Cations by Combining Photoelectron Spectroscopy, Quantum Chemical Calculations, and the Active Thermochemical Tables Approach*, U. Jacovella, B. Ruscic, N. L. Chen, H.-L. Le, S. Boyé-Péronne, S. Hartweg, M. Roy-Chowdhury, G. A. Garcia, J.-C. Loison, and B. Gans, *Phys. Chem. Chem. Phys.* **25**, 30838-30847 (2023); DOI: 10.1039/D3CP04244H

[10] *Dynamics of HCN, NHC, and HNCO Formation in the 193 nm Photodissociation of Formamide*, K. L. Caster, N. A. Seifert, B. Ruscic, A. W. Jasper, and K. Prozument, *J. Phys. Chem. A* (in press) (2024); DOI: 10.1021/acs.jpca.4c02232]

[11] *Accurate and Reliable Thermochemistry by Data Analysis of Complex Thermochemical Networks using Active Thermochemical Tables: The Case of Glycine Thermochemistry*, B. Ruscic and D. H. Bross, *Faraday Discuss.* (in press) (2024); DOI: 10.1039/D4FD00110A

Publications resulting from DOE sponsored research (2022 – present)

- *Accurate and Reliable Thermochemistry by Data Analysis of Complex Thermochemical Networks using Active Thermochemical Tables: The Case of Glycine Thermochemistry*, B. Ruscic and D. H. Bross, *Faraday Discuss.* in press (2024); DOI: 10.1039/D4FD00110A (part of the collection: *Data-Driven Discovery in the Chemical Sciences*)
- *Dynamics of HCN, HNC, and HNCO Formation in the 193 nm Photodissociation of Formamide*, K. L. Caster, N. A. Seifert, B. Ruscic, A. W. Jasper, and K. Prozument, *J. Phys. Chem. A* in press (2024); DOI: 10.1021/acs.jpca.4c02232
- *Active Thermochemical Tables (ATcT) Enthalpies of Formation Based on Version 1.202 of the Thermochemical Network*, B. Ruscic and D. H. Bross, Argonne National Laboratory, Lemont, Ill. (2024), https://atct.anl.gov/Thermochemical%20Data/version%201.202/index.php; DOI: 10.17038/CSE/2440256
- *Active Thermochemical Tables (ATcT) Enthalpies of Formation Based on Version 1.176 of the Thermochemical Network*, B. Ruscic and D. H. Bross, Argonne National Laboratory, Lemont, Ill. (2024), https://atct.anl.gov/Thermochemical%20Data/version%201.176/index.php; DOI: 10.17038/CSE/2440255
- *Active Thermochemical Tables (ATcT) Enthalpies of Formation Based on Version 1.172 of the Thermochemical Network*, B. Ruscic and D. H. Bross, Argonne National Laboratory, Lemont, Ill. (2024), https://atct.anl.gov/Thermochemical%20Data/version%201.172/index.php; DOI: 10.17038/CSE/2440254
- *Active Thermochemical Tables (ATcT) Enthalpies of Formation Based on Version 1.156 of the Thermochemical Network*, B. Ruscic and D. H. Bross, Argonne National Laboratory, Lemont, Ill. (2024), https://atct.anl.gov/Thermochemical%20Data/version%201.156/index.php; DOI: 10.17038/CSE/2440253
- *Active Thermochemical Tables (ATcT) Enthalpies of Formation Based on Version 1.148 of the Thermochemical Network*, B. Ruscic and D. H. Bross, Argonne National Laboratory, Lemont, Ill. (2024), https://atct.anl.gov/Thermochemical%20Data/version%201.148/index.php; DOI: 10.17038/CSE/2440252
- *Active Thermochemical Tables (ATcT) Enthalpies of Formation Based on Version 1.140 of the Thermochemical Network*, B. Ruscic and D. H. Bross, Argonne National Laboratory, Lemont, Ill. (2024), https://atct.anl.gov/Thermochemical%20Data/version%201.140/index.php; DOI: 10.17038/CSE/2440250
- *Importance Sampling within Configuration Space Integration for Adsorbate Thermophysical Properties: A Case Study for CH_3/Ni(111)*, K. Blöndal, K. Badger, K. Sargsyan, D. H. Bross, B. Ruscic, and C. F. Goldsmith, *Phys. Chem. Chem. Phys.* **26**, 17265-17273 (2024); DOI: 10.1039/D4CP01197J
- *Systematic Exploration of the Thermochemistry for a Set of Peroxy Hydroperoxy-Alkyl Radicals*, S. N. Elliott, C. R. Mulvihill, M. K. Ghosh, H. J. Curran, and S. J. Klippenstein, *Proc. Combust. Inst.* **40**, 105618 (2024); DOI: 10.1016/j.proci.2024.105618
- *The C_2H_4O Isomers in the Oxidation of Ethylene*, N. A. Seifert, B. Ruscic, R. Sivaramakrishnan, and K. Prozument, *J. Mol. Spectrosc.* **398**, 111847/1-8 (2023); DOI: 10.1016/j.jms.2023.111847 (*Colin Western Memorial Issue*)
- *Active Thermochemical Tables (ATcT) Enthalpies of Formation Based on Version 1.130 of the Thermochemical Network*, B. Ruscic and D. H. Bross, Argonne National Laboratory, Lemont, Ill. (2023), https://atct.anl.gov/Thermochemical%20Data/version%201.128/index.php; DOI: 10.17038/CSE/1997229
- *Active Thermochemical Tables (ATcT) Enthalpies of Formation Based on Version 1.128 of the Thermochemical Network*, B. Ruscic and D. H. Bross, Argonne National Laboratory, Lemont, Ill. (2023),

https://atct.anl.gov/Thermochemical%20Data/version%201.128/index.php; DOI: 10.17038/CSE/1997230

- *Refining the Thermochemical Properties of CF, SiF, and Their Cations by Combining Photoelectron Spectroscopy, Quantum Chemical Calculations, and the Active Thermochemical Tables Approach*, U. Jacovella, B. Ruscic, N. L. Chen, H.-L. Le, S. Boyé-Péronne, S. Hartweg, M. R. Chowdhury, G. A. Garcia, J.-C. Loison, and B. Gans, *Phys. Chem. Chem. Phys.* **25**, 30838-30847 (2023); DOI: 10.1039/D3CP04244H (with cover art)
- *Active Thermochemical Tables: Enthalpies of Formation of Bromo- and Iodo-Methanes, Ethenes and Ethynes*, D. H. Bross, G. B. Bacskay, K. A. Peterson, and B. Ruscic, *J. Phys. Chem. A* **127**, 704-723 (2023); DOI: 10.1021/acs.jpca.2c07897 (with cover art)
- *Sub 20 cm^{-1} Computational Prediction of the CH Bond Energy – A Case of Systematic Error in Computational Thermochemistry*, J. H. Thorpe, D. Feller, D. H. Bross, B. Ruscic, and J. F. Stanton, *Phys. Chem. Chem. Phys.* **25**, 21162-21172 (2023); DOI: 10.1039/D2CP03964H (selected as *PCCP Hot Article*; also, part of thematic issue: *Benchmark Experiments for Numerical Quantum Chemistry*)
- *High Accuracy Heats of Formation for Alkane Oxidation: From Small to Large via the CBH-ANL Method,* S. N. Elliott, M. Keçeli, M. K. Ghosh, K. P. Somers, H. J. Curran, and S. J. Klippenstein*, J. Phys. Chem. A* **127***,* 1512-1531 (2023); DOI: 10.1021/ac/jpca.2c07248 (with cover art, part of virtual issue *Combustion in a Sustainable World: From Molecules to Processes*; *ACS Editors' Choice Article*)
- *Group Additivity Values for the Heat of Formation of C_2-C_8 Alkanes, Alkyl Hydroperoxides, and their Radicals,* M. K. Ghosh, S. N. Elliott, K. P. Somers, S. J. Klippenstein, and H. J. Curran, *Combust. Flame* **257**, 112492 (2023); DOI: 10.1016/j.combustflame.2022.112492
- *Systematically Derived Thermodynamic Properties for Alkane Oxidation*, S. N. Elliott, K. B. Moore III, A. V. Copan, Y. Georgievskii, M. Keçeli, K. P. Somers, M. K. Ghosh, H. J. Curran, and S. J. Klippenstein, *Comb. Flame* **257**, 112487 (2023); DOI: 10.1016/j.combustflame.2022.112487 (*Jim Miller Memorial Issue*)
- *Group Additivity Values for Entropies and Heat Capacities of C2-C8 Alkanes, Alkyl Hydroperoxides, and their Radicals*, M. K. Ghosh, S. N. Elliott, K. P. Somers, S. J. Klippenstein, and Henry J. Curran*, Combust. Flame* **257**, 112706 (2023); DOI: 10.1016/j.combustflame.2023.112706
- *The Influence of Thermochemistry on the Reactivity of Propane, the Pentane Isomers, and n-Heptane in the Low Temperature Regime*, M. K. Ghosh, S. Panigraphy, S. Dong, S. N. Elliott, S. J. Klippenstein, and H. J. Curran, *Proc. Combust. Inst.* **39**, 601-609 (2023); DOI: 10.1016/j.proci.2022.08.086
- *High Accuracy Heats of Formation for Alkane Oxidation: From Small to Large via the CBH-ANL Method*, S. N. Elliott, M. Keçeli, M. K. Ghosh, K. P. Somers, H. J. Curran, and S. J. Klippenstein, *J. Phys. Chem. A*, **127**, 1512-1531 (2023); DOI: 10.1021/acs.jpca.2c07248
- *Ring-Opening Dynamics of the Cyclopropyl Radical and Cation: The Transition State Nature of the Cyclopropyl Cation*, N. Genossar, P. B. Changala, B. Gans, J.-C. Loison, S. Hartweg, M.-A. Martin-Drumel, G. A. Garcia, J. F. Stanton, B. Ruscic, and J. H. Baraban, *J. Am. Chem. Soc.* **144**, 18518-18525 (2022); DOI: 10.1021/jacs.2c07740
- *Configuration Space Integration for Adsorbate Partition Functions: The Effect of Anharmonicity on the Thermophysical Properties of CO–Pt(111) and CH_3OH–Cu(111)*, K. Blöndal, K. Sargsyan, D. H. Bross, B. Ruscic, and C. F. Goldsmith, *ACS Catalysis* **13**, 19-32 (2022); DOI: 10.1021/acscatal.2c04246
- *Mechanism, Thermochemistry, and Kinetics of the Reversible Reactions: $C_2H_3 + H_2 \rightleftarrows C_2H_4 + H \rightleftarrows C_2H_5$*, T. L. Nguyen, D. H. Bross, B. Ruscic, G. B. Ellison, and J. F. Stanton, *Faraday Discuss.* **238**, 405-430 (2022); DOI: 10.1039/D1FD00124H
- *Active Thermochemical Tables (ATcT) Enthalpies of Formation Based on Version 1.124 of the Thermochemical Network*, B. Ruscic and D. H. Bross, Argonne National Laboratory, Lemont, Ill. (2022), https://atct.anl.gov/Thermochemical%20Data/version%201.124/index.php; DOI: 10.17038/CSE/1885923
- *Active Thermochemical Tables (ATcT) Enthalpies of Formation Based on Version 1.122x of the Thermochemical Network*, B. Ruscic and D. H. Bross, Argonne National Laboratory, Lemont, Ill. (2022), https://atct.anl.gov/Thermochemical%20Data/version%201.122x/index.php; DOI: 10.17038/CSE/1885922
- *Active Thermochemical Tables (ATcT) Enthalpies of Formation Based on Version 1.122v of the Thermochemical Network*, B. Ruscic and D. H. Bross, Argonne National Laboratory, Lemont, Ill. (2022), https://atct.anl.gov/Thermochemical%20Data/version%201.122v/index.php; DOI: 10.17038/CSE/1885921

ARGONNE-SANDIA CONSORTIUM ON PRESSURE-DEPENDENT CHEMISTRY

Raghu Sivaramakrishnan, Ahren W. Jasper, Stephen J. Klippenstein, Robert S. Tranter
Chemical Sciences and Engineering Division, Argonne National Laboratory, Lemont, IL, 60439

Leonid Sheps, Craig A. Taatjes
Combustion Research Facility, MS 9055, Sandia National Laboratories Livermore, CA 94551-0969,
raghu@anl.gov, lsheps@sandia.gov

Program Scope

This project explores fundamental aspects of collisional energy transfer and chemical kinetics with the goal of developing accurate models for gas-phase chemistry spanning a range of pressures up to the high pressures of practical devices. We design and implement novel experiments, theory, and modeling to probe pressure-dependent kinetics from elementary reactions to comprehensive chemical mechanisms. We focus on sensitive time-resolved experimental probes of reaction intermediates, which enable direct studies of chemical systems of interest to DOE energy missions. We apply novel master equation and stochastic simulation methods to accurately predict the kinetics of key processes. The theoretical predictions and experimental observations are employed in high fidelity non-empirical chemical models, and, importantly, identify departures from standard chemical kinetics assumptions. Recently, we have been pursuing detailed understandings of non-equilibrium effects and of radical oxidation chemistry. We are currently integrating modeling, experiment, and theory (MET) through feedback loops at all levels of chemical complexity for small alkanes, alcohols, and ethers (including cyclic variants) as key prototype fuels. The consortium expands and enhances collaborations between Argonne's Chemical Dynamics Group and the Gas-Phase Chemical Physics Group in Sandia's Combustion Research Facility.

Recent Progress

High pressure oxidation: We continued our collaboration with Ju on high pressure oxidation (up to 100 atm) as observed in his novel JSR apparatus. Thus far, we have contributed to his efforts to model the oxidation data he has obtained for methanol, dimethyl ether, hydrogen, and most recently for a mixture of ammonia and methanol. Accurate modeling of the latter requires some consideration of the interaction of CH_3OH and CH_2O with NH_2 radical chemistry and of NH_3 with CH_2OH/CH_3O radical chemistry. Predicted third body collision efficiencies for H_2O_2 and HO_2 (+M) were used to minimize bath gas effects as a possible source of error at high pressures. New high level ab initio transition state theory (TST) based master equation rates were provided for the reaction of NH_2 with CH_3OH and CH_2O. For the first reaction, we predict a major difference in the branching between CH_3O and CH_2OH relative to that predicted by earlier lower-level efforts. For the second reaction, we predict order of magnitude larger rate constants than those in the literature. While the final model predictions show some improvement over other existing models, there are also a number of unresolved issues, which will require further model improvements. Notably, the reaction of H_2NO with various radicals appear to be generally important in NH_3 cofuel oxidation, and we are now pursuing high level treatments of these reactions.

Stereochemistry and butane oxidation: Stereochemistry significantly influences chemical processes yet is only rarely included in chemical models for oxidation and combustion. There are various challenges in doing so, mostly related to the additional degree of complexity it introduces. We developed a code for direct expansion of full mechanisms to incorporate all forms of stereochemical effects, and then applied this code in a large scale study of the butane oxidation system. Remarkably, the substitution of the resulting first principles stereochemically correct submechanism for the first and second stages of the radical oxidation yielded modeled predictions that were in equivalent or slightly better agreement with the experimental observations than those of a highly tuned butane oxidation mechanism of Curran. This modeling result indicates that our stereochemical implementation can accurately capture important aspects of the physics. We continued this work with a SCGSR funded collaboration with the Rotavera group (who is a leader in the experimental observation of stereospecific aspects of radical oxidation) on a study of stereochemical

effects in the oxidation of 2,3-dimethyloxirane. One notable finding was that prompt dissociation of the ring opened radicals dramatically affects the product distribution. We also demonstrated that the stereochemistry of the initial ring radicals is rapidly equilibrated through ring inversion processes. Preliminary simulation results suggest the need for additional rate calculations, which are now in progress. These projects provided a clear demonstration of the joint utility of our automated rate generation, automated prompt analysis, and automated stereo expansion methodologies.

Master equation code: We made a number of improvements to our MESS master equation system solver to increase its effectiveness. It is now possible to obtain more stable answers through the use of arbitrary precision solutions or alternatively to use a new algorithm that is particularly effective at low temperatures. Furthermore, the code has been ported to GPU based machines, with significant speedups observed. We expect to write this work up shortly. In the meantime, the code improvements are already available.

***Nonstatistical kinetics in H + HO_2*:** Quasiclassical trajectories (QCT) and global potential energy surfaces constructed using newly developed strategies were used to compute thermal and nonthermal rate constants for the H + HO_2 reaction. A significant fraction of trajectories that reached the H_2O_2 well promptly dissociated back to reactants instead of via the heavily statistically favored 2OH channel. This nonstatistical consequence of inefficient IVR was shown to increase with the initial vibrational energy of HO_2*, and a negative energy dependence in the nonthermal H + HO_2 rate constant was observed.

Pyrolysis of cycloalkanes: The pyrolysis of cyclohexane and its primary dissociation product 1-hexene were studied at reaction pressure up to 10 bar. The experiments were performed in the HRRST and analyzed by VUV-PIMS at the ALS. 1-hexene primarily dissociates to allyl and propyl radicals although other channels such as CH_3 elimination and the retro-ene reaction are not negligible. Thus, H and CH_3 are rapidly formed. These both attack the parent molecule and combine with radical products resulting in complex chemistry. A recent literature model for 1-hexene did not reproduce the experimental observations and insights into the reasons for this were gained. However, a recent model for methylcyclohexane pyrolysis which incorporates cyclohexane and 1-hexene did satisfactorily reproduce the experimental observations after several key rate coefficients were updated. The improved model also produced satisfactory agreement with the cyclohexane results. Some key observations include the importance of the cyclohexyl radical which rapidly dominates cyclohexane pyrolysis and the observation of a sequence of intermediate species in the dehydrogenation of cyclohexane to benzene. A more robust description of the chemistry of cyclohexane and 1-hexene at high pressures and temperatures was obtained.

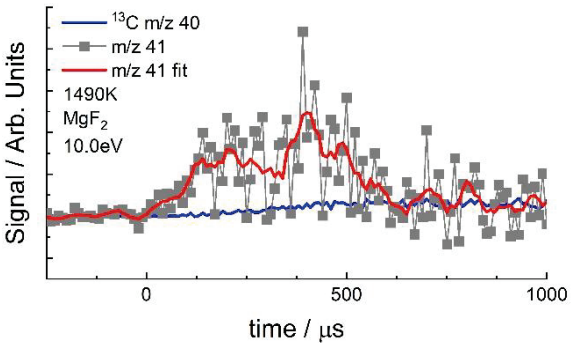

Figure 1: Time dependent effective concentration of allyl radical (squares) produced in the dissociation of cyclohexane (~9bar). There is a small contribution from the ^{13}C isotopologues of allene/propyne (blue).

***i^{2}PEPICO studies of PAH formation*:** In collaboration with Comandini and Chaumeix (CNRS-Orleans), we have continued investigations of PAHs (polyaromatic hydrocarbons) by HRRST/i^{2}PEPICO experiments at the SOLEIL synchrotron. Prior studies focused on the pyrolysis of individual species allowing differences in the PAH formed and the dominant paths to be elucidated; analyses of these data are still ongoing. We have recently performed additional studies where an aromatic molecule was pyrolyzed in the presence of propene. These studies allow synergistic effects on PAH production like those encountered in practical systems to be examined. The experiments spanned 1300-1800 K and pressures of 8-9 atm with 0.1% toluene and 0.2% propene dilute in argon. Additional experiments with pure m-xylene and benzene examined the effect of methyl substitution relative to toluene. Finally, experiments were performed with pure propene to obtain a reference dataset for the toluene/propene work. These detailed studies should ultimately result in

the development of generic mechanisms for PAH formation.

Role of HCO prompt dissociation in scramjet engine relevant flames: Combustion in high-speed ram-based propulsion engines occurs under thermodynamic conditions of high reactant temperatures (greater than 1000 K) and relatively low pressures (less than 5 atm). There is a lack of fundamental flame measurements at such conditions that result in adiabatic flame temperatures (T_{ad}) exceeding 2500 K. In a collaborative work with experiments led by Jayachandran (Worcester Polytechnic Institute-WPI), laminar flame speeds were measured for CH_4/oxidizer mixtures at high T_{ad} using oxygen enriched mixtures (25-75% O_2 in oxidizer) to probe the flame chemistry relevant to ram-based combustors. Simulations with recent literature kinetic models (FFCM-1) revealed increasing differences between data and model predictions with increasing T_{ad}, reaching up to 25%. Kinetic analyses reveal that at the thermodynamic conditions in these O_2-enriched flames, i.e., lower pressures and higher T_{ad}, the effects of HCO prompt dissociation are accentuated. Reaction path analysis for these flames revealed that approximately half of the reaction flux for HCO formation undergoes prompt dissociation to H + CO. Since prompt HCO dissociation is an inherent feature of our in-house Theory-informed kinetics (ThInK) model, simulations using this model was in closer agreement with these higher T_{ad} flame speed measurements. On the other hand, the simultaneous inclusion of fall-off in HCO dissociation coupled with prompt HCO dissociation was required in FFCM-1 to improve its predictive capability for these more exotic flames.

Theory informed kinetics model (ThInK): Theoretical chemical kinetics has become an indispensable tool in modeling the chemical interactions relevant in combustion such that one would be hard-pressed today to find a modern combustion kinetics model that does not include a single theoretical prediction for any of the elementary reactions and/or thermochemical/transport parameters. Over the course of several years now we have been actively involved in the development of a theory informed kinetics model (ThInK) that includes *a priori* high-level theoretical predictions for the elementary reactions as well as thermochemistry and transport parameters for species involved in small molecule combustion chemistry (H_2 and $C_0 – C_3$ species). In contrast to the adage “Models are to be used, not believed”, combustion kinetics models have been intended to be predictive in nature, at least over regimes where experimental data exist. The prodigious use of high-level theory in the present kinetics model is expected to facilitate predictive simulations of chemical reactivity, even in regimes of practical relevance that are poorly characterized by elementary kinetics and/or combustion experiments. Simulations using the ThInK model are in good agreement with measured laminar flame speeds and auto-ignition delays for the core species ($H_2 – C_3$).

A high-pressure FAGE instrument. We reported a new Fluorescence Assay by Gas Expansion (FAGE) apparatus for time-resolved detection of OH and HO_2 in pump-probe experiments at elevated pressures and temperatures. Our miniaturized instrument uses a novel sampling configuration with dilution flow to solve a long-standing challenge in FAGE applications, in which transport effects in the sampling nozzle degraded the experimental time resolution. We demonstrated quantitative detection of OH and HO_2 (with 10 μs resolution) from a pulsed laser photolysis reactor at pressures up to 50 bar, using benchmark chemical reactions OH + CH_4, OH + OH, OH + HO_2, and HO_2 + HO_2.

Reactions of oxygenated radicals, produced from methyl formate. We completed an MET study of the •CH_2OCHO and CH_3OC•O radicals, formed by the reaction of Cl• with methyl formate (MF, CH_3OCHO) following pulsed laser photolysis of Cl_2/MF/He mixtures at T = 400 – 750 K. Quantitative time-resolved measurements of MF, Cl_2, HCl, CO_2, •CH_3, CH_3Cl, CH_2O, and $ClCH_2OCHO$ were used to constrain a chemical model, anchored by theoretical calculations of the initial H abstraction rate coefficients, •CH_2OCHO and CH_3OC•O decomposition, and secondary reactions of •CH_2OCHO with Cl• and Cl_2. We found that CH_3OC•O dissociated with a >99% yield to CH_3 + CO_2 on μs timescales, faster than our time resolution, at all T. In contrast, •CH_2OCHO decomposed to CH_2O + •CHO on 1 – 10 ms timescales, which were resolved by our experiments. Our optimized rate parameters had significant impacts on modelling of the combustion of methyl esters, which are critical components or surrogates of biodiesel.

Quantification of intermediates in tetrahydrofuran oxidation. We extended our earlier study of THF oxidation to P = 10 bar and T = 450 – 675 K. The new measurements enabled the first quantification of the time-resolved concentrations of key intermediates in THF autoignition: RO_2, O_2QOOH, butanedial, and hydroperoxides. Comparisons with chemical models revealed that the prevailing mechanisms of THF combustion drastically over-estimated the $O_2QOOH \longrightarrow$ ketohydroperoxide + OH $\longrightarrow$ oxy-radical + 2 OH yields and the overall reactivity, echoing similar observations we made in related ethers and cycloalkanes.

Insights into mechanism optimization strategies. We further extended our chemical model optimization methodology via genetic algorithm fitting using literature cyclohexane combustion data from jet-stirred reactors. We confirmed our earlier finding of the critical role of $RO_2 \leftrightarrow QOOH$ as a rate-limiting step in the low-T oxidation of cycloalkanes, and also revealed the limitations of time-averaged speciation data in constraining complex reaction mechanisms.

Future Work

HRRST: We will continue to explore the pyrolysis of cyclic species at high pressures. Experiments have been conducted with cyclopentane and cycloheptane and their conjugate 1-alkenes and with cyclooctane. These are similar to the C6 studies and allow the effect of ring size and length of the 1-alkene to be explored. The data are being analyzed and should yield information guiding the development of rate/mechanism rules. We will also expand the range of heterocyclic species studied to include heteroatoms other than O.
Key areas for development of the PAH studies include improving the simulation of photoelectron spectra to more accurately identify isomeric compositions and uncertainties in assignments of isomers. Additional attention will be given to elucidating reaction paths leading to each isomer with a goal of generating generic rules for PAH growth.

Theory: We are in the process of a developing a first principles theory-based model for tetrahydrofuran (THF), which is a focus of ongoing experimental efforts by Sheps. This effort is proceeding beyond related efforts through the direct incorporation of prompt dissociation effects for the ketohydroperoxide and alkoxy radical channels, the explicit consideration of stereochemistry (including in the various fleeting transition states), the inclusion of up to third O_2 reactions, and explicit incorporation of all ring puckered states in the conformational analyses. The latter aspect has been the focus of a significant ongoing extension to the AutoMech code. As part of this effort, we will use the benchmarking and bootstrapping method pioneered in our collaboration with Lester for QOOH radical decomposition to obtain highly accurate energetics.
In collaboration with Rotavera, we are continuing to improve and expand upon our treatment of butane oxidation with related treatments of various submechanisms that arise later in the oxidation process. The ultimate goal is to have a fully first principles mechanism that includes a number of key additional physical phenomenon that are generally neglected. We are also planning work on roaming channels in neopentanol dissociation in collaboration with Tranter and Cavallotti.

Nonstatistical kinetics: To further explore the negative-energy-dependent kinetics observed for $H + HO_2$*, we performed additional QCT studies of $CH_2 + CH_3$* and O + OH*. All three systems feature a deep intermediate well, a barrierless entrance channel, and a low-lying exit channel with no reverse barrier. Together, the three systems allow us to study the importance of IVR as a function of system size. In preliminary work, we found that while inefficient IVR is observed for all three systems, negative energy dependence is observed only for $H + HO_2$. Compared to $H + HO_2$, inefficient IVR is relatively less important for the larger $CH_2 + CH_3$ system, as expected; while inefficient IVR is relatively more important for the smaller O + OH system, its effect is not significant enough to overcome the much stronger positive energy dependence in the statistical rate constant.

Collisional energy transfer in van der Waals systems: Quantifying collisional energy transfer in transient van der Waals (vdW) systems is relevant to our understanding of oligomerization reactions in the atmosphere as well as the radical-complex (chaperone) mechanism. An initial planned study involves developing accurate two- and three-body interaction potential energy surfaces for the $CH_2OO\cdots H_2O_2$ ($+H_2O$) system, which will be used in trajectory calculations characterizing the vdW complex lifetime and

collisional energy transfer with water. Initial calculations suggest that longer-lived vdW complexes show significantly less energy transfer than shorter lived complexes due to the differences in their partitioning of energy among intermolecular and intramolecular modes of the dimer.

Role of nonthermal reactions of HO_2* + CO/H_2 in syngas ignition: We propose to computationally explore the role of reactive collisions of HO_2* with stable species like CO (and H_2, H_2O). While the thermal reaction CO + HO_2 has a significant barrier ~18 kcal/mol and therefore slow rates, this reaction is known to substantially influence autoignition in syngas mixtures, where the initial reactants include large mole fractions of CO. In such a situation, we anticipate that CO + HO_2* should have much faster rates than CO + HO_2. We propose to characterize this initially using the effective temperature model (developed based on prior dynamics studies on CH_4*/H_2O* + X) coupled with master equation calculations. These results can then be used to drive combustion modeling studies on syngas auto-ignition. In a similar fashion, reactions of HO_2* with H_2 and H_2O may also be facile, and we propose to characterize these additional nonthermal reactions of hot radical complexes with stable species.

Non-Boltzmann effects in autoignition reactions. Building on our recent success in characterizing and quantifying transient reaction intermediates, we will focus on direct probing of non-Boltzmann reactions in THF oxidation as the experimental platform. This system includes two dominant O_2QOOH dissociation channels, leading to hydroperoxides cy-C_4H_5O-OOH + HO_2 and cy-$C_4H_5O_2$-OOH + OH. These pathways have exothermicities of ~ 40 and ~105 kcal/mol, respectively, and should thus exhibit very different non-Boltzmann contributions from chemically activated intermediates. In addition to RO_2, O_2QOOH, and butanedial, we previously quantified the sum of hydroperoxides in THF oxidation. Although we could not quantify independently the yields of cy-C_4H_5O-OOH and cy-$C_4H_5O_2$-OOH via photoionization mass spectrometry, we should be able to do so now using our new high-pressure FAGE diagnostic. Furthermore, we quantified the yields of fumaraldehyde and acrolein. We hypothesize that the source of these compounds is decomposition of cy-C_4H_5O-OOH and cy-$C_4H_5O_2$-OOH, providing potential markers for channel-specific probing of hydroperoxide decomposition. We are thus well-positioned to directly probe the kinetics of the entire THF oxidation sequence, including prompt non-Boltzmann processes.
We expect non-Boltzmann reactions to manifest as prompt formation of reaction intermediates on microsecond timescales. The yields of these prompt channels should be highly sensitive to temperature and pressure (i.e., collisional energy transfer rate), and we plan to explore these effects over pressures up to tens of bar and temperatures spanning the autoignition regime. The experimental results will enable detailed comparisons with theoretical predictions that were outlined above.

Automated optimization of theory-based reaction mechanisms. In collaboration with Zador (via the SNL Core GPCP program) we plan to create an automated workflow for efficient optimization of theory-based chemical mechanisms. The expected outcome is an open-source code that will perturb calculated molecular properties and collisional energy transfer parameters in user-supplied master equation (ME) inputs to optimize chemical model predictions against detailed experimental speciation data. This effort builds on our earlier applications of this idea to cyclopentane and cyclohexane oxidation, with several notable advances: i) enabling model benchmarking using diverse experimental results, including our own time-resolved speciation, jet-stirred reactor, and shock tube data; ii) exploring flexible optimization strategies, such as genetic algorithms, simplex algorithms, and related methods, and iii) allowing simultaneous optimization of coupled MEs.

Publications acknowledging support from this program, 2022 – present:

1. **Bayesian model calibration for vacuum-ultraviolet photoionisation mass spectrometry**, J. Oreluk, L. Sheps, H. Najm, *Comb. Theo. Mod.* **26,** 513 (2022).
2. **Methanol oxidation up to 100 atm in a supercritical pressure jet-stirred reactor,** Z. Wang, H. Zhao, C. Yan, Y. Lin, A. D. Lele, W. Xu, B. Rotavera, A. W. Jasper, S. J. Klippenstein, Y. Ju, *Proc. Combust. Inst.* **39**, 445 (2022).
3. **The role of collisional energy transfer in the thermal and prompt dissociation of 1-methylallyl**, J. Cho, Y. Tao, Y. Georgievskii, S. J. Klippenstein, A. W. Jasper, R. Sivaramakrishnan, *Proc. Combust. Inst.* **39**, 601 (2022).
4. **Formation of organic acids and carbonyl compounds in n-butane oxidation via γ-ketohydroperoxide decomposition**. D. M. Popolan-Vaida, A. J. Eskola, B. Rotavera, J. F. Lockyear, Z. Wang, S. M. Sarathy, R. L. Caravan, J. Zádor, L. Sheps,

A. Lucassen, K. Moshammer, P. Dagaut, D. L. Osborn, N. Hansen, S. R. Leone, C. A. Taatjes, *Angew. Chem. Int. Ed.* **61,** e202209168 (2022).

5. **Quantification of key peroxy and hydroperoxide intermediates in the low-temperature oxidation of dimethyl ether**. D. E. Couch, C. R. Mulvihill, R. Sivaramakrishnan, K. Au, C. A. Taatjes L. Sheps, *J. Phys. Chem. A* **126**, 9497 (2022).
6. **Inefficient intramolecular vibrational energy redistribution for the H + HO_2 reaction and negative internal energy dependence for its rate constant,** A. W. Jasper, D. R. Moberg, Y. Tao, S. J. Klippenstein, R. Sivaramakrishnan, *Front. Phys.* **10**, 1003010 (2022).
7. **Low- and intermediate-temperature oxidation of dimethyl ether up to 100 atm in a supercritical pressure jet-stirred reactor,** C. Yan, H. Zhao, Z. Wang, G. Song, Y. Lin, C. R. Mulvihill, A. W. Jasper, S. J. Klippenstein, Y. Ju**,** *Combust. Flame*, **236**, 112059 (2022).
8. **HO_2 + HO_2: High level theory and the role of singlet channels**, S. J. Klippenstein, R. Sivaramakrishnan, U. Burke, K. P. Somers, H. J. Curran, L. Cai, H. Pitsch, M. Pelucchi, T. Faravelli, P. Glarborg, *Comb. Flame* **243**, 111975 (2022).
9. **Effects of non-thermal termolecular reactions on detonation development in hydrogen (H_2)/methane (CH_4) - air mixtures** S. S. Desai, Y. Tao, R. Sivaramakrishnan, Y. Wu, T. F. Lu, J. H. Chen, *Combust. Flame* **244**, 112277 (2022).
10. **The role of energy transfer and competing bimolecular reactions in characterizing the unimolecular dissociations of allylic radicals**, J. Cho, A. W. Jasper, Y. Georgievskii, S. J. Klippenstein, R. Sivaramakrishnan**,** *Combust. Flame*, **257**, 112502 (2022).
11. **OH roaming during the ozonolysis of a-pinene: A new route to highly oxygenated molecules?** S. J. Klippenstein, S. N. Elliott, *J. Phys. Chem. A*, **127**, 10647 (2023).
12. **Genetic algorithm optimization of a master equation cyclopentane oxidation model against time-resolved speciation experiments**. M. Demireva, J. Oreluk, A. L. Dewyer, J. Zádor, L. Sheps, *Combust. Flame*, **257**, 112506 (2023).
13. **Automated identification and calculation of prompt effects in kinetic mechanisms using statistical models**, L. Pratali Maffei, K. B. Moore III, Y. Georgievskii, C. R. Mulvihill, S. N. Elliott, J. Cho, R. Sivaramakrishnan, T. Faravelli, S. J. Klippenstein, *Combust. Flame*, **257**, 112422 (2022).
14. **High-temperature dissociation of neopentanol: shock tube photoionization mass spectrometry studies**, C. Banyon, R. S. Tranter, *J. Phys. Chem. A* **127**, 1293 (2023).
15. **Effect of non-thermal termolecular reactions on wedge-induced oblique detonation waves,** S. S. Desai, Y. Tao, S. R. Sivaramakrishnan, J. H. Chen, *Combust. Flame*, **257**, 112681 (2023).
16. **Pyrolysis of cycloxane and 1-hexene at high temperatures and pressures – a photoionization mass spectrometry study**, R. S. Tranter, C. S. Banyon, R. E. Hawtoff, K. Kim, *Energies*, **16**, 7929 (2023).
17. **Bimolecular peroxy radical (RO_2) reactions and their relevance in radical initiated oxidation of hydrocarbons,** J. Cho, C. R. Mulvihill, S. J. Klippenstein, R. Sivaramakrishnan, *J. Phys. Chem. A*, **127**, 300 (2023).
18. **Theoretical kinetics predictions for reactions on the NH_2O potential energy surface**, S. J. Klippenstein, C. R. Mulvihill, P. Glarborg, *J. Phys. Chem. A*, **127**, 8650 (2023).
19. **Quantum and anharmonic effects in non-adiabatic transition state theory**, C. R. Mulvihill, Y. Georgievskii, S. J. Klippenstein, *J. Chem. Phys.*, **159**, 174104 (2023).
20. **Insights into constraining rate coefficients in fuel oxidation mechanisms using genetic algorithm optimization**, M. Demireva, L. Sheps, N. Hansen, *Energy Fuels*, ***37***, 14240 (2023).
21. **Modeling–experiment–theory analysis of reactions initiated from Cl + methyl formate,** J. Cho, D. Rösch, Y. Tao, D. L. Osborn, S. J. Klippenstein, L. Sheps, R. Sivaramakrishnan, *J. Phys. Chem. A* **127**, 9804 (2023).
22. **An experimental, theoretical, and kinetic modeling study of post-flame oxidation of ammonia**, J. Jian, H. Hashemi, H. Wu, Glarborg, A. W. Jasper, S. J. Klippenstein, *Combust. Flame*, **261**, 113325 (2024).
23. **High-pressure oxidation of hydrogen diluted in n_2 with added h_2o or co_2 at 100 atm in a supercritical-pressure jet-stirred reactor,** H. Zhao, C. Yan, G. Song, A. W. Jasper, S. J. Klippenstein, Y. Ju, *Combust. Flame* **266**, 113543 (2024).
24. **The role of stereochemistry in combustion processes**, S. N. Elliott, K. B. Moore III, C. R. Mulvihill, A. V. Copan, L. Pratali Maffei, S. J. Klippenstein, *WIREs, Comput. Mol. Sci.* **14**, e1710 (2024).
25. **Radical stereochemistry: accounting for diastereomers in kinetic mechanism development**, A. V. Copan, K. B. Moore III, S. N. Elliott, C. R. Mulvihill, L. Pratali Maffei, S. J. Klippenstein, *J. Phys. Chem. A*, **128**, 3711 (2024).
26. **High pressure ammonia/methanol oxidation up to 100 atm,** Z. Wang, B. Mei, N. Liu, A. Thawko, X. Mao, H. Zhao, P. Glarborg, S. J. Klippenstein, Y. Ju, *Proc. Combust. Inst.* **40**, 105489 (2024).
27. **Competing radical and molecular channels in the unimolecular dissociation of methylformate**, J. Cho, N. J. Labbe, L. B. Harding, S. J. Klippenstein, R. Sivaramakrishnan, *Proc. Combust. Inst.*, **40**, 105684 (2024).
28. **External standard calibration method for high-repetition-rate shock tube kinetic studies with synchrotron-based time-of-flight mass spectrometry,** F. E. Cano Ardila, S. Nagaraju, R. S. Tranter, S. Abid, A. Desclaux, A. Roque Ccacya, G. A. Garcia, N. Chaumeix, A. Comandini, *Analyst*, **149**, 1586 (2024).
29. **Time-resolved quantification of key species and mechanistic insights in low-temperature tetrahydrofuran oxidation**, M. Demireva, K. Au, N. Hansen, L. Sheps, *Phys. Chem. Chem. Phys.* **26**, 10343 (2024)
30. **New Instrument for time-resolved OH and HO_2 quantification in high-pressure laboratory kinetics studies**, L. Sheps, K. Au, *J. Phys. Chem. A* **128,** 3916 (2024)
31. **Systematic exploration of the thermochemistry for a set of peroxy hydroperoxyl-alkyl radicals,** S. N. Elliott, C. R. Mulvihill, M. K. Ghosh, H. J. Curran, S. J. Klippenstein, *Proc. Combust. Inst.* **40**, 105618 (2024).

Deciphering Complex Chemical Reaction Dynamics Induced by Non-Equilibrium Microplasma Discharges at High Pressures

Sayan Biswas
Mechanical Engineering Department, University of Minnesota Twin Cities, biswas@umn.edu

Project Background and Scope: Microplasma, confined to dimensions on the scale of millimeters or smaller, demonstrates remarkable stability even under high pressures, facilitating self-sustained and continuous operation [1-3]. This stability is attributed to the efficient energy transfer within the confined space, leading to heightened ionization and excitation processes [4]. With their cost-effectiveness, ease of operation, simplified hardware design, and portability, microplasmas find applications across diverse fields including materials processing, sensing, energy generation, environmental remediation, and chemical synthesis [5-10]. The behavior of ions, electrons, metastable species, excited atomic and molecular species dynamics in the transient streamers and early afterglow regimes of microplasma under *atmospheric* and *above-atmospheric pressures* is crucial for understanding its potential in complex reaction dynamics [11-13].

However, our current understanding of microplasma discharges at higher pressures is significantly constrained due to the scarcity of well-established experimental data on high-pressure microplasma kinetics. At elevated pressures, where the electron mean free path approaches the gap between electrodes, quenching processes become dominant. However, the onset of field emission in small gaps and the trapping of electrons in oscillatory motion between electrodes in microplasma discharges introduce deviations from classical plasma theory. The resulting plasma dynamics become stochastic and turbulent, leading to the predominance of short-lived plasma filaments at higher pressures. Free electrons, accelerated by the electric field, generate secondary electrons through gas particle ionization, leading to an electron avalanche and the creation of a self-induced electric field. The competing and counteracting processes in microplasma – quenching and secondary electron production under self-induced electric fields at high pressures produce an intricate nonadiabatic system that requires further investigation. In these filaments, channels are filled with metastable atoms and excited species, causing electron bombardment, electron-ion, and ion-neutral reactions that are not well understood [14, 15]. Excited Rydberg states [16] are key in plasma because they significantly influence the energy transfer, reaction pathways, and chemical dynamics within the plasma environment, leading to unique and often enhanced plasma chemistry. Much confusion exists currently in the literature about the branching ratio between metastable atoms and Rydberg molecules as products of dissociative recombination processes [17, 18]. In fact, no experimental branching ratio exists for many of these processes. The study will focus on understanding the electron-impact ionization and fragmentation of molecules such as methane and ammonia and the impact of Rydberg molecules on plasma chemistry and chemical reactions.

The presence of Rydberg states in microplasma significantly influences plasma chemistry pathways by providing alternative reaction channels. We hypothesize that the excitation of atoms or molecules to Rydberg states alters their reactivity, leading to the formation of unique chemical species and pathways not observed in non-Rydberg-excited plasmas. This hypothesis is based on the premise that Rydberg states possess distinct electronic structures and energy distributions, thereby governing the kinetics and thermodynamics of chemical reactions within the microplasma environment. Our experimental campaign will initially focus on investigating microplasma discharge in helium, a well-established plasma gas, before transitioning to methane or ammonia. The approach involves first identifying the Rydberg states for each gas, followed by a study of the chemical reactions involving these Rydberg states using spectroscopic and

laser diagnostics, such as Resonance-Enhanced Multiphoton Ionization (REMPI), Photoelectron Spectroscopy (PES), Fourier Transform Spectroscopy (FTS). This sequential approach is necessary due to the intricate nature of the processes involved. Quantitative laser diagnostics measurements will enable the assessment of methane and ammonia Rydberg molecule production rates during the discharge's active phase and early afterglow. We will delve into the fundamental processes governing the production of these species, including metastable and radiative pathways. Furthermore, we aim to elucidate the production channels of methane and ammonia metastable atoms, clarifying the branching ratio between metastable atoms and Rydberg molecules, a topic currently lacking experimental data in the literature. Our approach will involve developing a systematic methodology to enumerate all branching ratios.

The proposed research aims to unlock new chemical pathways in a gas-phase system by utilizing electrons, ions, and Rydberg molecules in a high-pressure non-equilibrium microplasma. Over a five-year span, the research trajectory will commence with focused studies on well-established gases like helium and/or argon during the initial two years. Subsequently, the scope will expand to encompass investigations into air, methane, and ammonia systems, particularly in the context of energy applications, in the latter three years. Through this progressive approach, the research aims to deepen our understanding of microplasma chemistry and its potential for transformative applications in various domains.

Future Work: Our first objective would be to perform a well-laid-out experimentation campaign to investigate the high-pressure microplasma behavior to explore kinetics and the scaling parameters. The objective is to use experiments and optical diagnostics to investigate high-pressure microplasma dynamics and characteristics. An optically accessible constant volume calorimeter with a high-pressure capacity (designed for up to 1000 bar) to delve into microplasma dynamics, illustrated in **Figure 1**. However, our investigation will narrow its focus to pressures ranging between 1 and 10 bar absolute. Presently, various electrode designs and geometries are undergoing scrutiny for tailored applications in energy and combustion projects. For this project, we will employ canonical electrode configurations like pin-to-pin or pin-to-plate, with meticulous attention directed toward refining electrode surface characteristics. This includes precise control over parameters such as tip radius for pin-to-pin discharges, surface roughness for pin-to-plate setups, and the ceramic surface for dielectric barrier discharges.

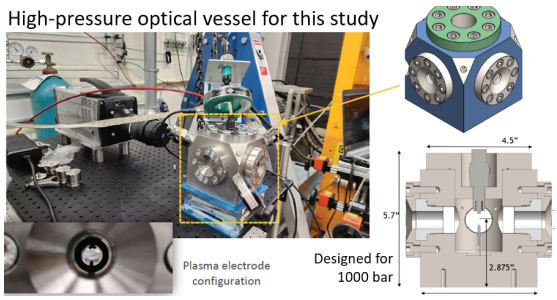

Figure 1. *Experimental setup for the proposed study.*

Once microplasma generation is achieved, our primary objective is to delineate the discharge transition boundary, scaling parameters, and elucidate its underlying physics. Pulsed discharges, such as nanosecond DC discharges, occurring at atmospheric or slightly above atmospheric pressure, exhibit intricate structures with non-uniformities at scales of tens of micrometers near the electrode surface. For instance, in dielectric barrier discharges, the initiation of streamers induces a substantial alteration in electron density (for negative polarity discharges) or positive ion concentration (for positive polarity discharges) on the surface, leading to a sharp decline in the electric field perpendicular to the surface. Concurrently, the electron density profile undergoes significant changes in proximity to the dielectric. During the first budget period, our objective is to thoroughly characterize various microplasma behaviors and utilize emission spectroscopy to gain insights into the overall plasma dynamics.

References

[1] J. A. Bittencourt, “Fundamentals of Plasma Physics,” Fundamentals of Plasma Physics. Springer, pp. 1–32, 2004. doi: 10.1007/978-1-4757-4030-1_1.

[2] M. A. Lieberman and A. J. Lichtenberg, “Principles of Plasma Discharges and Materials Processing: Second Edition,” Principles of Plasma Discharges and Materials Processing: Second Edition, pp. 1–757, Jan. 2005, doi: 10.1002/0471724254.

[3] A. Fridman and L. A. Kennedy, “ELEMENTARY PROCESSES OF CHARGED SPECIES IN PLASMA,” Plasma Physics and Engineering, Feb. 2010, doi: 10.4324/9780203334874_CHAPTER_2.

[4] R. Mahamud and T. I. Farouk, “Ion kinetics and self pulsing in DC microplasma discharges at atmospheric and higher pressure,” J Phys D Appl Phys, vol. 49, no. 14, p. 145202, Mar. 2016, doi: 10.1088/0022-3727/49/14/145202.

[5] K. H. Becker, K. H. Schoenbach, and J. G. Eden, “Microplasmas and applications,” J Phys D Appl Phys, vol. 39, no. 3, Feb. 2006, doi: 10.1088/0022-3727/39/3/R01.

[6] V. Karanassios, “Microplasmas for chemical analysis: Analytical tools or research toys?,” Spectrochim Acta Part B At Spectrosc, vol. 59, no. 7, pp. 909–928, Jul. 2004, doi: 10.1016/J.SAB.2004.04.005.

[7] X. Yuan, J. Tang, and Y. Duan, “Microplasma Technology and Its Applications in Analytical Chemistry,” Appl Spectrosc Rev, vol. 46, no. 7, pp. 581–605, Oct. 2011, doi: 10.1080/05704928.2011.604814.

[8] J. P. Boeuf, “Plasma display panels: Physics, recent developments and key issues,” J Phys D Appl Phys, vol. 36, no. 6, Mar. 2003, doi: 10.1088/0022-3727/36/6/201.

[9] K. Tachibana, “Current status of microplasma research,” IEEJ Transactions on Electrical and Electronic Engineering, vol. 1, no. 2, pp. 145–155, Aug. 2006, doi: 10.1002/TEE.20031.

[10] R. S. Houk, “Mass Spectrometry of Inductively Coupled Plasmas,” Anal Chem, vol. 58, no. 1, pp. 97A-105A, 1986, doi: 10.1021/AC00292A003.

[11] A. Von Engel and L. Marton, “ Ionized Gases ,” Phys Today, vol. 18, no. 10, pp. 64–64, Oct. 1965, doi: 10.1063/1.3046953.

[12] Y. Guo, S. Wu, X. Liu, L. Yang, and C. Zhang, “The Application of Microplasma in the Terahertz Field: A Review,” Applied Sciences 2021, Vol. 11, Page 11858, vol. 11, no. 24, p. 11858, Dec. 2021, doi: 10.3390/APP112411858.

[13] F. Meng, X. Yuan, X. Li, Y. Liu, and Y. Duan, “Microplasma-Based Detectors for Gas Chromatography: Current Status and Future Trends,” Appl Spectrosc Rev, vol. 49, no. 7, pp. 533–549, Oct. 2014, doi: 10.1080/05704928.2013.863778.

[14] J. Choi, F. Iza, J. K. Lee, and C. M. Ryu, “Electron and ion kinetics in a DC microplasma at atmospheric pressure,” IEEE Transactions on Plasma Science, vol. 35, no. 5 I, pp. 1274–1278, Oct. 2007, doi: 10.1109/TPS.2007.904827.

[15] H. C. Kim, F. Iza, S. S. Yang, M. Radmilović-Radjenović, and J. K. Lee, “Particle and fluid simulations of low-temperature plasma discharges: Benchmarks and kinetic effects,” J Phys D Appl Phys, vol. 38, no. 19, Oct. 2005, doi: 10.1088/0022-3727/38/19/R01

[16] G. M. Lankhuijzen and L. D. Noordam, “Rydberg Ionization: From Field to Photon,” Advances in Atomic, Molecular and Optical Physics, vol. 38, no. C, pp. 121–153, 1998, doi: 10.1016/S1049-250X(08)60051-8

[17] P. C. Stangeby and W. T. Wong, “Recombination in cold high pressure helium,” Phys Lett A, vol. 51, no. 5, pp. 312–314, Mar. 1975, doi: 10.1016/0375-9601(75)90462-4.

Chemical Kinetic Data of Benchmark Accuracy through Multi-Scale Informatics Strategies

Michael P. Burke

Department of Mechanical Engineering, Department of Chemical Engineering, & Data Science Institute
Columbia University, New York, NY 10027
mpburke@columbia.edu

Program Scope

The reliability of predictive simulations for advanced energy conversion devices depends on the availability of accurate data for thermochemistry, chemical kinetics, and transport. In that regard, accurate data are critically important for both their direct use in predictive simulations and for benchmarking improved theoretical methodologies that can similarly produce accurate data for predictive simulations. The use of informatics-based strategies for the determination of accurate thermochemical data with well-defined uncertainties, i.e. the Active Thermochemical Tables (ATcT),[1] has revolutionized the field of thermochemistry – ATcT provides thermochemical data of unprecedented accuracy for direct use in predictive simulation and has served as a key enabler of *ab initio* electronic structure methodologies of equally impressive accuracy. In this program, we are developing an analogous active database for *chemical kinetics* to establish high-accuracy kinetic data for predictive simulation and to evaluate emerging *ab initio*-based theoretical kinetics methods, using novel multiscale informatics strategies we are developing. Particular emphasis is placed on reaction systems for which non-thermal kinetic sequences arise and for which combining theoretical and experimental data is necessary to unravel complex reaction data into chemical information, where this program advances the state of the art in computational methodologies for those purposes.

Recent Progress

There are several significant challenges in deriving high-accuracy kinetic data of relevance to the complex reactions encountered in combustion, planetary atmospheres, and interstellar environments. First, even the most "direct" experimental rate constant determinations are often influenced by uncertainties in secondary reactions – leading to a complex web of interdependences among kinetic parameters for many reactions (and an opportunity to gain more information than has been attained previously, since uncertainties are seldom at the noise floor of the measurements). Second, there is rarely enough experimental data to constrain the full temperature, pressure, and composition (*T/P/*$\underline{X}$) dependence of many rate constants – rendering usual rate-parameter-based uncertainty quantification approaches ineffective. Third, many reactions of interest to various application domains and gas-phase theoretical chemistry involve non-thermal kinetic sequences[2-3,iii] – posing an additional problem for rate-parameter-based approaches.

During the past several years, we have been developing a multi-scale uncertainty quantification approach, MultiScale Informatics (MSI),[4,i,ii,iv,viii] to address the challenges involved in 1) unraveling the complex web of interdependences among reactions in complex systems data (by reinterpreting the raw data from multi-reaction systems used to determine rate constants experimentally), 2) sufficiently constraining the *T/P/*$\underline{X}$ dependence of rate constants (by incorporating theoretical calculations to extrapolate constraints imposed by limited data), and 3) analyzing data from reaction systems involving non-thermal kinetic sequences (by leveraging the physics-based framework to account for such processes). In this program, we are applying and expanding MSI to develop a high-accuracy kinetics database through carefully chosen reaction systems that serve to both anchor the database and grow it in ways leveraging its anchored foundations – while addressing outstanding scientific questions and identifying new ones.

$H + O_2 = O + OH$, $OH + H_2 = H_2O + H$, $O + H_2 = OH + O$, $H + HO_2$ = products, TBHP fragment kinetics, CH_2O kinetics, and other reaction systems. We have continued our massive simultaneous analysis of several hundred (raw) experimental and theoretical datasets spanning many dozens of reactions to unravel their dauntingly complex web of interdependences. This endeavor is intended to both anchor the active network and determine refined values for their rate constants and uncertainties (including for the first three reactions listed above, whose rate constants are generally well known but still hindered by secondary reaction uncertainties). For example, our analysis of data used to determine rate constants for OH + H_2 indicate strong influences from several reactions involving the decomposition fragments from the common OH-precursor tert-butylhydroperoxide (TBHP) including OH + CH_3COCH_3, CH_3 + CH_3, and CH_3 + OH.[ix]

The overall analysis has already yielded insights into rate constants, and discrepancies among data, for many reactions (only some of which are presented here as examples). These include both revisions to some of the best characterized reactions and resolution of controversies for highly debated reactions.

With regard to the former, we recently found that the *raw* data from the most precise rate constant determinations[5] for H + O_2 = OH + O can be reproduced using an MSI model with a ~10% lower rate constant than originally derived from the data (Fig. 1). This difference is mainly attributable to differences in the rate constants for secondary reactions, for which the MSI model better reproduces the associated theoretical and experimental data. Given that H + O_2 = OH + O is the most sensitive reaction in many combustion environments and in many rate constant determinations, even a small revision to its rate constant is very significant. For example, we have also found that the same MSI model reproduces the *raw* data from the rate constant determination for H + O_2 (+M) = HO_2 (+M) from Davidson et al.[6] with a much lower rate constant that (unlike the original interpretations[6]) is also consistent with recent *a priori* 2D-ME calculations.[7,8]

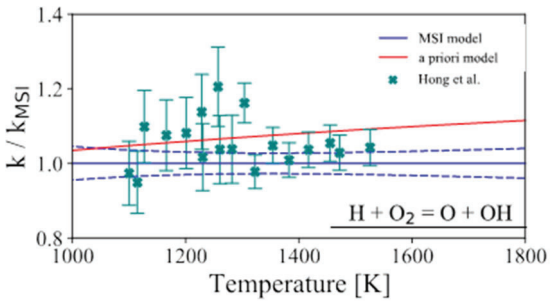

Fig. 1. Rate constants for H + O_2 = O + OH relative to the MSI model. Symbols show the original experimental interpretations[5] of raw data that the MSI model reproduces equally well.

With regard to the latter, our analysis has also identified consistent explanations of seemingly inconsistent data for HCO + O_2 = CO + HO_2. For example, our analysis revealed an alternative interpretation of experimental data used for rate constant determinations at high temperatures consistent with theoretical calculations.[10] While the original interpretations of the high-temperature experiments show high values and a sharp temperature dependence, the MSI model reproduces the raw data from those studies with a factor of three lower rate constant and mild temperature dependence consistent with theory.[10]

All told, the analysis contains hundreds of theoretical and experimental datasets for dozens of highly coupled reaction systems, whose interconnections can only be unraveled through *active* rather than *static* approaches, as demonstrated above. We are now writing up the results from these many inextricably coupled systems in a series of journal papers that we plan to submit in the coming months.

Representation of complex T/P/X dependence in MSI (and kinetic modeling codes). As part of both our ongoing MSI methodological developments, we have been conducting a major overhaul of how MSI and Cantera, which MSI uses for phenomenological kinetics/continuum-level simulations, treat the complex *T/P/X* dependence of complex-forming reactions. Previously, continuum-level chemical codes could not properly represent composition (*X*) dependence for the most common types of complex-forming reactions, including many non-equilibrium kinetic sequences and other "pressure-dependent" reactions.

We have been rewriting portions of the Cantera source code to address this. In collaboration with Ray Speth (MIT), we recently implemented[xii] our group's new reduced-pressure mixture rule[12-13] (validated against ME equations for broad classes of reactions), which enables an accurate treatment of *T/P/X* dependence, in Cantera.[11] We recently described this implementation in a journal paper[xii] and we plan for

it to be included in the next release of Cantera,[11] a software suite widely used for combustion, catalysis, chemical vapor deposition, atmospheric chemistry, plasmas, and a host of other applications.

Using this new version of Cantera, we were then able to incorporate data from the *a priori* 2D-ME calculations of Jasper[8] for the first time (since previous codes could not treat the complex $T/P/\underline{X}$ dependence). As demonstrated in Fig. 2, the kinetic model using these new *a priori* 2D-ME calculations reproduces the experimental data remarkably well (and certainly within experimental uncertainties)—providing an important test of *a priori* 2D-ME accuracy for polyatomics (like CO_2 and H_2O) which are often only studied in mixtures experimentally.[xii] Our other results[xii] (not shown) reveal similar reproduction of raw experimental data used to determine H_2O_2 (+M) for M = CO_2 and H + O_2 (+M) for M = NH_3, and indicate that inclusion of the 2D-ME data appears to resolve previous modeling difficulties for H_2 and NH_3 (carbon-free fuels of recent interest).

Sub-models for fluorinated precursors and related insights into destruction of PFAS. We have been continually expanding our kinetic sub-models for precursors that we use to reinterpret experimental data from precursor-initiated kinetics. Our expansions of these precursor sub-models into fluorine kinetics (relevant to experiments for H + HO_2, for example) led to the realization that low-temperature fluorocarbon oxidation pathways (known to the atmospheric chemistry community) influence fluorocarbon combustion within incinerators for PFAS (polyfluoroalkyl substances) destruction.

For context, essentially all combustion kinetic mechanisms for fluorocarbons to date find their basis in those developed for fluorocarbons as flame suppressants and likewise are primarily composed of high-temperature kinetic pathways. Yet, these same models have often been used to assess PFAS destruction in incinerators, which emphasize lower temperatures (~700–1400 K).

We recently showed that low-temperature oxidation pathways (mediated by peroxy radicals, RO_2) — not considered previously in PFAS incineration modeling — impact predictions of common surrogates for PFAS destruction (e.g. C_2F_6, Fig. 3), toxic products of incomplete combustion (e.g. CF_2O), and overall PFAS destruction efficiencies.[xi]

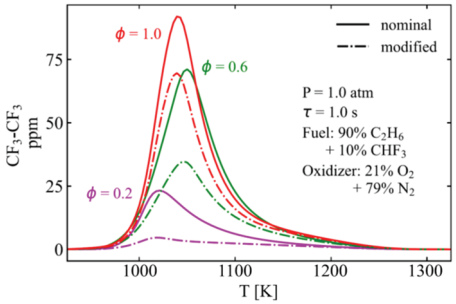

Fig. 3. Predicted CF_3-CF_3 mole fractions from isothermal plug flow reactor simulations for models with ("modified") and without ("nominal") CF_3O_2 kinetics.[xi]

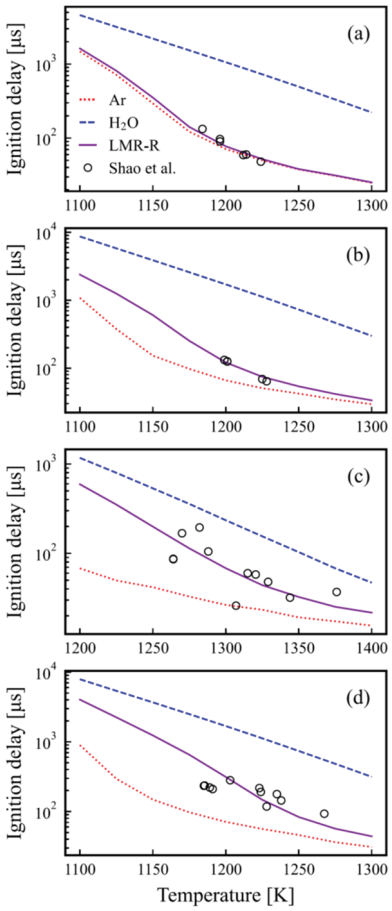

Fig. 2. Ignition delay times used to determine rate constants for H + O_2 (+M) = HO_2 (+M) for various bath gases.[xii] (a) 3% H_2/1.5% O_2/Ar, (b) 3% H_2/1.5% O_2/N_2, (c) 3% H_2/1.5% O_2/9% H_2O/Ar, and (d) 3% H_2/1.5% O_2/20% CO_2/Ar. Symbols denote experimental data.[9] Lines denotes predictions using the reduced-pressure mixture rule (LMR-R) and, for comparison, using pure Ar or pure H_2O as the third body, based on *a priori* 2D-ME data.[7,8]

CH_2O (+M) and CH_2O + O_2. Building on our master equation calculations[vi,vii] of the CH_2O + M/O_2 system reported previously, we have been conducting MSI analysis of data from pyrolysis, oxidation, and photochemical experiments, for which there is no shortage of discrepancies (and non-Boltzmann sequences). Of note, our current MSI model reproduces the raw data from pyrolysis/oxidation experiments[15,16] whose original interpretations were inconsistent with each other. We have also been analyzing data from photochemical experiments[17] that show evidence of a rovibrationally excited CH_2O^* + O_2 reaction, where we have also identified the role of a photoisomerization-assisted

$HCOH + O_2$ reaction[vi] and secondary reactions stemming from $CH_2O + HO_2$ that we plan to investigate.

Future Plans

We plan to venture next into the $CH_2O + HO_2$ reactions (to form $HCO + H_2O_2$ or $HOCH_2O_2$) important to some determinations for $H + O_2 = OH + O$ and $CO + OH = CO_2 + H$ and photochemical experiments[17] of $CH_2O^* + O_2$. These reactions and subsequent reactions of $HOCH_2O_2$, which we will study in tandem, are also broadly important to combustion and atmospheric chemistry (e.g. oxidation of hydroxymethyl hydroperoxide, HMHP, formed from reaction of the simplest Criegee intermediate with water). We also plan to explore phenomenological representations of the reactivity of molecular entities that react too quickly to be considered chemical species, building on our previous studies on HCOH,[vii] and representations of $T/P/\underline{X}$ dependence of non-Boltzmann kinetic sequences, building on our work discussed above.[xii] These efforts will also enable deeper integration of our AutoNonBoltzmann code[iii,v] into MSI.

References

1. B. Ruscic, et al. *J Phys Chem A* 108 (2004) 9979–9997.
2. M.P. Burke, S.J. Klippenstein. *Nature Chemistry* 9 (2017) 1078-1082.
3. N.J. Labbe, et al. *J. Phys. Chem. Lett.* 7 (2015) 85–89.
4. M.P. Burke. *Int J Chem Kinet* 48 (2016) 212–235.
5. Z. Hong, D.F. Davidson, E.A. Barbour, R.K. Hanson. *Proc Combust Inst* 33 (2011) 309–316.
6. D.F. Davidson, E. Petersen, M. Röhrig, R.K. Hanson, C.T. Bowman *Proc Combust Inst* 26 (1996) 481–488.
7. S.J. Klippenstein. *Proc Combust Inst* 36 (2017) 77–111.
8. A. W. Jasper. *Faraday Discussions* 238 (2022) 68–86.
9. J. Shao, R. Choudhary, A. Susa, D.F. Davidson, R.K. Hanson. *Proc Combust Inst* 37 (2019) 145–152.
10. S.J. Klippenstein, unpublished.
11. D.G. Goodwin, H.K. Moffat, I. Schoegl, R.L. Speth, B.W. Weber, Cantera, https://www.cantera.org.
12. M.P. Burke, R. Song. *Proc Combust Inst* 36 (2017) 245-253.
13. L. Lei, M.P. Burke. *J Phys Chem A* 123 (2019) 631-649.
14. J. Shao, R. Choudhary, A. Susa, D.F. Davidson, R.K. Hanson. *Proc Combust Inst* 37 (2019) 145–152.
15. S.S. Kumaran, J.J. Carroll, J.V. Michael. *Proc Combust Inst* 27 (1998) 125−133.
16. V. Vasudevan, D.F. Davidson, R.K. Hanson, C.T. Bowman, D.M. Golden. *Proc Combust Inst* 31 (2007) 175−183.
17. B. Welsh, M. Corrigan, E. Assaf, K. Nauta, P. Sebastianelli, M. Jordan, C. Fittschen, S. Kable. *Nat Chem* 15 (2023) 350.

BES-supported products (2021-present)

i. C.E. LaGrotta, M.C. Barbet, L. Lei, M.P. Burke, "Towards a High-Accuracy Kinetic Database Informed by Theoretical and Experimental Data: $CH_3 + HO_2$ as a Case Study," *Proceedings of the Combustion Institute* 38 (2021) 1043-1051.

ii. C.E. LaGrotta, L. Lei, M.C. Barbet, Z. Hong, D.F. Davidson, R.K. Hanson, M.P. Burke, "Towards Resolution of Lingering Discrepancies in the H_2O_2 Decomposition System: $HO_2 + HO_2$," 12th U.S. National Combustion Meeting, College Station, Texas, May 2021.

iii. L. Lei, M.P. Burke, "An Extended Methodology for Automated Calculations of Non-Boltzmann Kinetic Sequences: $H + C_2H_2$ + X and Combustion Impact," *Proceedings of the Combustion Institute* 38 (2021) 661-669.

iv. C.E. LaGrotta, M.C. Barbet, L. Lei, M.P. Burke. MSI: A Package for MultiScale Informatics. https://github.com/TheBurkeLab/MSI.

v. L. Lei, M.P. Burke. AutoNonBoltzmann: A Code for Automated Calculations of Non-Boltzmann Kinetic Sequences.

vi. M.P. Burke, "Master Equation Calculations to Assess the Role of Non-Thermal Bimolecular Reactions in Formaldehyde Photochemistry," American Geophysical Union Fall Meeting, December 2021.

vii. M.P. Burke, Q. Meng, C. Sabaitis, "Dissociation-Induced Depletion of High-Energy Reactant Molecules as a Mechanism for Pressure-Dependent Rate Constants for Bimolecular Reactions," *Faraday Discussions* 238 (2022) 355–379.

viii. C.E. LaGrotta, Q. Meng, L. Lei, M.C. Barbet, Z. Hong, M.P. Burke, "Resolving Discrepancies Between State-of-the-Art Theory and Experiment for $HO_2 + HO_2$ via Multiscale Informatics," *Journal of Physical Chemistry A* 127 (2023) 799–816.

ix. J.M. Pankauski, C.E. LaGrotta, J. Lee, M.P. Burke, "Resolving Discrepancies among Experimental and Theoretical Data for the CH_3 + OH Reaction using MultiScale Informatics," 2024 Spring Technical Meeting of the Eastern States Section of the Combustion Institute, Athens, Georgia, March 2024.

x. P. Signal, J. Lee, L. Lei, R.L. Speth, M.P. Burke, "Implementation of New Mixture Rules in Cantera and Implications for H_2 and NH_3 Combustion Simulations," 2024 Spring Technical Meeting of the Eastern States Section of the Combustion Institute, Athens, Georgia, March 2024.

xi. R.E. Cornell, M.P. Burke, "Low-Temperature Oxidation Pathways are Critical to Thermal Incineration of PFAS-Laden Materials," *Journal of Hazardous Materials Letters* 5 (2024) 100100.

xii. P.J. Singal, J. Lee, L. Lei, M.P. Burke, "Implementation of New Mixture Rules has a Substantial Impact on Combustion Behavior of H_2 and NH_3," *Proceedings of the Combustion Institute* (2024) in review.

Dynamics and Energetics of Elementary Reactions and Transient Species using Coincidence Spectroscopy
Grant DE-FG03-98ER14879

Robert E. Continetti (rcontinetti@ucsd.edu)
Department of Chemistry and Biochemistry, University of California San Diego
9500 Gilman Drive, La Jolla, CA 92093-0340

I. Program Scope

This research program has focused on experimental studies of fundamental chemical reactions that provide benchmarks for advancing our theoretical understanding of chemistry, in particular the potential energy surfaces (PESs) that govern the reactions, and computational predictions of the reaction dynamics. Some of the highlights of our efforts over the years have included important insights into the dynamics of the HOCO free radical[1] and the F + H_2O hydrogen exchange reaction.[2] The third generation of this experimental approach employs a photoelectron-photofragment coincidence (PPC) spectrometer equipped with a cryogenic octopole accumulator trap (COAT) for the preparation of anions thermalized below 20K. These cold anions are used to load an electrostatic ion beam trap (EIBT),[3] allowing the PPC measurement to be carried out on 7 keV ions, with the fast beam enabling detection in coincidence of photoelectrons, stable photoneutrals, and multiple photofragments. The PPC experiment is unique in that it yields a kinematically complete measurement of energy partitioning in reactions induced by photodetachment of precursor anions. During this project period, limited scientific progress was made, however, important technical advances in the implementation of a new generation of three-dimensional imaging detectors are now culminating as detailed below. In addition, we have refined our analysis of earlier experiments on the 1-photon dissociative photodetachment of the oxyallyl anion in work that will soon be submitted for publication, focusing on the roles of the low-lying triplet and singlet states induced by 1-photon absorption at 388 nm. The next generation of experiments are then discussed, including studies of fluoride complexes, carbon oxides and IR excitation experiments examining the excitation and isomerization of $HOCO^-$ as a new tool for manipulating the dynamics of the HOCO free radical and the H + CO_2 → OH + CO reaction.

II. Recent Progress

A. A New Photoelectron-Mulitiple-Photofragment Coincidence Detection System

This project was renewed following a year's hiatus in May of 2023 and we worked to bring this complex apparatus back on-line. A number of technical challenges have been faced, including the reliability of the laser system and the age of the photoelectron and multiple photofragment detector systems. We have worked with the laser vendor, Clark-MXR, to bring the kHz Ti:Sa regenerative amplifier laser system back to a state of reliable operation. To jump-start the scientific aspects of the project we were in the process of finalizing calibration experiments on O^-, O_2^- and O_3^- when the legacy data acquisition computer system for the apparatus failed. The quadrant crossed-delay line and wedge-and-strip-anode detectors used in this data acquisition system were interfaced through the CAMAC system, technology dating to the early 1970's, and regrettably it proved to not be feasible to bring the system back online despite considerable efforts. This called the question about moving forward with an important element of the grant proposal – the replacement of this 30-year old system with a state-of-the-art kHz CMOS camera-based system This detection scheme is based on an extensive body of work by Wen Li and co-workers at Wayne State University,[4] and we acknowledge his help with respect to adapting his data acquisition codes to our application. At this point, we have replaced both the electron and multiparticle photofragment detectors with multihit time- and position-sensitive detectors based on phosphor images recorded by kHz CMOS cameras coupled with timing information recorded with high bandwidth transient digitizers. **Figure 1** shows a schematic diagram of the implementation of the detector system on the apparatus.

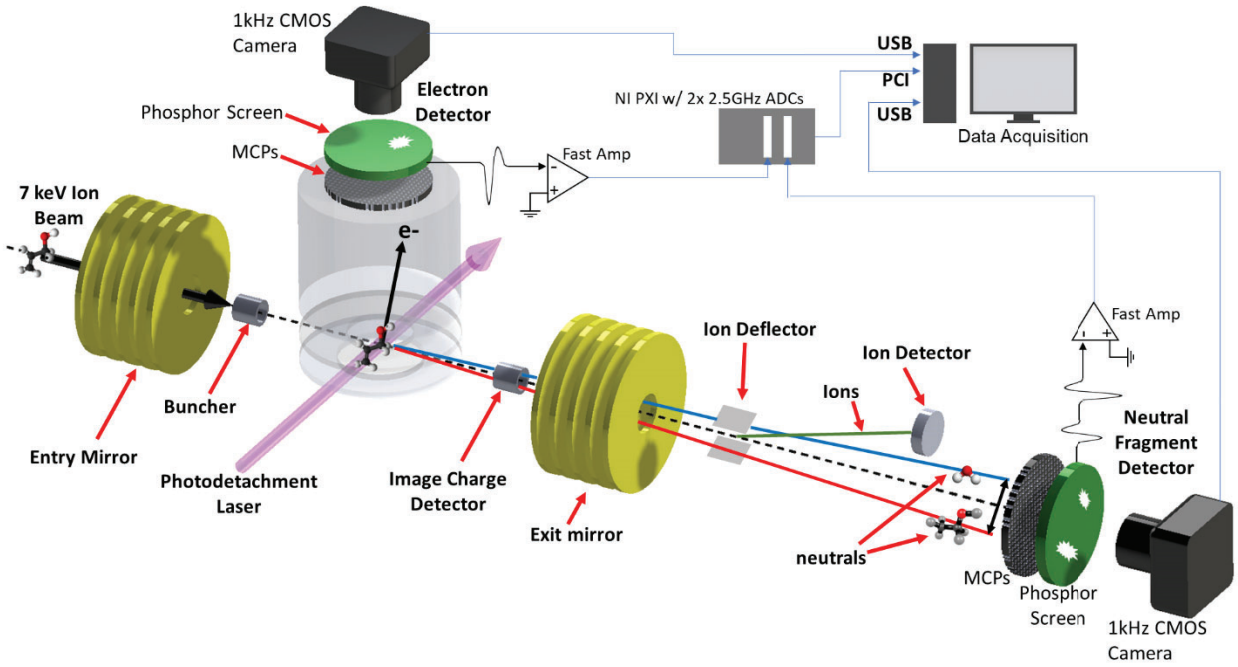

Figure 1. Schematic of the new multiparticle detectors as implemented on the PPC spectrometer used in these studies of dissociative photodetachment processes related to reactive intermediates and collision complexes.

The entry mirror, buncher, image charge detector and exit mirror compose the Electrostatic Ion Beam Trap (EIBT). This trap is filled with ions from a discharge ion source that have been accelerated to 7 keV and mass selected based on their time-of-arrival from the ion source. The ions can be cooled while stored in the EIBT as it is mounted on a cryogenic head. In the middle of the trap is an interaction region of the ps Ti:Sa laser beam with the stored ions. The ejected electrons are measured for both ejection direction and energy in photoelectron spectrometer which operates in a quasi-VMI mode which maintains the ejection angle in 3 space as well as measures usual 2d position. The neutral(s) produced by an electron ejection event then fly thru the exit mirror and their position and time of arrival is measured by the neutral fragment detector. Both the electron and all the neutral fragments are measured in 2d position using 1 kHz CMOS cameras imaging separate MCP-based phosphor detectors. Two high speed transient digitizers capture the electronic signal from the MCP to measure the time-of-arrival (3rd dimension) for each of the electron and neutral fragments. The images and digitizer information are captured and combined at 1kHz, same rate as the laser, in a LabView program yielding the 3D velocity vector for each of the neutral fragments as well as the electron which is then recorded for later analysis. This new detection system will open the way for an exciting new era for this experimental program studying the dissociative photodetachment (DPD) of transient species in the second half of the current grant period.

B. Revisiting the One-Photon DPD of the Oxyallyl Anion

While engaged in replacement of the imaging detector system, we have re-examined the data previously obtained on the one-photon DPD of the oxyallyl anion, $C_3H_4O^-$, at a photon energy of 3.2 eV (388 nm). At this photon energy there are three electronic states of the oxyallyl diradical that are accessed – the two low-lying and nearly degenerate $^1A_1$ and $^3B_2$ electronic states and a higher-lying $^3B_1$ excited state, as previously shown by anion photoelectron spectroscopy[5] and other experimental and theoretical techniques.[6] The $^1A_1$ state is predicted to be the lowest energy in the Franck-Condon region, and earlier theoretical work showed no evidence for a true minimum singlet C_{2v} structure indicating that photodetachment to the $^1A_1$ state essentially produces a transition state in the cyclization to the much more stable singlet cyclopropenone. This work builds on our previous study of the stable photodetachment channel at this photon energy that resulted

in the reassignment of the photoelectron spectrum reported to be ethylenedione (OCCO) to the oxyallyl diradical (C_3H_4O).[7] Our previous studies of the oxyallyl anion also included discovery of a resonance-mediated two-photon DPD at a photon energy of 1.6 eV (775 nm).[8] The latter study was remarkable as it showed not only non-Franck-Condon two-photon DPD but also revealed a strong delayed photoemission channel, both mediated by an excited anionic state, likely a dipole-bound state built on the zwitterionic $^1A_1$ core.

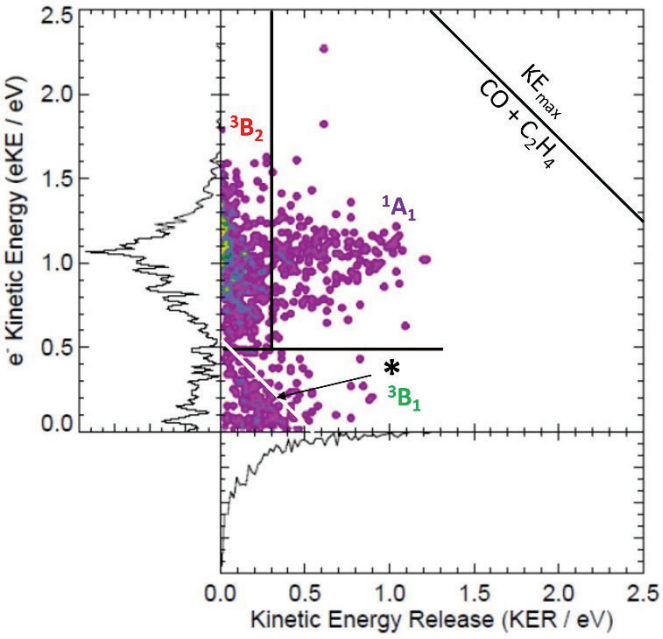

Figure 2. Coincidence plot for the dissociative data at 3.20 eV. Three channels can be seen: $^1A_1$ dissociation with a high KER, $^3B_2$ dissociation with a low KER weakly correlated with the eKE, and the $^3B_1$ excited state with a KER feature that aligns reasonably well with the diagonal line (*), corresponding to the

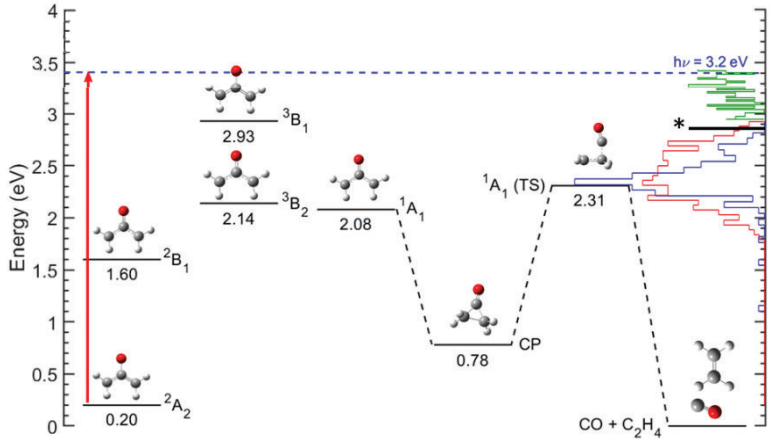

Figure 3. Energetics for the oxyallyl system plotted with the photoelectron spectra measured for each of the three electronic states of oxyallyl. The different photoelectron spectra, $^3B_2$ in red, $^1A_1$ in blue and $^3B_1$ in green, were resolved through KER gating in the PPC spectrum shown in Figure 2. The energetics of the CO + triplet C_2H_4 channel is noted by the asterisk.

In the present work, we have examined the minor (< 20 %) dissociative channel observed at 388 nm, confirming that at this photon energy the resulting neutral products are predominantly stable cyclopropanone with a minor dissociation pathway yielding equal mass fragments, consistent with the production of CO + C_2H_4. Using the PPC spectrometer, both stable and dissociative photoelectron spectra were measured at 388 nm. Relying on higher-resolution spectra measured by Lineberger and co-workers, we showed that at this wavelength two features were observed, one consisting of contributions from the low-lying $^1A_1$ and $^3B_2$ states of oxyallyl, with a smaller feature to the $^3B_1$ excited state. The real power of PPC spectroscopy is to resolve the dissociation dynamics of the system as a function of energy as determined by the eKE of the departing electron. This information is contained in the coincidence spectrum shown in **Figure 2**.

This coincidence spectrum shows that all three of the low-lying states exhibit differing dissociation dynamics in the minor dissociation channel. The $^1A_1$ state exhibits the highest kinetic energy release (KER), up to 1.2 eV. This is consistent perhaps with the determination that there is no bound $^1A_1$ state, and instead photodetachment to that state leads to facile ring closure to cyclopropanone, with some of the molecules surmounting the barrier and dissociating to the very stable closed-shell CO + C_2H_4 products. The $^3B_2$ state, however, exhibits a much lower KER, consistent with the fact that photodetachment to $^3B_2$ yields more significant vibrational excitation owing to a larger structural change from the anion, and relatively slow internal conversion to the singlet state could account for the channeling of more of the available energy to internal degrees of freedom. Finally, the

feature assigned to the excited $^3B_1$ state has a distribution that implies an inverse correlation between eKE and KER as is seen in direct DPD processes. A tantalizing possibility in this case is that dissociation of $^3B_1$ occurs on the triplet surface, producing CO + triplet C_2H_4. In studies of ethylene sulfide, Suits and co-workers have seen evidence for this triplet state 2.86 eV above ground state ethylene.[9] The diagonal line marked by an * is placed at that energy. The energetics governing this mechanism are summarized in the energetics diagram in Figure 3, which also shows the singlet and triplet state-resolved photoelectron spectra along the right vertical axis.

In summary, PPC spectroscopy allows determination of the contributions of the three low-lying electronic states of the oxyallyl diradical system to the minor dissociation channel as a result of the distinct energy partitioning they exhibit. Dissociation of each neutral state results in the formation of molecular products CO + C_2H_4, along with the production (80%) of singlet cyclopropanone. Photodetachment to the $^1A_1$ state leads to facile ring closure, with some CO + C_2H_4 products observed at high KER. Dissociation of the $^3B_2$ state must occur by relatively slow internal conversion, and leads to much higher apparent internal energies (low KER) in the CO + C_2H_4 products. Finally, it is interesting to note the possibility that the excited $^3B_1$ state dissociates on the neutral surface yielding CO + triplet C_2H_4. These results show considerable complexity in the chemistry of the oxyallyl diradical, and can perhaps motivate new theoretical studies of this prototypical molecule.

II. Future Plans

With the new imaging detectors now coming online we are prepared to carry out a new generation of PPC measurements on reactive species. In addition to further studies of the oxyallyl anion using higher photon energies to reveal new excited state phenomena, we will move on to our proposed studies of the effect of solvation by examining the $F^-(H_2O)_2$ system, other halide complexes, and oxidized carbon species, including CO_3^-, CO_4^- and HCO_3^-. The ultimate goal for this grant period, however, is to return to our goal of examining the effects of IR excitation in the anionic precursor on the DPD dynamics. The first experiments using IR excitation will examine promotion of the *cis*-$HOCO^-$/*trans*-$HOCO^-$ and HCO_2^-/$HOCO^-$ isomerizations and we will then pursue examination of mode-specific effects on the dissociation dynamics of HOCO by the DPD of vibrationally excited $HOCO^-$ anions as the culmination of this research program. We hope to provide thereby further state-of-the-art benchmark experimental results to guide the future development of quantum chemistry and dynamics theory on increasingly complex systems supporting further advancements in the fundamental understanding of chemical phenomena.

III. DOE-supported publications by this project 2022-2024

No new publications to report since 2022.

References

1. C. J. Johnson, R. Otto and R. E. Continetti, Phys. Chem. Chem. Phys. **16**, 19091-19105 (2014).
2. R. Otto, J. Ma, A. W. Ray, J. S. Daluz, J. Li, H. Guo and R. E. Continetti, Science **343**, 396 (2014).
3. C. Johnson, B. Shen, B. Poad and R. Continetti, Rev. Sci. Instrum. **82**, 105105 (2011).
4. G. Basnayake, Y. Ranathunga, S. K. Lee and W. Li, J. Phys. B. **55**, 023001 (2022).
5. T. Ichino, S. Villano, A. Gianola, D. Goebbert, L. Velarde, A. Sanov, S. Blanksby, X. Zhou, D. Hrovat, W. T. Borden and W. C. Lineberger, J. Phys. Chem. A **115**, 1634-1649 (2011).
6. V. Mozhayskiy, D. J. Goebbert, L. Velarde, A. Sanov and A. I. Krylov, J. Phys. Chem. A **114**, 6935-6943 (2010).
7. K. G. Lunny, Y. Benitez, Y. Albeck, D. Strasser, J. F. Stanton and R. E. Continetti, Angew. Chem. Int. Ed. **57**, 5394-5397 (2018).
8. Y. Albeck, K. G. Lunny, Y. Benitez, A. J. Shin, D. Strasser and R. E. Continetti, Angew. Chem. Int. Ed. **58**, 5312-5315 (2019).
9. C. Weeraratna, C. Amarasinghe, B. Joalland and A. G. Suits, J. Phys. Chem. A **124**, 1712-1719 (2020).

Ultrafast time-resolved bimolecular reactions of neutral and ionic species

DOE Grant No. DE-SC0025576

Marcos Dantus,

Department of Chemistry and Department of Physics and Astronomy, Michigan State University, East Lansing MI 48824. dantus@msu.edu

Project Scope

The rate of bimolecular reactions is determined by the time between molecular collisions, constrained by diffusion, and the likelihood that the encounter will result in product formation. Successful reactions depend on the relative orientation of the molecules and the energy they bring to bear into the collision, which also depends on the impact parameter. Given that collisions occur at random times, energies, and orientations, the study of bimolecular reactions by femtosecond time-resolved methods has been impeded. As a result, there is a knowledge gap in our understanding of the fundamental bond-forming, bond-breaking, and rearrangements occurring during gas-phase neutral and ionic bimolecular reactions. We plan to address this knowledge gap by performing time-resolved measurements on bimolecular reactions starting from weakly bound pairs of molecules. These pairs of molecules eliminate much of the initial orientation randomness, making it possible for an ultrafast laser pulse to initiate the reaction by ejecting a radical or a radical cation towards the adjacent molecule with specific kinetic energy dictated by the excitation laser pulse. The reaction is then monitored by a second laser that gently ionizes the collision complex or the products of the reactions as a function of the delay between the initial excitation pulse and the probe pulse. The time-dependent yield of the products reveals details about the fundamental bond-forming and bond-breaking processes that occur as the reaction proceeds from reagents to products. Theory in the form of high-level quantum mechanical simulations and molecular dynamic simulations will provide important insight into the experimental results. Findings from this work will provide valuable information regarding bimolecular reactions between neutral and ionic species. This information is important for improving our understanding and modeling of atmospheric chemistry and astrochemistry. In addition, this information is valuable for benchmarking computer programs designed to predict the outcome of bimolecular collisions.

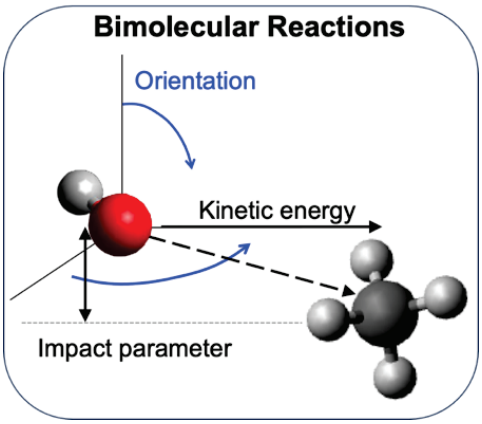

Bimolecular reactions depend on the orientation, kinetic energy, and impact parameters.

Recent Progress

This is a new project; the grant has just reached our university.

Future Plans

We are planning upgrades to our molecular beam, and gas handling to create the weekly bound dimers. We have a replacement laser arriving in early October that will be used for these experiments. We expect to carry the first measurements by the end of the year.

Peer-Reviewed Publications Resulting from this Project (2024)

None yet.

Reaction Dynamics of Organic Radicals and Carbenes

H. Floyd Davis

Dept. of Chem. & Chem. Biology, Cornell University, Ithaca, NY 14853-1301

hfd1@cornell.edu

I. Program Scope:

We are carrying out experimental studies of polyatomic free radicals and carbenes. In some studies, a crossed molecular beams apparatus employing "universal" vacuum ultraviolet (VUV) photoionization and electron impact detection of neutral species is used to measure product angular and velocity distributions. During the past year, we have carried out pump-probe time-resolved studies of photolytic carbene formation from various precursors using a single-beam apparatus. The reactions of radicals and carbenes typically involve multiple reaction intermediates and transition states, leading to competing product channels relevant to atmospheric chemistry, catalysis, combustion, and synthetic chemistry. Our experiments aim to provide key experimental benchmarks against which theoretical models, including the thermochemistry and potential energy barriers for key species and reactions, may be tested.

II. Recent Progress:

Alkyl-substituted carbenes have been remarkably elusive to experimental characterization. Lying ~ 300 kJ/mol (~ 3 eV) above their stable ground state alkene isomers, singlet alkylcarbenes, once produced, undergo rapid isomerization to alkenes via a 1,2-hydrogen atom shift.[1] Most previous attempts at formation of alkylcarbenes involved UV photodissociation of diazoalkanes (RN_2), or their cyclic alkyldiazirine isomers. The singlet alkylcarbenes photogenerated from these nitrogenous precursors are produced with high internal energies, leading to extremely short lifetimes, precluding their observation. To gain insight into carbene production from diazirine photolysis in the absence of carbene isomerization, we studied the photodissociation dynamics of the simplest diazirine, cyclo-CH_2N_2, which produces CH_2 + N_2.[2] The angular and velocity distributions of the CH_2 products were measured using both photoionization and electron impact. Dissociation occurs on subpicosecond timescales with a mean product internal energy of ~ 2 eV.

We have shown that near-UV excitation of alkyl-substituted ketenes ($R_1R_2C{=}C{=}O$) facilitates production of alkylcarbenes at relatively low levels of internal energy. Excitation of methylketene near 350 nm (or its isomer propenal, followed by a 1,3-H atom shift forming methylketene) leads to production of triplet ground electronic state methylcarbene, CH_3CH, also called ethylidene.[1] Owing to a high potential energy barrier for a 1,2-H atom shift, triplet methylcarbene with internal energies lying below the electronically excited singlet is *stable* in the absence of collisions (Fig. 1). Following our initial study, we have been systematically exploring related systems of greater complexity. For example, dimethylketene produces dimethylcarbene (CH_3CCH_3)[3] and ethylketene produces ethylcarbene (C_2H_5CH).[4] For both systems, studies at a range of excitation wavelengths

allowed us to assess the energy-dependent competition between carbene formation and direct production of propene. For the latter channel, we found that a significant fraction of the 3 eV exoergicity for propene formation is channeled into product translational energy. This clearly indicates that propene is formed prior to, or concurrently with, CO elimination, rather than from isomerization of the initially-formed carbene. Direct alkene formation from photolysis of carbene precursors has been termed "rearrangement in the excited state" (RIES) by the physical organic chemistry community. Although this process has been observed frequently, it remains poorly understood.[5]

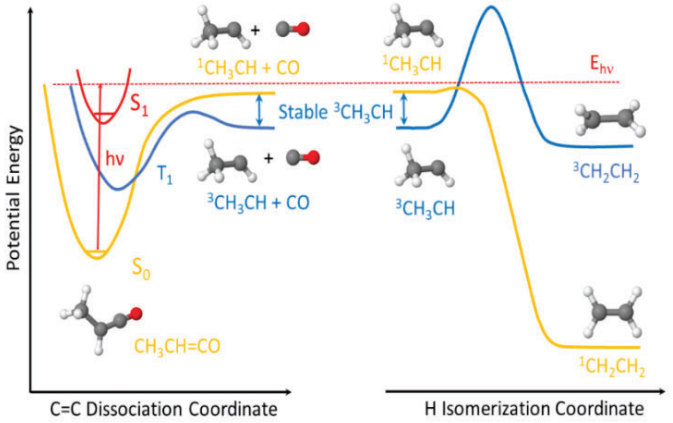

Fig. 1. *Methylketene photodissociation produces ethylidene + carbon monoxide.*

Time-resolved pump-probe studies of methylketene and propenal decomposition.

During the past year, we have carried out an extensive series of time-resolved pump-probe studies of ethylidene formation from methylketene and propenal as a function of excitation energy.[6] A near-UV pump laser (~7 ns pulse duration) prepares electronically excited methylketene S_1 which subsequently undergoes dissociation on S_0 or T_1 producing ethylidene + carbon monoxide. Since the ionization energy of ground state methylketene is 8.9 eV, no ionization of cold ground state methylketene is observed at 8.8 eV. However, methylketene excited by the UV laser is readily ionized at 8.8 eV, so we can monitor the population of dissociating hot methylketene parent molecules directly in real time. As illustrated in Fig. 2, we observe single-exponential decay with rate constants (k) strongly dependent upon excitation energy. Stephen Klippenstein is carrying out calculations on the C_3H_4O PES and is applying RRKM theory to calculate rate constants for

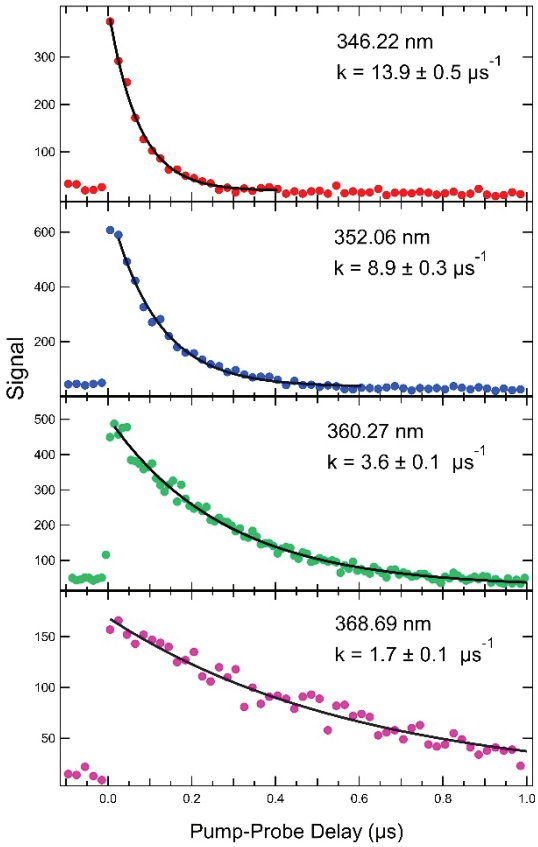

Fig. 2. *Time-resolved pump-probe measurements of methylketene decomposition following electronic excitation at indicated wavelengths.*

ethylidene + CO formation for comparison to our experimental measurements. A joint experimental/theoretical paper is currently in preparation.[6]

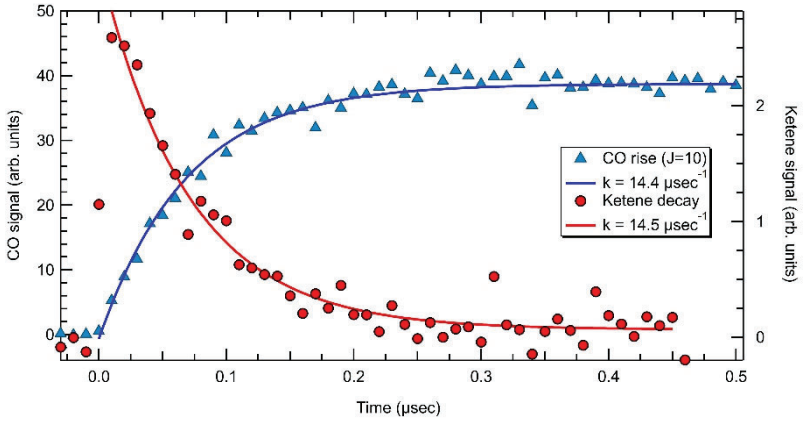

Fig. 3. *Time-resolved pump probe measurements of ketene decomposition following electronic excitation at 351.02 nm. Rise of CO (v=0, J = 10) product shown in blue; decay of hot ketene (m = 42) in red.*

Time-resolved studies of the unimolecular dissociation of gaseous molecules on microsecond timescales presents several experimental challenges. Most notably, "flyout" of dissociating molecules from the laser probe volume is a significant issue. Also, experimental probing of the time-dependent decay of hot parent molecules, rather than appearance of products, is a novel and relatively untested approach. To characterize and validate the method, we have carried out studies on several representative systems other than methylketene, including ketene, propenal, benzaldehyde, acetone, and pyruvic acid.[7] A paper describing these experiments is in preparation. Following UV excitation of ketene, 8.8 eV photoionization facilitates direct observation of dissociating ketene (CH_2CO) in real time. We have compared the rate constants for ketene decay to that for CO appearance under identical conditions in pump-probe studies. As illustrated in Fig. 3, these measurements are in mutual agreement and yield rate constants similar to those measured by C.B. Moore's group who monitored the timescale for CO production using VUV laser induced fluorescence.[8]

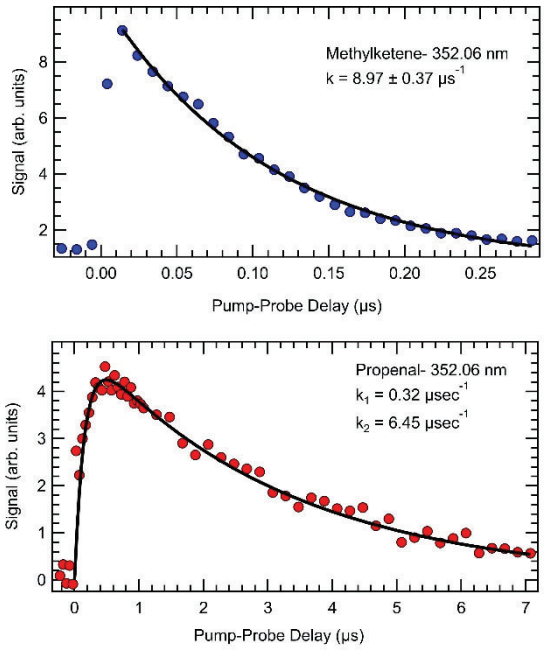

Fig. 4. *Time-resolved pump-probe measurements of hot methylketene populations following excitation of methylketene and propenal at the same wavelength. In lower figure, the initial rise is due to isomerization of propenal to methylketene. In both cases decay of methylketene forms ethylidene + CO.*

In the case of propenal, a 1,3- H atom shift produces hot methylketene, which subsequently dissociates. In time resolved experiments analogous to those described above for methylketene, we can monitor the *sequential* dynamics for propenal → methylketene → CH_3CH + CO, characterized by rate constants k_1 and k_2, respectively. In this case, the photon energy of the ionization laser (8.8 eV) lies well below the 10.1 eV ionization energy of propenal. Following excitation of propenal at time zero, we

monitor the formation of hot methylketene (rate constant k_1), and its decay to ethylidene + CO (rate constant k_2). For a given photon energy, the rate constants k_2 derived from experiments involving propenal are comparable to the dissociation rate constants k observed in the methylketene experiments (Fig. 4). Upon careful analysis, for a given excitation wavelength we observe slightly larger rate constants (k) in experiments involving methylketene than in experiments on propenal (k_2). We believe this is due to the slightly greater enthalpy of formation of methylketene and slightly greater initial thermal excitation in the parent methylketene molecular beam. A comparison of our experimental rate constants to calculations by Stephen Klippenstein reveal interesting aspects of the dynamics of the sequential reactions.[6]

We have studied and characterized "flyout" in microsecond pump-probe studies. An advantage of probing the decay of parent molecules, rather than formation of dissociation products with finite recoil energies, is that flyout can be minimized using heavy carrier gases. We have characterized a novel geometry with the excitation laser coaxial and counterpropagating to the molecular beam with the VUV laser at 90 degrees. For benzaldehyde in argon, which does not dissociate at 370 nm, we can monitor excited populations on timescales longer than 60 μs.[7]

III. Future Plans:

We plan to carry out analogous pump-probe studies on two related but somewhat more complex systems, dimethylketene and ethylketene. We will also study the photodissociation dynamics of several atmospherically-relevant molecules. The first is pyruvic acid, which dissociates to CH_3COH (hydroxymethylcarbene) + CO_2 and to CH_3CO + HOCO. For pyruvic acid, photofragment translational spectroscopy and time resolved pump-probe methods will be used. We will also continue our experiments using both experimental techniques on the atmospherically-relevant "enal" methacrolein, which isomerizes to dimethylketene following electronic excitation. This system will be compared to the analogous dynamics for crotonaldehyde, which isomerizes to ethylketene. Finally, we have recently demonstrated production of molecular beams containing cold triplet ethylidene by photolysis of methylketene or propenal. We hope to use this source to study bimolecular reactions of this simple carbene in crossed molecular beams.

IV. References (* denotes published articles acknowledging DOE support since 2022):

1. S. Datta and H.F. Davis, "Direct observation of ethylidene, the elusive high-energy isomer of ethylene", *J. Phys. Chem. Lett.* 2020, 11, 10476-10481.
2. S. Datta and H.F. Davis, "Photodissociation Dynamics of the Simplest Diazirine: cyclo-$CH_2N_2 \rightarrow CH_2 + N_2$", *J. Phys. Chem. A*, submitted Sept. 2024.
3. S. Datta and H.F. Davis, "Dimethylcarbene vs. Direct Propene Formation in Dimethylketene Photodissociation", *J. Phys. Chem. A.* **2021***, 125, 6940-6948.*

*4. S. Datta and H.F. Davis, "Ethylcarbene vs. Direct Propene Formation in the Near-UV Photodissociation of Ethylketene", *J. Phys. Chem. A.* **2023***, 127, 450-456.*

5. M. S. Platz, "A Perspective on Physical Organic Chemistry", *J. Org. Chem.* 79, 2341-2353 (2014).
6. L. J. Sauer, H.F. Davis and S.J. Klippenstein, manuscript in preparation.
7. L. J. Sauer and H.F. Davis, manuscript in preparation.
8. E.R. Lovejoy, S.K. Kim, and C.B. Moore, "Observation of Transition-State Vibrational Thresholds in the Rate of Dissociation of Ketene", *Science* **1992**, 256, 1541-1544.

Methods for the Construction of Multiple Coupled Potential Energy Surfaces with Applications to Nonadiabatic Molecular Dynamics

Richard Dawes, dawesr@mst.edu
Missouri University of Science and Technology
400 W. 11th street, Rolla, MO 65409

I. Program Scope:

The DOE Office of Science's priority interest in Quantum Information Science (QIS) is complemented by efforts to control and better understand the preparation and evolution of highly non-thermal quantum states in molecular systems. In particular, new methods to treat light-matter interactions will permit simulation of short, intense, shaped laser pulses as applied to molecules, that are now being realized experimentally. The use of multiple, ultrashort, shaped pulses, provides great flexibility in the set of reachable superposition states that can be prepared. The evolution of these states on multiple coupled potential energy surfaces (PESs), especially in the region of conical intersections, can vary widely in their dynamics, loss of coherence, and energy flow leading to bonding rearrangements. In addition to exploiting coherences and interference effects—to drastically affect, for example, reactivity—strong field control can significantly displace energy levels, PES-couplings, and indeed the entire energy landscape governing dynamics. Many of these phenomena lend themselves to spectroscopic observation, and these signatures are part of the set of predictions.

This project will develop electronic structure and artificial intelligence/machine learning (AI /ML)-based methods for fitting interaction energies, suitable to construct multiple coupled PESs for gas phase molecules (including radicals). To treat light-matter interactions, non-scalar property surfaces such as transition dipoles are also required. Special tools are needed and will be developed to conduct the overall workflow which combines generating robustly converged high-level electronic structure data, transforming to a suitable well-behaved diabatic representation, and accurately fitting into energy, property, and coupling-surface representations. Finally, these representations must be rendered into a form that is convenient for use in quantum dynamics simulations. The complete Hamiltonian that will be simulated via the quantum dynamics method of Multi Configurational Time-Dependent Hartree (MCTDH) includes not only the coupled potential energy operators just described but in some cases unusual kinetic energy operators—which include couplings such as those encountered in Renner–Teller molecules, and also a high-fidelity representation of the laser pulses (field operators).

The developed methods will be validated through comparisons with experiments. A series of chemical systems of increasing complexity and dimensionality will be tackled. This will push the limits of the new methods, and also provide insight into how aspects of the quantum dynamics such as coherence are impacted by rapidly increasing configuration space, state densities, and

degrees of freedom. Tools to aid experimental collaborators, such as those for spectral simulation, will also be developed. This project includes additional broader impacts surrounding the education and training of young scientists in these frontier areas.

Recent Progress: This Recent Progress: The award notice for this project was received on 09/18/2024 with an official start date of 08/15/2024, so since the project is just beginning, only the abstract is provided with this submission.

Grant Number and Title: Grant No. DE-SC0025420 Methods for the Construction of Multiple Coupled Potential Energy Surfaces with Applications to Nonadiabatic Molecular Dynamics.

A Captivating New Spin on Energy Storage

Dr. Leah G. Dodson, Assistant Professor
Department of Chemistry and Biochemistry
University of Maryland
College Park, MD 20742
ldodson@umd.edu

I. Program Scope

This research program broadly investigates the fundamental chemical physics of gas/surface interactions under cryogenic conditions, with a narrow focus on how porous materials adsorb small gaseous molecules. These interactions could affect the adsorbate's nuclear-spin properties resulting in more efficient nuclear-spin-isomer enrichment at low temperature. The ultimate goal for this work is to utilize porous materials such as metal-organic frameworks (MOFs) to generate enriched fuels—in initial stages H_2 while later efforts will focus on CH_4—in their lowest-energy nuclear-spin states for cryogenic storage and transportation solutions for alternative fuels. Access to enriched samples of nuclear-spin isomers enables fundamental chemical physics studies of nuclear-spin isomers—for example testing parity laws—and will inform industry partners developing optimum storage devices for alternative fuels.

Our ongoing efforts combine advancements made in two orthogonal fields: 1) The materials science community has made impressive strides in creating carefully functionalized MOFs and has wielded infrared spectroscopy as an effective tool for distinguishing the nuclear-spin state of molecules adsorbed in their pores;[1–3] while 2) The chemical physics community has crafted elegant tests of the effect of confinement and the resulting intermolecular potentials on nuclear-spin enrichment in systems such as surfaces or rare-gas and other inert cryogenic matrices.[4–12] We use these advances to optimize state-specific preparation of H_2 and CH_4.

II. Recent Progress

Temperature-dependent shifts in vibrational spectra of porous materials

In the first year of this Early Career award, we built and commissioned the primary instrumentation (Figure 1) necessary to observe and quantify the chemical physics of small-molecule adsorption to porous materials at cryogenic temperatures. At its core is a closed-cycle helium cryostat with a custom sample mount (Figure 2) capable of controlling the temperature of powdered samples between 25–450 K. The sample is probed (via transmission spectroscopy) from 600–4000 cm^{-1} by a commercial Fourier-transform infrared spectrometer (FTIR) revealing the vibrational modes of the sample and any adsorbed species. Important to the development of these techniques is the establishment of

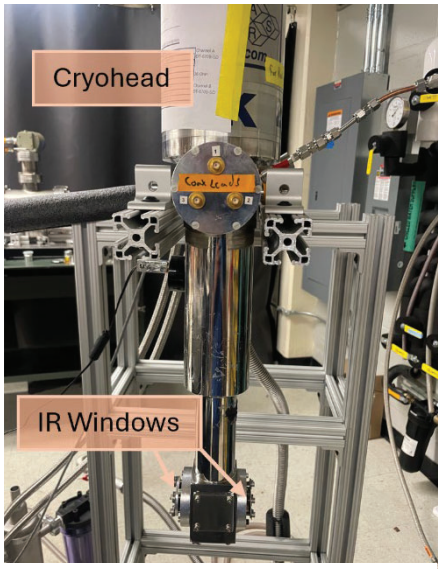

Fig. 1: Photo of the new instrumentation for cryogenic spectroscopy of porous materials. The entire instrument is mounted on a custom scaffold that can be rolled into a purged FTIR compartment for analysis.

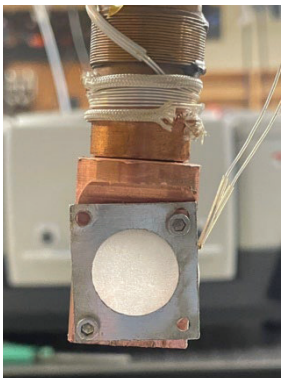

Fig. 3: Photo of the custom sample mount that can be cooled down to 25 K when enclosed in the shroud shown in Figure 1.

sample-preparation protocols to enable direct measurement of the transmission spectra of desired crystalline materials without complications from optical scattering or modifications to the material itself. Also important is to investigate the spectroscopy of the materials as a function of temperature in the absence of adsorbates, so that any temperature-dependent structural transformations of the material itself can be separated from those caused by/to any adsorbed small molecules. The design of the instrument is such that any powdered sample can be loaded into the sample mount, creating a broadly useable system.

Using our new instrument we carried out our first collaborative study with a synthetic chemistry group—also at the University of Maryland—to investigate the temperature dependence of prototypical porous materials while establishing robust sample-preparation methods.[13] Using samples of covalent organic framework materials synthesized by our collaborators in the Taylor lab, we prepared pressed samples of the materials doped into KBr pellets (Figure 3) and tested for shifts in the peak positions of key vibrational modes as a function of temperature. We observed that many—but not all—vibrational modes in the three covalent organic frameworks in question shift, and we were able to link the identity of the shifting modes with a proposed structural deformation that is known to occur in flexible porous materials. Specifically for COF-300, several vibrational peaks associated with the main subunits that link the framework together are seen to blue shift as the temperature of the sample is lowered to 30 K. Figure 4 shows a portion of the infrared spectrum observed for COF-300 as it evolves as a function of temperature, with key peaks labeled. Using quantum chemistry calculations, we assigned the main structural deformation as the material cools to an established "pedal motion" (visualized in Figure 4(a)) as the *N*-benzylideneaniline (Figure 4(b)) linker distorts with pore collapse. This motion is reversible, with the material recovering its original configuration when warmed back to room temperature. Comparing these findings with similar materials (like COF-300-amine, also shown in Figure 3) informed us on the role that different functionalization and structural motifs have on the behavior of these materials at low temperature.

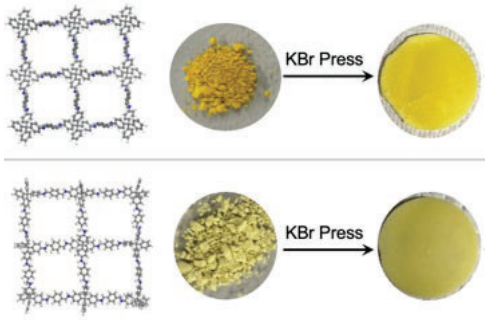

Fig. 2: Two of the covalent-organic frameworks investigated in this study, showing their structures and sample preparation. Top: COF-300; Bottom: COF-300-amine. (Taken from Ref. 13.)

In addition to the scientific knowledge that we contributed to the fundamental understanding of the structural dynamics in covalent organic framework materials, we also learned three important things for our overall research program: 1) The infrared spectrum of some materials do change as a function of temperature, necessitating control experiments when moving forward to observing temperature-dependent adsorption of small gaseous molecules; 2) Some porous materials have to be prepared in KBr glasses to reduce optical scattering losses, and we need to investigate the effect that the glass has on gas uptake; and 3) Theoretical methods can potentially be used to predict porous materials that will have ideal properties to adsorb the gases of interest.

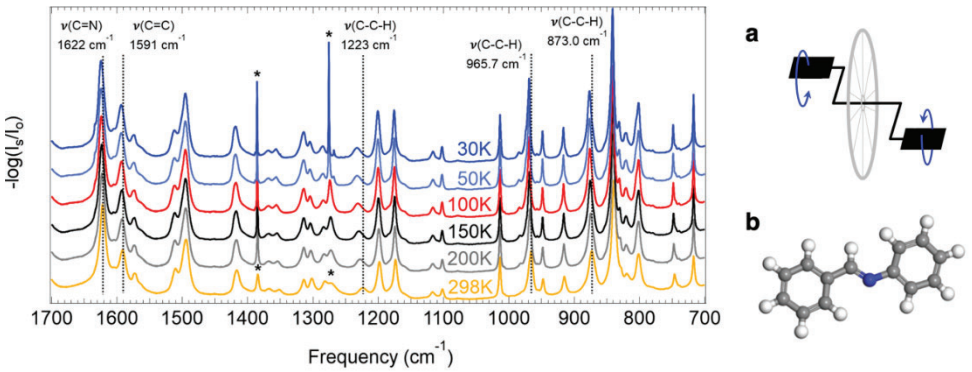

Fig. 4: (Left) Temperature-dependent infrared spectra of the covalent-organic framework COF-300. (Right) (a) Graphic of the pedal motion assigned to the observed structural change. (b) Small-molecule representation of the framework linker undergoing the transformation. (Taken from Ref. 13.)

Observation of ortho/para hydrogen conversion in mixed ices

In tandem with our studies investigating the spectroscopy and gas uptake of porous materials at cryogenic temperatures, we are carrying out complementary studies to develop our techniques for probing nuclear-spin isomers spectroscopically in confined environments. Molecular hydrogen is infrared-inactive but induced absorption features can be observed using FTIR spectroscopy in a polarizing environment. For example, H_2 has be observed in a carbon dioxide film, with peaks that enable distinction between *ortho* and *para* isomers in the infrared (~4150 cm^{-1}) using conventional FTIR.[14] To ensure quantitative detection of infrared-inactive molecules such as H_2 and CH_4 using our spectroscopy setup, we are carrying out a systematic study of these molecules under various matrix-isolated conditions using a separate instrument in our laboratory. We first reproduced the observations made by Yamakawa *et al*. to observe *ortho*-/*para*-H_2 in solid carbon dioxide (Figure 5) and are measuring the nuclear-spin conversion rate, with preliminary findings that the conversion rate significantly depends on the geometry of the pore. We have also collected preliminary data on the impact that the matrix-ice identity (argon, nitrogen monoxide, etc) has on both the spectroscopy and kinetics. This work is ongoing, and has provided valuable information in optimizing our spectroscopic methodology.

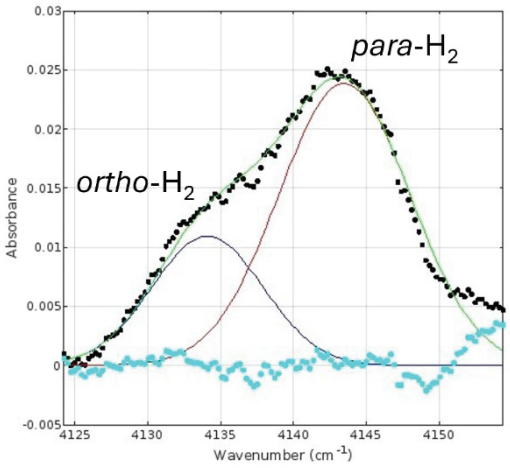

Fig. 5: Spectra collected in our laboratory showing induced-absorption peaks of H_2 trapped in solid carbon dioxide at 10 K. The peaks corresponding to the ortho (fit with the Gaussian shown in blue) and para (fit with the Gaussian shown in red) nuclear-spin isomers can be investigated quantitatively as a function of time and ice composition.

III. Future Plans

Now that we have established the protocols for cooling samples of porous materials, monitoring them spectroscopically as a function of temperature, and distinguishing adsorbed species by their nuclear-spin states, we have turned our attention to gas uptake in these porous materials. Adsorption isotherms are commonly reported for porous materials as they are a key

component of investigating these materials for a key design goal—maximizing gas separation and storage—and commercial technology is available to measure gas uptake (via monitoring the pressure of in the headspace above a material) at temperatures accessible with liquid nitrogen. Our goal is to design instrumentation that directly spectroscopically probes adsorbed species at low temperature. We have begun preliminary investigations adding a gas manifold to the chamber enclosing our sample mount (the gas line can be seen in the top right of Figure 1) and are testing pressure/temperature combinations to ensure stable conditions throughout prolonged experiments. We are also using computational methods to predict the best materials that combine several design elements: 1) Good gas uptake; 2) Ability to catalyze nuclear-spin conversion; and 3) Absence of absorption features in spectral windows needed to observe the adsorbed species.

In the longer term, we are developing a gas-phase detection system that enables us to monitor nuclear-spin enrichment of the small molecules of interest in the gas phase after the enriched gas samples have been removed from the porous materials.

DOE-Supported Products 2023-2024

- Frimpong, S.O., McLane, N., Dietrich, M., Bauer, G., Baptist, M, Dodson, L.G., Taylor, M.K., Temperature-Dependent Reversible Structural Dynamics in Covalent Organic Framework Revealed by Cryogenic Infrared Spectroscopy, *Phys. Chem. Chem. Phys*. **2024**, 26, 22252–22260.
- McLane, N., Frimpong, S., Taylor, M.K., Dodson, L.G., Cryogenic Characterization of Materials Using a Novel IR Spectroscopy System, Oral presentation at the 77th Annual International Symposium on Molecular Spectroscopy, June 18, 2024.

References

(1) Vitillo, J. G.; Regli, L.; Chavan, S.; Ricchiardi, G.; Spoto, G.; Dietzel, P. D. C.; Bordiga, S.; Zecchina, *J. Am. Chem. Soc.* **2008**, *130* (26), 8386–8396.
(2) Hadjiivanov, K. I.; Panayotov, D. A.; Mihaylov, M. Y.; Ivanova, E. Z.; Chakarova, K. K.; Andonova, S. M.; Drenchev, N. L. *Chem. Rev.* **2021**, *121* (3), 1286–1424.
(3) FitzGerald, S. A.; Hopkins, J.; Burkholder, B.; Friedman, M.; Rowsell, J. L. C. *Phys. Rev. B* **2010**, *81* (10), 104305.
(4) Beduz, C.; *et al*. *Proc. Natl. Acad. Sci. U.S.A.* **2012**, *109* (32), 12894–12898.
(5) Frayer, F. H.; Ewing, G. E. *J. Chem. Phys.* **1968**, *48* (2), 781–792.
(6) Hartl, M. *et al*. *Phys. Chem. Chem. Phys.* **2016**, *18* (26), 17281–17293.
(7) Hopkins, H. P.; Curl, R. F.; Pitzer, K. S. *J. Chem. Phys.* **1968**, *48* (7), 2959–2965.
(8) Kohl, J. E.; Semack, M. G.; White, D. *Phys. Rev. Lett.* **1979**, *42* (16), 1072–1075.
(9) Miyamoto, Y.; Fushitani, M.; Ando, D.; Momose, T. *J. Chem. Phys.* **2008**, *128* (11), 114502.
(10) Sliter, R.; Gish, M.; Vilesov, A. F. *J. Phys. Chem. A* **2011**, *115* (34), 9682–9688.
(11) Veber, S. L.; Bagryanskaya, E. G.; Chapovsky, P. L. *J. Exp. Theor. Phys.* **2006**, *102* (1), 76–83.
(12) Strom, A. I.; Anderson, D. T. *Chem. Phys. Lett.* **2020**, *752*, 137539.
(13) Frimpong, S. O.; McLane, N.; Dietrich, M.; Bauer, G. A.; Baptiste, M. R.; Dodson, L. G.; Taylor, M. K. *Phys. Chem. Chem. Phys.* **2024**, *26* (33), 22252–22260.
(14) Yamakawa, K.; Ishibashi, A.; Namiyoshi, T.; Azuma, Y.; Arakawa, I. *Phys. Rev. B* **2020**, *102* (4), 041401.

Theoretical and Experimental Studies of Elementary Hydrocarbon Species and Their Reactions (DE-SC0018412)

Gary E. Douberly and Henry F. Schaefer III
University of Georgia, Center for Computational Quantum Chemistry and Department of Chemistry, 1004 Cedar St., Athens, GA 30602-1546
douberly@uga.edu

Program Scope

New theoretical and experimental methods in chemical physics being developed by the PIs provide great opportunities for the study of molecular species and chemical reactions of fundamental importance in combustion processes. In this research, high level quantum mechanical formalisms are a significant source of critical predictions concerning molecular systems that may be challenging for experiments. Moreover, our helium droplet experiments have opened whole new vistas for the spectroscopic study of molecular species relevant to combustion environments. Theoretical developments proposed herein include a focus on obtaining highly accurate energetics for species pertinent to combustion reactions. Experimental developments focus on strategies to characterize transient combustion intermediates associated with low-temperature hydrocarbon oxidation processes, which have been difficult to probe with other methodologies. The combination of theory and experiment to solve problems inaccessible to either alone is a hallmark of this research.

Nearly all of the proposed non-methodological experimental research will benefit from state-of-the-art molecular electronic structure theory. In some cases, the experimental group needs theoretical predictions prior to beginning a new set of experiments. In other cases, experimental findings are puzzling and need theory for interpretation. We have an abundance of experiences with both sets of problems, and the PIs have already collaborated in several such situations. Some situations where theory-experiment interaction will be particularly important include: (i) the C_nH_m + $O(^3P)$ reactions, where predictions of structures, energetics, and spectroscopic properties of complexes and adducts on both singlet and triplet potential energy surfaces will be required; (ii) the spectroscopic studies of $(NH_2)_2$, NH-(NH_2), and other pre-reactive radical-radical complexes, where an interpretation will require computations of structures, energetics, and intersystem crossing rates; (iii) the near-IR and mid-IR studies of HOO-alkene complexes and related QOOH species, where computations of the excited state potential energy surface in the vicinity of the exit-channel complex will be essential; and (iv) the mid-IR studies of $\cdot C_nH_{2n+1}$ radicals, where the spectra are complicated by anharmonic and Coriolis resonances to an extent that the interpretation of these spectra will only be achievable through comparisons to effective Hamiltonian computations that employ highly accurate quartic force fields and Coriolis parameters.

Recent Projects

I. T. Beck, M. E. Lahm, G. E. Douberly, and H. F. Schaefer, "Convergent ab initio Analysis of the Multi-Channel HOBr+H Reaction," J. Chem. Phys. 160, 124304 (2024).

High-level potential energy surfaces for three reactions of hypobromous acid with atomic hydrogen were computed at the CCSDTQ/CBS//CCSDT(Q)/complete basis set level of theory. Focal point analysis was utilized to extrapolate energies and gradients for energetics and optimizations, respectively. The H attack at Br and subsequent Br–O cleavage were found to proceed barrierlessly. The slightly submerged transition state lies −0.2 kcal mol^{-1} lower in energy than the reactants and produces OH and HBr. The two other studied reaction paths are the radical substitution to produce H2O and Br with a 4.0 kcal mol^{-1} barrier and the abstraction at hydrogen to produce BrO and H2 with an 11.2 kcal mol^{-1} barrier. The final product energies lie −37.2, −67.9, and −7.3 kcal mol^{-1} lower in energy than reactants, HOBr + H, for the sets of products OH + HBr, H2O + Br, and H_2 + BrO, respectively. Additive corrections computed for the final energetics, particularly the zero-point vibrational energies and spin–orbit corrections, significantly impacted the final stationary point energies, with corrections up to 6.2 kcal mol^{-1}.

M.E. Lahm, M.A. Bartlett, T. Liang, L. Pu, W.D. Allen and, H.F. Schaefer, "The Multichannel i-Propyl + O_2 Reaction System: A Model of Secondary Alkyl Radical Oxidation," J. Chem. Phys. 159, 024305 (2023).

The i-propyl + O_2 reaction mechanism has been investigated by definitive quantum chemical methods to establish this system as a benchmark for the combustion of secondary alkyl radicals. Focal point analyses extrapolating to the ab initio limit were performed based on explicit computations with electron correlation treatments through coupled cluster single, double, triple, and quadruple excitations and basis sets up to cc-pV5Z. The rigorous coupled cluster single, double, and triple excitations/cc-pVTZ level of theory was used to fully optimize all reaction species and transition states, thus, removing some substantial flaws in reference geometries existing in the literature. The vital i-propylperoxy radical (MIN1) and its concerted elimination transition state (TS1) were found 34.8 and 4.4 kcal mol^{-1} below the reactants, respectively. Two β-hydrogen transfer transition states (TS2, TS2′) lie above the reactants by (1.4, 2.5) kcal mol^{-1} and display large Born–Oppenheimer diagonal corrections indicative of nearby surface crossings. An α-hydrogen transfer transition state (TS5) is discovered 5.7 kcal mol^{-1} above the reactants that bifurcates into equivalent α-peroxy radical hanging wells (MIN3) prior to a highly exothermic dissociation into acetone + OH. The reverse TS5 → MIN1 intrinsic reaction path also displays fascinating features, including another bifurcation and a conical intersection of potential energy surfaces. An exhaustive conformational search of two hydroperoxypropyl (QOOH) intermediates (MIN2 and MIN3) of the i-propyl + O_2 system located nine rotamers within 0.9 kcal mol^{-1} of the corresponding lowest-energy minima.

S.M. Goodlett, J.M. Turney, H.F. Schaefer, "Comparison of Multifidelity Machine Learning Models for Potential Energy Surfaces," Special Topic Issue for "Software for Atomistic Machine Learning," J. Chem. Phys. 159, 044111. (2023).

Multifidelity modeling is a technique for fusing the information from two or more datasets into one model. It is particularly advantageous when one dataset contains few accurate results and the other contains many less accurate results. Within the context of modeling potential energy surfaces, the low-fidelity dataset can be made up of a large number of inexpensive energy computations that provide adequate coverage of the N-dimensional space spanned by the molecular internal coordinates. The high-fidelity dataset can provide fewer but more accurate electronic energies for the molecule in question. Here, we compare the performance of several neural network-based approaches to multifidelity modeling. We show that the four methods (dual, Δ-learning, weight transfer, and Meng–Karniadakis neural networks) outperform a traditional implementation of a neural network, given the same amount of training data. We also show that the Δ-learning approach is the most practical and tends to provide the most accurate model.

C. J. Tang, A. G. Heide, A. D. Heide, G. E. Douberly, J. M. Turney, and H. F. Schaefer, "Exploring the Tl_2H_2 Potential Energy Surface: A Comparative Analysis with Other Group 13 Systems and Experiment," J. Comput. Chem. 45, 985-994 (2024).

Thallium chemistry is experiencing unprecedented importance. Therefore, it is valuable to characterize some of the simplest thallium compounds. Stationary points along the singlet and triplet Tl_2H_2 potential energy surface have been characterized. Stationary point geometries were optimized with the CCSD(T)/aug-cc-pwCVQZ-PP method. Harmonic vibrational frequencies were computed at the same level of theory while anharmonic vibrational frequencies were computed at the CCSD(T)/aug-cc-pwCVTZ-PP level of theory. Final energetics were obtained with the CCSDT(Q) method. Basis sets up to augmented quintuple-zeta cardinality (aug-cc-pwCV5Z-PP) were employed to obtain energetics in order to extrapolate to the complete basis set limits using the focal point approach. Zero-point vibrational energy corrections were appended to the extrapolated energies in order to determine relative energies at 0 K. It was found that the planar dibridged isomer lies lowest in energy while the linear structure lies highest in energy. The results were compared to other group 13 M_2H_2 (M = B, Al, Ga, In, and Tl) theoretical studies and some interesting variations are found. With respect to experiment, incompatibilities exist.

Ongoing Experimental Work and Future Plans

Sequential Capture of O(^{3}P) and Alkenes by Helium Nanodroplets: Infrared Spectroscopy and Ab Initio Computations of the Triplet Biradical Intermediates

According to Smith *et al*. [Smith, I. W. M.; Sage, A. M.; Donahue, N. M.; Herbst, E.; Quan, D. *Faraday Discuss.* **2006**, 133, 137.], for molecule + radical reactions, the energetic difference between the molecule's ionization energy (IE) and the radical's electron affinity (EA) can provide insight into the nature of the reaction barrier, either *above* or *below* the reactant asymptote. They propose that a difference (IE − EA) greater than 8.75 eV indicates a real barrier above the asymptotic limit, whereas a value below 8.75 eV indicates a submerged barrier. Indeed, this difference for the O(^{3}P) + HCN system is 12.2 eV. Accordingly, the barrier to oxygen insertion into the CN π system is ~10 kcal/mol above the reactant asymptote, and a van der Waals complex is observed when these species are brought together in a 0.4 K helium nanodroplet. However, O(^{3}P) reactions with *alkenes* are predicted to cross the postulated 8.75 eV threshold as the alkene substitution pattern evolves from ethene (no substitution) to propene (methyl group substitution) to butene (dimethyl substitution, of which there are four different isomers), and this trend was tested by Sabbah *et al.*
[Sabbah, H.; Biennier, L.; Sims, I.R.; Georgievskii, Y.; Klippenstein, S.J.; Smith, I. W. *Science* **2007**, 317, 102.]. Their findings corroborated the behavior predicted by Smith *et al.* The HCN + O(^{3}P) results presented recently by us demonstrate the feasibility for analogous alkene + O(^{3}P) spectroscopic studies, in which O(^{3}P) and alkenes of varying substitution are combined in helium droplets *via* the sequential capture scheme. As the *real* reaction barrier (*i.e.* for the ethene and propene reactions) evolves to being *submerged* below the asymptotic limit (*i.e*. for the butene reactions), one might expect that strongly bound reaction intermediates, such as triplet biradicals, will be observed in helium droplets, rather than van der Waals complexes. Given the fact that a 10,000 atom helium droplet can dissipate 140 kcal/mol, it should be possible to quench the internal energy of these reaction intermediates and probe them for the first time spectroscopically.

Joseph T. Brice, Peter R. Franke, Gary E. Douberly "Sequential Capture of O(^{3}P) and HCN by Helium Nanodroplets: Infrared Spectroscopy and Ab Initio Computations of the $^3\mathbf{\Sigma}$ O-HCN Complex" *Journal of Physical Chemistry A*, **121**, 9466-9473 (2017). Published: November 2017.

Selected Publications acknowledging DOE support (2022-2024):

1. S.M. Goodlett, J.M. Turney, G.E. Douberly, and H.F. Schaefer, "The Noncovalent Interaction Between Water and the 3P Ground State of the Oxygen Atom," Mol. Phys. 120, (2022). DOI: 10.1080/00268976.2022.2086934.

2. G.E. Douberly, "Infrared Spectroscopy of Molecular Radicals and Carbenes in Helium Droplets," pages 155-177 of Molecules in Superfluid Helium Nanodroplets, Editors A. Slenczka and J.P. Toennies, Springer (2022). https://doi.org/10.1007/978-3-030-94896-2_4

3. P. Vermeeren, M.D. Tiezza, M.E. Wolf, M.E. Lahm, W.D. Allen, H.F. Schaefer, T.A. Hamlin and F.M. Bickelhaupt, "Pericyclic Reaction Benchmarks: Hierarchical Computations Targeting CCSDT(Q)/CBS and Analysis of DFT Performance," Phys. Chem. Chem. Phys. 24, 18028-18042 (2022).

4. K.E. King, P.R. Franke, G.T. Pullen, H.F. Schaefer, and G.E. Douberly, "Helium Droplet Infrared Spectroscopy of the Butyl Radicals," J. Chem. Phys. 157, 084311 (2022). DOI: 10.1063/5.0102287

5. N. Kitzmiller, M.E. Wolf, J.M. Turney, and H.F. Schaefer, "Toward the Observation of Tin and Lead Analogs of Formaldehydes," MQM 2022 Special Issue of J. Phys. Chem. A 126, 7930-7937 (2022).

6. M.E. Lahm, N.L. Kitzmiller, H.F. Mull, W.D. Allen, and H.F. Schaefer, "Concordant Mode Approach for Molecular Vibrations," J. Amer. Chem. Soc. 144, 23271-23274 (2022).

7. G. Li, Y. Yao, Y. Lin, Y. Meng, Y. Xie, and H.F. Schaefer, "The Reaction Between the Bromine Atom and the Water Trimer: High Level Theoretical Studies," Phys. Chem. Chem. Phys. 24, 26164-26169 (2022).

8. J.M. Begley, G.J.R. Aroeria, J.M. Turney, G.E. Douberly, and H.F. Schaefer, "Enthalpies of Formation for Criegee Intermediates: A Correlation Energy Convergence Study," J. Chem. Phys. 158, 034302 (2023). DOI: 10.1063/5.0127588

9. N. Villegas-Escobar, P.R. Hoobler, A. Toro-Labbe, and H.F. Schaefer, "High Level Coupled Cluster Study of Substituent Effects in the H_2 Activation by Low Valent Aluminyl Atoms," J. Phys. Chem. A 127, 956-965 (2023).

10. A. Jiang, J.M. Turney, and H.F. Schaefer, "Tensor Hypercontraction Form of the Perturbative Triples Energy in Coupled Cluster Theory," J. Chem. Theory Comput. 19, 1476-1486 (2023).

11. A.K. Bralick, E.C. Mitchell, A.C. Doner, A.R. Webb, M.G. Christianson, J.M. Turney, B. Rotavera, and H.F. Schaefer, "Simulation of the VUV Absorption Spectra of Oxygenates and Hydrocarbons: A Joint Theoretical-Experimental Study," J. Phys. Chem. A. 127, 3743-3756 (2023).

12. K. Schueller, H.F. Mull, J.M. Turney, and H.F. Schaefer, "Butterfly, Vinylidene-Like, Monobridged, and Trans Structures of SiH_2^+. Comparison to the Well-Characterized Neutral Si_2H_2," Special Issue in Honor of Professor Helmet Schwarz, Israel J. Chem. (2023) e202300033.

13. M.E. Lahm, M.A. Bartlett, T. Liang, L. Pu, W.D. Allen and, H.F. Schaefer, "The Multichannel i-Propyl + O_2 Reaction System: A Model of Secondary Alkyl Radical Oxidation," J. Chem. Phys. 159, 024305 (2023).

14. S.M. Goodlett, J.M. Turney, H.F. Schaefer, "Multifidelity Machine Learning for Modeling Potential Energy Surfaces," Special Topic Issue for "Software for Atomistic Machine Learning," J. Chem. Phys. 159, 044111. (2023).

15. P. M. Tran, Y. Wang, M. E. Lahm, P. Wei, C. J. Molnar, H. F. Schaefer, and G. H. Robinson, "Germanium (II) Dithiolene Complexes," Chem. Eur. J. e202302258 (2023).

16. Y. Wang, P. M. Tran, M. E. Lahm, P. Wei, E. R. Adams, H. F. Schaefer, and G. H. Robinson, "From Carbene-Dithiolene Zwitterion Mediated B–H Bond Activation to BH_3•SMe_2-Assisted Boron-Boron Bond Formation," Organometallics 42, 3328-3333 (2023).

17. J. Jin, H. F. Mull, J. M. Turney, and H. F. Schaefer, "The Heavy Carbene Analogues SbH2+ and BiH2+: Convergent Quantum Mechanical Studies," Molecular Physics 121, e2271579 (2023).

18. C. J. Tang, A. G. Heide, A. D. Heide, G. E. Douberly, J. M. Turney, and H. F. Schaefer, "Exploring the Tl_2H_2 Potential Energy Surface: A Comparative Analysis with Other Group 13 Systems and Experiment," J. Comput. Chem. 45, 985-994 (2024).

19. R. H. Givhan, S. M. Goodlett, G. E. Douberly, J. M. Turney, and H. F. Schaefer, "$Pb_2H_2^+$: Convergent Quantum Mechanical Study of Seven Lead Hydride Cation Structures. Toward Laboratory Identification," Molecular Physics 122, e2307497 (2024).

20. I. T. Beck, M. E. Lahm, G. E. Douberly, and H. F. Schaefer, "Convergent ab initio Analysis of the Multi-Channel HOBr+H Reaction," J. Chem. Phys. 160, 124304 (2024).

21. P. M. Tran, Y. Wang, M. E. Lahm, P. Wei, H. F. Schaefer, and G. H. Robinson, "Unusual Nucleophilic Reactivity of Dithiolene-Based N-Heterocyclic Silane," Dalton Transactions 53, 6178-6183 (2024).

22. E. J. Poncelet, H. F. Mull, Y. Abate, G. H. Robinson, G. E. Douberly, J. M. Turney, and H. F. Schaefer, "A Wealth of Structures for the $Ge_2H_2^+$ Radical Cation: Comparison of Theory and Experiment," Physical Chemistry Chemical Physics 26, 12444 (2024).

23. P. M. Tran, Y. Wang, B. Dzikovski, M. E. Lahm, Y. Xie, P. Wei, H. F. Schaefer, and G. H. Robinson, "A Stable Aluminum Tris (dithiolene) Triradical," J. Amer. Chem. Soc. 146, 16340-16347 (2024).

Coordination and Solvation of Actinide Cations Studied with Selected-Ion Infrared Spectroscopy

DOE Award No. DE-SC0018835

Michael A. Duncan

Department of Chemistry, University of Georgia, Athens, Georgia 30602
maduncan@uga.edu

Program Scope

Actinide metal and metal oxide cation-molecular complexes are studied in the gas phase to investigate their bonding, ligand coordination and solvation. Cation-molecular complexes of the form $M^{n+}(L)_y$, where M = U or Th, n = 1 or 2, and L = small molecules such as H_2O, CO, N_2, CO_2, CH_3CN, or benzene are produced in a supersonic molecular beam by pulsed laser vaporization of solid metal targets. Similar methods produce metal oxide ions. Complexes containing a metal or oxide core ion with a specific number of ligand or solvent molecules are size-selected in a time-of-flight mass spectrometer and studied with different forms of laser photodissociation measurements. Tunable infrared laser spectroscopy reveal the shifts that occur for ligand/solvent vibrations upon binding to these metals and how these vary with the charge state, the number of ligands or solvent molecules present, the geometric and electronic structures of complexes, and the possible occurrence of ligand reactions mediated by the metal center. Additional experiments employ tunable laser UV-visible photodissociation spectroscopy to probe excited states and photodissociation thresholds. Photofragment kinetic energy analysis in a specially-designed ion imaging instrument also investigates cation-molecular bond energies. The experiments are complemented by computational chemistry, with careful attention to relativistic and spin-orbit effects. The goal of these studies is an increased understanding of the fundamental interactions involved in actinide bonding, coordination and solvation.

Recent Progress

Progress in the last year has been limited because we had to move our lab from the old Chemistry Building to the new STEM Building. Beginning in November 2023, we had to dis-assemble three molecular beam machines and their associated plumbing, wiring, electronic, and lasers. Packing, moving and re-assembling everything took about seven months. Most of the instruments are now working as they were before. The exception is our infrared laser system, which has required YAG laser repair. We have no new infrared data as a result of this.

In the new work since last year we have focused on photodissociation studies in the UV-visible region. For metals like uranium, analogous to transition metals like iron, we have

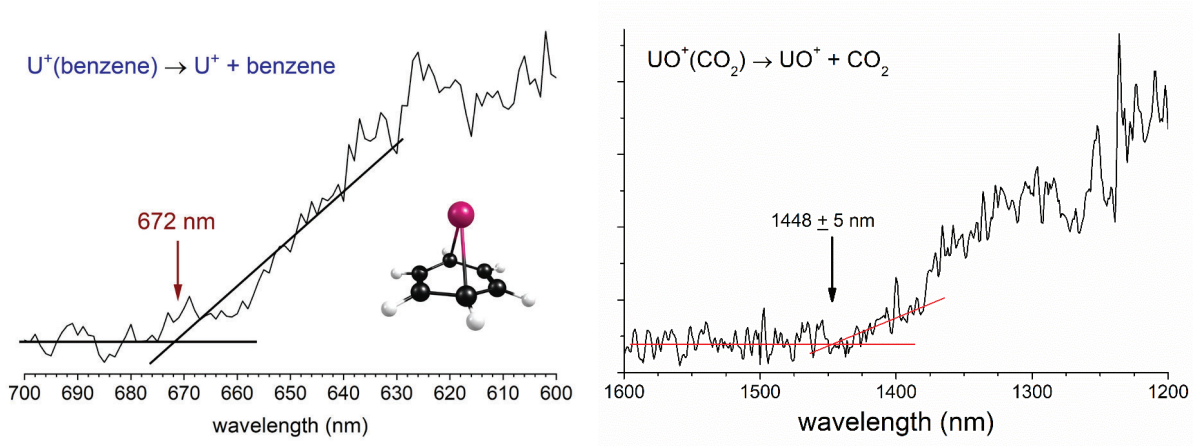

Figure 1. a) UV-visible photodissociation threshold for the U^+(benzene) complex. b) Near-IR laser photodissociation threshold for the $UO^+(CO_2)$ complex.

found that the density of excited electronic states is so great that M^+-L ion-molecule complexes have essentially continuous absorption spectra. If this is the case, and the excited states are strongly coupled, then dissociation will occur whenever the photon energy exceeds the bond energy. Measurement of the threshold for the appearance of dissociation is therefore equivalent to measuring the bond energy for the complex. We have now measured photodissociation spectra for U^+(benzene) (Figure 1a), UO^+(benzene), and UO_2^+(benzene) using a broadly tunable OPO laser system (Continuum Horizon II). In each of these cases photodissociation occurred by the elimination of the benzene ligand. We found no photodissociation at low energy, a threshold at which photodissociation could be observed, and then continuous photodissociation with no spectral structure at all energies above the threshold. Because of these characteristics, we assigned the photodissociation threshold energies to correspond to the bond energies for these complexes. The experimental values obtained for the benzene complexes [U^+–(benzene): 42.5 ± 0.3 kcal/mol; UO^+–(benzene): 41.0 ± 0.3 kcal/mol; UO_2^+–(benzene): 39.7 ± 0.3 kcal/mol] represent the first data for actinide cation-π thermochemistry. Computational studies were conducted at the DFT/B3LYP level using the Stuttgart/Köln fully relativistic 60 electron core potential (ECP60MDF) and the cc-pVTZ-PP basis set for uranium and the aug-cc-pVTZ level for C, H. and O for each of these complexes. Table 1 shows a comparison of the experimental and computed values for the dissociation energies.

Similar photodissociation threshold experiments were conducted on the UCO_3^+ ion made by ablation of uranium in a CO_2 expansion. This ion has two possible structures: $UO^+(CO_2)$ and $UO_2^+(CO)$; the latter is computed to be more stable by 43.7 kcal/mol. The dissociation energy for the oxide-CO_2 ion was predicted to be 16.6 kcal/mol, whereas that for the dioxide-carbonyl was predicted at 35.5 kcal/mol. A threshold for the elimination of the CO_2 ligand was measured at 1448 nm (19.7 kcal/mol) (Figure 1b), showing that most of the ions have the oxide-CO_2 structure, even though it is less stable. Apparently there is a barrier to the insertion reaction with CO_2. Experiments are in progress to make the ion with the same mass from a CO expansion,

Table 1. Computed vs experimental benzene binding energies for the ions in this study. DFT/B3LYP computations employed the ECP60MDF core potential and cc-pVTZ-PP basis set for uranium and the aug-cc-pVTZ basis set for C, H and O.

Ion	D_0(–Benzene) Theory (kcal/mol)	TPD Experiment. (kcal/mol)
U^+(benzene)	47.25	42.5 ± 0.3
UO^+(benzene)	41.01	41.0 ± 0.3
UO_2^+(benzene)	29.71	39.7 ± 0.3

which should favor the other isomer. This experiment shows that photodissociation thresholds can be used to distinguish isomers. It also shows that electronic spectroscopy on actinide cations may be limited by the high density and congestion of excited electronic states.

Future Plans

We will continue the infrared spectroscopy experiments by examining uranium-acetylene and uranium-benzene complexes as well as small uranium carbonyls. Uranium cations have been suggested previously to catalyze the cyclo-trimerization reaction to form benzene, but there is no spectroscopic evidence to confirm this. The structures produced by theory for the U^+, UO^+ and UO_2^+ complexes with benzene show distortion of the planarity of benzene and bending of the UO and OUO moieties. IR measurements can test these predictions. Additional threshold photodissociation experiments in the UV-visible region will be conducted on a variety of U^+-L, UO^+-L, and UO_2^+-L complexes to determine their bond energies.

BES Supported Publications (2022 – 2024)

1. N. J. Dynak, B. M. Rittgers, J. E. Colley, D. J. Kellar, M. A. Duncan, "Photofragment Imaging of Carbon Cluster Cations: Explosive Ring Rupture," *J. Phys. Chem. Lett*. **13**, 4786−4793 (2022). DOI: 10.1021/acs.jpclett.2c00950.

2. J. H. Marks, A. G. Batchelor, J. R. C. Blais, M. A. Duncan, "Cationic Complexes of Uranium and Thorium with Cyclooctatetraene: Photochemistry and Decomposition Products. *J. Phys. Chem. A* **126**, 4230−4240 (2022). DOI: 10.1021/acs.jpca.2c03035.

3. B. M. Rittgers, J. H. Marks, D. J. Kellar, M. A. Duncan, "Photoinduced Charge Transfer in the Zn-Methanol Cation Studied with Selected-Ion Photofragment Imaging," *J. Chem. Phys.* **157**, 114302 (2022). DOI: 10.1063/5.0108467.

4. J. E. Colley, A. G. Batchelor, M. A. Duncan, "Cation-π Bonding in Actinides: UO_x^+(Benzene) (x=0,1,2) Complexes Studied with Threshold Photodissociation Spectroscopy and Theory," *J. Phys. Chem. Lett.*, submitted.

TOWARDS MACHINE LEARNING MOLECULAR DYNAMICS: EFFECT OF DATA PARTITIONING ON MODEL RESULTS

C. Franklin Goldsmith, PI
Brown University

Program Scope

One of the grand challenges for the Department of Energy is the ability to simulate the complex interactions between fluid mechanics and chemical kinetics for gases at high pressures (e.g. 100 bar). Under these conditions, the ideal gas equation of state is not valid. Although considerable advances have been made regarding real-gas equations of state for thermodynamic properties, the same cannot be said of chemical kinetics under extreme pressures. The standard approach in computational kinetics assumes that reactions occur under isolated conditions. Real-gas behavior can have a profound effect on the chemical source terms in reactive flow simulations. These many-body interactions can change both the rate constants and the product branching fractions.

In this project, we are investigating different methodologies to quantify many-body effects on transition states and thence high-pressure effects on rate constants. The specific aims are: (i) develop chemically accurate surrogate potential energy surfaces for computational kinetics with explicit solvent molecules, and use this surrogate model within molecular dynamics simulations; (ii) quantify the effects of high pressures on rate constants for different reaction families; (iii) determine the pressure at which solvent cage effects will cause the branching fractions in bond-fission reactions to favor molecular elimination products; and (iv) analyze the results for possible trends that can be applied heuristically.

Recent Progress

Our initial focus was to develop a work flow for creating machine learning molecular dynamics. Since the last PI meeting, we published our first manuscript "High-Dimensional Neural Network Potentials for Accurate Prediction of Equation of State: A Case Study of Methane" M. Abedi, J. Behler, and C. F. Goldsmith. *Journal of Chemical Theory and Computation* (2023) DOI: 10.1021/acs.jctc.3c00469. In this manuscript, we presented a methodology to compute the mass density of methane as a function of temperature and pressure, $\rho(T,p)$. The method begins with ab initio molecular dynamics (AIMD) simulations with density functional theory (DFT). We started with the more traditional DFT approach of using periodic boundary conditions (PBC) with planewave basis functions. In addition, we also performed non‑PBC calculations with clusters of CH4 and repulsive walls. The latter approach, which is novel, allows us to use more accurate gaussian-type basis functions, which should be more reliable for accurate barrier heights. The results suggest that the non-PBC strategy is just as effective as the conventional PBC method. In both cases, we train a single neural network (NN) to the AIMD data. This NN potential is used in constant-temperature, constant-pressure (NPT-ensemble) molecular dynamics simulations. The resulting mass density is compared against experimentally-derived equation-of-state data. The NPT simulations with the NN potential can successfully reproduce the mass density to within a few percent error. This

approach suggests that we have a working computational strategy to compute the molar volume as a function of temperature and pressure, *V(T,p)*.

From there, we moved on to apply our method for a reaction with a first-order saddle point, $HO_2 + CH_3OH \rightarrow H_2O_2 + CH_2OH$, in collaboration with Prof. Yiguang Ju (Princeton). We computed a "real-gas correction" to the rate constant using the method of "change in volume of activation", $\mathbf{\Delta}V^{\ddagger}$,. As with the EoS results, we first compute the $V(T, p)$ using the *NPT* ensemble. The change in volume of activation is then given by $\mathbf{\Delta}V^{\ddagger}(T, p) = V_{TS}(T, p) - V_{OH}(T, p) - V_{CH3OH}(T, p)$. The real-gas correction had the correct trend, but it was too small to explain the observable difference in Prof. Ju's data.

Unfortunately, the postdoc, Dr. Abedi, decided to take a position in industry before we could finalize the results and submit them for publication. As a result, this project is on hold.

Per- and Polyfluoroalkyl Substances (PFAS)

We continue to work on our theory-based mechanism for PFAS incineration. Our first manuscript was recently published: "A Theory-based Mechanism for Fluoromethane Combustion I: Thermochemistry and Abstraction Reactions" Siddha Sharma, Kento Abeywardane, and C. Franklin Goldsmith, *Journal of Physical Chemistry A* (2023). In this manuscript, we extended the ANL0 methodology to include fluorine atoms. We found that the best results were obtained when using CF_4 as the reference species. We computed the thermophysical properties for 92 small molecules containing H/C/O/F (all species up to 2 carbon atoms). Additionally, we computed 40+ rate constants for H abstraction, and 30+ rate constants for F abstraction.

Since then, we have developed a new strategy to compute the enthalpy of formation for larger PFAS. This strategy combines different levels of theory with the connectivity based hierarchy of Raghavachari and coworkers. The most fundamental level, or tier 1, uses the ANL0 methodology from our previous paper. The ANL0 method is combined with CBH-1 (isodesmic) reactions to compute the enthalpy of formation for a 14 new species (in addition to the 92 species in our previous paper). This method is functionally identical to the ANL-CBH methodology of Sarah Elliott and Stephen Klippenstein. The ANL-CBH species provide a library of functional groups, which we use as reference values for the next level. The second tier uses UCCSD(T)-F12b/cc-pVTZ-f12//B2PLYPD3/cc-pVTZ level theory. 22 species were computed, including up to perfluorobutanoic acid (PFBA). Using the ANL-CBH tier 1 list as reference species, the enthalpy of formation for the F12 tier 2 list was computed using CBH-2 and CBH-3 schema. For any PFAS larger than PFBA, we used tier 3. This level used either DLPNO-CCSD(T)/aug-cc-pVQZ//ωB97dx/cc-pVTZ or DLPNO-CCSD(T)/aug-cc-pVQZ//M06-2X/cc-pVTZ.

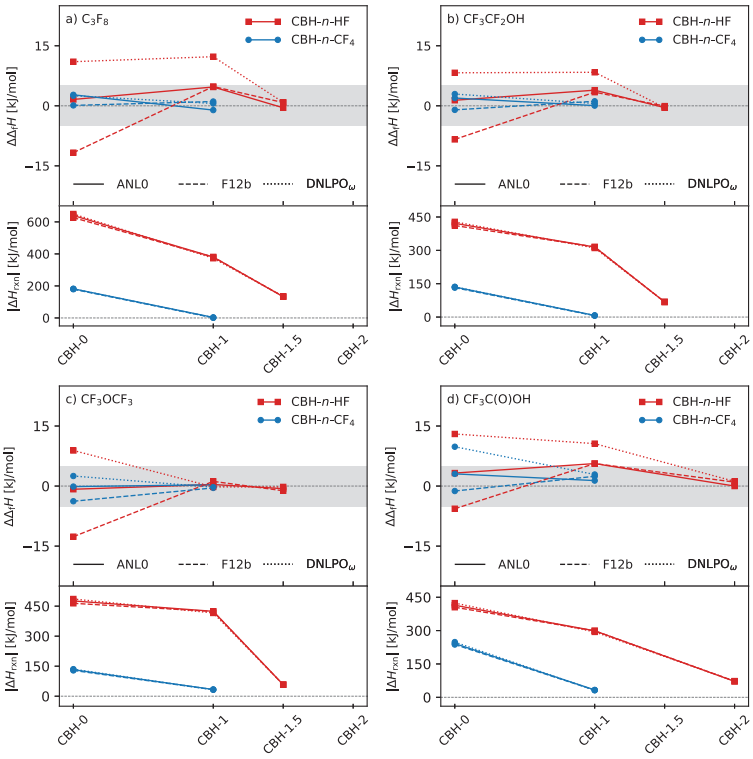

Figure 1: Comparison of the three different computational methods.

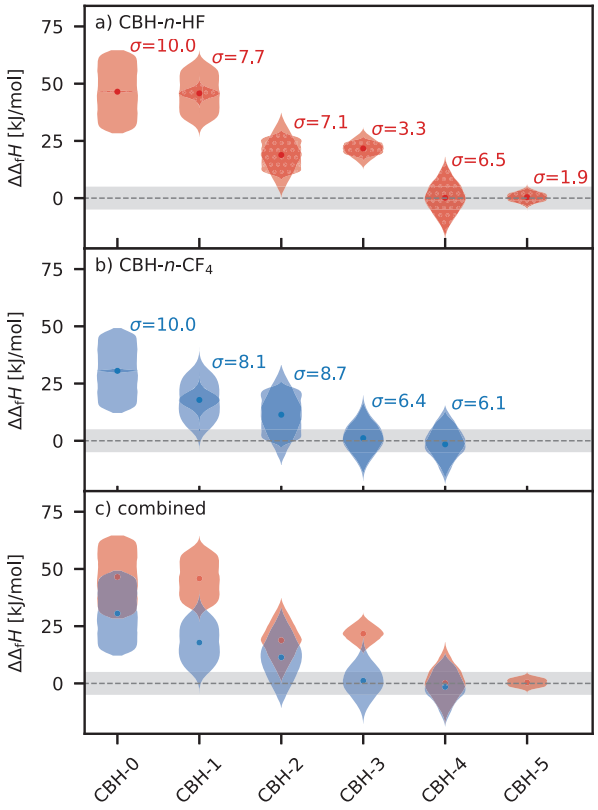

Figure 2: uncertainty quantification for PFOA.

Figure 1 summarizes some of the results for the four largest species considered in the tier 1 level, which each species containing an important functional group. Figure 2 presents our uncertainty quantification for the largest PFAS consider, perfluorooctanoic acid (PFOA). Overall, we believe that we can maintain chemical accuracy for species as large as PFOA. Although we developed the method for PFAS, it should be applicable to any large species in the gas phase. These results were recently published: "Accurate Enthalpies of Formation for PFAS from First-Principles: Combining Different Levels of Theory in a Generalized Thermochemical Hierarchy" Kento Abeywardane, and C. Franklin Goldsmith, *ACS Physical Chemistry Au* (2024).

We measured the impact of CH_2F_2 on the ignition delay time of propane. We created a new theory-based mechanism for the interaction of small fluorine-containing molecules with light hydrocarbons. The model was in excellent agreement with our measured ignition delay times. These results were presented at the recent International Symposium on Combustion and will be published the next issue of the *Proceeding of the Combustion Institute*.

We are also collaborating with Rob Tranter (Argonne) to measure PFAS decomposition kinetics using shock tube laser schlieren densitometry. A visiting student measured the decomposition kinetics for C_2F_6, C_3F_8, C_4F_{10}, and PFBA. We intend to publish the three perfluoroalkanes in one manuscript and the perfluoro-carboxylic acid separately. These experiments will be some of the few available shock tube data on PFAS decomposition.

Gas Surface Interactions

We are excited to begin a new project on the kinetics of gas-surface interactions (*e.g.* adsorption and desorption). The current state of the art for computing rate constants for adsorption is fixed (or harmonic) transition state theory. This approach is generally fine for adsorption reactions that have a first-order saddle point in potential energy along the reaction coordinate. Dissociated adsorption is a good example of reactions that typically have a barrier: $CH_4 + 2^* \rightarrow CH_3^* + H^*$. For many adsorbates, however, the potential is barrierless (*e.g.* $CO + ^* \rightarrow CO^*$). Much like radical-radical recombination in the gas phase, barrierless adsorption reactions require variational transition state theory. Previously in our group, we adapted the VaReCoF code from Yuri Georgievskii and Stephen Klippenstein to a new python version, rotdPy. We are now collaborating with Judit Zador on updating and improving the code for gas-phase reactions, and we are collaborating with Stephen Klippenstein on adapting the code to work on gas-surface interactions as well. Our goal is to create the first proper variational transition state theory code for applications in gas-surface systems.

Enabling Quantitative Predictions of Reacting Gas-Liquid Systems

William H. Green
Department of Chemical Engineering
Massachusetts Institute of Technology
Cambridge, MA 02139
whgreen@mit.edu

I. Program Scope

Many important systems are complex non-equilibrium mixtures of molecules where multiple reactions are occurring simultaneously in more than one phase; examples include conversion of waste plastic, smog chemistry, combustion of fuel sprays, and reactive capture of CO_2. In all of these systems reactions are occurring in both a gas/vapor phase and a liquid phase (and sometimes in a solid phase also). Most of the gas phase reactions will also occur in the liquid phase, but with different rates and equilibria due to solvent effects. (There are also often additional ionic reactions that are only significant in the liquid phase.) The movement of molecules between the phases affects the overall course of the reactions. At present, many of the models used to understand or improve these systems are oversimplified. This project is advancing the nascent capability to predict the gas-phase reactions, by computing solvent effects on the liquid-phase reactions, and by combining gas-phase and liquid-phase models into a unified simulation.

The goal of this project is to use Artificial Intelligence / Machine Learning methods based on quantum and statistical mechanics to make it possible to quickly construct high-fidelity computer models for two-phase reactive systems. These simulations would facilitate scientific understanding and speed design of new systems for tackling today's environmental and energy challenges. This project directly addresses DOE BES's priorities in **Artificial Intelligence and Machine Learning** and **Fundamental Science to Enable Clean Energy.** The project is part of the GPCP's research thrust on **Chemical Reactivity**.

II. Recent Results

A. Overview

This project involves several different lines of research:

1) Improve modeling methodology to allow us to tackle these complicated systems.
2) Develop improved methods for calculating/estimating k(T,P) & K_{eq}(T) for gas phase reactions
3) Develop improved methods for calculating/estimating solvent effects on k(T) and K_{eq}(T).
4) Develop models for gas, liquid, and two-phase systems & compare with experiments

Most of our estimation methods use machine-learning (ML) methods trained using data obtained from quantum chemistry and COSMO-RS calculations, supplemented by experimental data as possible. For a concise overview of our approach, showing both its successes and some challenges, see [12].

B. Improved Modeling Methodology and Software

We have developed a new general solver [11] for reactive multi-phase systems, including transport between the phases as well as complex kinetics within each phase, and demonstrated its utility.[29-30] We have made several improvements to the Reaction Mechanism Generator software package that make it easier to install, use, and modify, and several algorithmic improvements that make it easier to build useful kinetic models.[6,7,11,22,33] We also made many enhancements to the package's database and popular online tools at rmg.mit.edu [3]. We also demonstrated the practicality and value of automatic spawning of quantum chemistry calculations of species thermo as the model is being constructed.[26,29,30] Cumulatively these improvements have led to greatly increased use and development of the open-source package, so RMG is no longer primarily an MIT project but a real

community effort. We added the capability to include macromolecules in the simulations, and are now using it to model chemical recycling of waste plastic (pyrolysis of molten polyethylene).

C. Improved methods for gas-phase reactions

We used quantum chemistry to construct large datasets of computed transition state geometries and energies for training estimators that can be used to predict other reactions.[1,2,12] The process is iterative, using the current best estimator to estimate the barrier height of a proposed reaction to decide if the reaction is fast enough to be worth calculating, and to provide initial-guess geometries for the TS's of new reactions. This has been effective at bootstrapping the procedure from a very limited data set on small molecules to several data sets with $O(10^4)$ reactions, suitable for training accurate ML models. Along the way we discovered weaknesses in existing data sets and ML methods, and developed improved ML methods.[18-23] We also computed improved atom-energy and bond-additivity enthalpy corrections for several popular quantum chemistry methods, and developed an improved method for estimating thermochemistry of radicals.[9,10] We also developed improved methods for estimating the pressure-dependence of reaction rates, particularly for chemically-activated reactions on PES's with many wells, and addressed some technical issues in master equation methods.[5-8]

D. Solvent Effects on k(T) and K_{eq}(T)

Around the time this project started, we developed a good estimator for predicting T-dependent solvation energies of neutral closed shell organics in pure solvents, and so solvent effects on K_{eq}(T), by combining COSMO-RS calculations, experimental data, and asymptotic relations for thermochemistry near solvent critical points.[13,14] In those early models we assumed the solvated molecule has a single conformation, i.e. the same conformation as the gas-phase molecule, but that is not correct, so we developed a method for predicting the conformer energies in different solvents.[31] During the last 3 years we have extended that work to also predict solvation of transition states (and so solvent effects on kinetics); due to cancellation of errors between TS and reactants this turns out to be more accurate than predicting the absolute solvation energies [4,15,16,32]. We also developed methods to predict solvation energies of radicals. Recently we have also developed methods for predicting solvation energies in binary solvent mixtures, even for non-ideal solutions, using experimental vapor-liquid equilibrium data to fine-tune models originally trained by COSMO-RS calculations.

In liquid phase, ion energies are very different than they are in gas phase, drastically shifting reaction equilibria and introducing solvent-specific reaction barriers. We compiled a data set on the solvation energies of ions in water, and tested methods for computing those thermochemical values.[17] Our recent work has focused on developing fast, accurate predictors for thermochemical properties of ions in multiple solvents. We developed a machine learning model that predicts the solvation energies of ions in 9 different solvents with mean absolute errors of about 2 kcal/mol (more accurate than the widely-used COSMO-RS solvation models). We also developed a model for predicting pKa in those solvents that was accurate to within ~1 pKa unit for nearly all solvents tested. Finally, we developed a model to predict gas-phase acidities, which when combined with thermochemical data on the neutrals gives ion energies within 3 kcal/mol of the best numbers in the literature. The pKa's can be combined into thermochemical cycles to predict the energies of the ions in the solvents, and so Keq's involving the solvated ions. We plan to integrate these predictors into RMG for simulation of reacting systems with charged species. We are also developing methods for predicting solvent effects on rates of ionic reactions using quantum-chemical calculations. Our work has shown that relative solvent effects for S_N2 reactions can be predicted within 1 order of magnitude using low-cost methods. However, more work is needed to extend to other types of ionic reactions, and to make this approach more general and reliable.

E. Constructing kinetic models and comparing with experiment

To test and demonstrate our new computer methods, and to better understand the issues involved, we have constructed kinetic models for several different systems.[24-30] In most cases, we can compare the model predictions with experiment, to test our method. In a few cases where data is lacking, our published model predictions are a signpost for future experimental efforts.

III. Future Plans

Upgrading Automated Kinetic Model Construction including Solvation.. We are currently working to extend the work we have published on closed shell molecules and reactions to solvated free radicals and ions and their reactions, and incorporating them into RMG.

Upgrading Uncertainty Estimates. We are also examining the many types of errors in today's Machine Learning models, to provide more reliable estimates of the uncertainties in the model predictions (today most published error estimates on ML models are much smaller than the actual errors you are likely to encounter if you use the models). Next step is to integrate all this into RMG to make it possible to rapidly and automatically improve the kinetic models as they are being constructed, to more accurately represent all the effects of solvation, and to attach reliable uncertainty estimates to RMG's predictions.

Open-Source Software and Databases. We plan to release a new version of the Reaction Mechanism Generator software package by the end of 2024, and a new of the Chemprop (Machine-Learning for Chemistry) package by the end of October. We have generated several very large databases of transition state geometries, barrier heights, and molecular and radical thermochemistry, and are preparing them for publication.

Publications and submitted journal articles supported by DOE BES 2022-2024

1. K. Spiekermann, L. Pattanaik, W.H. Green. High Accuracy Barrier Heights, Enthalpies, and Rate Coefficients for Chemical Reactions. *Sci. Data* **9**, 417 (2022).
2. K. Spiekermann, L. Pattanaik, W.H. Green. Fast Predictions of Reaction Barrier Heights: Towards Coupled-Cluster Accuracy. *J. Phys. Chem. A* **126,** 3976-3986 (2022).
3. M.S. Johnson, et al. The RMG Database for Molecular Property Prediction. *J. Chem. Inf. Model* **62**, 4906-4915 (2022). https://doi.org/10.1021/acs.jcim.2c00965
4. W.H. Green. Concluding Remarks on Faraday Discussion on Unimolecular Reactions. *Faraday Discussion* **238**, 741-766 (2022). https://doi.org/10.1039/D2FD00136E
5. M. S. Johnson, W.H. Green. Examining the Accuracy of Methods for Obtaining Pressure Dependent Rate Coefficients. *Faraday Discussions* **238**, 380-404 (2022).
6. M.S. Johnson, A. Grinberg Dana, W.H. Green. A Workflow for Automatic Generation and Efficient Refinement of Pressure Dependent Networks. *Combustion & Flame* 257, 112516 (2023).
7. A. Grinberg Dana et al., Automated reaction kinetics and network exploration (Arkane): A statistical mechanics, thermodynamics, transition state theory, and master equation software. *Int. J. Chem. Kinet.* **55**, 300-323 (2023). https://doi.org/10.1002/kin.21637
8. F. Holtorf, W.H. Green. On the accuracy of the chemically significant eigenvalue method. *Journal of Chemical Physics* **159**, 144102 (2023). https://doi.org/10.1063/5.0158782
9. H.-W. Pang, X. Dong, M.S. Johnson, W.H. Green. Subgraph Isomorphic Decision Tree to Predict Radical Thermochemistry with Bounded Uncertainty Estimation. *J. Phys. Chem. A* **128**, 2891–2907 (2024). https://doi.org/10.1021/acs.jpca.4c00569
10. H. Wu, A.M. Payne, H.-W. Pang, A. Menon, C.A. Grambow, D. Ranasinghe, X. Dong, A. Grinberg Dana, W.H. Green. Towards Accurate Quantum Mechanical Thermochemistry: (1) Extensible Implementation and Comparison of Bond Additivity Corrections and Isodesmic Reactions. *J. Phys. Chem. A* **128**, 4335-4352 (2024). https://doi.org/10.1021/acs.jpca.4c00949
11. M.S. Johnson, H.-W. Pang, A.M. Payne, W.H. Green. ReactionMechanismSimulator.jl: A modern approach to chemical kinetic mechanism simulation and analysis. *Int. J. Chem. Kinet.* (2024).

12. W.H. Green. Perspective on Automated Predictive Kinetics using Estimates derived from Large Datasets. *Int. J. Chem. Kinet.* (2024). https://doi.org/10.1002/kin.21744

Other Literature Cited

13. Y. Chung *et al.* Group Contribution and Machine Learning Approaches to Predict Abraham Solute Parameters, Solvation Free Energy, and Solvation Enthalpy. *J. Chem. Inf. Model.* **62**, 433 (2022).
14. Y. Chung, W.H. Green. Computing kinetic solvent effects and liquid phase rate constants using quantum chemistry and COSMO-RS methods. *J. Phys. Chem. A* **127**, 5637-5651 (2023).
15. Y. Chung, W.H. Green. Machine learning from quantum chemistry to predict experimental kinetic solvent effects**.** *Chemical Science* **15**, 2410-2424 (2024).
16. J.W. Zheng, W.H. Green. Experimental Compilation and Computation of Hydration Free Energies for Ionic Solutes. *J. Phys. Chem. A* **127**, 10268-10281 (2023).
17. E. Heid, W.H. Green. Machine learning of reaction properties via learned representations of the condensed graph of reaction (CGR). *J. Chem. Inform. Model.* **62**, 2101–2110 (2022).
18. E. Heid, C.J. McGill, F.H. Vermeire, W.H. Green. Characterizing Uncertainty in Machine Learning for Chemistry. *J. Chem. Inf. Model.* **63**, 4012-4049 (2023).
19. K.A. Spiekermann, T. Stuyver, L. Pattanaik, W.H. Green. Comment on ``Physics-based representations for machine learning properties of chemical reactions", *Machine Learning Science & Technology* **4**, 048001 (2023).
20. E. Heid, K. Greenman, Y. Chung, S.-C. Li, D. Graff, F.H. Vermeire, H. Wu, W.H. Green, C.J. McGill. Chemprop: A Machine Learning Package for Chemical Property Prediction, *J. Chem. Inf. Model.* **64**, 9–17 (2024).
21. M.S. Johnson, W.H. Green. A machine-learning based approach to reaction rate estimation. *Reaction Chemistry and Engineering* **9**, 1364 (2024).
22. S.-C. Li, H. Wu, A. Menon; K.A. Spiekermann, Y.-P. Li, W.H. Green. When Do Quantum Mechanical Descriptors Help Graph Neural Networks Predict Chemical Properties? *J. Am. Chem. Soc.* **146**, 23103–23120 (2024).
23. F.H. Vermeire, S.U. Aravindakshan, A. Jocher, M. Liu, T.-C. Chu, R.E. Hawtof, R. Van de Vijver, M.B. Prendergast, K. Van Geem, W.H. Green. Detailed Kinetic Modeling for the Pyrolysis of a Jet A Surrogate. *Energy & Fuels* **36**, 1304 (2022).
24. G. Pio, X. Dong, E. Bolzano, W.H. Green. Automatically Generated Model for Light Alkene Combustion. *Combust. Flame* **241,** 112080 (2022).
25. X. Dong, G. Pio, F. Arafin, A. Laich, J. Baker, E. Ninnemann, S. Vasu, W.H. Green. Butyl Acetate Pyrolysis and Combustion Chemistry: Mechanism Generation and Shock Tube Experiments. *J. Phys. Chem. A* **127**, 3231-3245 (2023).
26. H.-W. Pang, M. Forsuelo, X. Dong, R.E. Hawtof, D.S. Ranasinghe, W.H. Green. Detailed Multiphase Chemical Kinetic Model for Polymer Fouling in a Distillation Column. *Ind. Eng. Chem. Res.* **62**, 14266–14285 (2023).
27. H.-W. Pang, X. Dong, W.H. Green. Oxygen Chemistry in Polymer Fouling: Insights from Multiphase Detailed Kinetic Modeling. *Ind. Eng. Chem. Res.* **63**, 1013-1028 (2024).
28. L. Pattanaik, A. Menon, V. Settels, K. Spiekermann, Z. Tan, F. Vermeire, F. Sandfort, P. Eiden, W.H. Green. ConfSolv: Prediction of solute conformer free energies across a range of solvents. *J. Phys. Chem. B* **127**, 10151-10170 (2023).
29. K.A. Spiekermann, X. Dong, A. Menon, W.H. Green, M. Pfeifle, F. Sandfort, O. Welz, M. Begeler. Accurately Predicting Barrier Heights for Radical Reactions in Solution using Deep Graph Networks. *J. Phys. Chem. A* (2024) accepted.
30. M.S. Johnson, H.-W. Pang, M. Liu, W.H. Green. Species Selection for Automatic Chemical Kinetic Mechanism Generation. *International Journal of Chemical Kinetics* (2024) accepted.

Nonadiabatic Photochemistry

DE-SC0015997

Hua Guo,[1] Donald G. Truhlar,[2] and David R. Yarkony[3]

[1]*Department of Chemistry and Chemical Biology, University of New Mexico, Albuquerque, New Mexico 87131.*

[2]*Department of Chemistry, University of Minnesota, Minneapolis, Minnesota 55455*

[3]*Department of Chemistry, Johns Hopkins University, Baltimore, Maryland 21218*

e-mail: hguo@unm.edu; truhlar@umn.edu; yarkony@jhu.edu

PROGRAM SCOPE

This project involves the development and application of theoretical methods for treating electronically nonadiabatic processes both with fitted diabatic potential energy matrices (DPEMs) and by direct dynamics in the adiabatic representation. The project includes both electronic structure theory and dynamics, and the dynamics involves both fully quantal and semiclassical theoretical method development and calculations.

PROGRESS SINCE 2022

Hua Guo

We collaborated with Jingsong Zhang and Richard Dawes to elucidate the nonadiabatic photodissociation dynamics of HCO in its *A* band.[1] Quantum wave packet calculations on an accurate set of potential energy surfaces (PESs) revealed that the predissociation rate and product distribution are sensitive to the parent rotational quantum numbers. This is due to the fact that the predissociation is facilitated by the Renner-Teller coupling, which is controlled by the projection of the total rotational angular momentum on to the molecular axis. This model satisfactorily explained experimental observations.

In collaboration with David Osborn and Xixi Hu, we investigated the photodissociation of SO_2 in the C-band near 193 nm.[2] We have mapped out the ground and excited state adiabatic PESs with a high-level ab initio method and confirmed the newly discovered S + O_2 channel. Our trajectory simulations on the ground state PES of this system revealed that the S + O_2 products are formed after nonadiabatic transitions from the C state via a conical intersection. The presence of this previously unknown channel might impact our understanding of the mass-independent fractionation of sulfur found in the geological record related to the great oxygenation event.

In collaboration with Yarkony, the internal conversion and intersystem crossing in NH_3 photodissociation are investigated using a newly constructed DPEM.[3] This DPEM not only includes coupling between states with the same spin-multiplicity, but also coupling between different spin manifolds. Since a diabatic representation is used, the derivative coupling and spin-orbit coupling can all be represented with smooth functions, paving the way for studying internal conversion (IC) and intersystem crossing (ISC). These DPEMs also enforce the permutation symmetry, which is important for systems with identical atoms. In this study both the molecular (NH + H_2) and radical (NH_2 + H) channels were investigated. A DPEM for the singlet manifold of H_2CS has also been developed,[4] which represents the first step towards a first principles

understanding of the competition between IC and ISC channels in this system. Future work will add triplets into the DPEM. Compared with H_2CO, the presence of sulfur in H_2CS is expected to enhance the ISC process. Quasi-classical trajectory calculations have been performed on the ground state H_2CS PES and significant roaming was found.

We are also involved in collaborative efforts with Truhlar on a recent work of constructing a DPEM for the $O_3(^3A')$ system,[5] which is important for the photodissociation of O_3 in the Huggins band. In addition, the OH(A) quenching dynamics by H_2 was studied using a semi-classical method on different DPEMs,[6] which helps to elucidate the competition between the non-reactive and reactive quenching channels. Our collaboration has also lead to construction of the $N + C_2$ PES with the recently proposed compressed-state multistate pair-density functional theory method which allows the investigation of the corresponding reaction dynamics.[7]

An international collaborative effort to take advantage of the multi-configuration time-dependent Hartree (MCTDH) approach for characterizing high-dimensional nonadiabatic photodissociation dynamics was made involving Fabien Gatti, Dieter Meyer, and Yarkony.[8] Several important advances were introduced to handle the symmetry properties of the DPEM within the MCTDH framework.

In collaboration with Daiqian Xie, we have constructed a two-state global DPEM for the HO_2 system based on high-level ab initio data,[9] suitable for studying the dynamics of the $H + O_2 \leftrightarrow OH + O$ reaction. This is an important reaction in both combustion and atmosphere and has been the subject of extensive experimental and theoretical investigations. The diabatization was achieved by using both angular momentum and CI mixing coefficients. It is more accurate than the existing DPEMs. More recently, we carried out the first quantum scattering calculations using this DPEM, and found a significant effect of the geometric phase in both ICS and DCS.[10]

With our collaborators, we have been continuing our investigations of dynamics of bimolecular scattering and reactions. These studies include a full-dimensional quantum scattering calculation for the inelastic scattering between Ar and H_2O,[11] which is a prototype for understand rovibrational energy transfer. In addition, we have studied the dynamics of the $O + HO_2$ reaction, which has two different pathways leading to the same products.[12] Furthermore, we have reinvestigated the nonadiabatic quenching of OH(*A*) by H_2 using semi-classical methods, in collaboration with both Truhlar and Yarkony.[6, 13] In the reactive quenching channel, the H_2O product was found to possess extensive vibrational excitation, in qualitative agreement with experimental observations. The origin of the vibrational excitation is identified using an extended Sudden Vector Projection model. However, we were unable to find significant insertion trajectories which called for further improvement of the DPEM.

Finally, we published a review with Yarkony and Daiqian Xie on quantum dynamics of photodissociation,[14] a review with Kopin Liu on the mode specificity in state-to-state reactivity,[15] and another review with Hongwei Song is about dynamics of reactions with submerged barriers.[16]

Donald G. Truhlar

Our recent work involves a generalization of the semiclassical Ehrenfest method and coherent switching with decay of mixing to use only information about adiabatic surfaces and their gradients without requiring nonadiabatic coupling matrices, overlap calculations, or any other information about adiabatic wave functions.[17] We have also developed a version of trajectory surface hopping with this feature.[18] These methods are called curvature-driven methods, κCSDM and κTSH. We validated these new methods for a diverse group of problems, including (but not limited to) photodissociation of ammonia[19] and 1,3-cyclohexadiene[20] and photo-induced ring opening of ***γ***-butyrolactone.[21] The κCSDM and κTSH methods have been made available to the whole community in the ANT 2023[22] and SHARC-MN[23] computer programs.

With Guo, we used machine learning to construct full-dimensional global 1 ^{2}A′ and 1 ^{2}A″ potential energy surfaces for the C_2N system by fitting the results of compressed multistate pair-density functional theory multireference method, and we used these surfaces for a quasiclassical-trajectory study of the reaction of N atom with the rovibrational ground state of C_2.[7] The trajectories predict that the reaction produces vibrationally excited CN.

We also improved our method for fitting coupled potential energy surfaces to analytic functions by adding parametrically managed activation functions[5] to the direct-diabatization-by-neural-networks method,[24] and we developed a new approach to such fitting based on Frobenius companion matrices.[25]

Other publications in the period 2022-2024 supported by this grant are

- a new gradient correction scheme for electronically nonadiabatic dynamics involving multiple spin states,[26]
- the kinetics of the unimolecular reactions of *anti*-glycolaldehyde oxide and its reactions with one and two water molecules[27] and the sulfur trioxide reaction with water vapor,[28]
- a Python library for analytic representations of potential energy surfaces and diabatic potential energy matrices,[29]
- a program for combined quantum mechanical and molecular mechanical modeling and simulations,[30]
- a study of density functional accuracy for multi-step organic reactions,[31]
- a method for improved conservation of local-mode zero-point energy in quasiclassical trajectories,[32]
- a theoretical and experimental study of bound clusters in resonantly stabilized radical reactions relevant to carbonaceous particle growth,[33]
- kinetics of the HO_2 reactions with aldehydes[34, 35] and singlet oxygen reactions with dimethyl ether.[36]
- a perspective article on diabatic states,[37]
- a master equation study of the reaction of OH with HCHO,[38]
- a semiclassical trajectory studies of reactive and nonreactive scattering of OH(A $^2\Sigma^+$) with H_2,[6]

- kinetics of the reactions of Criegee intermediates with *s-cis-syn*-acrolein, acetone, and formyl fluoride,[39-41]
- a new method for analyzing intramolecular vibrational redistribution (IVR),[42]
- an examination of the best orbitals for Green's function calculations of quasiparticle energies for ionization, electron attachment, and band gaps,[43]
- degradation of biofuel ketohydroperoxides by reaction with OH,[44]
- an improvement of the multistructural method with torsional anharmonicity by using delocalized torsions,[45]
- a perspective article on electronic decoherence and its role in electronically nonadiabatic dynamics,[46]
- a combined theoretical and experimental study of the determination of organic hydroperoxides in gas-phase autoxidation,[47]
- electronic excitation of *ortho*-fluorothiophenol.[48]

David R. Yarkony

Since the *A*-*X* transitions in OH are used to detect this radical, the reactions of OH(A^2S^+) with H_2 are of practical as well as fundamental importance. The dynamics of this collisional process involves at least 3 channels:

$$\begin{aligned} OH(A^2\Sigma^+) + H_2 &\rightarrow H_2O + H && \text{R1 reactive nonadiabatic quenching} \\ &\rightarrow OH(X^2\Pi) + H_2 && \text{R2 nonreactive nonadiabatic quenching} \\ &\rightarrow OH(A^2\Sigma^+) + H_2 && \text{R3 nonreactive adiabatic scattering} \end{aligned}$$

This prototypical nonadiabatic process was investigated by our DOE funded team using semiclassical surface hopping nuclear dynamics.[13, 14] These studies are enabled by DPEMs from nonadiabatic electronic structure data at a high level multireference configuration interaction with single and double excitations. In order to test the above suggestion a new four-state DPEM is needed which focuses on (getting to) the Jahn-Teller like Rydberg region. To that end we are developing a new fitting method which extends a procedure of Eisfeld and uses permutation invariant polynomials and neural networks.[49]

We have complete sets of ES data for formaldehyde 1,2 ^{1}A, 1^{3}A, which include singlet and triplet DPEMs, spin-orbit coupling and dipole matrix elements. For thiophenol, we have performed electronic structure calculations for 1,2 ^{1}A (at MRCIS).[4] We are also redoing the diabatization of the 1,2 ^{1}A states of formaldehyde.

We have collaborated with Guo on a number of other projects related to nonadiabatic processes.[8, 14]

FUTURE PLANS

Hua Guo

We plan to use a quantum mechanical method to investigate the internal conversion and intersystem crossing in H_2CO using the recent DPEM from Yarkony. This is an interesting system because of the two possible nonadiabatic routes, via internal conversion to the S_0 state and

intersystem crossing to the T_1 state. The calculated energies and lifetimes can be compared with a large set of experimental data. These nonadiabatic processes are also at the center of the roaming dynamics in the S_0 state.

We will continue to investigate the nonadiabatic dynamics of SO_2 photodissociation, in collaboration with David Osborn and David Chandler. Our focus will be on the non-adiabatic transitions leading to the newly discovered S + O_2 channel and the product state distribution. We plan to construct a new DPEM for this system and explore the possible dissociation pathways leading to this minor channel.

We plan to collaborate with Truhlar on the collision-induced excitation in O + O_2, using a recently developed DPEM that include the facile exchange. The dynamics will be carried out by the semiclassical curvature-driven coherent switching with decay of mixing method.

Finally, we plan use the new DPEM for the HO_2 system to understand the nonadiabatic dynamics of the H + O_2 ↔ OH + O reaction and cold H + O_2 collisions. This reaction is strongly affected by conical intersections. The availability of the DPEM will enable accurate quantum mechanical studies of the nonadiabatic dynamics, particularly in cold collisions.

Donald G. Truhlar

We are currently working on new methods for discovering and fitting diabatic potential energy matrices. In particular, we have developed a dual-level parametrically managed direct diabatization by neural network scheme for fitting diabatic potential energy matrices of complex molecules, and we are applying it to *o*-fluorothiophenol.

We are also working on a new method for conserving zero-point energy in semiclassical simulations of photochemical processes.

We are also working on making the companion matrix method for diabatization more stable, minimizing the input information for direct diabatization by neural network, and improving the final-state analysis in the open-source ANT code for nonadiabatic dynamics.

Finally, we are working on a theorem delimiting the permitted and unpermitted permutational invariance properties of diabatic potential energy surfaces.

David R. Yarkony

Light-induced conical intersections were introduced by Cederbaum and coworkers. It was appreciated that this could move conical intersections and modify the outcome nonadiabatic dynamics. We will investigate using lasers to change the outcome of chemical reactions. Cederbaum showed how the interaction of an electric field with a molecular dipole can accomplish this. The incorporation of molecular dipole moments into the full set of electronic structure data will facilitate study of this process. Using light-induced shifted potential energy surfaces, Yarkony will investigate the intensity and polarization and pulse sequences needed to successfully modify reaction products using lasers. The students will involve nonadiabatic nuclear dynamics in collaboration with the Guo group. We will use the modified PDEMs to be constructed by Yarkony's group. These DPEMs are well suited for the repeated use required in this project. This project will also use DPEMs obtained by methods introduced by the Truhlar group.

For applications we will start with systems that exhibit weak spin-orbit coupling due to a large singlet/triplet separation. We will then shift the abundant singlets to reduce the singlet/triplet separation and increase| the production of spin-forbidden products.

CITED PUBLICATIONS

(1) Sun, G.; Han, S.; Zheng, X.; Song, Y.; Qin, Y.; Dawes, R.; Xie, D.; Zhang, J.; Guo, H. Unimolecular dissociation dynamics of electronically excited HCO($\tilde{A}^2A''$): rotational control of nonadiabatic decay. *Faraday Discuss.* **2022**, *238*, 236-248.

(2) Rösch, D.; Xu, Y.; Guo, H.; Hu, X.; Osborn, D. L. SO_2 photodissociation at 193 nm directly forms $S(^3P) + O_2(^3\Sigma_g^-)$: Implications for the Archean atmosphere on earth. *J. Phys. Chem. Lett.* **2023**, *14*, 3084-3091.

(3) Wang, Y.; Guo, H.; Yarkony, D. R. Internal conversion and intersystem crossing dynamics based on coupled potential energy surfaces with full geometry-dependent spin–orbit and derivative couplings. Nonadiabatic photodissociation dynamics of $NH_3(A)$ leading to the $NH(X^3\Sigma^-, a^1\Delta) + H_2$ channel. *Phys. Chem. Chem. Phys.* **2022**, *24*, 15060-15067.

(4) Guan, Y.; Xie, C.; Guo, H.; Yarkony, D. R. Toward a unified analytical description of internal conversion and intersystem crossing in the photodissociation of thioformaldehyde. I. Diabatic singlet states. *J. Chem. Theo. Comput.* **2023**, *19*, 6414-6424.

(5) Shu, Y.; Akher, F. B.; Guo, H.; Truhlar, D. G. Parametrically managed activation functions for improved global potential energy surfaces for six coupled $^5A'$ states and fourteen coupled $^3A'$ states of $O + O_2$. *J. Phys. Chem. A* **2024**, *128*, 1207-1217.

(6) Han, S.; de Oliveira-Filho, A. G. S.; Shu, Y.; Truhlar, D. G.; Guo, H. Semiclassical trajectory studies of reactive and nonreactive scattering of $OH(A\ ^2\Sigma^+)$ by H_2 based on an improved full-dimensional ab initio diabatic potential energy matrix. *ChemPhysChem* **2022**, *23*, e202200039.

(7) Zuo, J.; Zhang, D.; Truhlar, D. G.; Guo, H. Global potential energy surfaces by compressed-state multistate pair-density functional theory: The lowest doublet states responsible for the $N(^4S_u) + C_2(a\ ^3\Pi_u) \rightarrow CN(X\ ^2\Sigma^+) + C(^3P_g)$ reaction. *J. Chem. Theo. Comput.* **2022**, *18*, 7121-7131.

(8) Han, S.; Schröder, M.; Gatti, F.; Meyer, H.-D.; Lauvergnat, D.; Yarkony, D. R.; Guo, H. Representation of diabatic potential energy matrices for multiconfiguration time-dependent Hartree treatments of high-dimensional nonadiabatic photodissociation dynamics. *J. Chem. Theo. Comput.* **2022**, *18*, 4627-4638.

(9) Wang, J.; An, F.; Chen, J.; Hu, X.; Guo, H.; Xie, D. Accurate full-dimensional global diabatic potential energy matrix for the two lowest-lying electronic states of the $H + O_2 \leftrightarrow HO + O$ reaction. *J. Chem. Theo. Comput.* **2023**, *19*, 2929-2938.

(10) Wang, J.; Xie, C.; Hu, X.; Guo, H.; Xie, D. Impact of geometric phase on dynamics of complex-forming reactions: $H + O_2 \rightarrow OH + O$. *J. Physi. Chem. Lett.* **2024**, *15*, 4237-4243.

(11) Yang, D.; Liu, L.; Xie, D.; Guo, H. Full-dimensional quantum studies of vibrational energy transfer dynamics between H_2O and Ar: theory assessing experiment. *Phys. Chem. Chem. Phys.* **2022**, *24*, 13542-13549.

(12) Chen, Q.; Zhang, S.; Hu, X.; Xie, D.; Guo, H. Reaction pathway control via reactant vibrational excitation and impact on product vibrational distributions: The $O + HO_2 \rightarrow OH + O_2$ atmospheric reaction. *J. Phys. Chem. Lett.* **2022**, *13*, 1872-1878.

(13) Han, S.; Zhao, B.; Conte, R.; Malbon, C. L.; Bowman, J. M.; Yarkony, D. R.; Guo, H. Nonadiabatic reactive quenching of OH($A^2\Sigma^+$) by H_2: Origin of high vibrational excitation in the H_2O product. *J. Phys. Chem. A* **2022**, *126*, 6944-6952.
(14) Han, S.; Xie, C.; Hu, X.; Yarkony, D. R.; Guo, H.; Xie, D. Quantum dynamics of photodissociation: Recent advances and challenges. *J. Phys. Chem. Lett.* **2023**, *14*, 10517-10530.
(15) Pan, H.; Zhao, B.; Guo, H.; Liu, K. State-to-state dynamics in mode-selective polyatomic reactions. *J. Phys. Chem. Lett.* **2023**, *14*, 10412-10419.
(16) Song, H.; Guo, H. Theoretical insights into the dynamics of gas-phase bimolecular reactions with submerged barriers. *ACS Phys. Chem. Au* **2023**, *3*, 406-418.
(17) Shu, Y.; Truhlar, D. G. Generalized semiclassical Ehrenfest method: A route to wave function-free photochemistry and nonadiabatic dynamics with only potential energies and gradients. *J. Chem. Theo. Comput.* **2024**, *20*, 4396-4426.
(18) Shu, Y.; Zhang, L.; Chen, X.; Sun, S.; Huang, Y.; Truhlar, D. G. Nonadiabatic dynamics algorithms with only potential energies and gradients: Curvature-driven coherent switching with decay of mixing and curvature-driven trajectory surface hopping. *J. Chem. Theo. Comput.* **2022**, *18*, 1320-1328.
(19) Zhao, X.; Shu, Y.; Zhang, L.; Xu, X.; Truhlar, D. G. Direct nonadiabatic dynamics of ammonia with curvature-driven coherent switching with decay of mixing and with fewest switches with time uncertainty: An illustration of population leaking in trajectory surface hopping due to frustrated hops. *J. Chem. Theo. Comput.* **2023**, *19*, 1672-1685.
(20) Zhang, L.; Shu, Y.; Bhaumik, S.; Chen, X.; Sun, S.; Huang, Y.; Truhlar, D. G. Nonadiabatic dynamics of 1,3-cyclohexadiene by curvature-driven coherent switching with decay of mixing. *J. Chem. Theo. Comput.* **2022**, *18*, 7073-7081.
(21) Zhao, X.; Merritt, I. C. D.; Lei, R.; Shu, Y.; Jacquemin, D.; Zhang, L.; Xu, X.; Vacher, M.; Truhlar, D. G. Nonadiabatic coupling in trajectory surface hopping: Accurate time derivative couplings by the curvature-driven approximation. *J. Chem. Theo. Comput.* **2023**, *19*, 6577-6588.
(22) Shu, Y.; Zhang, L.; Truhlar, D. G. ANT 2023: A program for adiabatic and nonadiabatic trajectories. *Comput. Phys. Commun.* **2024**, *296*, 109021.
(23) Shu, Y.; Zhang, L.; Truhlar, D. G. *SHARC-MN version 1.0 (https://sharc-md.org)*; University of Minnesota, 2020.
(24) Shu, Y.; Truhlar, D. G. Diabatization by machine intelligence. *J. Chem. Theo. Comput.* **2020**, *16*, 6456-6464.
(25) Shu, Y.; Varga, Z.; Parameswaran, A. M.; Truhlar, D. G. Fitting of coupled potential energy surfaces via discovery of companion matrices by machine intelligence. *J. Chem. Theo. Comput.* **2024**, *20*, 7042-7051.
(26) Shu, Y.; Zhang, L.; Wu, D.; Chen, X.; Sun, S.; Truhlar, D. G. New gradient correction scheme for electronically nonadiabatic dynamics involving multiple spin states. *J. Chem. Theo. Comput.* **2023**, *19*, 2419-2429.
(27) Sun, Y.; Long, B.; Truhlar, D. G. Unimolecular reactions of e-glycolaldehyde oxide and its reactions with one and two water molecules. *Research* **2023**, *6*, 0143.
(28) Long, B.; Xia, Y.; Zhang, Y.-Q.; Truhlar, D. G. Kinetics of sulfur trioxide reaction with water vapor to form atmospheric sulfuric acid. *J. Am. Chem. Soc.* **2023**, *145*, 19866-19876.

(29) Shu, Y.; Varga, Z.; Zhang, D.; Truhlar, D. G. ChemPotPy: A Python library for analytic representations of potential energy surfaces and diabatic potential energy matrices. *J. Phys. Chem. A* **2023**, *127*, 9635-9640.
(30) Lin, H.; Zhang, Y.; Pezeshki, S.; Duster, A. W.; Wang, B.; Wu, X.-P.; Zheng, S.-W.; Gagliardi, L.; Truhlar, D. G. QMMM 2023: A program for combined quantum mechanical and molecular mechanical modeling and simulations. *Comput. Phys. Comm.* **2024**, *295*, 108987.
(31) Li, H.; Mansoori Kermani, M.; Ottochian, A.; Crescenzi, O.; Janesko, B. G.; Truhlar, D. G.; Scalmani, G.; Frisch, M. J.; Ciofini, I.; Adamo, C. Modeling multi-step organic reactions: can density functional theory deliver misleading chemistry? *J. Am. Chem. Soc.* **2024**, *146*, 6721-6732.
(32) Shu, Y.; Truhlar, D. G. Improved local-mode zero-point-energy conservation scheme for quasiclassical trajectories. *J. Phys. Chem. A* **2024**, *128*, 3625-3634.
(33) Wang, H.; Guan, J.; Gao, J.; Zhang, J.; Xu, Q.; Xu, G.; Jiang, L.; Xing, L.; Truhlar, D. G.; Wang, Z. Direct observation of covalently bound clusters in resonantly stabilized radical reactions and implications for carbonaceous particle growth. *J. Am. Chem. Soc.* **2024**, *146*, 13571-13579.
(34) Gao, Q.; Shen, C.; Zhang, H.; Long, B.; Truhlar, D. G. Quantitative kinetics reveal that reactions of HO2 are a significant sink for aldehydes in the atmosphere and may initiate the formation of highly oxygenated molecules via autoxidation. *Phys. Chem. Chem. Phys.* **2024**, *26*, 16160-16174.
(35) Long, B.; Xia, Y.; Truhlar, D. G. Quantitative kinetics of HO_2 reactions with aldehydes in the atmosphere: high-order dynamic correlation, anharmonicity, and falloff effects are all important. *J. Am. Chem. Soc.* **2022**, *144*, 19910-19920.
(36) Zhong, H.; Meng, Q.; Mei, B.; Thawko, A.; Yan, C.; Liu, N.; Mao, X.; Wang, Z.; Wysocki, G.; Truhlar, D. G.; Ju, Y. Kinetics and mechanism of the singlet oxygen atom reaction with dimethyl ether. *J. Phys. Chem. Lett.* **2024**, *15*, 6158-6165.
(37) Shu, Y.; Varga, Z.; Kanchanakungwankul, S.; Zhang, L.; Truhlar, D. G. Diabatic states of molecules. *J. Phys. Chem. A* **2022**, *126*, 992–1018.
(38) Zhang, R. M.; Chen, W.; Truhlar, D. G.; Xu, X. Master equation study of hydrogen abstraction from HCHO by OH via a chemically activated intermediate. *Faraday Disc.* **2022**, *238*, 431-460.
(39) Xia, Y.; Long, B.; Lin, S.; Teng, C.; Bao, J. L.; Truhlar, D. G. Large pressure effects caused by internal rotation in the s-cis-syn-acrolein stabilized Criegee intermediate at tropospheric temperature and pressure. *J. Am. Chem. Soc.* **2022**, *144*, 4828-4838.
(40) Wang, P.-B.; Truhlar, D. G.; Xia, Y.; Long, B. Temperature-dependent kinetics of the atmospheric reaction between CH_2OO and acetone. *Phys. Chem. Chem. Phys.* **2022**, *24*, 13066-13073.
(41) Xia, Y.; Long, B.; Liu, A.; Truhlar, D. G. Reactions with criegee intermediates are the dominant gas-phase sink for formyl fluoride in the atmosphere. *Fundamental Res.* **2023**, *in press*.
(42) Zhang, R. M.; Xu, X.; Truhlar, D. G. Observing intramolecular vibrational energy redistribution via the short-time Fourier transform. *J. Phys. Chem. A* **2022**, *126*, 3006-3014.
(43) Zhang, L.; Shu, Y.; Xing, C.; Chen, X.; Sun, S.; Huang, Y.; Truhlar, D. G. Recommendation of orbitals for G_0W_0 calculations on molecules and crystals. *J. Chem. Theo. Comput.* **2022**, *18*, 3523-3537.

(44) Xing, L.; Lian, L.; Wang, Z.; Cheng, Z.; He, Y.; Cui, J.; Truhlar, D. G. Lowering of reaction rates by energetically favorable hydrogen bonding in the transition state. Degradation of biofuel ketohydroperoxides by OH. *J. Am. Chem. Soc.* **2022**, *144*, 16984-16995.
(45) Chen, W.; Zhang, P.; Truhlar, D. G.; Zheng, J.; Xu, X. Identification of torsional modes in complex molecules using redundant internal coordinates: The multistructural method with torsional anharmonicity with a coupled torsional potential and delocalized torsions. *J. Chem. Theo. Comput.* **2022**, *18*, 7671-7682.
(46) Shu, Y.; Truhlar, D. G. Decoherence and Its Role in Electronically Nonadiabatic Dynamics. *J. Chem. Theo. Comput.* **2023**, *19*, 380-395.
(47) Hu, Z.; Di, Q.; Liu, B.; Li, Y.; He, Y.; Zhu, Q.; Xu, Q.; Dagaut, P.; Hansen, N.; Sarathy, S. M.; et al. Elucidating the photodissociation fingerprint and quantifying the determination of organic hydroperoxides in gas-phase autoxidation. *Proc. Natl. Acad. Sci. U. S. A.* **2023**, *120*, e2220131120.
(48) Ning, J.; Truhlar, D. G. Electronic Excitation of ortho-Fluorothiophenol. *J. Phys. Chem. A* **2023**, *127*, 1469-1474.
(49) Guan, Y.; Yarkony, D. R.; Zhang, D. H. Permutation invariant polynomial neural network based diabatic ansatz for the (E + A) × (e + a) Jahn–Teller and Pseudo-Jahn–Teller systems. *J. Chem. Phys.* **2022**, *157*, 014110.

Integrated Data-driven Methods for Scientific Discovery of Non-equilibrium Thermochemical Processes in Complex Environments from Ultrafast X-ray Measurements at LCLS

Matthias Ihme, Stanford University (Principal Investigator) mihme@stanford.edu
Eric Darve, Stanford University (Co-Investigator)
Stefano Ermon, Stanford University (Co-Investigator)
Dimosthenis Sokaras, SLAC National Accelerator Laboratory (Co-Investigator)
Jana Thayer, SLAC National Accelerator Laboratory (Co-Investigator)
Adrianus van Duin, Penn State University (Co-Investigator)
Diling Zhu, SLAC National Accelerator Laboratory (Co-Investigator)

1 Program Scope

Recent advances achieved with the ultrafast coherent X-ray-Free Electron Laser at the Linac Coherent Light Source (LCLS) have enabled to probe non-equilibrium processes at atomistic scales with femtosecond (fs) temporal resolution. However, despite unprecedented LCLS capabilities, the enormous complexity, data volume, and experimental access constitute major challenges for scientific discovery. The proposed research will directly tackle this urgent issue by developing novel techniques to enable ultrafast X-ray Photon Correlation Spectroscopy (XPCS) measurements that are closely supported through atomistic-scale simulations to discover non-equilibrium processes and chemical reactions of fluids at supercritical conditions. In the following, we outline major research progress and scientific progress towards improving the fundamental understanding of ultrafast physico-chemical process in supercritical fluids, pertaining to non-polar interaction of mixtures, collective motion, transport processes, and ionization in water, CO2, Ethanol, and mixtures.

2 Research Progress

2.1 Examination of strong-field Ionization of water by ultrafast X-ray pump/X-ray probe

The radiolysis of liquid water is fundamental to several biological and engineering applications. While the ultrafast processes underlying valence ionization and excitation by laser and optical pulses has been studied in the past [Lin, 2021], the ultrafast structural response and decay subject to intense, high-energy X-ray radiation remains largely unknown. This is of relevance in nuclear power plant cooling and design in addition to long-duration space travel.

As part of an experimental campaign conducted at the SPring-8 Angstrom Compact free electron LAser (SACLA) in Japan, we conducted X-ray pump X-ray probe experiments on a sample of pure liquid water maintained at elevated (50, 150, and 225 bar) pressure and ambient temperature (30 C). The X-ray energy delivered to the sample was measured at 10 keV. By varying the time delay between the pump and probe pulses, the time evolution of the signal was recorded and analyzed. After background subtraction, the dynamics are isolated and plotted in **Figure 2.1.A**.

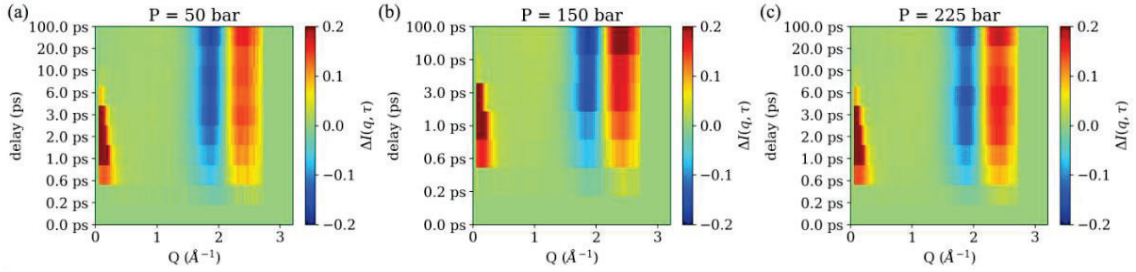

Figure 2.1: *Two-dimensional contour plots showing the response of liquid water as a function of Q and time delay. Contours are coloured by the difference in the normalized intensity from the equilibrium structure, ΔI; different panels show the response at different pressure conditions.*

From **Figure 2.1**, we note the appearance of a previously unseen structure in the low-Q domain between Q = 0.1 and 0.5 $Å^{-1}$. This relatively large nanoscale structure first becomes dominant at 600 fs. The signal shifts to lower Q values as the time delay increases, signifying an expansion in the system. On average, the collective motion of the ions is expanding at a rate of 400 m/s. At the same time, on the time scale of a few picoseconds, recombination and neutralization events in liquid water take place. This contributes to the diminishing of the signal and its decay after 6 ps.

In the high-Q domain surrounding the water peak, we note the presence of a negative of positive signature in the dynamics. This signifies the shift of the water peak to larger Q values, i.e., smaller O-O bond distances. The shift is in line with previous studies, and we quantify the temperature jump in the sample to be 20 K [Zarkadoula, 2022]. Together with the low-Q observations, we identify a new mechanism by which the water molecules relax. Moreover, we identify a region where the ionization is localized, and the remainder of the water molecules maintain their H-bond network albeit at a slightly elevated temperature.

2.2 X-ray Photon Correlation Spectroscopy of supercritical CO2

Supercritical fluids (SCFs), near the liquid-gas critical point, exhibit unique behavior in thermodynamic and transport properties, which makes them attractive for several engineering applications including carbon sequestration, polymer synthesis, chemical processing and biomass gasification. The variation in thermodynamic and transport properties in SCFs have been attributed to their structural heterogeneity which manifests as molecular clusters.

While the static structure of the clusters and their connection to thermodynamic properties have been studied rigorously using high energy X-ray and neutron scattering experiments, experimental studies on cluster dynamics and their influence on transport processes in SCFs are still missing. At the characteristic cluster length scales of about 1 nm, dynamics occur at picosecond timescales. Capturing such ultrafast motion has been the major challenge towards the study of cluster dynamics in SCFs.

We overcome this challenge by using the split pulse XPCS (sp-XPCS) technique [Li, 2021]. Combining this method with the high intensity 10 fs X-ray pulses at LCLS, we can achieve nanometer-picosecond spatiotemporal resolution. The measurements were carried out at the XPP instrument at LCLS. Using the sp-XPCS technique, we studied the cluster dynamics in supercritical CO2. The experimental setup is shown in **Figure 2.2 A (a)** wherein the XFEL pulse is split into two using the split delay optics and then passed through the sample which is maintained at 308.2 K and 7.5 bar using our pressure cell [Muhunthan, 2024]. The scattered signal is recorded using a set of four ePix100 detectors covering a Q range of 0.01 $Å^{-1}$ – 0.1 $Å^{-1}$. We measured the sample dynamics at 4, 8 and 13 ps. The results obtained here are the first direct observation of ultrafast cluster dynamics in SCFs.

The intermediate scattering function (ISF) is the primary quantity measured from XPCS. This is a density autocorrelation function and its decay with time delay gives information about the timescale and nature of the dynamics. We also obtained the ISF by performing large scale molecular dynamics (MD) simulations and the results from XPCS and MD are shown in **Figure 2.2 A (b)**. The ISF shows a non-exponential behavior which indicates the measured dynamics is not simple diffusion [Kawaski, 1970].

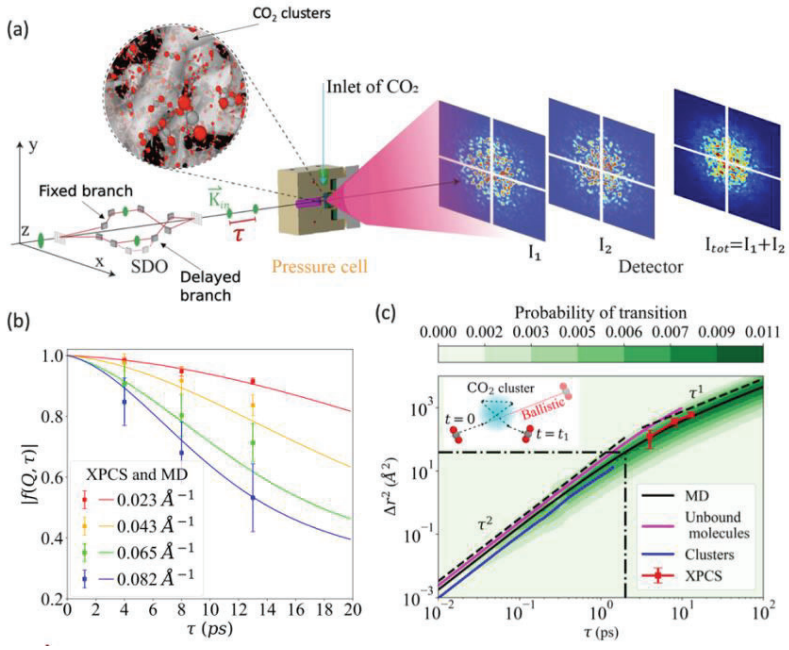

Figure 2.2 A: *(a) Schematic of sp-XPCS experiment. scCO2 was kept at 308.2 K and 7.5 MPa in the pressure cell and the scattered photons from the sample were recorded with an assembly of four ePix100 detectors. (b) Comparison of intermediate scattering function f (Q, τ) obtained from sp-XPCS measurements with MD trajectories for different Q values. (c) Mean square displacement ⟨Δr²(τ)⟩ vs. Time delay τ from sp-XPCS measurements and MD simulations. The contour plot shows the probability of transition to liquid phase for 500,000 molecular trajectories that are initially in the gas phase. The horizontal black dash-dotted line corresponds to the square of the gas molecule displacement before interacting with a cluster as obtained from kinetic theory. The inset in the top left corner shows a schematic of the interaction between an unbound molecule with a cluster between time t = 0 and t_1. The molecular trajectory is shown by the black dashed line. The red dotted line shows the ballistic trajectory of the molecule if it does not interact with the cluster.*

To further understand the origin of the observed dynamics, we analyze the MD trajectories and obtain the clusters in the system using Hill's energy criterion [Hill, 1955]. To characterize the dynamics, we also calculate the mean square displacement (MSD) from both MD and XPCS and the results are shown in **Figure 2.2 A (c)**. Based on the MSD, we conclude that the observed dynamics lies at the crossover region from ballistic motion to diffusion. This explains the observed non-exponential behavior. We also conclude, by obtaining the MSD for molecules inside and outside clusters, that the unbound molecules move faster than molecules bounded inside cluster. Upon obtaining the probability of transition of molecules from unbound state to cluster, we observe that the ballistic to diffusion crossover occurs when the probability of transition maximizes. Based on these results, we confirm that the ballistic to diffusion crossover occurs when unbound molecules interact with clusters and undergo a slowdown, as depicted by the schematic in **Figure 2.2 A (c)** inset. Our results showcase the influence of cluster dynamics on transport processes in SCFs and provide improved fundamental understanding about molecular motion in the presence of clusters.

2.3 Hard X-ray Transient Grating

The fundamental origin of the challenge studying dynamical processes in amorphous systems including gas and liquids lies in the lack of long-range periodicity, which prevents the efficient utilization of laser techniques to study dynamics of a specific length scales. If one can create an artificial periodicity in the sample on the length scale of interests, one could use coherence diffraction to study the sample dynamics.

We are particularly interested in the microscopic dynamics on the sub-10nm length scales and picosecond time scale. Therefore, we would like to create periodic perturbation of the sample on the sub-10nm length scales which is only enabled by the hard X-ray free electron lasers (FELs). The technique in which we implement this idea is summarized in **Figure 2.3 A**, which is called hard X-ray transient grating (TG) [Rouxel, 2024]. In the TG measurement, we overlap two coherent hard X-ray pulses on the sample in both space and time. Therefore, they generate an interference pattern. This interference pattern perturbs the sample periodically. When the third pulse, the probe pulse arrives at

the sample, the periodically perturbed sample will diffract the probe pulse as if a grating, which comes the name of transient grating.

In our demonstration experiment at XPP at LCLS, a crystalline sample $SrTiO_3$ is used for the simplicity of the data interpretation and the great potential of using $SrTiO_3$ as catalysis in chemical reactions. As shown in **Figure 2.3.A (d)**, with significant enhancement of the scattering intensity at the pixel corresponding to the TG periodicity on the detector indicates the generation of the long-range periodic perturbation of the $SrTiO_3$. For the first time, we obtain the capability to establish an artificial long range order in a bulk sample in a non-intrusive way.

By comparing the rocking curve of the Bragg peak of the crystal and the TG peak generated by the TG pump pulses, we can prove that the artificial long-range order from the interference pattern has a higher perfection and the crystalline order of $SrTiO_3$ since the angular divergence of the TG peak as shown in **Figure 2.3.A (d)** is dominated by the crystalline defects of the $SrTiO_3$ sample.

While currently, the technique is demonstrated in the crystalline sample, the optic principle and technique apply equally to amorphous systems including both gas phase and liquid phase conditions. Therefore, by applying this technique to gas phase and liquid phase samples, we expect to be able to measure the sub-10nm thermal [Hofmann, 2019] and chemical dynamics [Brown, 1999] which is beyond the reach of other techniques.

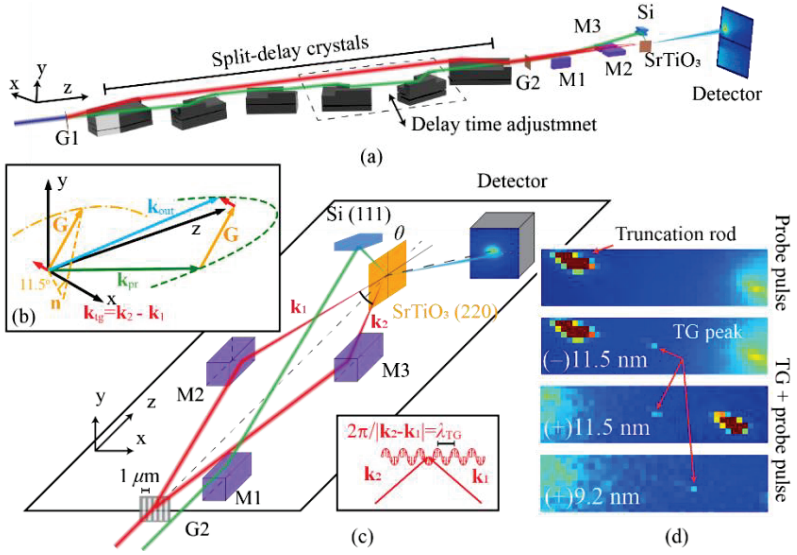

Figure 2.3.A: *(a) Schematics of the experiment downstream the focusing lens. The incident X-ray pulse propagates along the z axis and is shown with the dark blue line. Red lines indicate the pump pulse while the green line indicates the probe pulse. The two pump pulses generate an interference pattern on the sample after M2 and M3. The interference pattern perturbs the sample periodically which acts as if a grating which is the transient grating (TG). This TG diffracts the probe pulse which is recorded by the 2D detector. (b) Illustration of the phase matching condition of the TG signal. (c) Detailed schematics of the X-ray optics downstream of the split-delay crystals. (d) Measured TG signal on the 2D detector in 4 different scenarios. The (+) and (-) sign indicates the relative angular position of the sample crystal rotating around* ***n*** *as shown in Figure 2 (b). The number with unit indicates the corresponding TG period.*

2.4 Inelastic X-ray Scattering of CO2

A recent experimental study on supercritical water using Inelastic X-ray Scattering (IXS) showed that the SCFs near the Widom line simultaneously exhibit liquid-like and gas-like features by obtaining two acoustic modes in their measurement [Sun, 2020]. The low frequency mode corresponds to the gas-like component while the high-frequency mode corresponds to the liquid-like component. Their results also demonstrated that the high-frequency component becomes more dominant as one moves from gas-like thermodynamic conditions to liquid-like conditions across the Widom line.

While the two components exist in water and have been tied to the existence of hydrogen bond, not all SCFs have hydrogen bonds. However, molecular simulations show the presence of the two component dynamics in other SCFs as well [Sun, 2021]. Thus, the microscopic origin behind the existence of two component acoustic modes in SCFs is still unclear.

Our hypothesis behind the existence of two component dynamics is the presence of clusters in SCFs. These clusters create liquid-like and gas-like regions in the microstructure of SCFs, leading to the observation of two acoustic modes.

To verify this hypothesis, we performed IXS measurements of supercritical CO2. The experiments were carried out the ID28 beamline of the ESRF at Grenoble, France. The X-rays from the synchrotron were monochromatized using Si (11,11,11) backscattering monochromator and then passed through the sample which was stored in a pressure cell [Bencivenga, 2007]. The scattered signal is made to reflect from the Si (11,11,11) analyzer which provides an energy resolution of 1.5 meV. The sample was kept at 88.3 bars pressure and temperature varied from 283 K to 342 K. At each thermodynamic conditions, the intensity was measured from –25 meV to +25 meV energy range at Q range of 0.7 $Å^{-1}$ – 2.0 $Å^{-1}$. We also performed MD simulations to gain insight into the molecular motion in clusters. The results from IXS and MD are shown in **Figure 2.4 A**. The intensity obtained by the two methods show good agreement as observed in **Figure 2.4 A** (a). With increase in temperature, the intensity changes from a Lorentzian to a Gaussian shape, indicating a crossover from liquid-like to a gas-like behavior. The current correlation function, which is a correlation of momentum, is shown in **Figure 2.4 A** (b) for MD simulations for increasing temperature from blue to red curve. The blue curve shows a shoulder around 10 meV which gradually vanishes with rise in temperature. This feature corresponds to the high frequency liquid-like component while the low frequency peak, near 2.5 meV, corresponds to to the gas-like component. We perform non-negative matrix factorization (NMF) of the data and report the two components in **Figure 2.4 A** (c). The peak in current correlation function corresponds to acoustic mode and as such, the results from NMF analysis indicate the existence of two acoustic modes in the system. By performing cluster analysis on the MD trajectories, we obtain the liquid fraction x_L, which is defined as the fraction of molecules inside clusters of size 4 and above. Upon comparing the fraction of high-frequency component, denoted by f, with x_L in **Figure 2.4 A** (d) we observe a linear correlation between the two for both IXS and MD. This indicates that the existence of two-component dynamics is strongly coupled with the presence of clusters in the system.

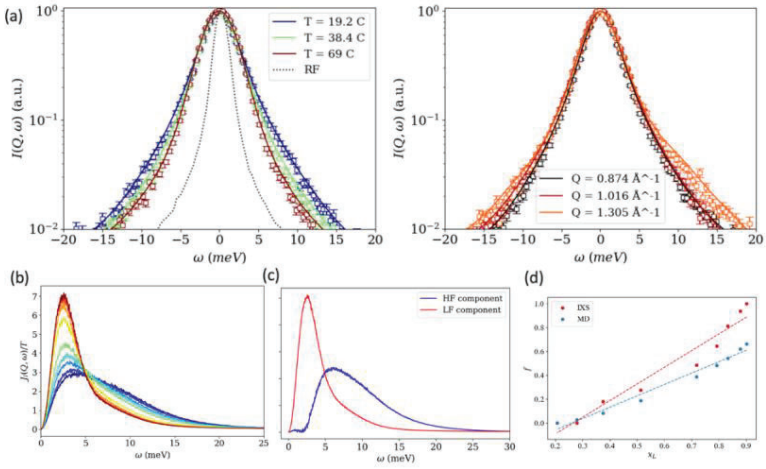

Figure 2.4 A: *(a) Intensity from IXS (symbols) and MD simulations (solid lines). Left panel shows the temperature trend at 88.3 bar pressure and Q = 1.016 $Å^{-1}$. The black dotted line shows the resolution function (RF). Right panel shows the variation of intensity with Q at P = 88.3 bars and T = 302 K. (b) Current correlation function from MD simulations at Q = 1.016 $Å^{-1}$ and P = 88.3 bar with increasing temperature from blue (293 K) to red (342 K). (c) Low frequency (LF) and high frequency (HF) component of the current correlation functions in (b) obtained via non-negative matrix factorization. (d) Fraction of HF component f for different temperatures compared against the liquid fraction x_L, which is the fraction of molecules inside clusters of size 4 and above. Both MD and IXS show a linear correlation between f and x_L.*

2.5 WAXS and MD simulation of supercritical ethanol-CO_2 mixture

While significant progress has been made on studying properties of pure fluids at supercritical conditions, fundamental questions concerning the microstructure and dynamic response in mixtures of

supercritical fluids remain. Among these systems, the binary mixture of ethanol and carbon dioxide has attracted considerable attention due to its relevance in a wide range of industrial processes, including supercritical extraction of thermal labile compounds, dehydration of alcohols using supercritical, and extraction of natural products using near critical solvents [Skarmoutsos, 2007]. The unique interactions between ethanol, a polar hydrogen-bonding molecule, and CO_2, a nonpolar molecule, give rise to complex molecular arrangements that are sensitive to temperature, pressure, and composition [Mareev, 2021].

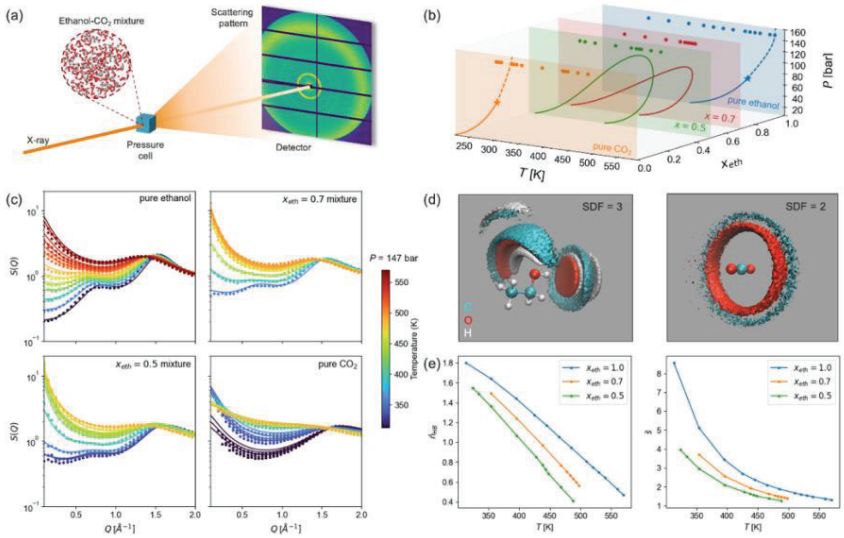

Figure 2.5 *(a) Schematic of the WAXS experiment. (b) Experimental conditions (dots) mapped onto the P-T-x phase diagram. (c) Structure factor of the mixture at different composition and thermodynamic conditions. Lines represent measurements from WAXS, and dots represent results from MD simulations. (d) Isosurfaces of the spatial distribution function (SDF) for the mixture (x = 0.5, P = 147 bar, T = 354 K). (e) The effect of temperature and compostion on the mean number of hydrogen bonds per ethanol molecule and mean number of ethanol molecules per hydrogen-bonded chain.*

We have performed Wide Angle X-ray Scattering (WAXS) investigations in the range of $0.1Å^{-1}<Q<2.0Å^{-1}$ to probe the microscopic structure of ethanol-CO_2 mixture under supercritical conditions across multiple mixing fractions, as illustrated in **Figure 2.5(a-b)**. The experiments were conducted at SSRL Beamline 4-2 at SLAC National Accelerator Laboratory. The structure factors, $S(Q)$, derived from the WAXS measurements are illustrated in **Figure 2.5(c)**. The emergence of a distinct inner peak in $S(Q)$ at $Q \approx 0.75$ $Å^{-1}$, attributed to correlations between hydrogen-bonded ethanol molecules [Tomšič, 2007], signifies that ethanol forms a non-ideal mixture with CO_2. This behavior is primarily driven by strong ethanol-ethanol interactions and the presence of hydrogen bonds.

To complement the experimental findings, molecular dynamics (MD) simulations were performed, and the binary interaction parameters of the force field were calibrated using the experimental $S(Q)$ values. The close agreement between the experimental and simulated $S(Q)$ confirms the accuracy of the model, allowing us to compute the spatial distribution functions (SDFs) for the mixtures, which provides information of the orientation and positioning of the local structure. **Figure 2.5(d)** presents a typical SDF, revealing the chain-like hydrogen bonding structures formed by ethanol molecules. To further explore the impact of CO_2 concentration on the structural arrangement of the mixture, we analyzed the hydrogen-bonding topology. The results, illustrated in **Figure 2.5(e)**, show a reduction in the number of hydrogen bonds per ethanol molecule and a decrease in the average size of hydrogen-bonded chains as the CO_2 fraction increases. Additionally, analysis of the partial SDFs suggests that the local arrangement of CO_2 around ethanol reduces the possibility of an ethanol molecule forming a hydrogen bond as an acceptor, thus disrupting the hydrogen-bonding network.

2.6 Small-Angle X-ray Scattering of CO2

Supercritical CO_2 (sCO_2) shows strong sensitivities to changes in thermodynamic properties and exhibits both liquid-like and gas-like behaviors. This anomalous behavior mainly arises from an increase in thermal density fluctuations [Nishikawa, 2004], which result from the molecular transfer between clusters in the fluid. With liquid-like density and gas-like viscosity, sCO_2 can be used as a green solvent in many chemical processes including polymer synthesis and hazardous waste destruction. We performed Small Angle X-ray Scattering (SAXS) measurements of sCO_2 (critical point 7.38 MPa, 304.2 K) at the SSRL Beamline 4-2 at SLAC National Accelerator Laboratory. SAXS enables the study of materials at microscopic dimensions (10^{-9} to 10^{-6} m). We use SAXS to characterize the structural heterogeneities (clusters) in supercritical CO_2 near the critical point and crossing the Widom line.

During the SAXS measurements, the sCO_2 was contained in a high-pressure cell. The pressurized fluid (CO_2, 99.999%) was supplied by a syringe pump (Teledyne ISCO 100DM) and confined between two 100 μm-thick diamond windows in the cell [Muhunthan, 2024]. Deviations in the temperature and pressure during one measurement were within $\Delta T = \pm 0.1$ K and $\Delta P = \pm 0.01$ MPa, respectively. The X-ray energy during the experiments was 15 keV, and the sample to detector distance was 2.5 m. For one P, T condition, the total measurement time was approximately 6 minutes. The 1-D SAXS curves were averaged over 50 data frames after background subtraction of scattering from the empty pressure cell.

The scattering intensity obtained between momentum transfer (Q) of 0.03-0.15 $Å^{-1}$ for sCO_2 at 308 K is plotted in **Figure 2.6(a)**. An increase in density fluctuations in sCO_2 near the critical point and near the Widom line leads to a non-monotonic increase in the SAXS scattering intensity with pressure. We used the Unified Fit [Beaucage, 1995] theory to analyze the size and shape of clusters formed in sCO_2. The size of the clusters was quantified by the radius of gyration, R_g, defined as the root-mean-squared distance from the cluster's center of gravity. **Figure 2.6(b)** plots the average cluster size R_g as a function of pressure and temperature. At each isotherm, lower pressures correspond to the low-density region of sCO_2. The R_g is small at these conditions, and the average cluster size is approximately 10 Å in this region (Fig. 2.6(b)). The R_g increases with increasing pressure, reflecting the formation of larger clusters close to the Widom line. The R_g decreases with further increases in pressure to the high-density region of sCO_2. Based on molecular dynamics (MD) simulations (Simeski 2023), this behavior may be due to the formation of large, percolating clusters in the fluid. Since SAXS is sensitive to electron density variations, the large percolating clusters essentially form a homogeneous medium in the fluid, and it is the smaller clusters not contained in the percolating clusters that lead to a decrease in R_g at high pressure.

The average shape of the clusters can also be determined from Unified Fit theory. **Figure 2.6(c)** plots the primary cluster shape at each condition. At 308 K and 310.5 K, the primary cluster shape is sphere-like for all pressures. However, at 313 K and 316 K, the primary cluster shape changes to disk-like for certain pressures above and below the Widom line. The R_g is small at these conditions, and the average cluster contains only a few CO_2 molecules. In this case, a disk-like shape may be the preferred configuration, since there are not enough molecules to form a higher-dimension shape such as a sphere. For conditions around the Widom line, the R_g is large, indicating the presence of larger clusters with more CO_2 molecules. In this case, a sphere-like cluster shape may be preferred, since this configuration minimizes the surface energy of the cluster and makes it more stable.

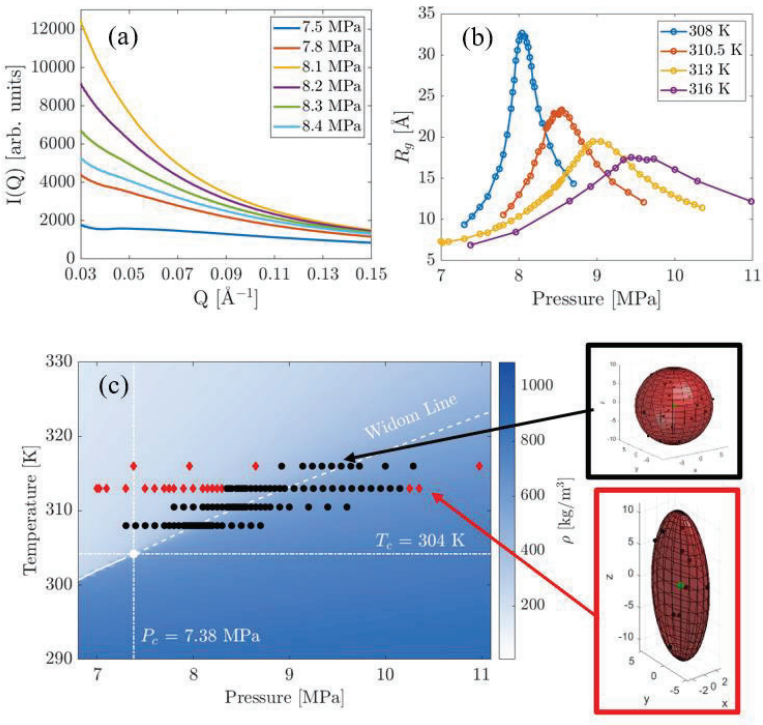

Figure 2.6.A (a) SAXS intensity curves for sCO_2 at 308 K. (b) Average cluster size (R_g) as a function of pressure and temperature. (c) Phase diagram and primary cluster shape of sCO_2. The symbol color indicates the primary shape of the cluster at that condition: sphere-like (black), disk-like (red). The white circle is the critical point of CO_2, the solid white line is the liquid-vapor coexistence line, and the dashed line is the Widom line, defined with respect to the maximum isobaric heat capacity. Density data and critical properties were retrieved from the NIST database.

Publications and visibility from this research

- M. Ihme, W. T. Chung, and A. A. Mishra, "Combustion machine learning: Principles, progress and prospects." Progress in Energy and Combustion Science, 91, 101010, 2022.
- K. Younes, M. Poli, P. Muhunthan, S. Ermon, and M. Ihme, "Rapid, online screening of complex phase spaces using Bayesian Optimization for SAXS measurements," Nuclear Inst. and Methods in Physics Research, A, 2023.
- P. Sharma, W. T. Chung, B. Akoush, and M. Ihme, "A Review of Physics-Informed Machine Learning in Fluid Mechanics." Energies, 16, 2343, 2023.
- N. Ly and M. Ihme, "Matters Arising: Stable Supercritical Interfaces Do Not Exist Without Surface Tension." Accepted Nature Communications, 2024.
- J. Z. Ho, M. Talei, D. Brouzet, W. T. Chung, P. Sharma, M. Ihme, "Predictions of instantaneous temperature fields in jet-in-hot-coflow flames using a multi-scale U-Net model." Proceedings of the Combustion Institute, 40, 2024, 105311.
- J.A.C. Kildare, W. T. Chung, M. J. Evans, Z. F. Tian, P. R. Medwell, and M. Ihme, "Predictions of instantaneous temperature fields in jet-in-hot-coflow flames using a multi-scale U-Net model." Proceedings of the Combustion Institute, 40, 2024, 105330.
- P. Muhunthan, H. Li, G. Vignat, E.R. Garza, K. Younes, Y. Sun, D. Sokaras, T. Weiss, I. Rajkovic, T. Osaka, I. Inoue, S. Song, T. Sato, D. Zhu, J. L. Fulton, M. Ihme. "A versatile pressure-cell design for studying ultrafast molecular-dynamics in supercritical fluids using coherent multi-pulse x-ray scattering." Review of Scientific Instruments, 2024. 95 (1): 013901.
- F. Li, W. Zhang, B. Bai, and M. Ihme, "Small-scale turbulent characteristics in transcritical wall-bounded flows." Journal of Fluid Mechanics, 986, A36, 2024.

- M. Ihme and W. T. Chung, “Artificial intelligence as a catalyst for combustion science and engineering.” Proceedings of the Combustion Institute, 40, 105730, 2024.
- F. Li, W. Zhang, and M. Ihme, “Mechanisms and models of the turbulent boundary layers at transcritical conditions” Under review.
- A. Majumdar, H. Li, P. Muhunthan, A. Späh, S. Song, Y. Sun, M. Chollet, D. Sokaras, D. Zhu, and M. Ihme. “Direct observation of ultrafast cluster dynamics in carbon dioxide at supercritical conditions using X-ray Photon Correlation Spectroscopy”, (Under review).
- J. Fan, N. Ly, and M. Ihme, “Cluster-structure dynamical model for describing nonlinear thermodynamic behavior in supercritical fluids.” Under review.
- Ihme, M. “Machine learning methods for reacting flows at macro and micro-scales.” Telluride workshop “Machine Learning and Informatics for Chemistry and Materials” September 2021.
- A. Majumdar, H. Li, Y. Sun, A. Späh, P. Muhunthan, D. Sokaras, D. Zhu and M. Ihme. "Examining molecular cluster dynamics of supercritical CO_2 using ultrafast XPCS. " APS March Meeting Abstracts 2023.
- M. Poli, S. Massaroli, E. Nguyen, D. Y. Fu, T. Dao, S. Baccus, Y. Bengio, C. Ré, S. Ermon "Hyena Hierarchy: Towards Larger Convolutional Models". roceedings of the 40th International Conference on Machine Learning, Honolulu, Hawaii, USA. PMLR 202, 2023.
- H. Li, S. Song, T. Sato, Y. Sun, N. Wang, S. She, A. Maznev, S. Teitelbaum, J. Hastings, K. Nelson, D. Reis, M. Ihme and D. Zhu. " Sub-10nm Hard X-ray Transient Grating and its Application in Crystalline Samples". 15th International Conference on Synchrotron Radiation Instrumentation, contributed talk, 2024
- K. Younes, H. Li, Y. Sun, S. Song, T. Osaka, I. Inoue, D. Zhu, M. Ihme, “Ultrafast Structural Reorganization of Supercritical Water Molecules Under XFEL Radiation”. Bulletin of the American Physical Society, 2024
- K. Younes, H. Li, Y. Sun, S. Song, T. Osaka, I. Inoue, P. Ho, D. Zhu, M. Ihme, “Observing the Ultrafast Structural Response of Liquid Water Subject to Strong XFEL Radiation”. 15th International Conference on Synchrotron Radiation Instrumentation, contributed talk, 2024.
- K. Younes, M. Poli, P. Muhunthan, S. Ermon, and M. Ihme, “Rapid, online screening of complex phase spaces using Bayesian Optimization for SAXS measurements,” 15th International Conference on Synchrotron Radiation Instrumentation, invited talk, 2024.
- A. Majumdar, H. Li, P. Muhunthan, A. Späh, S. Song, Y. Sun, M. Chollet, D. Sokaras, D. Zhu, and M. Ihme. "Examining molecular cluster dynamics in supercritical fluids using split-pulse XPCS." Bulletin of the American Physical Society, 2024.

References

1) Neiswanger, W., Wang, K. A., Ermon, S., Proceedings of the 38th International Conference on Machine Learning, PMLR 139:8005-8015 (2021)
2) Mareev, E.I., Sviridov, A.P., Gordienko, V.M., The Anomalous Behavior of Thermodynamic Parameters in the Three Widom Deltas of Carbon Dioxide-Ethanol Mixture. Int. J. Mol. Sci., 22, no. 9813 (2021)
3) Tsuzuki et al. Journal of Chemical Physics 109 (1998): 2169-2175
4) Lomb L, Barends T R M, Kassemeyer S, et al. Radiation damage in protein serial femtosecond crystallography using an x-ray free-electron laser. Physical Review B, 2011, 84(21): 214111.
5) Garrett B C, Dixon D A, Camaioni D M, et al. Role of water in electron-initiated processes and radical chemistry: Issues and scientific advances. Chemical reviews, 2004, 105(1): 355-390.
6) Carlson R W, Anderson M S, Johnson R E, et al. Hydrogen peroxide on the surface of Europa. Science, 1999, 283(5410): 2062-2064.
7) Blanc M, Andrews D J, Coates A J, et al. Saturn plasma sources and associated transport processes. Space Science Reviews, 2015, 192: 237-283.
8) Jahnke T, Guillemin R, Inhester L, et al. Inner-shell-ionization-induced femtosecond structural dynamics of water molecules imaged at an x-ray free-electron laser. Physical Review X, 2021, 11(4): 041044.
9) Bergh M, Tîmneanu N, van der Spoel D. Model for the dynamics of a water cluster in an x-ray free electron laser beam. Physical Review E, 2004, 70(5): 051904.

10) Inhester L, Hanasaki K, Hao Y, et al. X-ray multiphoton ionization dynamics of a water molecule irradiated by an x-ray free-electron laser pulse. Physical Review A, 2016, 94(2): 023422.
11) H. Li et al., "Design of an amplitude-splitting hard x-ray delay line with subnanoradian stability," Optics letters, vol. 45, no. 7, pp. 2086-2089, 2020.
12) Yoshii, N. and Okazaki, S. "A large-scale and long-time molecular dynamics study of supercritical Lennard-Jones fluid. An analysis of high temperature clusters," The Journal of chemical physics, vol. 107, no. 6, pp. 2020-2033, 1997.
13) Sikorski, M. et al., "Application of an ePix100 detector for coherent scattering using a hard X-ray free-electron laser," Journal of synchrotron radiation, vol. 23, no. 5, pp. 1171-1179, 2016.
14) Kawasaki, K., "Kinetic equations and time correlation functions of critical fluctuations," Annals of Physics, vol. 61, no. 1, pp. 1-56, 1970.
15) Rouxel, Jeremy R., et al. "Hard X-ray transient grating spectroscopy on bismuth germanate." *Nature Photonics* 15.7 (2021): 499-503.
16) M.-F. Lin, et al., Science 374, 92 (2021).
17) . Zarkadoula, Y. Shinohara, T. Egami, Physical Review Research 4, 013022 (2022).
18) Brown, Emily J., Qingguo Zhang, and Marcos Dantus. "Femtosecond transient-grating techniques: Population and coherence dynamics involving ground and excited states." *The Journal of chemical physics* 110.12 (1999): 5772-5788.
19) Hofmann, Felix, Michael P. Short, and Cody A. Dennett. "Transient grating spectroscopy: An ultrarapid, nondestructive materials evaluation technique." *Mrs Bulletin* 44.5 (2019): 392-402.
20) Nishikawa, K. Arai, A. A., and Morita, T. “Density fluctuation of supercritical fluids obtained from small-angle X-ray scattering experiment and thermodynamic calculation.” *The Journal of Supercritical Fluids,* 30, 3, (2004): 249-257.
21) Beaucage, G. “Approximations leading to a unified exponential/power-law approach to small-angle scattering.” *Journal of Applied Crystallography,* 28 (1995): 717-728.
22) Skarmoutsos, I., Dimitris D., and Jannis S. "Investigation of the local composition enhancement and related dynamics in supercritical CO2-cosolvent mixtures via computer simulation: the case of ethanol in CO2." The Journal of Chemical Physics 126.22 (2007): 224503.
23) Tomšič, M., et al. "Structural properties of pure simple alcohols from ethanol, propanol, butanol, pentanol, to hexanol: Comparing Monte Carlo simulations with experimental SAXS data." The Journal of Physical Chemistry B 111.7 (2007): 1738-1751.
24) Li, H. et al. Generation of highly mutually coherent hard-X-ray pulse pairs with an amplitude-splitting delay line. Phys. Rev. Res. 3, 043050 (2021).
25) Muhunthan, P. et al. A versatile pressure-cell design for studying ultrafast molecular-dynamics in supercritical fluids using coherent multi-pulse X-ray scattering. Rev. Sci. Instrum. 95, 013901 (2024).
26) Hill, T. L. Molecular clusters in imperfect gases. J. Chem. Phys. 23, 617–622 (1955).
27) Sun, Peihao, et al. "Two-component dynamics and the liquidlike to gaslike crossover in supercritical water." Physical Review Letters 125.25 (2020): 256001.
28) Sun, Peihao, et al. "Universal two-component dynamics in supercritical fluids." The Journal of Physical Chemistry B 125.49 (2021): 13494-13501.
29) Bencivenga, F., et al. "High-frequency dynamics of liquid and supercritical water." Physical Review E—Statistical, Nonlinear, and Soft Matter Physics 75.5 (2007): 051202.

Exploring Photon-Initiated Electron-Neutral Interactions in Strongly Correlated Lanthanide Complexes

Caroline Chick Jarrold
Department of Chemistry, Indiana University, 800 East Kirkwood Ave., Bloomington, IN 47405
cjarrold@iu.edu
Hrant P. Hratchian
Department of Chemistry and Chemical Biology, University of California, Merced, 5200 North Lake Road, Merced, CA 95343
hhratchian@ucmerced.edu
Lee M. Thompson
Department of Chemistry, University of Louisville, Louisville, Kentucky 40205, United States
lee.thompson.1@louisville.edu

I. Program Scope

The overarching goal of this project is to characterize the intrinsic electronic and magnetic properties of lanthanide (*Ln*)-based clusters, using experimental and theoretical approaches. Leveraging recent advances in our understanding of strong electron-neutral interactions, combined with new models in self-consistent field theory and nonorthogonal configuration interaction and developments in theory involving explicit time-propagation of the electronic structure, a range of homo- and hetero *Ln* oxides, borides, and nitrides are targeted for exploration.

These goals are being achieved in a series of new experiments and theoretical studies represented in **Figure 1**: We are capitalizing on our insights into how strong electron-neutral interactions are encoded in the gas-phase anion photoelectron (PE) spectra of these species, revealing both electronically- and magnetically-governed electron-neutral interactions. Our focus is on atomically precise cluster models of homo- and hetero-*Ln* materials, the composition of which, in turn, affects the magnetic properties of *Ln* metal centers. The premise underpinning this project is that the electronic and magnetic states of homometallic and bi-metallic *Ln* centers in clusters, oxides, nitrides, borides, and more complex molecular systems, can be probed, controlled, even switched, by interactions with free electrons, modeling the control of the properties in *Ln*-based single molecule magnets (SMMs) and spintronic devices. The "half-scattering" event picture of photodetachment as a model to current- and electric field-control of the energies and dynamic populations of excited magnetic and electronic states is being tested with cutting edge theory.

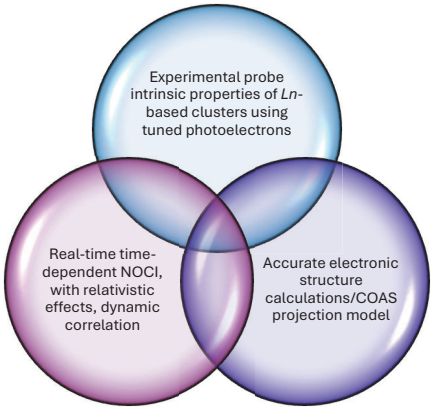

Figure 1. Interlocking experimental and theoretical contributions to the proposed research.

Accurate electronic structure calculations are laying the groundwork for understanding the electronic states of neutral lanthanide-based cluster systems from the manifold of low-lying states of the precursor anions, along with the constellation of neutral states that can potentially be accessed via the photoelectron-valence electron (PEVE) interactions that have become evident in nearly all of our past experimental studies in these systems.

The dynamics of electron detachment processes and how they drive electronic excitations in the remnant neutral are key areas of focus in the theoretical domain. The PEVE-driven neutral excitations we have observed experimentally generally have seemed strongly forbidden. However, by invoking a time-dependent depiction of the remnant neutral as photoelectrons are ejected reveal how the dynamics of the detachment process lend themselves to what a first glance should be a symmetry-forbidden process.

II. Recent Progress

II.A. Experimental progress

Experimental efforts have focused on (1) constructing a VMI detector assembly that will expedite data acquisition and enable higher-resolution studies on very low kinetic energy electrons, which is of central importance to this project; (2) expanding the range of lanthanides studied to elements that are more relevant in the single molecule magnet domain, and exploring new PEVE interactions that lead to anomalies in the photoelectron angular distributions (PAD); and (3) studying photodetachment in "simple" metal oxide systems in order to benchmark new computational advances in computing photoelectron angular distributions in polyatomic clusters. Topic (3) is primarily in service of theoretical progress.

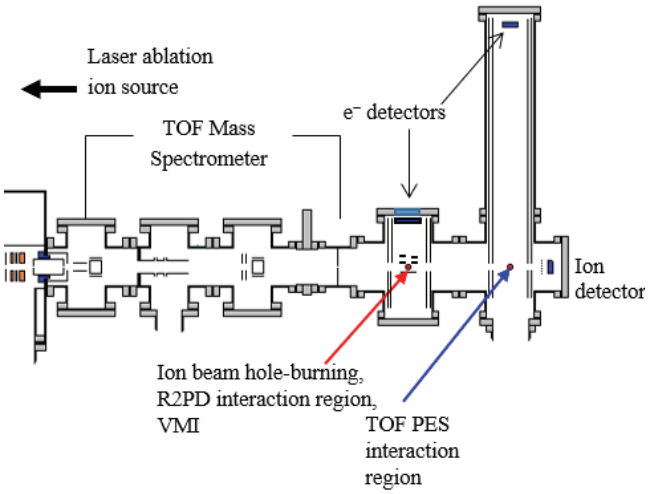

Figure 2. Schematic of instrument adapted with new VMI interaction region that will allow retention of ion beam hole-burning experiments, total cross section/R2PD measurements, and the time-of-flight e^-KE analysis for direct comparison between the two different modes (VMI and TOF) under the same source conditions.

II.A.1. Construction of the VMI assembly. As the primary experimental measurable is the electron kinetic energy-dependent intensities of multi-electron (nominally forbidden) transitions in the PE spectra of the lanthanide-based clusters, a velocity map imaging setup, which has a 100% PE collection efficiency and which maps out the PE angular dependence (PAD, see below) has been constructed and installed. This new portion of the instrument will allow for PE imaging measurements, which enable expeditious collection of two-dimensional PE spectra. These 2D PE spectra are constructed from the customary PE spectra of the anions measured over a range of photon energies. The heat maps used to display the 2D PE spectra readily show the evolution of forbidden transition intensities with e^-KE . PE imaging spectra are particularly amenable to measuring near-zero-kinetic energy electrons, which are of greatest interest in this experiment. These electrons naturally give the longest electron-neutral interaction times and may provide the most detailed insights into the types of PEVE interactions that govern the nominally forbidden processes observed frequently in these strongly correlated systems.

Note that the original e^-KE energy analyzer, which is a 1-m field-free drift tube remains in place and will enable continuation of ion-beam hole-burning studies to determine the presence of

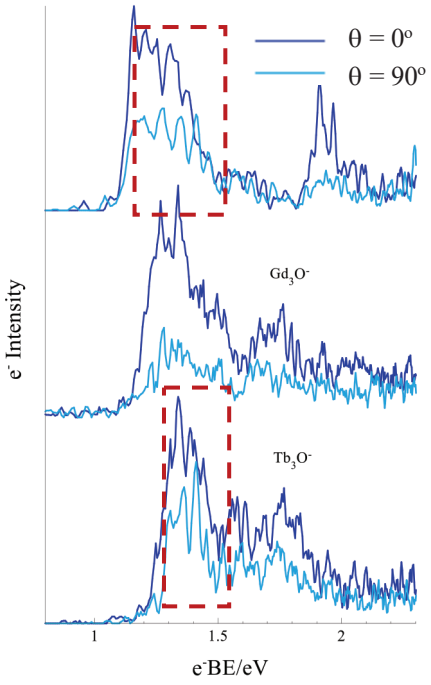

Figure 3. Anion PE spectra of Ln_3O^- anions. While the chemical properties of lanthanides are considered very similar, the relative stabilities of computed structures are different. Along the adjacent Ln elements, Sm, Gd and Tb, Gd is the unique element in that the $4f^7$ subshell occupancy results in zero orbital angular momentum. The spectra of Sm_3O^- and Tb_3O^- exhibit anomalous out-of-phase appearance of the spectra measured at different angles relative to the detachment laser E-field.

multiple structural isomers in the ion beam, but will also allow us to directly compare these two methods of e⁻KE analysis under identical source conditions.

II.A.2. Anomalies in the PADs measured in the PE spectra of $Ln_xO_y^-$ clusters. A striking effect observed in previous studies on small lanthanide oxide clusters in low oxidation states and high symmetry were anomalous PADs.[1] Specifically, PADs showed oscillations across what appeared to be a single electronic transition, which, based on electronic structure calculations, should have been uniformly "parallel," or more intense for photoelectrons measured in the direction parallel to the electric field vector of the laser. This effect was observed in cases where both degenerate orbitals and vibrations might have been involved with vibronic coupling resulting in the electrons being ejected with different angular momenta. However, the effect could also be rationalized as spin-orbit coupling between the ejected electron and the remnant neutral, and therefore tied to the magnetic properties of the cluster.

To further explore this phenomenon, we conducted a study on a series of near-Ln_3O^- neighbors in which the 4f subshells occupancies had incremental differences: *Ln* = Sm ($4f^6$), Gd ($4f^7$) and Tb ($4f^8$). Of these three elements, Gd is not viable in the SMM domain because of its isotropic $4f^7$ (^8S) subshell, whereas both Sm and Tb are (the latter being one of the more commonly explored in the SMM community). The PE spectra of these three Ln_3O^- clusters are shown in Figure 3. Of note, the spectra of the "magnetic" clusters show a striking out-of-phase appearance of structure in the spectra showing the relative intensities of electron signal ejected parallel (dark blue) and perpendicular (light blue) to the electric field vector of the detachment laser. Again, based on electronic structure, we would anticipate only parallel ejection in these clusters. This finding supports the hypothesis that the ejected electron can interact with the remnant neutral, driving transitions between m_s states at the expense of its angular momentum.[2]

II.A.3. Anion PE spectroscopy of stoichiometric zinc oxide clusters to benchmark computational efforts to predict angular distributions of photoelectrons. Our ongoing collaborative projects involving anion PE spectroscopy and electronic structure calculations have customarily taken advantage of our ability draw more quantitative comparisons between computational and experimental results using home-written spectral simulations codes that use computed parameters to simulate hypothetical appearance of the PE spectrum of a computed structure. To extend this capability in-house, we have developed new protocols to predict photodetachment pole strengths and photoelectron angular distributions based on the natural ionization orbitals (NIOs, see next section).

To fine tune the protocol and apply it to photoelectrons ejected from polyatomic metal oxide anions, we selected a system for which the HOMO or SOMO of the anion was easily characterized. Stoichiometric zinc oxide cluster anions, $Zn_xO_x^-$, were anticipated to have doublet anions and singlet neutrals, with the excess electron in the anion described as a totally symmetric combination of Zn 4s orbitals.[3] Figure 2 shows the anion PE spectra of a series of small stoichiometric $Zn_xO_x^-$ clusters (dotted blue lines), and spectral simulations based on computed spectroscopic parameters (solid lines) using our standard simulation codes, along with the computed NIOs. These orbitals, which are nearly identical to visualizations of the singly occupied orbital in the anion, are suitable models for photodetachment transitions in the lanthanide clusters in lower-than-traditional oxidation states, which are generally characterized as having primarily 6s parentage.

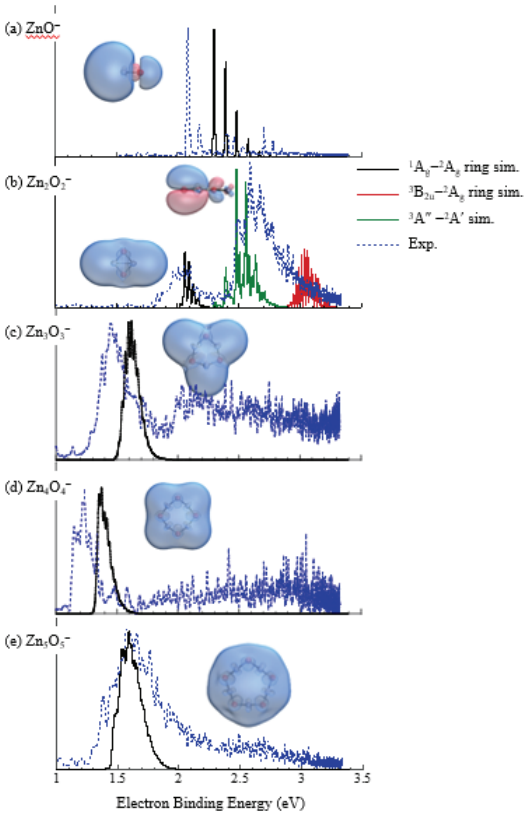

Figure 4. Anion PE spectra of small $Zn_xO_x^-$ clusters (blue dotted lines) with the computation-based simulations (solid lines) and the computed natural ionization orbitals shown as insets.

II.B. Theoretical progress

II.B.1. Expanded toolkit for synergies between computational and experimental studies. The NIO model provides a means for computing the ΔSCF (or other state-specific) Dyson orbital.[4] In our prior work, the NIO analysis was expanded to include pole strength evaluation.[5] In our zinc oxide study, we extended the model further to simulate the PADs. Specifically, we have employed a linear combination of atomic orbitals (LCAO) based approach using parameters taken from Hanstorp's simplification of the Cooper-Zare equation.[6,7] Despite its simplicity, this model provides qualitative results that align with conceptual expectations based on the nature and symmetry of the Dyson orbital given by the NIO model. Indeed, as shown in our published report,[3] the agreement between experimental and theoretical anisotropy parameters evaluated using this extension to the NIO model is very good.

II.B.2. Time-dependent simulations of electron detachment. To understand the observed dependence of transition intensities on the photon energy, real-time time dependent simulations of electron detachment are being developed. Initial work for simulating the effect of low kinetic energy photoelectrons on the remnant electron density has involved development of a real-time time-dependent configuration interaction approach in which the electron is treated as a point charge.[8] While the point charge model does not provide a quantum mechanical model of the electron, it provides an initial model in which the kinetic energy and electron detachment direction is well defined, while also accounting for the nonadiabatic nature of the detachment process. As a result it permits an understanding of the extent to which the remnant electron density is modified

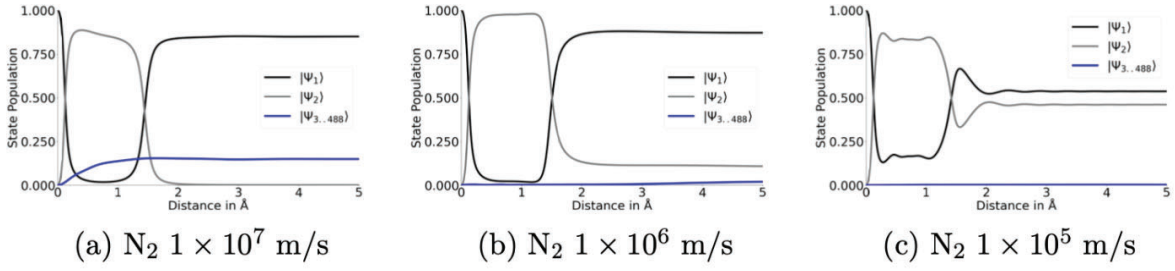

Figure 5. Kinetic energy dependence of remnant electronic structure in the photodetachment of $N_2 + h\nu \longrightarrow N_2^+ + e^-$ resulting in a superposition state primarily of $^2\Pi_u$ character. Faster electron detachment leads to larger populations of nonadiabatically excited states (blue line), while slower electron detachment leads to superposition in which the

by the electron-remnant interaction, the temporal and spatial range over which the interactions occur at different kinetic energies, as well as the effect of the photodetachment orientation. Figure 5 shows one of the results from our recent work for detachment from the π_u orbital of N_2 to form a final N_2^+ remnant wavefunction that is principally comprised of the $^2\Pi_u$ state. Faster electron detachment is less adiabatic and so the final remnant wavefunction contains small contributions from many states (panel a). Slower electron detachment inhibits nonadiabatic excitations but leads to a superposition in which the $^2\Pi_u$ states have similar weights (panel c). Detachment at 1×10^4 ms^{-1} results in an adiabatic detachment process, in which the wavefunction is in the $|\Psi_1\rangle$ stationary state at all time points. While it is expected that larger kinetic energy photoelectrons interact over a smaller temporal range, the simulations show that slower electrons also interact with the remnant molecule over a larger spatial range.

III. Future Plans

III.A. Heterolanthanide oxide cluster studies. In terms of theoretical developments needed to extend the time-dependent simulations to heterolanthanide oxide clusters, the code can already model systems of the size required for the study. However, as spin-orbit coupling is likely to play a role in governing the electron detachment events, implementation of these terms in the model is required.

III.B. Anisotropy parameter study and simulated VMI using the NIO model. As mentioned above, we have developed a simple approach for computing anisotropy parameters from the Dyson orbital using the NIO model. An alternate scheme using group theoretical based models to calculate anisotropy parameters within the NIO model will be examined. This will provide us with a more rigorous approach than the LCAO based method used in our zinc oxide study. We will carry out a thorough benchmark study of anisotropy parameters calculated using both models to fully examine their accuracy and reliability. With models in hand for evaluating anisotropy parameters, we will be able to simulate VMI spectra. Such modeling and simulation presents an important expansion of the degree of synergy and corroboration available for making assignments in PE spectra.

III.C. Improved simulated photoelectron description. Improvements in the time-dependent simulations will allow more realistic description of the detached electron. The current model treats the electron as a classical point charge, and so does not account for the quantum mechanical nature of the ionized electron or the extent to which electron-remnant interactions modify the photoelectron kinetic energy. The next step is to implement complex absorbing potentials to better describe the detachment process. Simulations can then proceed using an applied continuous field.

The potential issue with the proposed approach is that, owing to the laser field frequencies used in the experiment, the detachment of the electron is likely to require long simulation times. If the simulations prove infeasible, inspiration will be taken from rare-event dynamics simulations, in which the system can be biased towards the detachment. However, the best way of determining a valid biased initial state remains to be established.

III.D. Connecting real-time simulations to spectroscopy. Using our developed real-time time-dependent simulations, it is possible to extract densities, difference densities, natural orbitals, and density difference natural orbitals. As described in section II.B.1, these quantities have been shown by our recent work to correspond to the Dyson orbital which connects the electronic structure to the simulation. However, recovering the experimental spectrum from real-time time-dependent calculations requires consideration of an ensemble of simulations that average over detachment orientation and source orbital. Therefore, additional work developing the protocol that recovers the simulated spectrum from the time-dependent simulations is required. Additionally, for very slow electron kinetic energies, vibrational and rotational motion may occur on the same timescale as the detachment processes. While our current code allows for such effects to be examined, performing and analyzing these simulations will be carried out going forward.

IV. Publications resulting from this work

Huizenga, C.D.; Vaish, S.; Thompson, L.M., Jarrold, C.C. Electronic structures and potential spin frustration in Ln_3O (*Ln* = Ce, Sm, Gd) neutrals and anions determined by anion photoelectron spectroscopy. **Submitted**, *J. Chem. Phys*. September, 2024.

Kinyua, A.M.; Hratchian, H.P.; Jarrold, C.C.; Thompson, L.M. Understanding the time-dependent electronic response to low kinetic energy electron detachment events. **Submitted**, *J. Chem. Phys*. September, 2024.

Vaish, S.; Gyamfi, A.; Huizenga, C.D.; Hratchian, H.P.; Jarrold, C.C. Electronic Structures of Small Stoichiometric Zn_xO_x Clusters. *J. Phys. Chem. A* **2024**, *128*, 6450-6461. https://doi.org/10.1021/acs.jpca.4c03613

References

1. Mason, J.L.; Harb, H.; Abou Taka, A.; Huizenga, C.D.; Corzo, H.H.; Hratchian, H.P.; Jarrold. New Photoelectron-Valence Electron Interactions Evident in the Photoelectron Spectrum of Gd_2O^-. J. Phys. Chem. A **2021**, *125*, 9892-9903.
2. Huizenga, C.D.; Vaish, S.; Thompson, L.M., Jarrold, C.C. *ibid.*
3. Vaish, S.; Gyamfi, A.; Huizenga, C.D.; Hratchian, H.P.; Jarrold, C.C. *ibid.*
4. Thompson, L.M.; Harb, H.; Hratchian, H.P. Natural ionization orbitals for interpreting electron detachment processes. *J. Chem. Phys.* **2016**, *144*, 204117.
5. Harb, H.; Hratchian, H. P. ΔSCF Dyson orbitals and pole strengths from natural ionization orbitals. **2021**, *154*, 084104.
6. Hanstorp, D.; Bengtsson, C.; Larson, D.J. Angular Distributions in Photodetachment from O^-. *Phys. Rev. A*, **1989**, *40*, 670-675.
7. Grumbling, E.; Sanov, A. Photoelectron Angular Distributions in Negative-Ion Photodetachment from Mixed Up States. *J. Chem. Phys*. **2011**, *135*, 164302.
8. Kinyua, A.M.; Hratchian, H.P.; Jarrold, C.C.; Thompson, L.M. *ibid.*

Tracking the Mechanisms of Catalytic Reactions on Ligand-Protected Gold Nanoclusters

Christopher J. Johnson

Department of Chemistry

Stony Brook University

100 Nicolls Rd., Stony Brook, NY 11794-3400

chris.johnson@stonybrook.edu

Program Scope

We seek to understand the mechanisms driving catalytic CO_2 electroreduction on atomically-precise nanoclusters and to leverage their tunability to optimize their efficacy. Atomically-precise nanoclusters typically feature a metal or metalloid core of tens to hundreds of atoms surrounded by a stabilizing and solubilizing layer of organic ligands, yielding a nanoparticle with a total diameter of 1-2 nm. They merge desirable qualities of molecular and nanoscale catalysts: they can, in some cases, be synthesize or isolated with exact structures and formulae like molecules, but feature densities of states, redox properties, and compositions more consistent with nanoscale objects or bulk surfaces. Nanoclusters have been extensively pursued as potential designer catalysts, showing promise in a number of reactions.[3] For the electroreduction of CO_2, two prototypical nanoclusters in particular have shown enhanced activity that depends their composition.[1, 4] Specifically, we plan to:

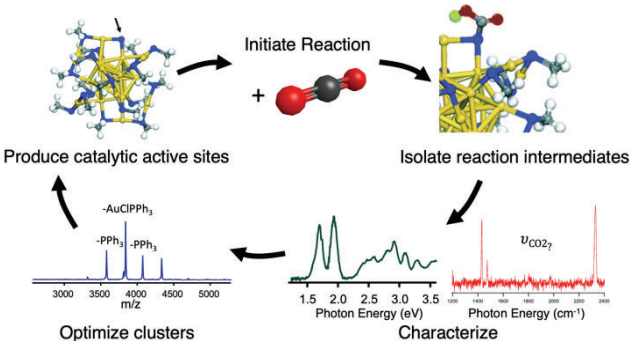

Figure 1: An overview of our experimental approach to understand and optimize CO_2 activation on metal nanoclusters.

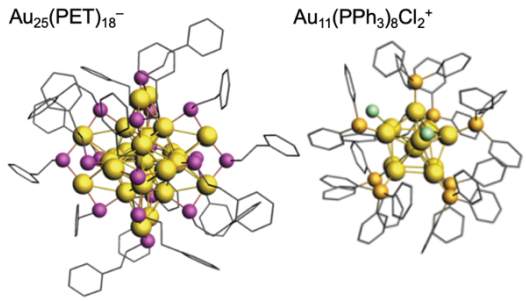

Figure 2: X-ray crystal structures of $Au_{25}(PET)_{18}^-$ (PET = phenylethantethiol) and $Au_{11}(PPh_3)_8Cl_2^+$ (PPh_3 = triphenylphosphine). Here gold = Au, pink = S, orange = P, and green = Cl.[1, 2]

1. Determine the active site for electrochemical CO_2 reduction by the ubiquitous $Au_{25}(SR)_{18}$ nanocluster,

2. Determine the mechanism of CO_2 reduction by Au_{11} nanoclusters with mixtures of PPh_3 and N-heterocyclic carbene ligands,

3. Synthesize nanoclusters with improved catalytic activity by tailoring active sites and optimizing electronic structure by ligand exchange and metal doping.

The $Au_{25}(SR)_{18}$ and $Au_{11}(PPh_3)_8Cl_2^+$ nanoclusters, shown in Figure 2, have been shown to be catalytically active towards CO_2 and the mechanisms have been investigated computationally. Quantum chemical calculations for $Au_{25}(SR)_{18}$ suggest that either a ligand or an R-group of a ligand dissociates, leaving an undercoordinated Au or S atom site that can bind CO_2 as a ligand.[5] Experimentally probing this proposed mechanism of CO_2 activation is challenging due to the inability to isolate and characterize the undercoordinated species. We use mass spectrometry as a general approach to produce and isolate this species and compare its activity towards CO_2 with that of the intact nanocluster. Mass spectrometry also allows us to track this activity as a function of exact metal doping number and site as well as ligand composition, both of which have been shown to increase activity. Once isolated in the mass spectrometer, we probe key elements of bonding, structure, and the degree of CO_2 activation in the nanocluster-CO_2 complexes using a combination of common chemical analysis tools adapted to mass selected ions.

Specifically, electronic spectroscopy yields key energetic information such as relative orbital energies and their dependence on the exact nanocluster composition, while infrared spectroscopy gives insight into structure and small molecule activation. We couple these techniques to variable-temperature ion traps, which give us access to key thermochemical information to characterize the reaction mechanisms driving elementary reactions catalyzed by these nanoclusters. These insights not only inform efforts to synthetically optimize nanoclusters, they also allow us to screen clusters for high activity. Given the difficulty of developing atomically-precise synthetic methods or purification protocols, our ability to propose specific clusters that are likely to be highly catalytically active will accelerate developments in this field.

Recent Progress

In the past year, we have focused on three thrusts: 1.) we have shown that individual ligand binding sites perturb specific peaks in the UV/vis spectrum, showing that it will be possible to determine which orbitals are involved in CO_2 binding; 2.) we have constructed and implemented two electrochemical flow cells in our electrospray ionization sources and shown that we can produce undercoordinated Au sites on Au_{25} via electroreduction that are active towards small molecules, and 3.) we have shown that the active state of Au_{11} for electroreduction of CO_2 requires more than just creation of undercoordinated sites, and thus the mechanism likely first involves reduction of the cluster itself.

Site-specific ligand control of nanocluster electronic structure

Using the $Au_8(PPh_3)_7^{2+}$ and $Au_9(PPh_3)_8^{3+}$ clusters as preparation for Au_{11}, we sought to develop an approach to determining the electronic spectral-manifestation of perturbations to specific ligand sites. Establishing a one-to-one correspondence between specific ligand sites and specific spectral features would allow us to explicitly probe the nanocluster orbitals involved in bonding and electron transfer with the CO_2 LUMO, the first step in its activation. We further used this test case to determine if it would be possible to use ligands to fine-tune the electronic structure of these nanoclusters to optimize their bonding.

We focused on the HOMO-LUMO transition of these clusters as a function of ligand identity and formed the clusters with three different ligands: PPh_3, and derivatives of it with Me and OMe substituted in the *para*- position. We previously showed that the HOMO-LUMO gap varied linearly with the Hammett parameter of the substituent, and thereby, its electron donating effect. While this showed that it would be possible to intentionally tune the HOMO-LUMO gap to optimize catalytic activity, it did not explain the mechanism for this control. Electron donating effects can come from two sources: resonance effects, in which the substituents change the contribution of different possible resonance structures, and inductive effects, in which electrostatic properties of the substituents induce electrostatic effects in the system that they are bound to. A classic physical organic chemistry experiment thus suggests substituting at the *meta* position, thereby eliminating resonance effects and isolating inductive ones. If the observed effect is still linear, then induction is the driving factor; if not, then resonance is. Figure 3 presents the primary results of this study: clearly, the *meta*-substituted clusters do not follow a linear trend, and thus resonance is dominant. This is somewhat surprising, because the HOMO and LUMO are both nominally localized on the Au atoms, and the ligand substituents are remote, yet they completely control the orbital energies.

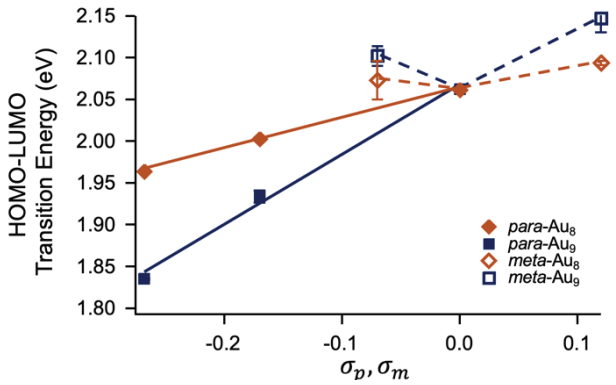

Figure 3: Results of a Hammett study for Au8 and Au9 nanoclusters, showing that resonance effects of the ligands drives shifts in the HOMO-LUMO gap.

The observation of resonance effects controlling the HOMO-LUMO gap then suggested that individual ligands likely have significantly different contributions. In other words, specific resonance structures are likely to involve specific ligands. Using capability unique to our instrument, we collected the electronic

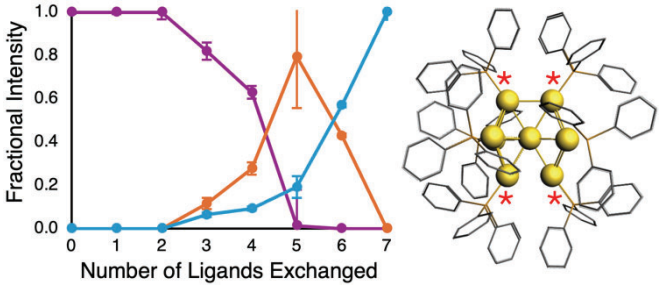

Figure 4: Evolution of the three components of the HOMO-LUMO transition with respect to ligands exchanged. (Right) The crystal structure of the nanocluster, with red * indicating the likely ligand sites responsible for shifting the HOMO-LUMO transition

spectra of clusters with exactly-known mixtures of PPh_3 and $OMe\text{-}PPh_3$ ligands, with the hypothesis that non-monotonic changes of the spectra with respect to ligand exchange would reveal ligand-site-specific resonance. Figure 4 summarizes the changes to the HOMO-LUMO transition with respect to number of ligands exchanged. We observe three distinct spectroscopic features in the vicinity of the transition, and Figure 4 tracks the relative intensities of these three features. It is clear that the first several exchanges have essentially no effect on the spectrum – presumably these sites are not involved in resonance structures for the HOMO or LUMO. Interestingly, the full shift we observed in Figure 3 is driven by only two ligand sites. Computational results suggest that the HOMO and LUMO both lie in a 4-atom plane of the cluster (shown inset in Figure 4, red *), suggesting that these are the sites primarily contributing to the putative resonance structures.

Electrochemical generation of catalytic active sites

Surface ligands protect and solubilize nanoclusters and are largely responsible for making them stable in solution, but this protection must be penetrated in order for them to actually do any chemistry. We implemented a nanoflow electrochemical flow cell for our electrospray ion source to generate these active sites and isolate the resulting clusters in the mass spectrometer prior to reaction with CO_2. Figure 5 shows a diagram of the setup and preliminary data for Au_{25}. Inset are models of the intact cluster and its activated analogue from DFT calculations.[5] With the cell potential on, we observe the loss of a single ligand radical and the creation of a putative active site. The nature of this site is confirmed by the observation additional masses representing activated solven molecules bound to the surface of the cluster. To our knowledge, this is the first direct observation of an electrochemically-generated active site on a ligand-protected nanocluster. With this capability in hand, we were ready to react these activated clusters with CO_2, either in the gas phase in an ion trap or in solution by dissolving CO_2 into the electrospray solvent. Unfortunately, due to unknown factors (potentially a change in building humidity due to air handler renovations), we have not been able to synthesize Au_{25} as we previously could. While we redevelop the synthetic method, we have begun a collaboration with Prof. Benjamin Lear at Penn State to supply us with more Au_{25} to continue this work.

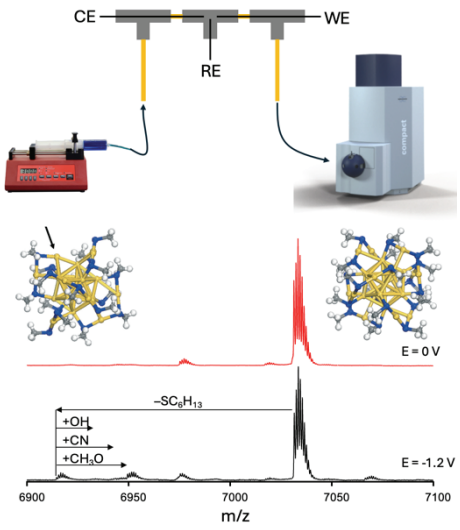

Figure 5: (top) A diagram of the nanoflow EChem-ESI setup. (bottom) Mass spectrometric isolation of activated Au_{25} nanoclusters: at a working voltage of 0 V, we observe the intact Au_{25}, while at -1.2 V, we observe the elimination of one SR ligand to produce an undercoordinated Au site as well as the activation of solvent molecules on that site to produce OH, CN, and MeO adducts.

Probing the reactivity of undercoordinated sites in Au_{11}

Undercoordinated sites are typically assumed to be the active sites for catalytic transformations on nanoclusters, but they are likely not sufficient. We formed a variety of undercoordinated sites on the $Au_{11}(PPh_3)_8^{3+}$ nanocluster by using gas phase collision induced dissociation to remove individual ligands or Au-PPh3 complexes from the cluster. We then exposed the clusters to trace CO_2 in a variable-temperature ion trap to evaluate the enthalpy and entropy of binding to each cluster in a shotgun approach. Figure 6 presents the results from one such experiment. We generally find that physisorbed (i.e., non-activating) CO_2 appears around 105 K, though the exact temperature depends on the change in entropy upon binding of free CO_2. In this example, we observe CO_2

adducts forming at 100 K, suggesting that these are indeed weakly-bound species and not activated. IR spectroscopy of these complexes in the mass spectrometer confirms this observation, with each showing a characteristic CO_2 asymmetric stretching band near the free value of 2350 cm^{-1}. This leads us to conclude that, at least for Au_{11}, it will likely be important to reduce the cluster electrochemically to induce CO_2 activation.

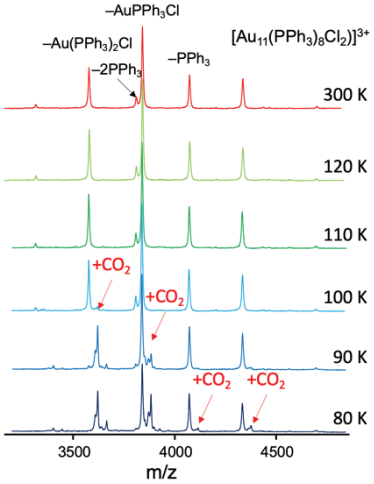

Figure 6: A shotgun variable-temperature mass spectrometry experiment to evaluate the binding affinity of CO_2 to a range of undercoordinated nanoclusters generated by collision induced dissociation. No cluster compositions showed notable activity towards CO_2.

Future Plans

We will obtain Au_{25} samples again and swiftly continue with the electrochemical reduction and CO_2 activation experiments using it. We intend to two important outstanding questions about this benchmark nanocluster catalyst: 1.) What is the active site? There are three possibilities that have been proposed, an Au atom in the icosahedral core, an Au atom in the ligand shell, or a bare S atom. 2.) What is the origin of increased catalytic efficacy of Ag-doped Au_{25}? Perturbations to our well-resolved spectra of Au_{25} upon CO_2 binding will identify the strength of electronic coupling while red shifts of the CO_2 asymmetric stretch will reveal the change in activation induced by Ag doping. We will further apply the same electroreduction scheme to the Au_{11} clusters, where we hypothesize that reductive elimination of Cl radicals will generate the desired active site. If this is not the case, collision-induced-dissociation production of active sites by elimination of PPh_3 ligands from the reduced precursor cluster will be pursued. If this is not successful, then the proposed mechanism for Au_{11}'s catalytic activity will be called into question. Finally, we will produce Au_{11} derivatives with N-heretocylic carbenes to investigate the mechanistic origins of the increased catalytic efficiency of these clusters upon ligand exchange.

Publications

Morales Hernández, H., Sun, Q., Rosati, M., Gieseking, R. L. M., and Johnson, C. J., "Bonding and Acidity of the Formal Hydride in the Prototypical $Au_9(PPh_3)_8H^{2+}$ Nanocluster," *Angew. Chem. Int. Ed.*, **62**, e202307723 (2023).

Morales Hernández, H., Ohtsuka, S., Mehmood, A., Bordenca, J., Wen, W., Levine, B. G., and Johnson, C. J., "Resonance Effects from Substituents on L-Type Ligands Mediate Synthetic Control of Gold Nanocluster Frontier Orbital Energies," *under review*. (ChemRXiv: 10.26434/chemrxiv-2024-csv33)

References

(1) Narouz, M. R.; Osten, K. M.; Unsworth, P. J.; Man, R. W. Y.; Salorinne, K.; Takano, S.; Tomihara, R.; Kaappa, S.; Malola, S.; Dinh, C.-T.; et al. N-heterocyclic carbene-functionalized magic-number gold nanoclusters. *Nat. Chem.* **2019**, *11* (5), 419-425.

(2) Heaven, M. W.; Dass, A.; White, P. S.; Holt, K. M.; Murray, R. W. Crystal Structure of the Gold Nanoparticle $[N(C_8H_{17})_4][Au_{25}(SCH_2CH_2Ph)_{18}]$. *J. Am. Chem. Soc.* **2008**, *130* (12), 3754-3755.

(3) Zhao, S.; Jin, R.; Jin, R. Opportunities and Challenges in CO_2 Reduction by Gold- and Silver-Based Electrocatalysts: From Bulk Metals to Nanoparticles and Atomically Precise Nanoclusters. *ACS Energy Lett.* **2018**, *3* (2), 452-462.

(4) Alfonso, D. R.; Kauffman, D.; Matranga, C. Active sites of ligand-protected Au_{25} nanoparticle catalysts for CO_2 electroreduction to CO. *J. Chem. Phys.* **2016**, *144* (18), 184705.

(5) Kauffman, D. R.; Alfonso, D.; Matranga, C.; Qian, H.; Jin, R. Experimental and Computational Investigation of Au_{25} Clusters and CO_2: A Unique Interaction and Enhanced Electrocatalytic Activity. *J. Am. Chem. Soc.* **2012**, *134* (24), 10237-10243.

Low Temperature Oxidation Kinetics of Ammonia with Oxygenates under Extreme Pressure

Yiguang Ju
Department of Mechanical and Aerospace Engineering, Princeton University, NJ 08540
Email: yju@princeton.edu

Proposal scope

Ammonia and carbon neutral oxygenated e-fuels and biofuels provide a great opportunity to lower carbon emissions. However, the kinetics of low temperature ammonia oxidation with oxygenated fuels at high pressure are not well known. The impact of HO_2 chemistry from oxygenated fuel oxidation on ammonia oxidation and NO_x chemistry has rarely been studied. The elementary reaction rates involving HO_2 and ammonia radicals have large uncertainties. Furthermore, the effects of strong intermolecular force of ammonia due to its hydrogen bonding and the resulting non-equilibrium kinetic effect at extreme pressure from multi-body collisions, reactive multi-molecular reactions, and severe deviation from Boltzmann distribution on reaction kinetics are not well understood. The objectives of this study are to examine the non-equilibrium kinetics of low temperature oxidation of ammonia with small oxygenated fuels such as alcohols, esters, and ethers at extreme pressure (up to 200 atm) by using a newly developed supercritical jet-stirred reactor (SP-JSR), to experimentally measure the rate and branching ratios of a key elementary reaction of $HO_2 + NH_2$ for considering HO_2, NO_x, and NH_3 chemistry interaction by using a new photolysis reactor with microsecond time-resolved mid-IR Faraday rotation spectroscopy, and to develop experimentally validated kinetic models and a new ab-initio trained machine-learning and molecular dynamics (aML-MD) method for high pressure non-equilibrium kinetics modeling. The proposed research will advance the fundamental understanding of non-equilibrium chemical kinetics of low temperature oxidation of ammonia with hydrogen and small oxygenated fuels at extreme pressure. It will provide an experimentally measured reaction rate and the branching ratios of a critical multi-channeled ammonia radical reactions with HO_2. Furthermore, it will develop a new ab-initio trained machine-learning molecular dynamics (aML-MD) method to examine the non-equilibrium kinetic effects at extreme pressure and enable direct comparison between experiments with modeling at extreme pressure.

Recent Progress

1.1. Development of ab-initio trained machine learning model (aML-MD) with multi-fidelity data for elementary rate determination

Machine learning (ML) provides a great opportunity for the construction of models with improved accuracy for classical molecular dynamics (MD). However, the accuracy of a machine learning trained model is limited by the quality and quantity of the training data. Generating large sets of accurate ab-initio training data can require significant computational resources. Furthermore, inconsistent or incompatible data with different accuracies obtained using different methods may lead to biased or unreliable ML models that do not accurately represent the underlying physics. In this work, ab-initio trained ML-based MD (aML-MD) models are developed through transfer learning using DFT data from multiple sources with varying accuracy within the Deep Potential MD framework. The accuracy of the force field is demonstrated by calculating rate constants for the $H + HO_2 \rightarrow H_2 + O_2$ reaction using quasi-classical trajectories. We show that the aML-MD model with transfer learning can accurately predict the

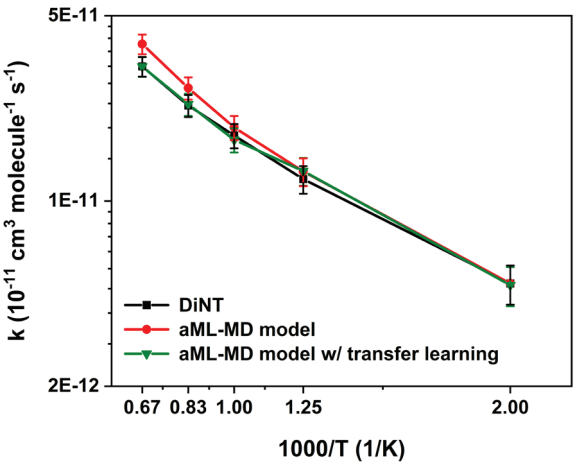

Fig. 1 Rate constants at different temperatures calculated by DiNT, aML-MD models with and without transfer learning.

rate constants while reducing the computational cost by more than 5 times compared to the use of more expensive quantum chemistry training datasets (Fig. 1) [1]. Hence, the aML-MD model with transfer learning shows great potential in using multi-fidelity data to reduce the computational cost involved in generating the training set for these potentials.

1.2. **Impacts of the Ammonia Economy on the Nitrogen Cycle and Climate**

Ammonia (NH_3) is an attractive low-carbon fuel and hydrogen carrier. However, losses and inefficiencies across the value chain could result in reactive nitrogen emissions (NH_3, NO_x, and N_2O), negatively impacting air quality, the environment, human health, and climate. A relatively robust ammonia economy (30 EJ/yr) could perturb the global nitrogen cycle by up to 65 Mt/yr, equivalent to 50% of the current global perturbation caused by fertilizers. Additionally, the emission rate of nitrous oxide (N_2O) at low combustion temperatures, a potent greenhouse gas and ozone-depleting molecule, determines whether ammonia combustion has a greenhouse footprint comparable to renewable energy sources or higher than coal (100-1400 gCO_2e/kWh). The success of the ammonia economy hence hinges on adopting optimal practices and technologies that minimize reactive nitrogen emissions. We discuss how this constraint should be included in the ongoing broad engineering research to reduce environmental concerns and prevent the lock-in of high-leakage practices. This study investigates the potential environmental risks associated with ammonia use in the energy sector. Our findings demonstrate that reactive nitrogen compounds released throughout the ammonia value chain can harm air quality, human health, ecosystems, climate, and stratospheric ozone depletion. However, we also show that optimal engineering practices and management strategies can effectively mitigate these concerns. Our research contributes to informed decision-making and the development of environmentally responsible ammonia energy systems [2].

1.3. **High pressure ammonia oxidation with alkanes and oxygenated fuels.**

Oxidation of NH3/n-heptane mixtures at pressures up to 100 atm and temperatures of 400-900 K was characterized experimentally in a laminar flow reactor and a jet-stirred reactor [3-4]. A detailed chemical kinetic model was developed, updating the hydrogen and amine subsets and introducing a subset for the chemical coupling with emphasis on the NH_2+n-heptane reaction. The kinetic model provided a good prediction of the ignition delay times measured in a rapid compression machine as well as the high pressure experimental data obtained in the present work. The results show that it is important to include updated rate constants for $NH_2 + HO_2$ and $NH_2 + n\text{-}C_7H_{16}$ to obtain reliable predictions for ignition and oxidation of NH_3/n-heptane mixtures at high pressure. The sensitivity analysis confirmed the effectiveness of implementing analogy rules for determining the rate constant of the key reaction $NH_2 + n\text{-}C_7H_{16}$. High pressure ammonia/methanol oxidation and NO_x formation were also investigated using a recently developed supercritical pressure jet-stirred reactor (SP-JSR) at 20 and 100 atm with temperatures between 550 and 950 K and equivalence ratios of 0.138 and 1.15 [5] (Fig. 2). The experimental results show that the NH_3 oxidation at high pressure is largely accelerated by the active OH radicals produced from CH_3OH oxidation. Furthermore, the kinetic interactions between NH_3 and CH_3OH are governed mainly by reactions $CH_3OH + NH_2 = CH_2OH + NH_3$, $CH_3OH + NH_2 = CH_3O + NH_3$, and $CH_2O + NH_2 = HCO + NH_3$. A HP-Mech model for high-pressure NH_3/CH_3OH oxidation was developed in this study. It consists of the most recently NH_3 and CH_3OH models as well as NH_3-CH_3OH interactions including some new reactions and updated rate constants from the literature. Our model with these updates improves the prediction for the experimental data at both 20 and 100 atm and reproduces well the ignition delay times in the literature and the measured N_2O/NO_x temperature dependence. In addition, the reaction pathway and sensitivity analysis show that N_2O/NO_x/HONO interaction with HO_2 are very important especially for a fuel-lean mixture at 100 atm. The HONO mole fraction for fuel-lean mixture at 100 atm was then measured by off-axis integrated cavity output spectroscopy (ICOS) at 6638.26 cm^{-1}. The experimental data show that HONO formation was very high at intermediate temperature and significantly underpredicted by numerical simulation at 100 atm. Therefore, the HONO related reactions such as NO + OH (+M) = HONO (+M), $H_2NO + NO_2 = HONO + HNO$, $HNO + NO_2 = HONO + NO$ need deeper exploration in the future.

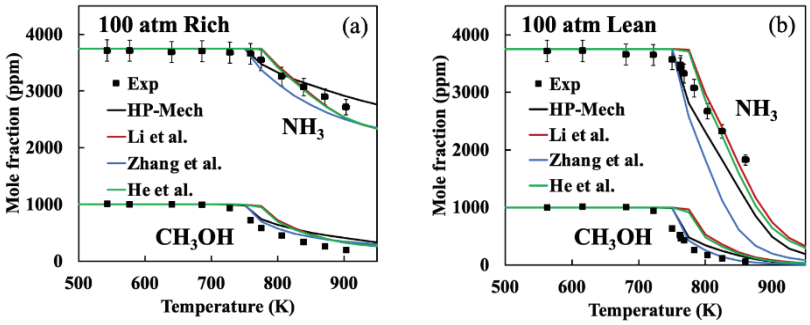

Fig. 2 Temperature evolutions of NH_3 and CH_3OH mole fractions for (a) fuel-rich and (b) fuel-lean mixtures [5]

1.4. **High pressure spray cool flame ignition and instability**

Experimental and numerical studies are performed on the non-premixed n-dodecane spray cool flames in a counterflow burner. A novel phenomenon of repetitive autoignition-extinction instability of near-limit non-premixed spray cool flames is observed and examined [6]. The spray cool flame is established by a polydisperse *n*-dodecane fuel spray generated from a twin-fluid atomizer, ranging from sub-micron sizes up to 400 μm with Sauter mean diameter of 109 μm. Digital Inline Holography is used to measure spray size distribution and quantify the fuel fraction in spray and gas phases at experimental conditions. The chemiluminescence of the excited formaldehyde molecule in spray cool flame is recorded by an Intensified-CCD (ICCD) camera to examine the repetitive cycles of autoignition and extinction, and to measure the spray cool flame stabilization time in each cycle. The repetitive autoignition and extinction cycles are found to be mostly caused by the competition between chemical heat release from low-temperature fuel oxidation, and heat loss in fuel spray vaporization in a counterflow, where the dynamics of large droplets in polydisperse spray play an important role. It is also found that with the increase of the oxygen mole fraction or the oxidizer temperature, the spray cool flame stabilization time increases and the cycles of autoignition and extinction become less frequent.

1.5. **Non-equilibrium depolymerization of plastics via dynamic spatiotemporal heating**

Depolymerization is a promising strategy for recycling waste plastics into their constituent monomers for subsequent polymerization in another lifecycle. However, many commodity plastics cannot be depolymerized with high selectivity using conventional thermochemical approaches as it is difficult to control the reaction progress and pathway, thereby often leading to a broad spectrum of products. Catalysts can be used to improve the selectivity, but they are susceptible to performance degradation. Herein, we developed a catalyst-free, far-from-equilibrium depolymerization method via electrified spatiotemporal heating that enables us to generate monomers from commodity plastics with high yields. The selective depolymerization is realized by two critical features to drive non-equilibrium kinetics: (1) a spatial temperature gradient and (2) a temporal heating profile. Using this approach, we depolymerized polypropylene and polyethylene terephthalate to their monomers with yields of ~36% and ~43%, respectively, which are among the highest compared to conventional thermochemical methods, even those that use catalysts [7].

Collaborations The work on aML-MD is conducted in collaboration with Drs. Stephen Klippenstein and Ahren Jasper at ANL. The high pressure ammonia oxidation with oxygenated fuels is collaborated with Drs. Stephen Klippenstein at ANL and Peter Glarborg at DTU.

Future Work We will study high pressure NH_3 oxidation with dimethyl ether, CH_2O, and methyl formate, develop aML-MD for key elementary reactions in involving pressure dependent reactions, and conduct elementary rate measurement of NH_2 with HO_2.

DOE Supported Publications 2022 - 2024

1. Zhiyu Shi, myself, Ahren W. Jasper, Stephen J. Klippenstein, and Yiguang Ju, Quasi-classical trajectory calculation of rate constants using an ab-initio trained machine learning model (aML-MD) with multi-fidelity data, The Journal Physical Chemistry, accepted, 2024. https://doi.org/10.1021/acs.jpca.4c00750
2. Matteo Bernard Bertagni, Robert H Socolow, John Mark Martirez, Emily A. Carter, Chris Greig, Yiguang Ju, Timothy Lieuwen, Michael Mueller, Sankaran Sundaresan, Rui Wang, Mark A. Zondlo, Amilcare Porporato, "Minimizing the Impacts of the Ammonia Economy on the Nitrogen Cycle and Climate", PNAS, 120 (46) e2311728120, 2023, doi: 10.1073/pnas.2311728120
3. Lauge Sven Thorsen, Malene Stryhn Thestrup Jensen, Mille Stub Pullich, Jakob Munkholt Christensen, Hamid Hashemi, Peter Glarborg, Vladimir A. Alekseev, Elna J.K. Nilsson∗, Ziyu Wang, Bowen Mei, Ning Liu, Yiguang Ju, High pressure oxidation of NH3/n-heptane mixtures, Combustion and Flame, Vol. 254, 12785, 2023. https://doi.org/10.1016/j.combustflame.2023.112785
4. Hamid Hashemi, Jakob M. Christensen, Peter Glarborg, Sander Gersen, Martijn van Essen, Ziyu Wang, Yiguang Ju, High-Pressure Oxidation of n-Butane, Int. J. Chemical Kinetics 2023: 55:688–706. DOI: 10.1002/kin.21678
5. Ziyu Wang, Bowen Mei, Ning Liu, Andy Thawko, Xingqian Mao, Hao Zhao, Peter Glarborg, Stephen J. Klippenstein, Yiguang Ju, High pressure ammonia/methanol oxidation up to 100 atm, Proceedings of the Combustion Institute, Volume 40, 2024, 105489. https://doi.org/10.1016/j.proci.2024.105489
6. Wenbin Xu, Ziyu Wang, Bowen Mei, Martin A. Erinin, M. Shyam Kumar, Yijie Xu, Jiarong Hong, Luc Deike, Yiguang Ju, Repetitive autoignition and extinction instability of non-premixed n-dodecane spray cool flames, Proceedings of the Combustion Institute, Volume 40, Issues 1–4, 2024, 105482. https://doi.org/10.1016/j.proci.2024.105482
7. Qi Dong, Aditya Dilip Lele, Xinpeng Zhao, Sichao Cheng, Yueqing Wang, Miao Guo, Mingjin Cui, Alexandra H Brozena, Tangyuan Li, Xin Zhang, Ioannis G. Kevrekidis, Jianguo Mei, Xuejun Pan, Dongxia Liu, Yiguang Ju*, Liangbing Hu*, Far-from-equilibrium Depolymerization of Plastics via Dynamic Spatiotemporal Heating, Nature, 616, pp.488–494 (2023). doi.org/10.1038/s41586-023-05845-8
8. Hao Zhao, Chao Yan, Guohui Song, Ziyu Wang, Ahren W. Jasper, Stephen J. Klippenstein, Yiguang Ju, High-pressure oxidation of hydrogen diluted in N2 with added H2O or CO2 at 100 atm in a supercritical-pressure jet-stirred reactor, Combustion and Flame, Vol. 266, 113543, 2024. doi.org/10.1016/j.combustflame.2024.113543
9. Robert L. McCormick, Gina M. Fioroni, Samah Y. Mohamed, Nimal Naser, Teresa L. Alleman, Seonah Kim, Ziyu Wang, Ying Lin, and Yiguang Ju, and Kenneth Kar, Fuel Property Evaluation of Unique Fatty Acid Methyl Esters Containing β-hydroxy Esters from Engineered Microorganisms, Fuel Communications, Vol. 19, 100120, 2024. https://doi.org/10.1016/j.jfueco.2024.100120
10. Yijie Xu, Ning Liu, Ying Lin, Xingqian Mao, Mikhail N Shneider, Yiguang Ju, Enhancements of Electric Field and Afterglow Discharge by Ferroelectric Electrode, Nature Communications, (2024) 15:3092. https://doi.org/10.1038/s41467-024-47230-7
11. Lele, Aditya; Lin, Ying; Ju, Yiguang, " Modelling the effect of surface charging on plasma synthesis of ammonia using DFT", Phys. Chem. Chem. Phys., 26, 9453-9461, 2024, DOI: 10.1039/d3cp06050k
12. Andrés Z. Mendiburu, João Carvalho, Yiguang Ju, FLAMMABILITY LIMITS: A COMPREHENSIVE REVIEW OF THEORY, EXPERIMENTS AND ESTIMATION METHODS", Energy & Fuels, 2023 37 (6), 4151-4197. DOI: 10.1021/acs.energyfuels.2c03598
13. Andy Thawko, Ziyu Wang, Ning Liu, Yiguang Ju, Observation of Two Different Cool Flame Regimes of Diethyl Ether in a Diffusion Counterflow Burner, Fuel, 346 (2023) 128269, doi: 10.1016/j.fuel.2023.128269
14. Burger, Christopher; Zhang, Angie; Xu, Yijie; Hansen, Nils; Ju, Yiguang, "Plasma-Assisted Chemical-Looping Combustion: Low-Temperature Methane and Ethylene Oxidation with Nickel Oxide", The Journal of Physical Chemistry A, 2023, 127, 3, 789–798. doi.org/10.1021/acs.jpca.2c07184
15. Ziyu Wang, Chao Yan, Bowen Mei, Ying Lin, Yiguang Ju, Study of Low Temperature Oxidation Kinetics of Diethyl Ether in a Supercritical Pressure Jet-stirred Reactor, The Journal of Physical Chemistry A, 2023, 127, 2, 506–516. doi.org/10.1021/acs.jpca.2c06182
16. Aditya Dilip Lele and Yiguang Ju, Assessment of the impact of reactor residence time distribution on non-equilibrium product selectivity of polypropylene pyrolysis using reactive molecular dynamics simulations, Fuel, 2023, 338, 127328. https://doi.org/10.1016/j.fuel.2022.127328

Probing the Reaction Dynamics of Hydrogen-Deficient Hydrocarbon Molecules and Radical Intermediates via Crossed Molecular Beams

Ralf I. Kaiser
Department of Chemistry, University of Hawai'i at Manoa, Honolulu, HI 96822
ralfk@hawaii.edu

1. Program Scope

The major goals of this project have been to explore in molecular beam experiments the fundamental reaction dynamics and underlying potential energy surfaces (PESs) of hydrocarbon molecules and their resonantly stabilized and/or aromatic radical precursors, which are relevant to the gas phase formation and molecular mass growth processes of mononuclear and polycyclic aromatic hydrocarbons (PAHs). *First*, reactions were initiated in crossed molecular beam experiments under single collision conditions by intersecting two supersonic reactant beams containing the open shell (radicals, atoms) and closed shell species under a well-defined collision energy and crossing angle (UH Manoa). By recording angular-resolved time-of-flight (TOF) spectra, we obtained unprecedented information on the reaction products, inferred intermediates involved, and extracted branching ratios of competing reaction channels, reaction energetics, and novel reaction mechanisms to (aromatic) hydrocarbon molecules along with their acyclic isomers. *Second*, reactions were conducted in a chemical microreactor at well characterized pressure and temperature distributions with reaction products interrogated isomer-selectively by tunable vacuum ultraviolet light (VUV) via photoionization (PI) coupled with a reflectron time-of-flight mass spectrometer (Re-TOFMS). These studies were conducted in collaboration with Dr. Musahid Ahmed (Advanced Light Source, Lawrence Berkeley National Laboratory) as well as Dr. Patrick Hemberger (Swiss Light Source, Paul Scherrer Institute) and merged with electronic structure calculations (Prof. Alexander M. Mebel, Florida International University). These studies have been of crucial importance to comprehend the fundamental gas phase formation mechanisms of two key classes of molecules involved in molecular mass-growth processes leading ultimately to carbonaceous nanostructures from the bottom up: resonantly stabilized free radicals (RSFRs) and polycyclic aromatic hydrocarbons (PAHs).

2. Recent Progress

2.1. Mechanistical Studies on the Gas Phase Formation of Aromatic Hydrocarbons

Exploiting molecular beams, four novel low- and high-temperature reaction mechanisms have been exposed leading to the formation of aromatic hydrocarbons carrying up to six rings: **R**adical-**R**adical **R**eactions (**RRR**) (**P4**, **P8, P9, P17, P18, P19, P26**), **P**ropargyl **A**ddition–**B**enz**A**nnulation (**PABA**) (**P22, P36**), **F**ulvenallenyl **A**ddition-**C**yclization **A**romatization (**FACA**) (**P27**), and **P**henylethynyl **A**ddition–**C**yclization-**A**romatization (**PACA**) (**P31, P33**). This mechanistical framework significantly expands synthetic routes to PAHs driven by **H**ydrogen **A**bstraction – C_2H_2 (acetylene) **A**ddition (**HACA**), Hydrogen **A**bstraction – **V**inylacetylene **A**ddition (**HAVA**), **P**henyl **A**ddition – Dehydro**C**yclization (**PAC**), and **M**ethylidyne **A**ddition – **C**yclization - **A**romatization (**MACA**) as elucidated in the 7/18-6/21 funding period.

2.2. Multi-Step Reaction Pathways to Aromatics

The elucidation of individual reaction pathways to PAHs (2.1) affords a unique opportunity of combining multiple mechanisms in complex, multi-step syntheses of aromatics [**P21, P24, P29**]. Coronene ($C_{24}H_{12}$) - a fundamental molecular building block of two-dimensional PAHs and graphene nanosheets – was prepared in a microchemical reactor via a combination of HACA, HAVA, and PAC [**P24**]. Finally, multi-step low temperature HAVA molecular mass growth processes lead to benzo-corannulene ($C_{24}H_{12}$) – a bowl-shaped PAH carrying seven rings. *In silico* studies provided compelling evidence that the benz-annulation mechanism can be expanded to pentabenzocorannulene ($C_{40}H_{20}$) followed by successive cyclodehydrogenation to the C40 nanobowl ($C_{40}H_{10}$) – a fundamental building block of buckyballs such as buckminsterfullerene (C_{60}) [**P21**]. These findings revealed that microreactor studies in conjunction with electronic structure calculations have advanced to such a level that complex, multi-step reaction pathways to aromatics carrying up seven rings can be elucidated.

2.3. Mechanistical Studies of the Incorporation of Methyl Groups in Aromatics

Exploiting crossed molecular beams experiments, the energetics and dynamics of the elementary reactions of the 1-propynyl radical (CH_3CC; C_3H_3) with isoprene ($H_2CCHC(CH_3)CH_2$; C_5H_8) revealed that two methyl groups can be incorporated barrierlessly into an aromatic system, i.e. m- and p-xylenes, under single collision conditions. The reaction dynamics are driven by a barrierless addition of the radical to the π electronic system (diene moiety) of isoprene (2-methyl-1,3-butadiene) followed by isomerization via hydrogen atom shifts and cyclization prior to unimolecular decomposition accompanied by aromatization via atomic hydrogen loss. This overall exoergic reaction affords a preparation of xylenes not only in high temperature environments such as in combustion flames and around circumstellar envelopes of carbon-rich Asymptotic Giant Branch (AGB) stars, but also in low-temperature cold molecular clouds (10 K) and in hydrocarbon-rich atmospheres of planets and their moons such as Triton and Titan with both methyl groups acting as spectators in the 1-propynyl radical and isoprene reactants. This study established a previously unknown gas phase route to xylenes and potentially more complex, disubstituted benzenes via a single collision event highlighting the significance of an alkyl-substituted ethynyl-mediated preparation of aromatic molecules [**P28**].

3. Future Plans

Our plan is to study elementary gas phase reactions forming phenyl (C_6H_5), benzene (C_6H_6), fulvenallenyl (C_7H_5), and fulveneallene (C_7H_6) as fundamental molecular building blocks of two- and three-dimensional carbonaceous nanostructures carrying six- and five-membered ring(s), respectively. Crossed molecular beam experiments are conducted under single-collision conditions and investigate the underlying energetics, dynamics, and potential energy surfaces (PESs) of reactions of key resonantly stabilized free radicals (RSFR, cyclopentadienyl, C_5H_5) and aromatic radicals (AR, phenyl, C_6H_5) as simplest representatives of five- and six-membered, cyclic hydrocarbon radicals, prototype 'aliphatic' radicals (methylidyne; CH), 'acetylenic' radicals (ethynyl, C_2H; butadiynyl, C_4H), and 'carbonaceous' transients (C, C_2, C_3) with unsaturated C2 to C5 hydrocarbons at the most fundamental, microscopic level.

4. Support

This work is supported by US Department of Energy (Basic Energy Sciences; DE-FG02-03-ER15411).

5. Publications Acknowledging DE-FG02-03ER15411 (2021–now)

P1 S. Doddipatla, G. R. Galimova, H. Wei, A. M. Thomas, C. He, Z. Yang, A. N. Morozov, C. N. Shingledecker, A. M. Mebel, R. I. Kaiser, Low-Temperature Gas-Phase Formation of Indene in the Interstellar Medium, *Sci. Adv.* **7**, eabd4044 (2021).

P2 C. He, A. A. Nikolayev, L. Zhao, A. M. Thomas, S. Doddipatla, G. R. Galimova, V. N. Azyazov, A. M. Mebel, R. I. Kaiser, Gas-Phase Formation of C_5H_6 Isomers via the Crossed Molecular Beam Reaction of the Methylidyne Radical (CH; $X^2\Pi$) with 1,2-Butadiene (CH_3CHCCH_2; X^1A'), *J. Phys. Chem. A* **125**, 126-138 (2021).

P3 L. Zhao, S. Doddipatla, R. I. Kaiser, W. Lu, O. Kostko, M. Ahmed, L. B. Tuli, A. N. Morozov, A. H. Howlader, S. F. Wnuk, A. M. Mebel, V. N. Azyazov, R. K. Mohamed, F. R. Fischer, Gas-Phase Synthesis of Corannulene - A Molecular Building Block of Fullerenes, *Phys. Chem. Chem. Phys.* **23**, 5740-5749 (2021).

P4 L. Zhao, W. Lu, M. Ahmed, M. V. Zagidullin, V. N. Azyazov, A. N. Morozov, A. M. Mebel, R. I. Kaiser, Gas-Phase Synthesis of Benzene via the Propargyl Radical Self-Reaction, *Sci. Adv.* **7**, eabf0360 (2021).

P5 L. Zhao, M. Prendergast, R. I. Kaiser, B. Xu, W. Lu, M. Ahmed, A. H. Howlader, S. F. Wnuk, A. S. Korotchenko, M. M. Evseev, E. K. Bashkirov, V. N. Azyazov, A. M. Mebel, A Molecular Beam and Computational Study on the Barrierless Gas Phase Formation of (Iso)quinoline in Low Temperature Extraterrestrial Environments, *Phys. Chem. Chem. Phys.* **23**, 18495-18505 (2021).

P6 A. A. Nikolayev, V. N. Azyazov, R. I. Kaiser, A. M. Mebel, Theoretical Study of the Reaction of the Methylidyne Radical (CH; $X^2\Pi$) with 1-Butyne (CH_3CH_2CCH; X^1A'), *J. Phys. Chem. A* **125**, 9536-9547 (2021).
P7 C. He, K. Fujioka, A. A. Nikolayev, L. Zhao, S. Doddipatla, V. N. Azyazov, A. M. Mebel, R. Sun, R. I. Kaiser, A Chemical Dynamics Study of the Reaction of the Methylidyne Radicals (CH, $X^2\Pi$) with Dimethylacetylene (CH_3CCCH_3, X^1A_{1g}), *Phys. Chem. Chem. Phys.* **24**, 578-593 (2022).
P8 R. I. Kaiser, L. Zhao, W. Lu, M. Ahmed, M. V. Zagidullin, V. N. Azyazov, A. M. Mebel, Formation of Benzene and Naphthalene through Cyclopentadienyl-Mediated Radical−Radical Reactions, *J. Phys. Chem. Lett.* **13**, 208–213 (2022).
P9 R. I. Kaiser, L. Zhao, W. Lu, M. Ahmed, V. S. Krasnoukhov, V. N. Azyazov, A. M. Mebel, Unconventional Excited-State Dynamics in the Concerted Benzyl (C_7H_7) Radical Self-Reaction to Anthracene ($C_{14}H_{10}$), *Nat. Commun.* **13**, 786 (2022).
P10 S. J. Goettl, C. He, D. Paul, A. A. Nikolavev, V. N. Azyazov, A. M. Mebel, R. I. Kaiser, Gas-Phase Study of the Elementary Reaction of the D1-Ethynyl Radical (C_2D; $X^2\Sigma^+$) with Propylene (C_3H_6; X^1A') Under Single-Collision Conditions, *J. Phys. Chem. A* **126**, 1889–1898 (2022).
P11 D. Paul, Z. Yang, S. J. Goettl, A. M. Thomas, C. He, A. G. Suits, D. H. Parker, R. I. Kaiser, Photodissociation Dynamics of Astrophysically Relevant Propyl Derivatives (C_3H_7X; X = CN, OH, HCO) at 157 nm Exploiting an Ultracompact Velocity Map Imaging Spectrometer: The (Iso)Propyl Channel, *J. Phys. Chem. A* **126**, 5768-5775 (2022).
P12 G. R. Galimova, A. M. Mebel, S. J. Goettl, Z. Yang, R. I. Kaiser, A Crossed Molecular Beams and Computational Study on the Unusual Reactivity of Banana Bonds of Cyclopropane (c-C_3H_6; X^1A_1') through Insertion by Ground State Carbon Atoms ($C(^3P_j)$), *Phys. Chem. Chem. Phys.* **24**, 22453-22463 (2022).
P13 D. Paul, Z. Yang, R. I. Kaiser, Photodissociation Dynamics of Xylene Isomers $C_6H_4(CH_3)_2$ at 157 nm using an Ultracompact Velocity Map Imaging Spectrometer – The C_7H_7 Channel, *Chem. Phys. Lett.* **807**, 140064 (2022).
P14 R. I. Kaiser, L. Zhao, W. Lu, M. Ahmed, M. M. Evseev, V. N. Azyazov, A. M. Mebel, R. K. Mohamed, F. R. Fischer, X. Li, Gas-Phase Synthesis of Racemic Helicenes and their Potential Role in the Enantiomeric Enrichment of Sugars and Amino Acids in Meteorites, *Phys. Chem. Chem. Phys.* **24**, 25077-25087 (2022).
P15 C. He, Z. Yang, S. Doddipatla, A. M. Thomas, R. I. Kaiser, G. R. Galimova, A. M. Mebel, K. Fujioka, R. Sun, Directed Gas Phase Preparation of Ethynylallene ($H_2CCCHCCH$; X_1A') via the crossed molecular beam reaction of the methylidyne radical (CH; $X^2\Pi$) with vinylacetylene ($H_2CCHCCH$; X^1A'), *Phys. Chem. Chem. Phys.* **24**, 26499-26510 (2022).
P16 Z. Yang, G. R. Galimova, C. He, S. Doddipatla, A. M. Mebel, R. I. Kaiser, Gas Phase Formation of 1,3,5,7-Cyclooctatetraene (C_8H_8) through Ring Expansion via the Aromatic 1,3,5-Cyclooctatrien-7-yl Radical ($C_8H_9^{\bullet}$) Transient, *J. Am. Chem. Soc.* **144**, 22470-22478 (2022).
P17 W. Li, L. Zhao, R. I. Kaiser, A Unified Reaction Network on the Formation of Five-Membered Ringed Polycyclic Aromatic Hydrocarbons (PAHs) and their Role in Ring Expansion Processes through Radical–Radical Reactions, *Phys. Chem. Chem. Phys.* **25**, 4141-4150 (2023).
P18 C. He, R. I. Kaiser, W. Lu, M. Ahmed, P. S. Pivovarov, O. V. Kuznetsov, M. V. Zagidullin, A. M. Mebel, Unconventional Pathway in the Gas-Phase Synthesis of 9H-Fluorene ($C_{13}H_{10}$) via the Radical–Radical Reaction of Benzyl (C_7H_7) with Phenyl (C_6H_5), *Angew. Chem. Int. Ed.* **62**, e202216972 (2023).
P19 C. He, R. I. Kaiser, W. Lu, M. Ahmed, Y. Reyes, S. F. Wnuk, A. M. Mebel, Exotic Reaction Dynamics in the Gas Phase Preparation of Anthracene ($C_{14}H_{10}$) via Spiroaromatic Radical Transients in the Indenyl–Cyclopentadienyl Radical–Radical Reaction, *J. Am. Chem. Soc.* **145**, 3084-3091 (2023).
P20 A. M. Mebel, M. Agúndez, J. Cernicharo, R. I. Kaiser, Elucidating the Formation of Ethynylbutatrienylidene (HCCCHCCC; X^1A') in the Taurus Molecular Cloud (TMC-1) via the Gas Phase Reaction of Tricarbon (C_3) with the Propargyl Radical (C_3H_3). *Astrophys. J. Lett.* **945**, L40 (2023).
P21 L. B. Tuli, S. J. Goettl, A. M. Turner, A. H. Howlader, P. Hemberger, S. F. Wnuk, T. Guo, A. M. Mebel, R. I. Kaiser, Gas Phase Synthesis of the C40 Nano Bowl $C_{40}H_{10}$. *Nat. Commun. 14*, 1527 (2023).

P22 C. He, R. I. Kaiser, W. Lu, M. Ahmed, V. S. Krasnoukhov, P. Pivovarov, V. N. Azyazov, A. N. Morozov, A. M. Mebel, Unconventional Gas Phase Preparation of the Prototype Polycyclic Aromatic Hydrocarbon Naphthalene ($C_{10}H_8$) via the Reaction of Benzyl (C_7H_7) and Propargyl (C_3H_3) Radicals Coupled with Hydrogen-Atom Assisted Isomerization. *Chem. Sci.* **14**, 5369 - 5378 (2023).
P23 S. J. Goettl, Z. Yang, S. Kollotzek, D. Paul, R. I Kaiser, A. Somani, A. P. González, W. Sander, A, A. Nikolayev, V. N. Azyazov, A.M. Mebel, Exploring the Chemical Dynamics of Phenylethynyl Radical (C_6H_5CC; X^2A_1) Reactions with Allene (H_2CCCH_2; X^1A_1) and Methylacetylene (CH_3CCH; X^1A_1). *J. Phys. Chem. A* **127**, 5723-5733 (2023).
P24 S. J. Goettl, L.B. Tuli, A.M. Turner, Y. Reyes, A. H. Howlader, S.F. Wnuk, P. Hemberger, A.M. Mebel, R.I. Kaiser, Gas Phase Synthesis of Coronene through a Directed Ring Annulation Framework. *J. Am. Chem. Soc.* **145**, 15443–15455 (2023).
P25 I. A. Medvedkov, A.A. Nikolayev, C. He, Z. Yang, A.M. Mebel, R.I Kaiser, A Combined Experimental and Computational Study on the Reaction Dynamics of the 1-Propynyl (CH_3CC, X^2A_1) – Propylene (CH_3CHCH_2, X^1A') System: Formation of 1,3-Dimethylvinylacetylene ($CH_3CCCHCHCH_3$, X^1A') under Single Collision Conditions. *Mol. Phys.* (Special Issue Timothy Lee) e2234509 (2023).
P26 Z. Yang, G. R. Galimova, C. He, S. J. Goettl, D. Paul, W. Lu, M. Ahmed, A. M. Mebel, X. Li, R. I. Kaiser, Gas phase Formation of the Resonantly Stabilized 1-Indenyl (C_9H_7) Radical in the Interstellar Medium. *Sci. Adv.* **9**, eadi5060 (2023).
P27 W. Li, L. Zhao, D. Couch, M. S. Marchi, N. Hansen, A.M. Mebel, R.I. Kaiser, Gas phase Preparation of Azulene ($C_{10}H_8$) via Reaction of the Resonantly Stabilized Fulvenallenyl ($C_7H_5^{\bullet}$) and Propargyl ($C_3H_3^{\bullet}$) Radicals. *Chem. Sci.* **14**, 9795-9805 (2023).
P28 I. A. Medvedkov, A.A. Nikolayev, C. He, Z. Yang, A.M. Mebel, R.I. Kaiser, One Collision – Two Substituents: Gas phase Preparation of Xylenes under Single-Collision Conditions. *Angew. Chem. Int. Ed.* **63**, e202315147 (2024).
P29 S. J. Goettl, A.M. Turner P. Hemberger, B.-J. Sun, A.H.H. Chang, R.I. Kaiser, Gas phase Preparation of the Dibenzo[e,l]pyrene ($C_{24}H_{14}$) Butterfly Molecule. *Chem. Comm.* **60**, 1404 - 1407 (2024).
P30 I. A. Medvedkov, Z. Yang, S. Goettl, A.M. Mebel, R.I. Kaiser, Elucidating the Chemical Dynamics of the Elementary Reactions of the 1-Propynyl Radical (CH_3CC; X^2A_1) with 2-Methylpropene ($(CH_3)_2CCH_2$; X^1A_1). *Phys. Chem. Chem. Phys.* **26**, 6448 - 6457 (2024).
P31 S. J. Goettl, Z. Yang, C. He, A. Somani, A. Portela-Gonzalez, W. Sander, A. M. Mebel, R. I. Kaiser, Exploring the Chemical Dynamics of Phenanthrene ($C_{14}H_{10}$) Formation via the Bimolecular Gas-Phase Reaction of the Phenylethynyl Radical (C_6H_5CC) with Benzene (C_6H_6). *Faraday Discuss.* (in press).
P32 Z. Yang, C. He, S. J. Goettl, A. M. Mebel, P. F. G. Velloso, M. O. Alves, B. R. L. Galvão, J.-C. Loison, K. M. Hickson, M. Dobrijevic, X. Li, R. I. Kaiser, Low-Temperature Formation of Pyridine and (Iso)quinoline via Neutral–Neutral Reactions. *Nat. Astron.* **8**, 856-864 (2024).
P33 S. J. Goettl, C. He, Z. Yang, R. I. Kaiser, A. Somani, A. Portela-González, W. Sander, B.-J. Sun, S. Fatimah, K. P. Kadam, A. H. H. Chang, Unconventional Gas-Phase Synthesis of Biphenyl and its Atropisomeric Methyl-Substituted Derivatives. *Phys. Chem. Chem. Phys.* **26**, 18321 (2024).
P34 A. M. Mebel, W. Li, L. P. Maffei, C. Cavallotti, A. N. Morozov, C.-Y. Wang, J.-Z. Yang, L. Zhao, R. I. Kaiser, Fulvenallenyl Radical ($C_7H_5^{\bullet}$) Mediated Gas-Phase Synthesis of Bicyclic Aromatic $C_{10}H_8$ Isomers: Can Fulvenallenyl Efficiently React with Closed-Shell Hydrocarbons? *J. Phys. Chem. A* **128**, 5707-5720 (2024).
P35 Z. Yang, I. A. Medvedkov, S. J. Goettl, A. A. Nikolayev, A. M. Mebel, X. Li, R. I. Kaiser, Low-Temperature Gas-Phase Formation of Cyclopentadiene in the Interstellar Medium. *PNAS* (under review).
P36 C.-Y. Wang, L. Zhao, R. I. Kaiser, Gas phase Preparation of the 14π Hückel Polycyclic Aromatic Anthracene and Phenanthrene Isomers ($C_{14}H_{10}$) via the Propargyl Addition–BenzAnnulation (PABA) Mechanism. *ChemPhysChem* **25**, e202400151, (2024).

Mechanistic Investigations of Heterogeneous Catalysis with Surface, In-Pore, and Gas-Phase Steps

Coleman X. Kronawitter and Ambarish R. Kulkarni
University of California, Davis

PROGRAM SCOPE

In heterogeneous systems, chemical events on catalyst surfaces are essential for controlling reaction kinetics and ultimately the overall process performance. For this reason, the vast majority of investigations and techniques have focused on interrogation of catalyst surfaces or chemical steps occurring thereon. However, by comparison there is a conspicuous knowledge gap regarding chemistry and speciation in the near-surface gas phase – a region distinct from the downstream reactor effluent that is characterized using conventional tools. A core objective of the work proposed here is to develop and implement an integrated experiment-theory approach to provide new insights into the interconnected roles of the surface, catalyst pores, and the near-surface gas phase in heterogeneous catalytic chemical upgrading, primarily through coupling reactions. The project seeks to connect well-defined active sites to primary product speciation reflected in the near-surface gas phase. This will be enabled by use of: (1) New research technologies, originally developed for the field of combustion science, which through recent collaborations with Sandia National Laboratories, now facilitate operando interrogation of the local, near-surface gas phase above catalyst surfaces; (2) Site-isolated supported metal catalysts (often atomically dispersed), comprehensively characterized to define active sites and minimize site heterogeneity over length scales of experimental interrogation; (3) Machine learning-accelerated DFT-derived microkinetic models to interpret reaction and materials characterization results from (1) and (2), deriving relationships between specific active site structures and local reaction outcomes.

Coupling reactions are a focus, because they are an essential aspect of small-molecule feedstock upgrading, which has recently seen resurgent interest in the context of growing environmental concerns and continuing relevance of shale gas resources in the U.S. Mixed-feed systems, such as those for alcohol cross-coupling or the co-reaction of natural gas mixtures are especially intriguing because of their potential to facilitate controlled construction of large platform molecules, including from unseparated or partially separated natural feeds. Coupling of both hydrocarbon fragments and oxygenates can occur through gas-phase, in-pore, and surface-mediated events, depending on the catalytic system and its operating conditions. The unique tools and strategies in this project are ideally suited to investigate these systems.

DE-SC0020320: Mechanistic Investigations of Heterogeneous Catalysis with Surface, In-Pore, and Gas-Phase Steps Students: Niko Hansen, Trevor Price, Saurabh Sivakumar

RECENT PROGRESS

Molecular beam mass spectrometry to investigate the gas phase during heterogeneous catalysis

We collaborate with Sandia National Laboratories' Combustion Research Facility (SNL-CRF), which involves UC Davis PhD students working alongside Sandia scientific staff. Our project utilizes a time-of-flight molecular beam mass spectrometer (TOF-MBMS) to investigate properties of the gas phase effluent evolving from a packed catalyst bed. We use photoionization at the Lawrence Berkeley National Laboratories' Advanced Light Source (ALS) which offers great advantages in species identification.

Continuous-flow ethane dehydroaromatization (DHA) reaction over a zeolite-supported platinum catalyst (Pt/HZSM-5)

Catalytic technology based on ethane dehydroaromatization (ethane DHA) has been proposed to utilize abundant natural gas resources for production of benzene, toluene, and xylene (BTX). Ethane DHA

proceeds over metal-modified zeolites catalysts, with a complex reaction pathway that occurs within the micropore volume. HZSM-5 is the zeolite most targeted because of the benefits afforded by its shape-selective properties. Its three-dimensional structure consists of two sets of intersecting channels: one nominally straight channel (~ 0.52 x 0.58 nm) and the other containing sinusoidal 10-membered rings (~ 0.51 x 0.55 nm) intersect to form a region approximately 0.89 nm in size;40 these properties facilitate the formation and diffusion of aromatics while restricting further growth. Our approach to study reactions and intermediates from complex mixtures with well-defined catalysts is ideally suited to study ethane DHA.

We have now performed extensive experiments using synchrotron photoionization MBMS at the ALS (Figure 1). To our knowledge, these are the first photoionization mass spectrometry experiments ever performed on any ethane DHA system.

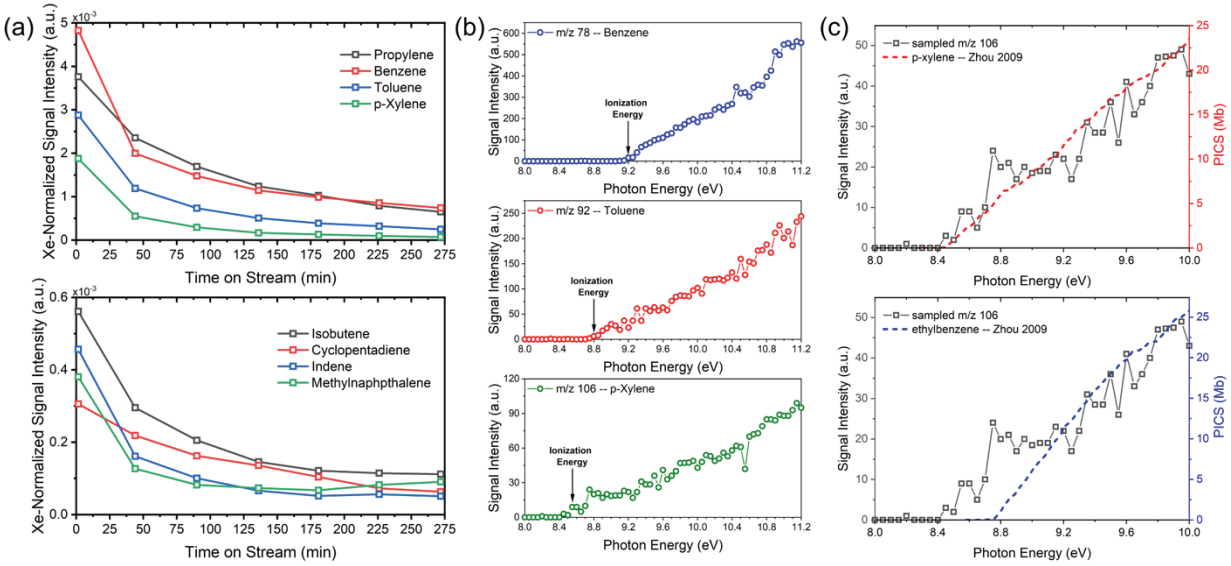

Figure 1. Continuous-flow ethane DHA studies with synchrotron photoionization MBMS with Pt/HZSM-5 [*J. Am. Chem. Soc.* 2022, 144, 13874–13887 and *ACS Catal.* 2024, 14, 4999−5005]. 200 mg; 10 sccm ethane, 10 sccm Ar, 1 sccm Xe; 375°C. (a) Photon-flux normalized signal vs. time-on-stream for select species; 12.4 eV. (b) PI spectra confirming aromatic identities through IE fingerprints. (c) PI spectra for C_8H_{10} species compared with literature spectra, [*Rapid. Commun. Mass. Spectrom.* 2009, 23 (24), 3994–4002] demonstrating isomer resolution.

Figure 1 shows representative results from continuous-flow ethane DHA experiments. The photon-flux normalized signals for eight species as a function of time-on-stream in Figure 1a shows that the catalyst deactivates, as expected, as there is a four-fold decrease in benzene, toluene, and xylene (BTX) signal within the first 4 h of time-on-stream. Further, the normalized signal of other species decreases similarly which suggests that the mode of deactivation is non-selective for the selected species. Exploring the relationship between specific species produced in pores and the deactivation process is a central goal of this aspect of our project.

Photoionization spectra (PI spectra), generated by collecting full mass spectra while scanning photon energies, provide fingerprints of observed m/z species to confirm their identities. Figure 1b shows PI spectra for BTX; the ionization energies indicated by these spectra are consistent with literature values. Figure 1c provides PI spectra for the signal for species composition C_8H_{10} compared with literature spectra [*Rapid. Commun. Mass. Spectrom. 2009, 23 (24), 3994–4002*] from two isomers with this composition, p-xylene and ethylbenzene. If both were produced in future experiments, measuring m/z 106 below 8.8 eV would selectively probe p-xylene. These results confirm that MBMS is a powerful tool for this application.

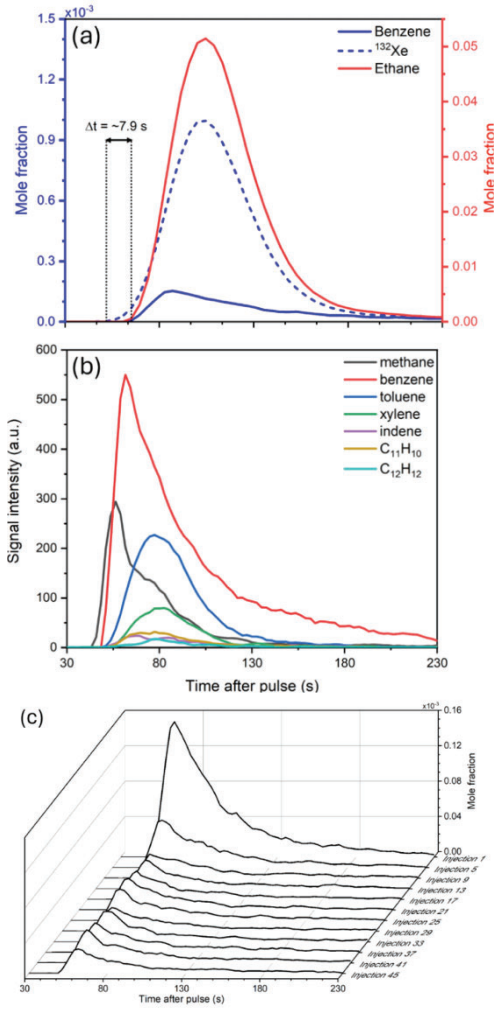

Figure 2. Reactant pulsing ethane DHA studies with synchrotron photoionization MBMS with unoptimized Pt/HZSM-5 [*J. Am. Chem. Soc.* 2022, 144, 13874–13887 and *ACS Catal.* 2024, 14, 4999−5005]. 250 mg; 20 mL reactant gas mixture; 47 vol% ethane, 47 vol% Ar, 6 vol% Xe; 500°C, 600 Torr. (a) Quantified time trace signal of xenon tracer gas compared to reactant (ethane) and product (benzene) time trace signals. (b) Signal intensity of time trace signal for various species collected simultaneously; 13.8 eV. (c) Quantified time trace signals of benzene as a function of injection number; 11 eV.

Reactant pulsing to study the ethane dehdroaromatization (DHA) reaction over a Pt/HZSM-5 catalyst

Data from the continuous-flow ethane DHA experiments above emphasize the importance of understanding catalyst deactivation for this reaction. This is known to the field – the key challenges associated with ethane DHA technology relate to controlling selectivity and avoiding/understanding catalyst deactivation.

The mechanisms of ethane DHA involve pools of intermediates within pores. These systems are effectively studied using time-resolved techniques – those that capture the release of products in the context of the hydrocarbon pool generated during the induction period and the autocatalytic dual-cycle period [*Top. Catal*. 2020, 63, 1463–1473]. In this period we have implemented a new approach to study the transient response of this system based on a reactant pulsing methodology. We designed experiments using a 6-port reactant sampling valve to pulse a precise metered volume of reactant gas through a catalyst bed. Early results are shown in Figure 2. We assume that catalyst deactivation proceeds as a function of the number of moles of carbon exposed onto the catalyst bed; therefore, small-volume reactant gas pulses significantly reduce the rate at which catalyst deactivation occurs. Use of gas pulses also adds a powerful temporal dimension to our product analyses. The relative onset time and breadth of the time trace curve for a particular species provides unique insights into its formation and interaction with catalytic sites.

Figure 2a shows quantified time trace signals for the reactant (ethane), desired product (benzene) and tracer gas (xenon), which provides a simple overview of the data obtained by our new experimental approach. The xenon time trace is representative of a non-interacting, inert species that only experiences inter-diffusive broadening and provides a zero point upon which to compare the relative onset times of different product species. The time traces shown in Figure 2b were compiled from mass spectra collected after a single reactant gas pulse which exhibits the power of the time-of-flight analyzer as it allows for the simultaneous collection of data for every relevant mass number. Analysis with a more standard quadrupole analyzer would dramatically diminish the time resolution of the collected time traces and collection of multiple species time traces during a single gas pulse would not be possible. Finally, Figure 2c shows quantified time traces for benzene as a function of injection number. Similarly to the continuous-flow experiments, the benzene signal exhibits rapid deactivation; however, using the reactant pulsing technique, the benzene signal achieves and maintains a steady state within a handful of injections. Steady state analysis of catalytic activity is vital and especially difficult for a reaction like ethane DHA that suffers greatly from deactivation. The capability of steady state analysis with our reactant pulsing technique presents great opportunity. Using

these approaches, we will bring new insights into the reaction mechanisms and events that lead to selective ethane upgrading and properties of the catalytic system that are associated with deactivation.

Oxidative methane coupling and soft oxidant methane coupling

In this period we also completed a study on the catalytic oxidative coupling of methane. In additional efforts, we have studied the use of CO_2 and N_2O as soft oxidants for methane coupling to produce ethylene. To accomplish this, we developed a ZnO-supported CaO catalyst, with varied loading of CaO. Our recent publication in this area [*J. Phys. Chem. C* 2024, 128, 1165−1176], led by Ph.D. student Leah Filardi and led by this grant, investigates the relationship between the local environment of Ca, studied through Ca K-edge XAS, and activity. Experiment and theory from ab initio full multiple scattering calculations showed that in sites particularly active for methane coupling, Ca primarily exists in an oxidized state that is consistent with the coordination environment of Ca ions in one- and two- dimensional clusters. The local Ca structure was correlated with methane coupling activity. Figure 3 provides a plot of C_2 product selectivity vs. Ca loading. This study provides a unique perspective on the relationship between catalyst physical and electronic structure and active sites for soft oxidant methane coupling, which informs catalyst development.

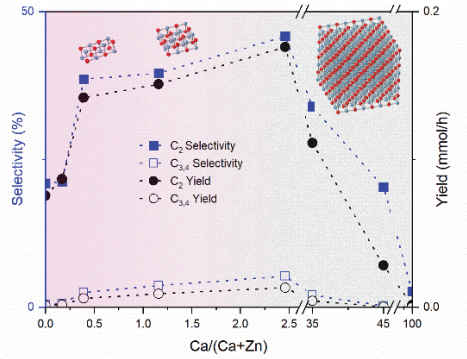

Figure 3. N_2O-assisted methane coupling C_2 selectivity vs. Ca loading in ZnO-supported CaO catalysts. From our publication [*J. Phys. Chem. C* 2024, 128, 1165−1176].

Progress in computational aspects

During this reporting period, we have made significant strides towards bridging the gap between atomistic calculations at the density functional theory (DFT) level and the development of first principles coupled gas-surface microkinetic models that can be experimentally verified. Primarily, this has been achieved by leveraging machine learning-based potentials (MLPs) to achieve DFT-level accuracy at a much-reduced computational cost. We have shown that these DFT-derived MLPs can be used to investigate many different physio-chemical processes such as diffusion, reactions, and desorption for simple metals (e.g., Ag) and for multi-metallic surfaces.

For example, first, we have demonstrated that MLPs can be used to calculate surface diffusivities directly through molecular dynamics (MD) simulations. This approach sidesteps the harmonic approximations that is required for diffusion barriers obtained using DFT-based nudged elastic band (DFT/NEB) methods. This work has been published [*J. Phys. Chem. C*, 2024, 128, 31, 13238–13248]. Second, we have used similar MLP-based workflow to investigate Ag-catalyzed oxidation of methanol. Specifically, we used the Pynta code – developed at Sandia – to iteratively develop a reactive MLP and exhaustively calculate all possible transition states for the relevant reactions – this work is currently being prepared for peer-review. Finally, as a step toward expanding the scope of our MLPs, we have generated DFT data for more complex multi-metallic surfaces such as high-entropy alloys and develop models to predict the binding energy of nitrogen containing molecules. Taken together, these results highlight the versatility of our MLP-based approaches in studying phenomena (e.g., diffusion and reaction barriers) at DFT-accuracies but at significantly reduced costs. Over the new few years, we will expand these methods to nanoporous material such as zeolites where the diversity of active sites and confinement effects will need to be considered.

Surface diffusivities using DFT/MLPs

The advent of machine learning potentials (MLPs) provides a unique opportunity to access simulation timescales and to directly compute physiochemical properties that are typically intractable using density functional theory (DFT). Supported by this award, we have used an active learning curriculum to train a generalizable MLP using the DeepMD-kit architecture. The resulting model, which provides DFT-level

(a)

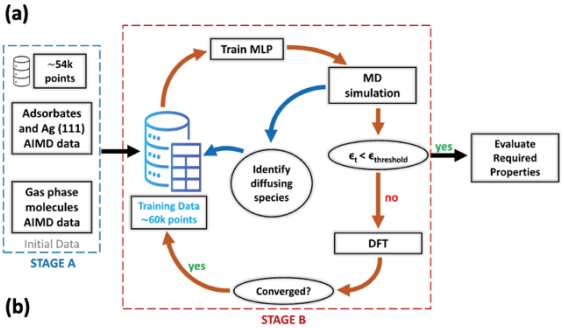

(b)

Adsorbate[a]	Diffusivity (400 K) × 10^{-9} (m^2/s)	Diffusivity (350 K) × 10^{-9} (m^2/s)	Diffusivity (300 K) × 10^{-9} (m^2/s)	E_d^{app} (eV)	Intercept ($\ln(D_0)$)
[CH3]	238.63	149.57	46.34	0.18	8.70
[CH2]	30.25	17.63	13.68	0.08	3.35
[CH]	3.42	3.06	1.06	0.12	2.71
[C]	2.07	1.46	0.94	0.08	0.80
[O]	3.97	2.16	0.95	0.14	3.37
[H]	44.17	32.73	16.03	0.11	4.61
[OH]	27.51	16.94	13.85	0.07	2.94
[CH2]C	67.34	57.84	33.71	0.07	4.07

Figure 4. (a) An active learning curriculum was used to develop a DeepMD-kit based machine learning potential for calculating diffusivity of surface bound intermediates. (b) Our results show that diffusivities obtained from MD are more accurate than those obtained using nudged elastic band calculations and traditional harmonic transition state theory.

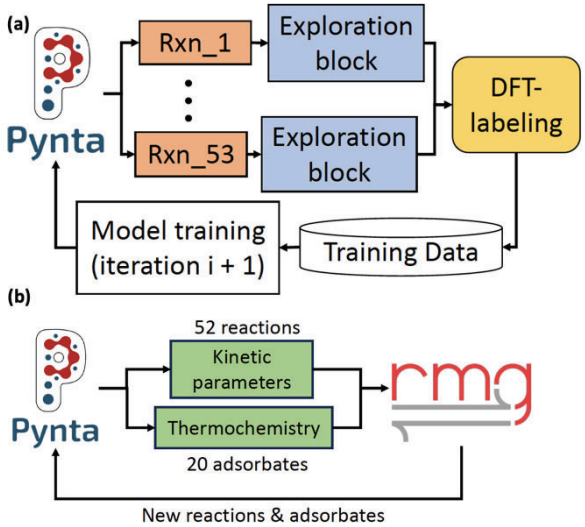

Figure 5. Schematic representation of using Pynta for (a) developing reactive MLPs for modeling surface reactions, and (b) for obtaining coupled gas-surface microkinetic models. This work was performed in collaboration Dr. Judit Zádor through a SCGSR fellowship.

accuracy, is used to investigate the diffusion of key surface-bound adsorbates on an Ag(111) facet using sufficiently long MLP-based molecular dynamics (MD) simulations. The MLP/MD-calculated diffusivities, obtained at three different temperatures, demonstrates the potential shortcomings of DFT-based nudged elastic band calculations that are widely employed to study diffusion. While this work has focused on a few adsorbates, the resulting model is transferable and can be fine-tuned to study other adsorbates not included in the initial training dataset.

Automated construction of reaction networks using DFT/MLPs

While microkinetic models (MKMs) can enable the rational design of new catalytic materials, the computational cost and manual nature of traditional approaches in their construction limits their applicability and transferability. Supported by this grant, we have used machine learning-based potentials (MLPs) and automated workflows to construct a comprehensive MKM describing the coupled gas and surface phase reactions for the partial oxidation of methanol over a silver catalyst. We use the open-source workflow tool Pynta to automate the DFT calculations of adsorbate thermochemistry and reaction kinetics. To accelerate these calculations, we demonstrate how Pynta can be used to iteratively train a reactive machine-learned potential (rMLP). We leverage the Reaction Mechanism Generator (RMG) to simulate this reaction and predict a set of important gas and surface phase reactions. These predictions inform new reactions and species to explore with Pynta so that we can generate new data for updating RMG to improve further simulations. We demonstrate iterative improvement of the model and a powerful framework for constructing comprehensive MKMs.

Modeling multi-metallic surfaces using ML-models

Finally, supported by this grant, we have worked on expanding the complexity of metal surfaces (such as Ag, studied above) to high-entropy alloys. This aims to address the challenge of developing interpretable ML-based models when access to large-scale computational resources is limited. Using CoMoFeNiCu high-entropy alloy catalysts as an example, we present a cost-effective workflow that synergistically combines descriptor-based approaches, machine learning-based force fields, and low-cost density functional theory (DFT) calculations to predict high-quality adsorption energies for H, N, and NH_x (x = 1, 2, and 3) adsorbates. This is achieved using three specific modifications to typical DFT workflows including: (1)

using a sequential optimization protocol, (2) developing a new geometry-based descriptor, and (3) repurposing the already-available low-cost DFT optimization trajectories to develop a ML-FF. Taken together, this study illustrates how cost-effective DFT calculations and appropriately designed descriptors can be used to develop cheap but useful models for predicting high-quality adsorption energies at significantly lower computational costs. We anticipate that this resource-efficient philosophy may be broadly relevant to the larger surface catalysis community.

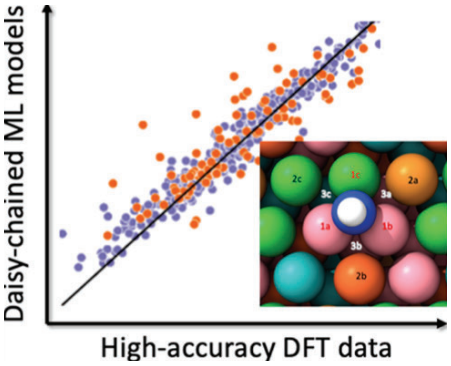

Figure 6. A parity plot illustrating that the binding energies predicted by our ML model align closely with the DFT-calculated values for the adsorption of NH_x species on CoMoFeNiCu high-entropy alloys.

FUTURE PLANS

Further integrate experiment and theory to develop a cohesive workflow for catalysis research

We will apply our integrated experiment-theory approach for studying coupling reactions with gas- and surface-mediated steps with the use of highly characterized catalysts with well-defined active sites. We seek to correlate catalytic activity for the reactions with the speciation of products and intermediates in the gas phase and with the atomic-scale structure of supported transition metal active sites. The goal of this work is to derive relationships between local composition/structure of (uniform) active sites and the local gas-phase universal speciation during reaction. Our next efforts emphasize the evolution of supported Pt catalysts. We find that we are able to stabilize both nanoparticulate and atomically dispersed Pt during reaction, which facilitates study of the structure- and Pt speciation-dependent activity of these systems. This accomplishment was essential because our computational and often experimental data analyses assume a defined catalyst state.

We also continue to work with SNL-CRF on optimization of experiments. We synthesize and characterize catalysts and study their activities in reactor studies. Our near-term experimental goals involve optimization of systems to include the new pulse-response experiments described above. To accomplish this, UC Davis PhD students work alongside Sandia scientists.

PUBLICATIONS APPEARING IN 2023-2024

1. The Photoionization of Methoxymethanol: Fingerprinting a Reactive C_2 Oxygenate in a Complex Reactive Mixture. *J. Chem. Phys.,* **2024**, 160, 124306. https://doi.org/10.1063/5.0197827.
2. Dynamic Structural Evolution of MgO-Supported Palladium Catalysts: From Metal to Metal Oxide Nanoparticles to Surface Then Subsurface Atomically Dispersed Cations. *Chem. Sci.,* **2024**, 15, 6454–6464. https://doi.org/10.1039/d4sc00035h.
3. Impact of Local Structure in Supported CaO Catalysts for Soft Oxidant-Assisted Methane Coupling Assessed through Ca K-edge X-ray Absorption Spectroscopy. *J. Phys. Chem. C,* 2024**,** 128, 1165−1176. https://doi.org/10.1021/acs.jpcc.3c06527.
4. Developing Cheap but Useful Machine Learning-Based Models for Investigating High-Entropy Alloy Catalysts. Langmuir, **2024**, 40, 3691–3701. https://doi.org/10.1021/acs.langmuir.3c03401.
5. Toward an Ab Initio Description of Adsorbate Surface Dynamics. *J. Phys. Chem. C,* **2024**, 128, 31, 13238–13248. https://doi.org/10.1021/acs.jpcc.4c02250.
6. Constraining Reaction Pathways for Methanol Oxidation through Operando Interrogation of Both the Surface and the Near-Surface Gas Phase. *Chem Catal*., **2023**, 3, 100782. https://doi.org/10.1016/j.checat.2023.100782.
7. A Pynta-based Curriculum for Accelerated Calculation of Reaction Barriers and Transition State Geometries for Surface Mediated Reactions, *Submitting* **2024**, (In preparation).

Molecular Reactivity in Complex Systems

Musahid Ahmed (mahmed@lbl.gov), Daniel Neumark (DMNeumark@lbl.gov), Kevin Wilson (krwilson@lbl.gov)

Chemical Sciences Division, LBNL, Berkeley, CA-94720

Background and Significance

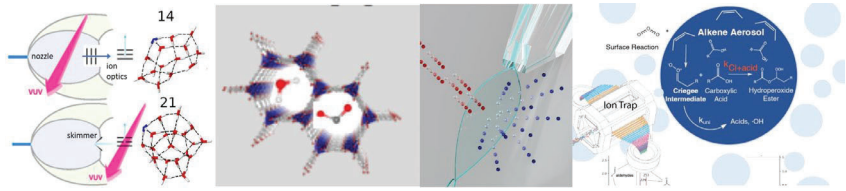

Fig. 1. Composite showing the themes that constitute this subtask from left to right. Photoionization of Clusters,[1-8] Gases in Confinement,[9-11] Dynamics in Liquid Jets[12-14] and Aerosol Chemistry.[15-18]

Our effort on molecular reactivity in complex systems targets multistep and multiphase chemical transformations built from isolated elementary bimolecular reactions to gas-surface reaction dynamics to coupled networks of elementary unimolecular and bimolecular pathways embedded at a gas/solid or liquid interface. In each of these areas, the gas phase is central for controlling the multiphase chemistry with additional kinetic processes, such as evaporation, condensation, and diffusion, playing a key role in governing the overall reactive outcome. (**Fig. 1**) Activities in this Subtask drive new theory and simulation, to enrich the molecular level interpretation of experiments with extensive use of DOE national user facilities such as the Advanced Light Source and NERSC.

Progress Report:

Photoionization Dynamics, Hydrogen Bonding and Reactivity in Molecular Beams: Van der Waals and hydrogen bonded clusters provide a template to probe ionization and solvation processes of paramount interest in thermal science, environmental and astrochemistry. Ahmed and co-workers tracked the appearance of a new magic number at 14, in addition to the traditional 21 in protonated water clusters.[4] Head-Gordon and coworkers performed meta-dynamics conformer searches coupled with state-of-the-art density functional calculations to identify the global minimum energy structures of protonated water clusters between n = 2 and 21, as well as the manifold of low-lying metastable minima. This methodology of combining mass spectrometry with electronic structure calculations was extended to a series of diol water clusters to understand how hydrogen bond networks evolve as one changes the positioning of methyl and hydroxyl groups over a similar backbone.[8] We discussed and suggested that the reactivity and photoionization of diols (ethylene glycol, 1,2 and 1,3 propylene glycols) in the presence of water is dependent on the size of the diol, the location of the hydroxyl group, and the number of water molecules clustered around the diol. In the case of formic acid water clusters, enhanced intensities are observed in the mass spectra for a number of clusters holding the following composition, $FA_1W_5H^+$, $FA_2W_4H^+$, $FA_3W_3H^+$, $FA_4W_2H^+$, $FA_5W_1H^+$ and $FA_6W_2H^+$ compared to their neighbors with one less or one more water component.[5] Our calculations shed light on these potentially stable structures, highlighting cyclic arrangements with molecules enclosed within the ring as the most stable structures, and demonstrate a decrease in the stability upon the addition of a water molecule. We close out this section reporting two recent studies of photoionization dynamics in methane-water clusters resulting in the formation of methanol and using PAH's as ionizer tags to decipher the electronic states of CO_2 clusters. Previous studies on methane-water clusters have primarily focused on the formation and structural information related to methane clathrates. We demonstrate that slight changes in our experimental conditions such as backing pressure and mixing ratios can generate water

rich or methane rich mixed clusters providing a fertile arena for probing these clusters at the molecular level. We experimentally demonstrated the formation of methanol within the methane-water cluster, following dissociative photo-ionization of a water moiety and subsequent extensive rearrangement.[6] We investigated the vacuum UV excitation of the naphthalene–CO_2 complex and observed excited states of CO_2 through a newly identified molecular electronic energy transfer ionization mechanism. We evaluated the spectral development upon cluster growth with time-dependent density functional theory and show that the photoionization spectrum of naphthalene–CO_2 closely resembles the photon-stimulated desorption spectrum of CO_2 ice.[7]

In collaboration with Ralf Kaiser (Hawaii), Ahmed seeks to understand the reactivity of long chain hydrocarbon fuel molecules on nanoparticle surfaces under high temperature and pressure conditions. This is a new direction for the radical-radical hot nozzle project.[19-24] A study to understand the fundamental bond breaking processes, reaction mechanisms, and kinetics involved in the oxidation of Jet Propellant-10 (JP10) jet fuel on aluminum oxide nanoparticles was completed.[25] We reveal an active low temperature heterogeneous catalytic surface chemistry commencing at 650 K involving the alumina (Al_2O_3) shell.[26] We also showed in a separate study that stress-altered aluminum nanoparticles exhibited distinctly different temperature-dependent reactivities towards catalytic decomposition of JP10.[27]

Evaporation and Molecular Beam Scattering from and on Liquid Jets: Molecular beam experiments in which gas molecules are scattered from liquids provide detailed, microscopic perspectives on the gas–liquid interface. Extending these methods to volatile liquids while maintaining the ability to measure product energy and angular distributions presents a significant challenge. The incorporation of flat liquid jets into molecular beam scattering experiments in the Neumark laboratory has allowed us to demonstrate their utility in uncovering dynamics in this complex chemical environment. Recent work on the evaporation and scattering of Ne, CD_4, ND_3, and D_2O from a dodecane flat liquid jet and first results on the evaporation and scattering of Ar from a cold salty water jet are described in a review article.[14] In the evaporation experiments, Maxwell–Boltzmann flux distributions with a cos(θ) angular distribution are observed. Scattering experiments reveal both impulsive scattering (IS) and trapping followed by thermal desorption (TD). Super-specular scattering is observed for all four species scattered from dodecane and is attributed to anisotropic momentum transfer to the liquid surface. In the IS channel, rotational excitation of the polyatomic scatterers is a significant energy sink, and these species accommodate more readily on the dodecane surface compared to Ne. Our preliminary results on cold salty water jets suggest that Ar atoms undergo some vapor-phase collisions when evaporating from the liquid surface. Initial scattering experiments characterize the mechanisms of Ar interacting with an aqueous jet, allowing for comparison to dodecane systems.

Aerosol and Multiphase Chemistry: Wilson and co-workers report efforts to understand the multiphase chemistry occurring at simple hydrocarbon aerosols. Criegee intermediates (CI) are central to the ozonolysis of unsaturated organic compounds, controlling the formation of small fragmentation reaction products and higher molecular weight oligomeric compounds through competing unimolecular and bimolecular pathways. We completed a series of aerosol flow tube studies of the ozonolysis of submicron organic aerosol containing mixtures of an internal *n*-alkene (Z-9-tricosene, Tri) and a saturated acid (2-hexyldecanoic acid, HDA).[18] The decay of the reactants and formation of reaction products are monitored using a custom-built aerosol interface to an Atmospheric Pressure Chemical Ionization mass spectrometer (APCI-MS). A sixfold-decrease in the reactive uptake (γ_{eff}) of ozone is observed with increasing acid concentration. Stochastic kinetic simulations are conducted

with different values of the CI + RCOOH rate constant to validate this result and show that the diffusion limited rate is indeed much too rapid to reproduce the experimental results.

Future:

Beyond Single Photon Ionization, Towards Excited States, Photo-Induced Energy and Electron Transfer: We propose to introduce laser spectroscopy to investigate the lower lying electronic properties of non-covalent complexes as well as to elucidate on their gas-phase structure as the ALS heads towards a shutdown. We propose to investigate structural rearrangements, internal conversion of energy and reactivity in clusters using our recently completed laser-based (Coherent Monaco pump laser coupled to Opera Optical Parametric Amplifier) mass spectrometer, which at its heart has a widely tunable femtosecond laser operating at up to 750 kHz. The probe pulse can be the second (517 nm), third (345 nm) or ninth (115 nm) harmonic of the fundamental. The ninth harmonic is generated in a Xe gas cell leading to VUV photon energy of 10.8 eV allowing access to ionization for a multitude of systems. One of our first undertakings will be to study the excited state dynamics of the anthracene dimer in collaboration with Eric Neuscamman (see Subtask 3) since its structure has been reported in the literature, while its excited state dynamics are a holy grail in the area of organic electronics because of possible singlet fission. Beyond that, clusters of interest are relevant to understanding and mitigating climate change (such as water-CO_2) or astrochemistry (methane-water, PAHs). The molecular configuration has a large effect on the electronic properties of molecules. Thus, we propose to use IR vibrational spectroscopy for structural elucidation. For pure water clusters, and mixed water clusters, this has been the method of choice, since the frequency of the infrared transitions, or position of the vibrational energy levels, are a direct result of the shape of the potential energy surface and hence their structure. One particular system of interest within our astrochemistry research line is CO_2-H_2O clusters, two of the most abundant ices in the interstellar medium. There is intense interest in carbon dioxide reduction, both as a fundamental science problem, as well as in light of the pressing challenges of rising CO_2 concentrations in the atmosphere which invites use of CO_2 as a feedstock. CO_2 reduction is thought to typically begin with formation of the radical anion CO_2^-, but the anion itself is a transient intermediate in reactive cascades and so is never experimentally characterized in catalytic cycles. We propose to perform cluster experiments and complementary quantum chemical calculations (MHG) on model clusters where the CO_2 anion can be generated either by spontaneous electron transfer, or by photoinduced charge transfer based upon suitable molecular ionizers (PAH's) and/or soft ionization methods. We propose to use the spectroscopic probes described earlier, particularly IR spectroscopy that would be very sensitive to the change in oxidation state of CO_2, as well as the strong change in geometry associated with charge transfer.

Leaky Nozzle Spectroscopy & Gases in Confinement: To probe gas phase molecules in confinement, Ahmed and co-workers are designing and implementing new devices that can be accommodated within mass spectrometers and laser based spectroscopic instruments. This is adapted from a previous design of a System for Analysis of Liquid Interfaces (SALVI) where liquids flow continuously in a reservoir and gases emanate through a 1 – 3 μm aperture to the vacuum chamber. These molecules evaporating through the aperture are interrogated by VUV photons and then detected by mass spectrometry. One such multimodal approach to probe both the gas phase and the gases within confinement is to interrogate the dynamics of the gas phase molecules (H_2O, CO_2, N_2) inside a metal organic framework (MOF) cavity using Raman spectroscopy (50-4000 cm^{-1}) allowing access to the lattice dynamics of the MOF cage in the THz regime, and the gas-organic linker functional group information in the IR region. A particularly exciting direction is that Qian and co-workers (Subtask 3) are developing methods to calculate X-ray, THz, IR and Raman spectra that will guide interpretation of the experimental results. Such an effort was also used to develop a computational model based on plane-wave KS-DFT to explain molecular details in Piedong Yang's (LBNL) Ag nanoparticle/ordered ligand interlayer (Ag-

NOLI) system to convert CO_2 in confinement. we could leverage an increasingly negative potential to induce the opening of a catalytically activated pocket. This pocket is formed by cleaving the O-Ag bonds between the tetradecylphosphonic (TDPA) ligand and the Ag nanoparticle one by one, from bi-dentate to mono-dentate and eventually resulting in a water intercalated non-dentate configuration.[28]

Evaporation and scattering from liquid jets: The Neumark group, in collaboration with the Wilson group, is transitioning from dodecane to water and has recently performed the first evaporation and scattering experiments with aqueous flat jets. Global concentrations of many key atmospheric species are governed by multiphase chemistry at aqueous interfaces. The complexity of these processes and their sensitivity to changing environmental conditions make laboratory studies essential for parametrizing kinetic models and evaluating field measurements. While aerosol experiments in the Wilson group focus on how multiphase chemistry affects droplet composition, molecular beam scattering probes the gas phase products produced at the liquid interface. Thus, for example, the Cl_2/aerosol uptake studies are highly complementary to Cl_2 scattering experiments from flat liquid jets. Within this context, the reactive uptake of N_2O_5 on aqueous surfaces is of particular interest. Neumark will carry out experiments scattering N_2O_5 from cold salty water flat jets, monitoring both the scattering and depletion of the initial molecular beam species as well as reaction products that are formed at the interface and ejected into the gas phase. Branching ratios for these reactions will be determined by assigning product formation channels to TD and IS mechanisms. Another reaction of interest is the hydration of SO_3 to form H_2SO_4, a major contributor to atmospheric acid rain formation and aerosol nucleation. By scattering SO_3 from a flat water jet, one can determine if it is immediately incorporated into the liquid or if the limited access to water molecules at the interface is sufficient to catalyze the formation of H_2SO_4 on the surface. Additionally, the cold salty water jet enables study of industrially relevant processes, such as the heterogeneous capture of CO_2. CO_2 capture is carried out by flowing flue gas through aqueous solutions containing nontoxic compounds such as monoethanolamine (MEA) via the following reaction: $2MEA + CO_2 \rightarrow MEACOO^- + MEAH^+$. It has been shown that neutral MEA preferentially exists at the surface of aqueous solutions while the products are mainly found in the bulk; unfortunately, a detailed understanding of the interfacial behavior of this system has not been developed. Thus, through the scattering of CO_2 from neat and amine-enriched water jets, the translational energy and angular distributions of CO_2 will be directly measured, giving insight into the underlying interfacial mechanisms.

Multiphase Aerosol Chemistry and non-covalent interactions: A new direction undertaken by Wilson is to use molecular simulations in collaboration with David Limmer (CPIMS program LBNL), to further explore the mechanism underlying the enhanced reactivity of Cl_2 with squalene in the presence of oxygenated molecules. The overall goal of this collaboration is to uncover the key molecular features at the air-liquid interface that could enhance/control the uptake and reaction of Cl_2. These are the first steps for ultimately developing a molecularly realistic kinetic model of the reaction, as described below**.** We propose to continue our simulation work on the Cl_2 + squalene reaction. Our overall goal is to build a realistic kinetic model that explains the enhanced reactivity of Cl_2 in the presence of oxygenated spectator molecules. To do this we will use the coarse grain stochastic reaction-diffusion kinetic framework that has been used extensively by the Wilson group to model multiphase reactions. The kinetic parameters in the model will be constrained by MD simulations. Once we have developed a realistic kinetic model that can accurately predict the experimentally observed uptake coefficient vs. temperature, we will incorporate oxygenated additives to the simulations. By combining kinetic and molecular simulations we hope to uncover the general principles that govern trace gas uptake and reaction at organic-air interfaces. For example, we hope to elucidate and predict where the multiphase reaction occurs (e.g. surface vs. bulk vs. subsurface).

Organic molecules in the environment oxidatively degrade by a variety of free radical, microbial and biogeochemical pathways. A significant pathway is autoxidation, in which degradation occurs via a network of carbon and oxygen centered free radicals. Recently, we found evidence for a new autoxidation mechanism that is initiated by hydroxyl (OH) radical addition to a carbon-carbon double bond and apparently propagated through pathways involving Criegee Intermediates (CI) produced from β-hydroxy peroxy radicals (β-OH-$RO_2^{\bullet}$). It remains unclear, however, exactly how CI are formed from β-OH-$RO_2^{\bullet}$, which could occur by a unimolecular or bimolecular pathway. We propose to test three mechanistic scenarios using kinetic models and multiphase OH oxidation measurements of squalene. Scenario 1 will assume that CI are formed by the unimolecular bond scission of β-OH-$RO_2^{\bullet}$, whereas Scenarios 2 and 3 test bimolecular pathways of β-OH-$RO_2^{\bullet}$ to yield CI. In parallel the Head-Gordon group will examine potentially new mechanisms using Quantum Chemistry. One such mechanism that looks potentially promising involves the formation for a primary ozonide via OH radical attack of β-OH-$RO_2^{\bullet}$. We will test the predictions of these scenarios against an extensive kinetics data set, which includes effective uptake coefficients vs. [OH] as well as the formation kinetics of the major products, which are aldehydes and secondary ozonides.

Ahmed and Wilson propose to explore the role of the gas-liquid interface in controlling the formation kinetics of zymonic acid (ZA). ZA is formed from a condensation reaction of two pyruvic acid (PA) molecules and only proceeds very slowly in bulk solutions (occurring over days to weeks). Preliminary mass spectrometry measurements of submicron aqueous droplets (radius ~ 100-300 nm) of PA show evidence that ZA is formed in minutes. We hypothesize that rapid ZA formation arises either from interfacial enrichment of reagents and/or a much larger rate coefficient for the surface reaction. To examine this hypothesis requires that the rate coefficient for ZA formation by condensation be quantified within a realistic kinetic description of the bulk-surface partitioning of PA and ZA. Furthermore, since PA is relatively volatile (vapor pressure = 175 Pa), there arises a natural competition of evaporation with the condensation reaction at the interface making this particular reaction a complex multiphase one. We will measure ZA formation kinetics in nano-sized droplets. Kinetics will be measured as a function of size and [PA]. We will build a realistic kinetic model of these kinetic measurements in an effort to constrain the mechanism, explain why this reaction appears to be accelerated in droplets and determine a surface rate coefficient.

Publications citing DOE-GPCP support in subtask 2@Berkeley Lab (2022-2024)

1 Lu, W. C., Mackie, C. J., Xu, B., Head-Gordon, M. & Ahmed, M. A Computational and Experimental View of Hydrogen Bonding in Glycerol Water Clusters. *J. Phys. Chem. A* **126**, 1701-1710 (2022). https://doi.org/10.1021/acs.jpca.2c00659

2 Molina, E. R., Xu, B., Kostko, O., Ahmed, M. & Stein, T. A combined theoretical and experimental study of small anthracene-water clusters. *Phys. Che. Chem. Phys.* **24**, 23106-23118 (2022). https://doi.org/10.1039/d2cp02617a

3 Zamir, A., Rossich Molina, E., Ahmed, M. & Stein, T. Water confinement in small polycyclic aromatic hydrocarbons. *Phys. Chem. Chem. Phys.* **24**, 28788-28793 (2022). https://doi.org/10.1039/d2cp04773j

4 Mackie, C. J. *et al.* Magic Numbers and Stabilities of Photoionized Water Clusters: Computational and Experimental Characterization of the Nanosolvated Hydronium Ion. *J. Phys. Chem. A* **127**, 5999-6011 (2023). https://doi.org/10.1021/acs.jpca.3c02230

5 Daniely, A. *et al.* A Vacuum Ultraviolet Photoionization Mass Spectrometry and Density Functional Calculation Study of Formic Acid-Water Clusters. *J. Phys. Chem. A* **128**, 6392-6401 (2024). https://doi.org/10.1021/acs.jpca.4c02875

6 Dias, N., Lemmens, A. K., Wannenmacher, A. & Ahmed, M. Vacuum Ultraviolet Photoionization of Methane-Water Clusters Leads to Methanol Formation. *ACS Earth Space Chem.* (2024). https://doi.org/10.1021/acsearthspacechem.4c00151

7 Lemmens, A. K., Wannenmacher, A., Dias, N. & Ahmed, M. Electronic energy transfer ionization in naphthalene-CO_2 clusters reveals excited states of dry ice. *Chemical Science* **15** (2024). https://doi.org/10.1039/d4sc03561e

8 Wannenmacher, A. *et al.* An experimental and computational view of the photoionization of diol-water clusters. *J. Chem. Phys.* **160**, 144303 (2024). https://doi.org/10.1063/5.0198162

9 Lu, W. *et al.* Probing growth of metal-organic frameworks with X-ray scattering and vibrational spectroscopy. *Phys. Chem. Chem. Phys.* **24**, 26102-26110 (2022). https://doi.org/10.1039/d2cp04375k

10 Devlin, S. W. *et al.* Agglomeration Drives the Reversed Fractionation of Aqueous Carbonate and Bicarbonate at the Air-Water Interface. *JACS* **145**, 22384-22393 (2023). https://doi.org/10.1021/jacs.3c05093

11 Glenna, D. M. *et al.* Carbon Capture: Theoretical Guidelines for Activated Carbon-Based CO2 Adsorption Material Evaluation. *J. Phys. Chem. Lett.* **14**, 10693-10699 (2023). https://doi.org/10.1021/acs.jpclett.3c02711

12 Lee, C. *et al.* Evaporation and Molecular Beam Scattering from a Flat Liquid Jet. *J. Phys. Chem. A* **126**, 3373-3383 (2022). https://doi.org/10.1021/acs.jpca.2c01174

13 Pohl, M. N. *et al.* Photoelectron circular dichroism in angle-resolved photoemission from liquid fenchone. *PCCP* **24**, 8081-8092 (2022). https://doi.org/10.1039/D1CP05748K

14 Yang, W. L. *et al.* Molecular beam scattering from flat jets of liquid dodecane and water. *Natural Sciences* **4** (2024). https://doi.org/10.1002/ntls.20240009

15 Rundel, J. A. *et al.* Production of Aliphatic-Linked Polycyclic Hydrocarbons during Radical-Driven Particle Formation from Propyne and Propene Pyrolysis. *Combust. Flame*, 112457 (2022). https://doi.org/10.1016/j.combustflame.2022.112457

16 Rundel, J. A. *et al.* Promotion of particle formation by resonance-stabilized radicals during hydrocarbon pyrolysis. *Combust. Flame* **243**, 111942 (2022). https://doi.org/10.1016/j.combustflame.2021.111942

17 Zeng, M., Liu, C.-L. & Wilson, K. R. Catalytic Coupling of Free Radical Oxidation and Electrophilic Chlorine Addition by Phase-Transfer Intermediates in Liquid Aerosols. *J. Phys. Chem. A* **126**, 2959-2965 (2022). https://doi.org/10.1021/acs.jpca.2c00291

18 Reynolds, R., Ahmed, M. & Wilson, K. R. Constraining the Reaction Rate of Criegee Intermediates with Carboxylic Acids during the Multiphase Ozonolysis of Aerosolized Alkenes. *ACS Earth Space Chem.* (2023). https://doi.org/10.1021/acsearthspacechem.3c00026

19 Kaiser, R. I. *et al.* Gas-phase synthesis of racemic helicenes and their potential role in the enantiomeric enrichment of sugars and amino acids in meteorites. *PCCP* **24**, 25077-25087 (2022). https://doi.org/10.1039/d2cp03084e

20 Kaiser, R. I. *et al.* Unconventional excited-state dynamics in the concerted benzyl (C(7)H(7)) radical self-reaction to anthracene (C(14)H(10)). *Nat Commun* **13**, 786 (2022). https://doi.org/10.1038/s41467-022-28466-7

21 Kaiser, R. I. *et al.* Formation of Benzene and Naphthalene through Cyclopentadienyl-Mediated Radical–Radical Reactions. *J. Phys. Chem. Lett.* **13**, 208-213 (2022). https://doi.org/10.1021/acs.jpclett.1c03733

22 He, C. *et al.* Unconventional Pathway in the Gas-Phase Synthesis of 9H-Fluorene (C(13) H(10)) via the Radical-Radical Reaction of Benzyl (C(7) H(7)) with Phenyl (C(6) H(5)). *Angew. Chem. Int. Ed. Engl.* **62**, e202216972 (2023). https://doi.org/10.1002/anie.202216972

23 He, C. *et al.* Exotic Reaction Dynamics in the Gas-Phase Preparation of Anthracene (C(14)H(10)) via Spiroaromatic Radical Transients in the Indenyl-Cyclopentadienyl Radical-Radical Reaction. *J. Am. Chem. Soc.* **145**, 3084-3091 (2023). https://doi.org/10.1021/jacs.2c12045

24 Yang, Z. H. *et al.* Gas-phase formation of the resonantly stabilized 1-indenyl radical in the interstellar medium. *Science Advances* **9** (2023). https://doi.org/10.1126/sciadv.adi5060

25 Biswas, S. *et al.* Efficient Oxidative Decomposition of Jet-Fuel exo-Tetrahydrodicyclopentadiene (JP-10) by Aluminum Nanoparticles in a Catalytic Microreactor: An Online Vacuum Ultraviolet Photoionization Study. *J. Phys. Chem. A* **128**, 1665–1684 (2024). https://doi.org/10.1021/acs.jpca.3c08125

26 Biswas, S. *et al.* Counterintuitive Catalytic Reactivity of the Aluminum Oxide “Passivation” Shell of Aluminum Nanoparticles Facilitating the Thermal Decomposition of exo-Tetrahydrodicyclopentadiene (JP-10). *J. Phys. Chem. Lett.* **14**, 9341–9350 (2023). https://doi.org/10.1021/acs.jpclett.3c02532

27 Biswas, S. *et al.* Stress-Alteration Enhancement of the Reactivity of Aluminum Nanoparticles in the Catalytic Decomposition of exo-Tetrahydrodicyclopentadiene (JP-10). *J. Phys. Chem. A* (2024). https://doi.org/10.1021/acs.jpca.4c02023

28 Shan, Y. *et al.* Nanometre-Resolved Observation of Electrochemical Microenvironment Formation at the Nanoparticle–Ligand Interface. *Nat. Catal.* (2024). https://doi.org/10.1038/s41929-024-01119-2

Fundamental Molecular Spectroscopy and Chemical Dynamics

Stephen R. Leone and Daniel M. Neumark
Lawrence Berkeley National Laboratory and Department of Chemistry,
University of California, Berkeley, California 94720
(510) 643-5467 srl@berkeley.edu
510-642-3502 dneumark@berkeley.edu

Scope of the Project: Decades of research into reaction rates, branching fractions, dissociation dynamics, and energetics have vastly improved our fundamental understanding of chemical processes. Measurements of radical spectroscopy and excited state dynamics comprise key future goals of this effort, especially the development of new ways to probe excited state dynamics developed by Neumark and Leone. For example, over past program cycles, the Neumark program pioneered high-resolution cold anion photoelectron spectroscopy and radical beam photodissociation product coincidence spectroscopy, and the Leone group exploited synchrotron photoionization for complex chemistry and intermediate detection, as well as extreme ultraviolet probing of photodissociation dynamics and intermediate state processes. Now the Leone and Neumark groups are pioneering femtosecond and attosecond time-resolved table-top X-ray spectroscopic probing of photochemical processes at sufficiently high photon energies to access carbon K-edge spectroscopy with unprecedented time resolution. In this subtask, ring opening has been investigated by X-ray and by electron diffraction at the SLAC UED facility, and Jahn-Teller distortion was observed in real time in the X-ray. This subtask describes progress and planned experiments by the Leone and Neumark groups to extend X-ray dynamic probing into new realms, including diradical species, coherent dynamics, and resonance stabilization of radicals Together with theorists Neuscamman and Head-Gordon, this program advances on multiple fronts the dynamics and energetics of reactive species.

Recent Progress:

Experiments during the last three years have focused on soft X-ray transient absorption spectroscopy (XTAS) measurements at photon energies ranging from 150-300 eV. The soft X-ray light is produced by tabletop laser systems capable of generating femtosecond or attosecond pulses. This range of photon energies enables one to access core-to-valence transitions in sulfur, chlorine, and carbon. Several of the experiments described below are pump-probe experiments in which an ultrafast 800 nm pulse serves as the pump pulse that initiates dynamics in the target molecule by impulsive stimulated Raman scattering (ISRS) or strong field ionization (SFI). ISRS initiates coherent vibrational motion on the electronic ground state of the target that appears as oscillatory motion in the X-ray transient absorption spectrum, while SFI initiates dynamics (Jahn-Teller distortion, dissociation) in the corresponding molecular cation. In both cases, the monitored core-to-valence transitions allow one to follow the dynamics with elemental specificity. Alternatively, many of the experiments utilize single photon initiation of photodynamics with 266 nm ultraviolet (UV) pulses created by nonlinear frequency mixing. This has the advantage of preparing a well-defined initial state based on the long history of well-known photochemistry. Some experiments are carried out with resonant - UV two-photon ionization and transient absorption detection. Finally, some experiments are performed with ultrafast electron diffraction.

Coherent Vibrations in Neutral SF_6. The potential energy surfaces (PESs) of a molecule dictate its coupled electron-nuclear dynamics following electronic excitation. In particular, PESs of core-excited states are of considerable interest due to core-level excitation being able to induce ultrafast nuclear motion on a timescale shorter than the few-femtosecond core-hole lifetime. Using attosecond X-ray probing of core level potentials, Barreau *et* al. mapped the inner shell PESs of SF_6 along the symmetric S-F stretch for several core sulfur L-edge excitations in the range of 170-200 eV. In this work, ISRS with a 6 fs 800 nm pulse excited coherent vibrational motion on the SF_6 ground state, yielding oscillations in the X-ray transient absorption spectrum at the frequency of the a_{1g} symmetric stretch ($\nu_1 = 775$ cm^{-1}, $T_1 = 43$ fs). The top panel of **Fig. 1** shows how vibrational wavepacket motion is imprinted on the X-ray transient absorption (XTA) spectrum; as the molecule vibrates, one observes oscillatory energy shifts in the XTA spectrum. Although other non-totally symmetric vibrational modes of SF_6 are Raman active, no signal from these modes is seen, which appears to be a general feature of ISRS/XTAS experiments due to symmetry considerations of the X-ray energy shift. **Fig. 1** (bottom) shows that the magnitudes of ν_1 oscillations in the XTA spectrum differ for the various core-to-valence transitions. From the magnitudes of the observed energy shifts in the X-ray transient absorption as a function of pump intensity, the relative slopes of the excited state PESs for various inner shell states are extracted as shown at the right of **Fig. 1.**

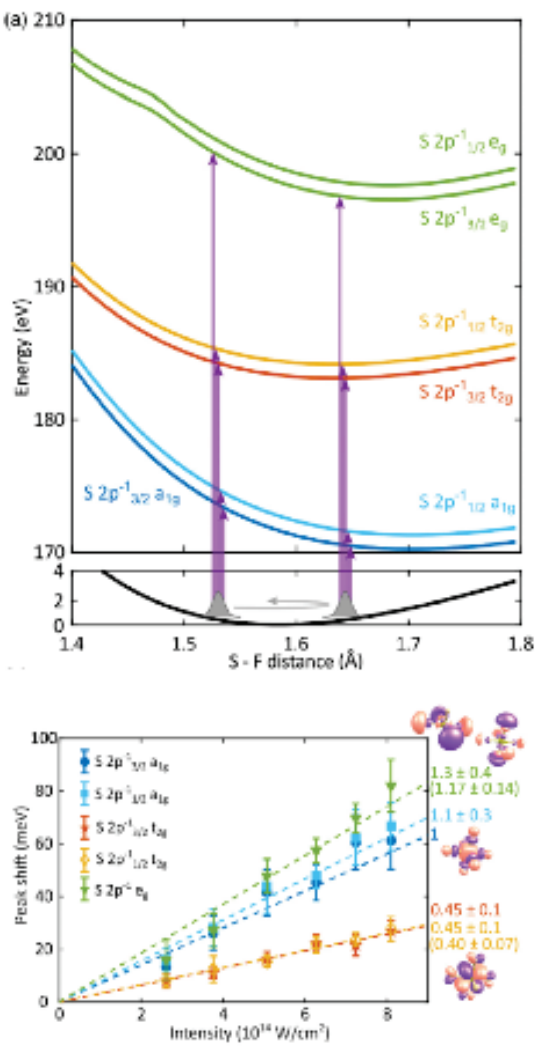

Fig. 1. (top) Principle of ISRS/XTAS experiment. (bottom) Potential energy surface slope mapping via the ν_1 vibrational mode in SF_6.

Signatures of the Bromine Atom and Open-Shell Spin Coupling in the X-ray Spectrum of Bromobenzene Cation. Exploiting the excellent sensitivity of tabletop soft X-ray spectroscopy, Epshtein *et al.* investigated the bromobenzene cation ($BrBz^+$) soft X-ray absorption around the carbon K-edge to explore the influence of halogenation on the X-ray absorption spectrum of the molecular cation as well as on the open-shell spin-coupling observed earlier in the benzene radical cation (Bz^+).[7, 8] The $BrBz^+$ cation was prepared in its electronic ground state by two-photon UV ionization of neutral bromobenzene (BrBz) with 267 nm pump pulses. A soft X-pulse generated via High Harmonic Generation (HHG) and temporally delayed by ~1 ps was used to record the absorption spectra. The dominating features of the spectrum of $BrBz^+$ are two peaks that arise due to core-to-SOMO [C1$s\rightarrow\pi^*$ and C*1$s\rightarrow\sigma^*_{(C^*\text{-Br})}$] transitions (C* is the specific carbon atom bonded to the Br). The identification of peaks as C*1$s\rightarrow\sigma^*_{(C^*\text{-Br})}$ transitions indicates a change in C*-Br bond length due to excitation of the C*-Br-stretch vibrational mode. Interestingly it was found that the influence of the bromine atom on the residual carbon atoms and in particular the C1$s\rightarrow\pi^*$ transition is small.

Femtosecond Symmetry Breaking and Coherent Relaxation of Methane Cations via X-ray Spectroscopy (Jahn-Teller Distortion). The experimental study that showcases the capabilities of our soft X-ray beamline perhaps the best is that by Ridente *et al.* on the direct time-domain observation of Jahn-Teller distortion in the methane cation published in *Science* in 2023 (**Fig. 2**). In conjunction with

important theoretical support from the Martin Head-Gordon group, the authors were able to directly and unambiguously reconstruct the dynamics following the removal of an electron from neutral CH_4 as it converts from its tetrahedral (T_d) shape to a lower-symmetry C_{2v} geometry. CH_4^+ is generated by strong field ionization at a very low power density with 800 nm optical pulses. The key to tracking the change is to observe the large shift in the transition energy of the C1s to SOMO X-ray feature observed in the time-resolved X-ray spectrum. This shift tracks the smallest angle of the H-C-H bond scissoring angle as the system distorts from 109.5º in the neutral tetrahedral to 55º in the Jahn-Teller distorted C_{2v} cation. During this angle change the bond orbital changes from a σ orbital on the CH group to a p-like orbital on the carbon, which is much higher in energy. The initial Jahn-Teller relaxation is essentially complete within (10 ± 2) fs and the motion activates coherent vibrational oscillations in the asymmetric scissoring mode of the CH_4 cation. These oscillations are damped within (58 ± 13) fs by redistribution of the released energy over other internal degrees of freedom. The frequency and damping of the oscillations are reproduced by theory, which also explains how the evolution of molecular orbitals in the cation leads to the observed Jahn-Teller distortion. Upon deuteration, the Jahn-Teller distortion is slowed by the predicted factor of 1.4 to 14 fs. This experiment represents a landmark in the study of molecular dynamics via femtosecond soft X-ray spectroscopy as it directly demonstrates the outstanding sensitivity of the technique to the ultrafast few-femtosecond dynamics in chemically relevant species.

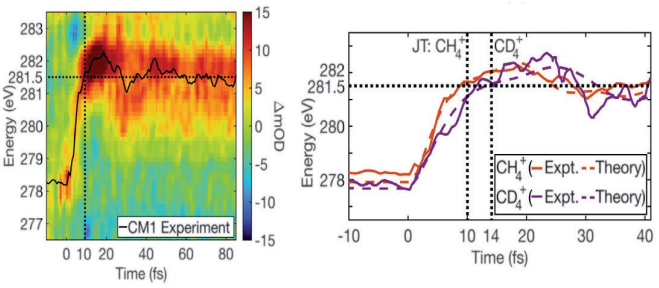

Fig. 2. Jahn-Teller distortion of the methane cation probed directly in the time domain via soft X-ray pump probe spectroscopy. Jahn-Teller distortion of the CH_4 cation occurs rapidly within (10 ± 2) fs upon ionization, activating coherent vibrations that decay within (58 ± 13) fs. Upon deuteration, the time shifts longer by 1.4.

Jahn-Teller Distortion and Dissociation of CCl_4^+ by Transient X-ray Spectroscopy Simultaneously at the Carbon K- and Chlorine L-edge.

In work by Ross *et al,* carbon tetrachloride cations (CCl_4^+) were prepared by strong-field ionization with an 800 nm pump pulse and probed at the carbon K-edge and chlorine L-edges with a soft X-ray pulse generated via high harmonic generation (HHG). The experiment tracked the evolution of the cation and revealed that its dynamics occur on three distinct timescales (**Fig. 3**): the cation undergoes Jahn-Teller distortion away from its highly symmetrical tetrahedral (T_d) shape within (6 ± 2) fs towards C_{2v} symmetry. Following this rapid geometrical transformation, the molecule transforms from a symmetry-broken covalently bonded species to a non-covalently bonded complex within (90 ± 10) fs. In the case of this halogen-substituted analog of methane, the complex dissociates by expelling a chlorine atom at long times τ > 800 fs. Both the symmetry-broken CCl_4^+ cation and the non-covalently bonded complex are short-lived intermediates that have not been observed in previous experiments. The noncovalently bonded $Cl–CCl_3^+$ complex is held together largely by the polarization of the neutral species, forming an ion-induced dipole complex with a lifetime significantly exceeding that of the covalent bond cleavage time. The observed long lifetime of the noncovalently bonded species is a potential explanation for otherwise unstable parent ions appearing in mass-spectra of ultra-short strong-field ionization.

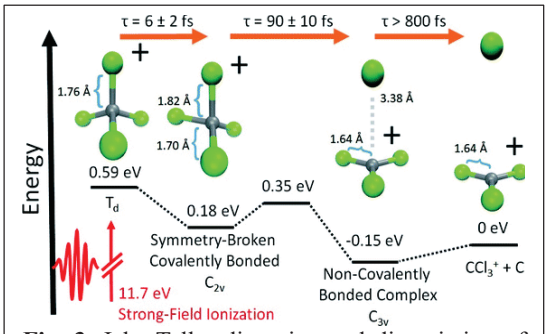

Fig. 3. Jahn-Teller distortion and dissociation of CCl_4^+ upon strong field ionization. Dynamics in CCl_4^+ upon strong-field ionization unfold on three different time scales: within (6 ± 2) fs the initially tetrahedral molecule Jahn-Teller distorts, followed by a transformation to a non-covalently bonded complex within (90 ± 10) fs. Ultimately the molecule dissociates for τ > 800 fs.

Coherent Vibrations in CCl_4 through the Eyes of Carbon and Chlorine. CCl_4 was studied as another candidate for mapping the core-excited state potential energy surfaces in an ultrafast soft X-ray transient absorption spectroscopy experiment via its vibrational properties. All of the modes are Raman active and have been studied in great detail. The experiment is able to clearly resolve the ν_1 mode in the soft X-ray transients at the chlorine L-edges as well as the carbon K-edge (albeit with lower signal-to-noise ratio) as seen in their Fourier transforms. Due to the CCl_4 sample not being isotopically pure in chlorine, it is expected that the experimental signal is a superposition of slightly detuned ν_1 vibrations with a recurrence time of ~10 ps. This recurrence is, in fact, observed in scans recorded at different times far from time zero. Importantly, the slopes of the core-excited potential energy surfaces could be determined (Cl $2p^{-1}$ $7a_1^*$: arbitrarily set to -1, Cl $2p^{-1}$ t_2^*: (-0.81 ± 0.08), C $1s^{-1}$ t_2^*: (-0.47 ± 0.05)) in excellent agreement with theory results of the Martin Head-Gordon group (yielding -1, 0.79 and 0.47, respectively). The results show that the projection of the relative forces of the potential energy surfaces, from the relative viewpoint of the Cl atom and the C atom, for the same stretching vibration, are markedly different, and accurately compare with Kohn-Sham calculations.

Capturing Ring Opening in Photoexcited Enolic Acetylacetone Upon Hydrogen Bond Dissociation by Ultrafast Electron Diffraction

Acetylacetone (AcAc) serves as a prototypical system within photochemistry as it displays a complex chemical relaxation pathway involving several conical intersections (CI) and a singlet-to-triplet intersystem crossing (ISC). AcAc also represents a classic example of keto-enol tautomerization where a significant number of rotational isomers play a key role in describing the equilibrium geometry following photoexcitation. These relaxation pathways are often the basis for photoinduced biological and chemical reactions within organic chromophores, such as AcAc. Ultrafast electron diffraction (UED) at the SLAC MeV-UED setup was employed as a structural probe of these relaxation pathways. In the gas phase, AcAc is predominantly found in a planar ring-like enolic form, which is stabilized by an extremely strong intramolecular hydrogen bond.[13-15] Upon excitation into its S_2 ($\pi\pi^*$) state via 266 nm light, acetylacetone undergoes rapid internal conversion followed by intersystem crossing, pathways that are associated with structural changes such as ring opening, deplanarization and bond elongation. Trajectory surface hopping calculations aided the analysis and interpretation of the UED data, providing a new perspective on the early time events occurring in the photoinduced nuclear dynamics of acetylacetone. The acetylacetone molecule is observed to undergo ring opening, deplanarization and bond elongation within the first 700 fs after excitation. These dynamics are associated mainly with the nuclear motion on the molecule's S_1 potential energy surface, occurring after rapid transfer from S_2 to S_1, allowing AcAc to reach the conical intersection between S_1 and T_1 for intersystem crossing.

Future Plans:

Some of the experiments described above involved non-linear pump schemes such as ISRS or SFI driven by an 800 nm or 266 nm pulse. Previous work by Leone with a longer pulse laser also involved single photon UV excitation to probe ring opening, singlet-to-triplet transfer, and bond breaking. New experiments focus more on the use of shorter UV pulses that access electronically excited states of target molecules via one-photon excitation. This capability enables "attosecond photochemistry" experiments in which the nature of the pump-induced excitation is well-defined. Using an attosecond soft X-ray probe pulse as before, one can then monitor element-specific electronic and vibrational dynamics as the photoexcited molecule undergoes non-adiabatic transitions via conical intersections, photodissociates, or isomerizes. Our current capabilities in this arena include the ability to generate sub-20 fs pulses with center wavelengths variable between 255 and 290 nm. We plan two experimental advances: the generation of sub-10 fs pulses out to 200 nm using resonant dispersive wave (RDW) emission, and the extension of the soft X-ray range to the nitrogen K-edge at 400 eV by means of two-color high harmonic generation schemes.

Recent Publications Acknowledging DOE GPCP Support (2022-2024):

- Garner, S.; Haugen, E.; Leone, S.R.; Neuscamman, E., "Spin Coupling Effect on Geometry-Dependent X-ray Absorption of Diradicals". J. Am. Chem. Soc., 146, 2387–2397 (**2024**). DOI: 10.1021/jacs.3c08002
- Leone, S.R., "Profile of Pierre Agostini, Anne L'Huillier, and Ferenc Krausz: 2023 Nobel laureates in physics". Proc. Natl. Acad. Sci. U. S. A. 121, e2321587121 (**2024**). DOI: 10.1073/pnas.2321587121
- Leone, S.R., "Reinvented - An Attosecond Chemist". Annu. Rev. Phys. Chem. 75, 1-19 (**2024**). DOI: 10.1146/annurev-physchem-083122-011610
- Ross, A.D.; Hait, D.; Scutelnic, V.; Neumark, D.M.; Head-Gordon, M.; Leone, S.R.. "Measurement of coherent vibrational dynamics of X-ray transient absorption spectroscopy simultaneously at the carbon K- and chlorine $L_{2,3}$-edges". Communication Physics (**2024**). DOI:1-.1038/s42005-024-01794-4
- Barreau, L.; Ross, A.D.; Kimberg, V.; Krasnov, P.; Blinov, S.; Neumark, D.M.; Leone, S.R., "Core-excited states of SF_6 probed with soft x-ray femtosecond transient absorption of vibrational wave packets". Phys. Rev. A 108, 012805 (**2023**). DOI: 10.1103/PhysRevA.108.012805
- Ridente, E.: Hait, D.; Haugen, E.A.; Ross, A.D.; Neumark, D.M.; Head-Gordon, M.; Leone, S.R., "Femtosecond symmetry breaking and coherent relaxation of methane cations via x-ray spectroscopy". Science 360, 713-717 (**2023**). DOI: 10.1126/science.adg4421
- Haugen, E. A.; Hait, D.; Scutelnic, V.; Xue, T.; Head-Gordon, M.; Leone, S.R., "Ultrafast X-ray Spectroscopy of Intersystem Crossing in Hexafluoroacetylacetone: Chromophore Photophysics and Spectral Changes in the Face of Electron-Withdrawing Groups". J. Phys. Chem. A. 127,3, 634-644 (**2023**). DOI: 10.1021/acs.jpca.2c06044
- Epshtein, M.; Tenorio, B. N. C.; Vidal, M. L.; Scutelnic, V.; Yang, Z.; Xue, T.; Krylov, A. I.; Coriani, S.; Leone, S. R., "Signatures of the Bromine Atom and Open-Shell Spin Coupling in the X-ray Spectrum of the Bromobenzene Cation". J. Am. Chem. Soc. 145, 6, 3554-3560 (**2023**). DOI: 10.1021/jacs.2c12334
- Popolan-Vaida, D. M.; Eskola, A. J.; Rotavera, B.; Lockyear, J. F.; Wang, Z.; Sarathy, S. M.; Caravan, R. L.; Zador, J.; Sheps, L.; Lucassen A.; Moshammer, K.; Dagaut, P.; Osborn, D. L.; Hansen, N.; Leone S. R.; Taatjes, C.A., "Formation of Organic Acids and Carbonyl Compounds in n-Butane Oxidation via γ-Ketohydroperoxide Decomposition". Angew. Chem. Int. Ed. 61, e202209168 (**2022**). DOI: 10.1002/anie.202209168
- Kobayashi, Y.; Leone, S. R., "Characterizing coherences in chemical dynamics with attosecond time-resolved X-ray absorption spectroscopy". J. Chem. Phys. 157, 1809014 (**2022**). DOI: 10.1063/5.0119942
- Ross, A. D.; Hait, D.; Scutelnic, V.; Haugen, E. A.; Ridente, E.; Balkew, M. B.; Neumark, D. M.; Head-Gordon, M.; Leone, S. R., "Jahn-Teller distortion and dissociation of CCl_4^+ by transient X-ray spectroscopy simultaneously at the carbon K- and chlorine L-edge". Chem. Sci., 13, 9310-9320 (**2022)**. DOI: 10.1039/D2SC02402K
- DeWitt, M.; Babin, M.C; Lau, J.A.; Solomis, T.; Neumark, D.M., "High Resolution Photoelectron Spectroscopy of the Acetyl Anion" J. Phys. Chem. A, 126, 7962–7970 (**2022**). DOI: 10.1021/acs.jpca.2c06214
- Chang, K. F.; Wang, H.; Poullain, S. M.; Gonzalez-Vazquez, J.; Banares, L.; Prendergast, D.; Neumark, D. M.; Leone, S.R., "Conical intersection and coherent vibrational drnamics in alkyl iodides captured by attosecond transient absorption spectroscopy". J. Chem. Phys. 156, 114304 (**2022**). DOI: 10.1063/5.0086775

- Chambreau, S. D.; Popolan-Vaida, D. M.; Kostko, O.; Lee, J. K.; Zhou, Z.; Brown, T. A.; Jones, P.; Shao, K.; Zhang, J.; Vaghjiani, G.L.; Zare, R. N.; Leone, S.R., "Thermal and Catalytic Decomposition of 2-Hydroxyethylhydrazine and 2-Hydroxyethylhydrazinium Nitrate Ionic Liquid". J. Phys. Chem. A. 126, 373-394 (**2022**). DOI: 10.1021/acs.jpca.1c07408

Theory of Electronic Structure and Chemical Dynamics

Martin Head-Gordon, Jin Qian, Eric Neuscamman
Chemical Sciences Division, Lawrence Berkeley National Laboratory, Berkeley, California 94720.
mhead-gordon@lbl.gov, jqian2@lbl.gov, eneuscamman@lbl.gov

Scope of the Project: To expand knowledge of transient species such as radicals relevant to combustion chemistry, atmospheric photochemistry, and other areas including catalysis, new theoretical methods are needed for reliable computer-based prediction of their properties. In electronic structure theory, focus centers on the development of new density functional theory methods and new wave function theories. Newly developed theoretical methods, as well as existing approaches, are employed to study prototype radical reactions, often in collaboration with experimental efforts in the related subtasks (see separate LBNL abstracts). These studies help to deepen understanding of the role of reactive intermediates in diverse areas of chemistry. They also sometimes reveal frontiers where new theoretical developments are needed in order to permit better calculations in the future.

Recent Progress

Due to length limitations, only a selection of projects can be summarized here.

High Accuracy Excited States and Monte Carlo Optimization. Neuscamman and co-workers have developed new methodology for diradical core states (Garner 2024) and excited-state-specific variational Monte Carlo (VMC) (Otis 2023a, Otis 2023b). The core state work leverages excited-state-specific complete active space self-consistent field theory and selected configuration interaction to tackle double excitations involving a core excitation to show how a geometry-dependent spin selection rule allows for richer interpretation time-resolved XAS spectra for diradical species. Work on VMC has improved excited-state-specific wave function optimization by showing that adaptive step size control stabilizes difficult cases and has demonstrated that excited state VMC maintains its high accuracy across singly excited, doubly excited, and charge transfer states. In contrast, other high level methods such as EOM-CCSD and CASPT2 perform well in some of these categories while struggling in others.

Assessing the predictive power of time-dependent DFT for electronic excited states. A large-scale benchmark assessment of more than 40 popular or recently developed density functionals for the calculation of 463 vertical excitation energies against the large and accurate QuestDB benchmark set was completed by the Head-Gordon group (Liang et al, J. Chem. Theory Comput. 2022). The functionals ωB97X-D and BMK are found to offer the best performance overall with a root-mean square error (RMSE) of around 0.27 eV, better than the computationally more demanding wavefunction-based methods. The Tamm-Dancoff approximation is recommended. These results provide useful updated guidelines for practical TDDFT calculations.

Analytical hessian evaluation for Van der Waals density functionals. What we believe to be the first analytical theory and implementation of the hessian for VV10-containing density functionals has been completed by the Head-Gordon group, and used to assess the quality of vibrational frequency predictions using modern VV10-containing functionals. VV10 contributes dispersion energy (the "-V" part) to today's leading density functionals, such as the most accurate hybrid meta-GGA (ωB97M-V). The additional compute cost of the VV10 contributions to analytical frequencies is shown to be small in all but the smallest basis sets for recommended grid sizes. Numerical assessments show that the contribution of VV10 to ωB97M-V harmonic frequencies is important for systems where weak interactions are significant.

Efficient real-space KS-DFT development: Key distinctions persist among the dominant practitioners of Kohn Sham-DFT (KS-DFT). On the one hand, quantum chemists favor orbital-like basis sets (usually gaussian type orbitals) and tend to focus their efforts on isolated molecular systems. In contrast, solid-state physicists leverage plane-wave basis sets (usually coupled with periodic boundary conditions) and tend to focus on descriptions of (quasi-) continuous solids and interfacial systems. Moving down the periodic table and building on our previous success for the 2nd row elements, Qian

and Head-Gordon (LBNL) collaborated on developing and benchmarking the real-space pseudopotential based XPS prediction capabilities for 3rd row elements (Liu et al., 2024). In this paper, we further discussed the implications of periodic boundary conditions (PBC) and carefully laid out an error cancellation strategy that accurately predicts XPS binding energies for large, periodic systems.

Ab initio regularization via size-consistent second order Brillouin-Wigner (BW2) perturbation theory. Beginning from a recent proposal to make second order Brillouin-Wigner perturbation theory extensive, the Head-Gordon has designed a new theory that is also size-consistent (Carter-Fenk et al, 2023a, 2023b), and ab initio in the sense that it depends only upon a novel repartitioning of the Hamiltonian to directly obtain size-consistent second order energies that are also stable (i.e. regular) in the zero gap limit. The repartitioning can be chosen such that the theory also captures an element of strong correlation by being exact for the problem of 2 electrons in 2 orbitals at dissociation. Alternatively the single parameter controlling the strength of the ab initio regularizing operator can be chosen to optimize performance for chemical problems. The results of these assessments are very encouraging, considering that the cost scales the same way as standard MP2 theory with molecular size.

Fantastical excited state structures from the Born-Oppenheimer separation. An excited state PES technically only exists within the realm of the Born-Oppenheimer separation of nuclear and electronic degrees of freedom. The Head-Gordon group (Talbot et al, 2023) has demonstrated through ab initio calculations and simple nonadiabatic dynamics that some excited state minimum structures are *fantastical:* they appear to exist as stable configurations only as a consequence of the PES construct, rather than being physically observable. Each fantastical structure exhibits an unphysically high predicted harmonic frequency and associated force constant, which is a result of being very close to the upper side of a conical intersection... That is a useful diagnostic of such non-observable structures!

Chemical Applications: Neuscamman's work on diradicals' core states (Garner 2024) has clarified a new spectroscopic handle in XAS and provides testable predictions for the furanone ring opening. In collaboration with Tod Pascal (UCSD) and Richard Saykally (UCB, LBNL), Qian applied the recently developed real-space KS-DFT XPS module (Xu et al., 2022) to study the gas-liquid interactions using the sodium carbonate nanoparticles as a surrogate model (Devlin et al, 2023). Leveraging plane-wave and real-space KS-DFT, Qian also studied the gas-solid interactions that guides the design of carbon capture solid sorber (Glenna et al, 2023) in collaboration with Haiyan Zhao (INL), Seth Snyder (INL) and Yingchao Yang (University of Maine). Head-Gordon's group has also completed a rich variety of chemical applications, including a collaboration with Musa Ahmed (LBNL) on hydronium-water clusters (Mackie et al, 2023), and analysis of the importance of Pauli repulsion in gold-I complexes (Wong et al, 2022), and a range of other recent applications (see publication list).

Future Plans:

Robust Excited State Guesses and Fast PES Exploration: Many excited-state-specific electronic structure methods amount to nonlinear optimization and, as such, depend strongly on the quality of the initial guess. In ground states, RHF and DFT usually provide excellent guesses, but their most widely used excited-state extensions (CIS and TDDFT) are much less reliable in this regard due primarily to a lack of excited state orbital relaxations. Work on a low-cost excited state initial guess generator that leverages advances in selected CI will fill this gap and enhance the impact of excited-state-specific electronic structure. In parallel with this effort, methods will be developed to accelerate ground and excited state explorations of potential energy surfaces by exploiting synergies that exist between atomic displacement energetics and local correlation methods.

Efficient real-space KS-DFT development: Qian will continue the development of real-space KS-DFT spectroscopic modules. The developmental effort is supported by a separate and synergistic ECRP award. The potential applications for this development involve core excitation predictions for finite systems from small (a few atoms) to large (>10,000 atoms), thermodynamics and kinetics predictions for gas in confined space (Subtask 2 with Musa Ahmed, LBNL). As we demonstrate the increased computational capabilities in simulating large systems, we will also develop efficient

algorithms navigating the complex energy landscape to prepare initial cluster structures as a prior step for these real-space KS-DFT calculations.

"Digital Twin" for XPS, Infrared, and Raman Spectroscopy: A "Digital Twin" is more than a "virtual mimic of the experiments". Indeed, the bidirectional feedback from the theory and experiment is central to "Digital Twin" and enables the dynamical growth of Qian's Digital Twin for Chemical Science (DTCS v.01) software platform. DTCS v.02 will be specially designed for gas phase experiments, where the input of "Digital Twin" will best mimic the real experimental settings, and output of "Digital Twin" will allow direct comparison between theory and experiment in the exact same format, such as XPS, Infrared, or Raman spectra. We envision that this development will facilitate planning of resource-heavy future experiments, interpret the observations on-the-fly, and intelligently guide the execution of subsequent experiments.

A Gold Standard Database for the development of a near-gold-standard functional? The Head-Gordon group has almost completed the development of new database of over 8000 highly accurate values spanning essentially all types of chemically relevant energy differences, both for main group elements and transition metals. Using this database we are attempting to improve hybrid density functionals, with the objective of surpassing the performance of the most accurate existing hybrid meta-GGA (ωB97M-V). Whether or not that is possible is an open question, but the result will be very interesting either way. There is some evidence that the limitations of earlier databases (e.g. no transition metals, and no direct assessments of density quality) could have adversely limited the accuracy of ωB97M-V for such problems. If the result is negative, then we will move on to consider functional design opportunities that differ more substantially from existing forms (e.g. see following paragraph).

Generalized size-consistent second order Brillouin-Wigner perturbation theory: Head-Gordon's recent development of BW-s2 can be dramatically generalized to include a rich variety of additional building blocks in the regularizing operator that is employed to repartition the Hamiltonian between unperturbed and perturbed parts. And this is without changing the size-scaling of the method: it still can scale the same as MP2 theory! We are fascinated by the resulting possibility of substantial additional improvements in the chemical performance of an optimally designed regularizer, and will pursue that problem. Viewed from a DFT standpoint, this also offers the chance to design rung 5 density functionals with a far richer set of descriptors for electron correlation than has hitherto been possible. That should synergize with the Head-Gordon group's DFT development plans mentioned above. There are also opportunities to extend the BW-s2 framework to excited states that we hope to pursue.

Collaborative chemical applications: Collaborative applications to understand XAS in glycerol solutions are approaching completion (Head-Gordon, with Musa Ahmed, LBNL). Ahmed and Head-Gordon are also planning a new collaboration on excited states of CO_2 in clusters and their connections to photo-driven chemistry. Head-Gordon's project on modelling oxidative chemistry of unsaturated hydrocarbons in aerosols (to connect with Wilson's experiments in the LBNL program) is now being written up for publication. The study of XAS for diradicals (Leone and Neuscamman) provides testable predictions for the furanone ring opening as well as a spin exchange model for thinking about which systems should exhibit observable geometry-dependent spin selection rules in diradicals' core spectra. Qian and Ahmed will continue their studies of CO_2 in metal–organic frameworks to understand the gas-confinement interactions. Collaborative research between Qian, Wilson, and Ahmed is ongoing to investigate the physical and chemical nature of ammonia sulfate aerosols.

Recent Publications Citing DOE Support (2022-2024)

- Aljama, H.; Head-Gordon, M.; Bell, A.T., Assessing the stability of Pd-exchanged sites in zeolites with the aid of a high throughput quantum chemistry workflow. Nature Comm. **2022**, *13*, 2910, DOI 10.1038/s41467-022-29505-z.
- Bergman, H.M.; Beattie, D.D.; Handford, R.C.; Rossomme, E.; Suslick, B.A.; Head-Gordon, M.; Cundari, T.R.; Liu, Y.; Tilley, T.D., Copper(III) Metallacyclopentadienes via Zirconocene-Transfer and Reductive Elimination to an Isolable Phenanthrocyclobutadiene. *J. Am. Chem. Soc*. **2022**, *144*, 9853−9858, DOI 10.1021/jacs.2c02581.

- Carter-Fenk K.; Head-Gordon, M., Repartitioned Brillouin-Wigner Perturbation Theory with a Size-Consistent Second-Order Correlation Energy. *J. Chem. Phys.* **2023,** 158, 234108. DOI 10.1063/5.0150033.
- Carter-Fenk, K.; Shee, J.; Head-Gordon, M., Optimizing the Regularization in Size-Consistent Second-Order Brillouin-Wigner Perturbation Theory. *J. Chem. Phys.* **2023**, 159, 171104. DOI 10.1063/5.0174923
- Chakraborty, R.; Talbot, J.J.; Shen, H.; Yabuuchi, Y.; Carsch, K.M.; Jiang, H.; Furakawa, H.; Long, J.R.; Head-Gordon, M., Quantum Chemical Modeling of Single and Multiple Hydrogen Binding in Metal Organic Frameworks: Validation, Insight, Predictions and Challenges. *Phys. Chem. Chem. Phys.* **2024**, 26, 6490-6511. DOI 10.1039/d3cp05540j.
- Devlin, S.; Jamnuch, S.; Xu, Q.; Chen, A.; Qian, J.; Pascal, T. A.; Saykally, R., Agglomeration Drives the Reversed Fractionation of Aqueous Carbonate and Bicarbonate at the Air-Water Interface. *J. Am. Chem. Soc.* **2023**, 145, 41, 22384–22393. DOI 10.1021/jacs.3c05093.
- Ganoe B.; Head-Gordon, M., The Doubles Connected Moments Expansion: A Tractable Approximate Horn-Weinstein Approach for Quantum Chemistry. *J. Chem. Theory Comput.* **2023**, 19, 9187-9201. DOI 10.1021/acs.jctc.3c00929.
- Garner, S. M.; Haugen, E. A.; Leone, S. R.; Neuscamman, E., Spin Coupling Effect on Geometry-Dependent X-ray Absorption of Diradicals. *J. Am. Chem. Soc.* **2024**, 146, 2387–2397. DOI 10.1021/jacs.3c08002.
- Glenna, D. M., Jana, A., Xu, Q., Wang, Y., Meng, Y., Yang Y., Neupane M., Wang, L., Zhao, H., Qian J., Snyder, S. W., Carbon Capture: Theoretical Guidelines for Activated Carbon-based CO2 Adsorption Material Evaluation. J. Phys. Chem. Lett. **2023**, 14, 10693. DOI 10.1021/acs.jpclett.3c02711
- Gobi, S.; Z. Lin, C. Zhu, M. Head-Gordon and R.I. Kaiser, "Oxygen Isotope Exchange Between Carbon Dioxide and Iron Oxides on Mars' Surface", J. Phys. Chem. Lett. 13, 2600−2606 (2022); doi: 10.1021/acs.jpclett.2c00289
- Hoberg, C.; Talbot, J.J.; Shee, J.; Ockelmann, T.; DasMahanta, D.; Novelli, F.; Head-Gordon, M.; Havenith, M., Caught in the Act: Observation of the Solvent Response that Promotes Excited-State Proton Transfer in Pyranine. *Chem. Sci.* **2023**, *14*, 4048–4058. DOI 10.1039/d2sc07126f.
- Leonhardt, B.E.; Head-Gordon, M.; Bell, A.T., The Effects of ≡Ti‑OH Site Distortion and Product Adsorption on the Mechanism and Kinetics of Cyclohexene Epoxidation over Ti/SiO_2. *ACS Catal.* **2024,** 14, 3049–3064. DOI 10.1021/acscatal.3c06073.
- Leonhardt, B.E.; Shen, H.; Head-Gordon M.; Bell, A.T., Experimental and Theoretical Evidence for Distorted Tetrahedral ≡Ti‑OH Sites Supported on Amorphous Silica and Their Effect on the Adsorption of Polar Molecules. *J. Phys. Chem. C* **2024**, 128, 129–145. DOI 10.1021/acs.jpcc.3c07027.
- Liang, J.; Feng, X.; Hait, D.; Head-Gordon, M., Revisiting the performance of time-dependent density functional theory for electronic excitations: Assessment of 43 popular and recently developed functionals from rungs one to four. *J. Chem. Theory Comput.* **2022**, *18*, 3460–3473, DOI 10.1021/acs.jctc.2c00160
- Liang, J.; Feng, X.; Head-Gordon, M., Analytical Harmonic Vibrational Frequencies with VV10-Containing Density Functionals: Theory, Efficient Implementation, and Benchmark Assessments. *J. Chem. Phys.* **2023**, *158*, 204109. DOI 10.1063/5.0152838.
- Liang, J.; Wang, Z.; Li, J.; Wong, J.; Liu, X.; Ganoe, B.; Head-Gordon, T.; Head-Gordon, M., Efficient Calculation of NMR Shielding Constants Using Composite Method Approximations and Locally Dense Basis Sets. *J. Chem. Theory Comput.* **2023**, *19*, 514–523. DOI 10.1021/acs.jctc.2c00933.
- Liu, L., Cunha, L., Xu, Q., Xin, H., Head-Gordon, M., Qian, J., Real-Space Pseudopotential Method for the Calculation of Third-Row Elements X-ray Photoelectron Spectroscopic (XPS) Signatures. J. Chem. Theory Comput. **2024**, 20, 14, 6134. DOI 10.1021/acs.jctc.4c00535

- Lu, W.; C.J. Mackie, B. Xu, M. Head-Gordon and M. Ahmed, "A computational and experimental view of hydrogen bonding in glycerol water clusters", J. Phys. Chem. A 126, 1701−1710 (2022); doi: 10.1021/acs.jpca.2c00659
- Mackie, C. J.; Lu, W.; Liang, J.; Kostko, O.; Bandyopadhyay, B.; Gupta, I.; Ahmed, M.; Head-Gordon, M., Magic Numbers and Stabilities of Photoionized Water Clusters: Computational and Experimental Characterization of the Nanosolvated Hydronium Ion. *J. Phys. Chem. A,* **2023**, 127, 5999-6011. DOI 10.1021/acs.jpca.3c02230.
- Otis, L.; Neuscamman, E., Optimization Stability in Excited-State-Specific Variational Monte Carlo. *J. Chem. Theory Comput.* **2023***,* 19, 767. DOI 10.1021/acs.jctc.2c00642.
- Otis, L; Neuscamman, E., A Promising Intersection of Excited-State-Specific Methods from Quantum Chemistry and Quantum Monte Carlo. *WIREs: Comp. Mol. Sci.* **2023**, e1659. DOI 10.1002/wcms.1659.
- Rettig, A.; J. Shee, J. Lee and M. Head-Gordon, Revisiting the Orbital Energy Dependent Regularization of Orbital Optimized Second Order Moller-Plesset Theory, *J. Chem. Theory Comput.* **2022** 18, 5382–5392; doi: 10.1021/acs.jctc.2c00641
- Rettig, A.; Lee, J.; Head-Gordon, M., Even Faster Exact Exchange for Solids via Tensor Hypercontraction. *J. Chem. Theory Comput.* **2023**, 19, 5773−5784. DOI 10.1021/acs.jctc.3c00407
- Shan, Y., Zhao, X., Guzman, M. F., Jana, A., Chen, S., Yu, S., Ng, K., Roh, I., Chen, H., Altoe, V., Corder, S. G., Bechtel, H., Qian, J., Salmeron, M., Yang, P., Nanometre-Resolved Observation of Electrochemical Microenvironment Formation at the Nanoparticle–Ligand Interface. *Nat. Catal.* **2024**, **7**, 422–431. DOI 10.1038/s41929-024-01119-2.
- Talbot, J.J.; M. Head-Gordon, W.H. Miller and S.J. Cotton, "Dynamic signatures of electronically nonadiabatic coupling in sodium hydride: a rigorous test for the symmetric quasi-classical model applied to realistic, ab initio electronic states in the adiabatic representation", Phys. Chem. Chem. Phys. 24, 4820–4831 (2022); doi: 10.1039/d1cp04090a
- Talbot, J.J. ; M. Head-Gordon, and S.J. Cotton, "The symmetric quasi-classical model using on-the-fly time-dependent density functional theory within the Tamm-Dancoff approximation", Mol. Phys. e215376 (2022); doi: 10.1080/00268976.2022.2153761
- Talbot, J.J.;Arias-Martinez, J. E.; Cotton, S.J.; Head-Gordon, M., Fantastical Excited State Optimized Structures and Where to Find Them. *J. Chem. Phys.* **2023**, 159, 171102. DOI 10.1063/5.0172015
- Wang, Z.; Liang, J.; Head-Gordon, M., Earth Mover's Distance as a Metric to Evaluate the Extent of Charge Transfer in Excitations Using Discretized Real-Space Densities. *J. Chem. Theory Comput.* **2023**, 19, 7704−7714. DOI 10.1021/acs.jctc.3c00894
- Wong, Z.R.; Schramm, T.K.; Loipersberger, M.; Head-Gordon, M.; Toste, F.D., Revisiting the Bonding Model for Gold(I) Species: The Importance of Pauli Repulsion Revealed in a Gold(I)-Cyclobutadiene Complex. Angew. Chem. **2022**, *61*, e202202019, DOI 10.1002/anie.202202019
- Wong, J.; Ganoe, B.; Liu, X.; Neudecker, T.; Lee, J.; Liang, J.; Wang, Z.; Li, J.; Rettig, A.; Head-Gordon, T.; Head-Gordon, M., An *In Silico* NMR Laboratory for Nuclear Magnetic Shieldings Computed via Finite Fields: Exploring Nucleus-Specific Renormalizations of MP_2 and MP_3. *J. Chem. Phys.* **2023**, *158*, 164116. DOI 10.1063/5.0145130.

SPECTROSCOPY AND DYNAMICS OF REACTION INTERMEDIATES IN HYDROCARBON OXIDATION

Marsha I. Lester
Department of Chemistry
University of Pennsylvania
Philadelphia, PA 19104-6323
milester@sas.upenn.edu

I. Program Scope

Our research aims to characterize important, yet often elusive, reaction intermediates in hydrocarbon oxidation using novel spectroscopic and dynamical methods. A recent thrust is focused on characterizing hydroperoxyalkyl radical intermediates (•QOOH) containing a carbon radical center (•Q), which are important intermediates in low temperature combustion of hydrocarbon fuels and atmospheric oxidation of volatile organic compounds. In addition, we continue to collaborate on experiments carried out at the Advanced Light Source that focus on carbonyl oxides (Criegee intermediates, $R_1R_2C{=}O^+O^-$), which are important intermediates in tropospheric hydrocarbon oxidation.

II. Recent Progress

A. Infrared spectroscopy and unimolecular dissociation dynamics of •QOOH

The atmospheric oxidation of volatile organic compounds (VOCs) and low-temperature (≤ 1000 K) combustion of hydrocarbon fuels proceed via a well-established sequence of radical reactions. These radical chain reactions are known to drive the formation and growth of secondary organic aerosols in the atmosphere and provide the key chain-branching pathways in low-temperature combustion and autoignition. Although most aspects of the reaction mechanism are understood, a critical class of carbon-centered hydroperoxyalkyl radical intermediates, commonly called •QOOH, have generally eluded direct experimental observation of their structure, stability, and dissociation dynamics. Our initial studies focused on the infrared (IR) fingerprint of •QOOH radicals transiently formed in isobutane oxidation, along with direct time-domain measurement of the •QOOH unimolecular dissociation rates over a wide range of energies.[1,2] Recently, my group obtained the IR spectroscopic signatures of carbon-centered •QOOH radicals transiently formed in the oxidation of cyclohexane and cyclopentane, along with their energy-resolved and time-dependent evolution to hydroxyl (OH) radical products.[3-5] In each case, the experimental results are complemented by state-of-the-art electronic structure calculations, statistical unimolecular rate calculations, and master equation modeling in collaboration with Stephen Klippenstein (Argonne).

Hydroperoxy-cyclohexyl radicals (•QOOH) transiently formed in cyclohexane oxidation have been stabilized, jet-cooled, and characterized through their IR action spectrum and unimolecular decay dynamics to OH products that are detected by UV laser-induced fluorescence.[3,4] The cyclohexane oxidation pathway leads to three nearly degenerate carbon-centered hydroperoxy-cyclohexyl isomers, β-, γ-, and δ-QOOH, which are prepared in the laboratory using photolytically generated Cl atoms to abstract an H-atom from corresponding ring sites of the cyclohexyl hydroperoxide precursor. The three isomers are predicted to have similar fundamental and overtone OH stretch transitions and combination bands, which differ from one another by only a few cm^{-1} in each spectral region based on anharmonic frequencies computed by second-order vibrational perturbation theory. This precludes definitive identification of the •QOOH isomer by IR spectroscopy alone. However, β-QOOH has a significantly lower transition state (TS) barrier to OH radical products compared to those for γ- or δ-QOOH, which has enabled isomer-specific characterization of β-QOOH at energies ranging from 10 to 20 kcal mol^{-1} (Figure 1).

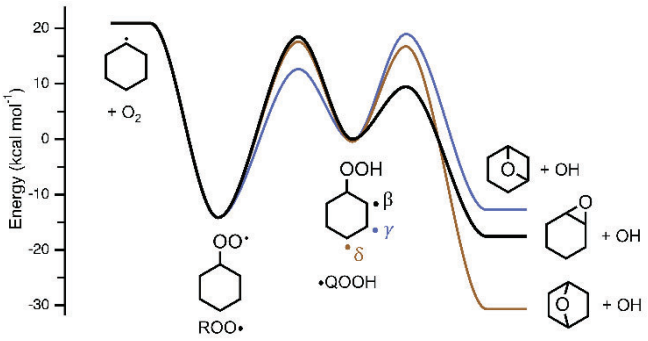

Figure 1. Schematic reaction pathway illustrating key minima and transitions states on the $C_6H_{11}O_2$ potential energy surface. The barriers leading to OH products differ considerably for β- (black), γ- (blue), and δ- (brown) QOOH, enabling isomer-selective detection of β-QOOH.

The energy-resolved unimolecular decay rates for β-QOOH, measured as the time-dependent appearance of OH products on a nanosecond timescale, increased 40-fold (5×10^6 s^{-1} to $\geq 3 \times 10^8$ s^{-1}) over the energy range explored (3500 to 7000 cm^{-1}; 10 to 20 kcal mol^{-1}), providing a stringent test of the corresponding TS barrier. Moreover, β-QOOH has near unity branching to OH products, while γ- and δ-QOOH are predicted to favor branching to ROO• and/or undergo much slower unimolecular decay to OH products than experimentally observed rates.

A benchmarking approach has been utilized to evaluate stationary point energies – most importantly the TS barriers leading to OH products – by comparison with the structurally similar, yet smaller, β-QOOH of $•CH_2CH_2OOH$, in which higher accuracy energies can be computed. The benchmark electronic structure calculations for β-QOOH in the $C_6H_{11}O_2$ system yielded a TS barrier of 9.49 kcal mol^{-1} and optimized TS barrier of 9.76 kcal mol^{-1}, which were utilized for statistical RRKM calculations. The computed microcanonical rates $k(E)$ were in excellent accord with the experimental rates measured for appearance of OH products. Heavy atom tunneling, involving O-O extension and C-C-O angle contraction for cyclization, was found to enhance the microcanonical unimolecular decay rates by ca. 20% or more. Master equation modeling was also utilized to compute thermal decay rates for β-QOOH over a wide range of temperatures and pressures. At 298 K, the thermal rate in the high pressure limit $k(T,P) \sim 2 \times 10^5$ s^{-1}, corresponding to a lifetime of 5 μs with 2-fold enhancement due to heavy atom tunneling, illustrates the transient nature of the •QOOH intermediates.

An analogous carbon-centered hydroperoxyalkyl intermediate (•QOOH) in the oxidation of cyclopentane has been identified by IR action spectroscopy with time-resolved unimolecular decay to hydroxyl (OH) radical products that are detected by UV laser-induced fluorescence.[5] Two nearly-degenerate •QOOH isomers, β- and γ-QOOH, are generated by H-atom abstraction of the cyclopentyl hydroperoxide precursor. Fundamental and first overtone OH stretch transitions and combination bands of •QOOH are observed and compared with anharmonic frequencies computed by second-order vibrational perturbation theory. An OH stretch transition is also observed for a conformer arising from torsion about a low-energy CCOO barrier. Definitive identification of the β-QOOH isomer relies on its significantly lower TS barrier to OH products, which results in rapid unimolecular decay and near unity branching to OH products. By contrast, γ-QOOH is predicted to decay to ROO• with high yield. A benchmarking approach is utilized to compute high-accuracy stationary point energies, most importantly TS barriers, for cyclopentane oxidation ($C_5H_9O_2$), again building on higher level reference calculations for ethane oxidation ($C_2H_5O_2$). The experimental OH product appearance rates are compared with computed statistical microcanonical rates, including heavy atom tunneling, thereby validating the computed TS barrier (9.76 kcal mol^{-1};727*i* cm^{-1}) for β-QOOH. The results are extended to thermal unimolecular decay rate constants at temperatures and pressures relevant to cyclopentane combustion via

master-equation modeling. At 298 K, the thermal rate in the high pressure limit, $k(T,P) \sim 2.2 \times 10^5$ s^{-1}, corresponds to a β-QOOH lifetime of 4.5 μs, which is enhanced 2-fold by heavy atom tunneling. The various torsional and ring puckering states of the wells and transition states are explicitly considered in these calculations.

B. Photoionization mass spectrometry studies

In the past year, we continued our collaboration with Caravan (Argonne), Taatjes (Sandia), and Klippenstein on the bimolecular chemistry of Criegee intermediates utilizing the Sandia Multiplexed Photoionization Mass Spectrometer (MPIMS) at the Advanced Light Source. We are examining the impact of water complexation on the reactions of CH_2OO and *syn*/*anti* conformers of CH_3CHOO with organic hydroperoxides. In the absence of water, these reactions proceed by 1,2 insertion mechanisms. We are using experiment and theory to address how water complexation influences the kinetics and product branching of these reactions. Further details and motivation are provided in Caravan's abstract.

III. Ongoing and Future Work

Current and future experiments are expanding our studies of •QOOH radicals to systems with additional functionality, e.g. OH substituents,[6] such as occur in isobutanol oxidation.[7] Preliminary calculations of IR transitions and unimolecular decay rates are in progress, which are used to guide IR spectral searches and dynamical measurements using an analogous IR pump-UV probe scheme. The experimental results will then be compared with computed anharmonic frequencies and unimolecular decay rates predicted by statistical RRKM theory.

We are also continuing our collaboration with Caravan and Taatjes to examine the rates and products of bimolecular reactions of Criegee intermediates – with and without extended conjugation – involving key atmospheric species (water vapor, SO_2, formic acid, NO_2). These bimolecular reactions involve remarkably different types of mechanisms, 1,2 addition, 1,4 addition, and secondary ozonide (SOZ) formation, which form more highly oxygenated products with greater mass.

IV. References

1. A. S. Hansen, T. Bhagde, K. B. Moore, D. R. Moberg, A. W. Jasper, Y. Georgievskii, M. F. Vansco, S. J. Klippenstein and M. I. Lester, *Science* **373**, 679 (2021).
2. T. Bhagde, A. S. Hansen, S. Chen, P. J. Walsh, S. J. Klippenstein, and M. I. Lester, *Faraday Discuss.* **238**, 575-588 (2022).
3. Y. Qian, T. K. Roy, A. W. Jasper, C. A. Sojdak, M. C. Kozlowski, S. J. Klippenstein, and M. I. Lester, *Proc. Natl. Acad. Sci* **121** (16) e2401148121 (2024).
4. T. K. Roy, Y. Qian, C. A. Sojdak, M. C. Kozlowski, S. J. Klippenstein, and M. I. Lester, *J. Chem. Phys.* **161**, 034302 (2024).
5. Y. Qian, T. K. Roy, D. S. Valente, E. M. Cruz, M. C. Kozlowski, A. Della Libera, S. J. Klippenstein, and M. I. Lester, submitted (2024).
6. K. H. Møller, T Kurtén, K. H. Bates, J. A. Thornton, and H. G. Kjaergaard, *J. Phys. Chem. A* **123**, 10620−10630 (2019)
7. M. J. Goldman, N. W. Yee, J. H. Kroll, and W. H. Green, *Phys. Chem. Chem. Phys.* **22**, 19802 (2020).

V. Publications supported by this DOE project (2022-present)

1. M. F. Vansco, M. Zou, I. O. Antonov, K. Ramasesha, B. Rotavera, D. L. Osborn, Y. Georgievski, C. J. Percival, S. J. Klippenstein, C. A. Taatjes, M. I. Lester, and R. L. Caravan, "Dramatic conformer-dependent reactivity of the acetaldehyde oxide Criegee intermediate with dimethylamine via a 1,2-insertion mechanism", *J. Phys. Chem. A* **126**, 710–719 (2022). https://doi.org/10.1021/acs.jpca.1c08941
2. T. Bhagde, A. S. Hansen, S. Chen, P. J. Walsh, S. J. Klippenstein, and M. I. Lester, "Energy-resolved and time-dependent unimolecular dissociation of hydroperoxyalkyl radicals (•QOOH)", *Faraday Discuss.* **238**, 575 – 588 (2022). https://doi.org/10.1039/D2FD00008C
3. T. N. V. Karsili, B. Marchetti, M. I. Lester and M. N. R. Ashfold, "Electronic Absorption Spectroscopy and Photoinitiated Chemistry of Criegee Intermediates", *J. Photochem. Photobiol.* (2022). http://doi.org/10.1111/php.13665
4. V. J. Esposito, T. A. McHenry, and M. I. Lester, "Photoionization energetics and dissociation pathways of hydroperoxyethyl formate produced in the reaction of CH_3CHOO + formic acid", *Chem. Phys. Lett.* **809**, 140179 (2022). https://doi.org/10.1016/j.cplett.2022.140179
5. T. Liu, M. Zou, A. Caracciolo, C. A. Sojdak, and M. I. Lester, "Substituent effects on the electronic spectroscopy of four-carbon Criegee intermediates", *J. Phys. Chem. A* 126, 6734-6741 (2022). https://doi.org/10.1021/acs.jpca.2c05502
6. G. Wang, T. Liu, M. Zou, C. A. Sojdak, M. C. Kozlowski, T. Karsili, and M. I. Lester, "Electronic Spectroscopy and Dissociation Dynamics of Vinyl-Substituted Criegee Intermediates: 2-Butenal Oxide and Comparison with Methyl Vinyl Ketone Oxide and Methacrolein Oxide Isomers", *J. Phys. Chem. A* **127**, 203–215 (2022). https://doi.org/10.1021/acs.jpca.2c08025
7. G. Wang, T. Liu, M. Zou, T. Karsili, and M. I. Lester, "UV Photodissociation Dynamics of the Acetone Oxide Criegee Intermediate: Experiment and Theory", *Phys. Chem. Chem Phys.* **25**, 7453-7465 (2023). https://doi.org/10.1039/D3CP00207A
8. T. Liu, S. N. Elliott, M. Zou, M. F. Vansco, C. A. Sojdak, C. R. Markus, R. Almeida, K. Au, L. Sheps, D. L. Osborn, F. A. F Winiberg, C. J. Percival, C. A. Taatjes, R. L. Caravan, S. J. Klippenstein, and M. I. Lester, "OH Roaming and Beyond in the Unimolecular Decay of the Methyl-Ethyl Substituted Criegee Intermediate: Observations and Predictions", *J. Am. Chem. Soc.* **145**, 19405-19420 (2023). https://doi.org/10.1021/jacs.3c07126 Correction: *J. Am. Chem. Soc.* **146**, 18184–18185 (2024). https://doi.org/10.1021/jacs.4c06089
9. M. Zou, T. Liu, M. F. Vansco, C. A. Sojdak, C. R. Markus, R. Almeida, K. Au, L. Sheps, D. L. Osborn, F. A. F. Winiberg, C. J. Percival, C. A. Taatjes, S. J. Klippenstein, M. I. Lester, and R. L. Caravan "Bimolecular rate and products of the methyl-ethyl substituted Criegee intermediate reaction with SO_2", *J. Phys. Chem. A* **127**, 8994–9002 (2023). https://doi.org/10.1021/acs.jpca.3c04648
10. Y. Qian, T. K. Roy, A. W. Jasper, C. A. Sojdak, M. C. Kozlowski, S. J. Klippenstein, and M. I. Lester, "Isomer-Resolved Unimolecular Dynamics of the Hydroperoxyalkyl Radical (•QOOH) in Cyclohexane Oxidation", *Proc. Natl. Acad. Sci.* **121** (16) e2401148121 (2024). www.pnas.org/doi/10.1073/pnas.2401148121
11. T. K. Roy, Y. Qian, C. A. Sojdak, M. C. Kozlowski, S. J. Klippenstein, and M. I. Lester, "Infrared Signature of the Hydroperoxyalkyl Intermediate (•QOOH) in Cyclohexane Oxidation: An Isomer-Resolved Spectroscopic Study", *J. Chem. Phys.* **161**, 034302 (2024). https://doi.org/10.1063/5.0219431

Chemistry of Nitrogen Species

Paul Marshall
Department of Chemistry and Center for Advanced Scientific Computing and Modeling
University of North Texas, 1155 Union Circle #305070, Denton, TX 76203
E-mail marshall@unt.edu

Program Scope

Measurements and quantum chemistry modeling are carried out to improve the fundamental understanding of the reactivity and thermochemistry of nitrogen-containing species. Reaction barriers and bond strengths control the behavior of short-lived radical intermediates, and this basic chemistry helps reveal general principles which influence the magnitude of rate constants and ratios of alternative pathways to different products. A goal is to improve our understanding of the physical chemistry of ammonia oxidation alone and in conjunction with hydrocarbons, and the behavior of oxidized nitrogen species.

An application of this work is to help analyze the use of ammonia as a carbon-free energy transfer fuel, when it is synthesized from green sources of energy such as wind, solar or hydroelectric. A near-term application may be for carbon-free cargo shipping. With a boiling point and vapor pressure similar to propane, ammonia is relatively easily transported (by comparison to liquid hydrogen) and can then catalytically decomposed to release hydrogen for use in fuel cells, or directly burned for energy release. It can serve as a substitute for diesel fuel. There are indications that ammonia's ignition and engine properties are improved by mixing with conventional fuel, which makes interactions between the chemical cycles of nitrogen and carbon species of interest. The aim is to develop a reliable chemical mechanism, so that engines can be modified or designed intelligently. One issue about the use of ammonia is the potential formation of nitrous oxide, a potent greenhouse gas. If it is not destroyed within the flame, N_2O emissions will cancel the environmental benefit of zero CO_2 formation, so N_2O chemistry will be examined.

Recent progress

Pulsed laser-photolysis to generate radicals followed by time-resolved laser-induced fluorescence to monitor their consumption has been applied to measure NH_2 radical kinetics under conditions (low concentration and short time) where single elementary reactions dominate the measured species profiles.

We applied this technique to study the reaction

$$NH_2 + H_2O_2 \rightarrow NH_3 + HO_2 \qquad (1)$$

at a single temperature and obtained the temperature dependence (see Fig. 1) via Multistructural Improved Canonical Variational Transition State Theory with Small Curvature Tunneling, with geometries and scaled frequencies obtained with M06-2X/6-311+G(2df,2p) theory, and single-point energies from CCSD(T)-F12b/cc-pVTZ-F12 theory, plus a term to correct approximately for electron correlation through CCSDT(Q). There was good agreement with the measurement at ~429 K and, via the reverse reaction (relevant to HO_2 chemistry connected to ignition delay), with the 1000 K value obtained by Cavalotti et al. with EStokTP.

A similar approach was taken with

$$NH_2 + N_2H_4 \rightarrow \text{products} \qquad (2)$$

where the rate constant k_1 was in good accord with the empirical estimate of Dean and Bozzelli, but much larger than the only other quantum chemistry work, by Li and Zhang, and much smaller than that measured by Gehring et al. In the latter case, modeling of their reaction conditions indicates low sensitivity to reaction 2.

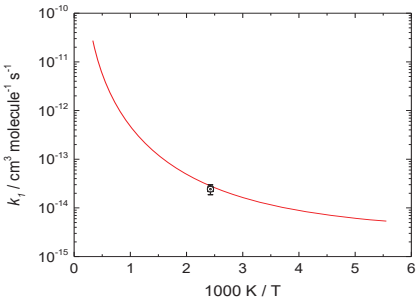

Figure 1. LP-LIF measurement and calculation (red curve) for $NH_2 + H_2O_2$.

Our measurements up to 640 K, plotted in Fig. 2, for

$$NH_2 + CH_2O \rightarrow \text{products} \quad (3)$$

indicate an activation energy E_a of ca. 19 kJ mol^{-1}, by contrast to computational predictions by Barone and coworkers of a barrierless path to $H + HCONH_2$. Our own computational work, based on B2PLYP-D3 density functional theory for geometries and anharmonic frequencies, combined with CCSD(T) results extrapolated to the complete basis set limit and with corrections for relativistic terms, core-valence correlation and further correlation through CCSDT(Q), leads to the potential energy diagram below.

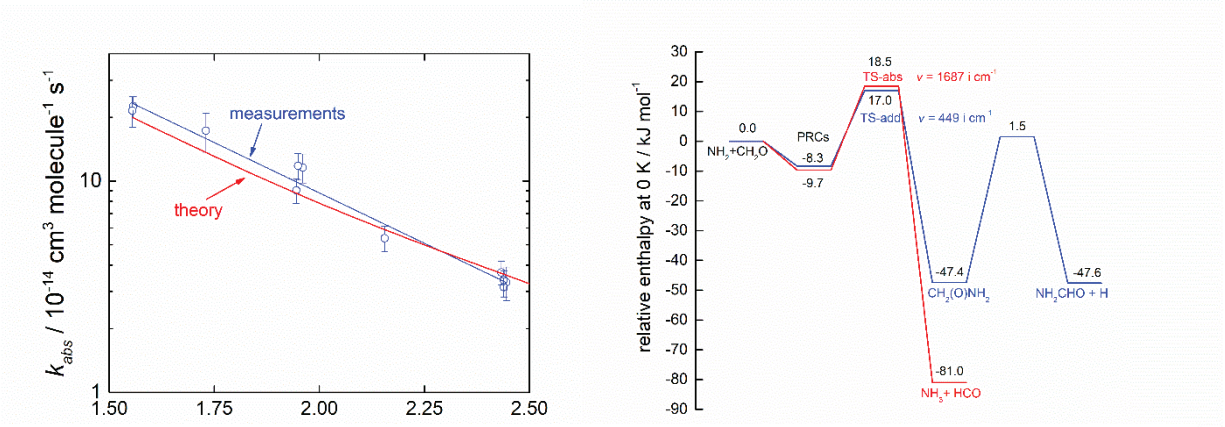

Figure 2. Arrhenius plot of PLP-LIF measurements for $NH_2 + CH_2O$ (left) and the PE diagram (right).

Variational Transition State Theory with internal torsions treated as uncoupled 1-D rotors, and tunneling assessed from the curvature at the top of the vibrationally adiabatic barrier and the Eckart model, yielded the theoretical rate constant plotted in Fig. 3. This revealed the dominant pathway is abstraction to form $NH_3 + HCO$ (97%), despite the higher barrier, because of greater tunneling enhancement of reactivity here than for the addition/dissociation channel (3%).

Further chemistry of NH_2 has been explored computationally, again based on M06-2X density functional and the 6-311++G(2df,2p) basis set for geometries and, after scaling, for zero-point vibrational energy and for fundamental frequencies used in partition functions. Relative enthalpies are obtained via direct extrapolation of coupled cluster CCSD(T) energies to the complete basis set limit via the CBS-APNO compound approximation. Mechanistic interpretation of experiments at Technical University of Braunschweig on ammonia/methanol mixtures was assisted by evaluation of k_{5a} and k_{5b} for

$$NH_2 + CH_3OH \rightarrow NH_3 + CH_2OH \quad (4a)$$

$$\rightarrow NH_3 + CH_3O \quad (4b)$$

based on Canonical Variational Transition State Theory with internal torsions treated as uncoupled 1-D rotors. Tunneling was assessed from the curvature at the top of the vibrationally adiabatic barrier and the Eckart model. It is planned to return to these processes using MS-CVT at a later date. Modeling indicated

that addition of methanol to ammonia fuel speeds ignition through increased [HO_2] and [OH] while recycling NH_2 back to NH_3 via reaction (4).

A recent theory/modeling study focused on the sometimes-included reaction $NH_2 + NH_3 \rightleftarrows N_2H_3 + H_2$ with the conclusion that there is no moderate barrier, direct pathway or one via an N_2H_5 intermediate, and that for several scenarios multireaction modeling can match literature observations without assuming this process.

Reactions (3), (4) implement coupling between C and N chemistry. There is also the possibility of forming C-N species in an ammonia/hydrocarbon flame, such as CH_3NH_2 from methyl + amidogen recombination. A product of attack on CH_3NH_2 is the imine CH_2=NH. This molecule is hard to handle and there are no experimental determinations of its reactivity with flame radicals such as H and OH. We have made measurements of hydroxyl kinetics with a more inert, fluorinated imine:

$$OH + (CF_3)_2C{=}NH \rightarrow \text{products} \qquad (5)$$

We monitored consumption of the imine and a reference compound, 1,1-difluoroethane, via FT-IR spectroscopy, in the presence of OH generated by UV photolysis of an ozone/hydrogen mixture. From the relative rates we derive the overall $k_5 \approx 4.4 \times 10^{-14}$ cm^3 molecule^{-1} s^{-1} at 298 K (incidentally, this leads to a 100-year Global Warming Potential of 90). This k_5 allows us to test computational evaluation of the rate constants for abstraction of H or addition at the C or N atoms. Initial results indicate addition to the C atom is favored. For H-atom reactions with this imine, theory yields predicted barriers for abstraction, C addition and N addition of 45, 29 and 17 kJ mol^{-1}, respectively. These H-atom values await experimental confirmation.

There has been some question about the high-pressure limit for

$$NH_3 + M \rightleftarrows NH_2 + H + M \qquad (6)$$

with shock-tube experiments interpreted to yield $k_{-6,\infty}$ values for NH_2 + H recombination of between 2×10^{12} to 2×10^{14} cm^3 mol^{-1} s^{-1}. Searches with multireference CASSCF-MP2 theory revealed no tight transition state for reaction (6) and classical capture theory based on long-range dispersion interactions yielded $k_{-6,\infty} \approx 6.5 \times 10^{14}$ cm^3 mol^{-1} s^{-1} at 298 K and proportional to $T^{1/6}$. This result supports the idea that most experiments are at the low-pressure limit for reaction 6 and a mechanism for ammonia pyrolysis that incorporates a recommended $k_{-6,\infty} = (4 \pm 2) \times 10^{14}$ cm^3 mol^{-1} s^{-1} has been published.

The high pressures and high NH_3 concentrations that arise with use of NH_3 as a fuel, rather than as a model for a fuel-nitrogen source of NO_x, mean that dinitrogen species may be formed. We have explored the PE surface for

$$N_2H_3 + O_2 \rightarrow \text{products} \qquad (7)$$

with the initial expectation of similarity to ethyl + oxygen which proceeds via the ethylperoxy intermediate and well-known ROO, QOOH chemistry. However, the isoelectronic $NH_2N(H)OO$ radical is computed to be thermodynamically unstable with respect to the reactants in reaction (7). The lowest barrier pathways appear to be abstractions leading to $N_2H_2 + HO_2$, with ROCCSD(T)/CBS barriers of ca. 60, 80 and 120 kJ mol^{-1} for attack at the three N-H bonds. This implies that the hydrazyl radical could be relatively long-lived, at least with respect to direct oxidation.

In the context of possible pathways for N_2O destruction, we note that Burke and coworkers recently discussed a significant role for NH_2 reaction with N_2O over 800-1100 K:

$$NH_2 + N_2O \rightarrow N_2H_2 + NO \qquad (8)$$

We have conducted experiments which yield an upper limit for overall NH_2 consumption of ca 1×10^{-15} cm^3 molecule^{-1} s^{-1} at 510 K, which is consistent with the empirically estimated $k_8 \sim 10^{-18}$ cm^3 molecule^{-1} s^{-1}. Investigation of the PE surface with modified CBS-APNO theory is summarized below in Fig. 3. The lowest barrier path leads to H_2NN rather than HNNH, following NH_2 attack at the terminal N of N_2O.

A second N_2O consumption route is

$$O + N_2O \rightarrow N_2 + O_2 \text{ and/or } 2\ NO \qquad (9)$$

and we recently published an evaluation of prior work in this area, attempting to resolve disagreements concerning product branching ratios.

Details of the current quantitative mechanism for oxidation and pyrolysis of NH_3, N_2H_4 and related compounds developed to date are contained in publications 2, 5 and 6 below.

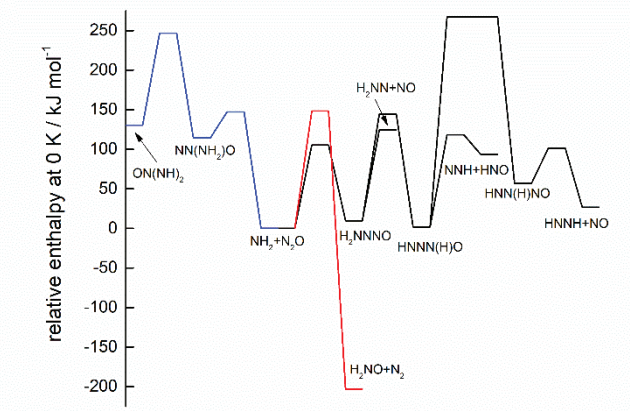

Figure 3. PE diagram for $NH_2 + N_2O$. Attack is possible at the O atom (red), central N atom (blue) and terminal N atom (black)

Future Plans

Experiments with resonance fluorescence detection of H atoms will be applied to the kinetics of $H + CH_3NH_2$. Theory will help assess H-abstraction from C-H vs N-H, and possible pathways to $CH_4 + NH_2$ and $CH_3 + NH_3$. Proposed extensions of NH_2 chemistry include its kinetics with unsaturated species, starting with ethylene and acetylene where addition to the pi bond is likely important, and with biofuels and diesel surrogates. Product studies of H and O-atom reactions with N_2O, a greenhouse gas potentially formed during ammonia oxidation, are aimed at improving understanding of these processes that destroy N_2O in flames. These product studies will include ca. 1 atm pressure discharge-flow experiments.

Our apparatus with FT-IR detection will be modified for high-temperature photochemistry, to investigate the reactivity and product formation for NH_3 and CH_3NH_2 reactions, initially with O atoms. Computationally, the unimolecular reactions of methylamine and ethylamine will be examined because the reverse of C-N bond breaking couples regular hydrocarbon chemistry and ammonia chemistry. Mechanism development in collaboration with Glarborg will continue, and species for further evaluation include NH_2O.

DOE Sponsored Publications 2022-2024

1. "Challenges in Kinetic Modeling of Ammonia Pyrolysis" P. Glarborg, H. Hamid and P. Marshall, Fuel Commun., 10, 100049 (2022).
2. "An Experimental and Modeling Study on Auto-Ignition Kinetics of Ammonia/Methanol Mixtures at Intermediate Temperature and High Pressure" M. Li, X. He, H. Hashemi, P. Glarborg, V.M. Lowe, P. Marshall, R. Fernandes and B. Shu, Combust. Flame, 242, 112160 (2022).
3. "Experimental and Computational Studies of the Kinetics of the Reaction of Hydrogen Peroxide with the Amidogen Radical" I.M. Alecu, Y. Gao and P. Marshall, J. Chem. Phys., 157, 014304 (2022).
4. "Reactions of Hydrazine with the Amidogen Radical and Atomic Hydrogen" Y. Gao, I.M. Alecu, H. Hashemi, P. Glarborg and P. Marshall, Proc. Combust. Inst., 39, 571 (2023).
5. "Re-Evaluation of Rate Constants for the Reaction N_2H_4 (+ M) ⇄ $NH_2 + NH_2$ (+ M)" C.J. Cobos, P. Glarborg, P. Marshall and J. Troe, Combust. Flame, 257, 112374 (2023).
6. "Probing high-temperature amine chemistry: Is the reaction $NH_3 + NH_2 = N_2H_3 + H_2$ important?" P. Marshall and P. Glarborg, J. Phys. Chem. A, 127, 2601-2607 (2023).
7. "Re-Examination of the $N_2O + O$ Reaction" P. Glarborg, J.S. Allingham, A.B. Skov, H. Hashemi and P. Marshall, J. Phys. Chem. A, 127, 6521 (2023).

Hydrogen Generation from Hydrocarbons via Radical-Driven Reactions

Hope A. Michelsen
Department of Mechanical Engineering and Environmental Engineering Program
University of Colorado Boulder
1111 Engineering Drive, UCB 427
Boulder, CO 80309
Hope.Michelsen@colorado.edu

I. Program Scope

This program is focused on the development of new approaches to hydrogen production from the conversion of hydrocarbons, including methane and bioderived hydrocarbons, with an emphasis on the basic chemistry of hydrogen generation. There is considerable interest in hydrogen production as a clean-energy source[1, 2] with carbon-negative hydrogen production as the ultimate goal for mitigating climate change. Hydrogen is currently almost entirely produced from fossil-fuel sources, predominantly via high-temperature catalytic conversion of hydrocarbons, primarily methane.[1] Most hydrogen (75%) is produced by steam reforming of methane from fossil-fuel sources, which also produces CO_2, limiting its utility as a carbon-neutral hydrogen source.

We are exploring how radical-driven reactions initiated by pyrolysis or photolysis can catalytically lower hydrogen-production temperatures. Our approach involves performing pyrolysis studies focused on identifying the chemical pathways and key intermediates in the radical-driven carbonization of gas-phase hydrocarbons and their gas-to-condensed-phase conversion. These studies are performed using a variable-temperature flow reactor to control and vary the conditions for gas-to-condensed-phase conversion. Observations of gas- and condensed-phase product evolution are made using in situ diagnostics, such as laser-induced incandescence (LII), elastic laser scattering (ELS), and elastic and inelastic X-ray scattering for particles and laser-induced fluorescence (LIF), time-resolved near-edge X-ray absorption spectroscopy (TR-NEXAFS), and X-ray Coulomb explosion imaging (CEI) for gas-phase intermediates. Gas-phase and particle products can be extracted for ex situ diagnostics, such as transmission electron microscopy (TEM), scanning mobility particle sizing (SMPS), and vacuum ultraviolet photoionization aerosol mass spectrometry (VUV-AMS) for particles and resonance-enhanced multiphoton ionization (REMPI) for gas-phase intermediates.

II. Recent Progress

A. Pyrolysis experiments

We performed experiments at Beamline 9.0.2 at the ALS in December 2023 and June 2024. In these experiments, we worked on the development of a calibration scheme for our VUV-AMS pyrolysis experiments. Aerosol mass spectra often have a plethora of mass peaks spanning a wide range of masses, and confidence in correctly identifying these peaks requires a calibration procedure. Large masses are difficult to calibrate, but their calibration is crucial for gaining insight into the chemistry of radical hydrocarbons and hydrocarbon clustering leading to solid phases. During the first ALS experiments of this project, we developed a scheme to generate regularly spaced and isolated polydimethylsiloxane (PDMS) peaks for use in calibrating mass spectra in the large-mass regime. These peaks are typically considered to be artifacts in mass spectrometry in which they appear as a result of contamination from silicone vacuum grease and valve lubricants. Conductive silicone tubing used for aerosol studies can also lead to contamination of aerosol mass spectra and is a particular problem when high-temperature mature soot is generated and heats the tubing in the sampling line to the aerosol mass spectrometer.[3] The peaks thereby generated by PDMS are reproducible, isolated, and span the range of masses typically observed in our experiments and thus make a good basis for mass calibration.

We can reproducibly generate these peaks in the VUV-AMS by producing highly carbonaceous particles and passing them through a section of PDMS tubing heated to ~150°C before sending them into the aerosol mass spectrometer. We typically use ethylene heated to 1050 – 1150 °C in our pyrolysis flow reactor to produce these carbonaceous particles. The peaks produced by these particles do not interfere with the siloxane calibration peaks, as shown in Fig. 1a.

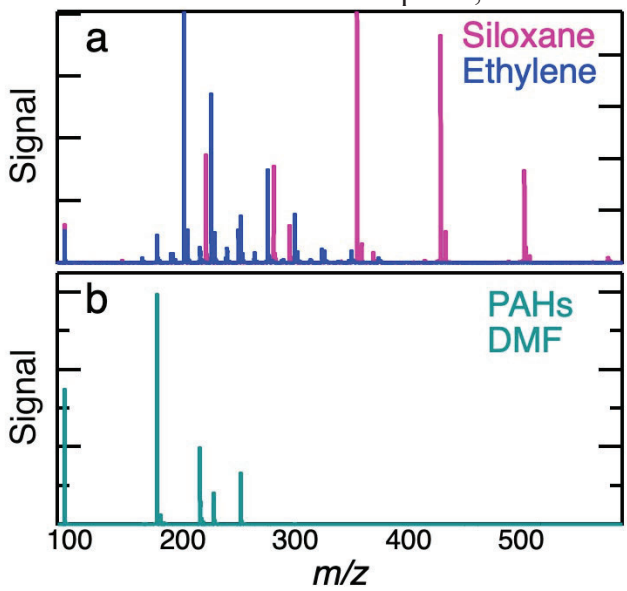

Figure 1. VUV-AMS mass spectra of peaks used in the calibrations. Mass spectra are shown for (a) carbonaceous particles generated by heating ethylene to 1150 °C in a flow reactor with (pink) and without (blue) heated silicone tubing in the sampling line between the flow reactor and the VUV-AMS and (b) selected PAHs, which included anthracene ($C_{14}H_{10}$, 178.08 u), 2,3-benzofluorene ($C_{17}H_{12}$, 216.09 u), chrysene ($C_{18}H_{12}$, 228.09 u), perylene ($C_{20}H_{12}$, 252.09 u), coronene ($C_{24}H_{12}$, 300.09 u), and 2,5-dimethylfuran (DMF) (C_6H_8, 96.06 u).

The smallest species in the first series of peaks appears at *m/z* 73.05, which has previously been identified as $Si(CH_3)_3$.[4] This series of peaks results from the repeated addition of dimethylsiloxane ($Si(CH_3)_2O$) with a mass of 74.02 u, yielding small peaks at *m/z* of 147.07, 221.09, 295.10, 369.12, and 443.14. Another series of small peaks is generated by the addition of dimethylsiloxane (DMS) to SiOH, starting with $(Si(CH_3)_2O)_4SiOH$ to give peaks at *m/z* of 341.06, 415.06, 489.09, 563.11, 637.13, and 711.15. The most prominent series of peaks repeatedly adds DMS to the base species $(Si(CH_3)_2O)_3Si(CH_3)O$, yielding peaks at *m/z* of 281.05, 355.07, 429.09, 503.11, 577.13, 651.15, 725.16, and 799.00. Together these peaks extend throughout our typical range of mass detection.

We have verified the calibration of these peaks using a set of polycyclic aromatic hydrocarbons (PAHs) that are stable at room temperature, have known masses, and cover a modest mass range. This set includes anthracene ($C_{14}H_{10}$, 178.08 u), 2,3-benzofluorene ($C_{17}H_{12}$, 216.09 u), chrysene ($C_{18}H_{12}$, 228.09 u), perylene ($C_{20}H_{12}$, 252.09 u), and coronene ($C_{24}H_{12}$, 300.09 u). We also add 2,5-dimethylfuran (DMF) (C_6H_8, 96.06 u) to the chamber for calibrating the photon flux during energy scans. This peak additionally provides a mass calibration peak. An example mass spectrum of these species is shown in Fig. 1b, and the calibration range of DMF and the PAHs is compared with that of the siloxanes in Fig. 2.

In addition, we performed preliminary experiments on methane pyrolysis, which requires high temperatures to initiate gas-to-solid conversion. This species does not possess any C-C bonds that can be readily broken, and the C-H bonds are relative strong. We were able to record aerosol mass spectra for methane pyrolysis at flow reactor temperatures above approximately 1050°C.

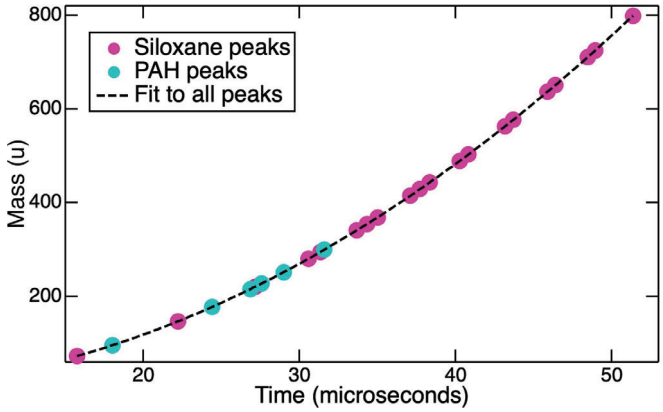

Figure 2. Comparison of calibration points for selected PAHs and siloxanes. The actual mass for each species is plotted against the detection time for the VUV-AMS. PAH points include data for anthracene ($C_{14}H_{10}$, 178.08 u), 2,3-benzofluorene ($C_{17}H_{12}$, 216.09 u), chrysene ($C_{18}H_{12}$, 228.09 u), perylene ($C_{20}H_{12}$, 252.09 u), coronene ($C_{24}H_{12}$, 300.09 u), and 2,5-dimethylfuran (DMF) (C_6H_8, 96.06 u).

B. Diagnostics development

In collaboration with colleagues at the Linac Coherent Light Source (LCLS), the X-ray free electron laser at the SLAC National Accelerator Facility, we are working on the development of Coulomb Explosion Imaging (CEI) and time-resolved near-edge X-ray absorption fine structure (NEXAFS) spectroscopy to measure reactive intermediates during hydrocarbon pyrolysis. We have written a proposal for beamtime at LCLS to study the formation and unimolecular decomposition of the phenoxy radical during anisole pyrolysis.

C. Theory and modeling

We performed a study focused on theoretical investigations of hydrogen-atom ejection during high-temperature hydrocarbon chain reactions driven by resonance-stabilized radicals (RSRs).[5] This work was performed in collaboration with Prof. Martin Head-Gordon and his group. Using quantum chemical theoretical approaches, we demonstrated that, during the types of chemical mechanisms involved in hydrocarbon radical-chain-reaction mechanisms, reaction barriers are low enough that hydrogen atoms can be ejected from intermediates species formed during these chain reactions. This result is important because it enables these radical-chain reactions to proceed even in the absence of large pools of free radical species that would otherwise be required to abstract these hydrogen atoms from such reaction intermediates.

III. Future Plans

A. Pyrolysis experiments

We will continue making and analyzing VUV-AMS pyrolysis measurements on methane, more complex hydrocarbons, and bioderived feedstocks. These experiments will be performed in collaboration with Dr. Kevin Wilson at LBNL. We will prioritize experiments aimed at reducing the temperature for hydrogen generation from such hydrocarbon feedstocks by doping them with direct RSR precursors, including indene and propyne. We will also design and build a new pyrolysis flow reactor with optical access for probing reactive intermediates during hydrogen generation.

B. Diagnostics development

We will build out our new lab space with laser-based diagnostics to detect H atom and molecular H_2 emitted during the gas-to-solid conversion. We will submit a proposal for beam time at LCLS to perform femtosecond wide-angle X-ray scattering (WAXS) measurements of the initial solid carbon particles formed as hydrogen is produced. These measurements will be performed in collaboration with Dr. Andy Aquila at LCLS.

C. Theory and modelling

We will develop a detailed chemical kinetic model of hydrogen generation during pyrolysis of different fuels. This work will involve identifying potential chemical kinetic mechanisms that contribute to hydrogen generation and solid carbon formation. Once potential mechanisms and intermediate species are identified, we will perform theoretical studies, in collaboration with Prof. Head-Gordon and his research group, to verify mechanisms and estimate rate constants for inclusion in the chemical kinetic model.

IV. References

(1) U.S. Department of Energy, Office of Science, Basic Energy Sciences Roundtable, Foundational Science for Carbon-Neutral Hydrogen Technologies, Technology Status Document; Accessed online: https://science.osti.gov/-/media/bes/pdf/brochures/2021/Hydrogen_Roundtable_Technical.pdf, 2021.

(2) U.S. Department of Energy, Office of Science, Basic Energy Sciences Roundtable, Foundational Science for Carbon-Neutral Hydrogen Technologies; Accessed online: https://science.osti.gov/-/media/bes/pdf/brochures/2021/Hydrogen_Roundtable_Report.pdf, 2021.

(3) Timko, M. T.; Yu, Z.; Kroll, J.; Jayne, J. T.; Worsnop, D. R.; Miake-Lye, R. C.; Onasch, T. B.; Liscinsky, D.; Kirchstetter, T. W.; Destaillats, H., et al., Sampling artifacts from conductive silicone tubing. *Aerosol Sci. Technol.* **2009,** *43*, 855-865.

(4) Dong, X.; Gusev, A.; Hercules, D. M., Characterization of polysiloxanes with different functional groups by time-of-flight secondary ion mass spectrometry. *J. Am. Soc. Mass Spectrom.* **1998,** *9*, 292-298.

(5) Hendrix, J.; Hait, D.; Michelsen, H. A.;Head-Gordon, M. P., Hydrogen ejection from hydrocarbons: Characterization and relevance in soot formation and interstallar chemistry. *Proc. Natl. Acad. Sci. U. S. A.* **2024**, in press.

V. Publications supported by this program 2022-2024

1. J. Hendrix, D. Hait, H. A. Michelsen, and M. Head-Gordon, "Hydrogen ejection from hydrocarbons: Characterization and relevance in soot formation and interstellar chemistry", *Proc. Natl. Acad. Sci. USA*, in press (2024).
2. J. A. Rundel, C. Martí, J. Zádor, P. E. Schrader, K. O. Johansson, R. P. Bambha, G. T. Buckingham, J. P. Porterfield, O. Kostko, and H. A. Michelsen,"The identity and chemistry of C_7H_7 radicals observed during soot formation", *J. Phys. Chem. A*, **127**(13), 3000-3019 (2023) DOI: 10.1021/acs.jpca.2c08949.
3. C. Martí, H. A. Michelsen, H. N. Najm, and J. Zádor,"Comprehensive kinetics on the C_7H_7 potential energy surface under combustion conditions", *J. Phys. Chem. A*, **127**(8), 1941-1959 (2023) DOI: 10.1021/acs.jpca.2c08035.
4. J. Zádor, C. Martí, R. Van de Vijver, S. L. Johansen, Y. Yang, H. A. Michelsen, and H. N. Najm, "Automated reaction kinetics of gas-phase organic species over multiwell potential energy surfaces", *J. Phys. Chem. A*, **127**(3), 565-588 (2023) DOI: 10.1021/acs.jpca.2c06558.
5. J. A. Rundel, K. O. Johansson, P. E. Schrader, R. P. Bambha, K. R. Wilson, J. Zádor, G. B. Ellison, and H. A. Michelsen, "Production of aliphatic-linked polycyclic hydrocarbons during radical-driven particle formation from propyne and propene pyrolysis", *Combust. Flame* **258**(1), 112457 (2023) DOI: 10.1016/j.combustflame.2022.112457.
6. H. A. Michelsen, E. Boigné, P. E. Schrader, K. O. Johansson, M. F. Campbell, R. P. Bambha, and M. Ihme, "Jet-entrainment sampling: A new method for extracting particles from flames", *Proc. Combust. Inst.*, **39**, 847-855 (2023) DOI: 10.1016/j.proci.2022.07.140.
7. H. A. Michelsen, M. F. Campbell, K. O. Johansson, I. C. Tran, P. E. Schrader, R. P. Bambha, E. Cenker, J. A. Hammons, E. Schaible, C. Zhu, and A. van Buuren, "Soot particle core-shell and fractal structures from small-angle X-ray scattering measurements in a flame", *Carbon*, **196**, 440-456 (2022) DOI: 10.1016/j.carbon.2022.05.009.
8. H. A. Michelsen, M. F. Campbell, I. C. Tran, K. O. Johansson, P. E. Schrader, R. P. Bambha, J. A. Hammons, E. Schaible, C. Zhu, and A. van Buuren, "Distinguishing gas-phase and nanoparticle contributions to small-angle X-ray scattering in reacting aerosol flows", *J. Phys. Chem. A*, **126**, 3015-3026 (2022) DOI:10.1021/acs.jpca.2c00454.
9. J. A. Rundel, C. M. Thomas, P. E. Schrader, K. R. Wilson, K. O. Johansson, R. P. Bambha, and H. A. Michelsen, "Promotion of particle formation by resonance-stabilized radicals during hydrocarbon pyrolysis", *Combust. Flame*, **243**, 111942 (2022) DOI:10.1016/j.combustflame.2021.111942.

Electronic Structure, Spectroscopy, and Bond Dissociation Energies of Small Actinide Molecules

PI: Michael D. Morse (morse@chem.utah.edu)
Department of Chemistry, University of Utah
315 S. 1400 East, Salt Lake City, UT 84112

Program Scope

In this experimental program, we seek to obtain detailed, precise information concerning the electronic structure, spectroscopy, and bond dissociation energies of small thorium and uranium molecules and ions that can be used to assess computational approaches for these systems. The work is focused on advancing our understanding of the role of the 6*d* and 5*f* electrons in the electronic structure of these species. Computational chemistry finds these molecules to be quite challenging, due to the high electronic state density and the highly correlated electronic motions in the partially filled 6*d* and 5*f* subshells. In addition, relativistic effects, including spin-orbit interactions, are of great importance in the actinides. Accurate benchmark data is critically needed to assess method developments in this field.

The major focus is the precise measurement of bond dissociation energies (BDEs) by the observation of a sharp predissociation threshold in a resonant two-photon ionization (R2PI) spectrum. The Morse group has successfully applied this technique to about 30 transition metal dimers and trimers and to more than 130 diatomics formed from *d*- and *f*-block metals bonded to *p*-block elements, with error limits generally below 0.01 eV. In this work our focus is to measure the BDEs of Th and U-containing species. This method can reduce the error limits on the currently accepted BDE values by factors of 10 to 100, thereby building up a compendium of precise values for testing computational models of the 5*f* and 6*d* electrons. Measurements of the BDEs of the actinide cations will also be conducted in a cryo-cooled ion photodissociation spectrometer. BDEs of the more strongly bound Th^+-O, Th^+-N, U^+-O, OU^+-O, *etc.* molecules will be measured by the observation of a sharp predissociation threshold at the two-photon level, using a resonant two-photon dissociation (R2PD) method. Combining the BDEs of the neutral and cationic molecules with precisely known ionization energies (IEs) from PFI-ZEKE work or from photoionization threshold measurements and the atomic IEs closes a thermochemical cycle, allowing tests for self-consistency. When the BDE of the neutral cannot be measured due to its high BDE and low IE (ThF, ThO, UF, and UO, for example), the thermochemical cycle will be used to determine the neutral BDE from the three other values. The resulting wealth of highly precise data will enable in-depth probes of computational methods and basis sets, allowing effective computational methods to be identified.

R2PI spectroscopy of actinide neutrals and R2PD spectroscopy of actinide cations will be used to learn about the electronic structure of these species and to provide experimental feedback for computational chemists. Rotationally resolved spectroscopy will be used to improve our understanding of species such as the ThB, ThC, UB, UC, and US molecules. The spectrum of UO_2 will be investigated in the near-IR, where the density of electronic states is expected to be low enough that meaningful spectra may be obtained. Likewise, spectroscopic work on ThO_2 will be pursued to investigate the extent to which this molecule resembles its TiO_2 and ZrO_2 congeners, for which spectra are known. Among the cations, rotationally resolved spectra of ThX^+ and UX^+ species will be measured using a resonant two-photon dissociation method. The UB and UN species are relevant to high-melting reactor substrates (uranium nitrides and borides), and the uranium halide species are relevant to molten salt reactors.

Recent Progress

Measurements of Bond Dissociation Energies: US_2, OUS, and USe

In a recently published study,[1] we have measured the bond dissociation energies of SU-S, OU-S, and U-Se as 4.910(3) eV, 5.035(4) eV, and 4.609(9) eV, respectively. For the triatomics, a delayed two-

color R2PI method was required to allow sufficient time for the molecules to dissociate prior to the ionization laser pulse. By introducing this delay, highly precise bond energies were obtained. This work has prompted Kirk Peterson's group to perform high-level calculations on these species, with results that are in excellent agreement with our measured BDE values.

Measurements of Bond Dissociation Energies: URh

After pursuing laser ablation studies of uranium compounds for a few months, my group turned to NSF-supported work to measure the ionization energy of RhC. In a serendipitous discovery, it was found that uranium that had been deposited within the laser ablation fixture was being vaporized and it reacted with the ablated rhodium to form diatomic URh. My students scanned over the bond dissociation threshold and quickly measured D_0(URh) = 5.472(3) eV, in good agreement with the 1978 Knudsen effusion measurement of 5.34(18) eV.[2] David Dixon has now calculated the molecule, and finds that URh has a $d\sigma^2\ d\pi^4\ d\delta^4\ s\sigma^2\ 5f\varphi^1\ 5f\delta^1\ 5f\pi^1$, $^4I_{4.5}$ ground state. The dσ, dπ, and sσ orbitals have contributions on both atoms and are bonding orbitals; the dδ orbitals are localized on Rh and are nonbonding. The 5f orbitals also remain localized on U and are nonbonding. The computed BDE of 5.37 eV (large core CCSD(T) method) is in excellent agreement with our measurement. A joint publication is in preparation.

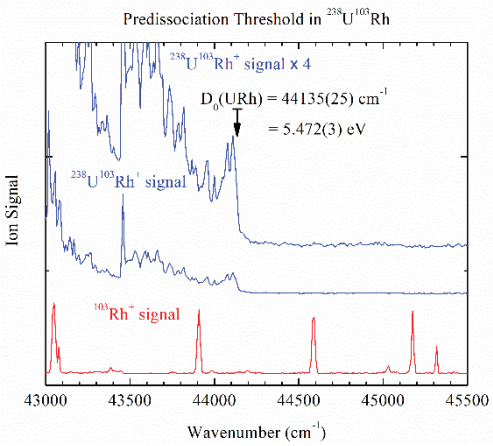

Fig. 1. Predissociation threshold measurement of the BDE of URh.

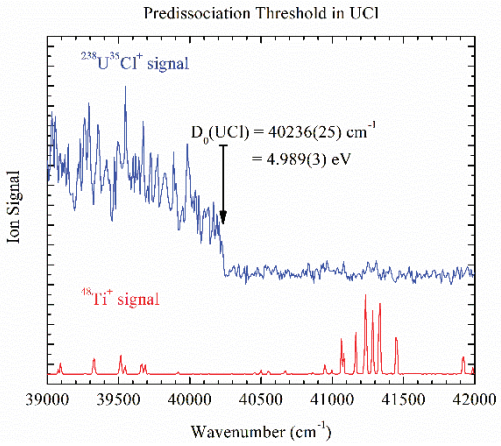

Fig. 2. Predissociation threshold measurement of the BDE of UCl.

Measurements of Bond Dissociation Energies: ThCl, ThBr, and ThI

My graduate students, Thomas Kawagoe and Dakota Merriles have measured the BDEs of the diatomic thorium halides, ThCl, ThBr, and ThI, obtaining values of 5.077(6) eV, 4.391(4) eV, and 3.537(8) eV, respectively. The value for ThCl is very close to a computational result by the Peterson and Heaven groups, who obtained 5.131 eV.[3] Similarly, it is in good agreement with a Knudsen effusion value of 5.03(6) eV.[4] The result for ThBr, however, differs substantially from Knudsen effusion values of Hildenbrand and Lau, who obtained 3.73(6) eV, revised to 3.87(6) eV in a subsequent review.[5, 6] The BDE of ThI has not previously been measured.

Measurements of Bond Dissociation Energies: UCl, UBr, and UI

Thomas Kawagoe has likewise measured the BDEs of UCl, UBr, and UI, obtaining values of 4.989(3) eV, 4.299(13) eV, and 3.449(8) eV, respectively. These compare to Knudsen effusion values of 4.64(9) eV, subsequently revised to 4.51(6) eV for UCl;[6, 7] and 3.87(8) eV, revised to 3.87(6) eV for UBr.[6, 8] No previous measurement exists for UI. From these two studies, we see that the Knudsen effusion BDE values for ThBr, UCl, and UBr significantly underestimate the strength of the AnX bond. A manuscript on these BDE measurements of ThCl, ThBr, ThI, UCl, UBr, and UI is in preparation.

Measurements of the Ionization Energies of ThCl and ThBr by R2PI

To measure the ionization energies (IEs) of the AnX molecules, we employed a resonant two-photon ionization scheme. In the first step, the first laser was scanned in the visible or near infrared while the second laser was set to a wavelength that could ionize any states that were excited by the first laser. This allowed excited vibronic states to be located. In a second step, the first laser was fixed on a wavelength to populate a given excited state, and the second laser was scanned to locate the ionization threshold of this particular excited state. The sum of the two photon energies, at the ionization threshold, provided the ionization energy of the molecule. For verification, the process was repeated using two other intermediate states. The process was tested on ThCl, which gave IE(ThCl) = 6.364(10) eV, in excellent agreement with Michael Heaven's value of IE(ThCl) = 6.3658(6) eV, measured by PFI-ZEKE spectroscopy.[3] We then applied it to ThBr, obtaining a value of IE(ThBr) = 6.336(11) eV.

Construction and Testing of the Cryo-Cooled Ion Photodissociation Spectrometer (CCIPS)

My graduate student, Joshua Ewigleben, is making good progress in bringing our CCIPS instrument online. We discovered that our initial ion source design, which employed laser ablation in a fairly high-pressure chamber (30 mTorr), transmission through an ion funnel, pre-trapping in a hexapole ion trap, and then travel through an octopole ion guide to a quadrupole mass filter simply doesn't work. Josh has now completely modified the design, moving the laser ablation source into higher vacuum (~10^{-5} Torr) and injecting the ions directly into the octopole ion guide. The new design works very well, yielding mass-selected atomic ion currents of roughly 0.5 nA, or 3×10^8 ions/pulse. He has turned the ions into the cryo-cooled ion trap and brought them to the conversion dynode detector, where at least 10^5 ions/pulse have been detected. Further design modifications are needed on the detection end of the instrument, but we anticipate our first thermochemical or spectroscopic measurements by the end of the year.

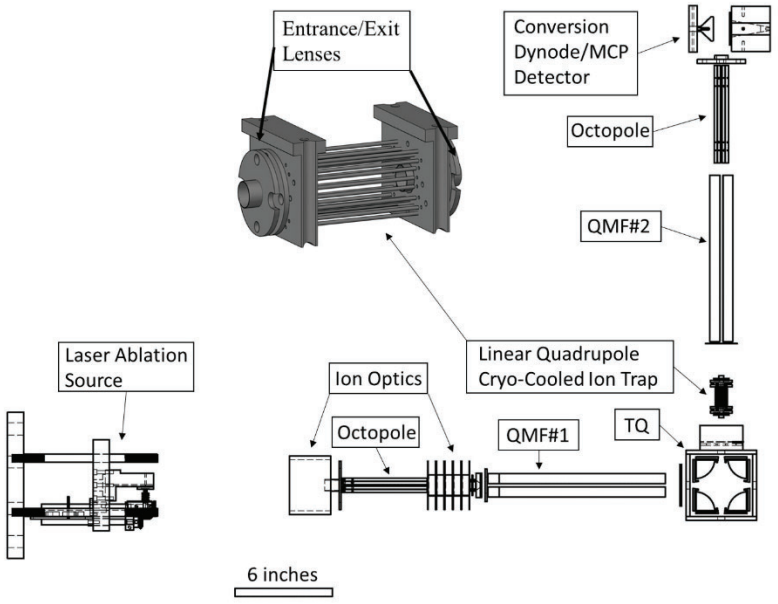

Fig. 3. Current design of the cryo-cooled ion photodissociation spectrometer.

Future Plans

Measurements on UC: BDE, IE, and Rotationally Resolved Spectroscopy

Thomas Kawagoe's current work in the laboratory is focused on diatomic UC. We have already measured D_0(UC) = 4.304(3) eV, in excellent agreement with the value of 4.26 eV obtained by the FPD composite method by the Peterson and Dixon groups.[9] We are in the process of setting up experiments to measure IE(UC) using the methods described above for ThCl and ThBr. Subsequently, we will begin attempts to measure rotationally resolved spectra of UC, to verify (or disprove) the computed ground state of $\Omega = 3$ and $r_e = 1.854$ Å.[9] This work is currently on hold due to some laboratory maintenance issues.

Measurements of other neutral molecule properties:

Among the other neutral molecule experiments we plan to attempt are (1) measurements of the BDEs of US, ThCN, UCN, possibly other actinide-transition metal diatomics, and possibly oxo species such as OUCl and OThCl. (2) measurements of the IEs of the remaining Th and U halides, and (3) rotationally resolved spectroscopy of other species, such as UCl and US.

Measurements of Cationic BDEs

Among the first tasks we plan for the cryo-cooled ion photodissociation spectrometer (CCIPS) are experiments to precisely measure the BDEs of thorium and uranium diatomic cations, such as MC^+, MN^+, MO^+, and MF^+ (M = Th, U). We anticipate that the carbides can be measured in a one-photon photodissociation experiment, while the remaining species will require a resonant two-photon dissociation experiment. We also plan to measure the remaining thorium and uranium halide cations, which if we are successful in measuring the neutral molecule IEs will flesh out the thermochemical cycle, providing a self-consistency check. An advantage of the CCIPS instrument is that we envision being able to make measurements of larger species, such as the series of UF_n^+, ThF_n^+, *etc*. cations. Unlike the neutral experiments, where we are limited by the possibility of larger molecular species fragmenting and falling into the mass channel of the species of interest, this will not be an issue in the cationic studies, because the cation will be mass selected prior to spectroscopic interrogation as well as mass analyzed following irradiation. Once in operation, we also plan to use resonant two-photon dissociation experiments to measure rotationally resolved spectra. Initial targets will the UF^+, UO^+, UN^+, and UO_2^+.

DOE Supported Publications 2021-2024

1. Tomchak, K. H.; Sorensen, J. J.; Tieu, E.; Morse, M. D. Predissociation-based measurements of bond dissociation energies: US_2, OUS, and USe. *J Chem Phys* **2024**, *161* (4). DOI: 10.1063/5.0220813.

References:

[1] K. H. Tomchak, J. J. Sorensen, E. Tieu, and M. D. Morse,"Predissociation-based measurements of bond dissociation energies: US_2, OUS, and USe," J Chem Phys **161** (2024)

[2] K. A. Gingerich, and S. K. Gupta,"Dissociation energies of the molecules rhodium-thorium (RhTh) and rhodium-uranium (RhU) from high temperature mass spectrometry and predicted thermodynamic stabilities of selected diatomic actinide-platinum metal intermetallic molecules," J. Chem. Phys. **69** (1978) 505-511.

[3] R. A. VanGundy, J. H. Bartlett, M. C. Heaven, S. R. Battey, and K. A. Peterson,"Spectroscopic and theoretical studies of ThCl and $ThCl^+$," J. Chem. Phys. **146** (2017) 054307.

[4] K. H. Lau, and D. L. Hildenbrand,"High-temperature equilibrium studies of the gaseous thorium chlorides," J. Chem. Phys. **92** (1990) 6124-6130.

[5] D. L. Hildenbrand, and K. H. Lau,"Thermochemistry of the gaseous thorium bromides," J. Chem. Phys. **93** (1990) 5983-5989.

[6] D. L. Hildenbrand, and K. H. Lau,"Trends and anomalies in the thermodynamics of gaseous thorium and uranium halides," Pure Appl. Chem. **64** (1992) 87-92.

[7] K. H. Lau, and D. L. Hildenbrand,"Thermochemical studies of the gaseous uranium chlorides," J. Chem. Phys. **80** (1984) 1312.

[8] K. H. Lau, and D. L. Hildenbrand,"Thermochemistry of the gaseous uranium bromides UBr through UBr_5," J. Chem. Phys. **86** (1987) 2949.

[9] G. F. de Melo, M. Vasiliu, G. Liu, S. Ciborowski, Z. Zhu, M. Blankenhorn, R. Harris, C. Martinez-Martinez, M. Dipalo, K. A. Peterson, K. H. Bowen, and D. A. Dixon,"Theoretical and Experimental Study of the Spectroscopy and Thermochemistry of $UC^{+/0/-}$," J. Phys. Chem. A **126** (2022) 9392-9407.

Spectroscopy, Kinetics, and Dynamics of Highly Reactive Species

JILA/NIST/Department of Chemistry/Department of Physics
University of Colorado, Boulder 80309
David. J. Nesbitt (djn@jila.colorado.edu)

Our DOE research program involves experimental and theoretical study of transient chemical species relevant to fundamental chemical processes. The work focuses on spectroscopy and unimolecular/bimolecular dynamics of complex (and often highly reactive) intermediates, combining i) high-resolution direct IR laser absorption methods with quantum shot noise limited detection, ii) high densities (10^{12}-10^{14} #/cm^3) of jet-cooled hydrocarbon radicals and molecular ions in slit supersonic discharge expansions, accompanied by iii) high-level *ab initio* potential surface and multidimensional quantum mechanics calculations. Over the past two years, our group has utilized and further developed ultrasensitive high resolution spectroscopy methods to achieve detailed characterization of atmospherically/astronomically important species, with a few selected highlights described below.

A. Spectroscopy and dynamics of metastable cis-HCOOH species

High-resolution direct absorption infrared spectra of metastable cis-formic acid (HCOOH) trapped in a cis-well resonance behind a 15 kcal/mol barrier are reported for the first time, with the energetically unstable conformer produced in a supersonic slit plasma expansion of trans-formic acid/H_2 mixtures.[1] We present a detailed high-resolution rovibrational analysis for cis-formic acid species in the OH stretch (ν_1) fundamental, providing first precision vibrational band origin, rotational constants, and term values, which in conjunction with a*b initio* calculations at the CCSD(T)/ANOn (n=0,1,2) level support the experimental assignments and establish critical points on the potential energy surface for internal rotor trans-to-cis isomerization. Relative intensities for a- and b-type transitions observed in the spectra permit the transition dipole moment components to be determined in the body fixed frame and prove to be in good agreement with *ab initio* CCSD(T) theoretical estimates but rather poor agreement with simple bond-dipole predictions. The observed signal dependence on H_2 in the discharge suggests the presence of a novel H atom radical chemical mechanism for strongly endothermic "up-hill" internal rotor isomerization between trans- and cis-formic acid conformers.[2]

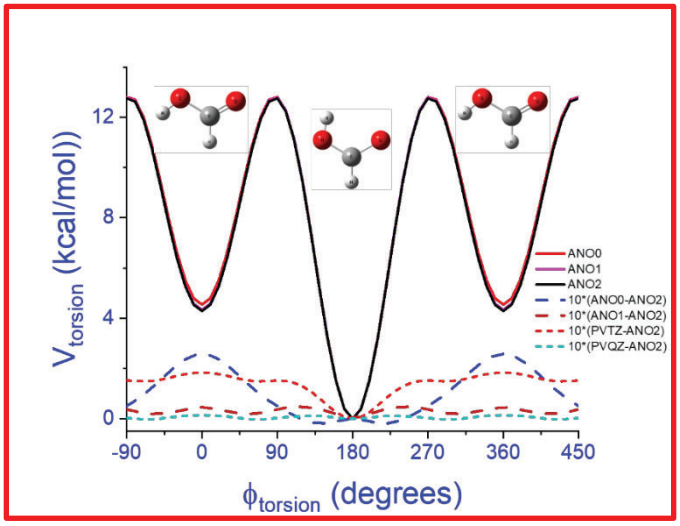

B. High-resolution infrared spectroscopy of gas-phase cyclobutyl radical in the α-CH stretch region: Structural and dynamical insights

Gas-phase cyclobutyl radical (*c*-C_4H_7) is generated at a rotational temperature of 25.6 ± 1.4 K in a slit-jet discharge mixture of 70% Ne/30% He and 0.5-0.6% cyclobromobutane (*c*-C_4H_7Br). The

fully rovibrationally resolved absorption spectrum of the α-CH stretch fundamental band between 3062.9 cm^{-1} to 3075.7 cm^{-1} is obtained and analyzed, yielding the first precision structural information for this radical species.[3] The α-CH stretch fundamental band origin is determined to be 3068.7887(4) cm^{-1}, which from previous infrared spectroscopic studies of cyclobutyl radicals in droplets implies a 0.8 cm^{-1} blue shift due to the presence of liquid helium. This value is also in good agreement with high-level *ab initio* calculations, which predicts an anharmonic frequency of 3076.4 cm^{-1} from second-order vibrational perturbation theory (VPT2). The 1D potential energy surface along the ring puckering coordinate computed at CCSD(T) level of theory with an ANO2 basis set shows double minima in C_s puckered geometry and a C_{2v} transition state, with a barrier height < 1 cm^{-1}. Eigenvalues and eigenfunctions for this 1D double minimum potential are solved using Numerov-Cooley methods. With calculated zero-point energy of the ground state above the interconversion barrier, a vibrationally averaged C_{2v} structure is predicted. Intensity alternation in the experimental spectrum due to nuclear spin statistics upon exchanging 3 pairs of identical fermionic hydrogen atoms (I_H = ½) matches the predicted $K_a + K_c$ = even : odd = 36:28 for a C_{2v} structure, providing the first experimental confirmation of the planar cyclobutyl radical ground state. The persistence of fully resolved high resolution infrared spectroscopy for such large cyclic polyatomic radicals at high vibrational state densities suggests a "*deceleration*" of IVR for a cycloalkane ring topology, much as low frequency torsion/methyl rotation degrees of freedom have demonstrated a corresponding "*acceleration*" of IVR processes in linear hydrocarbons. The results continue to suggest successful application of high-resolution infrared spectroscopy for even larger terpenyl, purinyl, pyradinyl, and polyaromatic ring radical systems.

C. Ergodicity breaking in rapidly rotating C_{60} fullerenes

Large buckminsterfullerene molecules with 60 identical ^{12}C atoms offer completely novel opportunities for long lived quantum control in many body spin systems, establishing a gas-phase molecular platform in principle capable of representing a 60-qubit entangled state with potential applications in quantum computation. As a necessary first step in this direction, quantum state-resolved spectroscopy has been demonstrated in a Nesbitt/Ye group collaboration for gas phase C_{60} molecules when cooled by buffer gas collisions and probed with a mid-infrared frequency comb. Spectroscopically achieving rovibrational quantum state resolution for the largest molecule on record is facilitated due the remarkable high (I_h) symmetry and rigidity of C_{60}, which also present fundamentally new opportunities and challenges with which to explore energy transfer between quantum states in this unique many-atom system. By way of first demonstration of these capabilities, we have combined state-specific optical pumping, buffer gas collisions, and ultrasensitive intracavity nonlinear laser spectroscopy to initiate and probe the rotation- vibration energy transfer and relaxation. This approach provides the first detailed characterization of C_{60} collisional energy transfer for a variety of

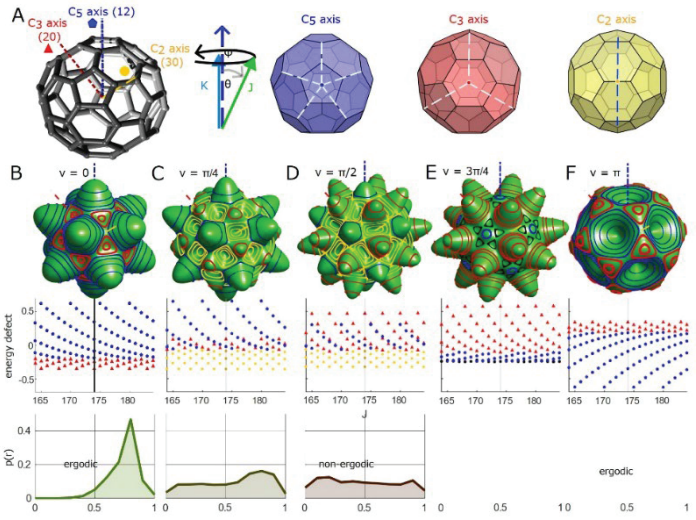

collision partners and determines rotational/vibrational inelastic and elastic collision cross sections.[4] These results establish a novel route towards quantum state control for creating quantum entanglement in a new class of unprecedentedly large gas phase molecules. Ergodicity, the central tenet of statistical mechanics, predicts that an isolated system will explore all of energetically available phase space. Mechanisms for violating ergodicity are of great interest for probing non-equilibrium states of matter and protecting quantum coherence in complex systems. For decades, polyatomic molecules have served as an intriguing and challenging platform for probing ergodicity breaking in vibrational energy transport, particularly in the context of controlling chemical reactions. Here, we report[5] the observation of rotational ergodicity breaking in an unprecedentedly large, symmetric molecule, $^{12}C_{60}$. This is facilitated by the first observation of icosahedral rovibrational fine structure in any physical system, which was theoretically first predicted for $^{12}C_{60}$ almost 4 decades ago but remained experimentally unobserved. The ergodicity breaking exhibits several surprising features: 1) there are multiple transitions between ergodic and non-ergodic regimes as the total angular momentum is increased, and 2) they occur well below the traditional vibrational ergodicity threshold (2). These peculiar dynamics result from the interplay of the molecules' unique combination of symmetry, size, and rigidity, highlighting the potential of fullerenes to discover emergent phenomena in mesoscopic quantum systems.

D. Novel laser ablation and buffer gas cooling methods in C_{60}: Spectroscopic observation of full contrast icosahedral Bose-Einstein statistics

We have recently developed a novel laser desorption vapor source with liquid N_2 buffer gas cooling to produce a cold sample of gas phase C_{60}. This allows us to measure the R branch rotational progression of $^{12}C_{60}$ from $J = 0$- 250 and beyond using cavity- enhanced high-resolution spectroscopy on the 8.4 μm rovibrational band, unambiguously demonstrating for the first time the remarkable intensity alternations (e.g. complete absence of J = 1, 2, 3, 4 5 states) predicted by ^{12}C (I=1/2) nuclear spin statistics for such a high symmetry species (I_h).[6] We characterize the rotational temperature of laser desorbed C_{60} and find that it reaches below 100 K using both Ar and He buffer gas cooling. Rotational and Doppler thermometry indicate that rotational and translational degrees of freedom are fully thermalized. We also observe large signal from cold C_{60} with He, indicating that in spite of the enormous mismatch in masses, small He-C_{60} rotational quenching cross section, and highly non thermal optical excitation by 532 nm photons, He buffer gas is able to efficiently cool all vibrational, rotational, and translational degrees of freedom in laser desorbed C_{60}. Our laser desorption and buffer gas cooling approach offers several unique features to enable high sensitivity molecular spectroscopy: 1) three orders of magnitude reduction in heat load on the cryogenic buffer gas cell compared to traditional oven sources; 2) stable pulse-to-pulse desorption yields, varying by less than 10%, due to the uniformity of the deposited C_{60} film thickness; 3) long duration (200 ms), low power (2 W) vs. > 10^6 W peak powers required with traditional ns pulsed lasers; 4) efficient collisional cooling by He; and 5) controllable, transient (3 0 ms response time) C_{60} yield, enabling rapid

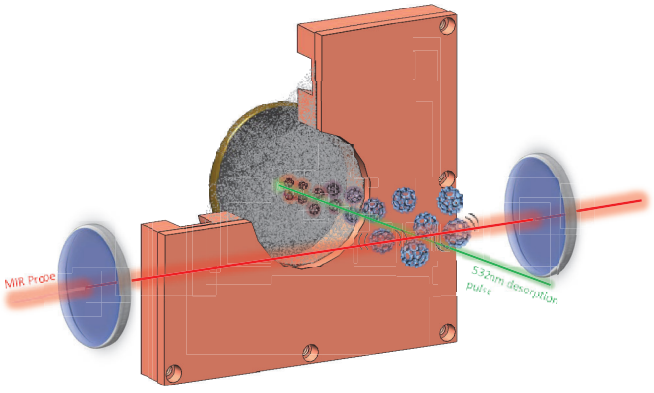

subtraction of probe light intensity fluctuations from absorption signal. This technique paves the way to cooling C_{60} and other large gas phase fullerene molecules (e.g. C_{70}, $^{13}C_{60}$) to even lower cryogenic (< 20K) temperatures, promising further advances in spectral resolution and sensitivity.

Papers published indicating DOE support (2022-2024)

1 K. D. Doney, A. Kortyna, Y.-C. Chan, and D. J. Nesbitt, "Formation and detection of metastable formic acid in a supersonic expansion: High resolution infrared spectroscopy of the jet-cooled *cis*-HCOOH conformer", J. Chem. Phys. **156**, 204309 (2022).

2 Y. C. Chan and D. J. Nesbitt, "High-resolution rovibrational spectroscopy of trans-formic acid in the ν_1 OH stretching fundamental: Dark state coupling and evidence for charge delocalization dynamics", J. Mol. Spec. **392**, (2023).

3 Y. C. Chan and D. J. Nesbitt, "High-resolution infrared spectroscopy of jet cooled cyclobutyl in the α-CH stretch region: Large-amplitude puckering dynamics in a 4-membered ring radical", Phys. Chem. Chem. Phys. (2024).

4 L. R. Liu, P. B. Changala, M. Weichman, Q. Liang, J. Toscano, S. Kotochigova, D. J. Nesbitt, and J. Ye, "Collision-induced C_{60} rovibrational relaxation probed by state-resolved nonlinear spectroscopy", Physical Review X Quantum. **3**, (2022).

5 L. R. Liu, D. Rosenberg, P. B. Changala, P. J. D. Crowley, D. J. Nesbitt, N. Y. Yao, T. V. Tscherbul, and J. Ye, "Ergodicity breaking in rapidly rotating C_{60} fullerenes", Science. **381**, 778 (2023).

6 Y. C. Chan, L. R. Liu, A. Scheck, D. J. Nesbitt, J. Ye, and D. Rosenberg, "Observation of full contrast icosahedral bose-Einstein statistics in laser desorbed, buffer gas cooled C_{60}", Physical Review Letters. (2024, in review).

An Ultracold Playground for Controlled Atom-Molecule Chemistry

Kang-Kuen Ni
Department of Chemistry and Chemical Biology, Harvard University
12 Oxford St., Cambridge, MA 02138
ni@chemistry.harvard.edu

Research Scope:
Combining the exquisite control over the state of certain molecules at ultralow temperatures (T $<$ 1 μK) via atomic, molecular, optical (AMO) physics tools and state-specific detection via physical chemistry tools recently have facilitated exploration of bimolecular reaction with unprecedented details. The specific model system under study has been the molecule-molecule reaction of KRb+KRb, where full product state distribution have been mapped and reaction intermediate lives for sufficiently long times (360 ns) have been probed. The state-to-state dynamics follows closely a statistical description due to the presence of the long-lived complex, but the detailed experimental scrutiny also reveals deviations that would require new calculations to explain, which are beyond the current state-of-the-art.

These studies have proven foundational to our understanding of chemistry in this temperature regime and allow us, on the one hand, begin to ask qualitatively new questions concerning the roles of phase, coherence, and entanglement despite the existence of a long-lived complex. On the other hand, we seek to explore the seemly more theoretically tractable atom-molecule Rb + KRb reaction, which is endothermic. Surprisingly, we observed an exceedingly long-lived KRb_2^* collisional complexes, with our experimentally measured complex lifetime ($\sim$ 400 μs) deviating from conventional theoretical calculations by *five orders* of magnitude. This discrepancy has motivated many explorations of possible underlying causes, though no model yet captures this phenomenon completely.

The focus of this work will be to understand and control Rb+KRb atom-molecule reactions and interactions. An aim is to dig into the origin of the long-lived KRb_2^* complex lifetime and develop means to control the outcome of the reaction complex. On this front, we will systematically vary the initial reactant states of both Rb and KRb as well as vary the external magnetic and electric fields to study the corresponding complex lifetimes. This work is on-going and we hope to report the fuller picture next year. A second aim is to explore qualitatively new features that did not exist in the ($^1\Sigma$)molecule-($^1\Sigma$)molecule reaction, namely the role of nuclear spin and its coupling to other degrees of freedom in collisions and a conical intersection that is accessible at the collisional energy. Because the atom in the Rb+KRb system has an electronic spin, it can couple to the nuclear spins of the system effectively and lead to different consequences, such as hyperfine-to-rotation energy transfer, which we report here. Considering the role of hyperfine spin coupling in the complex may be an important clue to solving the long-lived KRb_2* puzzle. A third aim is to explore the KRb+Rb* system where Rb atoms are excited to a Rydberg state. This system can give rise to rich phenomena including resonant energy transfer, (which is interesting on its own but can

also be leveraged for molecular qubit detection), ultra long-range Rydberg molecule formation, and ion-neutral reactions.

Recent Progress:
At sub-microkelvin temperatures, the chemical reaction between Rb and KRb is energetically forbidden (Fig. 1a), though the loss-rate of molecules is increased dramatically when atoms are introduced. In our previous work (Ref. [2]), we investigated the origin of this loss of the KRb $(v=0, N=0)$ + Rb $|F_a, M_{F_a}\rangle = |1,1\rangle$ system by directly observing the collisional complex KRb_2* and found the complex lifetime to be $\sim 400\ \mu$s, which is 5 orders of magnitude too long compared to theoretical RRKM estimates treating spins as "spectators".

Because sufficiently strong spin-dependent interactions can couple electron and nuclear spins to molecular rotations at short range, spins can dramatically increase the density of states of ultracold collision complexes and hence their RRKM lifetimes, potentially explaining the large discrepancy. We therefore designed an experiment to probe such spin-dependent hyperfine interactions and made state-to-state measurements of collisional processes specifically mediated by spin-dependent interactions. On the theory side, enormous rotational and spin basis sets have prevented rigorous atom-molecule quantum scattering calculations. In order to understanding these experimental results, theoretical collaborators continue to push the frontier of calculations. Our combined experimental and theoretical result is written up in Ref. [5].

Specifically, we directly probed the spin-dependent interactions in Rb + KRb collisions by activating the spin degree of freedom with the Rb atom prepared in an excited hyperfine state $|F_a, M_{F_a}\rangle = |2,2\rangle$ (Fig. 1b). Our collaborators calculated the underlying potential energy surfaces (Michal Tomza, University of Warsaw) and developed the formalism for rigorous quantum scattering calculations to model these collisions (Timur Tscherbul, University of Nevada, Reno). As

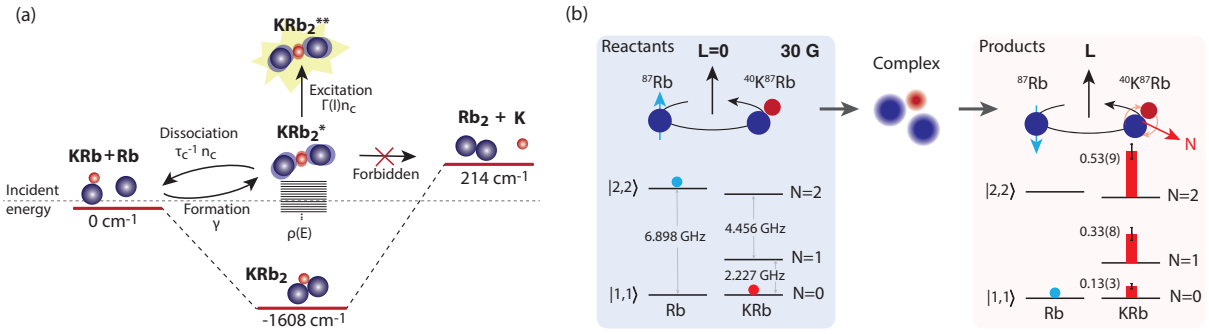

Figure 1: (a)Illustration of the KRb + Rb collision dynamics. The incident energy of one free electronic ground state Rb atom and one free KRb molecule in its rovibronic ground state is defined as the zero of energy. (b) Observations from the reaction of KRb + Rb in the $|2,2\rangle$ state. (left) Energy level diagram for the reaction as well as that for the lower-lying $|1,1\rangle$ state outlining the opening of rotationally-excited KRb (N = 0-2) channels. (right) Commensurate with this is the observation of rotationally excited KRb and de-excited Rb atoms. Measured branching ratio of rotationally-excited KRb.

the KRb + Rb $\rightarrow$ K + Rb_2 reaction is endothermic, only inelastic collision outcomes are allowed at ultracold temperatures. We directly measured the final states of the atoms and the molecules via REMPI detection, finding the excitation of molecules to all energetically allowed rotational levels ($N = 0, 1, 2$) commensurate with a relaxation of the atoms to their ground hyperfine states. This observation confirms the coupling between spin and mechanical rotation in the KRb_2 complex. To our knowledge, this is the first example of hyperfine-to-rotation energy transfer from one collisional partner to the next.

Furthermore, we quantified the branching ratio of the outcomes of the inelastic collisions with careful calibrations and found the product KRb rotational states $N = 2, 1$ and 0 to be $0.53(9) : 0.33(8) : 0.13(3)$. At a first glance, this looks statistical because of the number of m_N sub-levels are 5 : 3 : 1. However, this is only the case if all degrees of freedom are mixed, in particular, the nuclear spin is coupled strongly to the mechanical angular momentum of the system such that the mechanical angular momentum alone is no longer conserved. If such mixing does not take place, then the expected statistical outcome should have been 1 : 1 : 1 among the rotation states. From the *ab initio* calculated strengths of the short-range physical interactions by Tomza, we found that the interactions are a few orders of magnitude too weak to explain the breaking of the mechanical angular momentum conservation.

Putting the statistical picture aside, our collaborator Tscherbul made a heroic effort to develop new codes and approaches to the atom-molecule coupled-channel scattering calculations taking into account of spins and rotations. In order to converge the calculation, he included only the ground electronic potential and made the assumption of molecules as rigid rotors. Under these assumptions, his calculation again showed a major departure of the experimental observed branching ratio.

In electronic structure calculations by Tomza, we identified a conical intersection, which is energetically accessible and could play an important role in the collision dynamics. We note that fully converged scattering calculations including vibrational modes and CIs is beyond the current state-of-the-art. This joint experimental and theoretical efforts manifest the complexity of atom-molecule dynamics. We will continue to collaborate to provide necessary experimental benchmarks for more advanced theoretical and computational tools to study quantum scattering.

Returning to the puzzle of the previously measured exceptionally long lifetime of ground-state Rb-KRb complex (Ref. [2]), we now know one key ingredient, hyperfine spin coupling, that we have to take into account. This again will require a close experimental and theory collaboration.

Future Plans:
On the experimental side, we have also explored the impact on the complex lifetime of the m_F level within the $F = 1$ manifold. Here, the rotationally-excited exit channels are closed and we observed long-lived complexes. The m_F levels are split by 0.7 MHz/G, allowing us to explore the role of both the atomic state and energy by preparing atoms in various m_F levels and at different magnetic fields. Under constant magnetic field, we find that the complex lifetime drops by a factor of two when the Rb atoms are promoted from their ground $|1,1\rangle$ state, but is otherwise independent of the m_F level or the nuclear hyperfine level of KRb, see Figure 2(a). Importantly, however, we find

that when the magnetic field is varied, the complex lifetime can be continuously varied by a factor of five, with the lifetime saturating at higher fields, Figure 2(b). There also seems to be a critical electric field that contribute to the magnetic field dependence, Figure 2(c). A theoretical frame work that properly counting the increased density of states for the complex due to hyperfine spin coupling as well as the number of accessible open channels for the RRKM estimates, while also matching all the experimental data will be needed. We hope we can crack this puzzle soon, which is a goal for the next funding period.

Separately, we have implemented the necessary technical upgrades to excite Rb atoms to Rydberg states and to explore resonant energy transfer between Rydberg atoms and molecules. We hope to report on this soon.

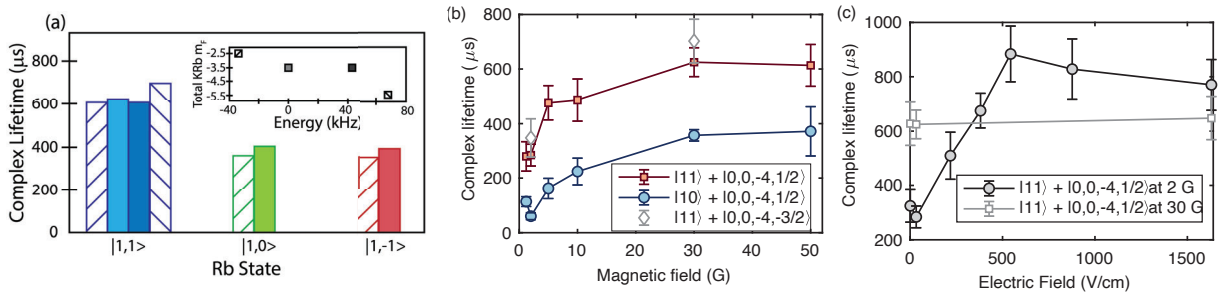

Figure 2: KRb_2^* Complex lifetime measurements (preliminary). (a) Measured complex lifetime as a function of Rb state, $|F, m_F\rangle$, and molecular nuclear hyperfine state, $|m_I^K, m_I^{Rb}\rangle$. Inset: KRb hyperfine level spacing. (b) Complex lifetime as a function of magnetic field for various Rb $|F, m_F\rangle$ + KRb $|-4, 1/2\rangle$ state-pair combinations. (c) Complex lifetime as a function of an applied electric field.

References to publications of DOE sponsored research 2022-2024:

1. Y. Liu, K.-K. Ni. Bimolecular chemistry in the ultracold regime. *Annu. Rev. Phys. Chem.*, 73:73-96, 2022.

2. M. A. Nichols, Y.-X. Liu, L. Zhu, M.-G. Hu, Y. Liu, and K.-K. Ni. Detection of long-lived complexes in ultracold atom-molecule collisions. *Phys. Rev. X*, 12, 011029, 2022.

3. J. Luke, L. Zhu, Y.-X. Liu, K.-K. Ni. Reaction Interferometry with Ultracold Molecules. *Faraday Discussions*, 251, 63 - 75, 2024

4. Y.-X. Liu*, L. Zhu*, J. Luke, J. J. A. Houwman, M. C. Babin, M.-G. Hu, K.-K. Ni. Quantum interference in atom-exchange reactions. *Science* 384, 1117, 2024

5. Y.-X. Liu*, L. Zhu*, J. Luke, M. C. Babin, T. V. Tscherbul, M. Gronowski, H. Ladjimi, M. Tomza, J. L. Bohn, K.-K. Ni. Hyperfine-to-rotational energy transfer in ultracold atom-molecule collisions, arXiv:2407.08891 (2024, under review)

Structure-Specific Radical Reactions at Model Catalytic Surfaces

G. Barratt Park (Principal Investigator)
Department of Chemistry and Biochemistry, Texas Tech University
Box 41061, Lubbock, TX 79409-1061
barratt.park@ttu.edu

Program Scope

The ability to efficiently convert natural gas to higher hydrocarbons is an urgently needed advance for the global environment and economy. The increasing and permanent scarcity of liquid petrochemical sources is leading to an inevitable reliance on natural gas sources for energy and as a feedstock for the industrial production of valuable chemicals. The primary component of natural gas, methane (CH_4), is the most abundant hydrocarbon in the earth's crust. Because methane is remarkably stable, advanced catalytic methods are required to activate methane's C–H bond in order to oxidize the molecule and convert it to higher hydrocarbons containing C–C bonds. This project aims to build a fundamental, microscopic understanding of the mechanism for key processes related to heterogeneous catalysis (i.e. chemistry that is catalyzed at gas-surface interfaces) for the conversion of single-carbon molecules to more valuable products.

One such class of reactions would provide revolutionary routes to efficient direct conversion of CH_4 to liquid fuels via oxidative coupling processes, thereby bypassing steam reforming, and saving tremendous amounts of energy. The resulting energetic bounty will necessarily have profound transformative global geopolitical and environmental consequences, for the betterment of humanity. It is increasingly clear that in order to make oxidative coupling of CH_4 (OCM) industrially viable, fundamental quantitative knowledge of elementary surface-site-specific reaction kinetics and dynamics is needed for designing better catalysts able to efficiently activate the C-H bond on one hand, while suppressing formation of undesired CO and CO_2 products on the other.

Another potential route to bypass steam reforming is the partial oxidation of methane to methanol, which can be followed by partial oxidation reactions that produce valuable and convenient products such as formaldehyde. A detailed understanding of such reactions will serve as a second target of the proposed research.

The ability of catalytic surfaces to achieve these transformations results from their remarkable ability to break bonds and stabilize the formation of reactive radical species. A major goal of the proposed work is to build a detailed understanding of how reactive radicals interact with surfaces and undergo reactions at high temperatures relevant to industrial processes. This approach has the potential to provide the first quantitatively accurate rate data for the formation and consumption of surface radical species under industrially relevant high-temperature conditions. The proposed research will systematically address challenges in heterogeneous catalysis with quantitative surface-site-specific approaches, offering universality and transferability. The results will provide first-principles understanding that can guide catalyst design beyond the trial-and-error "cook and look" based approaches employed today, and will serve as valuable benchmarks for theoretical treatment of surface reactions, a sorely needed component for 21st century advances. The ability to guide both further theoretical and practical progress in catalysis will have a wide global impact.

Recent Progress

This is a newly funded project. It is based on recent progress in the area of Velocity-Resolved Kinetics,[1] a technique for studying the kinetics and dynamics of surface reactions that was developed during the PI's post-doc. The approach combines surface science with gas-phase molecular beam techniques and ion-imaging based detection. The PI recently used this technique

for a detailed study on the kinetic energy, angular, and internal state distribution of the products of N_2O decomposition on Pd(110).[2] The results indicated two reaction channels, one giving rise to "thermal" N_2 product channel consistent with thermal desorption of N_2 from the surface and a second "hyperthermal" N_2 product channel that involved the direct release of N_2 from its transition state into the gas phase. (See Figure 1.) The hyperthermal channel featured a highly oriented angular distribution and a large amount of rotational excitation, but no vibrational excitation. Comparison of the results with *ab initio* calculations performed in collaboration with Hua Guo's group led to a detailed understanding of the reaction's transition state and post-transition state dynamics.

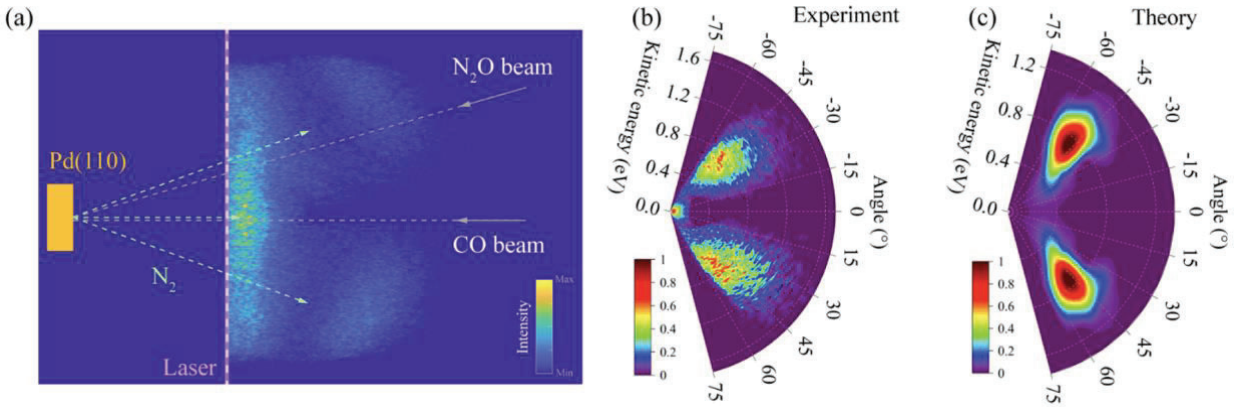

Figure 1. The decomposition of N_2O on a Pd(110) surface at T_{surf} = 550 K gives rise to a bimodal N_2 product distribution. (a) Slice ion image of the N_2 products in the selected quantum state J = 10 (v = 0). The laser position is indicated by a purple dashed line. The velocity vectors of incident N_2O and CO beams used in the study are labeled by gray arrows. The velocity vectors of N_2 products are shown in green arrows. The "thermal" channel appears close to the laser with a broad angular distribution. A "hyperthermal" channel appears at two locations far from the laser and centered at angles of approximately ±40° from the surface normal in the plane containing the [001] axis. (b) The experimentally derived kinetic energy and angular distribution of N_2 product derived from the ion image. (c) Kinetic energy and angular distributions obtained from theoretical trajectory simulations on a newly constructed potential energy surface. This figure is reproduced with permission from Ref. 2. More details are available in the reference.

Future Plans

The proposed work addresses two broad questions related to the special role of radicals in heterogeneously catalyzed chemistry. In most cases, radicals are believed to be formed and consumed on the surface in Langmuir-Hinshelwood processes. The chemical mechanisms for such processes have been studied in detail using traditional UHV surface science methodology based on temperature programmed reaction. Such studies require very low surface temperatures, typically far below the temperature at which industrial processes are performed. Reaction kinetics can be extracted from temperature programmed measurements, but the absolute determination of rate constants is crude at best. Studies performed at higher temperatures and under *operando* conditions are often capable of obtaining mechanistic insights through surface-sensitive spectroscopies, but are almost never capable of quantitative measurements of the rates of formation and depletion of reactive surface intermediates. The first objective is to apply newly developed techniques to measure highly accurate kinetics of reactions involving surface-bound radical intermediates at industrially-relevant temperatures. We will apply the Velocity-Resolved Kinetics (VRK) method. This technique will be coupled with Laser-Induced Desorption (LID) to probe the time-dependent kinetic traces of surface-bound radical intermediates. A primary focus

will be the partial oxidation of methanol to formaldehyde on model Ag and Cu catalyst surfaces. This is an industrial process that is performed on a large scale with Ag- and Cu-based catalysts, and whose importance is increasing due to rising global demand for C_1 chemistries that produce formaldehyde.

A second broad question deals with the potential role of surfaces in generating reactive *gas-phase* radical species. Under the high temperature conditions employed in many industrial reactors, it is possible for a catalytic surface to activate a reactant species, generating a reactive radical that is subsequently released into the gas phase, initiating homogeneous chemistry above the surface. Such a mechanism is known to play a central role in the oxidative coupling of methane above metal oxide catalysts and is likely important in the direct conversion of methane to methanol. Novel techniques that analyze the composition of the gas phase directly above the surface have detected gas-phase radicals that desorb during the partial oxidation of methanol to formaldehyde,[3] a process for which gas-phase radical reactions had never before been observed or considered, raising questions about how prevalent gas-phase radical reactions might be during high-temperature heterogeneous catalysis. Almost no detailed UHV surface science studies have investigated the mechanisms for desorption of reactive polyatomic radicals from catalytic surfaces. The second objective of this proposal is to investigate the interaction potentials of radicals with surfaces and how these influence the mechanism for the desorption of radicals from surfaces. Detailed experiments will investigate the scattering of methane radicals from OCM catalysts to probe the interaction potentials that governs the release of these radicals into the gas phase. Sticking coefficients of methyl radicals to these catalysts will be measured for a range of surface morphologies and oxidation states. Such experiments will provide information about the desorption mechanisms by means of microscopic reversibility and detailed balance arguments. Finally, desorption of surface-bound radicals will be probed over catalysts for partial oxidation of methanol to formaldehyde under high-temperature UHV conditions. These experiments will indicate whether high temperatures alone are sufficient to give rise to radical desorption or whether "pressure gap" effects play a deciding role. If radical desorption is observed in our experiments, it will provide a way forward for UHV surface science experiments to investigate cooperativity between surface and gas-phase radical chemistry in heterogeneously catalyzed processes.

References (from work prior to DOE award)

1. G. B. Park, T. N. Kitsopoulos, D. Borodin, K. Golibrzuch, J. Neugebohren, D. J. Auerbach, C. T. Campbell, A. M. Wodtke, "The kinetics of elementary thermal reactions in heterogeneous catalysis" *Nature Reviews Chemistry* **3**, 723-732 (2019), https://doi.org/10.1038/s41570-019-0138-7.
2. J. Quan, R. Yin, Z. Zhao, X. Yang, A. Kandratsenka, D. J. Auerbach, A. M. Wodtke, H. Guo, G. B. Park, "Highly Rotationally Excited N_2 Reveals Transition-State Character in the Thermal Decomposition of N_2O on Pd(110)" *J. Am. Chem. Soc.* **145**, 12044-12050 (2023), https://doi.org/10.1021/jacs.3c01127.
3. B. Zhou, E. Huang, R. Almeida, S. Gurses, A. Ungar, J. Zetterberg, A. Kulkarni, C. X. Kronawitter, D. L. Osborn, N. Hansen, J. H. Frank, "Near-Surface Imaging of the Multicomponent Gas Phase above a Silver Catalyst during Partial Oxidation of Methanol" *ACS Catalysis* **11**, 155-168 (2021), https://doi.org/10.1021/acscatal.0c04396.

Mechanistic Understanding of the Criegee Intermediates Reaction Networks in Atmospheric and Combustion Systems

Denisia M. Popolan-Vaida
Department of Chemistry, University of Central Florida, Orlando, FL 32816
denisia.popolan-vaida@ucf.edu

Program Scope

The reaction networks that describe the complex chemical processes involved in atmospheric and combustion systems are typically dominated by reactive intermediates that usually occur in small concentrations. Identification and quantification of these reactive species within complex reactive mixtures are key for the development of a fundamental, chemically accurate description of complex atmospheric and combustion systems. The objective of this program is to generate new mechanistic understanding of the reaction network of Criegee intermediates (CIs), which are important species formed during the ozonolysis of unsaturated organic compounds. CIs have the unique capability to add both carbon and oxygen mass to the co-reactant through either 1,3-dipolar cycloaddition or insertion mechanisms that can lead to the production of high-molecular-weight, low-volatility products, which have been linked to the formation of secondary organic aerosols (SOA), in just a few reaction steps. Therefore, this research also focuses on understanding the pathways by which CIs can drive the formation of high-molecular-weight, low-volatility SOA precursors, and eventually detect and identify the size and composition of SOA. To assess the competition between collisional stabilization and unimolecular reaction of the energy-rich CIs, the ozone-assisted oxidation reaction of selected acyclic and endocyclic unsaturated organic compounds is investigated as a function of unsaturated organic compound structure, functionality, carbon number, and reactive environment. The key questions this research program aims to answer are: (1) How does the mechanism of ozone-assisted oxidation change as a function of unsaturated organic compound carbon-number, functionality, and structure? (2) Is there a specific carbon-number that corresponds to a crossover between the radical production and secondary ozonide (SOZ) stabilization in the case of endocyclic compounds? (3) What is the role of CIs in gas-particle interconversion? and (4) Does high carbon-number facilitate the formation of organic particles.

Recent Progress

The reaction networks of Criegee intermediates formed in the ozonolysis on 1-butene, *trans*-2-pentene, cyclopentene, *trans*-2-hexene, and cyclohexene were investigated in an atmospheric pressure jet stirred reactor (JSR) to understand the effect of CIs carbon number and reactive environment on the products distribution and the formation of high-molecular-weight, low-volatility compounds. Molecular beam high-resolution mass spectrometry and tunable synchrotron single-photon ionization in conjunction with *ab initio* threshold energy calculation performed in

the group of Dr. Ahren Jasper were employed for the detection and identification of gas-phase reactive intermediates and final products. Temperature-dependent analysis employing DART ionization-Orbitrap mass spectrometry was used to facilitate the detection of high-molecular-weight, low-volatility reaction products.

Reaction networks of formaldehyde oxide and propanal oxide CIs formed in the ozone-assisted oxidation reaction of 1-butene: The reaction networks of two CIs intermediates of different carbon number, i.e., formaldehyde oxide (CH_2OO) and propanal oxide (CH_3CH_2CHOO), formed in the ozone-assisted oxidation of 1-butene were investigated in a range of conditions, such as temperature (300 K – 800 K), residence time (1 s - 3 s), equivalence ratios (0.5 - 1.2), and 1-butene concentration (0.5% - 3%) at a fixed ozone concentration of 1000 ppm. The mass spectra recorded at temperatures below 500 K were characterized by the presence of products characteristic to both 1-butene ozonolysis reactions and low-temperature oxidation reactions. Both CIs were observed to undergo rich chemistry with the co-products formed in the ozone-assisted reaction of 1-butene. For instance, products corresponding to the reactions of both CH_2OO and CH_3CH_2CHOO with species such as water, ketene, ethene, propene, 1-butene, formaldehyde, acetaldehyde, methanol, ethanol, acetone, and formic acid were detected and identified based on the measured ionization thresholds and calculated adiabatic ionization energies.

Measurements performed using DART-Orbitrap mass spectrometry at different DART temperatures revealed the formation of high-molecular-weight, low-volatility compounds. Interestingly, the signature of two different molecular growth channels have been identified corresponding to (i) CIs oligomerization products, marked by an increase in both oxygen and carbon numbers and (ii) highly oxygenated organic compounds (HOM), marked by an increase only in the oxygen number. The CIs oligomerization products observed in our experiments were exclusively due to sequential addition of CH_2OO CIs, and no clear evidence of products corresponding to CH_3CH_2CHOO oligomerization were observed. Sequential addition of CH_2OO was observed to species like ethene, 1-butene, formaldehyde, acetaldehyde, and formic acid. The sequential addition of up to six CH_2OO CIs have been observed for the reaction with ethene. In addition, products indicative of CH_2OO self-reactions that involve up to six CIs ($C_6H_{12}O_{12}$) were detected. Experiments are currently in progress to get more insights into the chemical identity of the high-molecular-weight, low volatility compounds using collision-induced dissociation mass spectrometry. HOMs such as $C_4H_6O_n$ and $C_4H_8O_n$ (n = 5-8) were also detected in our experiments. These products might originate from the autoxidation pathways via peroxy radical channels. Detection of species like methanol, ethanol, ketene, and hydroperoxide like methyl hydroperoxide and ethyl hydroperoxide confirms the existence of multiple oxidation channels. This work provides additional evidence that CIs are key intermediates in the formation of oligomeric species via the formation of hydroperoxides.

Reaction networks of CIs formed in the ozone-assisted oxidation reaction of C5 and C6 acyclic and endocyclic alkenes: To understand the effect of alkene structure and carbon number, as well as the role of the reactive environment on the CIs reaction networks, the ozone-assisted oxidation

reaction of C5 and C6 acyclic and endocyclic alkenes, i.e., *trans*-2-pentene, *trans*-2-hexene, cyclopentene, and cyclohexene, were investigated under various conditions. The ozonolysis of both *trans*-2-pentene and *trans*-2-hexene, leads to the formation of primary ozonides that subsequently undergo unimolecular decomposition to form a C2 (CH_3CHOO, aldehyde oxide) CI and a longer chain CI, such as C3 (CH_3CH_2CHOO, propanal oxide) and C4 ($CH_3CH_2CH_2CHOO$, butanal oxide), respectively. These investigations focused on understanding the chemical behavior of CH_3CHOO when produced in different reactive environments that include the presence of another longer chain Criegee intermediate. Products corresponding to both unimolecular and bimolecular reactions of all CIs have been observed under our experimental conditions. Bimolecular reactions with co-products like aldehydes, alkenes, and carboxylic acids were observed that lead to the formation of a variety of hydroperoxides.

Because the carbonyl and CI are bound together in a ring, the primary ozonides formed in the ozone-assisted oxidation of *trans*-2-pentene and *trans*-2-hexene cannot decompose into two distinct molecules and instead undergoes ring-opening to form long-chain CIs, i.e., glutaraldehyde oxide ($CHOCH_2CH_2CH_2CHOO$) and adipaldehyde oxide ($CHOCH_2CH_2CH_2CH_2CHOO$), respectively. This eliminates the significant complication of energy distribution between the bimolecular fragments inherent to acyclic alkenes, and it keeps the carbonyl group close to the CI. No products corresponding to $CHOCH_2CH_2CH_2CHOO$ and $CHOCH_2CH_2CH_2CH_2CHOO$ bimolecular reactions have been observed under our experimental conditions. Instead, the long chain CIs undergo unimolecular isomerization to vinyl hydroperoxides that rapidly dissociate into OH and acyl radicals. The formed acyl radicals can either add O_2 or decompose via CO splitting. Auto-oxidation of the acyl radical was observed to lead to the formation of HOMs with up to seven oxygen atoms, while the decomposition channel via CO splitting was observed to lead to the formation of smaller oxygenates and hydroperoxide species. Investigations are currently in progress to understand the chemical behavior of long chain CIs formed in the ozone-assisted oxidation of cyclohexene.

Future Plans

Structural differences between acyclic and endocyclic unsaturated organic compounds, as well as differences in carbon number and functionality, are expected to produce different high-energy intermediates and consequently different reaction kinetics. In addition, subtle changes around the C=C double bond of unsaturated compounds can have dramatic effect on OH formation yields. We hypothesize that, at a certain critical size (carbon number), the ozonolysis of acyclic and endocyclic alkenes is expected to switch from a pathway directed toward the preferential formation of OH radicals, to a secondary ozonide-directed pathway, presumably devoid of production of OH radicals, but potentially effective in SOA formation. To verify this hypothesis, future investigations will focus on understanding the impact of collisional stabilization of CIs induced by a progressive increase of the alkenes carbon number, on the CI reaction networks. A series of acyclic alkenes, such as trans-3-hexene, and trans-3-heptene as well as endocyclic alkenes, like 3,5-dymethylcyclopentene, 4,5-dimethylcyclohexene, cycloheptene, and 4,5-dymethylcycloheptene,

that have a common characteristic, i.e. only one C=C double bond, but different structures and carbon numbers will be investigated at different alkene concentrations. As the compound concentration is increased in the reaction mixture, radical-radical reactions will be enhanced. In particular, the reactions of the resonance-stabilized species will increase, which will be evident due to the formation of carbon-rich products. The ozone-assisted oxidation of unsaturated functionalize hydrocarbons, like acrolein, allyl alcohol, and crotyl alcohol, that lead to the formation of functionalized CIs will be also investigated to understand the changes that my occur in the reaction mechanism when CIs with different functionalities are present. Finally, by following the changes in the gas- and particle-phase mass spectra as a function of reagents concentration, we plan to correlate the formation of high-molecular-weight compounds with the onset of the organic particles.

Publications supported by this DOE project (2022-present)

- Alec C. DeCecco, Alan R. Conrad, Arden M. Floyd, Ahren W. Jasper, Nils Hansen, Philippe Dagaut, Nath-Eddy Moody, Denisia M. Popolan-Vaida, *"Tracking the reaction networks of acetaldehyde oxide and glyoxal oxide Criegee intermediates in the ozone-assisted oxidation reaction of crotonaldehyde"*, Phys. Chem. Chem. Phys., 2024, 26, 22319-22336.
- Arden M. Floyd, Alec C. DeCecco, Yitong Zhai, Ahren W. Jasper, Nils Hansen, Denisia M. Popolan-Vaida, "*Reaction networks of Criegee intermediates formed in the ozone-assisted oxidation of C5 acyclic and endocyclic alkenes*", submitted 2024.

Ultrafast Transient Absorption Spectroscopy of Hydrocarbon Radicals

Melanie Reber
Department of Chemistry, University of Georgia, Athens, GA 30602
mreber@uga.edu

Project Scope

We aim to complete an ultrafast cavity-enhanced transient absorption spectrometer and incorporate two sources of radicals in molecular beams and study the excited state dynamics of vinyl radical and allyl radical. The spectrometer consists of a home-built Ytterbium fiber laser frequency comb and Ytterbium fiber chirped-pulse amplification system that will generate ultrafast (about 100 fs pulse duration) pulses across much of the visible region. This light will be split into pump and probe beams and coupled into enhancement cavities housed in a vacuum chamber. Lock-in detection and noise subtraction techniques will be used during signal detection. With the increase in signal-to-noise with these techniques, it will be possible to perform ultrafast transient absorption spectroscopy in the visible and near-IR spectral regions of radical intermediates in molecular beams.

The overarching goal of this project is to study the excited state dynamics of vinyl, C_2H_3, and allyl, C_3H_5, radicals. The first excited state of allyl radical exhibits a broad absorption and is thought to connect to the ground state through several conical intersections. The upper state lifetime is less than 5 ps and excitation of this state results in the release of a hydrogen atom. Direct, time-resolved absorption spectroscopy could elucidate this mechanism. Similarly, the first excited state of vinyl radical has picosecond lifetimes, with a decrease in lifetimes with higher vibrational excitation. The frequency-resolved spectroscopy has the signature of ultrafast predissociation from the ground state. We hope to gain insight into these processes in vinyl radical with ultrafast transient absorption spectroscopy. This work will advance our knowledge of excited state processes in combustion intermediates and reactive species.

The first step of this project is to demonstrate the ability to take ultrafast transient absorption spectroscopy of the electronically excited states of radical intermediates. Specifically, there are three components of this goal. (i) The first part is to finish testing the new cavity-enhanced transient absorption spectrometer. (ii) The second part is to complete and test the differential pumping and vacuum system. (iii) The third part entails a proof-of-principle that we can study radicals with this spectrometer, which includes generating radicals with the Excimer laser in our new differential pumping setup.

Recent Progress

The new ultrafast, cavity-enhanced transient absorption spectrometer and molecular beam vacuum system was completed. In short, the spectrometer consists of a homebuilt Yb:fiber oscillator, which we recently published about[1], and a home-built chirped-pulse Yb;doped photonic crystal fiber amplifier. The light is split into pump and probe arms and frequency doubled to about 530 nm. The pump arm also has a third-harmonic generation capability to make about 355 nm. The probe is coupled into an enhancement cavity and locked using Pound-Drever-Hall locking techniques. Currently the pump is not in an enhancement cavity, although one is available to use in the future; it is modulated by a chopper for lock-in amplification. The cavity is

under vacuum pumped by a turbomolecular pump and enters a molecular beam region through slits. Molecular beam region is pumped by a Roots blower. The differential pumping system achieved almost three orders-of-magnitude pressure differential between the cavity region and molecular beam region with typical test molecular beam flows. The pump, probe, and excimer beams all cross at the molecular beam in this Roots blower region. The signal exits the probe enhancement cavity through the back of a cavity mirror and then goes to an auto-balanced detector along with a time-delayed reference beam for common-mode noise subtraction. Lockin amplification, and optionally, boxcar integration, are used to process the signal before recording it through a DAQ board on the computer.

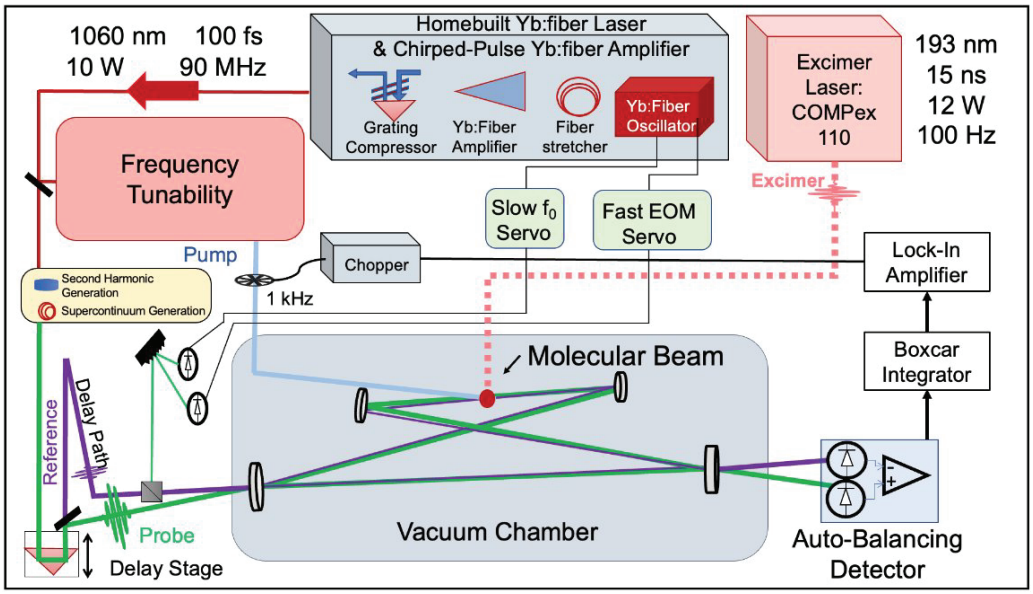

Figure 1: Minimalist schematic of the new ultrafast cavity-enhanced transient absorption spectrometer.

To test our newly-built cavity-enhanced transient absorption spectrometer, we started by looking at NO_2 as a stable test system that did not require the excimer to produce. After a day of taking data on NO_2 in November 2023, we had to pack everything into moving crates and put it into storage. It took about a month to pack everything into moving crates and load into storage.

In March 2024 we were able to start rebuilding and moving into the part of the lab that houses the laser tables. We are still unable to unpack about 1/3 of our equipment while we wait for our prep lab space to have casework, tables, and air conditioning. Nevertheless, we have been able to partially set back up the vacuum system as well as the Yb:fiber oscillator and some of the electronics. The vacuum system layout is very different and the laser lab is smaller, so there was a significant amount of redesign needed to set back up the vacuum system and excimer laser, including purchasing new components. Testing of the rebuilt vacuum system is underway.

Before the move we also investigated the feasibility of carrying out sum frequency generation between the ultrafast frequency comb laser and a continuous wave narrow-linewidth laser to create tunable, ultrafast frequency comb light at a range of frequencies [2]. With the influx of high- and moderate-power, narrow-linewidth, stable cw lasers at a variety of frequencies now commercially available for a moderate price, we wanted to investigate the

feasibility of using sum frequency generation (SFG) or difference frequency generation instead of an OPO/OPA system. Specifically, we used a Coherent Mephisto Nd:YAG laser as the narrow-linewidth cw laser and our amplified ultrafast comb laser and combined them in a BBO crystal in an autocorrelation geometry. The resulting SFG beam is an ultrafast frequency comb. Figure 2 shows the optical spectrum of the resulting SFG beam as well as the second harmonic (SHG) spectra of the cw YAG and ultrafast Yb:fiber laser. The RF spectrum of the SFG is also shown to illustrate that the beam is pulsed. It is also a frequency comb, just like the Yb:fiber laser. We were able to simulate the results using SNLO using the 2D-mix-SP program by approximating the cw laser as a long pulse. We then designed a mid-IR conversion system using SNLO and commercially available stable, narrow-linewidth solid-state lasers as an alternative to an OPO for ultrafast frequency comb generation and predict we could generate over 300 mW at 3.3μm.

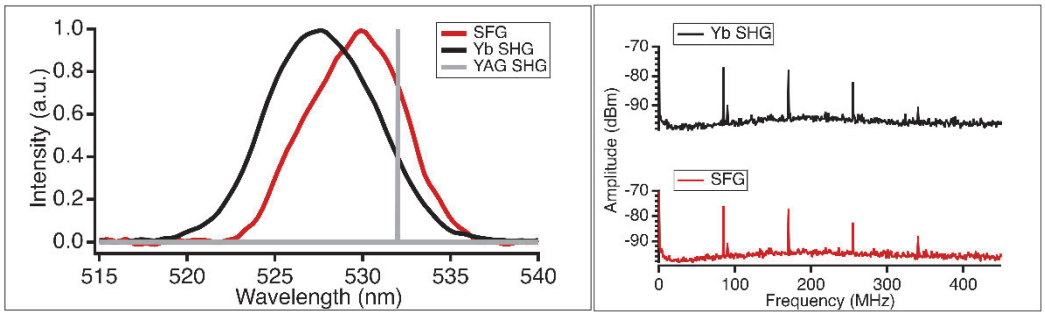

Figure 2: Optical spectra of mixed SFG and ultrafast SHG (experimental measurements), CW SHG (drawn) on a linear scale for clarity; b) RF spectra of mixed SFG and Yb:fiber SHG. The repetition rate of mixed SFG and Yb:fiber SHG is 85 MHz. 170 MHz, 255 MHz, and 340 MHz are harmonics of the repetition rate. The signal at 90.5 MHz is the local campus radio station. Widths are limited by the instrument bandwidth.

Future Plans

We are working to rebuild the vacuum chamber and pumping system. We also have to rebuild the chirped-pulse amplifier system and transient absorption spectrometer. We are still waiting to have full lab functionality, which will occur when UGA finishes the renovation of the other half of our lab space; there is currently no timeline for this that I am aware of. Once we have a working prep lab (electronics, test, machining, and building space), it will speed up our ability to rebuild the electronics and vacuum system. Also, the new pump room is adjacent to the laser lab and has no added sound dampening, instead of across a hall and surrounded by sound dampening as in our previous space, so we still need to test if there is enough sound and vibration damping to be able to run the roots blowers and our enhancement cavities.

Once the spectrometer and vacuum system is set back up, we will again be ready to study systems in molecular beams with the transient absorption spectrometer. We will go back to testing the spectrometer with a stable molecule, NO_2, with visible pump - visible probe and then azulene with UV pump - visible probe transient absorption spectroscopy as the final test of the spectrometer before making radicals.

The radicals will initially be generated through photolysis with an excimer laser, with a pyrolysis nozzle added eventually. Photolysis will be carried out with an Excimer laser, already set back up, that will be sent through the differential pumping slit and through the molecular beam. To incorporate photolysis into the ultrafast transient absorption spectrometer, a gated integration data acquisition program is being implemented and has been partially tested with simulated signals. The optics for coupling the excimer into the vacuum chamber and molecular beam have been designed and acquired and will be installed once the vacuum system is set back up. We will then start with studying the time-resolved excited state spectroscopy of vinyl and allyl radical. Experiments with a wide range of combustion radicals are planned for the future as well as increasing the spectral range of the spectrometer to include the infrared and mid-infrared region.

Publications

[2] Jie Zhan, Nicholas D. Cooper, and Melanie A. R. Reber, “Joint Experimental and Computational Characterization of Sum-frequency Generation between a Continuous Wave Laser and an Ultrafast Frequency Comb Laser for Tunable Laser Development”, Submitted 2024

[1] Nicholas D. Cooper, Uyen M. Ta, and Melanie A. R. Reber, "Spectral shaping of an ultrafast ytterbium fiber laser via a passive intracavity optical filter: a simple and reliable route to sub-45 fs pulses," Appl. Opt. 62, 2195-2199 (2023)

FUNCTIONAL GROUP EFFECTS ON UNIMOLECULAR QOOH REACTIONS AT HIGH PRESSURE USING HIGH-RESOLUTION ELECTRONIC ABSORPTION SPECTROSCOPY

Brandon Rotavera
College of Engineering | Department of Chemistry
University of Georgia
Athens, GA 30602

rotavera@uga.edu | (rotavera.uga.edu)

Program Scope

The primary goal of this research program is to produce new fundamental knowledge on connections between molecular structure of hydroperoxy-substituted carbon-centered radicals (ȮOOH) and selectivity towards specific unimolecular reaction pathways (**Figure 1**). This knowledge is derived in part from combustion experiments using a jet-stirred reactor that is employed to measure isomer-resolved species concentration profiles of multi-functional intermediates derived from ȮOOH formed via oxidation of the species in **Figure 2**. As a primary outcome, this research program expands gas-phase chemical kinetics knowledge on the effects of functional groups on chemical reactivity that is necessary to refine computational combustion models that support ongoing efforts to incorporate biofuels in current and future combustion systems. Additionally, owing to the complex combustion behavior of functionalized molecules, this program focuses on identifying new reaction pathways that are studied in greater detail using theoretical chemical kinetics computations, including potential energy surfaces and rate calculations. In addition, a primary focus of the program is to utilize experiments and chemical kinetics modeling to understand the effect of oxygen concentration on competing reactions of ȮOOH radicals formed from the species in **Figure 2**. In particular, experiments are conducted to examine product formation from unimolecular reactions versus from the second-O_2-addition step. The red-highlighted text in Figure 1 indicates the classes of species produced via the former reaction type, which involves constitutional isomers as well as stereoisomers and are important due to the connection to specific ȮOOH radicals that govern reactivity.

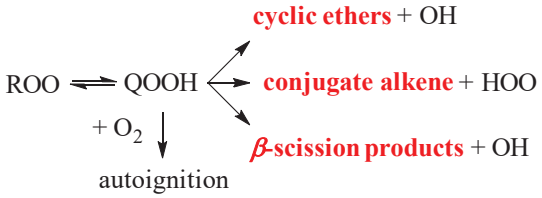

Figure 1. *Reaction mechanisms of ȮOOH radicals are central to understanding and developing modeling capabilities for hydrocarbon and biofuel oxidation. Accurately quantifying product formation from ȮOOH reflects the balance of chain-branching reactions (downward-pointing arrow) to chain-propagation and chain-inhibiting reactions (arrows pointing towards the right), each of which can produce an abundance of isomers.*

Direct measurements of such isomers, e.g. cyclic ethers, provide stringent benchmarks of ȮOOH chemistry and are therefore central to the development of robust chemical kinetics mechanisms. This program bridges knowledge gaps between molecular structure and ȮOOH reactivity for C4 and C5 molecules, namely the balance of unimolecular decomposition vs. bimolecular reaction with O_2.

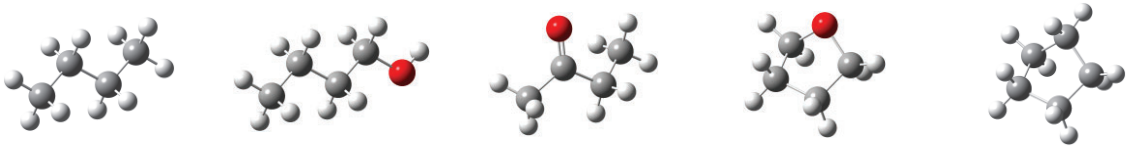

Figure 2. *Molecular structure of C4 species studied in this program (left to right): n-butane, 1-butanol, butanone, tetrahydrofuran, and cyclopentane.*

Recent Progress

Speciation experiments in a jet-stirred reactor: The jet-stirred reactor (JSR) at the University of Georgia is capable of experiments at pressures up to 50 atm and operates with a well-characterized temperature profile. Particular attention is paid to quantifying uncertainty in spatial temperature as well as in species concentration in the sampling region. Complete temperature characterization was accomplished using a systematic series of experiments conducted at residence times up to 4000 ms over a range of temperatures controlled independently in two distinct heating regions of the JSR, the reactor region and the pre-heating region. In all cases, owing to a custom-built, woven Inconel and ceramic insulation heating system, 1σ deviations in temperature are <1% of the nominal temperature (up to 1000 K) over a 3-cm sampling distance. Species quantification is accomplished with an uncertainty of ~10% in all cases and is achieved via tandem gas chromatography measurements via two independent detection methods (Figure 3). The first uses electron-impact (EI) mass spectrometry (Figure 3a). The second uses vacuum ultraviolet absorption spectroscopy (Figure 3b). The unique aspect of the tandem approach is that for each retention time, two molecular signatures are produced, an EI mass spectrum and an absorption spectrum measured from 5.167 – 9.920 eV, which enables resolution of both constitutional isomers and stereoisomers. An example of the latter is shown in **Figure 3** and is important due to stereochemical-dependent reaction chemistry [1-3].

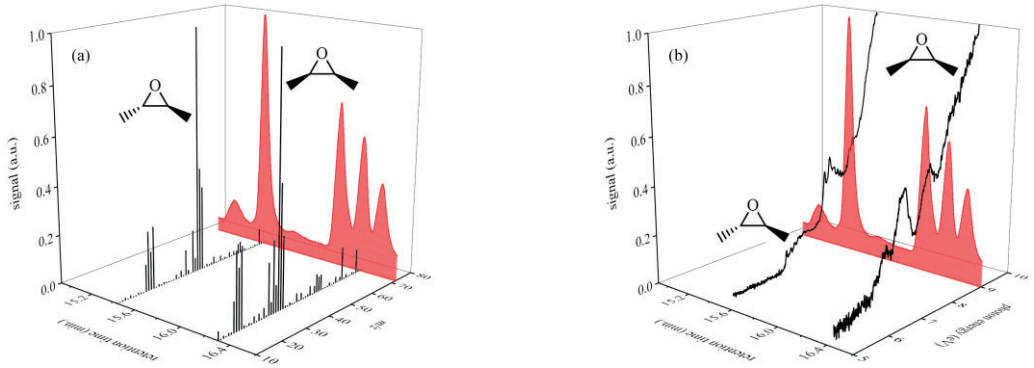

Figure 3. *EI mass spectra (a) and VUV absorption spectra (b) of 2,3-dimethyloxirane isomers.*

To examine the influence of temperature and oxygen concentration on intermediates from cyclopentane, similar to publications on *n*-butane [4], tetrahydrofuran [5], and tetrahydropyran [6], isomer-resolved speciation measurements were conducted at 835 Torr in a jet-stirred reactor (JSR) from 500 – 1000 K in Hill et al. [7]. **Figure 4** shows representative experimental results for the type of competing chemical pathways probed. The main objective of these experiments is to provide specific, quantitative targets for modeling ȮOOH-mediated chemistry over a range of oxygen concentration to interrogate the chemistry depicted in Figure 1, particularly species that are connected to the competition between ring-opening of cyclopentyl and reaction with O_2 (forming cyclopentyl peroxy). Similar experiments were conducted for diethyl ether and butanone.

Detailed sub-mechanisms of consumption reactions for 1,2-epoxycyclopentane (and for cyclopentane) were created using Reaction Mechanism Generator (RMG) and then integrated into the cyclopentane mechanism of Lokachari et al. [8]. The sub-mechanisms included all possible carbon-centered radicals for the first time. The purpose of the integration was to model the effect on reducing mechanism truncation error by including an expanded set of elementary reactions for subsets of intermediates connected to reactions of $\dot{R} + O_2$ and of ȮOOH. The degree to which model predictions of [O_2]-dependent species profiles were affected (**Figure 4b**) was significant and underscored the deficiencies in modeling several reaction types including the competition between cyclopentyl → products, cyclopentyl + O_2 → products, formally direct pathways, and site-specific rate coefficients for ȮH-initiated H-abstraction from the two intermediates.

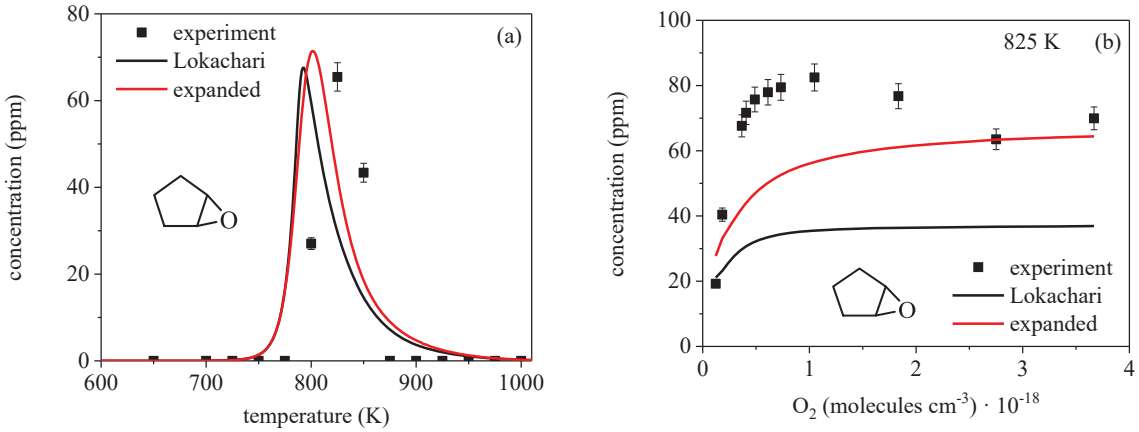

Figure 4. *Species profile measurements of ȮOOH-derived species, 1,2-epoxycyclopentane, produced from oxidation of cyclopentane at 835 Torr. (a) temperature dependence; (b) oxygen dependence at 825 K. Experimental measurements compared with predictions using Lokachari et al. [8] and an expanded version produced in Hill et al. [7] that prescribes additional, radical-specific consumption reactions neglected in [8].*

Reactions mechanisms and rates of cyclic ether radical stereoisomers: Reaction rates of *cis*- and *trans*- isomers of 2,3-dimethyloxirane, cyclic ethers produced from unimolecular decomposition of *β*-ȮOOH during *n*-butane oxidation (cf. Figure 3), were studied computationally. Isomer-resolved oxidation experiments in Doner et al. [1] detected species produced from peroxy radical-mediated reactions, including methyl vinyl ketone, diacetyl, and vinyl acetate. However, the formation pathways remain unclear as to whether the species form from O_2-addition to intact 2,3-dimethyloxiranyl radicals or to radicals produced from ring-opening. The calculations examined reaction rates for the competing pathways to provide clarity and fundamental insight on the reaction mechanisms of *cis*- and *trans*-2,3-dimethyloxirane. Stereochemical-dependent potential energy surfaces for 2,3-dimethyloxiranyl radicals were calculated using AutoMech and rate coefficients were computed using MESS for master equation modeling from 0.01 – 100 atm and 300 – 1000 K.

The rate calculations focused on the competition between reactions of *α*- and *β*- isomers of 2,3-dimethyloxiranyl (Ṙ), namely ring-opening to Ṙ′, including via prompt reactions, and O_2-addition to form ROȮ. The results showed that, across a broad range of pressures, ring-opening rates exceed O_2-addition unless $[O_2] > 10^{19}$ cm^{-3}. However, prompt effects are significant for H-abstraction from *cis*- and *trans*-2,3-dimethyloxirane above ~500 K. The implication of the latter result is that thermalization of Ṙ at combustion conditions is minimal, indicating that O_2 preferentially adds to carbon-centered radicals formed via ring-opening, even at high O_2 concentrations. From Dewey and Rotavera [9], inclusion of such pathways in chemical kinetics mechanisms of *n*-butane impacts ȮH populations, species profiles, and chain-branching reactions relevant to other alkyl radicals.

Future Work

Gas-phase chemical kinetics experiments: Speciation measurements of hydrocarbons and biofuels are continuing with acyclic species *n*-pentane and butanone, cyclic species cyclopentanol and cyclopentanone, and additional experiments on other C4 oxygenated species, 1,1-dimethoxyethane and 1,2-dimethoxyethane in collaboration with RWTH Aachen University, Ghent University, and Physikalisch-Technische Bundesanstalt (PTB). In addition, JSR experiments are being conducted at the University of Georgia on several intermediates including *cis*- and *trans*- isomers of 2,3-dimethyloxirane, 3,4-epoxytetrahydrofuran, cyclopentene, 1,2-epoxycyclopentane. The aim of the latter experiments is to provide quantitative modeling targets for the development of new, expanded sub-mechanisms.

Refining chemical kinetics mechanisms: The efforts above combine to achieve one of the primary goals of the program, which is increasing the quantitative prediction capabilities of chemical kinetics mechanisms by (i) providing new, benchmark experimental data, (ii) identifying new reaction pathways that may hold relevance to increasing the accuracy of modeling combustion, and (iii) computing theoretical rates. Future work on this topic will involve using existing mechanisms from the literature on the five species in **Figure 1** and refining via a combination of the efforts above.

Publications/Presentations Acknowledging Support from the Gas-Phase Chemical Physics Program, 2022 – Present:

1. **Probing O_2-Dependence of Cyclopentyl Reactions via Isomer-Resolved Speciation**, A. W. Hill, D. A. Moore, N. S. Dewey, S. W. Hartness, B. Rotavera, *Proceedings of the Combustion Institute*, Vol. 40, 2024.
2. **Nuclear Ensemble Approach for Substituted Oxiranes with Conformational Sampling: A Joint Theoretical–Experimental Study**, I. T. Beck, E. C. Mitchell, A. W. Hill, J. M. Turney, B. Rotavera, H. F. Schaefer III, *Journal of Physical Chemistry A (Special Issue – Rodney J. Bartlett Festschrift)*, 2024.
3. **O_2-Dependence of Unimolecular Reactions of 1,2-Dimethoxyethanyl and 1,2-Dimethoxyethanylperoxy Isomers**, N. S. Dewey, K. De Ras, R. Van de Vijver, S. W. Hartness, A. W. Hill, J. W. Thybaut, K. M. Van Geem, L. Sheps, B. Rotavera, *Combustion and Flame*, 2024.
4. **Alkylperoxy Radicals are Responsible for the Formation of Oxygenated Primary Organic Aerosol**, O. El Hajj, S. W. Hartness, G. W. Vandergrift, Y. Park, C. K. Glenn, A. Anosike, A. R. Webb, N. S. Dewey, A. C. Doner, Z. Cheng, G. S. Jatana, M. Moses-DeBusk, S. China, B. Rotavera, R. Saleh, *Science Advances*, Vol. 9, 1 – 12, 2023.
5. **Unimolecular Reactions of 2-methyloxetanyl and 2-methyloxetanylperoxy Radicals**, A. C. Doner, N. S. Dewey, B. Rotavera, *Journal of Physical Chemistry A (Special Issue – Marsha I. Lester Festschrift)*, Vol. 127, 6816 – 6829, 2023.
6. (*invited seminar*, March 2024) **Chemical Kinetics for Sustainable Transportation**, *Georgia Tech*.
7. **Simulation of the VUV Absorption Spectra of Oxygenates and Hydrocarbons**, A. K. Bralick, E. C. Mitchell, A. C. Doner, A. R. Webb, M. G. Christianson, J. M. Turney, B. Rotavera, H. F. Schaefer III, *Journal of Physical Chemistry A (Krishnan Raghavachari Festschrift)*, 2023.
8. (*invited seminar*, February 2023) **Combustion for Sustainable Transportation**, *University of Illinois*.
9. **Probing O_2-Dependence of Hydroperoxy-Butyl Reactions via Isomer-Resolved Speciation**, S. W. Hartness, N. S. Dewey, M. G. Christianson, A. L. Koritzke, A. C. Doner, A. R. Webb, B. Rotavera, *Proceedings of the Combustion Institute*, Vol. 39, 2023.
10. **Machine Learning Models for Binary Molecular Classification using VUV Absorption Spectra**, A. C. Doner, H. A. Moran, A. R. Webb, M. G. Christianson, A. L. Koritzke, G. D. Smith, B. Rotavera, *Journal of Quantitative Spectroscopy & Radiative Transfer*, Vol. 297, 2023.
11. **Probing O_2-Dependence of Tetrahydrofuranyl Reactions via Isomer-Resolved Speciation**, A. L. Koritzke, M. G. Christianson, S. W. Hartness, N. S. Dewey, A. C. Doner, A. R. Webb, B. Rotavera, *Combustion and Flame (Special Issue in Honor of Jim Miller)*, 2023.
12. **Vacuum-Ultraviolet Absorption Cross-Sections of Functionalized Four-Carbon Species**, A. C. Doner, A. R. Webb, N. S. Dewey, S. W. Hartness, M. G. Christianson, A. L. Koritzke, A. Larsson, K. M. Frandsen, B. Rotavera, *Journal of Quantitative Spectroscopy & Radiative Transfer*, Vol. 292, 2022.

References

[1] A.C. Doner, M.M. Davis, A.L. Koritzke, M.G. Christianson, J.M. Turney, H.F. Schaefer, L. Sheps, D.L. Osborn, C.A. Taatjes, B. Rotavera, *Int. J. Chem. Kin.*, 53 (2021) 127-145.
[2] A.D. Danilack, C.R. Mulvihill, S.J. Klippenstein, C.F. Goldsmith, *J. Phys. Chem. A*, 125 (2021) 8064-8073.
[3] A.C. Doner, J. Zádor, B. Rotavera, *Faraday Discuss*, 238 (2022) 295-319.
[4] S.W. Hartness, N.S. Dewey, M.G. Christianson, A.L. Koritzke, A.C. Doner, A.R. Webb, B. Rotavera, *Proc. Combust. Inst.*, 39 (2022).
[5] A.L. Koritzke, N.S. Dewey, M.G. Christianson, S. Hartness, A.C. Doner, A.R. Webb, B. Rotavera, *Combustion and Flame (Special Issue in Honor of Jim Miller)*, (2023).
[6] S.W. Hartness, M. Saab, M. Preußker, R. Mazzotta, N.S. Dewey, A.W. Hill, G. Vanhove, Y. Fenard, K.A. Heufer, B. Rotavera, *Proc. Combust. Inst.*, 40 (2024) 105528.
[7] A.W. Hill, D.A. Moore, N.S. Dewey, S.W. Hartness, B. Rotavera, *Proc. Combust. Inst.*, 40 (2024).
[8] N. Lokachari, S.W. Wagnon, G. Kukkadapu, W.J. Pitz, H.J. Curran, *Combust. Flame*, 225 (2021) 255-271.
[9] N.S. Dewey, B. Rotavera, *Combust. Flame*, 252 (2023) 112753.

CHEMICAL DYNAMICS METHODS AND APPLICATIONS

David W. Chandler, Laura M. McCaslin, David L. Osborn, Judit Zádor, Christopher Kliewer, Timothy S. Zwier
Sandia National Laboratories, MS 9051, Livermore, CA 94551-0969
chand@sandia.gov, lmmccas@sandia.gov, dlosbor@sandia.gov,
jzador@sandia.gov, cjkliew@sandia.gov, tszwier@sandia.gov

PROGRAM SCOPE

This program focuses on unraveling the mechanisms and timescales of dynamical processes in molecular systems via multiplexed experimental and theoretical techniques. These studies employ high-level electronic structure and dynamics theory alongside time-resolved spectroscopic tools to investigate rotational, vibrational, electronic, and reaction dynamics in molecular systems. The work reported here relates closely to studies performed in the Ultrafast Physics, Ultrafast Chemistry, Multiphase Interactions, and Electron-Driven Chemistry tasks, all of which encompass studies of energy flow within molecules, correlations between nuclear and electronic motion, and development of advanced optical techniques.

Highlights from our program include velocity-map imaging molecular beam studies of the photodissociation of SO_2, broadband microwave spectroscopy of tunneling dynamics, site-specific photochemistry mapped by IR spectra in the excited state, production of quantum-state and velocity selected molecular beams, and studies of electronic energy transfer between remote, near-degenerate chromophores.

RECENT PROGRESS

Direct observation of the carbene HCOH from methanol photodissociation[1]

In collaboration with the group of Leah Dodson (University of Maryland) we have explored the photodissociation of CH_3OH (methanol) at 193 nm using both the MPIMS approach.[2] We observed an unexpected minor photodissociation channel that produces a m/z 30.11 amu molecule with an ionization threshold of about 8.9 eV, well below the known ionization threshold of formaldehyde (CH_2O). The only other plausible isomer with this empirical formula is the carbene HCOH (hydroxymethylene). The photoionization spectrum we obtained from this work matches nearly quantitatively in onset and shape with our calculated photoionization spectrum at the CCSD(T)-F12/cc-pVQZ-F12//CCSD(T)-F12/cc-pVTZ-F12 level of theory. We also photodissociated the CH_3OD isotopomer, which produced the HCOD carbene, but not HCOH, indicating that the O-H bond in methanol stays intact in the product channel producing hydroxymethylene. HCOH is known to have a singlet ground electronic state with the lowest triplet lying 1.07 eV higher in energy. In the presence of excess O_2, the HCOH carbene is consumed, but only slowly. Although we were not able to obtain a rigorous rate coefficient for the HCOH + O_2 reaction, our results indicate it is on the order of 10^{-13} cm^3 $molecule^{-1}$ s^{-1}, a value that lies between that of $^1CH_2 + O_2$ and $^1HCF + O_2$. These observations suggest a correlation between the electron withdrawing capacity of the H, OH, F substituent in these three carbenes and the rate of their reactions with O_2. This work is the first experimental observation of HCOH in the gas phase and paves the way for further studies of the reaction chemistry of this simplest hydroxycarbene.

Velocity map imaging of SO_2 photodissociation

The photodissociation of SO_2 in the near ultraviolet region has received renewed attention after S atoms were detected with a flow reactor coupled to a PEPICO apparatus and assigned to a primary photodissociation process yielding S + O_2 at wavelengths around 193 nm.[3] Although this work concluded that only 2-4% of photoexcited SO_2 produced S + O_2, this yield implies that O_2 could have been produced from SO_2 and radiation that would have been abundant in Earth's early atmosphere. In our recent progress, we use resonance-enhanced multiphoton ionization (REMPI) to image of O and S atoms (taken at identical REMPI laser fluence) produced by exciting jet-cooled SO_2 to a C state resonance using 202.19 nm laser light (see figure below).

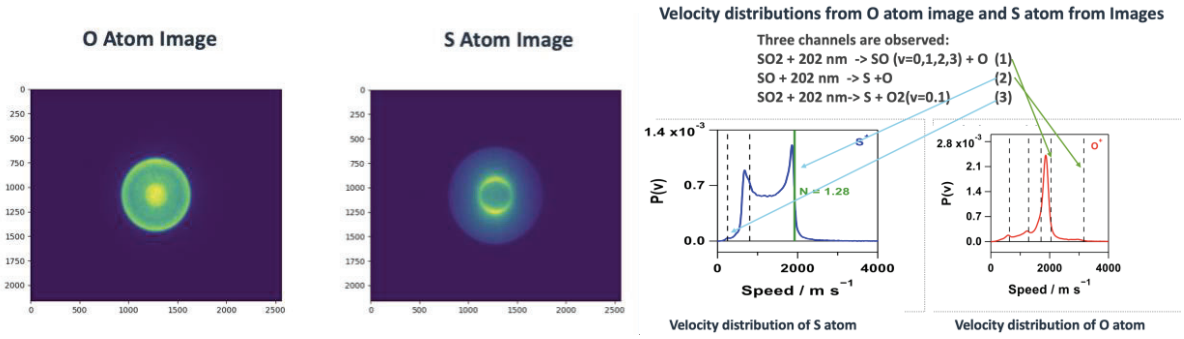

The inner rings of the O-atom image correspond to the primary one-photon dissociation $SO_2 \rightarrow O + SO$ (channel 1). Similarly, the innermost ring of the S-atom image corresponds to the primary one-photon dissociation $SO_2 \rightarrow S + O_2$ (channel 3). However, the outermost rings in the O- and S-atom images correspond to a secondary one-photon dissociation of the dominant SO reaction product: $SO \rightarrow S + O$ (channel 2). After Abel-inversion and angular integration, the resulting velocity distributions provide unbiased information on the relative intensity of each of the channels. The appearance of channel 2 in both images enables an elegant estimate of the target branching ratio between channels 1 and 3 without the need for precise O- and S-atom REMPI cross-sections. For example, at the experimental photofragmentation wavelength reported here, our preliminary analysis is that the primary $S + O_2$ channel is a small fraction (perhaps 1%) of the secondary dissociation channel. Similarly, the secondary dissociation channel is approximately 1% of the primary O + SO channel. Thus, one can visually estimate that approximately only 1-in-10,000 jet-cooled SO_2 molecules follow the newly discovered $S + O_2$ channel when excited at 202.19 nm. Precise branching ratios can be obtained by modeling the sequential dissociation image using the experimentally measured O-atom velocity distribution and the well-defined thermodynamic atomization energy of SO_2.

Simultaneous Velocity Selection and Vibrational Population of a Molecular Beam

Molecular beams have provided a wealth of chemical information about dynamic unimolecular (photochemical) and bimolecular (reactive and non-reactive scattering) processes. This is due to the supersonic cooling of the expansion which generates molecules with internal temperatures between approximately 2 K and 15 K. The resulting velocity spread is approximately 10% of the velocity of the supersonic beam, which translates to about 150 m/s for a He seeded beam. The typical molecular beam temperatures do not generally populate a single quantum state for dynamics to proceed from and their velocity spread causes averaging in the collision energy such that it is impossible to resolve closely spaced quantum states via their recoil. Eliminating both the thermal averaging of the velocity and internal state distribution are key for using molecular beams to study quantum-controlled chemical dynamics of more complex molecular systems.

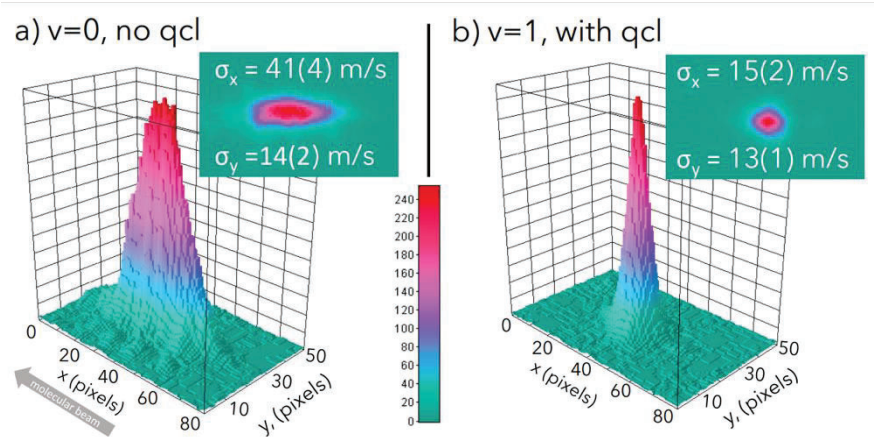

These shortcomings have motivated improvements such as the Stark decelerator, which can select a smaller velocity group of specific quantum states for molecules with low-field-seeking, large Stark shifts. While such techniques are effective, they are very time, money, and expertise intensive; in addition, they are

limited to the appropriate specific quantum states. We demonstrate a new technique that produces a molecular beam with a population of molecules comprising a single quantum state with a velocity selection dictated by the Doppler shift associated with the laser beam that excites the molecules. Specifically, we have used a Quantum Cascade (QC) laser, counterpropagating to a molecular beam, to prepare a single hyperfine state in the first vibrational level of NO (v=1 J=3/2) seeded in a molecular beam of either He or Ar. In both cases the velocity spread measured for the vibrationally excited molecules (~15m/s) is in good agreement with the expected time-averaged 3 MHz bandwidth of the QC laser. This average velocity spread represents a temperature of approximately 800 millikelvin -- significantly cooler than the typical molecular beam temperature defined by the rotational distribution of the molecules in the molecular beam. An average RMS velocity spread for a single shot is obtained by averaging many single-laser-shot images. Each single-shot measurement averages over approximately 50 milliseconds of IR laser excitation and gives a velocity spread of 9m/s or ~300 millikelvin temperature. The QC laser instability over time broadens the averaged velocity distribution. Below are velocity mapped ion images of the NO(v=0, J=1/2) molecular beam and the velocity mapped beam spot of a single hyperfine state of the NO(v=1 J=3/2) laser-excited species in the molecular beam. The size of the spot for the vibrationally excited species is limited by the actual size of a single ion strike on the detector and this must be deconvolved to obtain the true spot size. Improvements in the power supply that runs the QC laser and frequency locking of the laser will provide even more precise velocity selection, as well as long-term stability for molecular scattering experiments.

We believe this new technique will have significant impact for truly quantum-state resolved photochemistry as well as molecule-molecule scattering where the improved quantum state preparation and velocity resolution will allow one to study correlated product channels for scattering originating from a single, selectable quantum state.

Multi-dimensional Tunneling in 2,6-dimethyl phenol

Tunneling is a quintessential quantum mechanical process with important implications for such wide-ranging areas as quantum control and reaction kinetics. We use chirped-pulse Fourier Transform microwave (CP-FTMW) methods to probe molecules that are capable of tunneling, using the tunneling splittings to interrogate the tunneling dynamics. When more than one tunneling pathway is open to the molecule, interesting questions arise regarding the timescales on which these competing tunneling pathways occur and the extent to which the tunneling dynamics in one coordinate could be controlled by that in another coordinate. Over the past year, we have been puzzling over the effects of multi-dimensional tunneling on the spectroscopy of 2,6-dimethyl phenol (DMPhOH), which possesses one OH group and two symmetrically positioned CH_3 groups, all of which are capable of tunneling through an internal rotor barrier. The OH group tunnels in a two-fold potential with a calculated 1D barrier of V_2=1157 cm^{-1}. When the OH group is held in its in-plane minimum energy geometry, the two methyl rotors are inequivalent, with a V_3 barrier of 660 cm^{-1} for the methyl group toward which the OH is facing, while the 'backside' methyl has a barrier almost half that (V_3=376 cm^{-1}). We have recorded the broadband microwave spectrum of DMPhOH in the 7.5-17.5 GHz region and have a partial fit that provides a qualitative understanding of tunneling on this three-dimensional internal rotor surface. The spectrum is replete with rotational transitions split into triplets separated from one another by 48.5 MHz, seemingly violating selection rules that require a-type rotational transitions to be split by OH tunneling, but b-type transitions to be unsplit; that is, that individual rotational transitions will

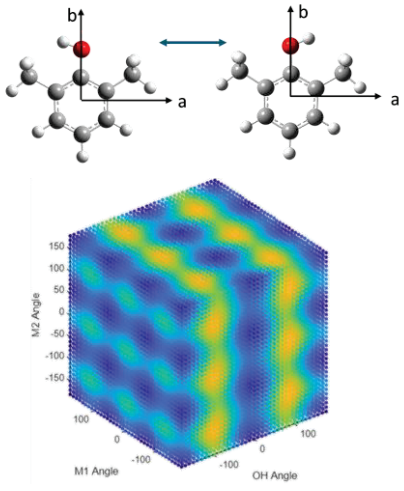

The OH tunneling coordinate in 2,6-dimethyl phenol and the calculated 3D surface for tunneling of the OH and two CH_3 groups.

either be split or unsplit. Importantly, the observed triplets arise because OH tunneling is possible in some of the methyl rotor states but is quenched in others. In particular, when one of the methyl groups is in the lowest methyl rotor tunneling state (with *a* symmetry in its local C_{3v} group) and the other in the next lowest methyl rotor state (with *e* symmetry in C_{3v}), OH tunneling is quenched, as OH tunneling would need to occur with a change in methyl rotor states of both methyl groups. Thus, 2,6-dimethyl phenol exhibits a state-dependent quenching of OH tunneling. We have mapped out the full 3D tunneling surface for DMPhOH and fit it to a properly symmetrized potential that retains the over-all symmetry of the two methyl groups on the full 3D surface with coupling terms that make the methyl rotor potentials asymmetric along 1D cuts through the surface. We are finalizing our analysis of the spectrum with a planned submission in Fall 2024.

Site- and Conformer-specific Photochemistry and Electronic Energy Transfer along a Protonated Peptide Scaffold[4]

Photoexcitation is a powerful means for initiating chemistry, yet the outcome of such excited state processes becomes harder to predict as the size and chemical complexity of the reactants grows. We are presently using a multi-stage mass spectrometer outfitted with a cryo-cooled octopole ion trap to explore the photochemistry of large, conformationally complex ions with multiple competing product channels. We use a well-studied protonated pentapeptide scaffold with an assigned starting structure to initiate the photochemistry by UV excitation through one or more aromatic chromophores. We have recently completed studies of protonated Leu-enkephalin (Tyr-Gly-Gly-Phe-Leucine, YGGFL) and chromophore-swapped analog FGGYL,[4] combining experimental studies of the excited state spectra and relative photochemical product yields with calculations that map out electronic state-specific structural changes via density functional theory (DFT) and time-dependent DFT (TDDFT).

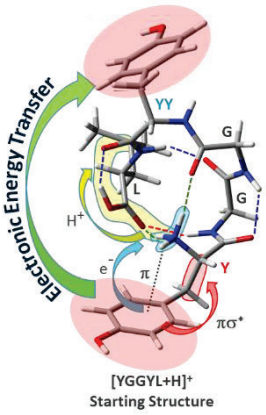

Over the past year, we have used similar methods to study the photophysics and photochemistry of YGGYL, with its two Tyr chromophores in unique local environments, separated from one another by 11 Å. We contrast these results with those from two selectively deuterated isotopologues (dY)GGYL and YGG(dY)L where 'dY' is a tyrosine chromophore perdeuterated on its aromatic ring. Whereas the undeuterated Tyr chromophores on the peptide scaffold have S_0-S_1 origins that are separated by 325 cm^{-1} from one another, upon deuteration at Y(1) or Y(4) increase or decrease this difference by 137 cm^{-1}. We track the relative product intensities following UV excitation and following IR enhancement in the excited state(s). We are collaborating with Lyudmila Slipchenko (Purdue) to model electronic energy transfer, vibronic coupling, intersystem crossing to the triplet manifold, and the product channels that follow.

FUTURE WORK

Super Rotor Dynamics

In order to develop our program's study of non-equilibrium systems, experiments involving highly rotationally excited molecules will be performed. While the effects of highly excited translational and vibrational states on chemical reactions are well-characterized, the effects of highly rotationally excited molecules are not as well understood. During the past year, the laser-based molecular optical centrifuge has been finished and demonstrated under the Ultrafast Physics section of our program. This year we plan to begin work on the photodissociation dynamics of N_2O super-rotors. We will expand N_2O in a supersonic jet to cool the rotational distribution to only the lowest few J states. This distribution will be accelerated to super-rotor states. We will dissociate N_2O at ~203 nm and observe the $O(^1D)$ and the N_2 fragments via resonance-enhanced multi-photon ionization coupled with VMI imaging. Beyond this direction observation of photodissociation dynamics starting from the unexplored initial condition of very high rotational excitation, these experiments will allow a direct test of whether rotation-to-vibration coherence transfer, as recently observed for CO_2 super-rotors, is a ubiquitous phenomenon. Furthermore, to better

understand the reactions of super-rotors and atoms, we will react rotationally excited N_2O and $O(^1D)$ to form NO, monitoring via VMI.

Tunneling dynamics

Using the extraordinary capabilities of modern microwave electronics, we seek to develop novel pulse sequences that can interrogate and even control quantum tunneling pathways in molecules capable of multi-dimensional tunneling. To do so, we need to expand both the experimental and theoretical modeling of multi-dimensional tunneling dynamics. In collaboration with L.V. Nguyen at Univ. Paris-Est Creteil, we will obtain FTMW spectra of 2,6-dimethyl phenol at higher resolution where methyl rotor splittings due to both methyl rotors will be resolved, thereby providing a direct spectroscopic link to the full 3D tunneling surface. In collaboration with Ned Sibert (UW-Madison), we will develop a model of the rotational-tunneling energy level structure on the 3D tunneling surface for comparison with experiment. From this foundational understanding of the energy level structure in the frequency domain, we will model and then experimentally verify tailor-made pulse sequences that interrogate tunneling in the time-domain.

Photodissociation of norbornadiene: a Molecular Solar Thermal storage candidate

A long-standing DOE mission goal is the efficient conversion of solar energy to stored chemical energy. One attractive approach to meeting this goal is Molecular Solar Thermal storage (MOST), in which a molecule absorbs sunlight that drives isomerization to a stable, higher enthalpy isomer. That isomer can then be stored and converted back to the more stable isomer, harvesting the exothermicity to do work, at a time of our choosing. Norbornadiene (bicyclo[2.2.1]hepta-2,5-diene) is a leading candidate for MOST systems, via photoconversion to its less-stable isomer quadricyclane. Surprisingly, there seems to be no published research on the photodissociation of norbornadiene in the gas phase. We propose to study photodissociation of the two C_7H_8 isomers norbornadiene and quadricyclane using our PEPICO apparatus. We hypothesize that, in contrast to photodissociation of acyclic and mono-cyclic closed-shell hydrocarbons, these multicyclic compounds may have a higher likelihood of forming closed-shell products instead of radical + radical products. In competition with bimolecular product formation, we expect some photo-induced isomerization. In the case of norbornadiene we expect to see quadricyclane, but we hypothesize that more stable isomers could also be formed. Starting from quadricyclane, given its more positive heat of formation compared to norbornadiene, it seems even more likely that photoisomerization to more stable isomers will occur, and we hope to discover what determines the branching between reversion to norbornadiene vs. isomerization to the global minimum (toluene) or other isomers.

Photodissociation of methanol at 193 nm

Despite its canonical nature as the smallest alcohol, the photodissociation of methanol is not well documented. A number of literature studies using end product analysis conclude that in the first absorption band, $S_1 \leftarrow S_0$ from 165 – 200 nm, the dominant products are CH_3O + H from simple O-H bond fission. Not surprisingly, for 193 nm excitation, where the photon contains 6.42 eV of energy, many other product channels are thermodynamically allowed. In an early paper, Wittig et al. report that these other product channels comprise 14 ± 10% of the total products. The Wittig experiments clearly detect H atoms and measure their kinetic energy via Rydberg H-atom time-of-flight spectroscopy. They attribute most of the H atoms to the CH_3O + H product channel, but could not rule out secondary photodissociation of CH_3O, CH_2O, and CH_3 species producing H atoms. We plan to use the PEPICO and MPIMS apparatuses to provide a more universal probe of the many possible product channels in this photodissociation. New calculations from Joel Bowman's group on an analytical CH_3OH potential energy surface will provide theoretical guidance on this system. Our observation of HCOH in this system (see Progress Report) is clear evidence that other product channels are active. We also plan to study the $O(^1D)$ + CH_4 reaction as an alternative way to create highly vibrationally excited CH_3OH on the ground electronic state, with less available energy than is possible from 193 nm excitation of methanol.

REFERENCES

1) Hockey, E.K.; McLane, N.; Martí, C.; Duckett, L.; Osborn, D.L.; Dodson, L.G. Direct observation of gas-phase hydroxymethylene: photoionization and kinetics resulting from methanol photodissociation. *J. Am. Chem. Soc.* **2024**, *146* (21), 14416-14421, Article. DOI: 10.1021/jacs.4c03090.
2) Osborn, D.L.; Zoe, P.; Johnsen, H.; Hayden, C.C.; Taatjes, C.A.; Knyazev, V.D.; North, S.W.; Peterka, D.S.; Ahmed, M.; Leone, S.R. The multiplexed chemical kinetic photoionization mass spectrometer: a new approach to isomer-resolved chemical kinetics. *Rev. Sci. Instrum.* **2008**, *79*(10), 104103, Article. DOI: 10.1063/1.3000004.
3) Rösch, D.; Almeida, R.; Sztáray, B.; Osborn, D.L. High-resolution double velocity map imaging photoelectron photoion coincidence spectrometer for gas-phase reaction kinetics. *J. Phys. Chem. A* **2022**, *126* (10), 1761-1774, Article. DOI: 10.1021/acs.jpca.1c10293.
4) Foley, C.D.; Lee, C.; Abou Taka, A.; Au, K.; Chollet, E.; Kubasik, M.; McCaslin, L.M.; Zwier, T.S. Site-specific photochemistry along a protonated peptide scaffold. *J. Am. Chem. Soc.* **2024**, *146* (19), 13282-13295, Article. DOI: 10.1021/jacs.4c01576.

BES-SPONSORED PUBLICATIONS (2022 -- PRESENT)

1) Savee, J.D.; Sztaray, B.; Hemberger, P.; Zádor, J.; Bodi, A.; Osborn, D.L. Unimolecular isomerization of 1,5-hexadiyne observed by threshold photoelectron photoion coincidence spectroscopy. *Faraday Discuss.* **2022**, *238*, 645-664, Article. DOI: 10.1039/D2FD00028H.
2) Fischer, J.L.; Blodgett, K.M.; Harrilal, C.P.; Walsh, P.S.; Choi, S.H., Zwier, T.S. Conformer-specific spectroscopy and IR-induced isomerization of a model γ-peptide: Ac-γ4-Phe-NHMe. *J. Phys. Chem. A* **2022**, *126* (11), 1837-1847, Article. DOI: 10.1021/acs.jcpa.2c00112.
3) Lawler, J.T.; Harrilal, C.P.; DeBlase, A.F; Sibert III, E.L.; McLuckey, S.A.; Zwier, T.S. Single-conformation spectroscopy of cold, protonated ^{D}PG-containing peptides: switching β-turn types and formation of a sequential type II/II' double β-turn. *Phys. Chem. Chem. Phys.* **2022,** *24,* 2095-2109, Article. DOI: 10.1039/D1CP04852J.
4) Hernandez-Castillo, A.O.; Calabrese, C.; Fritz, S.M.; Uriarte, I.; Cocinero, E.J.; Zwier, T.S. Bond length alternation and internal dynamics in model aromatic substituents of lignin. *ChemPhysChem* **2022**, 23, e202100808, Article. DOI: 10.1002/cphc.202100808.
5) Rösch, D.; Almeida, R.; Sztáray, B.; Osborn, D.L. High-resolution double velocity map imaging photoelectron photoion coincidence spectrometer for gas-phase reaction kinetics. *J. Phys. Chem. A* **2022**, *126* (10), 1761-1774, Article. DOI: 10.1021/acs.jpca.1c10293.
6) Rösch, D.; Xu, Y.; Guo, H.; Hu, X.; Osborn, D.L. SO_2 photodissociation at 193 nm directly forms $S(^3P) + O_2(^3\Sigma_g^-)$: implications for the archean atmosphere on earth, *J. Phys. Chem. Lett.* **2023**, *14* (12), 3084-3091, Article. DOI: 10.1021/acs.jpclett.3c00077.
7) Foley, C.D.; Lee, C.; Abou Taka, A.; Au, K.; Chollet, E.; Kubasik, M.; McCaslin, L.M.; Zwier, T.S. Site-specific photochemistry along a protonated peptide scaffold. *J. Am. Chem. Soc.* **2024**, *146* (19), 13282-13295, Article. DOI: 10.1021/jacs.4c01576.
8) Hockey, E.K.; McLane, N.; Martí, C.; Duckett, L.; Osborn, D.L.; Dodson, L.G. Direct observation of gas-phase hydroxymethylene: photoionization and kinetics resulting from methanol photodissociation. *J. Am. Chem. Soc.* **2024**, *146* (21), 14416-14421, Article. DOI: 10.1021/jacs.4c03090.

Chemical Kinetics for Complex Systems

Jacqueline H. Chen, Nils Hansen, Habib N. Najm, David L. Osborn, Leonid Sheps, Craig A. Taatjes, Judit Zádor, and Timothy S. Zwier
Sandia National Laboratories, MS 9055, Livermore, CA 94551-0969
jhchen@sandia.gov, nhansen@sandia.gov, hnnajm@sandia.gov, dlosbor@sandia.gov, lsheps@sandia.gov, cataatj@sandia.gov, jzador@sandia.gov, tszwier@sandia.gov

Program Scope

We employ experiment and theory to elucidate mechanisms of elementary chemical reactions, which impacts the research theme of Reaction Pathways in Diverse Environments. This task extends the high-resolution view of Sandia's "Chemical Dynamics" task to encompass complex interactions in collisional environments, and it provides a basis for the interface studies in Sandia's "Multiphase Interactions" subtask. Analytical tools that use tunable vacuum ultraviolet light from the Advanced Light Source synchrotron at Lawrence Berkeley National Laboratory and chirped pulse microwave spectroscopy enable sensitive and isomer-specific detection of reactant and product molecules sampled from chemical reactions. These individual reaction studies are linked to controlled measurements of more complex reaction systems as found in well-defined laboratory scale zero- and one-dimensional reactors. We use automated *ab initio* master equation workflows to study elementary kinetics, a particle-based approach for non-thermal effects at the mesoscale, and Bayesian statistics for optimal experimental design.

Recent progress

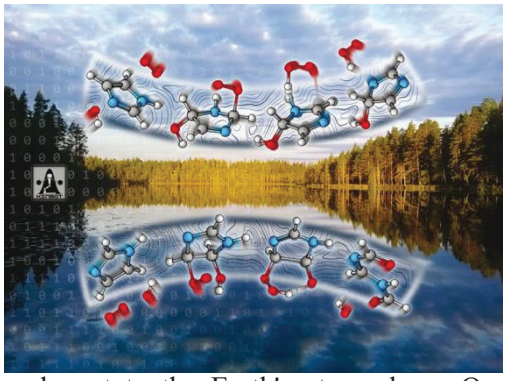

Oxidation reactions of imidazole explored using automated kinetics Imidazoles are present in Earth's atmosphere in both the gas-phase and in aerosol particles and have been implicated in the formation of climate-forcing of brown carbon aerosols. Yet, its atmospheric gas-phase sinks are unknown. We employed KinBot to investigate the reaction mechanism and kinetics of imidazole's OH-initiated gas-phase oxidation in the presence of O_2 and NO_x. The explored mechanism included reactions available to first-generation RO_2 radicals, as well as alkoxyl radicals produced from RO_2 + NO reactions. Product distributions were obtained by assembling and solving a master equation, under conditions relevant to the Earth's atmosphere. Our calculations show a complex, branched reaction mechanism, which nevertheless converges to yield two major closed-shell products: 4H-imidazol-4-ol and N,N′-diformylformamidine. This work also revealed fast O_2-migration pathways between the α-N-imino peroxyl radical isomers, a new prototype pathway that should be considered during the atmospheric oxidation of unsaturated organic nitrogen compounds in general.[1]

Mechanism and kinetics of carbene reactions The short lifetimes of carbenes largely prevent their direct investigation despite their fundamental importance in many gas-phase environments. Here we carried out an unprecedented direct gas-phase study of a model carbene reaction, $CH_3\ddot{C}OH$ + CD_3CDO, using our previously established strategy to produce singlet-methylhydroxycarbene ($CH_3\ddot{C}OH$). Carbenes are often assumed to react via insertion. However, previous work from Peter Schreiner's group concluded that $CH_3\ddot{C}OH$ + CD_3CDO occurs via a H-bonded complex followed by a simultaneous H-transfer and C-C addition step. By resolving the isomeric nature of the product, and kinetically linking the product to the reactant via its time history, we have confirmed that the reactivity is completely dominated by the proposed pathway, with no evidence for insertion. To determine the relevant barrierless rate coefficient, we modified the variable-reaction coordinate transition state theory (VRC-TST) code of Goldsmith (Brown U) and coupled it to KinBot. Our calculations confirm that this reaction is fast (near gas-kinetic) at very low

temperatures, where long-range attraction dominates. The submerged barrier separating the pre-reactive complex from the acetoin product become the rate-limiting step at higher temperatures. This work shows that singlet carbenes, when hydrogen bonding is possible, may not react via insertion pathways. Manuscript is in preparation.

Automated theoretical characterization of sulfur atom reactions with dienes In collaboration with Arthur Suits (U. Missouri), we investigated the fundamental chemistry and kinetics of $S(^3P)$ + 1,3-butadiene and $S(^3P)$ + isoprene reactions using automated high-level ab initio methods. Channels were found to be closed on the upper triplet PES. Instead, they proceed on the lower singlet PES upon ISC near the geometry of the initial adduct. Remarkably, our calculations show that cyclization forming (methyl)thiophene dominates under single collision conditions, in striking contrast with the analogous $O(^3P)$ reaction, but in agreement with the crossed-beam experiments. Our detailed modeling proposed further significant products, such as thioketene and thioformaldehyde, which were detected using the chirped-pulse mmW spectroscopy in uniform flows (CPUF) technique in the Suits laboratory.[4,10] Our work provides fundamental mechanistic insight into triplet and singlet sulfur chemistry and nonadiabatic reactions in general.

Fundamental studies of the reactivity of Criegee intermediates We have continued our collaboration spearheaded by Caravan (ANL) on the reactivity of carbonyl oxide Criegee intermediates. In the last year we investigated reactions of butanone oxide (methyl-ethyl Criegee intermediate, MECI) with Klippenstein (ANL), Lester (U. Penn), and collaborators from the Jet Propulsion Laboratory, identifying mechanistic pathways facilitated by the unusual electronic configurations of carbonyl oxides. By measuring isomerization products with synchrotron photoionization mass spectrometry, we were able to identify hydroxybutanone formation that arises from novel roaming pathways in MECI unimolecular reactions.[21] Comparison of the reactivity of MECI with SO_2 to the reaction of methyl vinyl ketone oxide (MVKO), a resonance-stabilized Criegee intermediate product of isoprene ozonolysis, showed that resonance stabilization substantially reduces the bimolecular reactivity of the carbonyl oxides.[20]

Non-thermal chemistry/termolecular reactions Molecular simulations of H_2-air detonations under chemical equilibrium but vibrational non-equilibrium were performed using DSMC to verify that a stochastic particle-based method works well in the continuum regime for processes that include complex chemical interactions and strong thermal non-equilibrium. To include vibrational and rotational non-equilibrium, an effective temperature model was employed. We validated this model for key H_2-air reactions in a 0-D thermal bath, and it was then used to simulate 1-D hydrogen-air detonations.[6] Two-dimensional high fidelity macro-scale simulations were performed for H_2/O_2 mixtures at 950 K and 5 atm to assess the significance of non-thermal reactivity induced by radical-molecule association and radical-radical recombination reactions on the initiation, propagation, and structure of planar detonation waves (PDWs). Non-thermal effects were found to increase the cell irregularity and marginally increase the detonation cell width and length from birth to death.[8] In the overdriven keystone region, where the most extreme conditions appear, termolecular reactions arising due to rovibrationally excited HO_2* were found to be the most active and contribute the most to heat release rate at the reaction front, while termolecular reactions arising due to rovibrationally excited H_2O* are most active far into the reaction zone. The increase in peak heat release rate in the keystone region is on the order of 60%, which is quantitatively correlated to the contribution of termolecular reactions. Both effects promote consumption of radicals and production of fuel.

Bayesian Optimal Experimental Design We achieved operational mode for our Bayesian optimal experimental design (BOED) for the HP-PIMS apparatus: starting from available HP-PIMS data, we are using BOED to propose new experimental conditions in the pursuit of increased expected information gain on targeted rate coefficients, proceeding to take measurements at these conditions, and iterating on this loop. Based on preliminary data from this activity, we enhanced the modeling framework with an *embedded* model error construction, aside from the already implemented additive model error setup. This combination

of embedded and additive model error constructions, along with improved capture of the correlation structure of the data, have both been useful in reducing bias in the instrument model, and in better informing uncertainty on inferred rate coefficients. A manuscript is in preparation.

Future Work

The role of singlet and triplet PESs in bimolecular reactions Interactions of two doublet radicals can lead to dynamics on singlet or on triplet surfaces, with the possibility of crossing at various points past the entrance channel. The ubiquitous reactions of peroxy radicals (ROO) with OH, HO_2, RO, or other ROO fall into this category. We propose to conduct experimental and computational studies to elucidate the mechanisms of ROO self-reactions and the details of the of ISC process in determining the branching among the possible product channels. We will focus on small model systems with alkyl and oxygenated R. We will quantify RO, ROOH, and ROOR using PIMS by measuring the observed product yields as a function of $[O_2]$. We hypothesize that systematic variation of $[O_2]$ will allow us to constrain the yields of ROO, RO, ROOH, and ROOR from the overall C atom balance. We will also probe the ROO self-reactions at elevated temperatures where ROOH and ROOR become thermally unstable, providing additional constraints on speciation measurements and on the mechanism. The proposed experiments will be closely coupled to calculations for kinetics and branching on ^{3}RO-OR and ^{1}RO-OR PESs as well as ROO + HO_2 and ROO + R kinetics. We will first establish the methods by which these complicated reactions can be systematically and effectively studied and implement these developments in our automated kinetics workflow code, KinBot, to allow us to then extend the calculations more easily to larger, more complex systems, and understand how for instance the structure of R influences the kinetics.

Detection and Characterization of Reactive Intermediates The reactivity of many chemical intermediates often depends strongly on their structure, and accurate knowledge of their isomer and conformer distributions is therefore critical to unraveling the mechanisms of complex reaction networks. Microwave (MW) spectroscopy readily distinguishes among conformers and powerfully complements photoionization detection, which is sensitive but may lack structural selectivity. However, MW spectroscopy suffers from the small population differences among adjacent rotational levels at typical reaction temperatures. A common way of shifting the rotational Boltzmann peak into the MW region is cooling via supersonic expansions, but this drastically lowers the sample density. As an alternative, we are commissioning a cryo-cooled buffer gas cell (BGC) designed for (i) continuous sampling out of high *T* chemical reactors, (ii) trapping the reactive intermediates for 100 times longer than in a supersonic expansion, and (iii) interrogation of the sampled molecules at $T_{rot} < 20$ K. In addition, a low-noise amplifier on the cold head lowers the noise floor by almost a factor of 8 relative to room temperature. Finally, continuous operation combined with broadband MW excitation enables detection at 50 kHz, 250 times faster than in our pulsed supersonic expansion. Together, these advances will achieve the sensitivity needed to detect short-lived reaction intermediates. Next year, we plan to couple MW detection in the BGC to a high-pressure, high-temperature reactor developed by Sheps at al. (*J. Phys. Chem. A* **2021,** 125 (20), 4467-4479) with the goal of characterizing the key intermediates in hydrocarbon oxidation. We will benchmark our approach by detecting a hydroperoxide compound HPMF (HO_2CH_2OCHO), which was previously identified by photoionization as a key intermediate in high-*P* dimethyl ether oxidation and which has only one structural isomer. Subsequently, we will extend our method to larger hydrocarbons cyclopentane, diethyl ether, and tetrahydrofuran, aiming to determine the isomeric distribution of peroxy radical and hydroperoxide intermediates that is key to unraveling the multi-channel oxidation reactions of these compounds.

Oxidation of norbornadiene: a Molecular Solar Thermal (MOST) storage candidate A long-standing DOE mission goal is the efficient conversion of solar energy to stored chemical energy. One attractive approach to meeting this goal is MOST storage, in which a molecule absorbs sunlight that drives isomerization to a stable, higher enthalpy isomer. That isomer can then be stored and converted back to the more stable isomer, harvesting the exothermicity to do work, at a time of our choosing. Norbornadiene (bicyclo[2.2.1]hepta-2,5-diene) is a leading candidate for MOST systems, via photoconversion to its less-

stable isomer quadricyclane. However, little is known about the oxidation chemistry of norbornadiene and quadricyclane, which will be important to understand when considering their use in a MOST system. We propose to use our PEPICO apparatus to study the time-resolved reactions of OH and $O(^3P)$ with norbornadiene and quadricyclane. Both molecules are bicyclic with ring strain, but norbornadiene is a non-conjugated diene, whereas quadricyclane is a high-strained alkane. It is therefore likely that their oxidation chemistries will be quite distinct. From a fundamental point of view, we are interested in the chemical reactions of multi-cyclic molecules as a function of increasing ring-strain, which will be a generally relevant topic for chemical energy storage systems. We anticipate that automated potential energy surface exploration via KinBot will play an important role in this research.

Stereoisomer-specific kinetics for barrierless reactions Our goal is to experimentally determine the nascent branching fractions of diastereomeric peroxy radicals formed from a series of cyclic organic precursors. We will use both TOFMS detection via PIMS analysis and CP-FTMW spectroscopy in the cryo-cooled buffer gas cell as complementary detection schemes. The broadband microwave spectra will be used for structure identification and to quantify the abundances of products using computed dipole moments that determine the intensities of rotational transitions. The aim of the experiments is to determine the branching and to serve as a benchmark and advance calculations. Our first targets are going to be substituted cyclopentyl or cyclohexyl radicals. At room temperature, O_2 addition produces a menagerie of distinct peroxy radicals in competition with one another. Furthermore, addition in *syn* or *anti* position can lead to diastereomeric products, with distinguishable rotational spectra.

Further developments for automated kinetics. We successfully coupled KinBot to rotdPy, the VRC-TST code of Goldsmith (Brown U), but several open questions remain. VRC-TST is an accurate theoretical framework, which, when applied correctly, can yield errors in the 10-20% range for total rate coefficients. However, for larger systems, theory needs to make compromises in things like basis set and number of sampled points. Moreover, the branching fractions can be sensitive to the location of the dividing surfaces and to dynamic effects. To this end, we will continue our work on automating barrierless calculations in collaboration with Goldsmith and use the stereoisomer-specific experimental results to benchmark our results. We are developing automatic approaches to place pivot points that go beyond just the local geometry of the radical center and will test approaches to select the multireference method automatically as well as implement multidimensional correction potentials.

Criegee chemistry We will continue to explore the chemistry of carbonyl oxide CIs, focusing on the powerful capability of synchrotron PIMS to characterize product channels, including continued collaboration on work led by Rebecca Caravan (ANL), Klippenstein (ANL) and Lester (Penn). We will continue investigations begun this past year on the role of water as a chaperone (or catalyst) for bimolecular reactions of CIs with other species.

Non-thermal processes in heterogeneous environments A neural-network-based machine learning method for non-equilibrium reaction modeling in DSMC based on the quasi-classical trajectory (QCT) calculations was developed and tested on the chain branching reaction $H + O_2 = OH + O$. Further such calculations will enable DSMC to treat fully non-equilibrium reacting flow systems. Three-body recombination reaction models will also be developed and validated in DSMC. New strategies will be devised to include pressure dependence of the recombination reaction rate modelling in DSMC for reactions such as $H + O_2 = HO_2$. our goal is to simulate reacting non-equilibrium systems including 2-D Kelvin–Helmholtz instabilities and 3-D turbulent multi-scale reacting flows using fully integrated non-equilibrium chemistry models.

While chemical non-equilibrium arising due to rovibrationally excited HO_2* and H_2O* was implemented through a phenomenological chemical-kinetics model in macro-scale simulations,[14] the effect of other complexes like H_2O_2* is still unknown. We will use DSMC to assist our macroscale simulations in determining the magnitude of thermal non-equilibrium, and whether to include additional termolecular

reactions. The effect of non-thermal termolecular reactions on the multi-zonal structure of edge-induced oblique detonation wave (ODW) for a stoichiometric H_2-air mixture at scramjet-relevant conditions will be studied with macroscale simulations. Preliminary results show a significant effect of non-thermal reactivity on the location of the transition between different zones in the ODW. The structure of the ODW (i.e., angle of the wave, initiation length, structure of the cellular structure, etc.) is related to the stability of it, which is important for the correct operation of relevant propulsion systems. The underlying mechanism and its effects on cellular structure and hydrodynamics in the flow will be characterized by statistical analysis.

BES-sponsored publications, 2022–present

1. Almeida, T. G.; Martí, C.; Kurtén, T.; Zádor, J.; Johansen, S. L., Theoretical Analysis of the OH-Initiated Atmospheric Oxidation Reactions of Imidazole, *Phys. Chem. Chem. Phys.*, **2024,** 26, 23570-23587.
2. Yuan, E. C.-Y.; Kumar, A.; Guan, X.; Hermes, E. D.; Rosen, A. S.; Zádor, J.; Head-Gordon, T.; Blau, S. M., Analytical ab initio Hessian from a Deep Learning Potential for Transition State Optimization. *Nature Communications*, **2024,** Accepted., https://arxiv.org/abs/2405.02247
3. Doner, A. C.; Zádor, J.; Rotavera, B., Stereoisomer-dependent rate coefficients and reaction mechanisms of 2-ethyloxetanylperoxy radicals. *Proc. Combust. Inst.*, **2024,** In press https://doi.org/10.1016/j.proci.2024.105578
4. Lang, J.; Foley, C. D.; Thawoos, S.; Behzadfar, A.; Liu, Y.; Zádor, J.; Suits, A. G., Reaction dynamics of S(^{3}P) with 1,3-butadiene and isoprene: Crossed beam scattering, low temperature flow experiments, and high-level electronic structure calculations. *Farad. Discuss.*, **2024**, 251, 550-572.
5. Rieth, M.; Gruber, A.; Hawkes, E. R.; Chen, J. H., Direct numerical simulation of low-emission ammonia rich-quench-lean combustion. *Proc. Combust. Inst.* **2024.** In press https://doi.org/10.1016/j.proci.2024.105558.
6. S. Trivedi; J. S. Salinas; M. Lee; S. Desai; M. A. Gallis; J. K. Harvey; J. H. Chen., Comparison of DSMC and multi-temperature simulations of thermal nonequilibrium in a supersonic Kelvin-Helmholtz shear layer. *AIAA SciTech* **2024**. https://doi.org/10.2514/6.2024-2722.
7. Rodhiya, A.; Gruber, A.; Bothien, M. R.; Chen, J. H., Spontaneous ignition and flame propagation in hydrogen/methane wrinkled laminar flames at reheat conditions: Effect of pressure and hydrogen fraction. *Combust. Flame* **2024**, 269, 113695.
8. Salinas, J. S.; Baranwal, A.; Chen, J. H.; Desai, S.; Tao, Y.; Poludnenko, A., Non-thermal termolecular reactions effects on hydrogen-air planar detonation. *AIAA SciTech* **2024**. https://doi.org/10.2514/6.2024-2783.
9. DeCecco, A. C.; Conrad, A. R.; Floyd, A. M.; Jasper, A. W.; Hansen, N.; Dagaut, P.; Moody, N.-E.; Popolan-Vaida, D. M., Tracking the Reaction Network of Acetaldehyde Oxide and Glyoxal Oxide Criegee Intermediates in the Ozone-Assisted Oxidation Reaction of Crotonaldehyde. *Phys. Chem. Chem. Phys.,* **2024,** 26, 22319-22336.
10. Li, H.; Lang, J.; Foley, C. D.; Zádor, J.; Suits, A. G., Sulfur (^{3}P) reaction with conjugated dienes gives cyclization to thiophenes under single collision conditions. *J. Phys. Chem. Lett.,* **2023,** *14,* 7611–7617.
11. Zádor, J.; Martí, C.; Van de Vijver, R.; Johansen, S. L.; Yang, Y.; Michelsen, H. A.; Najm, H. N., Automated reaction kinetics of gas-phase organic species over multiwell potential energy surfaces. *J. Phys. Chem. A* **2023,** *127,* 565–588.
12. Doner, A. C.; Zádor, J.; Rotavera, B., Unimolecular reactions of 2,4-dimethyloxetanyl radicals. *J. Phys. Chem. A* **2023,** *127* (11), 2591–2600.
13. Hellmuth, M.; Chen, B.; Bariki, C.; Cai, L.; Cameron, F.; Wildenberg, A.; Huang, C.; Faller, S.; Ren, Y.; Beeckmann, J.; Leonhard, K.; Heufer, K. A.; Hansen, N.; Pitsch, H., A comparative study on the combustion chemistry of two bio-hybrid fuels: 1,3-dioxane and 1,3-dioxolane. *J. Phys. Chem. A* **2023,** *127* (1), 286-299.
14. Desai, S.; Tao, Y.; Sivaramakrishnan, R.; Chen, J. H., Effects of non-thermal termolecular reactions on wedge-induced oblique detonation wave. *Combust. Flame* **2023,** *doi:10.1016/j.combustflame.2023.112681*.
15. Rieth, M.; Gruber, A.; Chen, J. H., The effect of pressure on lean premixed hydrogen-air flames. *Combust. Flame* **2023,** *250*, 112514.
16. Rieth, M.; Gruber, A.; Chen, J. H., A direct numerical simulation study on NO and N2O formation in turbulent premixed ammonia/hydrogen/nitrogen-air flames. *Proc. Combust. Inst.* **2023**.
17. Hu, Z.; Di, Q.; Liu, B.; Li, Y.; He, Y.; Zhu, Q.; Xu, Q.; Dagaut, P.; Hansen, N.; Sarathy, S. M.; Xing, L.; Truhlar, D. G.; Wang, Z., Elucidating the photodissociation fingerprint and quantifying the determination of organic hydroperoxides in gas-phase autoxidation. *Proc. Nat. Acad. Sci.* **2023,** *120* (10), e2220131120.
18. Rösch, D.; Jones, G. H.; Almeida, R.; Caravan, R. L.; Hui, A.; Ray, A. W.; Percival, C. J.; Sander, P. S.; Smarte, M. D.; Winiberg, F. A. F.; Okumura, M.; Osborn, D. L., Conformer-dependent chemistry:

Experimental product branching of the vinyl alcohol + OH + O2 reaction. *J. Phys. Chem. A.* **2023,** *127* (14), 3221–3230

19. Kohse-Höinghaus, K.; Ferris, A.M.; Zetterberg, J.; Lacoste, D. A.; Fjodorow, P.; Wagner, S.; Cai, L.; Rudolph, C.; Zádor, J.; Li, Y.; Ruwe, L.; Gaiser, N.; Wang, Z.; Geigle, K., P., *Chemistry diagnostics for monitoring.* In Combustion Chemistry and the Carbon Neutral Future: What will the next 25 years of research require?" Elsevier, **2023**.

20. Zou, M. J.; Liu, T. L.; Vansco, M. F.; Sojdak, C. A.; Markus, C. R.; Almeida, R.; Au, K. D.; Sheps, L.; Osborn, D. L.; Winiberg, F. A. F.; et al. Bimolecular Reaction of Methyl-Ethyl-Substituted Criegee Intermediate with SO_2. *J. Phys. Chem. A* **2023**, *127* (43), 8994-9002.

21. Liu, T. L.; Elliott, S. N.; Zou, M. J.; Vansco, M. F.; Sojdak, C. A.; Markus, C. R.; Almeida, R.; Au, K. D.; Sheps, L.; Osborn, D. L.; et al. OH Roaming and Beyond in the Unimolecular Decay of the Methyl-Ethyl-Substituted Criegee Intermediate: Observations and Predictions. *J. Am. Chem. Soc.* **2023**, *145* (35), 19405-19420.

22. Oreluk, J., Sheps, L., and Najm, H., Bayesian model calibration for vacuum-ultraviolet photoionization mass spectrometry, *Combust. Theory Model.*, **2022**, 26(3):513-540.

23. Im, H.; Chen, J. H.; Apsden, A., Direct numerical simulation perspective. In *Turbulent combustion physics*, Swaminathan, N. B., X.-S.; Fureby, C.; Haugen, N. E. L.; Brethouwer, G., Ed. Cambridge University Press: **2022**.

24. Kang, S.; Liao, W.; Sun, W.; Lin, K.; Liao, H.; Moshammer, K.; Dagaut, P.; Hansen, N.; Yang, B., Exploring low-temperature oxidation chemistry of 2- and 3-pentanone. *Combust. Flame* **2022**, 112561.

25. Huang, C.; Zhao, Y.; Roy, I. S.; Chen, B.; Hansen, N.; Pitsch, H.; Leonhard, K., Pathway exploration in low-temperature oxidation of a new-generation bio-hybrid fuel 1,3-dioxane. *Proc. Combust. Inst.* **2022**.

26. Demireva, M.; Oreluk, J.; Dewyer, A. L.; Zádor, J.; Sheps, L., Genetic algorithm optimization of a master equation cyclopentane oxidation model against time-resolved speciation experiments. *Combust. Flame* **2022**, 112506.

27. Doner, A. C.; Zádor, J.; Rotavera, B., Stereoisomer-dependent unimolecular kinetics of 2,4-dimethyloxetanyl peroxy radicals. *Faraday Discuss.* **2022,** *238* (0), 295-319.

28. Popolan-Vaida, D. M.; Eskola, A. J.; Rotavera, B.; Lockyear, J. F.; Wang, Z.; Sarathy, S. M.; Caravan, R. L.; Zádor, J.; Sheps, L.; Lucassen, A.; Moshammer, K.; Dagaut, P.; Osborn, D. L.; Hansen, N.; Leone, S. R.; Taatjes, C. A., Formation of organic acids and carbonyl compounds in n-butane oxidation via γ-ketohydroperoxide decomposition. *Angew. Chem. Int. Ed.* **2022,** *61* (42), e202209168.

29. Rieth, M.; Gruber, A.; Williams, F. A.; Chen, J. H., Enhanced burning rates in hydrogen-enriched turbulent premixed flames by diffusion of molecular and atomic hydrogen. *Combust. Flame* **2022,** *239*, 111740.

30. Vansco, M. F.; Zou, M.; Antonov, I. O.; Ramasesha, K.; Rotavera, B.; Osborn, D. L.; Georgievskii, Y.; Percival, C. J.; Klippenstein, S. J.; Taatjes, C. A.; Lester, M. I.; Caravan, R. L., Dramatic conformer-dependent reactivity of the acetaldehyde oxide Criegee intermediate with dimethylamine via a 1,2-insertion mechanism. *J. Phys. Chem. A* **2022,** *126* (5), 710-719.

31. Desai, S.; Tao, Y.; Sivaramakrishnan, R.; Wu, Y.; Lu, T.; Chen, J. H., Effects of non-thermal termolecular reactions on detonation development in hydrogen (H2)/methane (CH4) - air mixtures. *Combust. Flame* **2022,** *244*, 112277.

32. Caster, K. L.; Lee, J.; Donnellan, Z.; Selby, T. M.; Osborn, D. L.; Goulay, F., Formation of a resonance-stabilized radical intermediate by hydroxyl radical addition to cyclopentadiene. *J. Phys. Chem. A* **2022,** *126* (48), 9031-9041.

33. Valorani, M.; Malpica Galassi, R.; Ciottoli, P. P.; Najm, H.; Paolucci, S., The spectral characterisation of reduced order models in chemical kinetic systems. *Combust. Theory Model.* **2022,** *26* (7), 1185-1216.

34. Han, X.; Najm, H. N., Modeling fast diffusion processes in time integration of stiff stochastic differential equations. *Comm. App. Math. Comp. Sci.* **2022,** *4* (4), 1457-1493.

ELECTRON-DRIVEN CHEMISTRY

David W. Chandler, Jonathan H. Frank, Laura M. McCaslin, Krupa Ramasesha, Tim Zwier
Sandia National Laboratories, MS 9051, Livermore, CA 94551-0969
chand@sandia.gov, jhfrank@sandia.gov, lmmccas@sandia.gov, kramase@sandia.gov, tszwier@sandia.gov

PROGRAM SCOPE

Electron-driven chemistry, which we define as chemical transformations driven by an initial charge separation or addition, underpins many areas of interest to the DOE. The goal of this program is to deepen understanding of reactivity that is driven by motion of charges. We will apply a combination of sophisticated experimental and theoretical methodologies to provide detailed time- and state-resolved views of complex charge-transfer processes. These investigations will illuminate phenomena that defy the common simplifying assumptions of the Hartree-Fock and Born-Oppenheimer approximations and will aid in developing more sophisticated descriptions of coupled electron and nuclear motion. This work extends the research we have done on neutral processes, using quantum state-resolved experiments that provide detailed information about molecular potential energy landscapes and the dynamics involving coupled potential energy surfaces. We pursue experiments that include: 1) induced charge separation in an isolated molecule, 2) dynamics following attachment of a free electron to a neutral molecule or cluster, and 3) coupled chemical and physical evolution of a laser-induced plasma. In each area, we apply advanced techniques, including techniques presently being developed, to provide a new and deeper understanding of chemical physics processes. This effort complements research being performed in the Solar Photochemistry and Condensed-Phase and Interfacial Molecular Sciences programs and addresses BES Grand Challenges associated with the study of the nature of excited electronic states and the breakdown of the Born-Oppenheimer approximation. This research is closely tied to other work in our program. The study of ultrafast intramolecular charge transfer dynamics of large conjugated systems has strong connections to the ultrafast non-adiabatic dynamics and the detection schemes being developed in the Ultrafast Chemistry and Physics subtask. Research described in this subtask extends the work performed under the Chemical Dynamics subtask to investigate inelastic collisions of electrons with molecules and charge transfer and reaction after photoexcitation of a molecule.

RECENT PROGRESS

Advances in apparatus for Velocity Mapped Imaging of electron interactions

Our recently developed VMI apparatus for high-resolution electron scattering and excited-state dissociative electron attachment (DEA) has enabled studies of the dynamics of electron-driven chemistry in well-controlled, field-free conditions. We previously demonstrated VMI imaging of photoelectrons in a Kr plasma using electrically grounded fine metal meshes to create a field-free interaction region that was shielded from the electric field produced by the electrostatic imaging lens. However, for imaging of cations and anions, these meshes cause substantial blurring and reduce velocity resolution. We have since removed these meshes and demonstrated that high quality VMI images can be obtained using a pulsed imaging lens that is initially grounded to create a field-free interaction region and then rapidly energized during the ion extraction process. Figure 1 shows a direct comparison of VMI images of methyl cations generated from photo-dissociation of CH_3I followed by REMPI of the methyl radical species, taken with continuous extraction (where ion optic voltages are on continuously) and "field-free" pulsed extraction (where ion optic voltages are pulsed on after the interaction). The methyl cation

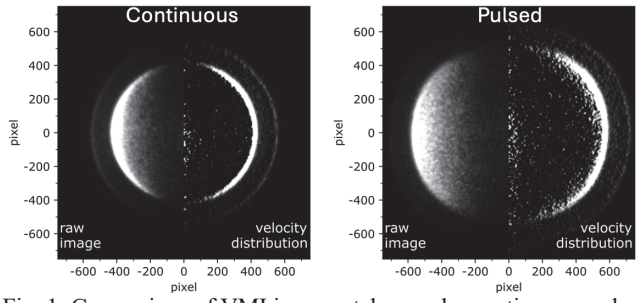

Fig. 1: Comparison of VMI images, taken under continuous and field-free pulsed extraction, of methyl cations from two-color photodissociation experiments on methyl iodide. The raw image and the image after Abel transform are shown on the left and right halves of each plot, respectively.

images show two distinct rings that are clearly captured in both approaches with only differences in the magnification of the overall image. The capability to record high-resolution VMI images under field-free conditions is critical to all the proposed electron-driven chemistry experiments.

The next stage of electron-driven chemistry VMI experiments requires that the electron, laser, and molecular beams be spatially and temporally overlapped in the interaction region. We identify this overlap condition by generating NO^+ cations in the interaction region with 1+1 REMPI using 226.25 nm photons and electron impact ionization using 20 eV electrons. The laser traverses vertically, intersecting the molecular beam and forming the line shaped spatial image shown in Fig. 2a. The electron beam traverses horizontally, forming a diffuse cloud of cations shown in Fig. 2b due to the much larger beam diameter (2-3 mm) of the electron beam. When both the laser and electron beams are present, the REMPI process initiated by the laser depletes the available parent NO molecules in the molecular beam, leading to a decrease in ion signal where the beams overlap, as shown in Fig. 2c. This method for precisely overlapping the beams has facilitated our ongoing studies of increasingly complex electron-driven processes, such as interactions with excited-state molecules and radicals.

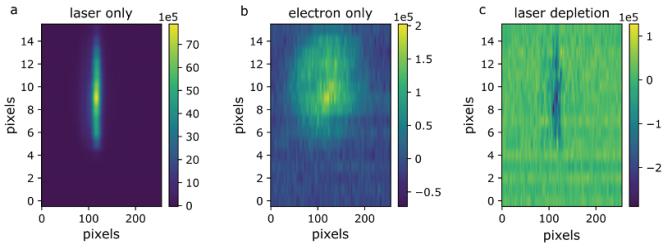

Fig. 2: Depletion of NO^+ signal confirms spatial overlap of electron, laser, and molecular beams on three orthogonal axes. Images are binned vertically by 128 pixels and horizontally by 8 pixels. (a) Spatial image of NO^+ generated through 1+1 REMPI with 226.25 nm photons. (b) Spatial image of NO^+ generated by electron impact with 20 eV electrons. (c) Spatial image of NO^+ generated by both 226.25 nm photons and 20 eV electrons after subtracting the laser only (a) and the electron only (b) backgrounds.

Formation of NO_2^- by electron transfer in Rydberg collisions

Recent experiments on electron transfer in Rydberg collisions build on our previously demonstrated ability to monitor the temporal evolution of ionic species in an ultracold plasma of NO/SF_6, where laser-excited NO Rydberg states can transfer an electron to SF_6 and form SF_6^- anions and NO^+ cations. The addition of electron acceptors such as SF_6 provides a means to tune the properties of a plasma by dramatically limiting electron-driven relaxation processes such as dissociative and three-body recombination. To further our studies of electron accepters in plasma systems, we investigated NO_2 as an electron acceptor, which has an electron affinity of 2.25 eV, approximately twice that of SF_6. Another key difference between NO_2 and SF_6 is the number of internal degrees of freedom that are available for energy partition upon electron attachment. Upon direct attachment of a low energy electron, SF_6^- is formed as a long-lived stable anion, whereas NO_2^- is transient with a ~13 ns lifetime due to autodetachment of the electron. Stable NO_2^- is only formed through three-body processes where excess energy is partitioned into translational degrees of freedom of NO_2^- and its partner in a Van der Waals cluster. The black trace in Fig. 3a shows an action spectrum of the NO^+ cation extracted 60 ns after two-color ($\omega_1 + \omega_2$) excitation of NO in a pulsed supersonic molecular beam of 10% NO in He. The ω_1 frequency is tuned to the $A \leftarrow X\, Q_1(0.5)$ transition, and the ω_2 frequency is varied to excite transitions in the f Rydberg series of NO that converges to the second rotational state of the cation ($N^+ = 2$). The NO^+ cations are formed by field-ionization of the Rydberg state NO molecules, and the observed series of discrete peaks confirms the formation of Rydberg states. The onset energy at which these peaks blend to form a continuum is dependent on the residual weak electric fields in the interaction region, which causes l-mixing of the different Rydberg series. The observed onset energy of the continuum is around 30515 cm^{-1}, which is higher than our previous measurements (near 30500 cm^{-1}), indicating that the residual fields are further eliminated in the interaction region with the field-free pulsed extraction scheme compared to shielding electric fields with metal meshes.

To investigate Rydberg electron transfer to the electron acceptor NO_2, we perform similar experiments with a supersonic beam of 7% NO and 2% NO_2 in He. The red trace in Fig. 3a shows the NO_2^- anion signal under identical experimental parameters except for the polarity of the ion optics. While the signal is more than an order-of-magnitude weaker than that of NO^+, clear bursts of NO_2^- signals are observed at the resonant frequencies of the Rydberg states of NO, indicating that Rydberg electron transfer is the primary mechanism

in the formation of the NO_2^- anion. We measured the VMI images of the NO_2^- anion at two distinct regions of the Rydberg spectra, as shown in Fig. 3b for the $n = 58$ state of the f Rydberg series of NO and in Fig. 3c for high lying Rydberg states of NO near the ionization potential. The images appear quite similar and show a clear ring. By performing an inverse Abel transform and angularly integrating the ion counts, we obtain the integrated velocity distribution shown in Fig. 3d. The integrated velocity distributions of the NO_2^- anions at the two Rydberg regions are identical to within experimental accuracy and show a recoil that peaks at 0.5 eV with a shoulder extending to approximately 1 eV. The upper threshold is consistent with the expected excess energy release from the electron affinity of NO_2. The broad recoil distribution could be due to a distribution of cluster sizes and partition of energy into internal degrees of freedom. Experiments that vary the molecular beam conditions are ongoing to provide further insights.

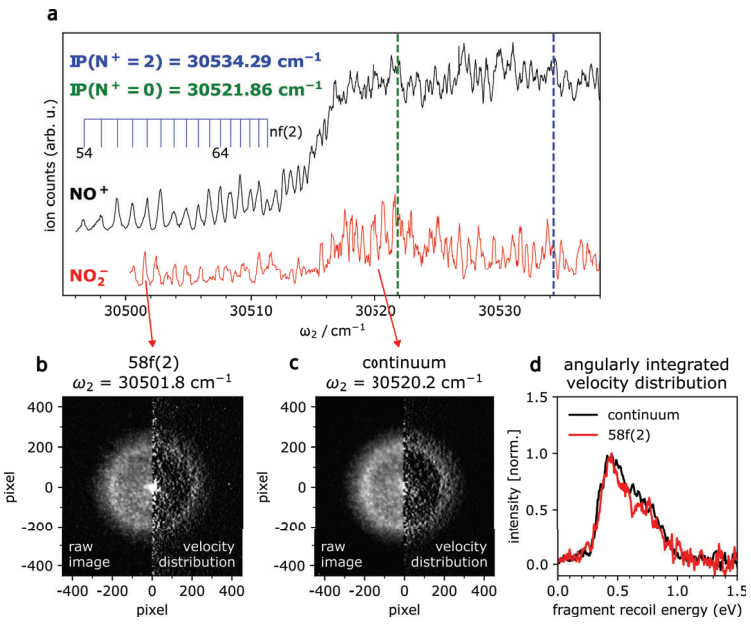

Fig. 3: (a) (black) NO^+ signal extracted from supersonic expansion of 10% NO in He 60 ns after two-color ($\omega_1 + \omega_2$) excitation of NO. (red) NO_2^- signal for 7% NO and 2% NO_2 in He. ω_1 excites $A \leftarrow X\ Q_1(0.5)$ transition of NO. Green and blue vertical dashed lines mark the ground state ionization potential of NO and the N=2 convergence limit of the f Rydberg series of NO, respectively. Predicted energy of nf(N=2) Rydberg series of NO are also shown. (b) Raw VMI image of NO_2^- (left half) and corresponding velocity distribution (right half) obtained from inverse Abel transform for the $n = 58$ state of the N=2 f Rydberg series of NO. (c) Raw VMI image of NO_2^- (left half) and the corresponding velocity distribution (right half) near the convergence limit of the N=2 f Rydberg series of NO. (d) Radially integrated velocity distribution of the NO_2^- images shown in (b) and (c).

Planned experiments include comparisons of NO/SF_6 with similar mixing ratios to the present NO/NO_2 study. Previous NO/SF_6 at 20% SF_6 concentration showed only SF_6^- signals at the highest lying Rydberg states, which we attributed to the formation of ion pairs of NO^+ and SF_6^- that trap the anion when the anion-cation separation distance is small. In contrast, the NO_2^- anion is observed across a wide range of Rydberg states, possibly due to the large recoil energy of the NO_2^- anions enabling them to escape from the ion pair potential. Direct comparison between electron acceptors with different electron affinities at various concentrations will shed light on the role of three-body processes in these systems.

Unraveling the role of intramolecular charge transfer driving singlet-triplet inversion in thermally activated delayed fluorescence materials

In the quest to design highly efficient organic light emitting devices (OLEDs), materials can be designed to exhibit thermally activated delayed fluorescence (TADF). TADF materials are designed such that the S_1-T_1 energy gap (ΔE_{ST}) is very small, enabling reverse intersystem crossing (RISC) from the T_1 to the S_1 state, where delayed fluorescence can occur. A new class of molecules, deemed inverted singlet-triplet molecules (INVEST), have been designed such that the S_1 state is lower in energy than the T_1 state. These molecules are often designed with alternating atoms in a core aromatic moiety such that the HOMO electron density is localized on one set of atoms and the LUMO on another. However, efficient and reliable quantum chemistry calculations of the negative quantity ΔE_{ST} in INVEST molecules are challenging due to the necessity of including double excitations in treatment of the electron correlation. This means that workhorse methods such as time-dependent density functional theory (TDDFT) cannot determine the correct sign of ΔE_{ST}. Development of high-throughput screening procedures for proposing novel INVEST molecules

require chemical rules and reliable quantum chemistry methods. To this aim, we have generated a novel test set of INVEST molecules by functionalizing a heptazine core, which is known to exhibit a negative value of ΔE_{ST}. Additionally, we have identified two metrics that quantify the degree of intramolecular charge transfer and find that they linearly correlate with ΔE_{ST}, resulting in new orbital structure-function relationships for design of next-generation INVEST molecules. Future directions include testing our charge transfer metrics on other classes of INVEST systems as well as searching for new ones.

FUTURE WORK

Laser-produced plasma initiation dynamics

The combination of VMI with well-controlled laser-generated plasmas opens many opportunities for detailed studies of chemical reactions of molecules in plasmas with tunable electron energy distributions. In the next year, our plasma-chemistry studies will focus on nitric oxide (NO), which can be used both to generate the plasma and to study plasma chemistry.

We will form plasmas either through excitation of NO Rydberg states or by laser ionization of NO molecules. This is done by first exciting the NO(A) state, which has a 200 ns lifetime. A second laser then excites from the A state either a long-lived Rydberg that evolves into a plasma or excites the NO(A) with sufficient energy to directly ionize it. After the plasma forms and is thermalized (tens of nanoseconds), we will send in another laser pulse to generate more Rydberg state molecules or add electrons of a known energy within the plasma as we do not deplete the NO(A) state population when we form the plasma. These perturbations will be monitored by imaging the electrons.

There are several interesting processes that are thought to happen within the early times of these plasmas that generate neutral N and O atoms. One process is the electron capture of some of the electrons by NO^+ cations forming an excited dissociative state of NO. A second mechanism is the Penning ionization that occurs when two Rydberg excited NO molecules (denoted as NO(R)) collide and one NO(R) generates a cation-electron pair and the second NO(R) is deactivated and dissociates. Both processes can be studied and differentiated by laser ionization of the N and O atoms and velocity imaging them. In this manner, the quantum state populations of the fragments will be determined. These processes are expected to be Rydberg number dependent as the size and velocity of the electrons may contribute to these processes. For instance, large Rydberg state molecules, high N, require only a small amount of energy transfer to ionize and they are much more likely to encounter either a free electron and ionize or another Rydberg and Penning ionize. This physics will be directly measured and quantified.

Dynamics following attachment of a free electron to a neutral molecule: Experimental studies

Detailed insights into the fundamental chemical interactions that occur in charge distributions such as plasmas can be obtained by investigating the dynamics following attachment of free electrons to isolated molecules or clusters. For these studies, our electron scattering apparatus has two characteristics that we are taking advantage of. One is the high energy resolution of the electrons dictated by the frequency spread of the laser beam. This allows us to scan the frequency of the laser and thereby scan the energy of the electrons with approximately 0.5 cm^{-1} (0.06 meV) resolution. This feature is essential for resolving narrow low energy resonances. In the next year, these studies will focus on DEA of nitric oxide and sulfur dioxide.

To better understand dynamics of electron attachment to ground state NO followed by detachment, we will scan the energy of the electrons through low energy resonances of NO. We will then use 1+1 REMPI to detect the formation of vibrationally excited NO. In this manner, we will measure the natural linewidth of the resonances associated with production of vibrationally excited ground state transient ions and determine the lifetime of the transient anions. We will also take advantage of the time resolution of using pulsed lasers to produce the electrons. The electrons traverse the molecular beam in a time that is shorter than the laser pulse duration. Therefore, all transient anions will be formed during the 5-ns laser pulse as the electrons encounter molecules in the molecular beam. As we have control over the time of the electron generation, we can excite a molecule in the molecular beam prior to the electron production. In this manner, we will study the production of transient anions from electronically excited states of NO and SO_2.

Dissociative electron attachment to nitric oxide exhibits significant changes for attachment to the ground and electronically excited states that require a more detailed understanding. DEA to ground state NO requires a minimum electron energy of approximately 7.5eV. In contrast, DEA to electronically excited NO in the $A^2\Sigma^+$ state (5.48 eV) is exothermic by 0.45eV, and the DEA cross sections are three orders of magnitude larger for the electronically excited state.[1] This extraordinary enhancement in the cross section is associated with a Feshbach resonance. The dissociation channel in the excited state also differs from that of ground state NO. DEA to ground state NO primarily produces $N(^2D) + O^-(^2P)$, and DEA to electronically excited NO(A) produces $N(^4S) + O^-(^2P)$.[2] The sensitivity of the DEA enhancement and branching of dissociation channels to varying levels of vibronic excitation are not well established. We plan to investigate the enhancement and branching ratios of DEA to excited-state NO by selective laser excitation to different vibronic states prior to electron attachment.

Electronic excitation of sulfur dioxide, SO_2, has profound effects on the dissociation channels following electron attachment, resulting in nearly complete suppression in the production of some ionic fragments. For DEA to SO_2 in the excited electronic state ($\tilde{B}^1B_1$), the cross sections for formation of products O^- and SO^- are enhanced by factors of 6 and 1.5, respectively, while the formation of S^- is almost entirely suppressed.[3] Previous studies of these effects of DEA to excited state SO_2 primarily focused on using time-of-flight mass spectrometry (TOFMS) and included limited investigation into the sensitivity of cross sections and product channels to different levels of excitation. We will conduct a series of detailed studies of DEA to SO_2 using velocity mapped imaging to provide mass selective detection of the kinetic energy and angular distribution of the DEA fragments following laser excitation of the parent molecule.

Dynamics following attachment of a free electron to a neutral molecule: Theoretical studies

We will pair experimental studies with theoretical investigations of the DEA processes in excited-state molecules. In order to probe the underlying dynamics and electronic structure involved in the vibrational- and electronic-state dependence of reactions such as $SO_2 + e^-$, non-adiabatic mixed quantum-classical (NA-MQC) dynamics calculations will be performed. Though these are relatively small systems, the electronic structure is quite difficult to describe due to the multiconfigurational nature of the wavefunctions. Electronic structure methods such as equation-of-motion coupled cluster in its electron-attachment variant (EOM-EA-CCSD) will be benchmarked against methods that incorporate treatments of both static and dynamic electron correlation such as MRCI in order to identify methods with an appropriate balance of accuracy and computational efficiency for employment in dynamics calculations.

Electron attachment to free radicals

The dynamics following electron attachment to free radicals are not well understood. To expand our studies of radicals beyond NO, we plan to investigate electron attachment to fluorocarbon radicals such as trifluoromethyl (CF_3). Interactions of CF_3 with low-energy (<20 eV) electrons have proven challenging to model, and there is a need for more detailed understanding because CF_3 plays a central role in plasma etching for microelectronics fabircation. For example, calculated differential cross sections significantly underestimated measured cross sections at electron energies of 20 eV and below.[4] In addition, some theory calculations previously suggested that CF_3 would not undergo DEA due to a lack of low-lying resonances, but experiments have shown both dissociative and non-dissociative electron attachment to CF_3.[5] We will form CF_3 in the interaction region of the VMI appartus by photodissociation of trifluoroiodomethane (CF_3I) in a similar manner to our recent experiments that used CH_3I as the photolytic precursor for CH_3. We will measure the products following electron attachment to CF_3 and the kinetic energy distirbutions to provide insights into the energy partitioning of the products. Electron attachment to the CF_3I precursor will also be investigated to improve fundamental understanding of its electron interactions. The CF_3I molecule has been suggested as a candidate alternative insulating gas in high voltage discharges for the impending phase-out of SF_6 usage. However, further insights into the dynamics following CF_3I electron attachment are needed.

Site-specific reactivity governed by unpaired electron spin density

Resonance-stabilized radicals such as the ground state of the phenoxy radical, distribute their unpaired spin density throughout the extended π cloud of the singly-occupied molecular orbital. The unpaired spin density, in turn, couples to other sources of angular momentum, most notably the over-all rotational angular momentum and the unpaired nuclear spins of ^{1}H, ^{14}N, or ^{13}C atoms, leading to splittings in the rotational transitions of the free radical that reflect these unpaired spin densities. We have recently recorded a preliminary CP-FTMW spectrum of the *ortho*-pyridoxy radical over the 7.5-17.5 GHz range after forming the radical in a pulsed electric discharge of 2-methoxy pyridine. Given the large number of angular momentum coupling terms, each rotational transition is split into almost 100 individual transitions spread over several MHz in the spectrum, which are partially resolved at our resolution. We have a preliminary fit to the spectrum that requires further refinement. Calculations predict that the unpaired spin density at the nitrogen site is far smaller than at the corresponding *ortho* carbon in phenoxy radical, and this is consistent with our experimental best fit. This shift in unpaired spin density will redirect further reaction to the remaining three sites (*ortho*- and *para*-C and O) of principle unpaired spin density based on resonance structures, which are shown in Fig. 4.

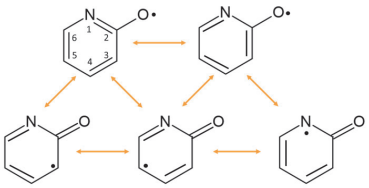

Fig. 4: Resonance structures of 2-pyridoxy radical.

BES-sponsored publications, 2022-present

1. Smoll, E. J.; Jana, I.; Frank, J. H.; Chandler, D. W., Velocity-mapped imaging of electron dynamics in an ultracold laser-induced plasma. *Phys. Rev. A* **2023**, *108* (4), L041301.

References

1. Kuo, C. T.; Hardwick, J. L.; Moseley, J. T., Low-energy-electron attachment to excited nitric oxide. *J. Chem. Phys.* **1994,** *101* (12), 11084-11085.
2. Kuo, C. T.; Ono, Y.; Hardwick, J. L.; Moseley, J. T., Dissociative attachment of electrons to the A $^{2}\Sigma^{+}$ state of nitric oxide. *J. Phys. Chem.* **1988,** *92* (18), 5072-5074.
3. Krishnakumar, E.; Kumar, S. V. K.; Rangwala, S. A.; Mitra, S. K., Dissociative-attachment cross sections for excited and ground electronic states of SO_2. *Phys. Rev. A* **1997,** *56* (3), 1945-1953.
4. Brunton, J. R.; Hargreaves, L. R.; Buckman, S. J.; García, G.; Blanco, F.; Zatsarinny, O.; Bartschat, K.; Brunger, M. J., Anomalously large low-energy elastic cross sections for electron scattering from the CF3 radical. *Chem. Phys. Lett.* **2013,** *568-569*, 55-58.
5. Shuman, N. S.; Miller, T. M.; Friedman, J. F.; Viggiano, A. A.; Maergoiz, A. I.; Troe, J., Pressure and temperature dependence of dissociative and non-dissociative electron attachment to CF3: Experiments and kinetic modeling. *J. Chem. Phys.* **2011,** *135* (5).

IMAGING THE NEAR-SURFACE GAS PHASE: A NEW APPROACH TO COUPLED GAS-SURFACE CHEMISTRY

Jonathan H. Frank, Nils Hansen, Christopher J. Kliewer, David L. Osborn
Sandia National Laboratories, Livermore, CA
jhfrank@sandia.gov, felgaba@sandia.gov, nhansen@sandia.gov, cjkliew@sandia.gov, dlosbor@sandia.gov
Coleman Kronawitter and Ambarish Kulkarni
Department of Chemical Engineering, University of California, Davis
ckrona@ucdavis.edu, arkulkarni@ucdavis.edu

PROGRAM SCOPE

The chemical reactivity of gases with solid surfaces is ubiquitous in natural and industrial energy transformation. Cooperative effects that couple gas phase chemistry with surface chemistry are critical for foundational understanding but challenging to probe experimentally and theoretically. Heterogeneous catalysis is an ideal field to expose and isolate the fundamental chemical physics of these cooperative effects. Our program seeks to characterize gas-surface coupling through chemically specific, temporally, and spatially resolved probes of both reacting surfaces and the near-surface gas phase. The program combines optical spectroscopy with mass spectrometry and photoelectron spectroscopy of both gas phase and surface species. The long-term goal is to elucidate the fundamental mechanisms of cooperative gas-surface chemistry, influencing DOE mission research in catalysis, synthesis, and energy transformation.

Our research explores two key physical mechanisms of gas-surface coupling – transport and reaction – and employs a range of chemical complexity and control over the model catalyst surface. First, we probe how molecular transport in the gas phase mediates coupling between different domains on a surface without gas-phase chemical reactions. This work employs well-controlled reactions on atomically cleaned crystalline and polycrystalline surfaces prepared under ultra-high vacuum (UHV) conditions, with reactivity studied under pressures of 10^{-6} to 760 Torr. Second, we add the complexity of reactive coupling, with bond breaking and formation among intermediates occurring in the gas phase as well as on the surface. This work utilizes both polycrystalline films and more complex surfaces (e.g., doped metal oxides, and bifunctional supported catalysts), with reactivity studied at elevated temperatures (400 - 1250 K) and pressures of 1 - 760 Torr.

RECENT PROGRESS

Development of a Sensitive Scheme for Near-surface Imaging of H_2O: Rydberg Resonant Femtosecond Laser Induced Photofragmentation Fluorescence One of the simplest, and oldest known gas-surface catalytic reactions is H_2 + O_2 over Pt and Rh. Over Pt(111), recent velocity-resolved kinetics work demonstrated that, within currently accepted microkinetic models, we either do not yet consider the appropriate reaction site for H (s) + O (s) → OH (s), or there must be an as-of-yet unconsidered reactive intermediate pathway to the formation of H_2O (s). In recent work, we have developed a new scheme for the sensitive detection and imaging of water vapor produced by this reaction. This important capability now allows us to explore the effect of step and defect density on local catalytic activity, which will unambiguously point to whether or not steps are involved in the discrepancy between current models and observed reaction rates for this reaction network. Even though there is much interest in measuring and imaging water distributions, this species does not have a strong laser induced fluorescence transition. The accessible excited states of water are short lived and undergo non-radiative relaxation pathways. The most studied of these weak fluorescent pathways is the $\tilde{C} \rightarrow \tilde{A}$ transition. Studies at atmospheric pressure and in flames show that the detection limit is ~0.2%–0.4% of atmospheric pressure (~5 × 1016 molecules/cm3) per single shot. This sensitivity was not sufficient for our planned studied over multi-domain and curved Pt and Rh crystals. Single photon absorption studies have shown excitations to highly excited Rydberg resonances at ~19, 25, 28, and 31 eV. These high-energy transitions can lead to neutral dissociation into excited states of the photofragments (H and OH). Specifically, the 19 eV Rydberg state has been seen to

produce H atoms in excited states up to n = 9. These fragments can then be sensitively detected with their fluorescence. The most detectable set of emission lines are the Balmer series, which correspond to radiative relaxation from n > 2 to the n = 2 level of hydrogen. The lowest energy Balmer series line is at 656.279 nm and the higher lines asymptotically approach 364.5 nm, with frequencies predicted by the Rydberg formula.

We recently showed that by using femtosecond UV pulses of light, H_2O can be detected using 2 + 2 femtosecond laser induced photofragmentation fluorescence (fs-LIPF). Two different channels, OH(Ã) and H atom Balmer series emission can be excited at the same time from the same color of light, as shown in Figure 1. This resonant intermediate state allows for efficient coupling into the highly excited Rydberg state that leads to the Balmer fluorescence. This emission (from both channels) can be used to image water down to ~10^{12} cm^{-3} densities. During the present year, we are using this new approach to quantify catalytic turnover for hydrogen oxidation as a function of step density to clarify mechanistic deficiencies.

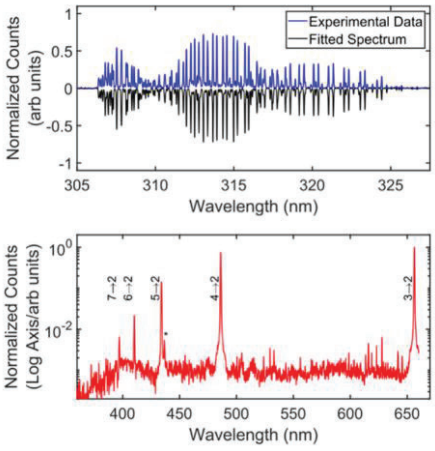

Figure 1. *Emission spectrum of H_2O photofragmentation. Top: OH(Ã) emission spectrum. Bottom: Balmer series hydrogen emission.*

Metal surface restructuring and phase change driven by the chemical potential of high pressure oxygen

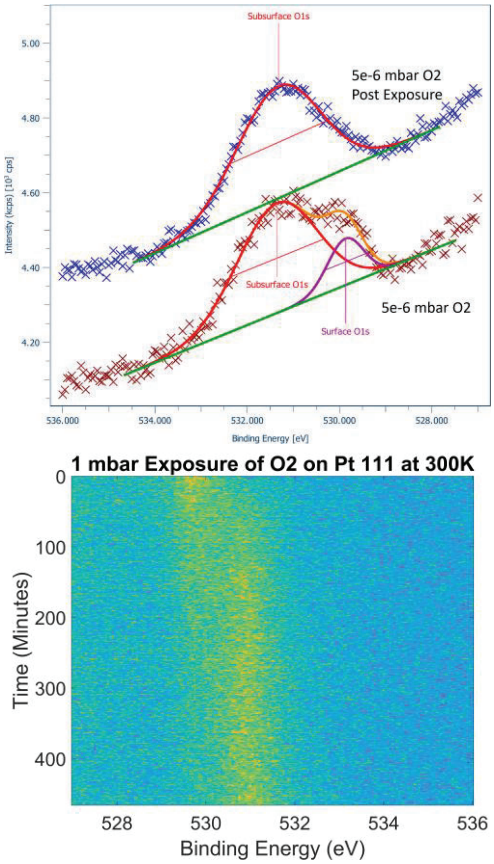

Figure 2. *(top) AP-XPS spectra of Pt(111) exposed to 5*10^{-6} Torr O_2 both before and after the chamber was evacuated. (bottom) Time-resolved exposure of Pt(111) to 1 Torr of O_2*

In high pressure environments (near atmospheric pressure or higher) new surface-bound phases and metal structures are formed at metal surfaces. This is one of the most glaring pieces of evidence of the so called "pressure gap", in that measurements under UHV conditions could never replicate such surface phases. One such system is the interaction of molecular oxygen with the surface of Pt. While this system has been studied for decades, consensus has not yet been reached on the structure of the Pt surface under high pressure exposure to O_2 during reaction conditions. We have recently performed AP-XPS experiments using our in-house instrument to study the evolution of the Pt(111) surface during high pressure gas exposure to O_2. This understanding will serve as the starting point to tackle the reactive H_2+O_2 system. In collaboration with Dr. Judit Zador (Sandia) and Dr. Jin Qian (LBNL), we have undertaken to interpret the O(1s) XPS spectrum under oxygen exposure from UHV to atmospheric pressure. DFT simulations using the Pynta automated reaction network code as well as simulation of the expected O(1s) spectra are being carried out. By comparison to low energy electron diffraction (LEED) data in our system, we can assign the 529.8 eV binding energy peak from O(1s) to the surface 2x2 adsorption overlayer of atomic O. Under higher pressure exposure, a new peak (or peaks) grow in at 531.2 eV and this peak has been tracked in time as the high-pressure environment causes a phase-change to the metal surface. We assign this peak to the formation of sub-surface O. Such formations clearly modify the surface free energy and reactivity of the Pt surface and will be ubiquitous during reactions at catalysis relevant pressures. Upon evacuating

the chamber, the high energy XPS peak remains, while the 2x2 overlayer disappears. Dr. Jin Qian (LBNL) is simulating these XPS spectra from DFT calculations based upon structures for sub-surface oxide formation and surface buckling calculated with Pynta. This is the first definitive assignment of the O(1s) peaks over Pt that differentiates the formation of the new surface phase. As we move forward, these spectra will also provide the basis for assignment of adsorbed (OH) during catalytic hydrogen oxidation and the reverse reaction, water splitting.

Diagnostic for Near-Surface Imaging of Methyl Last year, we reported preliminary 2-dimensional maps of gas-phase methyl (CH_3) radicals that had desorbed from an active catalyst surface. Because CH_3 radicals do not fluoresce after electronic excitation due to strong predissociation, we used the technique of photofragmentation laser-induced fluorescence (PF-LIF) to visualize their spatial distribution via the photodissociation channel CH_3 + 216 nm → CH + H_2. The CH radicals are then probed by laser-induced fluorescence. We now report the first operando imaging of methyl radical mole fraction in the near-surface gas phase over Ag/SiO_2 catalysts during partial oxidation of methanol. Methyl is mapped within 2 mm of the surface at single digit ppm concentrations. The temperature dependence of the methyl mole fraction in the gas phase follows the methyl surface coverage predicted by a computational study from the Norskov group, whereas gas-phase formaldehyde (measured by planar LIF) shows a negative correlation with its predicted surface coverage. We propose that this positive or negative correlation with coverage is due to the different binding energies of the adsorbates (stronger binding for CH_3, weaker binding for CH_2O). These results suggest that measurements of the near-surface gas phase can serve as a reporter of surface species and provide understanding of the impact of gas-phase radicals in catalyzed chemical processes. For the studied catalytic system, we gain insight into the fate of methyl produced on the catalyst surface and speculate on the role of methyl radicals for the formation of C_2-species. Methyl PF-LIF imaging could be used in a wide variety of gas conditions and chemistries, including oxidative coupling of methane where methyl radicals play a central role. A manuscript describing this work is currently in peer review.

Quantitative Measurements of Electronic Collisional Quenching of CH(A) Extracting quantitative mole fractions of CH_3 radicals in collisional gas-phase environments via PF-LIF requires measurement of electronic quenching cross sections with relevant collision partners. We have measured the collisional quenching rates of CH(A) by methanol, methane, oxygen, nitrogen, and acetone at temperatures between 300 and 600 K. The CH(A) quenching rate by methanol, which is highly relevant in catalysis, has not previously been studied. The quenching rates for acetone, which is used as a precursor to photolytically produce methyl, and methane have been studied but not at elevated temperatures. We find that methanol and acetone both have high quenching rate coefficients with only a small temperature dependence. By contrast, the quenching rate of CH(A) by methane has a significant temperature dependence between 300 - 600 K. The quenching rates determined in this work will be valuable for laser-induced fluorescence studies of catalysis, plasmas, and combustion. A manuscript describing this work is currently in peer review.

Cooperative Mechanisms in Nanoscale Smoothing of metals: adatom diffusion and step nucleation[1] Many heterogenous chemical processes induce and are affected by metastable surface morphology. At moderate temperatures, the morphology of crystalline solids often does not reach the lowest energy, equilibrium surface structure because the kinetics to do so are too slow. At the same time, it is often step edges, corners, and dislocations on crystalline surfaces that are the most active catalytic sites. In this work we studied the factors that control the metastability of a common feature of rough surfaces: random arrangements of "hillocks" or "mesas" consisting of three-dimensional stacks of two-dimensional islands. We used low energy electron microscopy (LEEM) to follow the evolution of the individual atomic steps in hillocks on Pd(111). The changing reflectivity of electrons from the surface as a function of time revealed a process in which adatoms move downhill from a hillock, eventually exposing a new, larger diameter terrace in the layer below. We find that the uppermost island in the stack often adopts a static, metastable configuration until the critical vicinal angle of the hillock sides reaches a maximum, at which point the topmost step is released. Modeling this result shows that the degree of the metastability depends on the configuration of steps dozens of atomic layers below the surface, highlighting how mesoscale morphology

evolves into metastable structures. Our model allows us to link surface metastability to the atomic processes of surface evolution.

Fingerprinting methoxymethanol, a reactive oxygenate in complex mixtures[3] Methoxymethanol (CH_3OCH_2OH) is a reactive two-carbon ether-alcohol formed in both heterogenous and homogeneous chemical systems. The presence of this species can be an important indicator of the chemical pathways forming C2 and larger oxygenates. Although a closed-shell species, it is typically challenging to detect due to its short lifetime in combustion and catalytic reactors. When detected via the sensitive technique of mass spectrometry, the few reports in the literature conclude that methoxymethanol in not observed at its parent m/z 62, but primarily after loss of a neutral H atom, at m/z 61. However, photoionization spectra were not previously available. To better characterize detection methods for this important molecule, we produced methoxymethanol from partial oxidation of methanol over a Pd/MgO catalyst. Our photoionization (PI) spectra show no production of the parent ion at m/z 62, but a clean PI spectrum at m/z 61.029, consistent with $[C_2H_5O_2]^+$, with an appearance energy of 10.24 ± 0.05 eV. To provide additional insight to the unimolecular fragmentation of this cation, we performed automated electronic structure calculations to identify key stationary points on the cation potential energy surface and computed conformer-specific microcanonical rate coefficients for the important unimolecular processes. The lowest energy calculated H-atom dissociation pathway arises from loss of an H atom from the CH2 group, forming a $[C_2H_5O_2]^+$ fragment ion with a predicted appearance of 10.21 eV, in excellent agreement with experimental results. Together, the experiments and computation provide a well-defined fingerprint for identification of methoxymethanol by photoionization or PEPICO spectroscopy in future chemical reactivity studies.

FUTURE PLANS

Hydrogen oxidation over Pt and Rh– a simple gas-surface reaction with rich dynamics and many open questions In our ongoing work, we have employed imaging AP-XPS and have found evidence of both OH (s) and H_2O (s) in the O(1s) XPS spectral range. In our initial work, we compared two single crystals mounted together- Pt(111) and Pt(557) - to elucidate the effect of step-density. Our hypothesis is that if defects, or steps, provide a near-barrierless route to H (s) and O (s) combination, then surfaces with higher step density should yield more observed OH (s) or H_2O (s). We propose to expand this work in several directions. We will first incorporate a curved Pt crystal that continuously increases the density of steps. This will allow our imaging approaches to sample a range of step densities under identical conditions simultaneously. We will incorporate H, OH, and O atom femtosecond LIF in the near-surface gas phase to monitor for these related intermediates. Heterodyne SFG-VS will be used to monitor the OH stretching region for surface adsorbed species/moieties. We have discovered a new PF-LIF approach for measuring near-surface H_2O with high sensitivity. Our gas-phase and surface diagnostics will reveal the role of steps and defects on H_2O formation rate as well as monitor the surface and near-surface gas phase for unexpected intermediates.

On Rh foil polycrystals the kinetic picture becomes significantly more complex. H_2 oxidation of Rh polycrystals has been shown to follow time-varying kinetics and kinetic oscillations that clearly depend on the local crystallographic termination and grain boundaries. The reaction rate follows oscillatory behavior between active and inactive states, and it is thought that the feedback mechanism is related to the formation and depletion of subsurface oxygen. The mechanism of communication and diffusion between domains remains unclear, and certainly a correlated measurement of localized product desorption and surface oxidation state remains elusive. We will attack this problem with our suite of correlated near-surface gas phase and surface-specific imaging probes to elucidate the mechanism of kinetic oscillation, unambiguously identify the more active state, and begin to understand communication between catalytic domains.

Correlated Measurements of Surface Oxidation State and Gas-Phase Structure using AP-XPS and Optical Spectroscopy To date, more than two dozen catalytic reactions have been reported to demonstrate nonlinear oscillatory and spatially inhomogeneous kinetics from UHV to atmospheric pressure conditions, and more reports are made nearly every year. Although many plausible kinetic models can create time-varying oscillations in agreement with macroscopic experiments, incisive experimental tests of these

theories require coupling local measurements of the surface and gas-phase over different domains of a catalyst. Our powerful combination of new and developed optical approaches will simultaneously probe the local gas-phase composition, surface intermediates, and surface oxidation state. We will first probe CO oxidation catalyzed by Pd and Ru catalysts. The catalytic oxidation of CO has been studied extensively over transition-metal catalysts due to the industrial relevance of catalytic treatments of automobile exhaust streams as well as the rich dynamics induced by this reaction over many surfaces and scientific debate over the origins of kinetic nonlinearities and oscillations. For instance, while catalytic oscillations have been observed for CO oxidation over Pd(110), the exact mechanisms are still debated, and it is not certain whether metallic Pd or PdO is the phase of higher reactivity for CO oxidation. In part, this depends on which mechanism is invoked to explain the time-dependent kinetics. Kinetic oscillations may result from subsurface oxygen, switching between stable solutions of the Langmuir-Hinshelwood equations, or a Mars-van Krevelen mechanism in which the reaction proceeds through two cycles. This sort of literature disagreement highlights the need for our novel experimental approach. By combining spatially resolved imaging of gas-phase products and reactants, in this case CO, O_2, and CO_2 with correlated AP-XPS imaging measurements of the surface oxidation state, we can close the kinetic loop with clear evidence for which oxidation states are present and correspond to a given catalytic activity. **The key to this breakthrough in mechanistic understanding is the combination of surface and gas-phase imaging diagnostics.**

Probing Chemical Mechanisms Through Photolysis Perturbation One approach to deciphering the chemical mechanisms and complex interactions of catalytic and gas-phase reactions is to introduce perturbations to the chemistry in a well-controlled manner and monitor the response. We propose to develop an apparatus for *in situ* measurements of the temporal response of an *operando* catalytic reactor to a transient perturbation of the gas composition using laser photolysis of a precursor molecule to generate a pulse of reactive species at a prescribed distance from the catalytic surface.

In preliminary work, we demonstrated the transient addition of CH_3 radicals by laser photodissociation of acetone vapor diluted in N_2 in the near-surface region above a vanadium pentoxide (V_2O_5) catalyst using the stagnation flow reactor operated at 10 Torr (Fig. 3). Catalytic reactions of CH_3 with V_2O_5 are known to produce methanol and formaldehyde. We combine methyl PF-LIF and formaldehyde LIF imaging to monitor the transient response of both reactants and products in this catalytic system (Fig. 3). To differentiate between gas-phase and surface-mediated reactions that impact the consumption of the laser-generated methyl and the production of formaldehyde, we compare the response of these species using the V_2O_5 catalyst and a significantly more inert surface: fused silica. In both experiments, the two materials are at the same temperature. At 300K, the rate of CH_3 consumption and CH_2O production are very similar with the two different materials (Fig. 3). However, when the surfaces are heated to 500K, a clear difference is observed between the two materials with the rates of CH_3 consumption and CH_2O production significantly enhanced by the presence of the heated V_2O_5 catalyst. Although the complete chemistry of this system is unclear at present, this enhanced chemical activity provides a measure of the impact of surface-mediated reactions with V_2O_5.

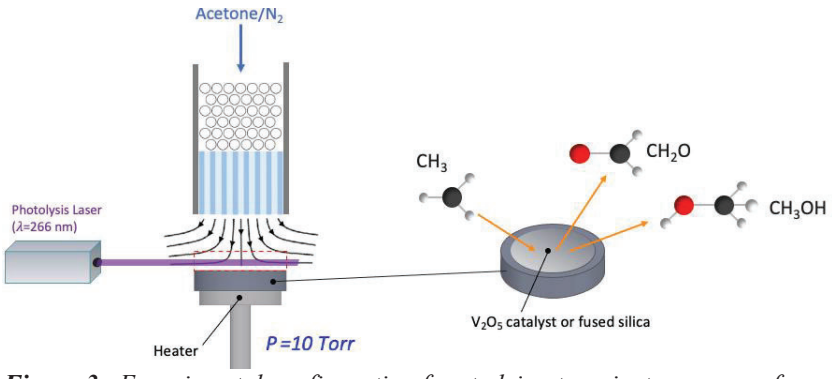

Figure 3. *Experimental configuration for studying transient response of catalytic systems to laser perturbation of the near-surface composition.*

We propose using this experimental approach of laser-induced perturbations to the near-surface composition in combination with time-dependent simulations by Olaf Deutschmann's group to provide mechanistic insights into the transient response of gas-surface interactions in catalytic systems.

We will also consider other transient perturbations beyond methyl. For example, we can generate additional OH radicals by photodissociation of a precursor (e.g., added H_2O_2) at a time (10 ns precision) and place (10s of μm precision) of our choosing. A probe laser will then monitor the chemical response by laser-induced fluorescence measurements at different time delays relative to the photolysis pulse. Separate MBMS experiments in the same chamber will quantify CH_4 conversion and C2 selectivity. Finally, our approach enables new, incisive methods to *perturb* mechanisms. **Monitoring of transient, spatial response to a pulse of OH radicals via PLIF and MBMS will provide new critical tests of mechanisms.**

Probing the Near-Surface Gas Phase using PhotoElectron PhotoIon Coincidence Spectroscopy In the coming year we will leverage the unique capabilities of our PEPICO spectrometer that was developed under our core Gas Phase Chemical Physics Field Work Proposal for studies of heterogeneous catalysis systems. This work is in collaboration with Drs. Patrick Hemberger and Andras Bodi of the Paul Scherrer Institute, Switzerland. We will couple existing sources of co-axial flows over a catalyst bed, followed by supersonic expansion of the gas with our PEPICO spectrometer. Initial studies will focus on the fundamental chemistry of plastic valorization and the precursors to coke formation (carbonaceous deposits). The systems will be initial tested at Sandia National Laboratories using a discharge lamp for production of vacuum ultraviolet photons, followed by experiments at the Advanced Light Source Synchrotron using tunable VUV photons.

Oxidative Coupling of Methane with Soft Oxidants Oxidative coupling of methane (OCM) is a potentially transformative catalytic process for production of valuable C2 species, such as ethane and ethylene. However, the selectivity of OCM towards C2 products is limited by over-oxidation as the desired C2 products react with O_2 to form CO and CO_2. One approach to improving the selectivity is to replace O_2 with "softer" oxidants, such as N_2O that moderate the degree of oxidation. Previous work has shown that compared to O_2, N_2O results in larger conversion rates and improved selectivity. However, the use of such alternative oxidants in OCM is much less studied than the use of O_2, and significant gaps remain in the mechanistic understanding of the improved selectivity afforded by other oxidants. For example, the role of the gas phase after surface activation of N_2O is not clear. We propose fundamental studies of OCM with N_2O using complementary MBMS and laser imaging diagnostics. These results build on those from the Kronawitter lab that focus on co-upgrading CO_2 and alkanes, including through CO_2-OCM.

The use of N_2O in OCM impacts the formation or oxidation of methyl. We propose to investigate the different pathways of methyl consumption using laser imaging diagnostics to probe the near-surface gas phase above OCM catalysts with N_2O or O_2 as the oxidizer. We will measure the methyl distributions using photofragmentation LIF and detect distributions of products OH, CH_2O, CH_3O using LIF imaging. Using these measurements in a series of studies with different catalysts and operating conditions combined with chemical kinetic simulations, we will provide mechanistic insights into the enhanced selectivity of OCM with N_2O as an oxidant. Quantitative N_2O-OCM reactor experiments will be performed in the Kronawitter lab at UC Davis to complement data from the near-surface.

BES-sponsored publications, 2022 – present

1) L. Fernandes Cauduro, F. El Gabaly, and N. C. Bartelt, Cooperative mechanisms behind nanoscale smoothing on metal surfaces: From adatom diffusion to step nucleation, *Phys. Rev. B* DOI:10.1103/PhysRevB.00.005400
2) T. A. Livingston Large and C. J. Kliewer, Sensitive detection and imaging of H_2O density through Rydberg resonant femtosecond laser induced photofragmentation fluorescence *J. Chem. Phys*. **160**, 201102 (2024).
3) N. A. Hansen, T. D. Price, L. R. Filardi, S. M. Gurses, W. Zhou, N. Hansen, D. L. Osborn, J. Zádor, C. X. Kronawitter, The photoionization of methoxymethanol: Fingerprinting a reactive C2 oxygenate in a complex reactive mixture, *J. Chem. Phys.*, **160**, 124306 (2024)
4) S. M. Gurses, N. Felvey, L. R. Filardi, A. J. Zhang, J. Wood, K. van Benthem, J. H. Frank, D. L. Osborn, N. Hansen, C. X. Kronawitter, Constraining reaction pathways for methanol oxidation through operando interrogation of both the surface and the near-surface gas phase, *Chem Catalysis* **3**, 100782 (2023)
5) S. A. Steinmetz, A. T. DeLaRiva, C. Riley, P. Schrader, A. Datye, E. D. Spoerke, and C. J. Kliewer, Gas-Phase Hydrogen-Atom Measurement above Catalytic and Noncatalytic Materials during Ethane Dehydrogenation, *J. Phys. Chem. C* **126**, 3054 (2022).

GAS PHASE INTERACTIONS WITH OTHER PHASES

David W. Chandler, Nils Hansen, Christopher J. Kliewer, Laura M. McCaslin,
Habib N. Najm, David L. Osborn, Leonid Sheps, Craig A. Taatjes, Timothy S. Zwier
Combustion Research Facility, Sandia National Laboratories, Livermore, CA 94551-0969

chand@sandia.gov, nhansen@sandia.gov, cjkliew@sandia.gov, lmmccas@sandia.gov,
hnnajm@sandia.gov, dlosbor@sandia.gov, lsheps@sandia.gov, cataatj@sandia.gov, tszwier@sandia.gov

PROGRAM SCOPE

This research program encompasses experimental and computational investigations of a wide range of multiphase phenomena, investigating the formation of particulates in gas-phase reaction systems, measuring and modeling the gas-phase processes at reactive interfaces and probing the physical and chemical interactions between phases. Understanding reactions that lead to particle formation and calculating surface reactions draw on work in the Sandia "Chemical Kinetics for Complex Systems" task, and experiments employ innovations from the "Ultrafast Physics: Nonlinear Optical Spectroscopy and Diagnostics" task. Recent emphasis is on chemically controlled gas-to-particle conversion; proposed new directions will extend work into understanding the interactions of gas-phase molecules with liquid and solid surfaces. These initiatives complement the catalytic surface investigations in Sandia's "Imaging the Near-Surface Gas Phase" program.

RECENT PROGRESS

Molecular weight growth and particle formation

1. ***Hydrocarbons***[1,5] We continued to investigate the scope of hydrocarbon molecular-weight growth through radical-radical chain reactions, focusing on the role of the propargyl (C_3H_3) radical at ambient to high temperatures. In our work, we used controlled pyrolysis in a SiC microreactor in combination with molecular-beam mass spectrometry and mass-selected threshold photoelectron spectroscopy PEPICO (photoelectron photoion coincidence). Following work reported in last year's abstract, in which we described the investigation of the well-skipping and dissociation channels in the cyclopentadienyl + phenyl reaction, we now studied the recombination reaction of propargyl radicals with fulvenallenyl (C_7H_5) and *o*-benzyne (C_6H_4) by dilute pyrolysis at low pressure near 30 Torr and intermediate temperatures of 800-1600 K. In combination with Kaiser (University of Hawaii), we reported on the very first gas phase preparation of azulene by probing the gas-phase reaction between two resonantly stabilized radicals, fulvenallenyl (C_7H_5) and propargyl (C_3H_3). Augmented by electronic structure calculations by Mebel (Florida International University), the novel reaction mechanism affords a versatile concept for introducing the azulene moiety into polycyclic aromatic systems thus facilitating an understanding of barrierless molecular mass growth processes of saddle-shaped aromatics and eventually carbonaceous nanoparticles.

In collaboration with colleagues from the DLR Stuttgart (Germany) and the Swiss Light Source at the PSI (Switzerland), we reported the identification of the indenyl (C_9H_7) radical – the simplest aromatic hydrocarbon radical carrying an adjacent five- and six-membered ring, as the major product of the *o*-benzyne (*o*-C_6H_4) reaction with propargyl (C_3H_3). We studied this reaction in a resistively heated microtubular SiC reactor at controlled conditions of 1150 K and a pressure near 10-20 Torr. We identified the reactants and the indenyl radical isomer-selectively utilizing photoion mass-selected threshold photoelectron spectroscopy (ms-TPES). The experimentally observed predominant formation of indenyl radicals finally confirms the theoretical predictions of Matsugi and Miyoshi [Phys. Chem. Chem. Phys. 14 (2012), 9722-9728] and highlights a versatile route for the formation of five-membered rings and curved PAHs via reactions of *o*-benzyne that favor the formation of multi-ring species over aliphatically substituted aromatic species.

2. ***Criegee intermediates***[3] In a broad collaboration led by Rebecca Caravan (ANL) and Carl Percival (Jet Propulsion Laboratory) we characterized the chemistry of Criegee intermediate oligomerization reactions that could build highly oxygenated species and contribute to secondary organic aerosol (SOA) formation precursors in Earth's atmosphere (see also ANL kinetics abstract). These SOA change Earth's radiation balance but their formation processes remain uncertain. Sequential Criegee intermediate additions to small oxygenated species like acids or alcohols have been demonstrated in laboratory experiments, and masses that would correspond to similar sequences have been observed in Amazon field experiments led by some of the collaborators in this work. In order to assess the extent to which the field observations could reflect Criegee intermediate oligomerization, we focused on the sequential addition of CH_2OO (formaldehyde oxide) to formic acid (HCOOH), which we observed in jet-stirred reactor measurements of ethene ozonolysis. The initial reaction of CH_2OO with HCOOH forms hydroperoxymethyl formate, as established by earlier work in our group and others, and subsequent reactions with CH_2OO retain an -OOH moiety that is susceptible to further reaction with CH_2OO. Most of the reactions in the sequence are not amenable to direct kinetics measurements, so we measured analogous reactions of CH_2OO with hydroperoxides and compared with state-of-the-art theoretical kinetics from Stephen Klippenstein (ANL). In addition to determining rate coefficients, our measurements confirmed the insertion mechanism by observing the hydroperoxide products in both direct kinetics and sampling from jet-stirred reactor ozonolysis experiments. Having established the accuracy of the theory for hydroperoxide reactions that could be measured, theoretical rate coefficients from the Argonne group were employed to model the effect of the oligomerization under field conditions. Although the oligomerization reactions are more prominent than previous models had assumed, the best estimates of their contribution in the Amazon still fall several orders of magnitude short of explaining the observed concentrations in the field measurements. This indicates either that Criegee intermediate rate coefficients (and Criegee intermediate concentrations) are substantially higher than current estimates, or that some other oxidation processes are dominant in forming the aerosol precursors that have been observed.

Ion imaging above reactive surface[8] Last year we reported on a new microscope based on a combination of velocity mapped ion imaging and spatial imaging that allowed us to measure the position of a surface that an ionized product was formed with approximately 50-micron resolution. This microscope uses a laser to state-selectively ionize molecules above a reactive surface, velocity map images the ions at a plane containing a pinhole (allowing only those moving perpendicular to the surface to pass), and then expands the ion cloud onto an imaging detector providing an image of the laser focus where the intensity is mapped to production of the ionized molecules on the surface. We have designed and are building a next generation microscope that will also provide velocity information on the arrival time of the products from the surface to the laser ionization position. This is possible if one uses a short energizing pulse to initiate the surface reactivity. This can be accomplished for example by photons from a laser pulse or a voltage pulse depending on the catalyst. By measurement of the time delay between the energizing pulse and the arrival time of the products at the laser focus one obtains velocity information to add to the spatial information we have previously demonstrated. As a demonstration we have studied 266-nm photodissociation of $MnBr(CO)_5$ spin coated onto the surface of the repeller plate of a velocity mapped ion-imaging apparatus. After 266 nm excitation the pentacarbonyl will contain enough energy to dissociate and produce 5 CO molecules that are detected by 2 +1 REMPI through the CO B $^1S^+$ state at 230 nm. The velocity distribution of CO photofragments shows the fastest CO is about 9000 m/s corresponding to an arrival time of about 15 μs. CO is observed to continue to arrive for up to 600 μs, implying trapping and subsequent desorption of thermalized CO from the surface. This new instrument is the subject of a patent application, and the apparatus will be employed to study photocatalytic processes once it is fully functional.

Non-adiabatic dynamics of photosensitizing reactions at environmental air-water interfaces In our aim to unravel the non-adiabatic photochemical mechanisms and timescales of photosensitizing reactions of fatty acids and solvated ions at environmental air-water interfaces, we have begun experimental and theoretical study of size-selected clusters of model photosensitizers and water. Photosensitizers are

molecules that absorb light and undergo electronic excitation; internal conversion and intersystem crossing processes may occur before energy transfer from the photosensitizer to a nearby acceptor molecule. Photosensitizing processes involve UV-Vis excitation of a photosensitizing molecule such as 4-benzoylbenzoic acid (4-BBA) and subsequent internal conversion before excited energy transfer to a nearby fatty acid or halide, causing proton or electron transfer. The details of these photosensitizing processes at air-water interfaces are largely unknown, including the electronic states involved, competition between internal conversion and intersystem crossing, and timescales of photosensitizing. We have teamed with Prof. Joseph Fournier (Wash U.) and Ahren Jasper (Argonne) to measure and characterize the IR and UV spectra of size-selected clusters of 4-BBA^-/nH_2O and 4-BBA^+/nH_2O (n=0-2), employing cryogenic ion action spectroscopies and density functional theory to predict and analyze the experimental spectra. Theoretically we are comparing the IR and UV signatures of 4-BBA^-/nH_2O/Cl (n=1-2) to identify signatures of the photosensitization process. We aim to perform non-adiabatic mixed quantum-classical dynamics calculations (NA-MQC) of these and other clusters to identify the electronic states and timescales involved in photosensitization reactions at air-water interfaces.

Vibrational Signatures of Polyaromatic Hydrocarbon Interactions with Water In collaboration with Prof. Mathias Weber (CU Boulder, JILA) and Prof. Joel Eaves (CU Boulder), we are predicting the IR spectra of anionic clusters of polyaromatic hydrocarbons (PAHs) and water molecules. Comparisons of experimental IR spectra and computational harmonic spectra show evidence of many anharmonic and nuclear quantum effects. The vibrational spectra of anionic pyrene + H_2O were computed from molecular dynamics (MD) employing classical molecular potentials and significantly overestimate the intensity of the H_2O antisymmetric stretch, which does not appear in the experimental spectrum. One remedy for this is to employ molecular potentials from quantum chemistry calculations (e.g. density functional theory (DFT)) due to their higher accuracy and ability to incorporate effects of charge fluctuation in the PAH. However, performing DFT calculations on-the-fly in MD is computationally prohibitive, as many nanoseconds of dynamics are needed to obtain converged spectra. We are working to solve this issue by fitting a machine learning (ML) model to DFT energies and gradients of the system, with training sets gathered from classical MD calculations and via sampling along 1- and 2-normal mode displacements. Once trained, we will employ these ML models to compute the MD and extract the vibrational density of states via the autocorrelation function of the velocities. We compute the dominant molecular motion (i.e. a generalized normal coordinate) underlying the vibrational features of interest and compute the IR intensities by taking the derivative of the DFT dipole along these generalized normal coordinates and scale the computational spectral features accordingly. We are also currently working to develop reduced dimensional models for computing the role of nuclear quantum effects in these spectra via multi-configuration time-dependent Hartree methods (MCTDH).

Enhanced Conformer Trapping During Cryogenic Matrix Formation[4] In collaboration with Prof. Leah Dodson's group (U. Maryland), we have revealed how the dynamics of cryogenic matrix formation consisting of bath gases N_2, Ar, or Xe, can change conformer abundances of CH_3ONO from their gas-phase levels. We find that when CH_3ONO is deposited onto a cold substrate, the cis conformer is enhanced relative to the expected gas-phase levels. To unravel the competition between differing binding energies vs. conformer size effects driving this enhancement, we performed calculations of the 1:1 complexes employing coupled cluster theory with single, double, and perturbative triple excitations (CCSD(T)). Through these we did not identify significant differences in stabilizing interactions between the bath gases and conformers of CH_3ONO. We therefore concluded that the enhancements are likely structural and due to the smaller van der Waals radius of cis-CH_3ONO compared to the trans conformer.

Kinetic Monte Carlo for stiff surface kinetics[2] We have completed a study targeting development and analysis of adaptive time integration in the context of stochastic Kinetic Monte Carlo (KMC) simulations for stiff gas-surface kinetics. We targeted development of adaptive time stepping versions of the "tau-leap" method, which is an approximate stochastic simulation algorithm that models the cumulative effect of fast

processes over slow time scales, originally developed for gas phase chemistry. Tau-leap has been used in the context of KMC for surface kinetics, albeit with a fixed time step size. We developed two algorithms for proposing the time step size adaptively, one based on an extension of similar methods in well-mixed gas phase systems, and another based on estimated dynamics of the average-state probability field[19]. We examined the performance of the methods relative to fixed time step constructions, both in terms of accuracy and computational speed, for a model problem involving catalytic decomposition of ammonia. Results highlight the utility of adapting the time step while retaining accuracy once the residual computational costs of either of the time-step selection algorithms can be suitably addressed.

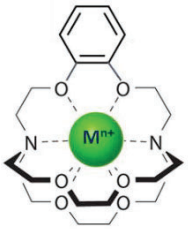

Periodic Trends in Ions Bound inside Molecular Cages Cryptands are three-dimensional molecular cages that selectively bind cations in their interiors, discriminating between atomic cations based on their size and charge state. We have carried out a study of the spectroscopy and structures of [2.2.2]-benzocryptand (BzCrypt) with M^{n+} = Na^+, K^+, Rb^+, Sr^{2+}, and Ba^{2+} under cryo-cooled conditions in the gas phase, in order to discern periodic trends in the absence of thermal, solvent or packing effects. We incorporate the aromatic ring in the cryptand cage to provide a UV chromophore for IR-UV double resonance. In each case, a single dominant conformation of the cage is formed. In the infrared, the imbedded ion produces significant shifts and splittings in the alkyl CH stretch infrared spectrum (2800-3000 cm^{-1}) that are also unique to the imbedded ion. In collaboration with Ned Sibert (UW-Madison), we employ an anharmonic local mode model of the manifold of CH stretch transitions to assign the experimentally observed structures. All five ions are bound inside the cage primarily by the six O-atoms in the three alkyl ether bridges, with secondary binding to the two tertiary amines. There is a strong correlation between phenyl ring orientation and the end-to-end N-N distance, with smaller cations (Na^+, Sr^{2+}) twisting the phenyl ring to nearly perpendicular to the N-N axis, thereby shortening the N-N distance from 6.08-6.12 Å in K^+-BzCrypt and Ba^{2+}-BzCrypt to 5.31 Å in Na^+-BzCrypt and 5.45 Å in Sr^{2+}-BzCrypt. Finally, Rb^+-BzCrypt takes up the same structure as in K^+-BzCrypt, with both UV and IR spectra that are closely similar to those in the latter complex.

FUTURE WORK

Molecular weight growth and particle inception The cyclopentadienyl radical is known to have a multifaceted chemistry. For example, the recombination of two C_5H_5 radicals and its potential to form naphthalene has been the focus of much previous work. This route would in fact make it possible to bypass the formation of single-ring aromatic species by directly forming naphthalene, the simplest PAH. The reaction $C_5H_5 + C_3H_3$ has been proposed to be a source of styrene through a ring-enlargement reaction that converts the five-membered into a six-membered ring. However, experimental datasets for this reaction are still scarce. In collaboration with colleagues from the DLR Stuttgart (Germany) and the Swiss Light Source (PSI, Switzerland), we studied this reaction at high temperatures using i^2PEPICO spectroscopy. The isomer-resolving capabilities of the i^2PEPICO end-station are necessary to differentiate between the different isomers by measuring mass-selected photoelectron spectra as a function of temperature. We are currently in the process of analyzing the experimental data and of comparing them with results of the potential energy surface exploration and kinetics study performed by Zádor *et al.*

We will continue to study the formation of five-membered ring species via *ortho*-benzyne (*o*-C_6H_4) as an essential molecular building block in molecular-weight growth reactions. We will study the reaction of *o*-C_6H_4 with benzyl (C_7H_7) radicals in a well-controlled flash pyrolysis experiment. Using molecular-beam time-of-flight mass spectrometry, we will trace the product formation and compare our experimental results with earlier theoretical calculations by Matsugi and Miyoshi [*PCCP,* 2012, **14,** 9722-9728], who predicted the formation of fluorene ($C_{13}H_{10}$) + H to be the dominant reaction channel.

Oligomerization reactions of larger Criegee intermediates may be more likely than the CH_2OO oligomerization already studied to lead to aerosol precursor formation in real tropospheric conditions. We will continue our collaboration with Caravan (ANL), Klippenstein (ANL), Lester (Penn), and Percival

(JPL) with studies of kinetics and product formation in sequential reactions of methyl vinyl ketone oxide with atmospheric species, comparing measurements in our photoionization mass spectrometric experiments with theory, modeling, and field observations.

Machine Learning and Uncertainty Quantification in Computational Chemistry Machine learning developments, and their applications in computational chemistry, have continued to advance at a remarkable rate. At the same time, there are clear and well-recognized indications of the need for vigilance in the assessment of quality of predictions from ML constructions, particularly in out-of-distribution extrapolative scenarios. With necessary approximations, uncertainty quantification methods have indeed been used to provide a measure of confidence in ML predictions. However, despite the extent of work in this area, there has been relatively little attention paid to the uncertainty in the data itself, and the consequent uncertainty in predictions from the trained neural network (NN). This issue is of particular relevance in the context of computationally generated training data relying on approximate models. In the computational chemistry context, DFT is often the main source of data for NN training. Given the large requisite training data sizes, it is typically necessary to use DFT computations at low levels of theory, with associated resulting uncertainties in the computed data used for NN training. These uncertainties are particularly large for gas-surface kinetics, as opposed to gas phase systems. We propose to address the challenge of estimating uncertainty in DFT predictions of surface kinetics, making use of Bayesian inference and Gaussian process models in the context of fitting of the BEEF functional. With this done, we will use BEEF-DFT to generate NN training data with associated uncertainties and will estimate the corresponding predictive uncertainties in trained NN predictions on model surface-kinetics systems.

Nano-Confinement: The Spectroscopy of Ions in Molecular Cages. Unlike the alkali metal and alkaline earth cations, which are bound to the cryptand cage almost entirely by electrostatics, the protonated cryptand cage has the proton chemically bound by a covalent bond to the cage at one of the capping nitrogen atoms. We have recorded preliminary UV and IR-UV spectra of both $[H+BzCrypt]^+$ and $[2H+BzCrypt]^{2+}$ and are presently collaborating with Daniel Tabor (Texas A&M) on the conformational analysis and anharmonic local mode calculations to assign the spectra. Not surprisingly, the singly protonated BzCrypt cage is most challenging, since it has one proton binding site filled and one empty, resulting in several low-energy conformers. Experimentally, we have observed two conformers of $[H+BzCrypt]^+$ and a single conformer of the doubly protonated counterpart. In the coming year, we will be completing our analysis and writing up a manuscript describing this work.

When we use barium acetate as the salt for making up solutions of the Ba^{2+}-BzCrypt complex, we see $Ba^{2+}(OAc)^{-1}$-Bzcrypt in the mass spectrum. Without the presence of the BzCrypt cage, $Ba^{2+}(OAc)^{-1}$ would constitute a contact ion pair. However, in the presence of the benzocryptand cage, the Ba^{2+} cation is imbedded in the cage, with the acetate anion bound to it. We have recorded both UV photofragment spectra and IR-UV double resonance spectra of this ion pair complex in order to understand the structural consequences and binding energy changes that are induced by the cryptand cage. We are collaborating with Daniel Tabor on the conformational and spectroscopic analysis of our data.

Publications acknowledging support from this project 2022 –

1. N. Hansen, T. Bierkandt, N. Gaiser, P. Oßwald, M. Köhler, P. Hemberger, "Formation of Five-Membered Ring Structures via Reactions of o-Benzyne", *Proc. Combust. Inst.*, **2024,** *40*, 10562. doi: 10.1016/j.proci.2024.105623
2. Che, T., Zhou, Y., Han, X., and Najm, H.N., Adaptive τ-leaping methods for microscopic-lattice kinetic Monte Carlo simulations, *J. Chem. Phys.*, **2024**, *161,* 084107. doi.org/10.1063/5.0218471
3. Caravan, R. L.; Bannan, T. J.; Winiberg, F. A. F.; Khan, M. A. H.; Rousso, A. C.; Jasper, A. W.; Worrall, S. D.; Bacak, A.; Artaxo, P.; Brito, J.; et al. Observational evidence for Criegee intermediate oligomerization reactions

relevant to aerosol formation in the troposphere. *Nat. Geosci.* **2024**, *17*, 219–226, Article. DOI: 10.1038/s41561-023-01361-6.

4. E.K. Hockey, N. McLane, K. Vlahos, L.M. McCaslin, L.G. Dodson, "Matrix-Formation Dynamics Dictate Methyl Nitrite Conformer Abundance", *J. Chem. Phys.***2024** *160*, 094303. doi.org/10.1063/5.0188433
5. W. Li, J. Yang, L. Zhao, D. E. Couch, M. M. San Marchi, N. Hansen, A. N. Morozov, A. M. Mebel, R. I. Kaiser, "Gas-Phase Preparation of Azulene ($C_{10}H_8$) via Reaction of the Resonantly Stabilized Fulvenallenyl (C_7H_5) and Propargyl (C_3H_3) Radicals", *Chem. Sci.*, **2023,** 14, 9795-9805. doi:10.1039/D3SC03231K
6. L. M. McCaslin, A. W. Götz, M. A. Johnson, R. B. Gerber, "Effects of Microhydration on the Mechanisms of Hydrolysis and Cl− Substitution in Reactions of N_2O_5 and Seawater", *ChemPhysChem* **2023***, 25,* e202200819. doi:10.1002/cphc.202200819.
7. D. E. Couch, G. Kukkadapu, A. J. Zhang, A. W. Jasper, C. A. Taatjes, N. Hansen, "The role of radical-radical chain-propagating pathways in the phenyl + propargyl reaction", *Proc. Combust. Inst.* **2023** *39*, 643-651. https://doi.org/10.1016/j.proci.2022.09.012
8. Chandler, D. W.; Fournier, M.; Smoll, E. J.; Kliewer, C. J. Velocity-selected spatial map ion imaging spectrometer for direct imaging of near-surface catalytic activity. *Appl. Phys. Lett.* **2023**, *122*, 251603, Article. DOI: 10.1063/5.0152985.
9. H. A. Michelsen, M. F. Campbell, K. O. Johansson, I. C. Tran, P. E. Schrader, R. P. Bambha, E. Cenker, J. A. Hammons, C. H. Zhu, E. Schaible, A. van Buuren, "Soot-particle core-shell and fractal structures from small-angle X-ray scattering measurements in a flame", *Carbon* **2022,** *196*, 440-456. doi:10.1016/j.carbon.2022.05.009.
10. K. C. Kalvakala, P. Pal, J. P. Gonzalez, C. P. Kolodziej, G. Kukkadapu, S. Wagnon, R. Whitesides, N. Hansen, S. K. Aggarwal, "Numerical Analysis of Soot Emissions from Gasoline-Ethanol and Gasoline-Butanol Blends under Gasoline Compression Ignition Conditions", *Fuel* **2022**, 319, 123740. doi:10.1016/j.fuel.2022
11. H. A. Michelsen, M. F. Campbell, I. C. Tran, K. O. Johansson, P. E. Schrader, R. P. Bambha, J. A. Hammons, E. Schaible, C. H. Zhu, A. van Buuren, "Distinguishing Gas-Phase and Nanoparticle Contributions to Small-Angle X-ray Scattering in Reacting Aerosol Flows", *J. Phys. Chem. A* **2022**, 126, 3015-3026. doi.org/10.1021/acs.jpca.2c00454
12. D. E. Couch, A. W. Jasper, G. Kukkadapu, M. M. San Marchi, A. J. Zhang, C. A. Taatjes, N. Hansen, "Molecular weight growth by the phenyl + cyclopentadienyl reaction: Well-skipping, ring-opening, and dissociation", *Combust. Flame* **2022,** 112439. doi: 10.1016/j.combustflame.2022.112439 (2022).
13. H. Michelsen, E. Boigné, P. E. Schrader, K. O. Johansson, M. F. Campbell, R. P. Bambha, M. Ihme, "Jet-entrainment sampling: A new method for extracting particles from flames," *Proc. Combust. Inst.* **2023**, *39,* 847-855. doi:10.1016/j.proci.2022.07.140 (2022).
14. J. A. Rundel, C. M. Thomas, P. E. Schrader, K. R. Wilson, K. O. Johansson, R. P. Bambha, H. A. Michelsen, "Promotion of particle formation by resonance-stabilized radicals during hydrocarbon pyrolysis," *Combust. Flame* **2022,** *243,* 111942. doi:10.1016/j.combustflame.2021.111942 (2022).

ULTRAFAST CHEMICAL PHYSICS: NON-EQUILIBRIUM DYNAMICS IN GAS-PHASE MOLECULES AND COHERENT MOLECULAR CONTROL

Christopher J. Kliewer, Krupa Ramasesha, Laura M. McCaslin
Combustion Research Facility, Mail Stop 9055; Sandia National Laboratories, Livermore, CA 94550
cjkliew@sandia.gov, kramase@sandia.gov, lmmcas@sandia.gov

Program Scope

This program applies ultrafast techniques and theoretical calculations to investigate fundamental gas-phase chemical dynamics. Our research uses diverse experimental probing techniques to follow coupled electronic and nuclear motion on femtosecond to picosecond timescales in gas-phase molecules, as well as advanced quantum chemical calculations to investigate these dynamics and predict experimental observables. The coupling of electronic and nuclear degrees of freedom, representing a breakdown of the Born-Oppenheimer approximation, gives rise to complex pathways for non-radiative energy dissipation in electronically excited molecules, often involving participation of multiple electronic states. Identifying the motions that couple electronic states, the timescales and dynamics of excited state population relaxation, and the role of coupled vibrational modes of a molecule in guiding energy flow is crucial to our understanding of non-equilibrium dynamics, and it forms the mainstay of this program. This is a core thread that runs through all of the complex photochemical systems that are studied and detailed below. *Ultrafast Chemistry* is one of the synergistic research themes of CSGB and this work addresses two key aspects of the Grand Challenges for Basic Energy Sciences: (1) investigating the nature of electronic excited states, and (2) exploring the breakdown of the Born-Oppenheimer approximation.

The interaction of intense pulsed laser fields with atoms, molecules, and surfaces induces a coherent response in the material. At especially high intensities, the material response becomes nonlinear and gives rise to a wealth of approaches to both *control* and to *probe* molecular processes in gas-phase and interfacial chemical physics, even processes very far from chemical equilibrium. As part of this program, our goal is to develop ultrafast optical methods to both measure and control matter at the molecular level and on molecular timescales. On the measurement side, ultrafast nonlinear approaches are advanced for the detection of transient reactive molecular species. In addition, broadband approaches enable the sampling of many spectroscopic transitions at once, allowing for the assessment of instantaneous molecular energy partitioning and energy transfer. A critical aspect of our research includes the study of fundamental spectroscopy, energy transfer, molecular dynamics, and photochemical processes. This aspect of the research is essential to the development of accurate models and quantitative application of techniques to complex environments. We are uniquely positioned to study molecular systems driven far from equilibrium, as well as relaxation rates and pathways. Time-resolved collisional dephasing measurements provide insight into the local chemical environment as well as inform spectroscopic models for quantitative interpretation.

Recent Progress

Femtosecond core-level spectroscopy reveals involvement of triplet states in the dissociation of gas-phase $Fe(CO)_5$ The photochemistry of $Fe(CO)_5$ has garnered intense interest as an excellent model for studying metal-ligand binding and reactivity in organometallic molecules, serving as a valuable starting point for understanding more complex systems relevant to photocatalysis. Previous work had shown that this molecule experiences sequential loss of two CO ligands in the gas phase when excited at 266 nm, but spectroscopic detection of the electronic and structural dynamics governing this dissociation had long eluded experimental observation, hindering a complete understanding of the photochemistry of this system. Researchers had thus explicitly disregarded the role of triplet states in the ultrafast photochemistry of $Fe(CO)_5$ in the gas phase. Our work unveiled the coupled electronic and structural dynamics of $Fe(CO)_5$ photodissociation at 266 nm using cutting-edge experiment and theory. Our experiments used ultrafast extreme ultraviolet (XUV) transient absorption spectroscopy near the Fe $M_{2,3}$ edge, which, via Fe 3*p*-to-

valence transitions, provided element-specific information on the femtosecond valence excited state dynamics during $Fe(CO)_5$ photodissociation. Our theory employed electronic structure to predict the key core-level spectroscopic signatures of the species involved in the dynamics and identify them in the experiment. Our work, for the first time, revealed spectroscopic signatures of transient singlet metal-centered excited states during the ultrafast first CO loss from $Fe(CO)_5$ along with spectroscopic signatures of vibrationally hot photoproducts, $Fe(CO)_4$ and $Fe(CO)_3$, formed on their first singlet excited states. Crucially, our work provided key spectroscopic evidence for the involvement of triplet states in the ultrafast photodissociation of gas-phase $Fe(CO)_5$, challenging decades-old presumptions that dissociation of this molecule proceeds exclusively on the singlet manifold.
This was a collaboration with Martin Head-Gordon's group (UC-Berkeley).

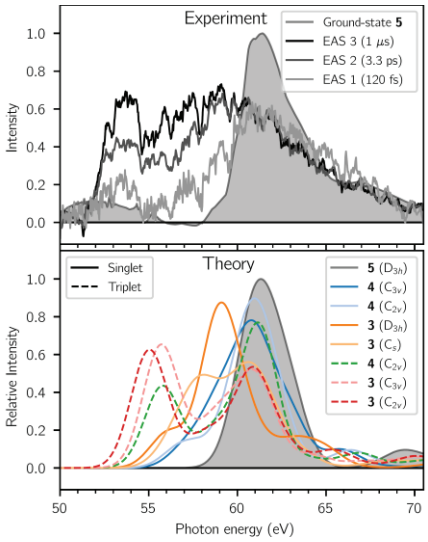

Figure 1: (Top) Experimental XUV spectra near the Fe $M_{2,3}$-edge of $Fe(CO)_x$ after 266 nm excitation of $Fe(CO)_5$. (Bottom) Theory predicted XUV absorption spectra of $Fe(CO)_x$ in the indicated geometries and on singlet and triplet electronic states.

Ultrafast production of NiCO and Ni following 197 nm dissociation of $Ni(CO)_4$ We studied the excited state photodissociation dynamics of gas-phase nickel tetracarbonyl – a unique model system to explore ligand binding and transition metal electronic structure – following deep-ultraviolet excitation at 197 nm. The existing literature on the ultrafast photodynamics of transition metal carbonyls at these high excitation energies is sparse due to challenges associated with a high density of electronic states and multiple competing pathways for dissociation. Using ultrafast transient infrared absorption spectroscopy to probe the bound C≡O stretching vibrations alongside equation-of-motion coupled cluster calculations of potential energy cuts, our work suggests picosecond production of $Ni(CO)_2$ and NiCO and the production of bare Ni on a 50-ps time scale, revealing more complex ultrafast photodynamics than previously thought.

Competing pathways in the ultrafast photodissociation of dimethyl disulfide Dimethyl disulfide (DMDS) is the simplest model system for the disulfide (S–S) bond, an important moiety in tertiary protein structure. Despite its central role in maintaining the structural integrity of proteins, the disulfide bond is photolabile with several electronic excited states proposed to be dissociative along the S–S and C–S bonds; we are investigating the competing pathways in the deep UV-induced dissociation of this molecule. We performed ultrafast electron diffraction (UED) at the SLAC MeV-UED facility to probe the competing pathways in the ultrafast photodissociation of DMDS following 200 nm excitation. Our theoretical work revealed that 200 nm populates S_5, which is characterized by transitions from n_S to primarily Rydberg orbitals, with minor contribution from transitions to $\sigma^*_{C\text{-}S}$. Following this excitation, experimental results show prompt appearance of negative signal at 2 Å and 3 Å interatomic distances, corresponding to the loss of C–S/S–S distances and the second-nearest neighbor C---S distances, respectively. This prompt response is followed by subtle evolution on a 1.5 ps timescale at interatomic distances between 2 and 3 Å. To complement our UED experiments, Vasilios Stavros' group (U. Birmingham) performed ultrafast photofragment velocity-mapped ion imaging of the CH_3 fragment; these results also show evidence for C–S and S–S bond dissociations, with possible existence of a second, slower C-S dissociation channel. These slower picosecond dynamics may be indicative of intersystem crossing or slow fragment velocities due to formation of electronically excited co-fragments.

To help interpret experimental results, we performed computational studies of the photodissociation of DMDS with electronic structure and non-adiabatic dynamics calculations. To this end, we compared the

performance of equation of motion coupled cluster theory with single and double excitations (EOM-CCSD) and extended multi-state complete active space second-order perturbation theory methods (XMS-CASPT2) with the two active spaces – (8e,8o) and (10e,10o). Specifically, we investigated these methods' ability to predict UV-Vis spectra, capture Rydberg character of excited states in the Franck-Condon region, and predict dissociation energies along the S-S and C-S coordinates. We also predicted the excitation and dissociation potential energy curves with a new equation-of-motion coupled cluster method that includes triples corrections, EOM-CCSD(T)(a)*. We find that EOM-CCSD is the superior method for predicting the UV-Vis spectra, including excited state energies and oscillator strengths at the Franck-Condon geometry, and it captures the Rydberg and mixed Rydberg-valence character of states S_3-S_6. We find that XMS-CASPT2(8e,8o) and (10e,10o) are reasonable at predicting these energies and Rydberg character but exhibit greater deviations from the experimental UV-Vis spectra than EOM-CCSD. Along the S-S and C-S dissociation coordinates, we find numerous dissociation pathways due to the large number of excited states and energetically available pathways. XMS-CASPT2 better predicts the asymptotic dissociation energies compared to EOM-CCSD and EOM-CCSD(T)(a)*. Further, we find spin-orbit coupling to be larger than 50 cm^{-1} at the Franck-Condon geometry and numerous singlet and triplet states that exhibit quasi-degeneracy, indicating a high likelihood of intersystem crossing during photodissociation. Our non-adiabatic dynamics simulations from the S_5 state (100 trajectories for 300 fs) at the XMS-CASPT2(8e,8o)/aug-cc-pVDZ level of theory show 63% S-S bond dissociation, 16% C-S bond dissociation, 18% three-body dissociation into S + SCH_3 + CH_3, and the final 5% of trajectories dissociating along other multi-body dissociation pathways. Given these trajectories, analysis of the experimental data is underway.

Dynamics of molecular alignment and spin-rotation coupling of super-rotors coupled to a magnetic field We have recently developed an optical molecular centrifuge for the study of molecular dynamics and reactivity in extreme angular momentum states. In our first demonstration[11], we optically trapped molecular CO_2 in the centrifuge pulse and angularly excited to J = 364, corresponding to a rotational energy of 6.14 eV. As these high angular momentum states relaxed, we directly observed rotational-to-vibrational energy exchange, with as much as 6 quanta detected in the bending mode of CO_2. The high angular momentum states are prepared by combining two oppositely chirped left- and right- circularly polarized beams on the sample, generating a linear polarization that rotates and ever-increasing angular velocity. This corkscrew shaped pulse traps molecules that possess polarizability anisotropy, and accelerates such molecules to very high angular momentum through successive ΔJ=2 transitions. To probe the distribution of states excited by the centrifuge, we scatter from the generated rotational coherence with either a picosecond or seeded nanosecond laser pulse. The picosecond pulse provides frequency resolution of ~0.2 cm^{-1}, while the nanosecond pulse is used for the resolution of finely spaced transitions. In CO_2, this enabled the monitoring of vibrational population through the slight shift in rotational

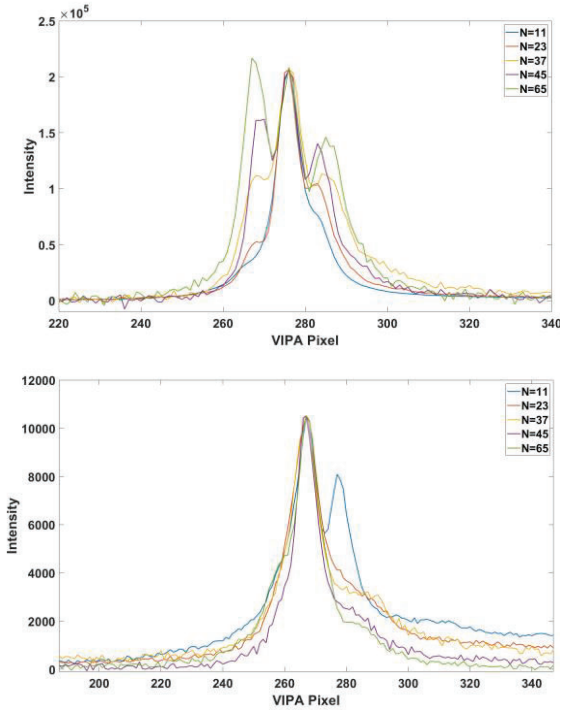

Figure 2: N-dependence of the resolved spin-multiplet (J = N-1 leftmost peak, J=N middle peak, J=N+1 rightmost peak) for oxygen (paramagnetic) unidirectionally spinning super-rotors with applied magnetic field of (a) 0.3 Tesla along the centrifuge laser pulse propagation axis and (b) 1T perpendicular to the propagation axis.

constant for each additional vibrational level populated. Molecular oxygen provides a model system with nonzero electronic spin in the ground state that couples to the nuclear motion through spin-spin and spin-rotation coupling. The optical centrifuge induces spin polarization, which in turn may generate a net magnetic field depending on the dynamics of the distribution of the spin states. Each rotational level in paramagnetic oxygen is split by the nondegenerate spin multiplicity into a total angular momentum of J = N, N+/-1, where N is the rotational angular momentum. Exciting molecular oxygen in molecular centrifuge in the presence of an external magnetic field allows for the investigation of magnetic coupling to spin polarization and molecular alignment. We conducted experiments with both cylindrically hollow magnets and disc magnet pairs to generate a magnetic field, **B**, either along the angular momentum axis of the unidirectionally spinning super-rotors or perpendicular to it. Magnetic fields between 0 and 4 Tesla were explored. Figure 2 shows a rich dynamics of molecular realignment of super-rotors and spin-flipping transitions in the presence of a magnetic field that were tracked as a function of angular momentum, and we are presently developing the model to correctly predict the observed dynamics.

Future Work

Photoisomerization and ring-opening in 1,3,5-triazine Knowledge of the photochemistry of aromatic heterocycles is crucial to a bottom-up understanding of the photostability of these fundamental building blocks of life. In particular, the role of conical intersections in the non-adiabatic dynamics of these heterocyclic rings has been the subject of intense study for several decades. While the photochemistry of pyridine and pyrimidine is well studied, the related system 1,3,5-triazine (*c*-$C_3H_3N_3$, *sym*-triazine, ST) has received less attention. ST is both an important model biochromophore and is a prototypical example of three-body dissociation. Photodissociation of ST only occurs following internal conversion (IC) to the ground electronic state, with conflicting evidence for synchronous *vs*. asynchronous concerted three-body dissociation mechanisms. Also, there is no information on the ST structural changes that accompany IC. To understand the excited state structural dynamics and the role of photoisomerization versus ring-open intermediates in ST, we recently performed UED following 266 nm excitation of sT at SLAC MeV-UED. Analysis is underway by comparing data to predicted differential scattering intensities and pair distribution functions for the ring-closed and ring-open intermediates and the three-body dissociation products.

Deep-UV induced dynamics in propargyl bromide Propargyl bromide is a photolytic precursor to the propargyl radical, which is an important precursor to the formation of aromatic molecules in flames. Being a multi-chromophore system—excitation at 200 nm can prepare states of mixed ππ*, πσ* and nσ* character—propargyl bromide has also attracted considerable interest for understanding excited state dynamics arising from UV excitation. Previous work near this excitation wavelength using velocity map imaging showed a bimodal translational energy distribution of the Br and Br* generated from C-Br bond dissociation. A few explanations have been put forth to explain the production of slow and fast Br atoms, including the involvement of triplet states in the dissociation and the formation of electronically excited C_3H_3 co-fragment. With the aim of shedding light on this issue, we recently performed ultrafast XUV spectroscopy near the Br $M_{2,3}$-edge, which reveals instantaneous formation of Br and Br* within 200 fs, with no further evolution of transient signal out to our longest time delay of 1.2 ns. We will perform ultrafast soft X-ray spectroscopy near the C K-edge to probe the fate of the propargyl radical, with particular attention to whether it is formed on an electronic excited state. Anna Krylov's group (USC) is performing theory and core-level spectral predictions.

Ultrafast soft X-ray transient absorption spectroscopy of excited state dynamics in the dissociation of dimethyl disulfide Our current work on DMDS suggests complex valence excited state dynamics, particularly on picosecond timescales when intersystem crossing and dynamics on triplet states may play a role. We will experimentally study the valence excited state dynamics using ultrafast soft X-ray transient absorption spectroscopy simultaneously near the S L-edge and C K-edge following 200 nm excitation of DMDS. Immediately following excitation, we expect new, strong pre-edge features arising from transitions

out of the S 2s and 2p orbitals to the now-partially-occupied localized non-bonding orbital of sulfur, as well as reduction in intensity of the S and C core level transitions to the newly populated σ^*_{CS} and Rydberg orbitals. As the molecule relaxes through singlet and triplet excited states characterized by transitions out of the two non-bonding sulfur orbitals to σ^*_{SS}, σ^*_{CS} and Rydberg states, the time-dependent evolution of corresponding transitions from the S 2s and 2p core orbitals to n_{S1}, n_{S2}, σ^*_{SS}, σ^*_{CS}, Rydberg orbitals and the C 1s core orbital to σ^*_{CS} and Rydberg orbitals will report on the relaxation dynamics prior to dissociation. Finally, C–S and S–S bond dissociations will result in a red-shift to the core level transitions due to the increase in electron density on the S and C atoms and the corresponding decrease in core binding energies. Given the sensitivity of X-ray absorption spectroscopy to the nature of valence excited states, these experiments promise to shed light on the electronic dynamics. In parallel, core-level absorption spectra of the sulfur 2s-to-valence, 2p-to-valence and carbon 1s-to-valence transitions will be calculated for valence excited state configurations predicted by our dynamics trajectories.

Optical centrifuge of N_2O for photodissociation dynamics studies In the coming year, planned work at Sandia involves the study of the photodissociation of N_2O super-rotors. This work is described in the "Chemical Dynamics" abstract of the Sandia Gas-Phase Chemical Physics program. To enable these studies, we need to tailor our optical centrifuge for efficient centrifuging of the N_2O molecule. In order to efficiently trap target molecules, the optical centrifuge must be tailored to the molecular system such that $8\pi\delta/E^2 < \Delta\alpha/I$, where δ is the rate of optical acceleration, E^2 is the laser intensity, $\Delta\alpha$ is the molecular polarizability anisotropy, and I is the molecular moment of inertia. Thus, for each new molecule studied, the pulse shaper must be once again optimized. An important aspect of the design is the effective turn-on time for the optical centrifuge pulse. Prior to interaction with the laser pulse, the gas-phase ensemble of molecules will be isotropically oriented about the laboratory coordinate. As the optical centrifuge turns on, it will begin exerting an aligning force on these molecules. If the turn-on time is too fast, the molecule will not have time to respond and become adiabatically trapped within the potential well created by the laser. In angular coordinates, the laser must cover π radians during the turn-on period to effectively trap all orientations. If the turn-on is too slow, the angular frequency will be too fast by the time the pulse is at full intensity and will not be able to retain the molecules, i.e. the kinetic energy of the molecules gained during centrifuge turn-on must be always less than the current potential well depth induced by the laser pulse. Spanner and Ivanov have proposed a method to derive these upper and lower limits, and have found that $(2\pi/\delta)^{\wedge}.5 < t_{on} < (U_0/[I\delta^2])$ allows for molecules to be effectively coupled into the centrifuge. Here, again, δ is the angular acceleration rate of the trap, t_{on} is the pulse turn-on time, U_0 is the potential well depth felt by the molecule from the laser, and I is the molecular moment of inertia. This year we will demonstrate efficient driving of N_2O to $J > 150$.

Study of coherence and rotation-to-vibration transfer of N_2O Our recent work has demonstrated the unique finding that molecules can undergo rotation-to-vibration collisional energy transfer without disrupting the phase of the rotations of the molecule that gains vibrational energy. This behavior was unexpected, as traditionally collisional energy transfer has been assumed to disrupt the phase or an ensemble of prepared rotors, and therefore those molecules are removed from the coherence and contribute to collisional coherence dephasing. However, this finding opens the possibility for detailed studies of energy relaxation across the entire populated manifold in other nonequilibrium systems using the same approach. We will study the centrifugation and relaxation pathways first for N_2O. It has been previously found during measurements of centrifuged N_2O that one quanta of bending vibration is likely excited during relaxation of the high angular momentum excitation. But this measurement was made over a limited range of populated rotational levels, and the multiplex approach demonstrated in our lab will provide more complete relaxation information. This information will first serve to validate whether coherence transfer during rotation-to-vibration energy exchange is a ubiquitous finding or unique to the particular case of CO_2. Laura McCaslin will further perform quantum chemical calculations to study how rotational phase disruption follows from rotation-to-vibration energy transfer for comparison to our results for both CO_2 and N_2O.

These results will be compared to semi-classical trajectory calculations from collaborator Ahren Jasper (Argonne National Laboratories). Further, the understanding of energy transfer pathways and timescales for N_2O will be critical foundational understanding leading into the superrotor photodissociation and bimolecular collision experiments proposed in the Chemical Dynamics subtask.

Selective rotational ladder climbing in polyatomics Up until now, we have only attempted to trap and accelerate linear molecules in the optical centrifuge. When a polyatomic molecule is placed in an aligning field, the most polarizable axis of the molecule will align with the laser polarization direction, provided the molecule possesses polarizability anisotropy. Thus, when incorporated into the molecular trap, the molecule will be accelerated such that the angular momentum vector is perpendicular to this, most polarizable, axis. However, in a polyatomic molecule, a powerful approach that may open the door to a more selective chemistry is to drive the polyatomic molecule along a different principal rotational axis. For instance, in chemical dynamics studies it will be interesting to weaken a particular bond through centrifugal distortion and follow how this modifies reaction probabilities. It has been recently theoretically proposed, yet never demonstrated, that pulse shaping the centrifuge excitation pulse could achieve this goal. Consider an asymmetric top molecule. Given that each rotation axis is likely to have a differing rotational constant, β, and therefore a different rotational period, one or both arms of the trap can be tailored to match a particular molecular axis. If the excitation pulse is shaped such that intensity maxima are present at pulse times where the $\Delta\omega$ frequency between the two arms of the centrifuge pulse matches the next sequential Raman transition frequency along the desired excitation axis of the molecule, the sequential Raman transitions will be preferentially excited along. Between those time positions, the pulse is minimized. As an initial demonstration, we will attempt to accelerate H_2S along the "a" and "c" principal rotational axes selectively.

BES-sponsored publications (2022-present)

1. S.A. Steinmetz, C.J. Kliewer, "Gas detection sensitivity of hybrid fs/ps and fs/ns CARS" *Opt. Lett.*, **2022,** *47*, 1470-1473
2. Cole-Filipiak, N. C.; Troß, J.; Schrader, P. E.; McCaslin, L. M.; Ramasesha, K., Ultrafast Infrared Transient Absorption Spectroscopy of Gas-Phase $Ni(CO)_4$ Photodissociation at 261 nm, *J. Chem. Phys.*, **2022**, *156* (14), 144306
3. Schnack-Petersen, A. K.; Tenorio, B. N. C; Coriani, S.; Decleva, P.; Troß, J.; Ramasesha, K.; Coreno, M.; Totani, R; Röder, A, Core Spectroscopy of Oxazole, *J. Chem. Phys.,* **2022**, *157* (21), 214305
4. T.Y. Chen, N. Liu, C.J. Kliewer, A. Dogariu, E. Kolemen, Y Ju, "Simultaneous single-shot rotation-vibration non-equilibrium thermomemtry using pure rotational fs/ps CARS coherence beating" *Opt. Lett*., **2022,** *47*, 1351-1354 *Highlighted as an "Editor's Pick" article
5. T.Y. Chen, C.J. Kliewer, "Numerical study of pure rotational fs/ps CARS coherence beating at high pressure and for multi-species rotation-vibration non-equilibrium thermometry" *J. Chem. Phys*., **2022,** *157,* 164201
6. S.A. Steinmetz, T.Y. Chen, B.M. Goldberg, C.M. Limbach, C.J. Kliewer*, "Resolved rotation–vibration non-equilibrium with rotational VIPA-CARS" *Opt. Lett,* **2022,** *47*, 5429-5432
7. Troß, J.; Carter-Fenk, K.; Cole-Filipiak, N. C.; Schrader, P. E.; Word, M.; McCaslin, L. M.; Head-Gordon, M.; Ramasesha, K., Excited State Dynamics during Primary C-I homolysis in Acetyl Iodide Revealed by Ultrafast Core-Level Spectroscopy, *J. Phys. Chem. A*, **2023**, 10.1021/acs.jpca.3c01414
8. Chen, T. Y.; Steinmetz, S. A.; Patterson, B. D.; Jasper, A. W.; Kliewer C. J.; Direct observation of coherence transfer and rotational-to-vibrational energy exchange in optically centrifuged CO_2 super-rotors, *Nat. Comm.,* **2023**, *14*, 3227
9. Troß, J; Arias-Martinez, J. E.; Carter-Fenk, K; Cole-Filipiak, N. C.; Schrader, P.; McCaslin, L. M.; Head-Gordon, M; Ramasesha, K; Femtosecond core-level spectroscopy reveals involvement of triplet states in the photodissociation of gas-phase $Fe(CO)_5$, *J. Am. Chem. Soc.,* **2024**, 146 (32), 22711-22723
10. Cole-Filipiak, N. C.; Troß, J.; Schrader, P.; McCaslin, L. M.; Ramasesha, K; Ultrafast production of NiCO and Ni following 197 nm photodissociation of nickel tetracarbonyl, *ACS Phys. Chem. Au (Letter),* **2024,** DOI: 10.1021/acsphyschemau.4c00033
11. Rishi, V.; Cole-Filipiak, N. C.; Ramasesha, K**;** McCaslin, L. M.; Excited State Electronic Structure of Dimethyl Disulfide Involved in Photodissociation at ~200 nm, *Phys. Chem. Chem. Phys.,* **2024**, DOI: 10.1039/D4CP02505A

Quantum Chemistry of Radicals and Reactive Intermediates

John F. Stanton
Quantum Theory Project
Departments of Chemistry and Physics
University of Florida
Gainesville, FL 32611
johnstanton@ufl.edu

Scope of Research

My research group works in the area of theoretical chemical physics, especially on the thermodynamics, spectroscopy and chemistry of organic radicals and other reactive intermediates. This research follows a number of paths, including first-principles calculation of bond energies and other thermochemical information (as well as development of methodology needed for such calculations), methods for the simulation and analysis of molecular spectra (especially those relevant to experiments that can be used to glean thermochemical information), the development of *ab initio* quantum chemical methods needed for the accurate treatment of fundamental aspects of electronic structure and potential energy surfaces, and computational kinetics including semiclassical transition state theory and master equation modeling of chemical reactions.

Summary of Selected Recent Accomplishments and Future Plans

• While a number of researchers around the world have worked in the area of nonadiabatic effects in spectroscopy (albeit far less than those that have focused on areas such as "quantum chemistry"), there is a class of problems that have rarely been studied. Specifically, when the coupled states have the same electronic symmetry, the so-called coupling modes are totally symmetric. In most examples – including classic problems such as the coupling in NO_2 ($^2B_2$ and $^2A_1$) and between the $^2A_2'$, $^2E''$ and $^2E'$ states of NO_3 – the coupled vibrational modes (which belong to symmetry species contained in the direct product of the two irreducible representations of the coupled electronic states) are separate from the Franck-Condon active (totally symmetric modes). In a case where the electronic states have the *same* symmetry, this clean separation is spoiled, and every feature in their spectra exhibit a mixture of simple Franck-Condon phenomena as well as vibronic coupling. This results in a qualitatively different and considerably more difficult problem for those that wish to model the spectra.

Motivation for research in this direction comes from the Active Thermochemical Tables (ATcT) project, in which our group plays a role as a member of a vital task force. Specifically, a current area of focus for the task group involves carbonic acid (H_2CO_3), and molecules

such as the (notoriously difficult) CO_3 singlet group state and the neutral and anionic states of HCO_3. The latter two can be viewed as the neutral and anionic forms of the hydroxy-formyloxy radical – an OH-substituted version of the notorious HCO_2 radical that has been extensively studied by members of the GPCP program (D.M. Neumark and R.E. Continetti, along with our group). While the parent species is now quite well understood in terms of a powerful coupling between its $^2B_2$ and $^2A_1$ electronic states (the adiabatic gap[1] between the two is 318 cm^{-1}), the hydroxy group in the parent species breaks the C_{2v} nuclear framework symmetry to C_s, and the two states so strongly and profoundly coupled in HCO_2 are both now $^2A'$ states. As a result, it is extremely difficult – impossible, really – to construct the vibronic Hamiltonian in the way that my group and I have done for the last two decades. However, behind the initiative of postdoctoral scholar Dr. Greg Jones (PhD, Caltech, with Okumura), a new approach[2] has been developed for constructing vibronic Hamiltonians based on the equation-of-motion coupled-cluster (EOM-CC) method that performs so well for vibronically coupled systems[3]. This work – which is still in progress – will help us to confidently assign the origin band in a previously recorded negative-ion photodetachment study of the HCO_3 anion[4], which will ultimately lead to improved thermochemical knowledge of this biologically important series of molecules.

• A controversy in the spectroscopy community has been raging for about fifteen years. It centers on the assignment of the degenerate stretching (ν_3) vibration of the NO_3 radical. In short, a number of theorists *and* experimentalists have favored the original – and high – value of 1492 cm^{-1} recorded long ago by Hirota in the infrared, while many theoreticians and a few experimentalists have favored a lower value near 1050 cm^{-1}. Despite a very low signal-to-noise recording of an IR-allowed – but very weak – band in this region by Kawaguchi[5] experimental work by the Neumark group at Berkeley together with a decade of calculations by my group as well as Bowman and Emory and Eisfeld in Germany, the problem remains visible in the annual International Symposium for Molecular Spectroscopy (now held in Urbana, IL). However in the last year, we have collaborated with the Newmark group yet again on this problem. And this time with spectacular success. In short, the Neumark group has developed a variation of anion photoelectron spectroscopy in which vibrational preexcitation of the anion is achieved prior to photodetachment. By these means and a truly fortuitous near coincidence of the ν_3 fundamental and sublevels of its first two overtones for NO_3^-, extremely rich information about the vibrational structure of the neutral molecule has been recorded. Although it is virtually useless to think about the spectra from the perspective of the Franck-Condon principle (vibronic bands completely dominate the spectra of $\nu_3 = 1, 2$ and 3 levels of the anion) simulations of the spectrum based on a model Hamiltonian developed in our group a decade earlier absoutely confirm the latter (low) assignment of ν_3, which convincingly settles the longstanding debate in the community. This work will soon be submitted for publication.

[1]E. Garand, K. Klein, J.F. Stanton, J. Zhao, T. Yacovitch and D.E. Neumark *J. Phys. Chem. A* 114, 1374 (2010).

[2]Dr. Jones' approach is closely related to the work done by Cave roughly a decade ago [R.J. Cave and J.F. Stanton *J. Chem. Phys.* 140, 214112 (2012).]

[3]See A.I. Krylov *Ann. Rev. Phys. Chem.* 59, 433 (2003).

[4]X.-B. Wang and S. Xantheas *J. Phys. Chem. Lett.* 2, 1204 (2011).

[5]K. Kawaguchi, J. Tang and N. Akakusa *Chem. Phys. Lett.* 765, 138315 (2021).

• In a very recent piece of work, we have studied the surprisingly fascinating anion of the BH_3 molecule. The electron photodetachment spectrum of the corresponding molecular anion was recorded about twenty years ago by Ellison and coworkers, who found an electron affinity of 0.038±0.015 eV, which is one of the smallest electron affinities ever recorded for a molecule. As a postdoctoral, your narrator ran calculations on this system and ultimately gave up, informing the authors of that work that they much have made a mistake. However, my excellent postdoc Peter Franke dug deeply into this problem, going down paths that his mentor had never tried and reside outside his sphere of knowledge. It turns out that BH_3 is a – perhaps uniquely in the following sense – interesting molecular ion. It is electronically unbound (*i.e.* the lowest electronic state of BH_3^- is the BH_3 molecule here and an additional electron at infinite separation), but bound by zero-point energy. To compute the electron affinity of such a species, it is necessary to look at the potential energy surface of the electronic resonance state that becomes bound – again by zero-point vibrational energy – only in regions that are above the minimum of the resonance state (see below). Using the RAC (resonance analytic continuation) approach suggested to us by T. Sommerfeld (U. Southeastern Louisiana), an expert in this area, Dr. Franke has carried out an extensive set of calculations and find an electron affinity of 43 meV, nicely inside the error bounds of the Ellison experiment. This is a beeautiful piece of work, and we plan to submit it to a high-profile journal.

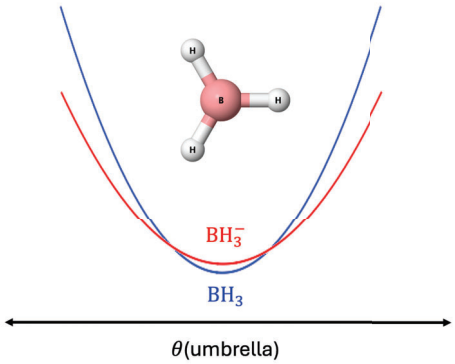

The qualitative nature of the potential energy surfaces of the ground state of BH_3 and the BH_3^- resonance state. The latter becomes bound when zero-point effects are included, due to a (small) lengthening of the BH bond distance upon electron attachment which lowers the zero-point energy of the anion enough that the total energy (electronic + zero-point effects) falls below that of the neutral at the anion equilibrium geometry.

All additional DOE-supported research can be found in the publications listed in the final section of this document.

Students and Postdoctoral Supported:

M.B. Bentley (student)
P.R. Franke (postdoc)
G. Jones (postdoc)

References from 5/2023-9/2024 citing BES-GPCP grant

P.R. Franke and J.F. Stanton "Rotamers of Methanediol: Composite Ab Initio Predictions of Structures, Frequencies, and Rovibrational Constants" *J. Phys. Chem. A* 924 (2024) (Early Access).

T.L. Nguyen and J.F. Stanton "The reaction of methylidyne with methane: role of the quartet electronic state" *Mol. Phys.* 122 (2024).

Y.J. Qian, T.L. Nguyen, P.R. Franke, J.F. Stanton and M.I. Lester *J. Phys. Chem. Lett.* 15, 6222 (2024).

N.P. Sahoo, P.R. Franke and J.F. Stanton *J. Comp. Chem.* "On the performance of composite schemes in determining equilibrium molecular structures" 45, 1419 (2024).

P.R. Franke and J.F. Stanton Influence of fourth-order vibrational corrections on semi-experimental (reSE) structures of linear molecules

T.L. Nguyen, J. Peeters, JF Woeller, A. Perera, D.H. Bross, B. Ruscic and J.F. Stanton "Methanediol from cloud- processed formaldehyde is only a minor source of atmospheric formic acid" Proc. Nat'l. Acad. Sci. 120, e2304650120 (2024).

B.J. Esselman, M.A. Zdanovskaia, A.N. Owen, J.F. Stanton, R.C. Woods and R.J. McMahon "Precise Equilibrium Structure of Benzene" *J. Amer. Chem. Soc.* 145, 21785 (2024).

P.B. Changala, P.R. Franke, J.F. Stanton, G.B. Ellison and M.C. McCarthy "Direct Probes of -Delocalization in Prototypical Resonance-Stabilized Radicals: Hyperfine-Resolved Microwave Spectroscopy of Isotopic Propargyl and Cyanomethyl" *J. Amer. Chem. Soc.* 146, 1512 (2024).

N.B. Jaffey, J.F. Stanton and M.C. Heaven "Photoelectron Velocity Map Imaging Spectroscopy of the Beryllium Trimer and Tetramer" *J. Chem. Phys. Lett.* 14, 8339 (2023).

Universal and State-Resolved Imaging Studies of Chemical Dynamics

Arthur G. Suits
Department of Chemistry, University of Missouri, Columbia MO 65211
suitsa@missouri.edu

1. Program Scope

The focus of this program is on combining universal ion imaging probes providing global insight with high-resolution state-resolved probes providing quantum mechanical detail, to develop a molecular-level understanding of chemical phenomena. Particular emphasis is placed upon elementary reactions involving transient species and in revealing new aspects of reaction mechanisms and the dynamical behavior of molecules. Much of the current effort here is in generalizing the lessons from simple systems as we investigate the behavior of larger polyatomic molecules and radical-molecule reactions. This research is conducted using state-of-the-art molecular beam machines, photodissociation, reactive scattering, and vacuum ultraviolet lasers in conjunction with velocity map ion imaging and other techniques we develop. One focus of our effort remains crossed-beam reactive scattering of polyatomic molecules. These are supplemented in some cases by complementary Chirped-Pulse Fourier-Transform mmWave spectroscopy studies in a uniform supersonic flow (CPUF). In addition, new directions in ultrafast time-resolved studies of photochemical processes are also underway taking advantage of the MeV UED facility at SLAC.

2. Recent Progress

2.1 Crossed Beam S(^{3}P) Reactive Scattering

We continue our ongoing studies of bimolecular reaction dynamics using crossed-beam velocity map imaging with single-photon 157 nm detection. In last year's report we described our initial investigations of ground state sulfur atoms in reaction with conjugated hydrocarbons studied in collaboration with Dr. J. Zádor at Sandia. Our results, supported by theory, show that the reaction proceeds by barrierless addition on the triplet surface which is followed by intersystem crossing to the singlet then to products. This synergistic collaboration led to deep insight into the products and pathways as described below and reported in two publications.

Until our recent work there appear to have been no fundamental studies of the reaction dynamics of ground state sulfur atoms using modern methods. We have performed crossed molecular beam imaging of S(^{3}P) reaction with unsaturated hydrocarbons focusing on 1,3-butadiene (13BD), and isoprene (2-methyl-1,3-butadiene), but including a survey of many others. In our Abstract last year we reported the open shell products of these reactions which are readily detected using our 157 nm probe. These include the H loss pathway from 13BD giving the resonantly stabilized 2-H-thiophen-5-yl (2HT) radical, the same radical product resulting from methyl loss for isoprene. H loss from isoprene was also readily observed and we have now identified this product as 2H-3methyl-thiophen-5yl (2H3MT) or 2H-4methyl-thiophen-5yl (2H5MT) radicals (or both) which have similar energies.

Detailed predictions of the product pathways and energetics using KinBot prompted us to attempt imaging of many of the closed shell channels. For the 13BD reaction at our 13.6 kcal/mol collision energy, KinBot predicted ~80% branching to thiophene + H_2, ~20% to thioketene + ethene, and only 0.2% to H loss. In favorable cases we find the closed shell products may be detected by focusing our 157 nm laser, which we assume are ionized by 1+1 REMPI through high-lying Rydberg states. Fig. 1A shows the reactive scattering image of the H_2-loss product (thiophene) at m/z=84 resulting from S(^{3}P) reaction 13BD with the Newton diagram superimposed. The recoil velocity distribution is obtained by projection onto the x-axis, from which translational energy distribution shown in Fig 1C is derived. The distribution peaks near 20 kcal/mol and extends to 75 kcal/mol consistent with the exit barrier predicted by theory for this product. We could

detect the predicted thioketene only very weakly so we could not obtain translational energy distributions for this product. However, this is one of the products we did detect using CPUF as described further below.

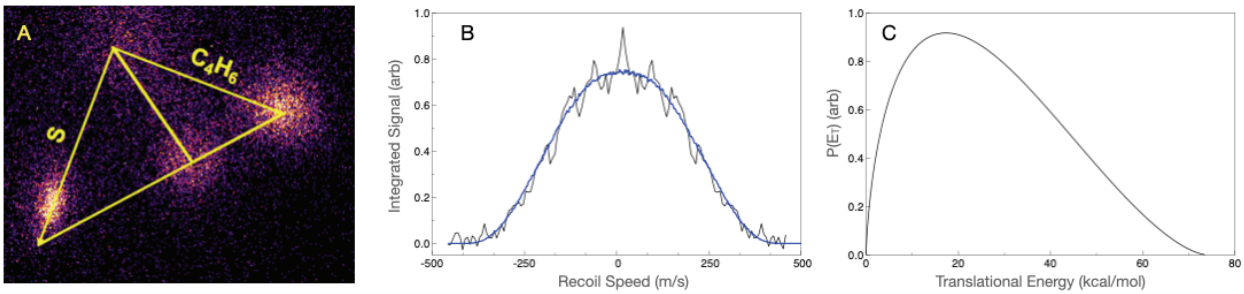

Figure 1. *A) Velocity map image of the 84 u product (thiophene) of the crossed-beam reaction of S(^{3}P) with 1,3-butadiene at 13.6 kcal/mol collision energy. The most probable Newton diagram is superimposed on the image showing the beam velocities and the center-of-mass velocity of the system. B) Recoil speed distribution following projection onto x-axis. C) Total translational energy distribution determined for the reaction based on the measured recoil velocity distribution in the image.*

We also performed the analogous experiment for S(^{3}P) reaction with isoprene. In this case theory predicts a rich array of open product channels, but we have only obtained bottleneck barriers to identify likely products, not detailed branching. For the isoprene reaction, 3-methyl thiophene (H_2 elimination) had the lowest bottleneck barrier 12.2 kcal/mol below the entrance channel, and it is likely the dominant channel by analogy with the 13BD reaction. The image and translational energy distribution (not shown) are very similar to those in Fig. 1. The translational energy distribution again shows evidence of the substantial exit barrier predicted by theory. We also obtained an image at 72 u corresponding to ethene elimination. We initially assumed this was methyl thioketene by analogy with the 13BD reaction. Theory showed, however, the limiting barrier height to be 2.3 kcal/mol lower for thioacrolein. The latter also has the lowest ionization energy among the possible 72 u products, 8.3 eV, which is consistent with our ability to detect it. The results highlight the powerful combination of KinBot with crossed-beam velocity map imaging employing VUV detection.

2.2 CPUF studies of S(^{3}P) Reactions

To complement the crossed-beam studies, we also used broadband rotational spectroscopy in a uniform supersonic flow at 20 K. Although we could barely detect reactive scattering leading to the predicted thioketene product in the 13BD reaction suggested by theory at mass 58 u, we could see it clearly in the 20 K flow. Under these conditions, the products are rotationally (and, to a more limited extent, vibrationally) cooled in the flow for detection by rotational spectroscopy. We detected the thioketene product on the $7_{0,7}$ – $6_{0,6}$ transition at 78.424 GHz as shown in Fig. 2a. This result shows that thioketene is formed in the reaction at 20 K, consistent with the potential surface that shows no barrier above the reactant energy *en route* to products. We then searched unsuccessfully for thiophene, which is predicted to dominate branching at zero collision energy by 130:1. Simply on the basis of linestrength and the 20 K rotational partition function, we would expect the thiophene signal to be nearly 50 times larger than thioketene. However, given the large exoergicity and the much hotter expected internal energy distribution for thiophene *vs*. thioketene, we believe the non-detection of thiophene in the low temperature experiment is due to the large difference in the effective vibrational partition function. We have also looked for products from the isoprene reaction in the flow. In this case we detected thioformaldehyde as shown in Fig. 2b. Interestingly, theory predicts four possible coproducts for thioformaldehyde with similar barrier energies, although 1,3-butadiene is the

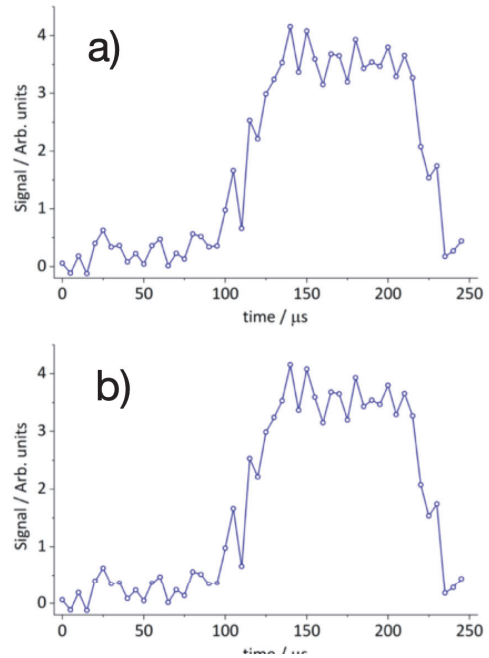

Figure 2. Time-dependent integrated line intensity for a) thioketene at 78.424 GHz from the 13BD reaction and b) thioformaldehyde at 69.747 GHz from the isoprene reaction. The laser is fired at 15 us.

lowest at -2.0 kcal/mol. Although the conditions in the flow are vastly different from the high energy crossed beam scattering, they are important to confirm the appearance of these products and the barrierless (or nearly so) addition leading to ISC.

2.3 Product Branching and Ultrafast Dynamics in Oxazole Photodissociation

Several years ago, we applied the CPUF method to determine the asymptotic product branching in the UV photodissociation of isoxazole, c-C_3H_3NO, an interesting heteronuclear aromatic with a weak N-O bond in the ring. We identified and quantified seven products involving five different reaction channels in that system, and argued, based on comparison to pyrolysis and ultrafast surface hopping studies, that some arose from direct excited state decomposition while others involved internal conversion and a more extended exploration of the ground electronic state. This previous work led us to propose to study this molecule at the MeV UED facility at SLAC. We happened to learn that Daniel Rolles and his team from the McDonald lab at KSU were also interested in this system. We joined forces and had very productive beamtime last January led by our post-doc Bryn Downes-Ward.

Isoxazole and oxazole are both five-membered heterocyclic molecules with an oxygen and a nitrogen atom. In isoxazole the heteroatoms are neighbors, in oxazole, they are separated by a carbon atom. Both molecules undergo ring opening following excitation at 200 nm followed by subsequent fragmentation. In the case of isoxazole, the dissociation dynamics are expected to be controlled by a low-lying intermediate state near the S_1/S_0. No equivalent structure exists for oxazole, however relaxation via a bicyclic intermediate is expected to be possible in oxazole. While the ring opening process is thought to be similar in both molecules we expected to see differences in the intermediate structures and timescales. We studied the early time dynamics using diffraction by a relativistic electron beam. Surprisingly we observed similar timescales for both molecules. We observe clear time-dependent signal changes that we believe are associated with the ring open structure and a possible three-membered ring structure. Preliminary results for isoxazole are shown in Fig. 3. We also observe a possible electronic signature at early times. We are still in the process of analyzing the data which will be compared to theoretical nonadiabatic dynamics from Prof. Christine Aiken at KSU.

We also studied the asymptotic products and their branching using CPUF. The detected photoproducts and respective branching fractions (%) are the following: HCN (70.4), HCO (22.8), CH_2CN (4.2), CH_2CO (1.0), CH_3CN (1.0), HNC (0.9), HNCO (0.08). We believe the discrepancy between the HCO and CH_2CN yield is owing to the formation of the other isomer, CH_2NC which we did not yet probe. We also studied the relaxation of vibrational excited HCN in a range of vibrational levels, obtaining the effective rate coefficients at 20 K.

3. Future Plans

$S(^3P)$ reactions. We will explore reactions first with butene isomers, both in crossed beams and with CPUF. We will continue to collaborate with Dr. Zádor at Sandia in these studies. We have plans to use two color 1+1' probe of the closed shell products in the crossed beam studies using VUV + VIS to enhance our

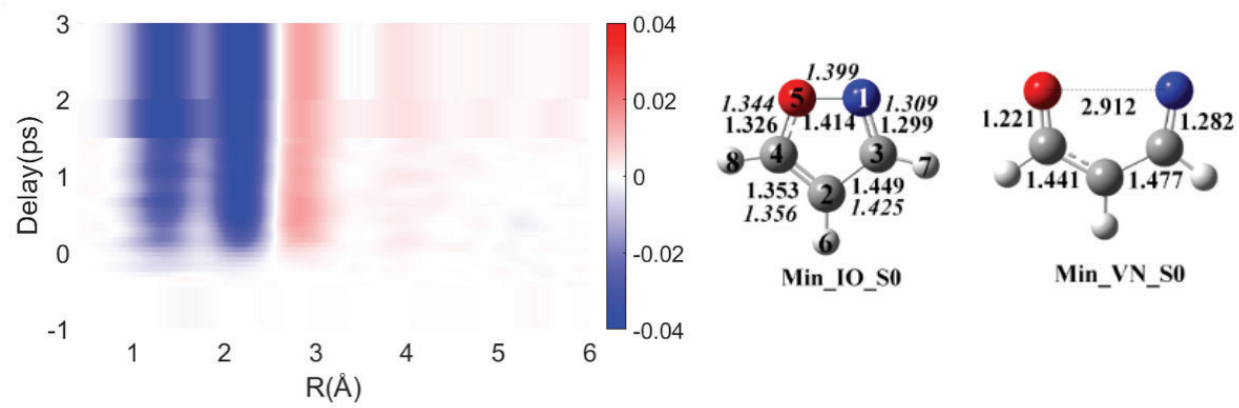

Figure 3. Left: The time-dependent difference pair distribution function of isoxazole. Blue indicates loss of bond and red indicates gain of a bond. Bonds are lost a 1.4 Å and 2.2 Å corresponding to neighboring and opposite atom distance in the ring closed molecule respectively. Right: Structures of the ground state equilibrium geometry and ring-opened minimum are shown from J. Cao, J. Chem. Phys. 142 (2015) 244302.

sensitivity in these experiments.

Oxazole and Isoxazole. We will complete the analysis of the oxazole and isoxazole results from the MeV UED facility and we plan to look for the isocyanomethyl radical from oxazole photodissociation once we locate the rotational transitions in the mmWave regime.

4. DOE Publications 2022-present

D. Paul, Z. Yang, A. G. Suits, D. H. Parker, R. I. Kaiser, "Photodissociation Dynamics of Xylene Isomers $C_6H_4(CH_3)_2$ at 157 nm using an Ultracompact Velocity Map Imaging Spectrometer – The C_7H_7 Channel," *Chem. Phys. Lett.* (2022) 807, 140064. https://doi.org/10.1016/j.cplett.2022.140064

H. Li, J. Lang, C.D. Foley, J. Zádor and A. G. Suits, "Sulfur (^{3}P) Reaction With Conjugated Dienes Gives Cyclization to Thiophenes Under Single Collision Conditions," *J. Phys. Chem. Lett.* (2023) DOI: 10.1021/acs.jpclett.3c01953.

J. Lang, C. D. Foley, S. Thawoos, A. Behzadfar, Y. Liu, J. Zádor, and A. G. Suits, "Reaction dynamics of S(^{3}P) with 1,3-butadiene and isoprene: Crossed beam scattering, low temperature flow experiments, and high-level electronic structure calculations," *Faraday Discuss.* (2024) **251**, 550-572

N. Dias, N. Suas-David, S. Thawoos, and A. G. Suits, "Broadband Rotational Spectroscopy in Uniform Supersonic Flows: CPUF for Reaction Dynamics and Low Temperature Kinetics," *Acc. Chem. Res.* (accepted).

B. Downes-Ward, A. Behzadfar, S. Thawoos, A. G. Suits, "Product branching in the photodissociation of oxazole detected by broadband rotational spectroscopy," *Phys Chem Chem Phys* (accepted).

Nanostructure Evolution During TCD with Regeneration by Partial Oxidation for Maintaining Autocatalytic Activity

Mpila Nkiawete[1], Randy Vander Wal[1,2], Adri van Duin[2] and Margaret Kowalik[2]
[1]The EMS Energy Institute and [2]The Dept. of Mechanical Engineering
Penn State University
University Park, PA 16802
Emails: ruv12@psu.edu, acv13@psu.edu

1.0 Program Scope

1.1 Motivation for Thermo-catalytic Decomposition

Hydrogen is envisioned as the energy carrier (fuel) of the future and is a crucial feedstock for various manufacturing industries. Thermo-catalytic decomposition (TCD) of methane can produce CO_X-free hydrogen for PEM fuel cells, oil refineries, ammonia and methanol production [1]. Recent research has focused on enhancing the production of hydrogen by the direct thermo-catalytic decomposition of methane to form elemental carbon and hydrogen as an attractive alternative to the conventional steam reforming process [2].

Carbon as a catalyst has many advantages compared to other catalytic materials: a) fuel flexibility, b) insensitivity to sulfur poisoning and c) high temperature resistance. TCD offers 100% carbon capture with the solid, high purity carbon useful as electrode material for energy storage [3]. Despite these advantages, carbon as a catalyst also problematically deactivates. Ideally the deposited carbon would be autocatalytic but all studies with methane find that *the deposited carbon is not as active a catalyst as the original carbon.*

1.2 Addressing TCD and Regeneration Research Needs

High fidelity parallels exist between TCD and soot processes. The TCD rate may be viewed as equivalent to a soot particle growth rate. Both reactions add mass via heterogenous radical-driven reactions. In a flame environment, variables affecting growth are highly coupled. In TCD these factors may be disentangled, and their contributions resolved. Of particular interest are the relationships between nanostructure, active sites and growth rate. These same connections apply to TCD. Nanostructure governs active site number. In turn, active sites determine kinetic rates. Additionally, deposition conditions determine nanostructure and thus kinetic rates. The overall project goal is to connect active sites, nanostructure and deposition rates in concert with reactive force field (ReaxFF) based modeling.

2.0 Recent Progress

2.1Packed Bed

The principal advantage of the packed bed is its scale enables monitoring reaction kinetics by reaction products with standard instrumentation. Product analyses furnish reaction metrics of yield, (product) selectivity and (catalyst) stability. Particular parameters of interest include reaction selectivity, yield and stability.

The challenge in determining each of these metrics lies in the intermediate regime where both the initial carbon catalyst and evolving TCD carbon both contribute to the overall reaction/conversion. Depending upon the relative reactivity of the two different carbons, varied time behaviors can be observed for the reaction rate and conversion yield with time. At longer durations it can be safely assumed that only the deposited carbon is contributing to the observed activity – due to complete coverage of the initial catalyst and asymptotic behavior of the observed reaction rate.

Approach

Starting carbon catalyst(s) are placed in a U-shaped quartz tube held in a vertical reactor. Mass flow controllers regulate the flow mixtures consisting of a mixture of inert carrier and hydrocarbon gas or mixture for TCD or inert plus oxidizer, such as CO_2, H_2O or O_2 for regeneration. The synthetic natural gas consisted of 85% (v/v) methane, 10% ethane and 5% propane. Reactants and products from either TCD or regeneration (RGN) are continuously monitored by on-line calibrated FTIR. Oxidation levels are gauged by integration of measured CO/CO_2 oxidation products. The experimental procedure was designed to evaluate the performance of the carbon catalyst through a cycle of TCD – RGN – TCD to test regeneration effectiveness for regaining (or increasing) TCD activity after loss following the 1st TCD cycle.

Results

Figure 1a shows the concentrations of the unreacted components of natural gas emerging from the bed during 2 TCD cycles; in each cycle the temperature is ramped as indicated by the dotted black line, reaching 900 ℃ after ~ 45 minutes as seen for the 1st cycle. At this temperature the methane drops by ~ 8% while the ethane and propane components drop substantially, reaching nearly full conversion. In this abbreviated run minimal carbon deposition has occurred incurring minimal loss of catalytic activity whereas in our previous reports significant catalyst deactivation was observed at longer reaction durations. After the this 1st TCD cycle regeneration was performed to remove deposited TCD carbon with likelihood of concurrently increasing the activity of the nascent carbon catalyst. Integration of the evolved CO/CO_2 products (shown in Fig. 1c) yielded an estimated 9 wt.% loss of carbon from the bed, based on the initial catalyst mass, effectively a small partial oxidation across the temperature range of 750 – 500 ℃. In prior studies the increase in active site concentration for R250 was measured for varied levels of partial oxidation by activated O_2 chemisorption followed by XPS analysis for O-atom content and oxygen functional group identification and relative contents. For the estimated 9 wt.% carbon loss the projected increase in active sites would by ~ 2-fold relative to the nascent R250. However the 2nd TCD cycle did not reveal any significant change in the TCD reaction conversions, as monitored by SNG component concentrations. A possible explanation is that the TCD carbon was preferentially removed while the nascent R250 catalyst was merely brought back to its initial activity level. Tests at longer TCD duration are on-going to evaluate the reactivity (preferentially) of the TCD deposited carbon.

The middle panel, **Fig. 1b** shows the byproduct gases emerging from the packed bed during both TCD stages. As with **Fig. 1a**, the temperature ramp is marked by the dotted black lines. The ethylene and propylene products are the dehydrogenation products of their respective SNG aliphatic components and not the result of gas and/or surface recombination reactions. The fast decay their concentrations to a steady-state value reflects the balance of their formation and loss (via TCD) rates. Meanwhile the benzene derives from 2 reactions paths with precursors of ethylene or propylene; each requiring several steps of hydrogen abstraction/loss to reach the prerequisite radicals for recombination.

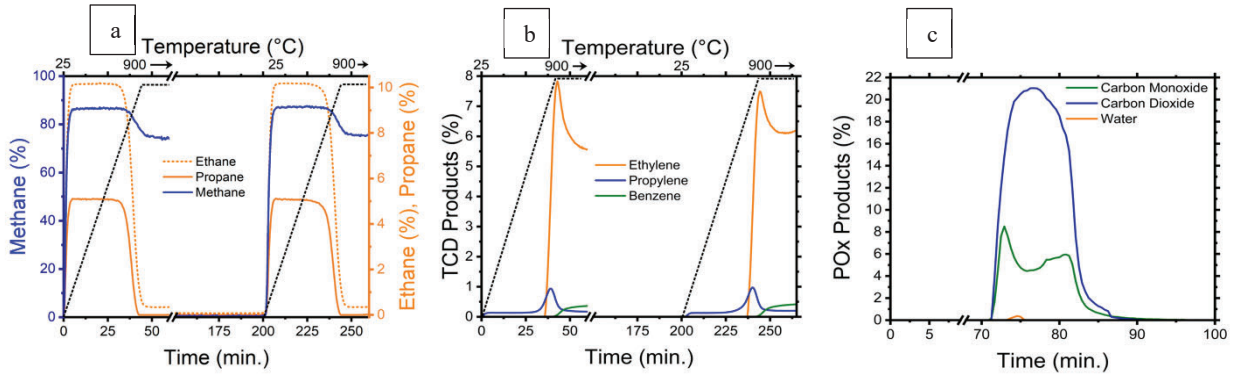

Figure 1. Graph (a) illustrates the decomposition kinetics of methane, ethane, and propane during thermal catalytic decomposition, (with notable differences in their reactivity and rates of consumption for the cycles as indicated), pyrolysis products (b) and intervening regeneration stage (c) with reaction products as shown.

2.2 Seeded Carbon Aerosol

Motivation

A packed bed reactor is well designed for kinetic measurements, and global reaction metrics such as conversion, yield and selectivity. However the gas percolating through the bed undergoes a time-varying history, assuming uniform temperature throughout the bed, in addition to the gas being at the bed temperature upon entry. Gas-phase pyrolysis reactions can occur in addition to surface catalyzed reactions contributing to apparent reaction metrics. gas-phase chemistry. With a finely packed bed material, e.g. carbon black, the uniformity of exposure during the course of reaction is unclear. Last, the mechanical actions of sampling and dispersal of bed material for TEM analysis raises the question of potential perturbation of the TCD deposited carbon.

TCD Aerosol Advantages

Suspending the catalyst as an aerosol provides uniform particle compositional exposure and temperature, permitting best assessment of particle catalyzed TCD carbon. A diluted hydrocarbon concentration can mitigate pyrolysis product

impacts on hydrocarbon decomposition and carbon deposition. Alternatively the hydrocarbon concentration can be increased to study the "self-catalyzed" carbon particle formation for comparison to seeded catalyst particles, e.g. carbon blacks.

To address concerns associated with post-mortem diagnosis of packed bed material and to test active sites in a more direct manner, a seeded aerosol approach was employed. Aerosolized unoxidized carbon blacks, partially oxidized (i.e. re-activated) carbon blacks, activated carbon and fullerenes were tested. Suspended in a carrier flow of inert plus hydrocarbon reactant, such as ethylene, the mixture flowed through a process tube at 1500 ℃, wherein pyrolysis reactions ensued. Carbon aerosol outflow was collected using 2 micron pore size Teflon Whatman filters in a Gelman filter holder. Collected carbons were dispersed in ethanol using ultrasound prior to deposition upon a TEM grid for analysis.

Research Questions

The intended research questions were as follows.

1. What is the deposited carbon nanostructure dependence upon the feed hydrocarbon?
2. What is the deposited carbon nanostructure dependence upon the carbon catalyst nanostructure?

The former can be addressed by varying the hydrocarbon (HC) for the same carbon seed nanostructure while the latter can be evaluated by varying the carbon seed nanostructure for the same HC feed.

Results

As the TEM images in **Fig. 2** show, the Ketjenblack is a partially oxidized carbon, accounting for its appearance; hollow interior voids and increased graphenic structure in its outer shell. Both structural aspects are hallmarks of low-temperature oxidation. Significantly the hollow interior voids necessitate the presence of pores and channels through bordering lamellae that enabled oxidizer inflow and product outflow. Upon seeding this "activated" carbon within the reactive gas at elevated temperature, carbon deposition occurred, as shown in **Fig. 3**. Surprisingly, instead of forming additional outer lamellae, the interior densified while coral-like graphenic sheets formed around the particle perimeter. The dark segments appearing within the particle are interpreted as the original lamellae forming the interior voids, appearing with greater contrast due to their orientation to the beam axis. Other carbon formed by TCD within the particle appears less structured and with lower contrast. The outward directed graphenic sheets on the particle surface resemble sails, both flat and folded. These images document secondary carbon growth upon carbon catalysts, by a gas-surface heterogenous reaction sequence, using preformed (and pre-oxidized) carbon black as an aerosol. As seen, the nanostructure of the catalyst carbon appears to account for the structure of the TCD carbon.

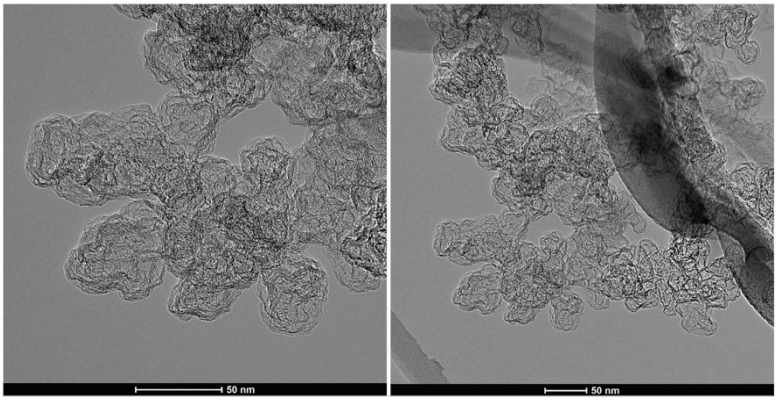

Figure 2. TEM images of nascent AkzoNobel carbon black, prior to seeding.

In sharp contrast, the ethylene within the carrier flow formed independent, smaller carbon particles with lamellae arranged concentrically, in the usual core-shell fashion. Notably these particles exhibited no unusual structure with no external, outward directed graphenic sheets on the particle surface, unlike the seeded Ketjenblack. Formed by pyrolysis, at high temperature, unseeded tests confirmed their identity by size and structure. In comparison to the Ketjenblack, the nanostructure of the catalyst carbon appears to account for the structure of the TCD carbon.

To test the capability of ReaxFF-based molecular dynamic simulations, a model carbon structure analogous to a "cotton sphere" is being tested under reactive environments, namely 25% ethylene at 1500 ℃.

These experiments directly address whether the form of TCD carbon is dependent upon the initial catalyst. The fixed bed and CVD tests used mature particles as the initial catalyst; non-uniform carbon "outgrowth" structures resulted, referred to here as "carbon coral". By the aerosol approach we can test the dependence of such coral growth upon

other carbon catalysts not readily incorporated into beds and with far more uniform exposure. Moreover, the same catalyst particles as studied earlier can also be seeded to test whether similar outgrowths are observed without the encumbrances of variable and unknown gas exposure as in a packed bed.

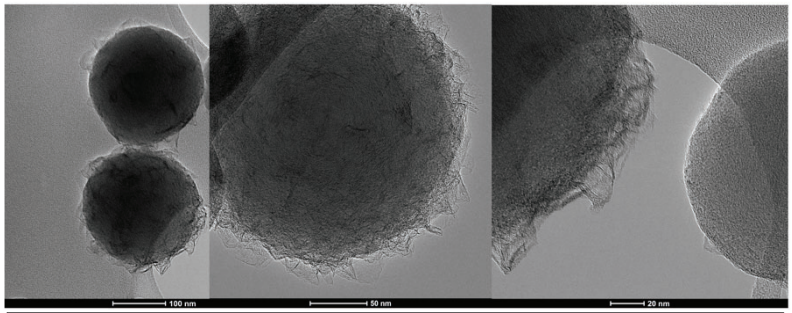

Figure 3. TEM images of AkzoNobel carbon black after exposure to 1500 °C under 25% C_2H_4 in Ar carrier.

Soot growth modelling with use of the ReaxFF method

To gain a better understanding on the experimentally observable differential growth of deposited carbon due to the structural variation in the carbon black seeding, the series of the reactive molecular dynamics simulations, with use of the ReaxFF method, are proposed. The ReaxFF method was shown to be adequate atomistic simulation approach in modelling pyrolysis processes and soot formation [4,5]. Additionally, ReaxFF has been applied to differentiate and identify the parameters characteristic for the physical and chemical nucleation in the presence of a metal cluster [6], a range of the precursors, e.g. acetylene [4] e.g. from 2, 5-dimethylfuran [7], as well in the presence of an external electric field [8]. Here we turn our attention to the model carbon black seeding to compare with the experimental.

The initial structures begin with an initial density equal 0.98 g/cm^3, 1.27 g/cm^3 and 2.3 g/cm^3 placed in the middle of the simulation box filled with the synthetic natural gas (SNG) are shown in **Fig. 4a**. In the case of the presented snapshots there are 50 molecules of propane, 100 molecules of ethane and 850 molecules of methane, representing the SNG composition are placed randomly in the simulation box as seen in **Fig. 4b**. The systems with the same model carbon black seeding and only 850 methane molecules will be also considered, as well as two more simulation boxes: with only SNG and only methene molecules in our next comparisons. For these the simulation scenario will be comparable to previously proposed steps: the initial equilibration at room temperature; heating from 300K to the range of the final temperatures: 1800K, 2500K, 3000K; pyrolysis simulations for minimum 10ns; cooling down to 300K and finally equilibration simulations at 300K. The possible variation in the soot growth will be analyzed, by assessing

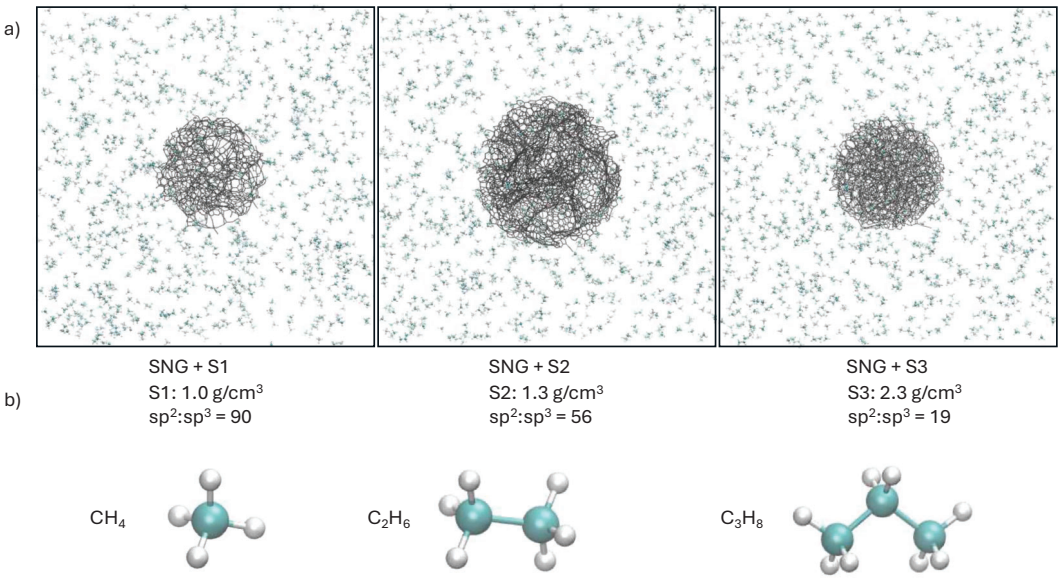

Figure 4. Atomistic models. a) The initial structures of the considered model carbon seedings, where all carbon-carbon bonds are indicated with the black sticks and the gas molecules, where carbon atoms are indicated as cyan and hydrogen spheres. b) The atomistic representation of the components of the synthetic natural gas: methene, ethane and propane.

possible changes: in particle mass; structure, and by comparing possible shifts in the radial pair distribution functions, sp^2:sp^3 ratio and ring statistics.

3.0 Future Plans

Reactive force-field (ReaxFF) based simulations will be used to gauge evolution of deposition carbon structure during both TCD and RGN reactions as well as probe the dependence of initial deposition upon the underlying carbon nanostructure. It should be noted that these simulations begin with a structural model and need benchmarks for comparison during development. We anticipate that models of active sites at different reaction stages coupled with TCD and RGN rates will serve to capture the range of TCD formed nanostructures.

Experimentally we also plan to further connect active sites with kinetic rates using the packed bed reactor across TCD and RGN reactions. Pairing TCD with RGN in a cyclic, iterative manner is planned in order to test the equivalency of active sites between RGN and TCD reactions. As a cross-check, pulsed chemisorption using acetylene is being evaluated for comparative active site determination. Finally, additional seeded aerosol tests are planned given the decided advantages of uniform conditions, direct observations of deposited carbon forms and connection with modeling efforts.

4.0 Publications and Presentations Acknowledging DOE_BES Support (2024-2022)

Nkiawete, M. M., & Vander Wal, R. L. (2024). Metal-Catalyzed Thermo-Catalytic Decomposition and Continuous Catalyst Generation. *Catalysts*, *14*(7), 414.

Nkiawete, M. M., & Vander Wal, R. L. (2024). Metal-Catalyzed Thermo-Catalytic Decomposition and Continuous Catalyst Generation. *Catalysts*, *14*(7), 414.

Nkiawete, M. M., & Vander Wal, R. (2023). Thermo-Catalytic Decomposition Comparisons: Carbon Catalyst Structure, Hydrocarbon Feed and Regeneration. *Catalysts*, *13*(10), 1382.

Mpila Nkiawete, James Heim II, and Randy Vander Wal. Thermo-catalytic Decomposition of Natural Gas for Clean Hydrogen and Premium Carbon. Program topical area: Clean Hydrogen. 2024 International Pittsburgh Energy and Carbon Management Conference. Oct. 7-9, 2024. Pittsburgh, PA (virtual conference).

Mpila Nkiawete, Randy Vander Wal. Thermo-catalytic Decomposition: Hydrocarbon Feed, Carbon Catalyst Structure, and Regeneration Comparisons. Paper M4.263. Session: Hydrogen Production and Industrial Uses. Monday, June 17th. TechConnect World Innovation Conference, National Harbor, MD, USA. June 17-19, 2024.

Randy Vander Wal, Mpila Nkiawete. Thermo-catalytic Decomposition of Natural Gas and Regeneration: An Overview. Paper M4.262. Session: Industrial Decarbonization: CCS & Hydrogen. Monday, June 17th. TechConnect World Innovation Conference, National Harbor, MD, USA. June 17-19, 2024.

Vander Wal, R., & Nkiawete, M. (2023, November). Carbon Catalyzed Decarbonization of Natural Gas for Clean Hydrogen and Solid Carbon. Orlando FL. In *2023 AIChE Annual Meeting*. AIChE.

Mpila Nkiawete, Randy Vander Wal Thermo-catalytic Decomposition of Methane to Produce hydrogen Using Carbon as Catalyst. Paper M4.444. Session: Industrial Decarbonization: CCS & Hydrogen. Monday, June 19th. TechConnect World Innovation Conference, National Harbor, MD, USA. June 19-21, 2023.

Mpila Nkiawete, Randy Vander Wal Carbon Catalyzed Thermo-catalytic Decomposition of Methane: Connecting Nanostructure to Deposition Conditions and Rates. Session: Industrial Decarbonization – Posters. Paper M8.521. Monday, June 19th. TechConnect World Innovation Conference, National Harbor, MD, USA. June 19-21, 2023.

Mpila Nkiawete, Randy Vander Wal Clean Hydrogen Production By Decarbonizing Natural Gas By Carbon-Catalyzed Thermal Decomposition. Session: Hydrogen. The 47th International Technical Conference on Clean Energy. Sheraton Sand Key, Clearwater, Florida, USA July 23 to 27, 2023.

Nkiawete, M., and Vander Wal, R. L., Thermo-catalytic Decomposition of Methane: Connecting Deposition Rates, Nanostructure, and Active Sites. Division: Division of Energy and Fuels. Symposium: Advances in Energy and Fuel.

Session: Thermal Catalysis for Natural Gas and CO_2 Conversions. Paper ID: 3821924. ACS Spring 2023 – Crossroads of Chemistry. Indianapolis, IN March 26-30, 2023. Oral-Virtual.

Nkiawete, M., & Vander Wal, R. (2022, November). Thermo-Catalytic Decomposition of Decarbonization of Natural Gas. Phoenix AZ. In *2022 AIChE Annual Meeting*. AIChE.

Nkiawete, M., and Vander Wal, R., Thermo-catalytic decomposition of methane: Focus on nanostructure Session/Paper 2A15: 149NEC-0118. 2022 Spring Technical Meeting, Eastern States Sections of The Combustion Institute, University of Central Florida Orlando, Florida March 6-9, 2022.

5.0 References

1. Muradov N. (2002). Thermo-catalytic CO_2-free production of hydrogen from hydrocarbon fuels. U.S. DOE Hydrogen Program Review. U.S.: Department of Energy (DOE); NREL/CP-610-32405.
2. Ahmed, S., Aitani, A., Rahman, F., Al-Dawood, A., and Al-Muhaish, F. (2009). Decomposition of hydrocarbons to hydrogen and carbon. *Applied Catalysis A: General*, *359*(1), 1-24.
3. De Falco, M., Basile, A. (Eds.). (2015). *Enriched Methane: The First Step Towards the Hydrogen Economy*. Springer.
4. Zhang C, Zhang C, Ma Y, Xue X. Imaging the C black formation by acetylene pyrolysis with molecular reactive force field simulations. *Physical Chemistry Chemical Physics. 2015;17(17):11469-80*.
5. Mao Q, Van Duin AC, Luo KH. Formation of incipient soot particles from polycyclic aromatic hydrocarbons: A ReaxFF molecular dynamics study. *Carbon. 2017 Sep 1;121:380-8*.
6. Shabnam S, Mao Q, Van Duin AC, Luo KH. Evaluation of the effect of nickel clusters on the formation of incipient soot particles from polycyclic aromatic hydrocarbons via ReaxFF molecular dynamics simulations. *Physical Chemistry Chemical Physics. 2019;21(19):9865-75*.
7. Zhang X, Di N, Xu L, Chen H, Shu X, Wang Y, Lin Y. Study on the formation process of soot from 2, 5-dimethylfuran pyrolysis by ReaxFF molecular dynamics. *Journal of Thermal Analysis and Calorimetry. 2023 Sep;148(17):9145-66.*
8. Lv P, Zhou W, Yang L, Jia Z. Soot evolution in ethylene combustion catalyzed by electric field: experimental and ReaxFF molecular dynamics studies. *Carbon. 2024 Oct 1;229:119443*.

Probing Nonvalence Excited States of Anions Using Photodetachment and Photoelectron Spectroscopy

Lai-Sheng Wang
Department of Chemistry, Brown University, Providence, RI 02912
Email: lai-sheng_wang@brown.edu

Program Scope

This project is aimed at obtaining energetic, electronic, and vibrational information about O- and N-containing polycyclic aromatic hydrocarbon (PAH) species, which are important in atmospheric and combustion chemistry, using new anion spectroscopic techniques. Highly diffuse nonvalence states can exist in anions as a result of long-range interactions between the extra electron and the neutral molecular cores, including charge-dipole, charge-quadrupole, or charge and induced-dipole interactions. The goal of this program is to search nonvalence excited states that exist in anions of functionalized PAH species. The nonvalence excited states are used as a new means to obtain energetic and spectroscopic information of the underlying neutral PAH radicals and molecules. The weakly-bound nature of the nonvalence excited states in the anions implies that vibrational excitation can induce autodetachment through vibronic coupling. The PI's lab has built a high-resolution photoelectron imaging apparatus equipped with an electrospray source and a cryogenically-cooled ion trap. Photodetachment spectroscopy is used to search for nonvalence excited states of anions. It is combined with resonant photoelectron spectroscopy to yield energetic, electronic, and vibrational information about the underlying neutral species, as well as information about vibronic coupling leading to autodetachment. Three types of anionic species are targeted: 1) Nitrophenoxide anions; 2) Quinone anions; and 3) Large O- and N-containing PAH anions.

Recent Progress

The Role of Polarization Interactions in the Formation of Dipole-Bound States.[13] Even though there is a critical dipole moment required to support a dipole-bound state (DBS), how molecular polarizability may influence the formation of DBSs is not well understood. Pyrrolide, indolide, and carbazolide provide an ideal set of anions to systematically examine the role of polarization interactions in the formation of DBSs. We investigated carbazolide using cryogenic photodetachment spectroscopy and high-resolution photoelectron spectroscopy (PES). A polarization-assisted DBS was observed at 20 cm^{-1} below the detachment threshold for carbazolide, even though the carbazolyl neutral core has a dipole moment (2.2 D) smaller than the empirical critical value (2.5 D) to support a DBS. Photodetachment spectroscopy revealed nine vibrational Feshbach resonances, as well as three intense and broad shape resonances. The electron affinity of carbazolyl was measured accurately to be 2.5653 ± 0.0004 eV (20,691 ± 3 cm^{-1}). The combination of photodetachment spectroscopy and resonant PES allow fundamental frequencies for fourteen vibrational modes of carbazolyl to be measured. The three shape resonances were due to above-threshold excitations to the three low-lying electronic states (S_1–S_3) of carbazolide. Resonant PES off the shape resonances was dominated by autodetachment processes. Ultrafast relaxation from the S_2 and S_3 states to S_1 was observed, resulting in constant kinetic energy features in the resonant PES. This study provided decisive information about the role that polarization plays in the formation of DBSs, as well as rich spectroscopic information about the carbazolide anion and the carbazolyl radical.

Probing Dipole-Bound States Using Photodetachment Spectroscopy and Resonant Photoelectron Imaging of Cryogenically-Cooled Anions.[14] Molecular anions with polar neutral cores can support highly diffuse dipole-bound states below their detachment thresholds due to the long-range charge-dipole interaction. Such nonvalence states constitute a special class of excited electronic states for anions and were observed in early photodetachment experiments to measure the electron affinities of organic radicals. Recent experimental advances in the PI's lab, primarily supported under this program, have allowed the investigation of dipole-bound excited states at a new level. For the first time, the zero-point level of dipole-bound excited states can be observed via resonant two-photon detachment; and resonant photoelectron spectroscopy can be performed via the above-threshold vibrational levels (Feshbach resonances) of the dipole-bound states. The PI was invited to write a perspective article to describe recent progresses in the investigation of dipole-bound states in the PI's lab using the third generation electrospray photoelectron spectroscopy apparatus equipped with a cryogenically-cooled Paul trap and high-resolution photoelectron imaging.

Probing the Dynamics and Bottleneck of the Key Atmospheric SO_2 Oxidation Reaction by the Hydroxyl Radical.[15] SO_2 is the major precursor to the production of sulfuric acid (H_2SO_4), contributing to acid rain and atmospheric aerosols. Sulfuric acid formed from SO_2 generates light-reflecting sulfate aerosol particles in the atmosphere. This property prompted geoengineering proposals to inject sulfuric acid or its precursors into the Earth's atmosphere to increase the planetary albedo to counteract global warming. SO_2 oxidation in the atmosphere by the hydroxyl radical HO to form $HOSO_2$ is a key rate-limiting step in the mechanism for forming acid rain. However, the dynamics of the HO + SO_2 $\rightarrow$ $HOSO_2$ reaction and its slow rate in the atmosphere were poorly understood. We use photoelectron spectroscopy of cryogenically-cooled $HOSO_2^-$ anion to access the neutral $HOSO_2$ radical near the transition state of the HO + SO_2 reaction (**Fig. 1**). Spectroscopic and dynamic calculations were conducted on the first *ab initio*-based full-dimensional potential energy surface to interpret the photoelectron spectra of $HOSO_2^-$ and to probe the dynamics of the HO + SO_2 reaction. In addition to the discovery of a new pre-reaction complex (HO…SO_2) directly connected to the transition state, dynamic calculations revealed that the accessible phase space for the HO + SO_2 $\rightarrow$ $HOSO_2$ reaction is extremely narrow, forming a key reaction bottleneck and slowing the reaction rate in the atmosphere, despite the low reaction barrier. This study underlined the importance of understanding the full multidimensional potential energy surface to elucidate the dynamics of complex bimolecular reactions involving polyatomic reactants.

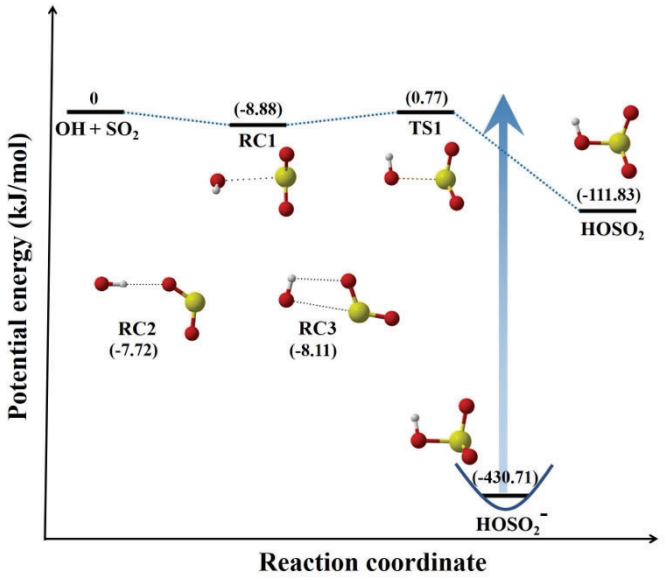

Fig. 1. Energetics for the photodetachment of $HOSO_2^-$ and reaction pathway for the HO + SO_2 system. The energies in kJ/mol are relative to the reactant asymptote HO + SO_2 at the UCCSD(T)-F12a/aug-cc-pV(T+d)Z level and are zero-point energy corrected values. RC: reaction complex. TS: transition state.

Observation of Bound Valence Excited Electronic States of Deprotonated 2-Hydroxytriphenylene using Photoelectron, Photodetachment, and Resonant Two-Photon Detachment Spectroscopy of Cryogenically-Cooled Anions.[16] Polycyclic aromatic hydrocarbons (PAHs) are common atmospheric pollutants, and they are also ubiquitous in the interstellar medium. We investigated a complex O-containing PAH anion, the deprotonated 2-hydroxy-triphenylene (2-OtPh$^-$), using high-resolution photoelectron imaging and photodetachment spectroscopy of cryogenically-cooled anions. Vibrationally resolved photoelectron spectra yielded the electron affinity of the 2-OtPh radical as 2.629(1) eV and several vibrational frequencies for its ground electronic state. Photodetachment spectroscopy revealed bound valence excited electronic states for the 2-OtPh$^-$ anion, with unprecedentedly rich vibronic features (**Fig. 2**). Evidence was presented for a low-lying triplet state (T_1) and two singlet states (S_1 and S_2) below the detachment threshold. Single-color resonant two-photon photoelectron spectroscopy uncovered rich photophysics for the 2-OtPh$^-$ anion, including vibrational relaxation in S_1, internal conversion to the ground state of 2-OtPh$^-$, intersystem crossing from S_2 to T_1, and a long-lived autodetaching shape resonance about 1.3 eV above the detachment threshold. The rich electronic structure and photophysics afforded by the current study suggests that 2-OtPh$^-$ would be an interesting system for pump-probe experiments to unravel the dynamics of the excited states of this complex PAH anion.

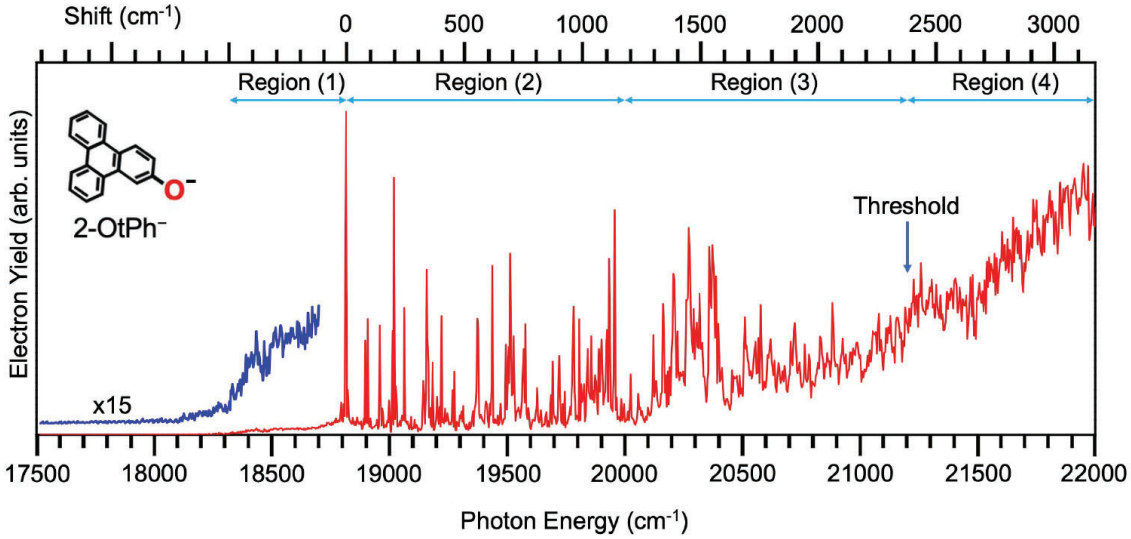

Fig. 2. The photodetachment spectrum of 2-OtPh$^-$ in the spectral range of 17,500 cm^{-1} (2.1697 eV) and 22,000 cm^{-1} (2.7277 eV). The detachment threshold at 21,204 cm^{-1} (2.629 eV) is indicated by the downward arrow. The upper axis gives the shift relative to the strong peak 0 at 18,816 cm^{-1} (i.e. the 0-0 transition to S_1). Four spectral regions are marked as Region (1) to Region (4). From ref. 16.

Future Plans

Experiments on dipole-bound excited states will be continued on O- and N-containing PAH anions. We have found that 5-memebered N-heteroring systems have rich spectroscopy and complicated vibronic couplings, which can be interrogated using our cryogenic ion trap and high-resolution photoelectron imaging.[6,8,9] We will continue this effort on 5-membered ring systems with different substituents. Another interesting finding is the observation of rich bound excited states in the 2-OtPh$^-$ anions containing four phenyl rings (Fig. 2).[16] We will extent this work to other large PAH systems, as well as nitro-containing PAH species.

Publications resulted from the BES-GPCP sponsored research (2021-2024)

1. Photodetachment Spectroscopy and Resonant Photoelectron Imaging of Cryogenically-Cooled 1-Pyrenolate" (C. H. Qian, Y. R. Zhang, D. F. Yuan, and L. S. Wang) *J. Chem. Phys*. **154**, 094308 (2021). DOI: 10.1063/5.0043932
2. "Probing the Dipole-Bound State in the 9-Phenanthrolate Anion by Photodetachment Spectroscopy, Resonant Two-Photon Photoelectron Imaging, and Resonant Photoelectron Spectroscopy" (D. F. Yuan, Y. R. Zhang, C. H. Qian, Y. Liu, and L. S. Wang), *J. Phys. Chem. A* **125**, 2967-2976 (2021). DOI: 10.1021/acs.jpca.1c01563
3. "Observation of A Dipole-Bound Excited State in 4-Ethynylphenoxide and Comparison with the Quadrupole-Bound Excited State in the Isoelectronic 4-Cyanophenoxide" (Y. R. Zhang, D. F. Yuan, C. H. Qian, and L. S. Wang), *J. Chem. Phys*. **155**, 124305 (2021). DOI:10.1063/5.0065510
4. "Resonant Two-Photon Photoelectron Imaging and Adiabatic Detachment Processes from Bound Vibrational Levels of Dipole-Bound States" (D. F. Yuan, Y. R. Zhang, C. H. Qian, and L. S. Wang), *Phys. Chem. Chem. Phys*. **24**, 1380-1389 (2022). DOI: 10.1039/D1CP05219E
5. "Observation of Core-Excited Dipole-Bound States" (Y. R. Zhang, D. F. Yuan, and L. S. Wang), *J. Phys. Chem. Lett*. **13**, 2124-2129 (2022). DOI: 10.1021/acs.jpclett.2c00275
6. "Probing the Electronic Structure and Spectroscopy of the Pyrrolyl and Imidazolyl Radicals using High Resolution Photoelectron Imaging of Cryogenically-Cooled Anions" (Y. R. Zhang, D. F. Yuan, and L. S. Wang), *Phys. Chem. Chem. Phys*. **24**, 6505–6514 (2022). DOI: 10.1039/D2CP00189F
7. "Probing the Electronic Structure and Bond Dissociation of SO_3 and SO_3^- using High-Resolution Cryogenic Photoelectron Imaging" (D. F. Yuan, T. Trabelsi, Y. R. Zhang, J. S. Francisco, and L. S. Wang), *J. Am. Chem. Soc*. **144**, 13740-13747 (2022). DOI: 10.1021/jacs.2c04698
8. "Probing the Strong Nonadiabatic Interactions in the Triazolyl Radical Using Photodetachment Spectroscopy and Resonant Photoelectron Imaging of Cryogenically-Cooled Anions" (Y. R. Zhang, D. F. Yuan, and L. S. Wang), *J. Am. Chem. Soc*. **144**, 16620-16630 (2022). DOI: 10.1021/jacs.2c07167
9. "Dipole-Bound State, Photodetachment Spectroscopy, and Resonant Photoelectron Imaging of Cryogenically-Cooled 2-Cyanopyrrolide" (D. F. Yuan, Y. R. Zhang, and L. S. Wang), *J. Phys. Chem. A* **126**, 6416-6428 (2022). DOI: 10.1021/acs.jpca.2c04405
10. "Investigation of the Electronic and Vibrational Structures of the 2-Furanyloxy Radical using Photoelectron Imaging and Photodetachment Spectroscopy via the Dipole-Bound State of the 2-Furanyloxide Anion" (Y. R. Zhang, D. F. Yuan, and L. S. Wang), *J. Phys. Chem. Lett*. **13**, 11481-11488 (2022). DOI:10.1021/acs.jpclett.2c03382
11. "Observation of a Polarization-Assisted Dipole-Bound State" (D. F. Yuan, Y. Liu, Y. R. Zhang, and L. S. Wang), *J. Am. Chem. Soc*. **145**, 5512-5522 (2023). DOI: 10.1021/jacs.3c00246
12. "Cryogenic Photodetachment Spectroscopy and High-Resolution Resonant Photoelectron Imaging of Cold *para*-Ethylphenolate Anions" (D. F. Yuan, Y. R. Zhang, C. H. Qian, G. Z. Zhu, and L. S. Wang), *Precis. Chem*. **1**, 161-174 (2023). DOI: 10.1021/prechem.2c00012
13. "The Role of Polarization Interactions in the Formation of Dipole-Bound States" (Y. R. Zhang, D. F. Yuan, C. H. Qian, G. Z. Zhu, and L. S. Wang), *J. Am. Chem. Soc*. **145**, 14952-14962 (2023). https://doi.org/10.1021/jacs.3c04740
14. . "Probing Dipole-Bound States Using Photodetachment Spectroscopy and Resonant Photoelectron Imaging of Cryogenically-Cooled Anions" (Y. R. Zhang, D. F. Yuan, and L. S. Wang), *J. Phys. Chem. Lett*. **14**, 7369-7381 (2023). https://doi.org/10.1021/acs.jpclett.3c01994
15. "Probing the Dynamics and Bottleneck of the Key Atmospheric SO_2 Oxidation Reaction by the Hydroxyl Radical" (D. F. Yuan, Y. Liu, T. Trabelsi, Y. R. Zhang, J. Li, J. S. Francisco, H. Guo, and L. S. Wang), *Proc. Natl. Acad. Sci*. (USA) **121**, e2314819121 (2024). https://doi.org/10.1073/pnas.2314819121
16. "Observation of Bound Valence Excited Electronic States of Deprotonated 2-Hydroxytriphenylene using Photoelectron, Photodetachment, and Resonant Two-Photon Detachment Spectroscopy of Cryogenically-Cooled Anions" (J. Kang, E. I. Brewer, Y. R. Zhang, D. F. Yuan, G. S. Kocheril, and L. S. Wang), *J. Chem. Phys*. **160**, 184301 (2024). https://doi.org/10.1063/5.0209948

Experimental and Computational Study of Quantum Nuclear and Many-Body Effects in Water Network Formation and Water-Surface Interaction in PAH-Water Cluster Ions

J. Mathias Weber[1,2] and Joel D. Eaves[2]

[1] JILA, Univ. of Colorado Boulder, 440 UCB, Boulder, CO 80309-0440

[2] Department of Chemistry, Univ. of Colorado Boulder, 215 UCB, Boulder, CO 80309-0215

weberjm@jila.colorado.edu; joel.eaves@colorado.edu

Program Scope – This research program employs a combined experimental and theoretical approach to quantify interactions between water molecules and aromatic hydrocarbons (PAHs). We study the interaction of water molecules with charged PAHs in mass selected cluster ions of the form $PAH^{-}\cdot(H_2O)_n$, employing infrared (IR) photodissociation spectroscopy, and comparing the experimental results with theoretical predictions.

PAHs are important in many areas of chemistry, such as soot formation, astrochemistry, and materials chemistry, where they are valuable model systems for both neutral and doped graphene as well as their chemical derivatives. In addition to collective effects from the polarization of the liquid, the wetting properties of surfaces are also influenced by molecular effects, such as the formation of H-bonds to the surface and H-bonded networks among the water molecules.

Experimentally probing the molecular level details of the interaction of single-layer graphene with water is challenging, and the debate over the hydrophobicity of graphene is not settled. Using hydrated PAH cluster ions circumvents many of the problems associated with condensed phase environments. From a theoretical and computational point of view, current water-carbon model potentials are not robust. Changes in the minimum energy of the van der Waals potential between water and graphitic carbon atoms that are on the 0.5 k_BT at room temperature can mean the difference in hydrophobicity between superhydrophobic and complete wetting. We aim to obtain a detailed theoretical description of water-PAH interaction, which will be the basis of a cost-effective computational model that can represent water-carbon interactions even for extended, condensed phase systems.

Recent Progress

Overview – We published three papers on pyrene anion and its interactions with water [1-3]. In our experiments we are using a home build photodissociation spectrometer [2] schematically shown in Figure 1. Target ions of the form $PAH^{-}\cdot(H_2O)_n\cdot Ar_m$ or $PAH^{-}\cdot(H_2O)_n$ were injected into a tandem time-of-flight mass spectrometer (TOF-MS). After mass-selection in the first space focus of the TOF-MS, target ions were irradiated with the output of a tunable, pulsed IR light source. With target ions containing Ar adducts, we monitored the photoinduced loss of Ar according to

$$PAH^{-}\cdot(H_2O)_n\cdot Ar_m + h\nu \rightarrow PAH^{-}\cdot(H_2O)_n + m\ Ar, \quad (1)$$

as a function of IR frequency, to measure their photodissociation spectra. For species without Ar tagging, we used instead the loss of water molecules in the process

$$PAH^{-}\cdot(H_2O)_n + h\nu \rightarrow PAH^{-}\cdot(H_2O)_{n-1} + H_2O. \quad (2)$$

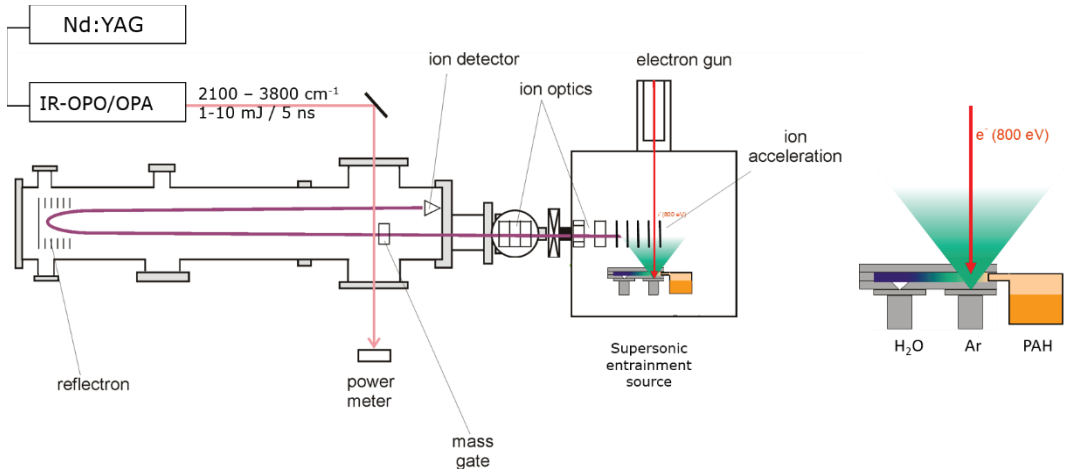

Figure 1. Schematic of the experimental setup used (left) with detail of the supersonic entrainment ion source (right).

Fragment ions were separated from the undissociated parent ions using a reflectron, and the fragment ion intensity was monitored on a dual multichannel plate as the light source was tuned.

The spectra obtained in this way were interpreted using density functional theory and molecular dynamics calculations. The former were performed using commercial quantum chemistry software. For the latter, we (1) developed a flexible water-PAH potential and implemented two methodological improvements that (2) take the simulation of small clusters into the thermodynamic limit and (3) allow the system to equilibrate in the presence of kinetic traps. The potential is simple, pairwise, and designed to be transferrable to other systems, including other PAH systems. To model these phenomena, we compute the IR spectrum directly from classical molecular dynamics in the PAH-water potential using a time-correlation function theory. The IR spectrum is proportional to a Fourier transform [4],

$$I(\tilde{\nu}) \propto \int_{-\infty}^{\infty} dt\, e^{\frac{2\pi i \tilde{\nu} t}{c}} \langle \dot{\boldsymbol{\mu}} \cdot \dot{\boldsymbol{\mu}}(t) \rangle , \qquad (3)$$

where $\dot{\boldsymbol{\mu}}(t)$ is the time derivative of the dipole moment of the entire system at time t. Eq. 3 relies on a number of approximations, and one of them is a high temperature one. As a result, the theory will work better for a narrow spectral width relative to $k_B T$ [2].

The potential that we developed is a flexible intramolecular potential for the water molecule and an intermolecular potential based on the DREIDING force field for the water-pyrene interactions [5]. The intermolecular water-water potential and geometry is the canonical TIP4P/2005 model [6]. The intramolecular potential is adapted from the Reimers and Watts [7] local mode potential parameterized to fit gas phase vibrational data in water that has been used to describe linear and nonlinear IR spectroscopy of HOD in D_2O.

Results on Pyrene-Water Clusters – We have engaged in a comprehensive campaign to investigate pyrene anion (Py^-) and its water clusters. Comparing spectra based on Ar loss from $Py^- \cdot (H_2O)_n \cdot Ar_m$ with those based on water loss from $Py^- \cdot (H_2O)_n$ yields insight into the temperature dependence of the behavior of these clusters, even though the temperature control is rather coarse.

Figure 2 shows a comparison of the photodissociation spectra for $Py^{-}\cdot(H_2O)_n\cdot Ar_2$ (n = 1 – 4), together with the lowest energy structures for each cluster size, calculated using DFT [1, 2]. The OH stretching region is rich in infrared bands that encode the interaction of the water molecules with each other and with the π-system of the PAH anion. Water molecules condense into water networks on the PAH surface. At each cluster size, multiple conformers are populated, although for n = 3 and 4, the spectra mostly resemble those predicted for n-membered water ring structures. The relative energies of the lowest lying structures are very close for n = 1 and 2 (below 20 meV), while the minimum energy structures are well separated from higher energy geometries for n = 3 and 4, indicating that the higher lying conformers are populated during cluster growth and kinetically trapped. All OH groups are engaged in H-bonds with other water molecules or with the π system. Three- and four-membered rings form robust structural subunits for n = 3 and 4. The frequency order of the vibrational modes in $Py^{-}\cdot(H_2O)_n$ clusters strongly suggests that the water-water H-bonds in the system are stronger than the water-π H-bonds, despite the fact that the π system accommodates the majority of the excess negative charge. This observation is consistent with earlier results on $Np^{-}\cdot(H_2O)_n$ and is testament to the strength of water networks.

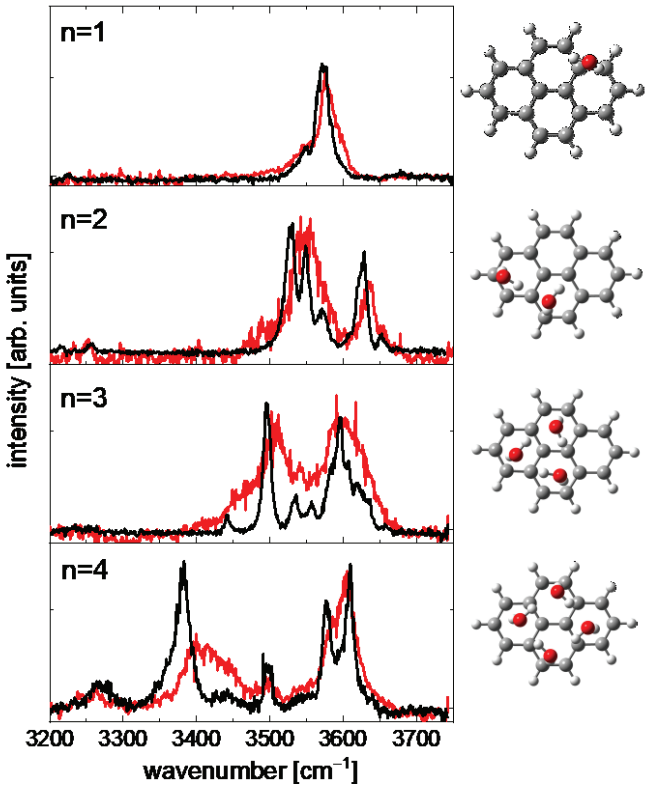

Figure 2. Photodissociation spectra of $Py^{-}\cdot(H_2O)_n\cdot Ar_2$ (black traces, from [1]) and of $Py^{-}\cdot(H_2O)_n$ (red traces, to be published) for n = 1 – 4. The structures shown on the right are the minimum energy structures obtained from DFT calculations.

The monohydrate of pyrene anion, $Py^{-}\cdot H_2O$, provides an interesting case study for water-PAH interactions and dynamics [2]. DFT calculations suggest that the potential energy surface for the motion of a single water molecule on the surface of a pyrene anion is very flat, resulting in the water adduct exploring a large conformational space. MD calculations show the importance of anharmonic and finite temperature effects in aqueous hydrocarbon cluster spectroscopy and offer important lessons for calculations of cluster spectra in other systems. Even $Py^{-}\cdot H_2O$, which is a relatively simple system with few degrees of freedom, can be nonergodic and exhibit kinetic trapping on computationally-accessible timescales. Our parallel tempering strategy minimizes the intrinsic problems with kinetic trapping and yields free energy surfaces consistent with the

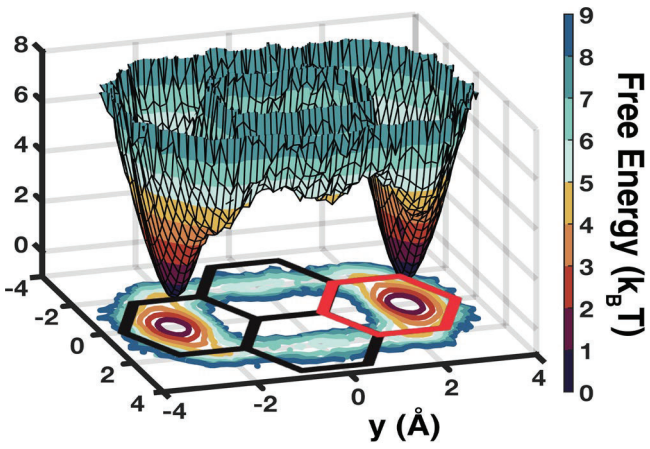

Figure 3. MD simulation at 50 K of a single water molecule starting above the red ring of the Py^- ion. The free energy surface and its depiction as a contour diagram is superimposed on a wireframe of the pyrene molecule. Taken from [2].

symmetry of the system (Figure 3). Interestingly, while the DFT calculations show that there is no local minimum for the water molecule above the two central rings of Py^- in the potential energy surface, the MD simulation shows such a local minimum in the free energy surface, indicating that entropy contributions are significant, and that the static DFT calculations do not offer a complete picture of the relevant water-π interactions.

The challenges in the computational treatment of even a seemingly simple system as $Py^-\cdot H_2O$ are significant, and the present description from neither DFT nor from MD simulations yield a fully satisfactory picture. The simulated IR spectrum from the MD simulation of $Py^-\cdot H_2O$ captures the width and shape of the symmetric stretching signature reasonably well, but the relative intensities of the symmetric and antisymmetric OH stretching modes suggest that the water-Py^- potential energy surface from the current classical parametrization is incomplete. The MD simulated spectra for $Py^-\cdot(H_2O)_n$ clusters are in good agreement with n = 3 and 4, where the water-water interactions are more important than for n = 1 and 2 (Figure 4). The DFT description of the $Py^-\cdot H_2O$ binary complex has yielded an ambiguous result regarding the minimum energy structure of the complex, since results with different functionals (ωB97XD and B3LYP) show significant differences. Neither of the methods used so far have been able to fully describe the IR spectrum of this complex. In particular, a prominent low-energy shoulder on the signature of the symmetric OH stretching mode remains unexplained [2], with quantum nuclear effects or different conformers being possible origins of this feature.

Results on Perylene-Water Clusters – We have acquired IR photodissociation spectra of perylene anion (Per^-) and its hydrated clusters, $Per^-\cdot(H_2O)_{1\text{-}4}$ and $Per^-\cdot(H_2O)_{1\text{-}2}\cdot Ar_2$ (Figure 4). While the computational analysis of the structures is not complete, the overall band pattern suggests similar behavior, i.e., the formation of water subclusters on the surface of the Per^- frame. Interestingly, the line width of the symmetric stretching mode of the Ar-tagged monohydrate, $Per^-\cdot H_2O\cdot Ar_2$, is significantly narrower than that of the analogous pyrene monohydrate [2], and similar to that of naphthalene monohydrate [8]. This suggests that dynamic effects are less pronounced, in hydrated Per^-, possibly restricting the water adducts to one of the naphthalene subunits of the Per frame. MD simulations to explore this possibility are planned.

Results on CH Stretching Vibrations in PAH Anions – The CH stretching region is interesting in its own right, particularly in the context of the possible existence of PAH anions in astrochemical objects. The theoretical description of this region is challenging, since the CH stretching modes

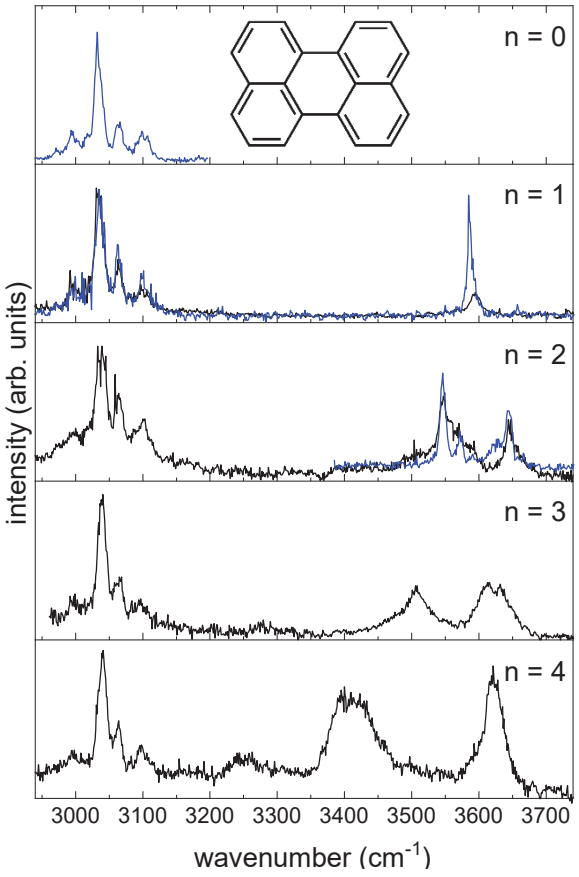

Figure 4. Photodissociation spectra of $Per^{-}\cdot(H_2O)_n\cdot Ar_2$ (blue traces) and of $Per^{-}\cdot(H_2O)_n$ (black traces) for n = 1 – 4. The structure of Per is shown in the upper panel.

are very close in energy to overtones and combination bands of CH bending modes, resulting in the formation of Fermi resonances. This necessitates the use of anharmonic calculations for an accurate assignment of vibrational transitions. We engaged in an (unfunded) collaboration with Dr. Anne B. McCoy (University of Washington, Seattle) and obtained a detailed description of the spectrum of Py^{-} [3], using IR photodissociation of $Py^{-}\cdot Ar_m$ clusters and vibrational perturbation theory (VPT2). We were also able to measure the IR spectra of Ar-tagged perylene and anthracene anions in the CH stretching region. We are currently working on measurements involving fluoranthene anions and are finalizing the VPT2 calculations of all three spectra.

Theory Development – As mentioned above, recent results on water-anionic pyrene clusters indicate that, when using conventional parameterized force fields, the vibrational spectrum in the OH region is accurate for the tri- and tetra-hydrate, where the water-water potential dominates. The results for mono- and di-hydrate clusters are not quantitative compared to experiments. Because Born-Oppenheimer molecular dynamics (BOMD) are infeasible due to the size of the system, we are developing scalable machine-learned (ML) potentials trained on configurations where one can compute the electronic structure to high accuracy. Dynamics using the ML models are orders of magnitude faster than BOMD and can be much more accurate. For the charged water-PAH interactions based on equivariant atomic cluster expansions coupled with graph neural networks and Behler-Parrinello feed-forward neural networks. Hydrated PAH clusters offer essential insights into training efficiency and convergence criteria for ML methods. These efforts are performed in collaboration with Dr. Laura McCaslin (Sandia National Laboratories).

Future Plans – We plan to finalize current experiments on fluoranthene anion and its hydrated clusters, and to publish our earlier results on untagged hydrated tretracene clusters, $Tet^{-}\cdot(H_2O)_{1\text{-}4}$, as well as the results on the CH stretching regions of anthracene and perylene. In addition, we expect to publish our work on $Per^{-}\cdot(H_2O)_{1\text{-}4}$ and $Per^{-}\cdot(H_2O)_{1\text{-}2}\cdot Ar_2$. We also plan to publish results from ML based MD simulations on $Pyr^{-}\cdot(H_2O)_{1\text{-}4}$ together with those involving our earlier model

potential and the experimental spectra of the untagged clusters to describe the temperature dependence of the spectra and dynamics on these systems. We expect overall at least four additional publications from past work.

With the start of the new funding period a few weeks ago, we plan to perform experiments on $Pyr^{-}{\cdot}HDO{\cdot}Ar_m$ to gain insight into quantum nuclear effects. We will begin with the implementation of a cryogenic ion trap to achieve temperature control over the cluster ions under study. In addition, we will use a quantum cascade laser to be purchased with funds from this proposal to perform hole burning spectroscopy, and we will use H/D isotope labeling to investigate quantum nuclear effects spectroscopically. In the theoretical part of the program, we will expand our ML efforts to PAH systems beyond Py and begin work on the description of quantum nuclear effects through path integral molecules dynamics and by solving the vibrational problem directly using a vibrational exciton model, a mixed quantum-classical method.

Publications Sponsored by This Award

1. N. LeMessurier, H. Salzmann, R. Leversee, J. M. Weber, J. D. Eaves, "Water-Hydrocarbon Interactions in Anionic Pyrene Monohydrate", J. Phys. Chem. B **128** (2024) 3200 – 3210.
2. H. Salzmann, A. P. Rasmussen, J. D. Eaves, J. M Weber, "Competition Between Water-Water Hydrogen bonds and Water-π Bonds in Pyrene-Water Cluster Anions", J. Phys. Chem A **128** (2024) 2772 – 2781.
3. H. Salzmann, A. B. McCoy, J. M. Weber, "The Infrared Spectrum of Pyrene Anion in the CH Stretching Region", J. Phys. Chem. A, **21** (2024) 4225–4232.

References

1. H. Salzmann, A.P. Rasmussen, J.D. Eaves, and J.M. Weber, *Competition Between Water-Water Hydrogen bonds and Water-π Bonds in Pyrene-Water Cluster Anions.* J. Chem. Phys. A **128** (2024) 2772-2781.
2. N. LeMessurier, H. Salzmann, R. Leversee, J.M. Weber, and J.D. Eaves, *Water-Hydrocarbon Interactions in Anionic Pyrene Monohydrate.* J. Phys. Chem. B **128** (2024) 3200 – 3210.
3. H. Salzmann, A.B. McCoy, and J.M. Weber, *The Infrared Spectrum of Pyrene Anion in the CH Stretching Region.* J. Phys. Chem. A (2024).
4. R. Iftimie and M.E. Tuckerman, *Decomposing total IR spectra of aqueous systems into solute and solvent contributions: A computational approach using maximally localized Wannier orbitals.* J. Chem. Phys. **122** (2005) 214508.
5. S.L. Mayo, B.D. Olafson, and W.A. Goddard, *DREIDING: a generic force field for molecular simulations.* J. Phys. Chem. **94** (1990) 8897-8909.
6. J.L.F. Abascal and C. Vega, *A general purpose model for the condensed phases of water: TIP4P/2005.* J. Chem. Phys. **123** (2005) 234505.
7. J.R. Reimers and R.O. Watts, *A local mode potential function for the water molecule.* Mol. Phys. **52** (1984) 357-381.
8. B.J. Knurr, C.L. Adams, and J.M. Weber, *Infrared Spectroscopy of Hydrated Naphthalene Cluster Anions.* J. Chem. Phys. **137** (2012) 104303.

Fundamental chemical kinetics of siloxane and silicon compounds

DOE BES Grant #18SC503179
Margaret S. Wooldridge (PI)
University of Michigan, Department of Mechanical Engineering, 2350 Hayward St., Ann Arbor, MI, 48109-2125, mswool@umich.edu
Andrew B. Mansfield
Eastern Michigan University, College of Engineering and Technology, Ypsilanti, MI, 48197, amansfi3@emich.edu,
Robert S. Tranter
Chemical Sciences and Engineering Division, Argonne National Laboratory, Argonne, IL, 60439, tranter@anl.gov

Program Scope

Siloxanes and other silicon compounds play significant roles as impurities in land-fill gas and as primary feedstock materials for high-value and large-volume products, yet the fundamental reaction chemistry of gas-phase silicon compounds remains largely unexplored. This research program integrates complementary experimental efforts to significantly advance the science of gas-phase silicon reaction chemistry. The primary research focus is on the elementary reactions of siloxanes and their decomposition products with a progression in the chemical structure of the compounds studied to elucidate the effects of bond structure. An additional area of interest is the interaction of gas-phase species with silica nanoparticles that are formed naturally as products of the thermal reactions of siloxanes and during oxidation.

Recent Progress

Experimental Approach

The experimental approach leverages the strengths of the University of Michigan (UM) rapid compression facility (RCF) and atmospheric burners and the diaphragmless shock tube (DFST) and the high-repetition rate shock tube (HRRST) at Argonne National Laboratory for advancing understanding of siloxane chemistry. The combination of experimental approaches allows an extensive and complementary range of state conditions to be studied with temperatures in the range of 700-2000 K and pressures of 0.1-50 bar. The studies focus on broad categories of chemical kinetics, including oxidation and pyrolysis reactions.

This past year, we further expanded the conditions and mixtures of the RCF experiments. We measured time-histories of OH radicals using continuous-wave, narrow-line laser absorption during ignition of H_2 and CO with and without the addition of different amounts of trimethyl silanol ($(CH_3)_3SiOH$, TMSO) and hexamethyldisiloxane ($(CH_3)_3SiOSi(CH_3)_3$, HMDSO). OH is the radical chain carrier in these ignition systems, and the impact of TMSO and HMDSO on the syngas system is significant. The OH measurements provide new insight into the reaction kinetics affected by the silicon-compounds.

We also completed analysis of the second set of experiments conducted last year at Argonne using the Advanced Photon Source (APS) facilities to study the mixing and temperature fields via krypton x-ray fluorescence of a Hencken, multi-element diffusion (MEDB) burner equipped with a central fuel tube for introducing nanoparticle precursors such as siloxanes. Analysis of the APS data led to a hypothesis on the potentially critical role of diffusive H-atom transport in the flames systems. We evaluated this hypothesis via collaboration with Kulatilaka at Texas A&M University and femtosecond two photon laser induced fluorescence (fsTPLIF) measurements of H-atom concentrations in the MEDB flames with and without HMDSO. Brief summaries of these efforts are provided here. Additional details can be found in the associated references.

RCF OH absorption studies

Last year, we had recently completed time-resolved OH measurements during ignition studies of mixtures of H_2 and CO (syngas) with the addition of TMSO to the reference syngas mixture. Our progress this past year includes expanding the OH data to ignition studies with higher concentrations of TMSO and mixtures with HMDSO. Comparison of the effects on the autoignition delay times, on pressure time-histories and

OH time-histories during ignition are presented in **Figures 1-3**, respectively, for a nominal temperature of 1020 K and pressure of 5 atm.

The TMSO and HMDSO have significant impact on the ignition delay times of the mixtures, with both TMSO and HMDSO accelerating reaction (**Figure 1**), increasing heat release rates (**Figure 2**) and increasing post-ignition pressures (**Figure 2**). The ignition delay time is a good global metric quantifying the overall reactivity of the mixtures. The data presented in **Figure 1** show, as seen in prior RCF studies, even small quantities of siloxane addition accelerate reaction.

The pressure time histories (**Figure 2**) show siloxane addition systematically increases both the pressure rise rate and the final pressure of the reactant mixture. The final pressure of ignition experiments is generally defined by thermal equilibrium (e.g., enthalpies of formation and assumptions of complete combustion), and not reaction kinetics; whereas, the rate of pressure rise (and heat release rate) is determined by the reaction chemistry. Regarding thermal equilibrium, the siloxane can increase pressure by producing more product species (increasing the number of moles) or by increasing the energy content in the mixture (due to the additional heating value of TMSO or HMDSO and the energy released by the formation of combustion products). Importantly, the siloxanes produce condensed-phase silica (SiO_2), and the condensation process is highly exothermic. Adiabatic equilibrium calculations assuming condensed-phase SiO_2 is formed indicate over a factor of two increase in pressure from the initial 5 atm of the experiments to post-ignition pressure (13-18 atm post ignition). However, much lower final pressures are observed, which is attributed to, in part, heat losses that occur in the experiments. The equilibrium calculations also indicate increase in the post-ignition pressure with increasing amount of TMSO, which is observed in the RCF pressure data. Specifically, the experimental results indicate ~20% increase in post-ignition pressure with 1000 ppm TMSO compared with the post-ignition pressure for syngas with no siloxanes, which consistent the ~14% increase predicted by the equilibrium calculations. The experimental observations indicate particle condensation occurs very rapidly in these siloxane systems and is likely the source of the higher post-ignition pressures.

While the peak OH values appear to systematically increase with increasing TMSO in **Figure 3**, the maximum OH values are within the uncertainty of the

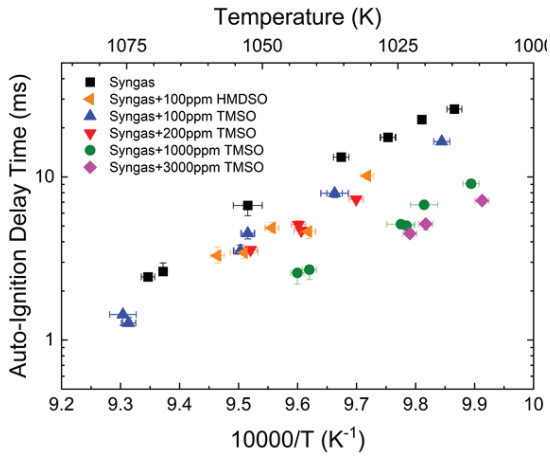

Figure 1. Comparison of ignition delay time measurements of H_2 and CO mixtures (1.2% H_2, 2.8% CO, φ = 0.1) with and without TMSO or HMDSO.

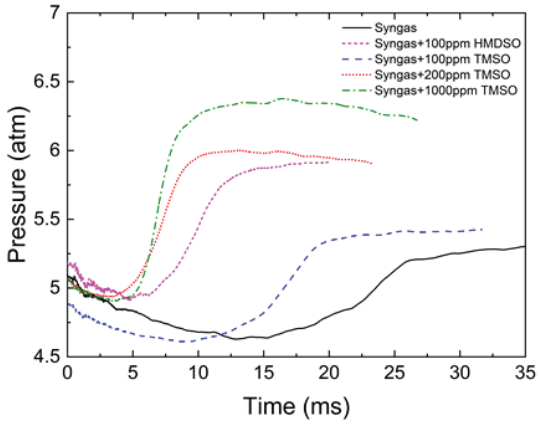

Figure 2. Pressure time-histories during ignition of syngas mixtures (1.2% H_2, 2.8% CO, φ = 0.1) with TMSO or HMDSO, for an average temperature of 1020 K.

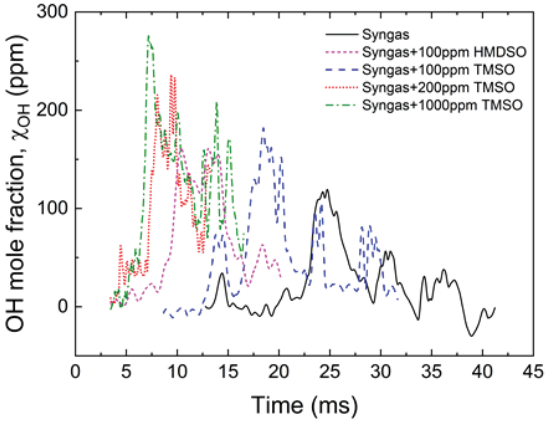

Figure 3. OH time-histories corresponding to the pressure data presented in **Figure 2**.

measurements for the syngas baseline mixture for the mixtures with 200 ppm and lower amounts of TMSO. Only 1000 ppm of TMSO addition led to maximum OH values outside the uncertainty limits of the measurements. The change in OH profiles indicates a shift in the OH chemistry with the larger amounts of TMSO.

In **Figure 4**, the OH mole-fraction time histories for the TMSO syngas mixtures are shifted in time to directly compare the rate of OH formation near the time of ignition. For clearer visual comparison of the relative shapes, the peak OH levels shifted to zero. At 1020 K, the addition of TMSO in syngas mixtures promotes the rate of OH formation, even though the rate at which OH is consumed post-ignition remains consistent for the different TMSO concentrations. At this temperature, it is probable that the hydroxyl group in TMSO directly contributes to the formation of OH radicals or plays a significant role in the reactions which are producing OH radicals. At 1050 K, lower concentrations of TMSO do not significantly influence the rate of OH formation. However, for 1000 ppm TMSO, the formation and consumption of OH radicals occur more rapidly compared with the lower concentration cases. This indicates additional OH production reactions are promoted at the higher temperature and higher TMSO concentrations of the experiments.

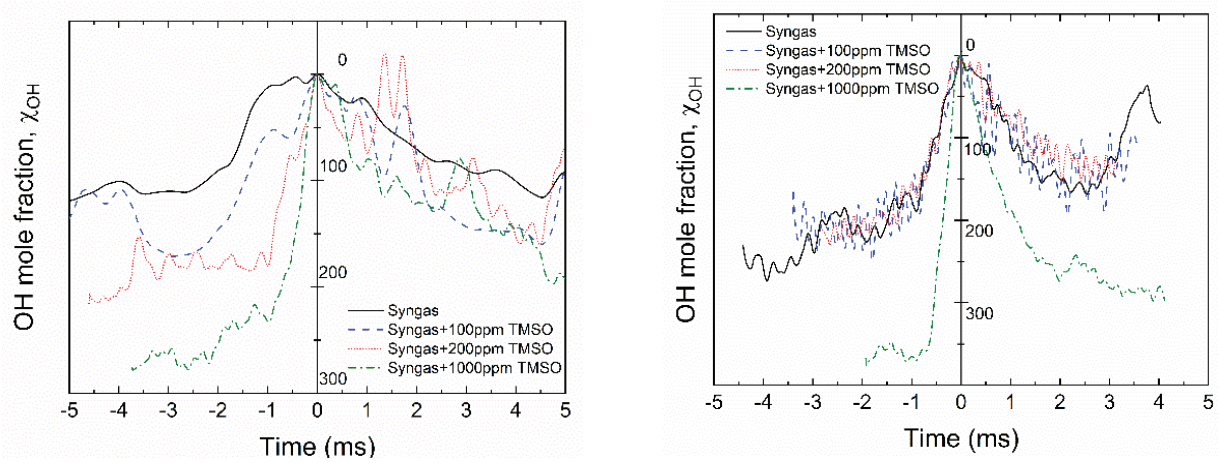

Figure 4: Comparison of trends in OH characteristic features for (a) T_{avg} = 1020 K and (b) T_{avg} = 1050 K for syngas mixtures (1.2% H2, 2.8% CO, and φ = 0.1) with TMSO. The OH mole fraction time histories were shifted to directly compare the relative shape of profiles. Specifically, the peak OH values of each profile were set to zero and y-axis represents the absolute magnitude of the OH mole fraction.

Reaction kinetics modeling

Detailed modeling of the reaction kinetics describing the RCF OH absorption studies is presently underway. The initial modeling approach combines detailed models of syngas combustion kinetics with those developed for tetramethylsilane ($Si(CH_3)_4$, TMS) decomposition in flames. While freezing the syngas kinetics, the TMSO kinetics within the TMS mechanism were systematically modified using a genetic algorithm, with experimental observations of ignition delay time and maximum OH mole fraction as the optimization targets. Initial results reveal good overall agreement (within the experimental uncertainty) between the new model predictions and experimental results for the 1000 ppm TMSO mixtures. Rate of production analysis using the updated kinetic model suggests TMSO can act as a catalyst to enhance the rate of H_2 to H conversion, enhancing overall reactivity with strong involvement of the OH radical pool. The pronounced effect of TMSO may be explained by its regeneration, as illustrated by the reaction path diagram suggested by the new reaction model and presented in **Figure 5**. As shown, TMSO regenerates and remains chemically active until a methyl group is lost, at which time the compound proceeds on a

pathway to form Si polymers. These initial results will be expanded upon and interrogated as part of our current and future work. The genetic algorithm optimization approach and the specific results are an excellent basis to evaluate and integrate other siloxane reaction chemistry as more fundamental understanding is advanced.

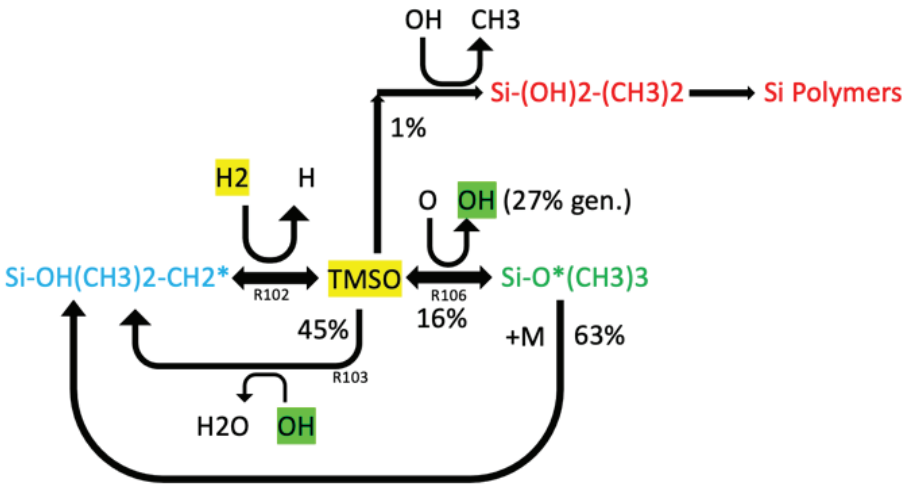

Figure 5: Hypothetical reaction path diagram for TMSO developed using genetic algorithm optimization of the siloxane reaction chemistry based on an initial detailed chemical kinetic model for TMS. The diagram is based on rate-of-production analysis at 50% H_2 consumed for syngas (1.2% H_2, 2.8% CO, and $\varphi = 0.1$) with 1000ppm TMSO at 1010 K, 4.9 atm.

X-ray fluorescence imaging of flames for nanoparticle formation

As described last year, we employed an x-ray fluorescence (XRF) technique with krypton as the fluorescence agent at the APS to measure temperature and gas mixing in the MEDB flame system with and without the addition of siloxanes. The XRF diagnostic has exceptional spatial fidelity (measurement volume of 6 x 4 x 325 μm) and our work demonstrated the XRF measurements were not impeded by the silica nanoparticles rapidly formed in the flame systems. The XRF results for the siloxane flame systems were analyzed in detail and the results are presented in Meng et al. Briefly, while HMDSO and TMSO yielded similar temperatures near the surface of the burner (height above the burner, HAB < 4 mm), the TMSO produced higher temperatures compared with HMDSO at HAB > 4 mm). The centerline temperature was also affected by the equivalence ratio of the main flame. **Figure 5** shows this variation with HMDSO in the jet and strong difference of the temperature profiles compared to the undoped jet. The small changes in

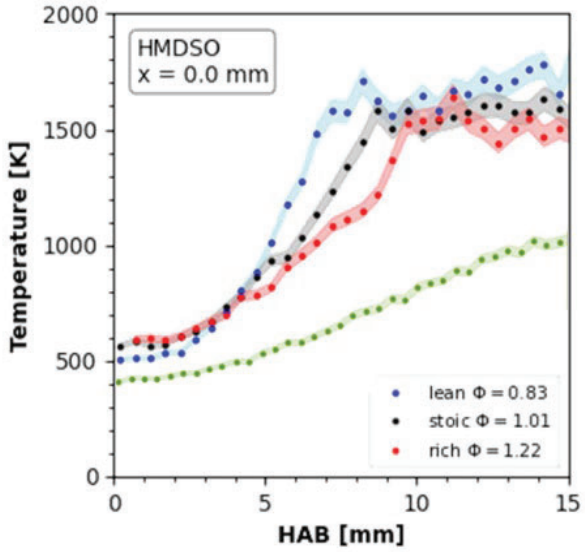

Figure 6. Temperature profiles along the MEDB jet centerline measured using Kr XRF with and without HMDSO in the jet. The primary flames were methane and air with ϕ = 0.8, 1.0 and 1.2. Green points represent the undoped case.

main flame temperatures at different conditions indicated that heat transfer was not a major factor contributing to the changes in centerline temperature. In addition to the temperature measurements, by doping the central flow with Kr, mixing between the central flow and the main flow was visualized and quantified. The results showed that mixing was similar between the different HMDSO and TMSO flames. When the temperature and mixing results are considered together, the findings suggested the changes in centerline temperature are due to the reaction chemistry of HMDSO and TMSO, and that reaction with these compounds is initiated close to the central jet exit where the gas temperature is too low for pyrolysis to occur. We hypothesized reaction is possibly initiated by H and OH radicals from the methane main flame penetrating into the central flow.

Figure 7. Image of nanoparticles being produced in the diffusion flame created when HMDSO precursor is introduced via an inert gas jet in the center of the MEDB. The primary flame is a lean (ϕ = 0.8) methane and air flame.

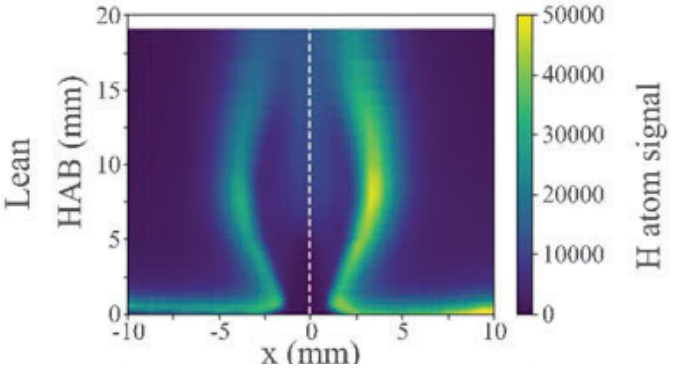

Figure 8. Relative H-atom concentration (arbitrary units) in the HMDSO diffusion and methane flames for lean (ϕ = 0.8) methane and air conditions.

This past year, to test our hypothesis, we collaborated with Kulatilaka at Texas A&M University to make fsTPLIF H-atom measurements of the siloxane flames. An image of one of the HMDSO-doped MEDB flame systems is shown in **Figure 7**, and typical H-atom concentration results are provided **Figure 8**. The data provide clear evidence supporting the transport of H-atoms into the central jet region. This evidence substantiates the hypothesis that the pyrolysis of HMDSO within the central jet is initiated at low temperatures by hydrogen atoms diffusing from the surrounding flame. The significant concentrations of H-atoms observed in the nitrogen jets at various heights above the burner, coupled with the dependency on methane flame stoichiometry, underline the importance of radial diffusion in the flame system. Moreover, the transition from over-ventilated to under-ventilated diffusion flames for lean and rich methane cases, respectively, as well as the significant H-atom production within the jet during lean flame conditions, enrich our understanding of the underlying reaction mechanisms important in these systems. It is likely that other species such as O and OH also penetrate the central jet, although to a lesser degree than H-atoms.

Future Plans

Our planned work includes additional RCF, shock tube and flame studies. We plan to expand our RCF studies to mixtures of H_2/CO and CH_4 (to lower ignition sensitivity to temperature and thus change reaction kinetics), expand to include gas-sampling from RCF ignition and MEDB studies (providing new measurements of stable intermediates), conduct complementary laminar flare speed studies (to further consider transport effects on the siloxane chemistry), and we hope to add TMS to the test matrix (time-permitting). HMDSO and TMS have chemical structures that when compared with TMSO can provide

hierarchal understanding of this class of compounds. Additionally, HMDSO and TMS have direct relevance to semiconductor and other materials manufacturing and biogas systems. We will also continue to probe the source of reaction in the MEDB jets, further leveraging our collaboration with Kulatilaka at Texas A&M to obtain absolute rather than relative H-atom concentrations within the jet and flame. We will also expand the study to include OH concentrations and possibly O-atom measurements.

Progress is being made in developing reaction mechanisms for the pyrolysis of HMDSO and TMSO based on experimental data taken previously. In the last year, we have identified traces of key species in mass spectra taken with the miniature shock tube at the Advanced Light Source. These traces indicate decomposition is proceeding through highly reactive intermediates that rapidly lead to SiOx species. This is consistent with the observation that at high temperatures and pressures no organosilicon species larger than the reagent HMDSO are formed. Interpretation of the experimental data is somewhat impeded by dissociative ionization due to small amounts of photons at high harmonics of the selected ionization energy at the T2 endstation. Consequently, we intend to repeat some experiments at T4 which should minimize dissociative ionization. In collaboration with Sivaramakrishnan we will perform theoretical and experimental studies on TMS and hexamethyldisilane (HMDS) to gain a better understanding of the reaction mechanisms of trimethylsilyl groups which are key structural features of HMDSO and TMSO.

DOE publications supported by this project

Journal publications

Kim, K., Hay, M., Meng, Q., Wooldridge, M.S., Kulatilaka, W.D., Tranter, R.S., (2024) "Hexamethyldisiloxane pyrolysis: probing H-atom initiation by femtosecond two-photon LIF," *Proc. Combust. Inst.*, **40**, 105640, pp. 1-7.

Meng, Q., Banyon, C., Kim, K., Kim, J.H., Kastengren, A.L., Wooldridge, M.S., Tranter, R.S., (2024) "In-situ two-dimensional temperature measurements using x-ray fluorescence spectroscopy in laminar flames with high silica particle concentrations," *Combust. Flame*, 113564, pp. 1-8.

Meng, Q., Banyon, C., Kastengren, A. L, Wooldridge, M. S., Tranter, R. S., (2023) "Experimental Measurement of the Rapid Mixing of Fuel and Air in a Multi-Element Diffusion (Hencken) Burner," *Combust. Flame*, 251, 112686.

Theses

Kim, John, 2024, *Investigations of the Combustion Chemistry of Iso-Propanol, Siloxanes and Syngas Fuels*, Ph.D. Thesis, University of Michigan, Ann Arbor.

Meng, Qinghui (Sylvia), 2023, *Fundamental Studies of Organic Silicon Combustion Chemistry and Characterizing the Presence of Silicon Species in Landfill and Sludge Gas*, Ph.D. Thesis, University of Michigan, Ann Arbor.

Schwind, Rachel, 2019, *Understanding the Combustion Chemistry of Siloxanes: Reaction Kinetics and Fuel Interactions*, Ph.D. Thesis, University of Michigan, Ann Arbor.